REPORT 2014 - 07

VERMONT AGENCY OF TRANSPORTATION

Research & Development Section
Research Report

PERFORMANCE MONITORING OF JOINTLESS BRIDGES

PHASE III

Report 2014 – 07

May 2014

PERFORMANCE MONITORING OF JOINTLESS BRIDGES
PHASE III

Report 2014 – 07

May 2014

Reporting on SPR-RAC-985

STATE OF VERMONT
AGENCY OF TRANSPORTATION

RESEARCH & DEVELOPMENT SECTION

BRIAN R. SEARLES, SECRETARY OF TRANSPORTATION
CHRIS COLE, DIRECTOR OF POLICY, PLANNING AND INTERMODAL DEVELOPMENT
JOE SEGALE, P.E./PTP, PLANNING, POLICY & RESEARCH
WILLIAM E. AHEARN, P.E., RESEARCH & DEVELOPMENT

Prepared By:

UMass Transportation Center
Scott Civjan PhD, PE, Associate Professor, Dept. of Civil and Environmental Engineering
Sergio Breña PhD, Associate Professor, Dept. of Civil and Environmental Engineering
Emre Kalayci, Graduate Student, UMass Amherst Structural Engineering Department
Brooke Quinn, Graduate Student and Research Assistant, UMass - Amherst

University of Massachusetts Amherst
UMass Transportation Center
214 Marston Hall
Amherst, MA 01003
Website: http://www.ecs.umass.edu/umtc

University of Massachusetts Transportation Center

The information contained in this report was compiled for the use of the Vermont Agency of Transportation (VTrans). Conclusions and recommendations contained herein are based upon the research data obtained and the expertise of the researchers, and are not necessarily to be construed as Agency policy. This report does not constitute a standard, specification, or regulation. VTrans assumes no liability for its contents or the use thereof.

Technical Report Documentation Page

1. Report No.	2. Government Accession No.	3. Recipient's Catalog No.
2014-07	- - -	- - -

4. Title and Subtitle	5. Report Date
PERFORMANCE MONITORING OF JOINTLESS BRIDGES – PHASE III - FINAL REPORT	May 2014
	6. Performing Organization Code

7. Author(s)	8. Performing Organization Report No.
Scott Civjan, PhD, PE Emre Kalaycı Sergio Breña, PhD Brooke Quinn	2014-07

9. Performing Organization Name and Address	10. Work Unit No.
University of Massachusetts Amherst UMass Transportation Center 214 Marston Hall Amherst, MA 01003	11. Contract or Grant No. RSCH017-985

12. Sponsoring Agency Name and Address		13. Type of Report and Period Covered
Vermont Agency of Transportation Materials and Research Section 1 National Life Drive National Life Building Montpelier, VT 05633-5001	Federal Highway Administration Division Office Federal Building Montpelier, VT 05602	Final 2008 – 2014
		14. Sponsoring Agency Code

15. Supplementary Notes

16. Abstract

Part I:

The third phase of a research project investigating the field performance of jointless bridges is reported. Three integral abutment bridges in Vermont, US have been instrumented and monitored as part of this research. General descriptions of the bridges are reported along with the final instrumentation plan for each bridge. Installation procedures are described along with data obtained during the construction process. As the bridges were completed a series of load tests were performed. The live load truck positions and collected data are reported. Three dimensional finite element models of each bridge were developed and are described. The data collected during construction stages and live load testing are analyzed and compared with the results of finite element models.

Part II:

The third phase of a research project investigating the field performance of jointless bridges is reported. Three integral abutment bridges in Vermont, US have been instrumented and monitored as part of this research. The long term data collected including seasonal thermal fluctuations are analyzed and compared with the results of finite element models.

17. Key Words	18. Distribution Statement
Integral Abutment Bridges, Bridge Monitoring, Finite Element Modeling, Live Load Testing, Construction Analysis	No Restrictions.

19. Security Classif. (of this report)	20. Security Classif. (of this page)	21. No. Pages	22. Price
- - -	- - -	347	- - -

PERFORMANCE MONITORING OF JOINTLESS BRIDGES

PHASE III

Report 2014 – 07

PART I

TABLE OF CONTENTS

Page

LIST OF TABLES

Table Page

LIST OF FIGURES

Figure Page

1 INTRODUCTION

1.1 Project Overview

Integral abutment bridges (IABs) have been constructed by State Departments of Transportation for a number of years. These bridges have been found to be cost effective from both an initial cost and life-cycle cost analysis. However, common design guidelines are lacking and non-uniform limitations on IAB design are imposed by different agencies. In order to evaluate design guidelines, the Vermont Agency of Transportation (VTrans) has initiated a program of field instrumentation and analysis to evaluate the performance of three IABs currently under construction. The research components are being conducted by the University of Massachusetts at Amherst. Three bridges are included, a straight bridge with 43 m (141 ft) span, a 15 degree skew bridge with 37 m (121 ft) span, and a curved two-span continuous structure with 11.25 degrees of curvature and 68 m (221 ft) total bridge length. The bridges are instrumented with 83, 89, and 131 gages, respectively. Instrumentation includes strain gages, pressure cells, displacement transducers, inclinometers, tiltmeters and thermistors. This report describes the project scope, bridge details and instrumentation of these sites as well preliminary finite element modeling and live load testing.

1.2 Background

In recent years integral abutment bridges (IABs) have become increasingly common. Most U.S. transportation agencies have developed and adopted their own policies for design and construction of IABs in absence of AASHTO guidelines. As a part of VTrans' research program related to IABs, a literature review was conducted by Wiss, Janney, Elstner (WJE) Associates, Inc. (2002). The literature review included temperature effects, skew and curvature issues, soil structure interaction, construction and performance issues and related topics. The report also compiled a list of questions that should be addressed in future research and was a direct precursor to this project. A detailed survey (Maruri and Petro 2005) reported the numbers of IABs and their design criteria in 39 different states. With a total number of 9,000 IABs and 4,000 semi-integral abutment bridges, the number of jointless bridges has tripled in 10 years compared with results of a similar survey carried out in 1995. Design criteria were noted for each State related to maximum span, maximum total bridge length, maximum skew angle and maximum curvature for bridges. The survey also noted the distribution of IAB design and construction practices among the regions of the United States with northern states reporting a dramatic increase in the number of IABs. Approximately 75 percent of agencies reported integral or semi-integral abutment bridges were the preferred design when possible. In Canada each Province has generally employed its own design procedure for construction of IABs (Iles 2006). In a United Kingdom survey (Iles 2006) it was noted that the ratio of IAB to traditional bridges constructed

increased to 64 percent in 2004. Those designed as jointed bridges were typically long span or highly skewed bridges.

Considering the volume of IABs being constructed, there has been relatively little consistency in design practice or verification of current design provisions. Past surveys of IAB practice have found that existing design provisions vary significantly, often based on each State's experience (Kunin 2000) (Soltani 1992). In general, the limits imposed on design have been gradually relaxed if the bridge field behavior is deemed adequate. This has resulted in variations in span length, skew and curvature limitations for IAB design among states. For example, the maximum IAB total length allowed in different states ranges from approximately 45 m (131 ft) to 200 m (656 ft) for steel girders with longer spans allowed in concrete girder bridges (Maruri and Petro 2005). The maximum skew angle restrictions vary from to 15 to 70 degrees depending on the agency, with most states at the lower end of this spectrum. The most recent report noted IAB girder curvature was only allowed by 4 states and limited to 10 degrees (Maruri and Petro 2005).

Construction details vary for IABs (Maruri and Petro 2005) (Kunin 2000) (Soltani 1992) (Conboy 2005). For instance, details may include driving piles in the existing subgrade, providing a pre-augered hole infilled with a variety of materials (sand, natural bentonite, bentonite slurry, pea stone, crushed stone, or no infill) prior to pile driving, or providing pipe materials to retain the select backfill material. Piles may be oriented about their strong or weak bending axis. Variations appear to be design preferences rather than driven by soil considerations. The lack of standardized details makes blanket comparison of data difficult and limits the relevancy of some studies.

Uncertainties in IAB behavior exist, such as abutment lateral and rotational response, soil-structure interactions under skewed and repeated loading, the inelastic response and moment distribution in piles, importance of orientation and installation methods of piles, effects of wing wall orientation and continuity with abutment, influence of construction methods, appropriate temperature ranges and importance of thermal gradients in the superstructure. With systematic evaluation of these issues one can re-evaluate IAB limitations (bridge length, skew angles, curvature) and determine the applicability of AASHTO design requirements. Though computer modeling capabilities have significantly improved, analysis alone is not sufficient. Calibration to field data is required to validate assumptions of bridge performance and to validate design and modeling techniques. Therefore, the structures described in this report provide a systematic approach of instrumentation and analysis of three progressively more complicated structures in order to evaluate their design and performance.

2 DESCRIPTION OF BRIDGES

A straight, a skewed and a curved steel girder IAB were selected for the monitoring project. Each bridge was constructed to replace an existing aging jointed bridge. To benefit from reduced maintenance costs, the bridge superstructures were designed to be integral with abutments and wing walls. Girders are built up sections of Grade 345W (50W) steel and include two rows of 22 mm (0.86 in) diameter by 180 mm (7.1 in) long shear studs for composite action. Girders are braced by steel angle cross frames. Piles are compact sections of Grade 345 (50W) steel driven directly into the subgrade. Piles are equally spaced across the abutment and oriented to bend about their weak axis when subjected to bridge longitudinal expansion and contraction. This was done to provide maximum deformation capacity under thermal displacements. Detailed descriptions of the bridges are given in the following sections.

2.1 Middlesex Bridge

The straight IAB is located on VT12 over Martin's Brook in Middlesex, VT. The bridge has a single span with length of 43.0 m (141.1 ft) from bearing to bearing and width of 10.2 m (33.5 ft) to outside of fascia. The structure has a 220 mm (8.7 in) concrete deck supported on five plate girders. Each girder web is 1170X14 mm (46.1X0.6 in) with a top and bottom flange plates of 510X25 mm (20.1X1.0 in) and 510X54 mm (20.1X2.1 in) respectively. The girders are evenly spaced every 2.05 m (6.7 ft) across the bridge starting 1.00 m (3.28 ft) from each deck fascia. A total of 376 shear studs are provided per girder. Galvanized steel guardrails are provided along the bridge deck edge with concrete supports. The steel girders are embedded into the abutment walls at both ends of the bridge, and supported by anchor bolts. Cross frames are provided throughout the length of the bridge at 5.50 m (18.05 ft) spacing. Each abutment wall is supported on 5 HP 310X125 (HP 12X84) steel piles. The piles are embedded 1.00 m (3.28 ft) into the bottom of the abutment and extend approximately 9.00 m (29.53 ft) below the abutment. The abutment has a total thickness of 1.00 m (3.28 ft) and extends 4.00 m (13.12 ft) to 4.20 m (13.78 ft) from the bottom of abutment to top of concrete (total depth of abutment concrete) at the fascia and center of roadway, respectively. Wing walls are integral with the abutment, have a thickness of 0.45 m (1.48 ft) and extend 3.00 m (9.84 ft) perpendicular to the abutment. A 6.0 m (19.7 ft) long approach slab of 380 mm (15 in) thickness is provided at each end of the structure. Figure 2-1 shows the bridge after construction is over. Figure 2-2, Figure 2-3, Figure 2-4 and Figure 2-5 show a plan view of the bridge, an elevation view of the bridge, plan and elevation view of abutment and a deck section view, respectively.

At the Middlesex Bridge, deck concrete placement was done in three stages. The center portion of the deck was placed in a day and separated from the ends of bridge by temporary formwork plugs located 3.3 m (10.8 ft) away from the abutments. Once the center portion of the deck hardened, the ends were cast to build a monolithic connection between deck, girders, and

abutment stem. This concrete pour sequence allowed rotation of the girder ends under self-weight of the deck and locks the deformed shape after deck concrete placement is finalized.

Figure 2-1: Middlesex Bridge

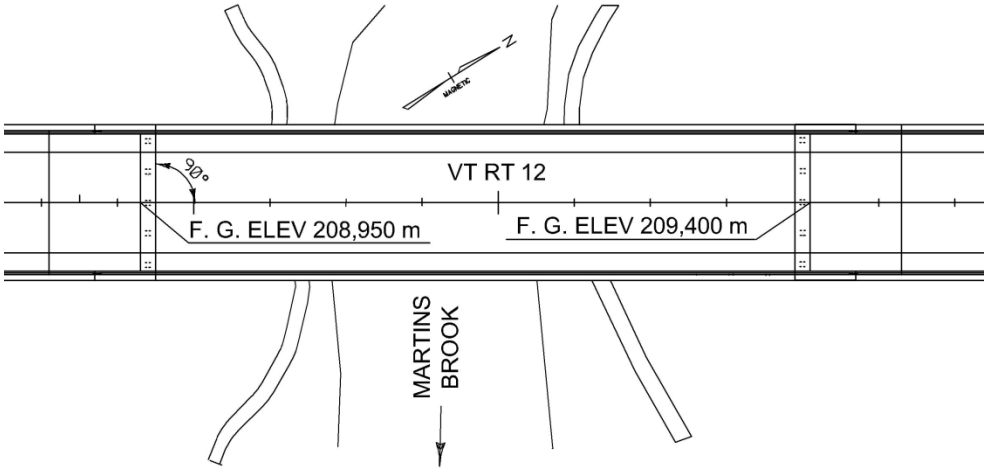

Figure 2-2: Plan View of Middlesex Bridge

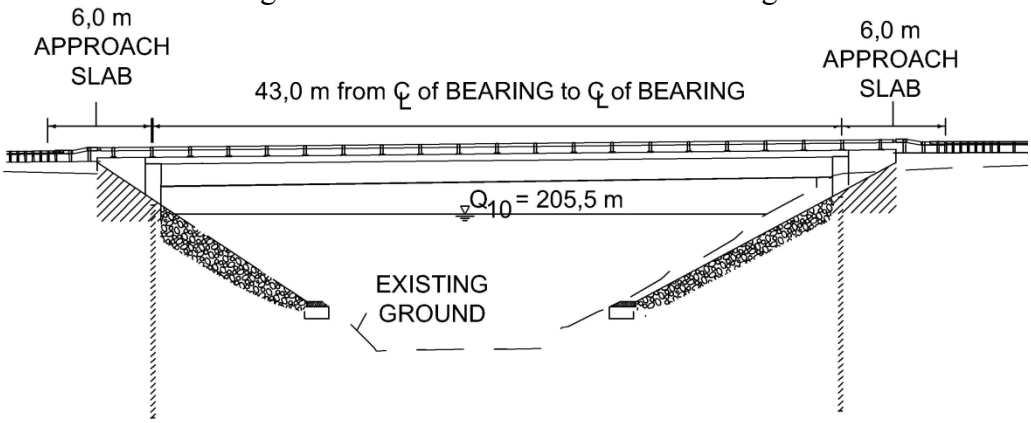

Figure 2-3: Elevation View of Middlesex Bridge

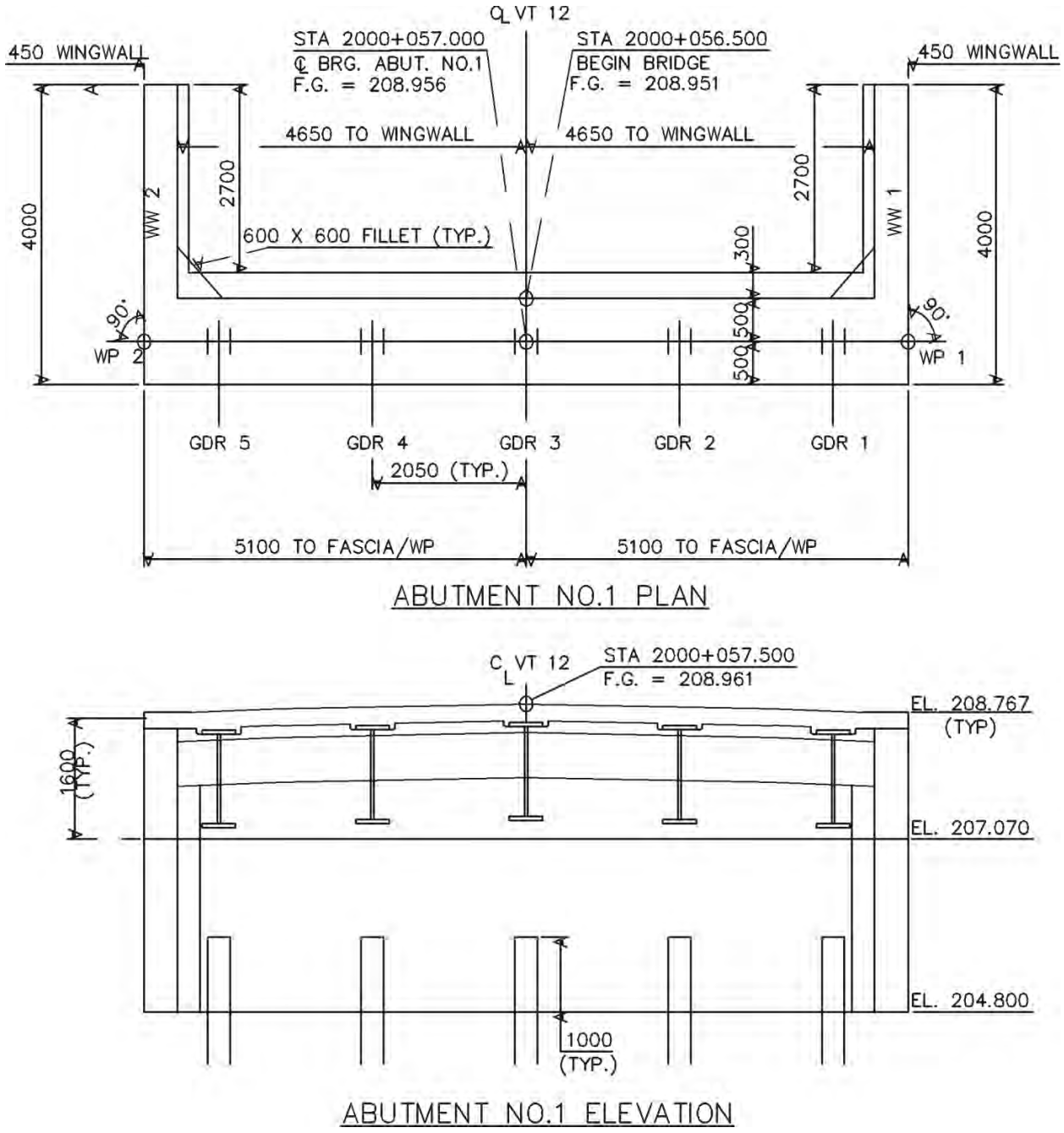

Figure 2-4: Plan and Elevation View of Abutment 1 at Middlesex Bridge

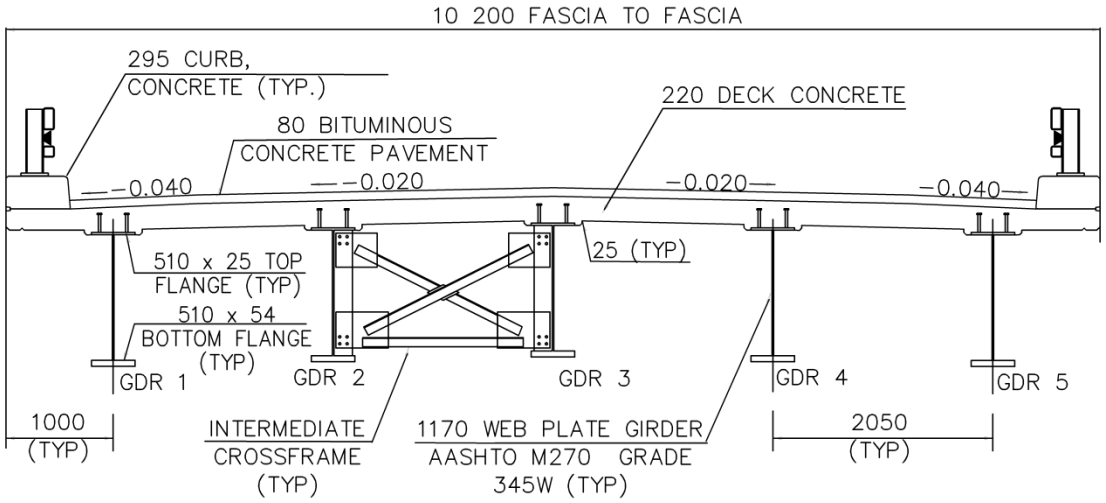

Figure 2-5: Middlesex Bridge Deck Section

2.2 East Montpelier Bridge

The skewed IAB is located on US2 over the Winooski River in East Montpelier, VT (Figure 2-6). It is a single span structure with a bridge skew of 15 degrees. The bridge has a single span with length of 37.0 m (121.4 ft) from bearing to bearing and width of 14.2 m (46.6 ft) to outside of fascia.

Figure 2-7, Figure 2-8, Figure 2-9 and Figure 2-10 show a plan view of bridge, an elevation view of bridge, plan and elevation view of abutment and a deck section view, respectively. The structure includes a 220 mm (8.7 in) concrete deck supported on five plate girders. Each girder web is 1346X16 mm (53X0.6 in) with top and bottom flange plates of 457X22 mm (18X0.87 in) and 457X41 mm (18X1.6 in), respectively. The girders are evenly spaced every 3.00 m (8.84 ft) across the bridge starting 1.10 m (3.61 ft) from each deck fascia. A total of 372 shear studs are provided per girder. Galvanized steel guardrails are provided along the bridge deck edge with concrete supports. The steel girders are embedded into the abutment walls at both ends of the bridge, and supported on a steel reinforced elastomeric pad. Cross frames are provided throughout the length of the bridge at 4.63 m (15.19 ft) spacing. Each abutment wall is supported on 5 HP 310X125 (HP 12X84) steel piles. The piles are embedded 0.60 m (1.97 ft) into the bottom of the abutment and extend approximately 38 m (125 ft) below the abutment. The abutment has a total thickness of 0.90 m (2.95 ft) and extends 3.90 m (12.80 ft) to 4.05 m (13.29 ft) from the bottom of abutment to top of concrete (total depth of abutment concrete) at the fascia and center of roadway, respectively. Wing walls are integral with the abutment, have a thickness of 0.45 m (1.48 ft) and extend 2.80 m (9.19 ft) from the centerline of the abutment at a 15 degree skew. The wing walls are tapered below the abutment construction joint at an angle of 45 degrees. A 6.0 m (19.7 ft) long approach slab of 380 mm (14.96 ft) thickness is provided at each end of the structure.

At the East Montpelier Bridge, the deck pour sequence differed from the scheduled construction plan. The initial plan was to pour the deck continuously including the abutment stems to have a monolithic connection between all superstructure components. However, due to problems encountered during deck concrete placement significant differences occurred. The deck concrete pour started from one abutment and continued to midspan. The process was then halted for a required modification in cross bracing. Hardened concrete was removed from the abutment through the first 6.1 m (20 ft) of the span. Subsequently, the remainder of the deck and the far abutment stem was poured monolithically.

Figure 2-6: East Montpelier Bridge

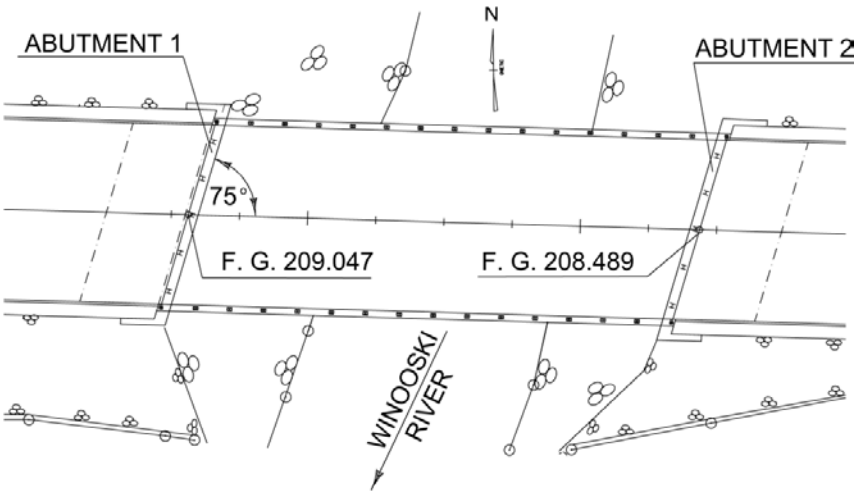

Figure 2-7: Plan View of East Montpelier Bridge

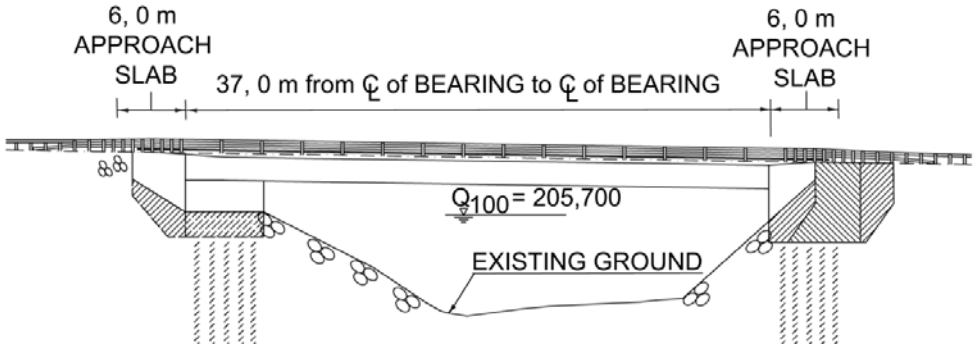

Figure 2-8: Elevation View of East Montpelier Bridge

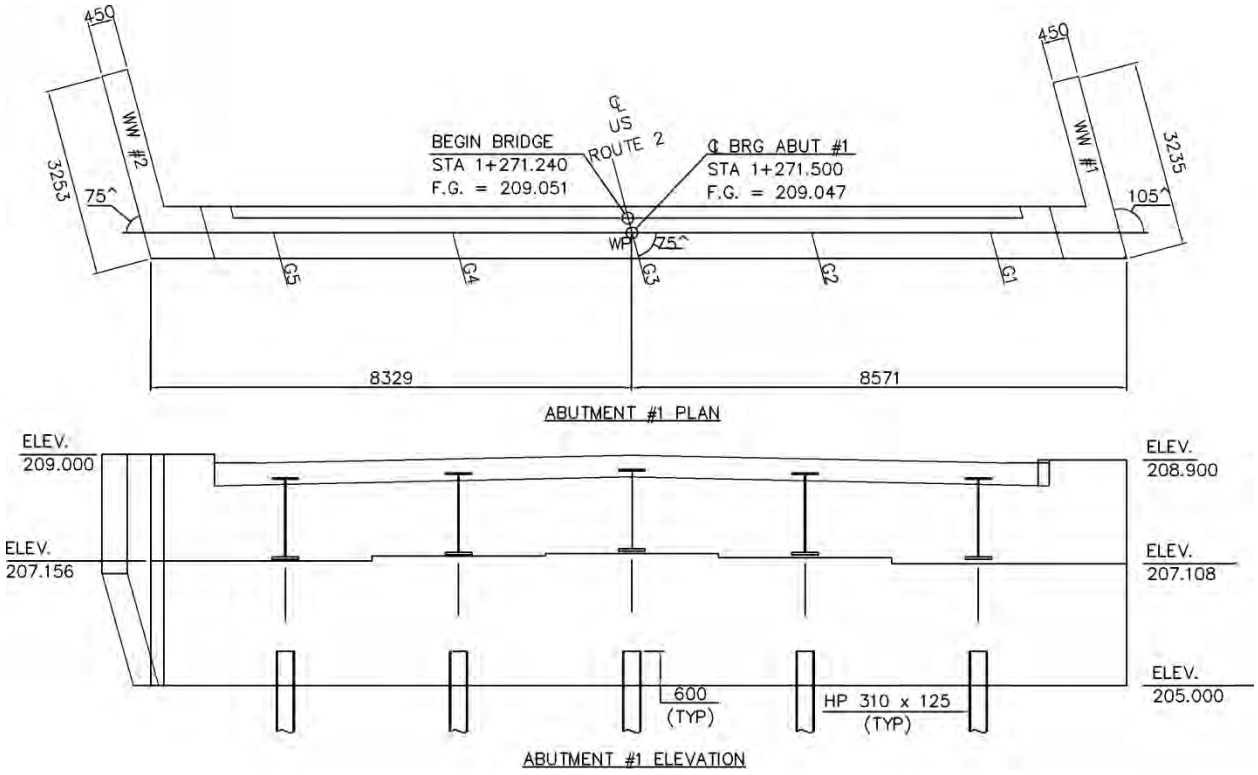

Figure 2-9: Plan and Elevation View of Abutment 1 at East Montpelier Bridge

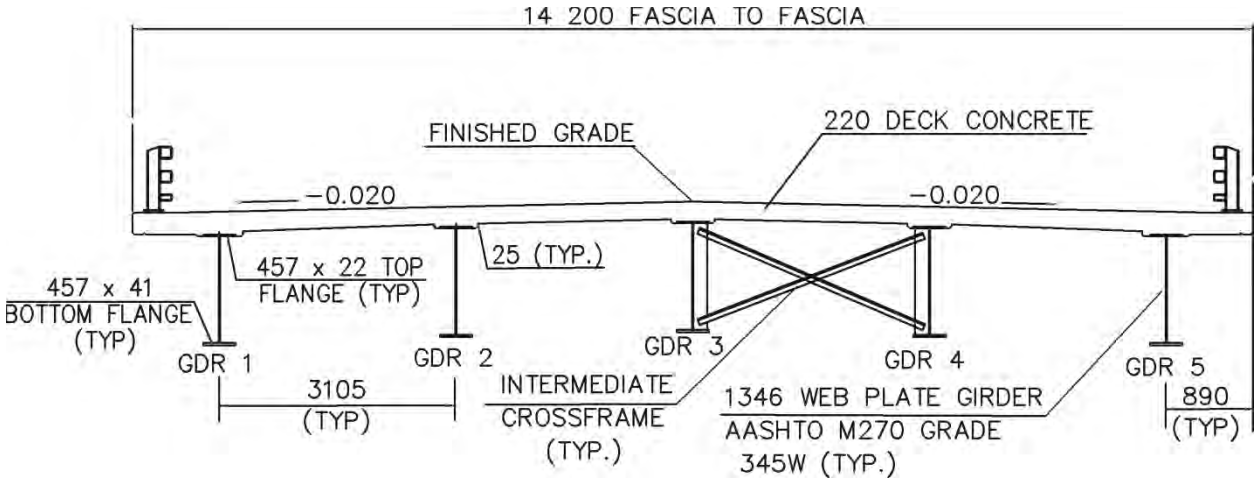

Figure 2-10: East Montpelier Bridge Deck Section

2.3 Stockbridge Bridge

This curved girder bridge is located on VT Route 100 and crosses the White River in Stockbridge, VT (Figure 2-11). It has a length of 67.6 m (222.0 ft) along its curved centerline. The degree of curvature along the bridge alignment is 11.25 degrees. A center pier is included with guided bearings positioned on the top of the pier cap beam to support each steel girder. Bearing constraints differ for Girders 1 to 3 (longitudinal displacement restrained) and Girders 4 and 5 (displacements in all directions restrained). At the road level, there is a superelevation of 6 percent and a vertical elevation difference between start and end of the bridge of 1.3 m (4.3 ft). Figure 2-12, Figure 2-13, Figure 2-14 and Figure 2-15 show a plan view of bridge, an elevation view bridge, plan and elevation views of abutment and a steel framing layout, respectively. The bridge width is 11.3 m (37.1 ft) to the fascia and has a composite deck with a 203 mm (8 in) thickness of reinforced concrete and built-up steel plate girders. Five girders with variable cross section along and across the bridge support the concrete deck spaced at 2.36 m (6.70 ft). Girders are numbered from outer (Girder 1) to inner (Girder 5). Web dimensions are constant at 1170X16mm (46X0.6 in). Flange dimensions differ among girders and vary along the span as shown in Figure 2-16 and Figure 2-17, respectively for Section 1 and Section 2. A total of 638 to 676 shear studs are provided per girder (interior and exterior girder respectively). Thirteen cross frames are provided along the bridge, with spacing varying from 2.6 m (8.5 ft) near the interior bent to 5.8 m (19.0 ft) over the rest of the structure. The abutments have a thickness of 0.90 m (3.00 ft) and an average depth of 6.30 m (20.70 ft). Wing walls are oriented at 85 degrees and 110 degrees from the abutment and are tapered below construction joints. Wing walls have a thickness of 0.45 m (1.5 ft) and extend 3.00 m (10 ft) and 4.30 m (14.00 ft) from the centerline of Abutment 1 and Abutment 2, respectively. Each abutment is supported on five HP 360X174 (HP 14X117) steel piles. The piles are embedded 0.60 m (2.00 ft) into the bottom of the abutment and extend approximately 23 m (7.5 ft) below the abutment.

At the Stockbridge Bridge, the deck and abutment stems were poured in a three step procedure. Firstly, the deck itself was separated from the ends of bridge by temporary formwork located at 1.8 m (6.0 ft) away from the abutments. This part of the deck was poured in 8 hours. Once it was hardened, the ends of the girders were monolithically cast with the abutment stem.

At the Stockbridge Bridge, geofoam material was applied at the abutment backwalls in this structure prior to backfilling. The design purpose was to reduce peak earth pressures on abutments.

Figure 2-11: Stockbridge Bridge

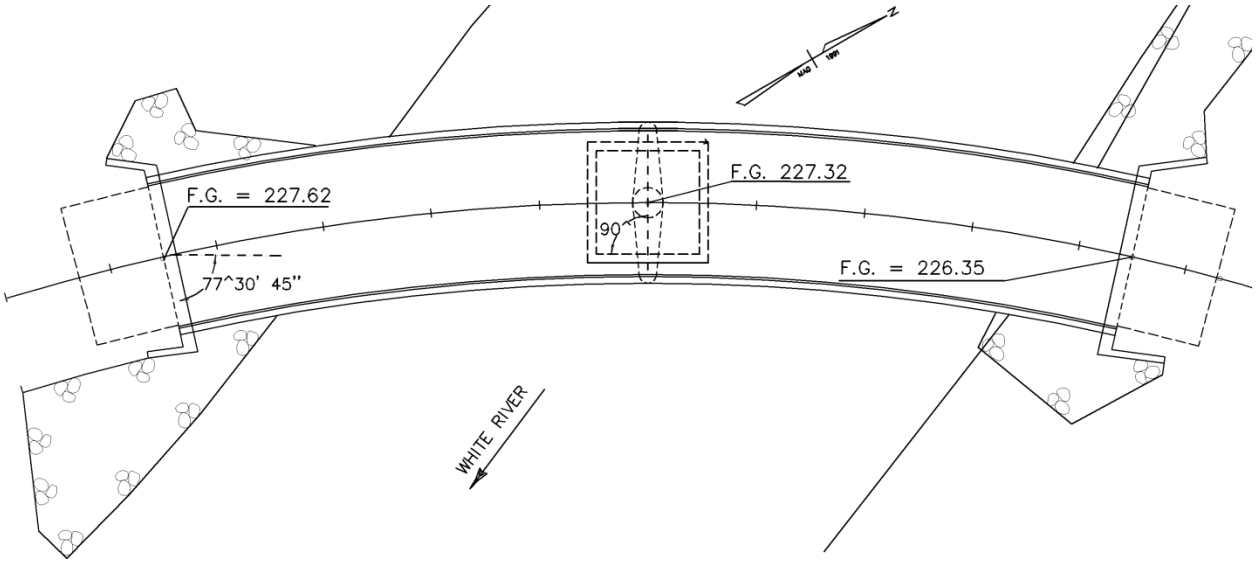

Figure 2-12: Plan View of Stockbridge Bridge

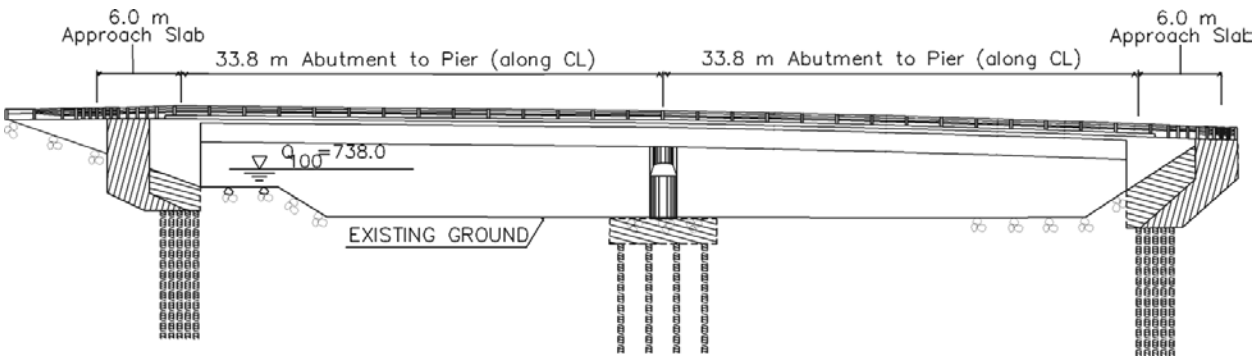

Figure 2-13: Elevation View of Stockbridge Bridge

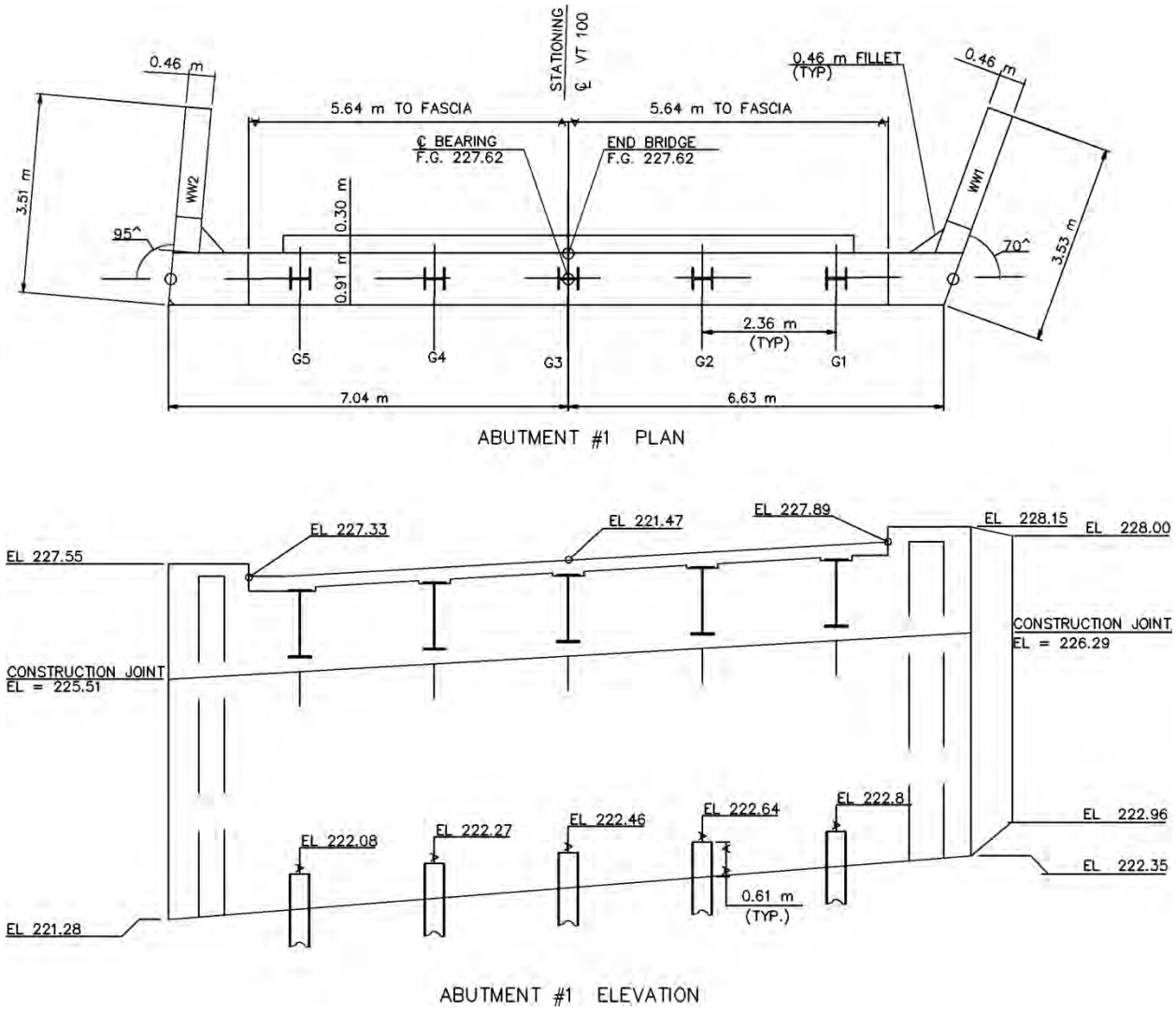

Figure 2-14: Plan and Elevation Views of Stockbridge Bridge Abutment 1

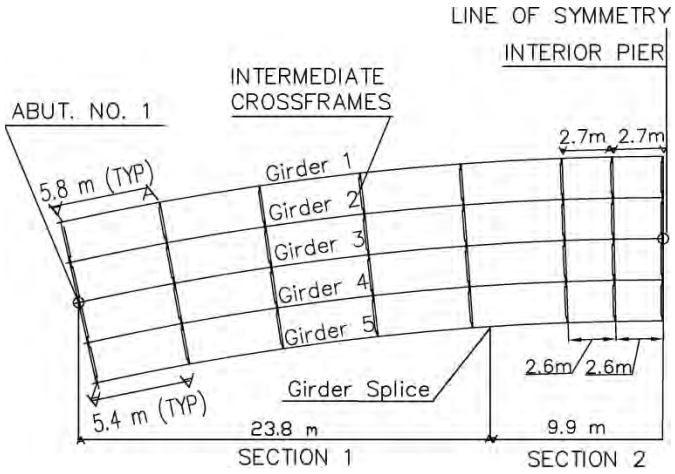

Figure 2-15: Stockbridge Framing Layout

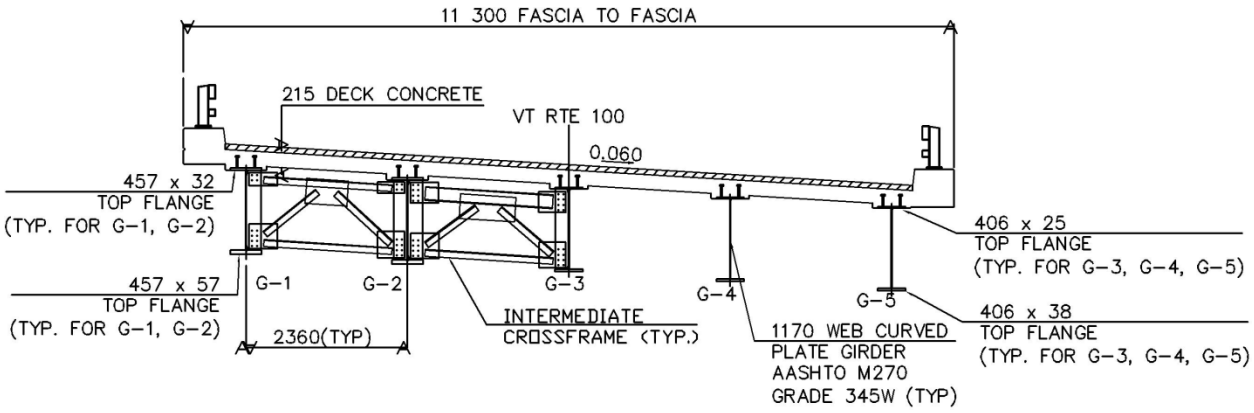

Figure 2-16: Stockbridge Deck Section 1

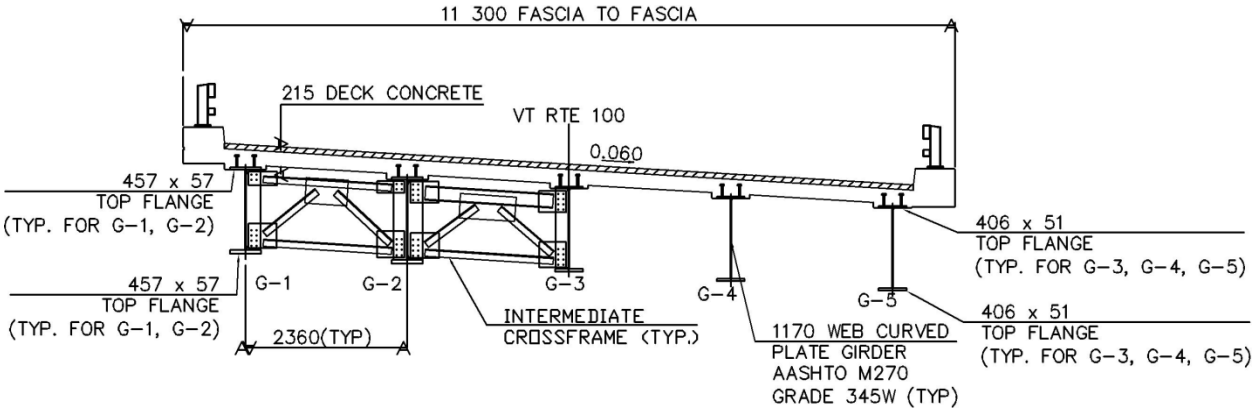

Figure 2-17: Stockbridge Deck Section 2

3 INSTRUMENTATION OF BRIDGES

3.1 Introduction

All three IABs were constructed with an array of permanent sensors and data logging equipment. Seasonal thermally induced response is the primary focus of the instrumentation plans, although daily fluctuations will also be monitored and static live-load testing of the structures will also be investigated. Monitoring of each structure will continue for a minimum period of two years following the end of construction with data collected every 6 hours. Each instrumentation system consists of Geokon gages and multiplexers and Campbell Scientific CR1000 and CR10X data loggers allowing for automated data collection and remote access.

The types of instruments utilized in the three bridges are similar, although the locations and functions vary depending on the instrumentation objectives for each bridge. Instrumentation of each IAB is focused on determining passive and active pressures at the abutment and wing walls, abutment movements (lateral, longitudinal and rotational), pile strains to monitor yielding and locations of positive and negative moments, strains in girders at critical locations and pile deformations. Gage locations were selected using two criteria. First, the significance of data was to be optimized based on expected IAB behavior. Second, a degree of redundancy was built into the instrumentation plans to allow verification of gage readings and mitigate loss of data from gage malfunction throughout the monitoring period. The instrumentation plans with gage locations at each bridge is summarized in the subsequent sections.

Two different types of instruments are used in the project – vibrating wire (VW) gages and microelectromechanical system (MEMS) gages. MEMS gages have the advantage of having more than one internal unit that can collect data. Therefore, whenever multiaxial response of a structural component is expected, MEMS gages are preferred over VW gages. In this project, MEMS gages are used to monitor the pile displacements at East Montpelier Bridge, pile and abutment displacements at Stockbridge Bridge. All the MEMS used in instrumentation planning were biaxial.

Vibrating wire pile strain gages were placed on the HP piles supporting each abutment, attached to the inside face of flanges. These instruments are located in the top 1.5 m (5 ft) to 3.0 m (10 ft) of the piles. These instruments are used to measure strains in the piles from which approximate stresses and moments can be calculated, indicating the location and extent of any pile yielding. Strain gages were also placed on girders at the inside face of top and bottom flanges at locations of expected critical positive and negative moments and can be used to determine neutral axis location to evaluate composite action. In Stockbridge, concrete strain gages were embedded in the center pier concrete to monitor bending of the pier.

Earth pressure cells are located behind abutment walls and wing walls to measure the distribution of pressures behind the walls, both across the abutment and at various depths. Recent reports have noted that fluid pressure cell readings can fluctuate with temperature (Daigle 2005). In this type of cells, temperature correction factors account only for vibrating wire properties but not for temperature effects on the fluid/cell interaction. To account for potential fluctuations in readings with changing temperature, a reference pressure cell was installed on a concrete block placed under one of the approach slabs. Reference cells were located away from the bridges as much as possible to minimize the effects of earth pressure fluctuation in the soil caused by bridge movements. Therefore, these reference cells can be used to implement appropriate correction factors for other pressure cells installed behind the abutments.

Tiltmeters and inclinometers were used to monitor the rotations of bridge substructures. Tiltmeters monitor the rotations of the abutments directly. They are anchored into the surface of the abutment with expansion anchors. Inclinometers are configured to reference rotation between wheel contact points within a casing which is rigidly attached to abutment piles. A linked string of these instruments provides data on the pile rotation between reference points and is used to evaluate pile deformations. At the Middlesex and Stockbridge Bridges, in order to enable gage removal/replacement in the future, the inclinometer casings were extended to the roadway level. At the top of the casing, a steel water-tight cover was installed. In the East Montpelier Bridge, however, the casings were cut at the construction joint in the abutments. Therefore the gages were embedded into concrete after the concrete pour. Before the pour, the top of the casing was sealed and the gage cables routed to their multiplexer location. Because of this, it will be impossible to service or replace these gages.

Displacement transducers measure longitudinal and transverse displacements of the abutments relative to a reference pile. Reference piles were driven near the outer face of abutments. They were driven to a depth of approximately 4.6 m (15 ft) with their flanges parallel to abutment alignment. Piles were offset laterally from the abutment and assumed to be minimally affected by abutment movements. A concrete enclosure with manhole access at the top of the enclosure protects the gages. The enclosure bottom was left open (bare soil) to allow for water drainage. Details and dimensions of these enclosures and reference piles differ between the bridges due to VTrans designer decisions and contractor preferences.

All instruments include an internal thermistor. Thermistors will provide local temperatures at gage locations (for gage thermal corrections) and allow for some evaluation of temperature fluctuations throughout the structure (thermal gradients).

Gage cables are routed to multiplexers located in enclosures on the face of each abutment between girders. Multiplexer cables are then routed to a single enclosure containing data logging equipment with electrical and phone service. All cables were secured in PVC or metal conduit or

encased in the abutment concrete. In order to protect data acquisition system against lighting and power surges, multiplexers and dataloggers were grounded using 10-AWG cable and 13 mm (0.5 in)-diameter grounding rods. The datalogger enclosure didn't have any protection against high and low outside temperature. However, water and weather proof enclosure is providing the required insulation that keeps the inside temperature within the working temperature range provided by datalogger manufacturer.

A summary of gage types and monitored responses corresponding to each gage type are given in Table 3-1. A total of 83, 89 and 131 gages were used for the Middlesex, East Montpelier and Stockbridge bridges, respectively. The total number of each gage type installed is provided in Table 3-2 for all three bridges.

Table 3-1: Summary of Gage Types

GAGE TYPE	**GAGE TYPE**	**GAGE MODEL (Geokon)**	**MONITORED RESPONSE**
Pier Strain Gage	Vibrating Wire	4200	Strains in pier column (only at Stockbridge Bridge)
Girder Strain Gage	Vibrating Wire	4050	Strains on girders
Pile Strain Gage	Vibrating Wire	4000	Strains on piles
Earth Pressure Cells	Vibrating Wire	4810 & 4815	Abutment Backfill Pressures
Displacement transducers	Vibrating Wire	4420	Abutment displacements
Inclinometers (Uniaxial)	Vibrating Wire	6350	Pile deformations
Tiltmeters (Uniaxial)	Vibrating Wire	6350	Abutment Rotations
Inclinometers (Biaxial)	MEMS	6150	Pile deflections
Tiltmeters (Biaxial)	MEMS	6160	Abutment Rotations (only at Stockbridge Bridge)

Table 3-2: Total Number of Gages in Each Bridge

	Strain Gage			Pressure Cell			Displacement Transducer	Tiltmeter	Inclinometer	Total Number of Gages
	Pile	Girder	Pier	Abutment	Wingwall	Reference				
Middlesex	37	18	NA	11	1	1	4	2	9	83
East Montpelier	32	20	NA	12	1	1	5	2	16	89
Stockbridge	60	24	8	16	4	1	6	2	10	131

3.2 Middlesex Bridge Instrumentation

Instrumentation at the Middlesex Bridge is concentrated on the middle and exterior piles and girders, providing information on variations of response across the abutment. Instrumentation is placed primarily at one abutment (Abutment 1) and corresponding girder end. The other abutment (Abutment 2) includes fewer instruments, but will allow verification of specific readings and provides information on variations that occur in ostensibly identical situations (due to factors such as construction variability, temperature gradients and variable soil conditions).

Data will be used to verify the applicability of an assumed symmetric two dimensional model (commonly used for design) and will allow comparison of deformations and stresses obtained from analyses. Figure 3-1 shows the data acquisition system installed at the Middlesex Bridge. Multiplexers are attached to the abutment wall whereas the datalogger box, phone lines and power are located on a concrete pad next to the approach to the bridge. Figure 3-2 shows the cable routing on an abutment, while Figure 3-3 schematically shows the cable routing for the entire structure. The elevation view of substructure instrumentation is shown in Figure 3-4, which indicates the gages located at each abutment.

Earth Pressure cells are attached to the backfill face of the abutments. All installed earth pressure cells are located below the abutment construction joints. The bottom row of gages is located at 0.3 m (1 ft) above the bottom of abutments. Abutment 1 has a second row of 3 gages located at 0.8 m (2.6) away from the bottom row of gages. The gages at the edges are 0.8 m (2.6 ft) away from abutment-wingwall connection. Both abutments have a single pressure cell positioned right below the construction joint at the center of the abutment. A single wingwall pressure cell is attached to Wingwall 3 as shown in Figure 3-5. The reference pressure cell is located 1 m (3 ft) below the approach slab. The concrete block encasing the gage is positioned vertically while the gage is facing towards the centerline of the roadway. The concrete block is located at 6.0 m (19.7 ft) away from the bridge end and 3.3 m (10.8 ft) away from the centerline of roadway. Position of the reference pressure cell is shown in Figure 3-6.

Pile strain gages are mounted on the inner side of the pile flanges as shown in Figure 3-7. . They are installed as 3 or 4 gages at each pile cross section in order to observe both weak and strong axis bending moments on the piles. The spacing between the flange edge and centerline of the gage is 77 mm (3.0 in).

The Middlesex Bridge girders have three sets of gages along their length. These girder strain gages are located at midspan of the bridge and near both ends of the bridge (Figure 3-8). At the ends of the bridge, the distance between gage location and ends of steel girder sections was 4.50 m (14.75 ft). The gages at the midspan are 22.7 m (74.5 ft) away from the end of the steel girder sections at Abutment 1. Two or four girder strain gages are attached to each instrumented girder cross section. The gages are positioned close to the edge of girder flange.

The spacing between the edge of the flange and the gages is 5 cm (2 in). Girder cross sections with 2 and 4 strain gages are shown in Figure 3-8.

One tiltmeter is located at the center of each abutment wall. At the Middlesex Bridge, the tiltmeters are mounted 0.5 m (1.65 ft) below bottom of girder flange. Inclinometers were installed on only one end of the bridge. The inclinometer casings were extended to the roadway level to allow gage removal/replacement after construction. At the top of the casing, a steel water-tight cover was placed. Abutment 1 has one inclinometer string with 4 gages and another one with 5 gages that are attached to piles below Girder 2 and Girder 4, respectively. The piles are instrumented on the pile flanges facing toward centerline of the roadway. A pile cross section showing the inclinometer casing attached to the pile flange is shown in Figure 3-9. The top wheel of the gage assembly is located at the bottom of the abutment. Distance between inclinometer gages is 0.6 m (2 ft), 0.9 m (3 ft) and 1.2 m (4 ft) (for the remaining spacings) starting from the bottom of the abutment. Therefore, the maximum depths of monitored pile deflections are 4.0 m (13 ft) and 5.2 m (17 ft) for Pile 2 and Pile 4, respectively. Since maximum pile moment will occur close to the bottom of abutment, the spacing between gages was decreased from 1.2 m (4 ft) to 0.6 or 0.9 m (2-3 ft) at the top of the pile to increase the number of readings in regions of high moment and to allow a detailed deflected shape to be constructed in this region of the pile.

The Middlesex Bridge is instrumented with 4 displacement transducers which are located only at the North side of the abutments. Both longitudinal and transverse measurements are taken at these locations. Displacement transducers with 50 mm (2.0 in) gage lengths are used to measure the displacements. The enclosure at Middlesex Bridge is significantly smaller than the enclosures at the other two bridges. Moreover, at the Middlesex Bridge the reference piles are encased with a circular concrete section over the top 3 m (9.8 ft) to decrease pile flexibility with the top 10 cm (4 in) of the steel pile exposed to enable gage attachment to the reference piles. Figure 3-11 shows the displacement transducers installed at both ends of the bridge.

a) Multiplexers at Abutment

b) Datalogger at Approach

Figure 3-1: Data Acquisition System in Middlesex Bridge

Figure 3-2: Cable Routing on the Abutment

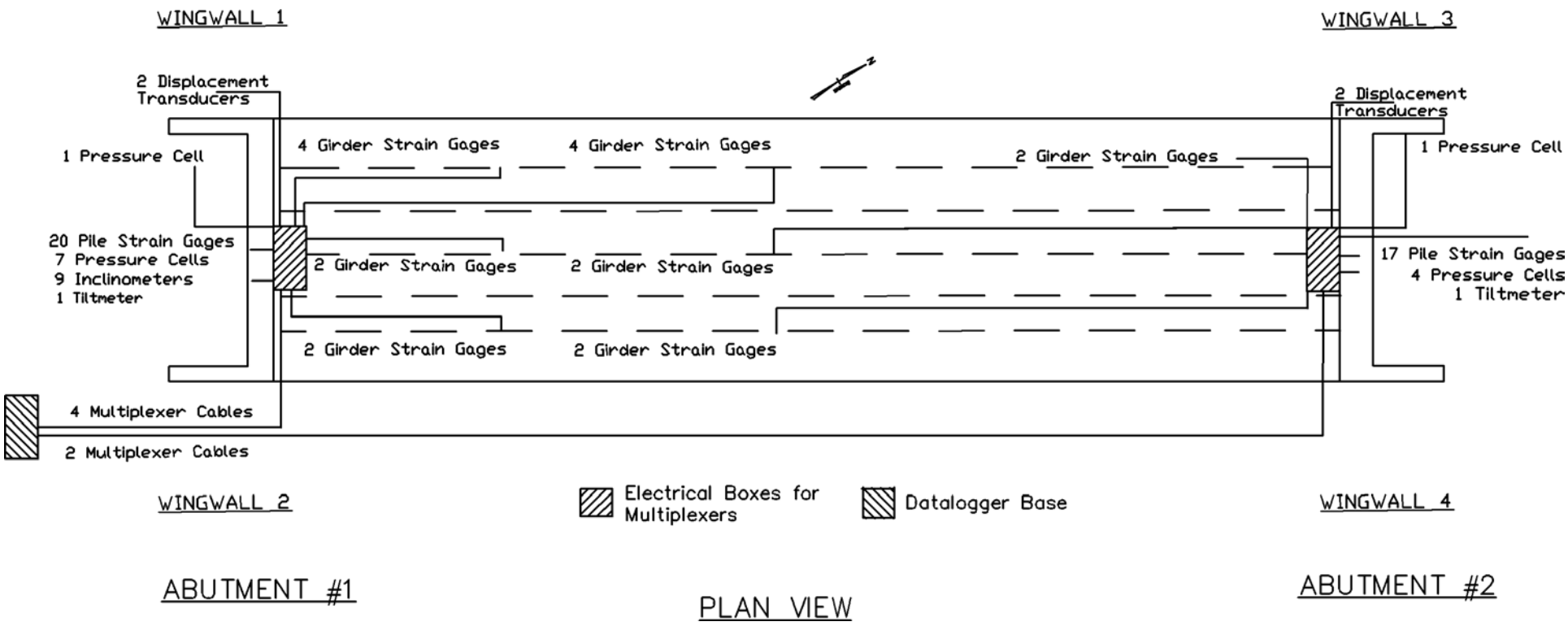

Figure 3-3: Overview of Instrumentation in Middlesex Bridge

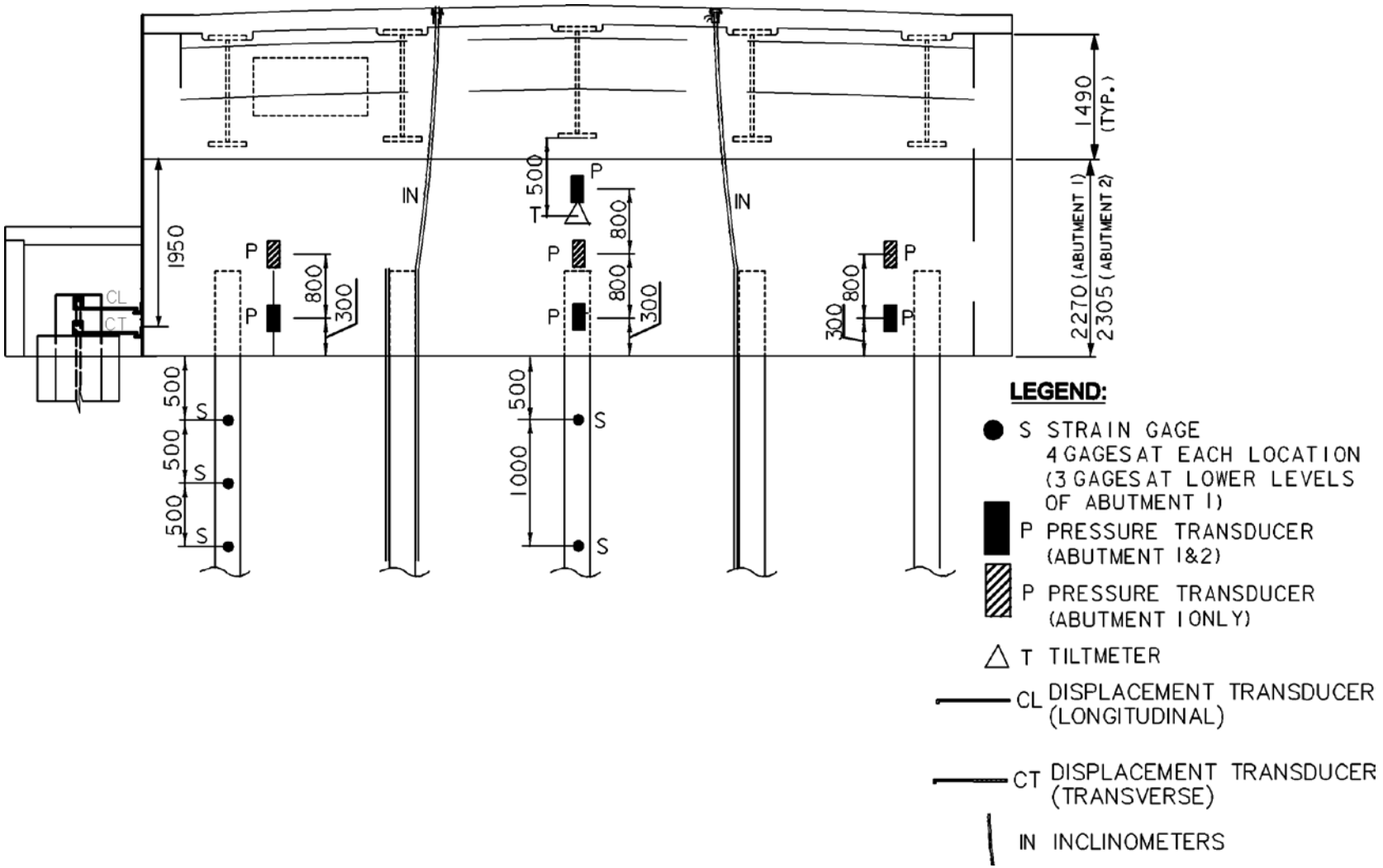

Figure 3-4: Instrumentation at Middlesex Bridge

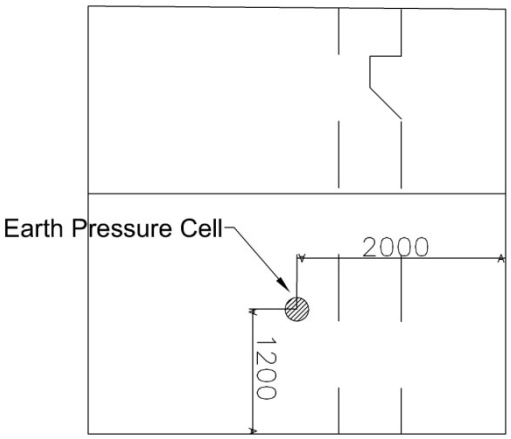

Figure 3-5: Wingwall Earth Pressure Cell at Middlesex Bridge

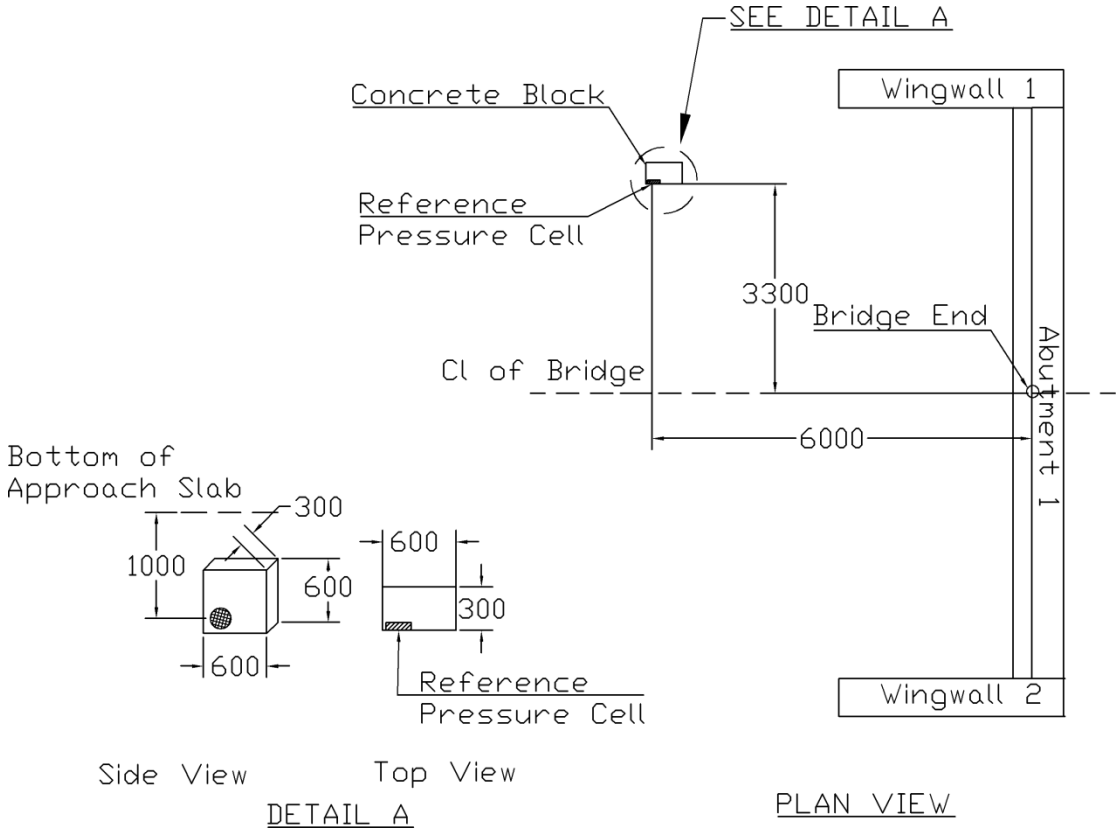

Figure 3-6: Reference Earth Pressure Cell at Middlesex Bridge

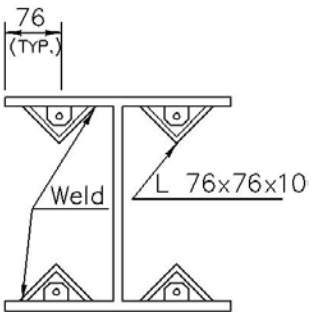

4 Gages at Cross Section (not to scale)

Figure 3-7: Pile Strain Gages at Middlesex Bridge

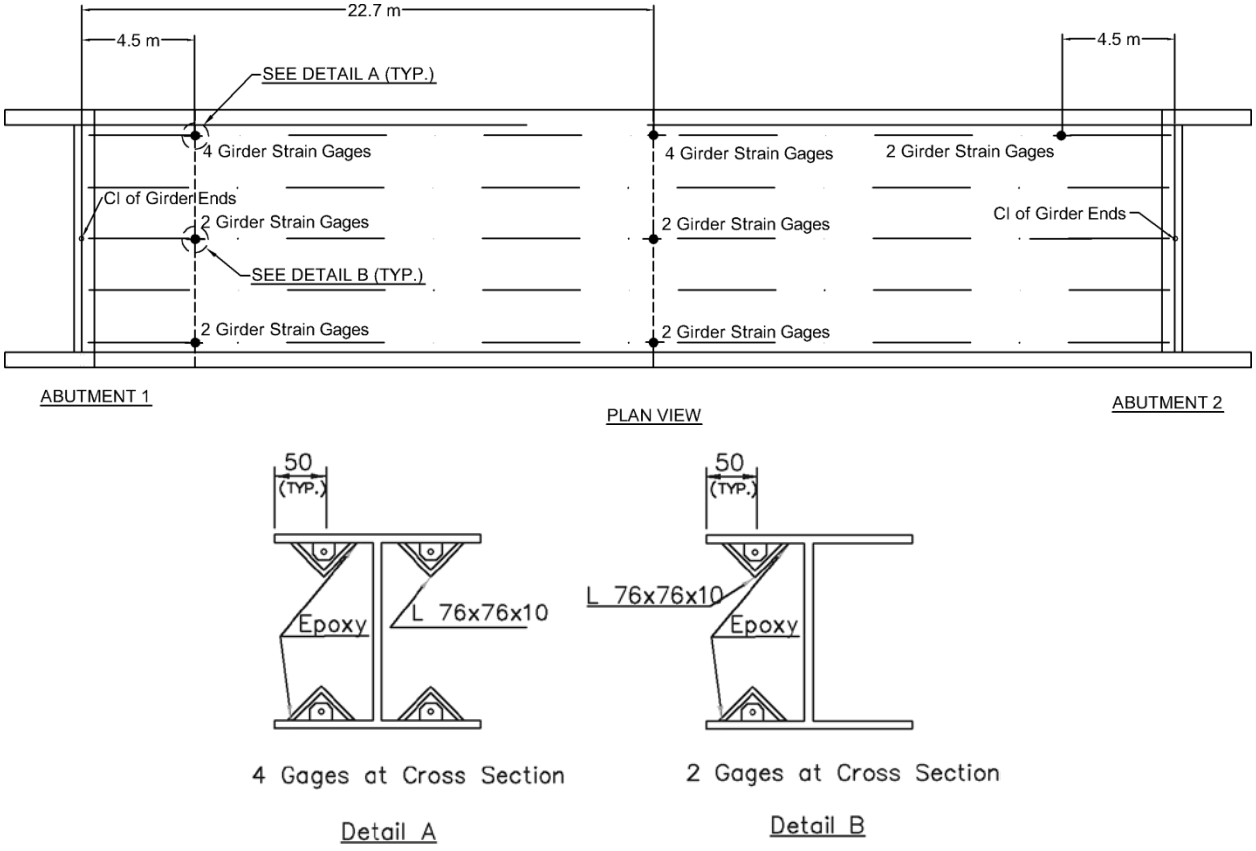

Figure 3-8: Girder Strain Gages at Middlesex Bridge

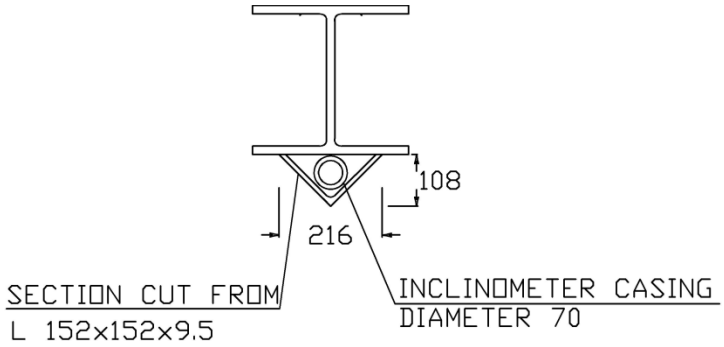

DETAIL FOR PILES BELOW GIRDER 2 and 4

Figure 3-9: Inclinometers at Middlesex Bridge

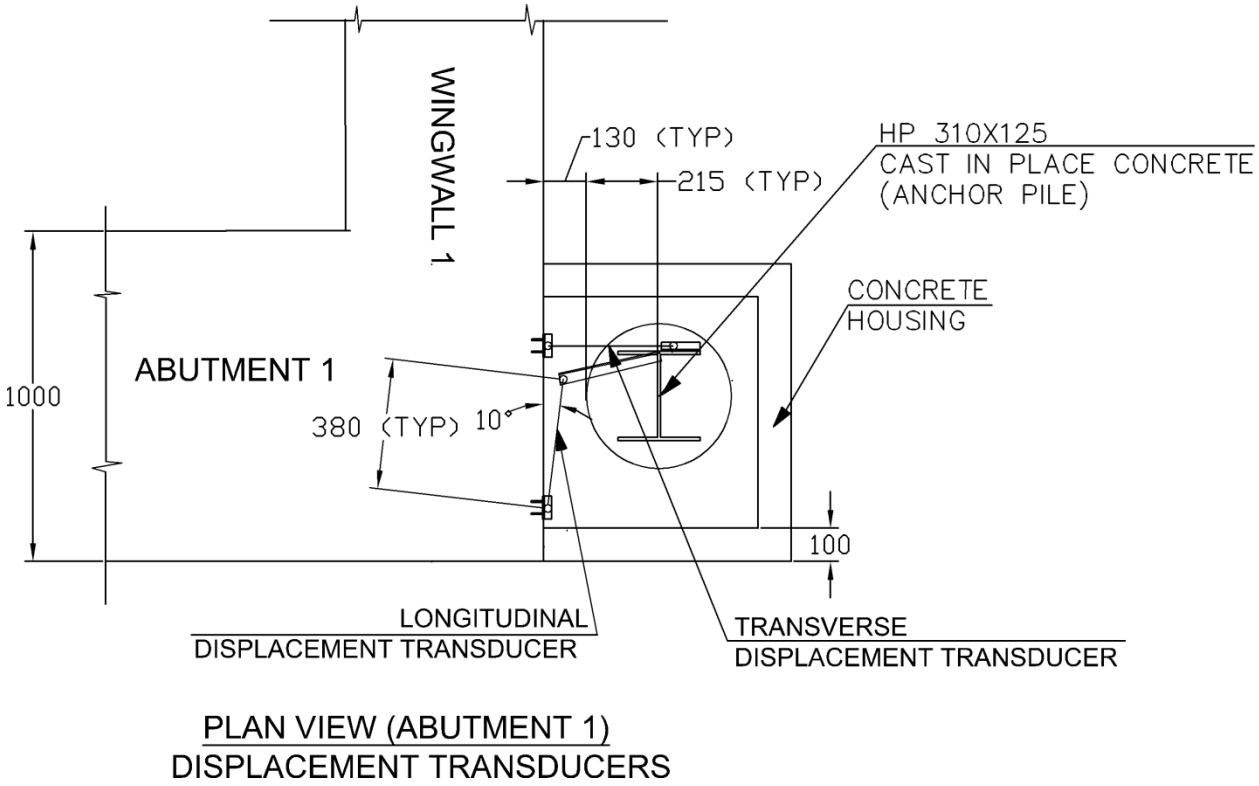

Figure 3-10: Displacement Transducers at Middlesex Bridge

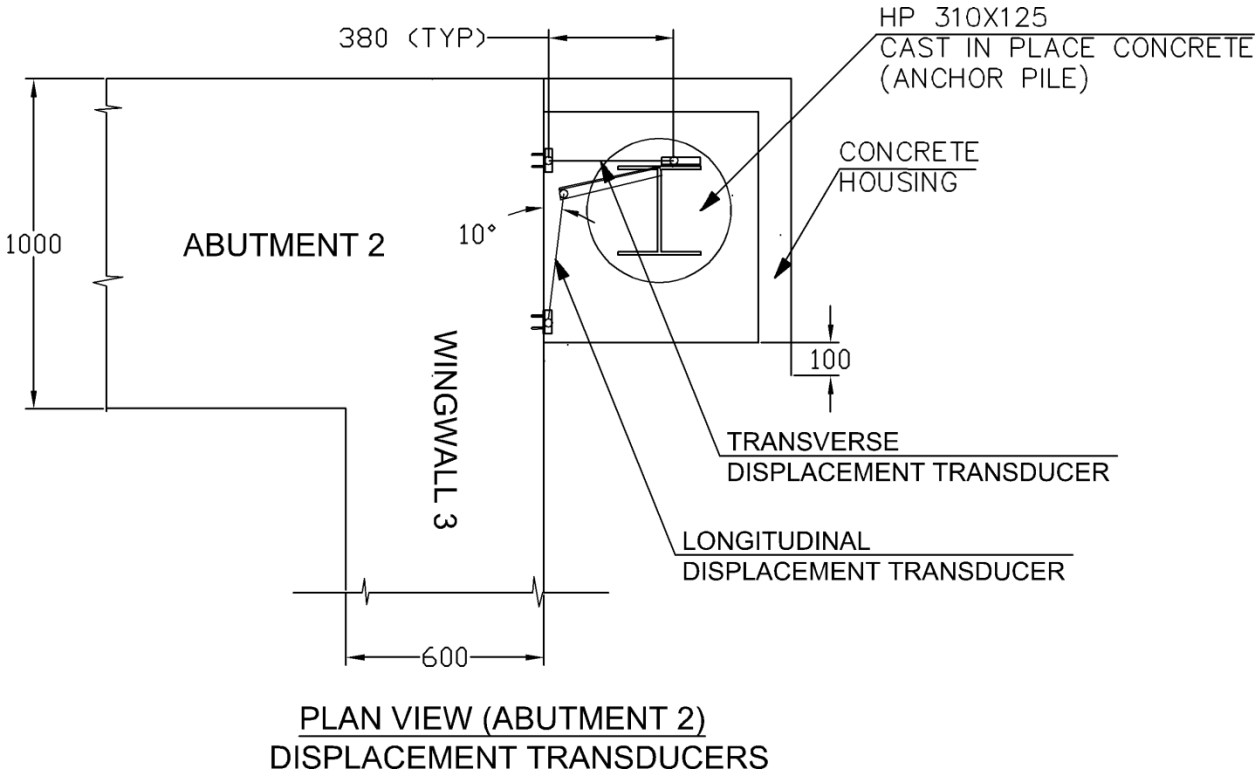

Figure 3-11: Displacement Transducers at Middlesex Bridge (cont.)

3.3 East Montpelier Bridge Instrumentation

Instrumentation for the skewed East Montpelier Bridge concentrated on outer piles and girders to determine the variation of behavior at interior and exterior skew angles. It was assumed that the performance of intermediate piles would approximately follow a linear variation between measurements taken at edge piles. In evaluating the distribution of pressures behind the skewed abutment and determining wing wall pressures the significance of skew angle on design procedures will be evaluated. For the relatively small skew angle of 15 degrees studied, a major objective will be to determine if the response across the structure varies significantly or could be captured by using a two dimensional analytical model.

Figure 3-12 shows the data acquisition system installed in the field. Both multiplexers and datalogger boxes are attached to the abutment wall. Figure 3-13 shows the plan view of instrumentation listing the number of gages at each location. The elevation view of substructure instrumentation is given in Figure 3-14, which indicates the gages located at each abutment.

Earth Pressure cells on the abutments are aligned with the exterior piles and the center pile. Abutment No. 1 has three rows of gages with a total of 8 gages, while Abutment No. 2 has 4 gages that are located along the exterior pile alignment (Figure 3-14). The bottom row of gages is located at 0.4 m (1.3 ft) above the bottom of abutments. The locations of the second and third

row of pressure cells were modified due to constructability problems in the field. With the revisions, the second row (only Abutment 1) and third rows of pressure cells are located at 0.6 m (2.0 ft) and 1.2 m (4.0 ft) from the bottom row of cells, respectively. A single wingwall pressure cell is attached to the wingwall that is located on Wingwall 1 as shown in Figure 3-15. The reference pressure cell is located 1.0 m (3.3 ft) below the approach slab. The concrete block encasing the gage is located closely to the end of approach slab and positioned vertically while the gage is facing towards Abutment 1. Approximate location of the reference pressure cell is shown in Figure 3-16.

Pile strain gages are mounted on the interior face of the pile flanges as shown in Figure 3-17. The spacing between the flange edge and centerline of the gage is 51 mm (2.0 in). Four gages are installed at each pile cross section. Abutment 1 has a total of 24 gages whereas Abutment 2 has only 8 gages. The gage spacing changes between the abutments (Figure 3-14). The gage spacing is 0.5 m (1.7 ft) for piles on Abutment 1, whereas the spacing was increased to 1.0 m (3.3 ft) for Abutment 2 pile gages by eliminating the middle instrumented section.

Two or four gages were attached to each instrumented girder cross section. Centerlines of the gages are located 11.5 cm (4.5 in) from the tip of the girder flange as shown in Figure 3-18. Figure 3-18 also shows the gage locations along the bridge. Instrumented cross sections are located at midspan and near the ends of the bridge. The spacing between instrumented sections and the ends of steel girder sections is 4.35 m (14.30 ft). Gages at midspan are 18.5 m (61 ft) away from the ends of the steel girder sections.

At the East Montpelier Bridge, the inclinometers are biaxial (Geokon 6150) whereas the tiltmeters are uniaxial (Geokon 6350). Inclinometers that measure the pile inclinations along and perpendicular to the roadway alignment are micro-electro-mechanical systems (MEMS), while tiltmeters that measure the abutment rotation are vibrating wire instruments. The bridge has one tiltmeter at the center of each abutment wall. The gage is attached to the abutment vertically at 0.5 m (1.6 ft) below the bottom of middle girder flange. Inclinometers are attached to the exterior piles located below Girder 1 and Girder 5 as shown in Figure 3-19. Abutment 2 inclinometers are located on the pile flanges facing the centerline of the roadway, whereas the inclinometers that are installed on Abutment 1 are attached to the pile flanges that are facing the fascia of the bridge. Each inclinometer string consists of 4 gages. The gages are placed at 0.6 m (2 ft), 0.9 m (3 ft), 1.2 m (4 ft) and 1.2 m (4 ft) spacings starting from the bottom of the abutment except for the string attached to pile below Girder 5 at Abutment 2 where the bottom gages are 0.9 m (3 ft) apart. Unlike the Middlesex and Stockbridge bridges where the inclinometer casings extended to the roadway surface, the inclinometer casings in this bridge were terminated below the abutment construction joints. This procedure was necessary to avoid openings on the roadway because the East Montpelier Bridge is part of the “Highways for Life” program, including stainless steel reinforcement used in the deck. Penetrations through the deck were not allowed. Therefore,

before deck concrete placement, the top of the casing was sealed and inclinometer gages were embedded into the abutment concrete.

At the East Montpelier Bridge 100 mm (3.9 in) gage lengths were used to measure both longitudinal and transverse displacements of the abutments. The bridge has a total of 5 displacement transducers. Both longitudinal and transverse measurements are taken at the North side of each abutment, while only longitudinal readings are taken at the south side of Abutment 1. Displacement transducers are shown in Figure 3-21.

a) Multiplexers at Abutment b) Dataloggers at Abutment

Figure 3-12: Data Acquisition System for East Montpelier Bridge

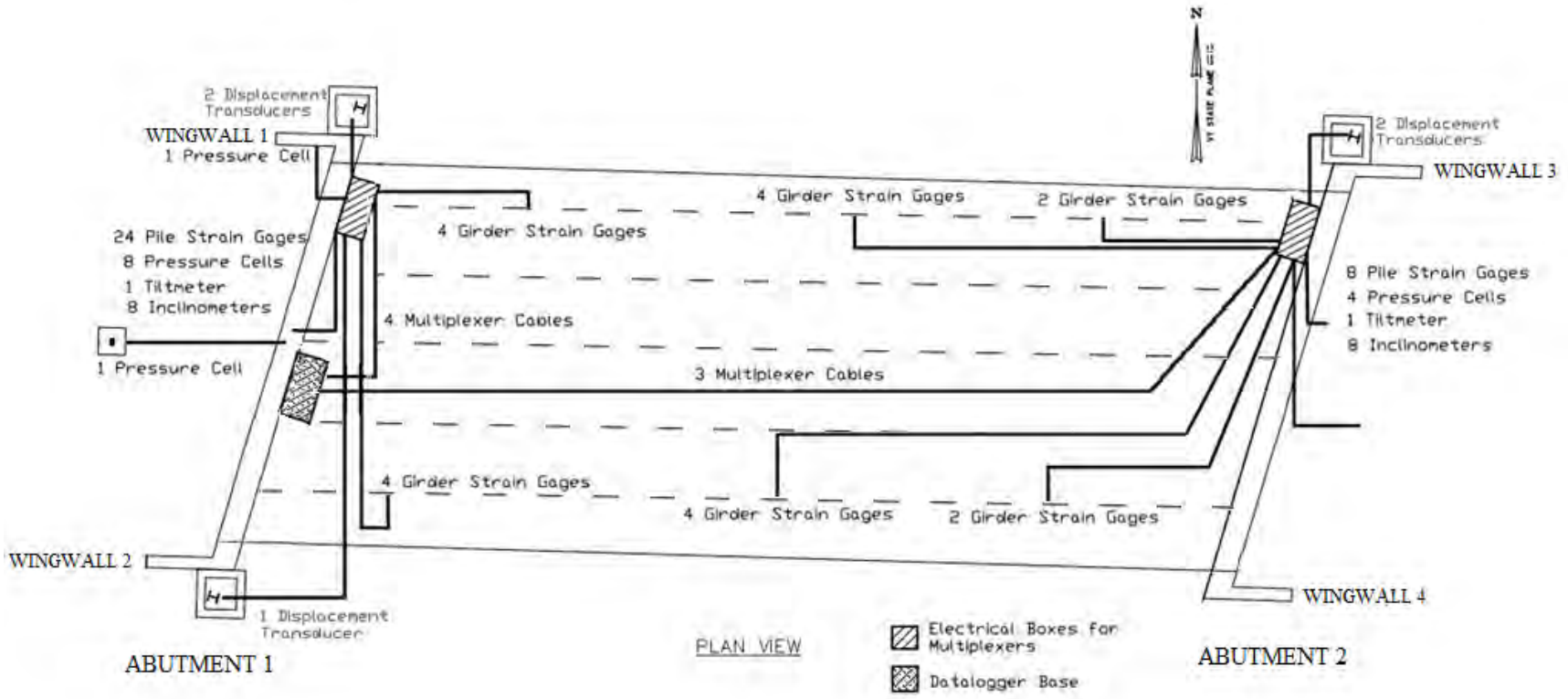

Figure 3-13: Overview of Instrumentation in the East Montpelier Bridge

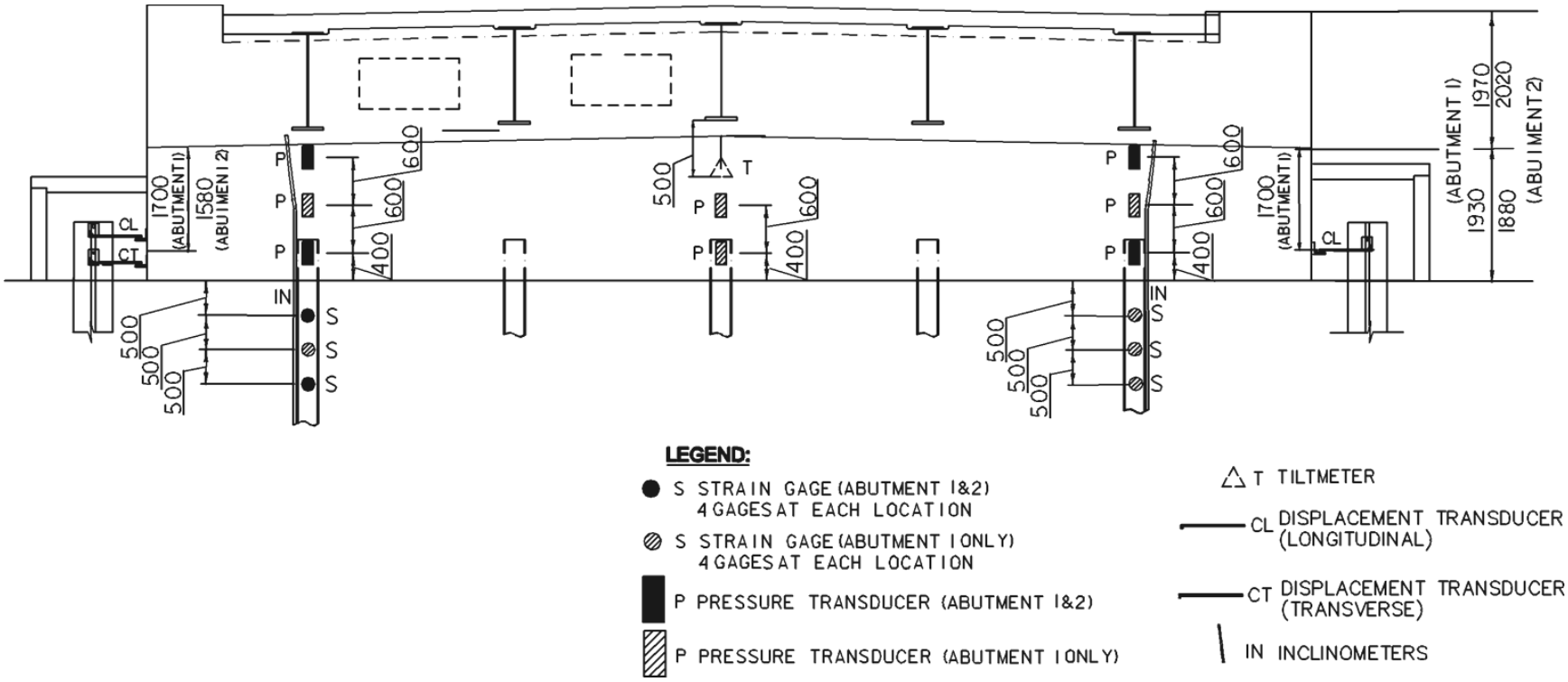

Figure 3-14: Instrumentation at the East Montpelier Bridge

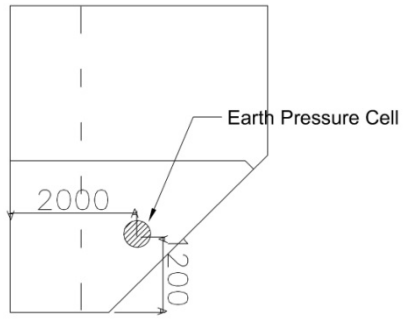

Figure 3-15: Wingwall Earth Pressure Cell at the East Montpelier Bridge (Wingwall 1)

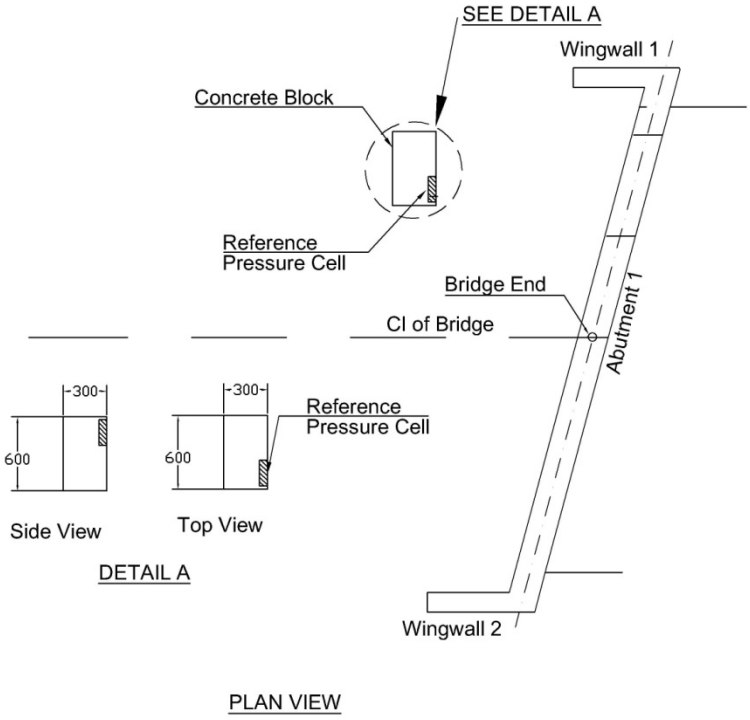

Figure 3-16: Reference Earth Pressure Cell at the East Montpelier Bridge

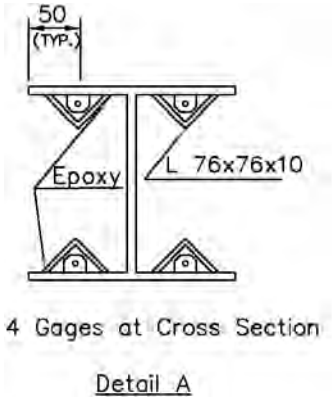

Figure 3-17: Pile Strain Gages at the East Montpelier Bridge

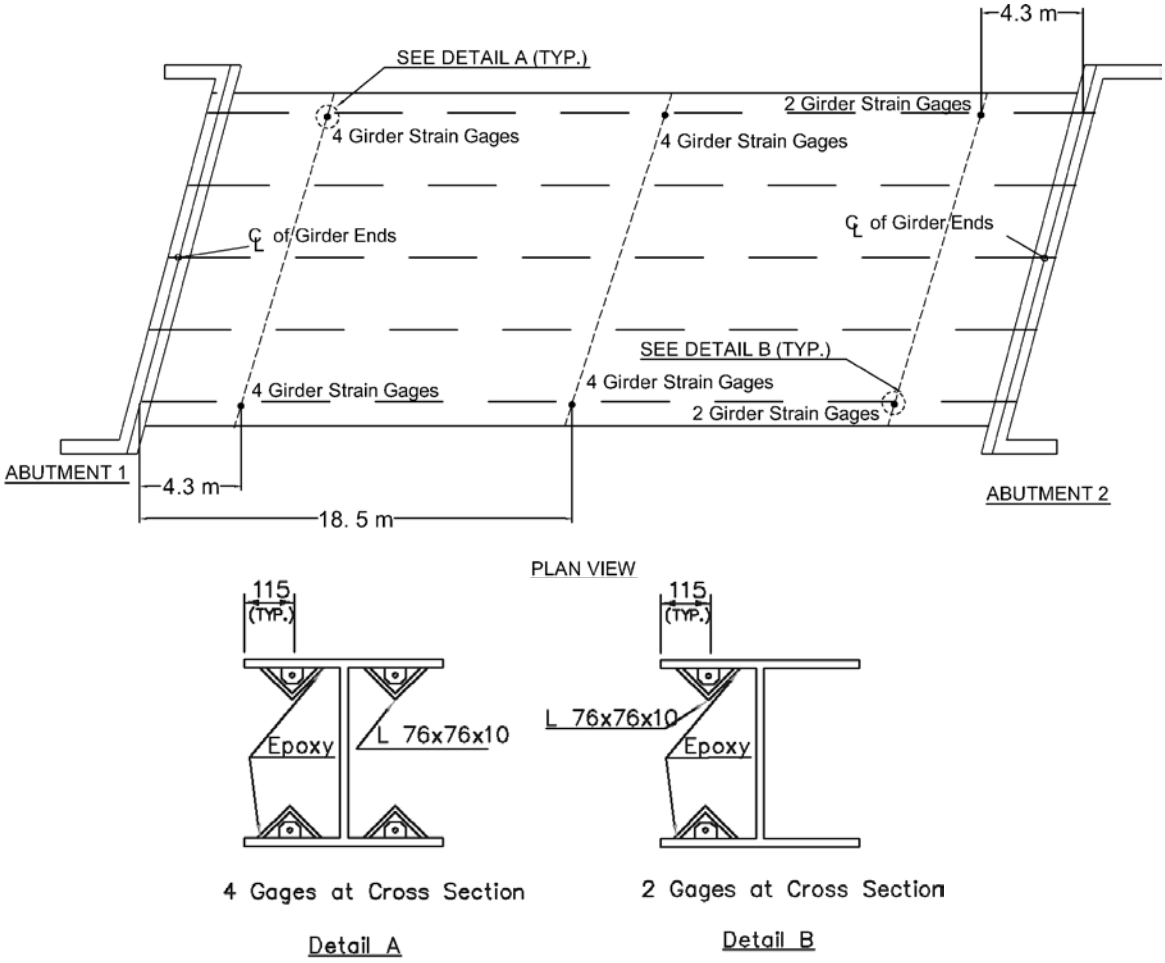

Figure 3-18: Girder Strain Gages at the East Montpelier Bridge

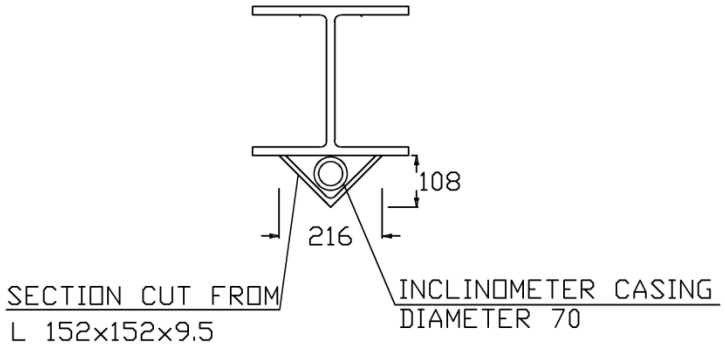

DETAIL FOR PILE 1 and 5

Figure 3-19: Inclinometers at the East Montpelier Bridge

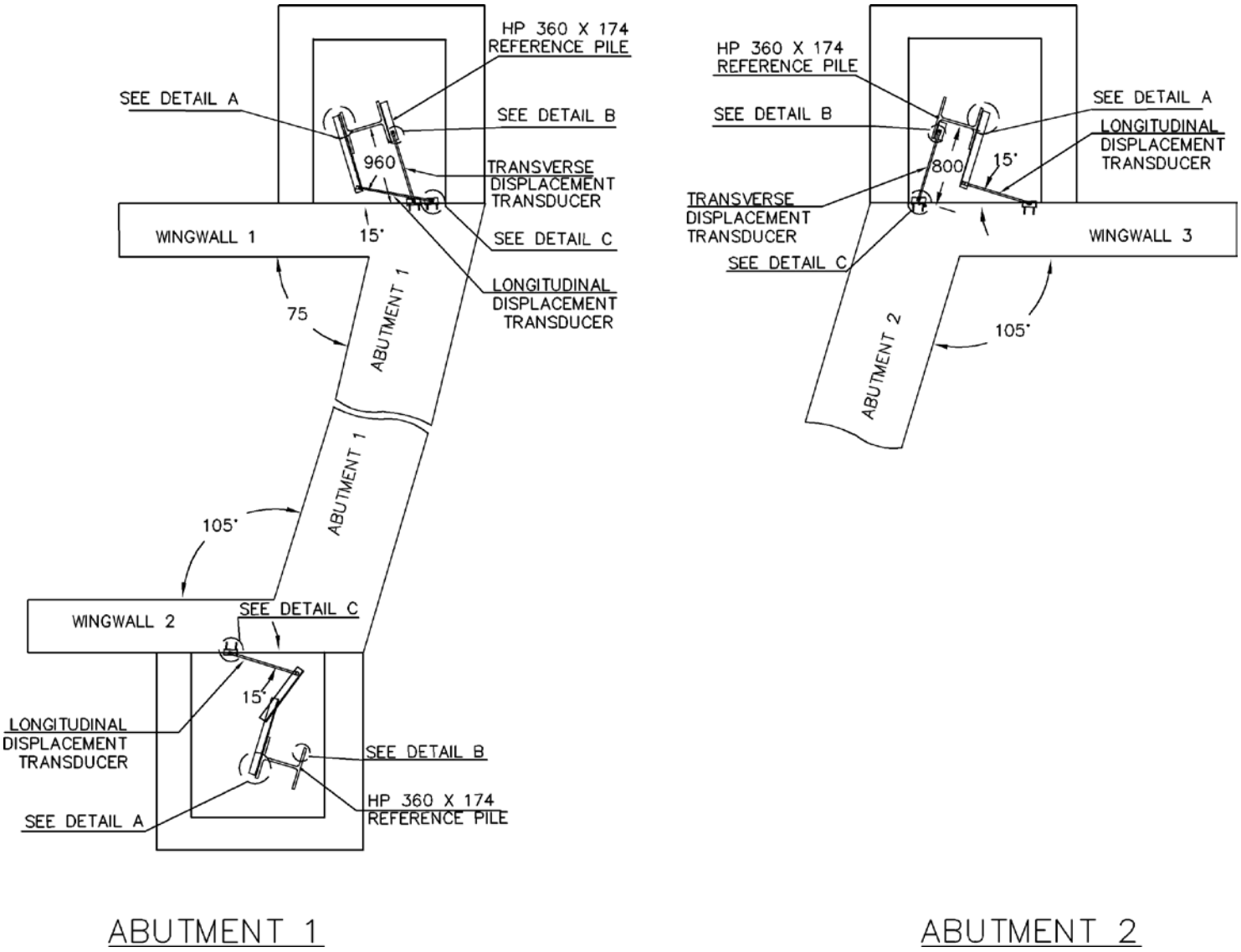

* Details are shown in Figure 3-21.

Figure 3-20: Displacement Transducers at East Montpelier Bridge

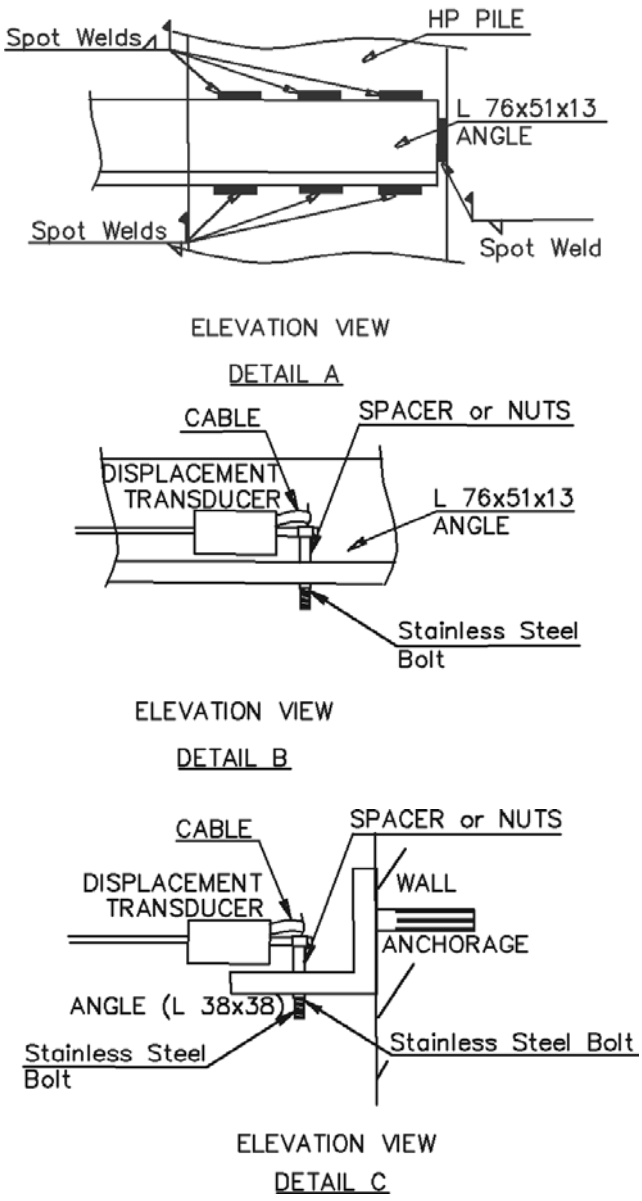

Figure 3-21: Attachment Details for Displacement Transducers at East Montpelier Bridge

3.4 Stockbridge Bridge Instrumentation

The Stockbridge Bridge instrumentation is unique due to the bridge curvature. Due to the lack of field data for curved IABs the instrumentation plan was extensive and similar at each abutment. The instrumentation plan was designed to measure variation in soil pressures at the abutment and wing walls, associated abutment displacements and rotations, and biaxial response of piles and pier bending. Girder strain gages were concentrated near mid-spans and at a section above the interior pier.

Figure 3-22 shows the data acquisition system installed in the field. Multiplexers were attached to the abutment wall whereas the datalogger box (with phone line and electrical service) was placed on a concrete pad next to the approach on Abutment 2 side of the bridge. Figure 3-23 shows a plan view of the bridge instrumentation listing the total number of gages at each location. The elevation view of substructure instrumentation is given in Figure 3-24, which indicates the gages that were used at each abutment.

Earth Pressure cells on the abutments are positioned at the center and at both edges of the abutment (Figure 3-24). The gages at the edges are 1 m (3 ft) away from abutment-wingwall connection. Both abutments have a total of 8 gages. The bottom row of pressure cells is located at 0.6 m (2.0 ft) above the bottom of abutments. The second row from the bottom of each abutment is located 1.5 m (5.0 ft) from the bottom row of gages. A single wingwall pressure cell is attached to the each wingwall as shown in Figure 3-25. The reference pressure cell is located 1 m (3 ft) below the approach slab on Abutment 1 side of the bridge. The concrete block encasing the gage is positioned horizontally while the gage is on top surface of the block. The concrete block is located at 1.5 m (4.9 ft) away from the bridge end right at the centerline of roadway. The position of the reference pressure cell is shown in Figure 3-26.

Pile strain gages were mounted on the interior face of pile flanges as illustrated in Figure 3-27. Each instrumented cross section consisted of 3 or 4 gages. The spacing between the flange tip and gage centerline is 6.4 cm (2.5 in). The gages are attached to the piles at a longitudinal spacing of 0.9 m (3.0 ft).

Four girder strain gages were attached to the each girder cross sections as shown in Figure 3-28. The spacing between the tip of the flange and the gage centerline is 64 mm (2.5 in). There were three instrumented girder cross sections: one on top of the interior pier and the other two located at midspan in each span. Midspan sections are located 17.4 m (57 ft) and 16.2 m (53 ft) away from the ends of steel girder sections, respectively, measured along exterior and interior girders (Figure 3-28).

The interior pier in the Stockbridge Bridge has a total of 8 strain gages in two different sections – 305 mm (1 ft) from the top and bottom of the pier column (Figure 3-29). Four gages in each section are oriented to record longitudinal strains in directions parallel and perpendicular to the roadway alignment. Strain gages were tied to longitudinal reinforcement in the pier during construction.

One biaxial MEMS tiltmeter is located at the center of each abutment wall. The vertical location of the gage is defined from the bottom of the middle girder. The tiltmeters were positioned 1 m (3 ft) below the bottom of girder flange. At the Stockbridge Bridge, exterior piles located below Girder 1 and Girder 5, were instrumented with inclinometers (Figure 3-30).

Inclinometer casings were attached to the pile flanges facing the roadway centerline. Each instrumented pile has a 5-gage-string. The top wheel of the gage assembly coincides with the bottom of the abutments. The gage spacing is 0.6 m (2 ft), 0.9 m (3 ft) and 1.2 m (4 ft) (for the rest of gages) starting from the bottom of the abutment. The total depth of monitored pile deformations is therefore limited to 5.2 m (17 ft). In order to enable gage removal/replacement after construction, the inclinometer casings were extended to the roadway level. At the top of the casing, a steel water-tight cover was placed.

The number of displacement transducers installed at each bridge depended on the complexity of each structure. In order to investigate the effects of curved alignment, the Stockbridge Bridge was instrumented with 6 displacement transducers. Both longitudinal and transverse measurements are taken at the North side of each abutment, while only longitudinal readings are taken at the south side of abutments. Longitudinal displacement transducers have a 100 mm (3.9 in) gage length whereas transverse gages have a 50 mm (2.0 in) gage length. Location and orientation of each displacement transducer is shown in Figure 3-32. Figure 3-33 shows the attachment details.

Figure 3-22: Data Acquisition System (Loggers) near Approach Slab

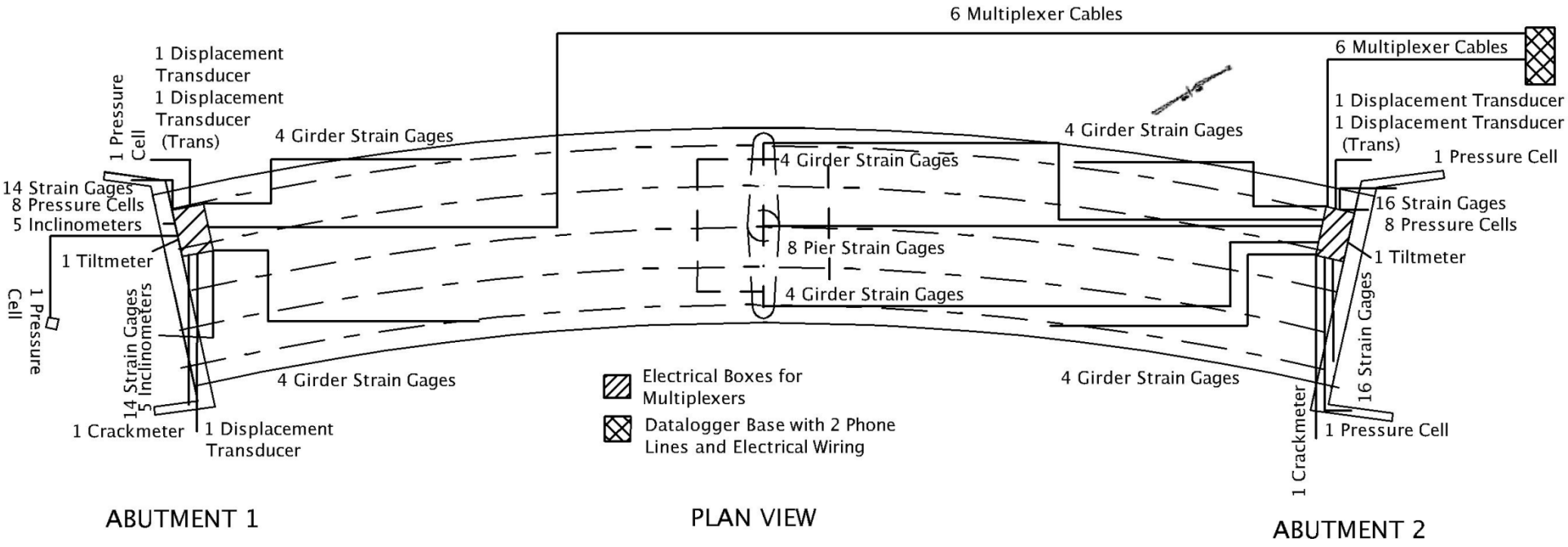

Figure 3-23: Instrumentation at the Stockbridge Bridge

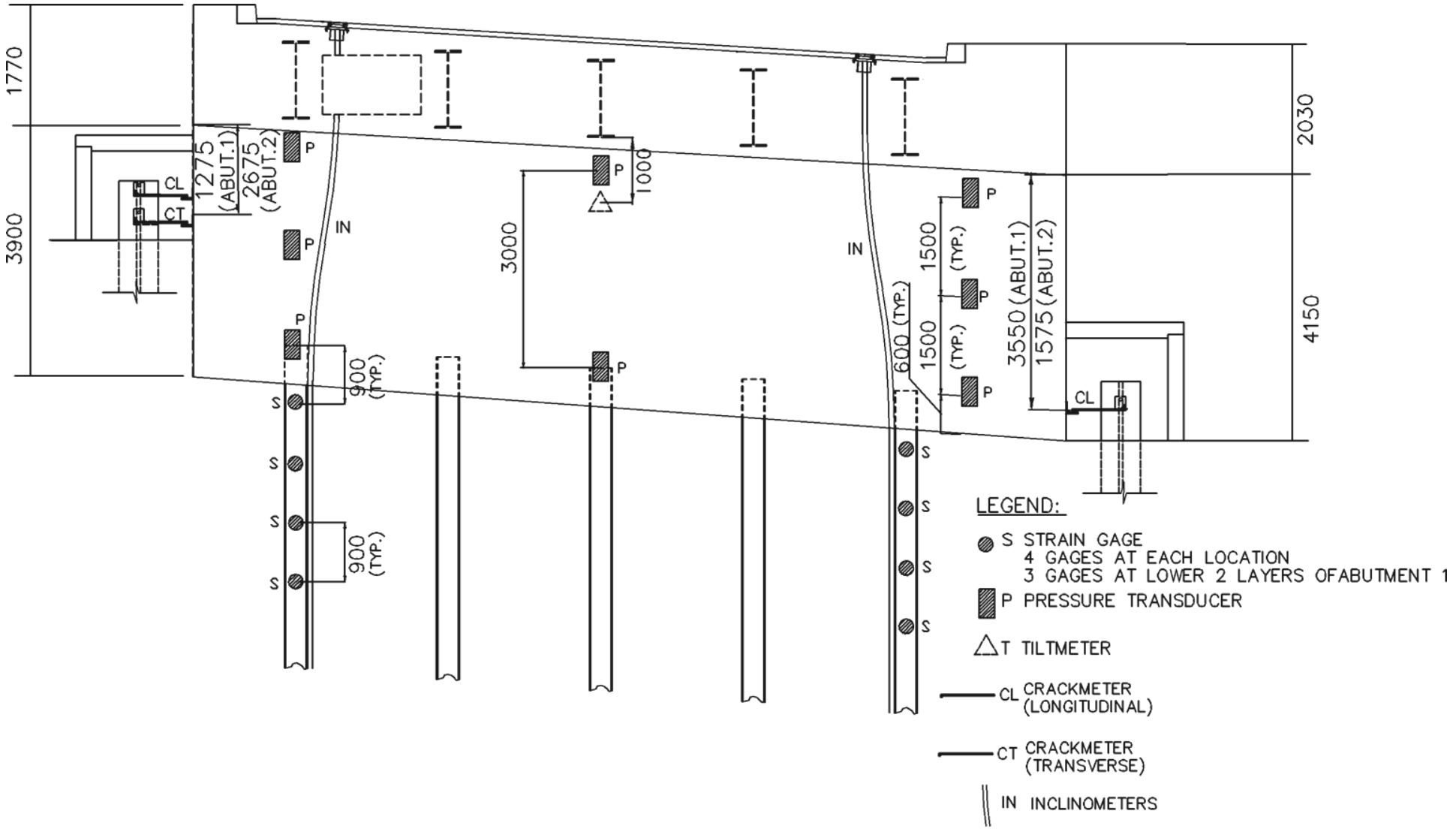

Figure 3-24: Abutment Instrumentation at Stockbridge Bridge

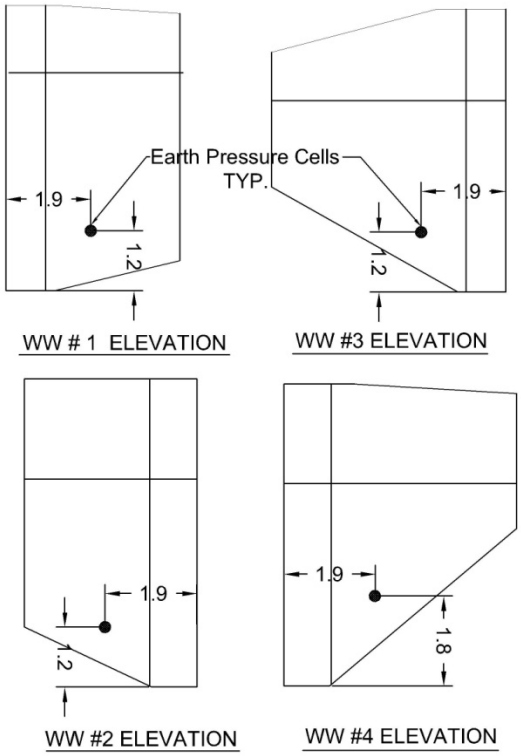

Figure 3-25: Wingwall Earth Pressure Cells at the Stockbridge Bridge

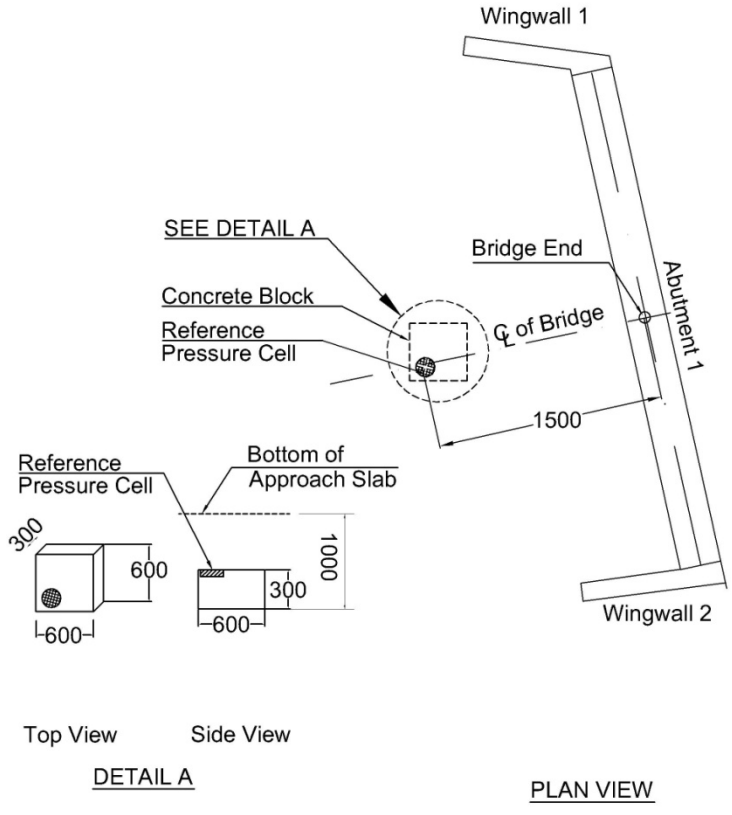

Figure 3-26: Reference Earth Pressure Cells at the Stockbridge Bridge

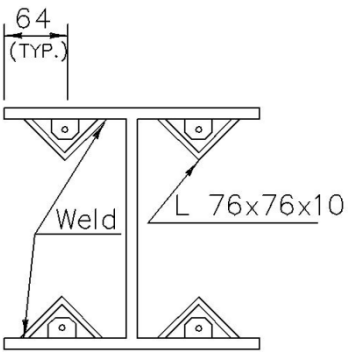

4 Gages at Cross Section

Figure 3-27: Typical location of Pile Strain Gages at the Stockbridge Bridge

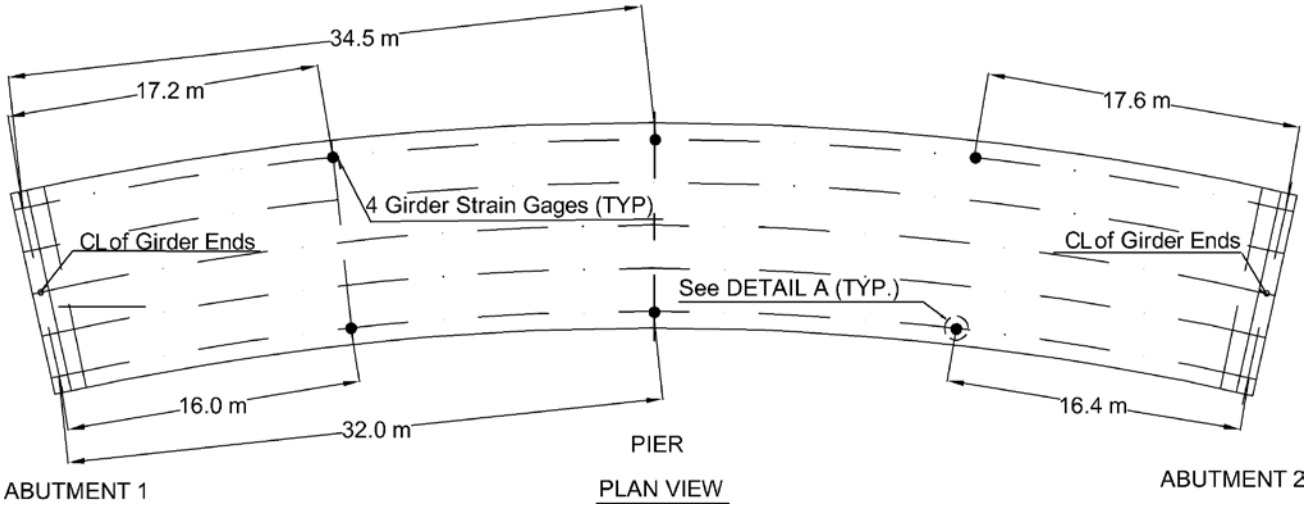

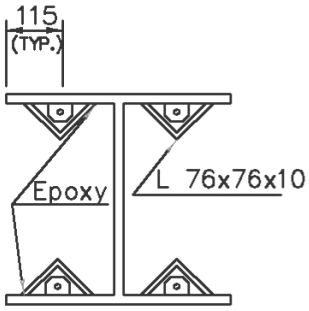

4 Gages at Cross Section

Detail A

Figure 3-28: Location of Instrumented Girder sections at the Stockbridge Bridge

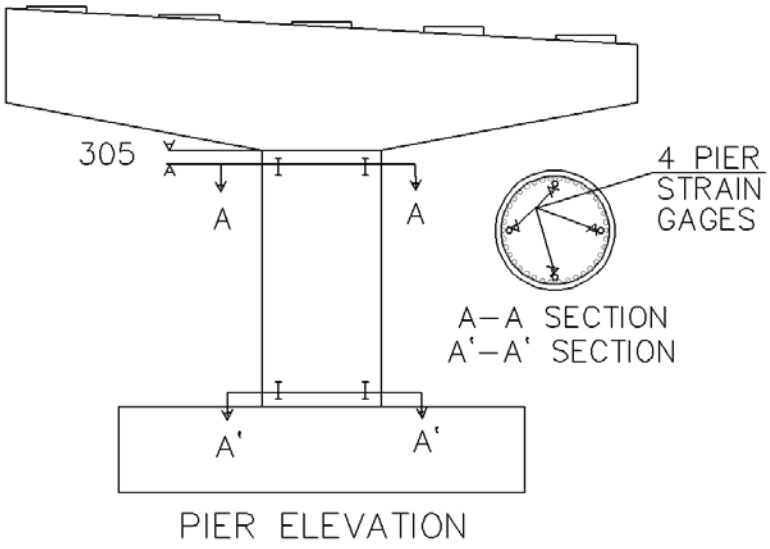

Figure 3-29: Pier Strain Gages at the Stockbridge Bridge

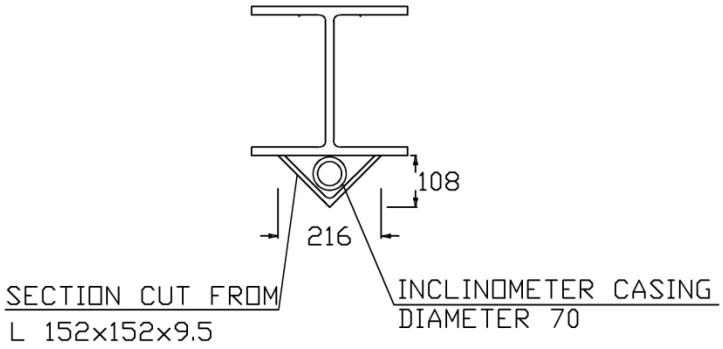

DETAIL FOR PILES BELOW GIRDER 1 and 5

Figure 3-30: Attachment of Inclinometer Casings for Piles in Stockbridge Bridge

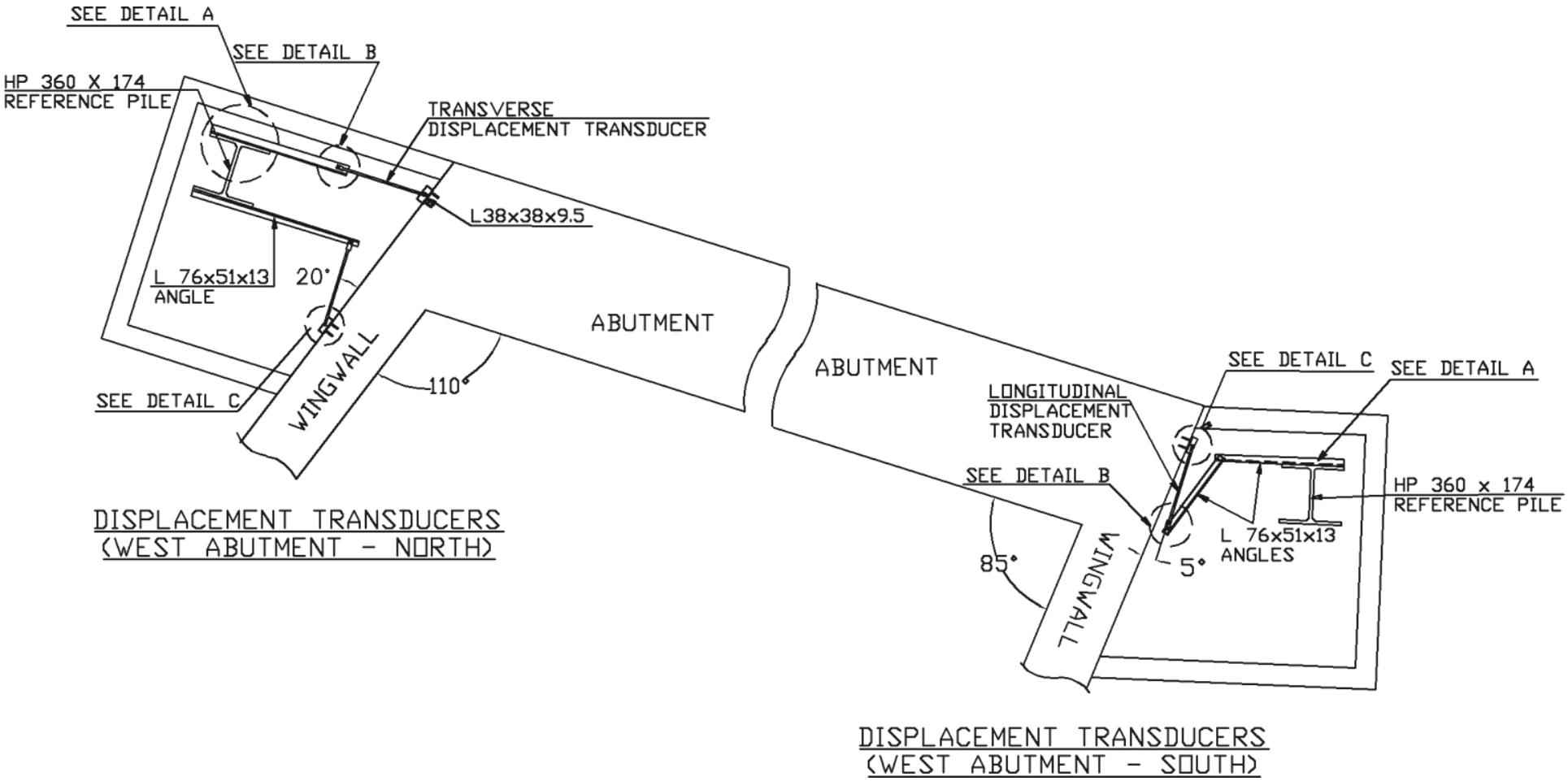

* Details are shown in Figure 3-33.

Figure 3-31: Displacement Transducers at the Stockbridge Bridge Abutment 1

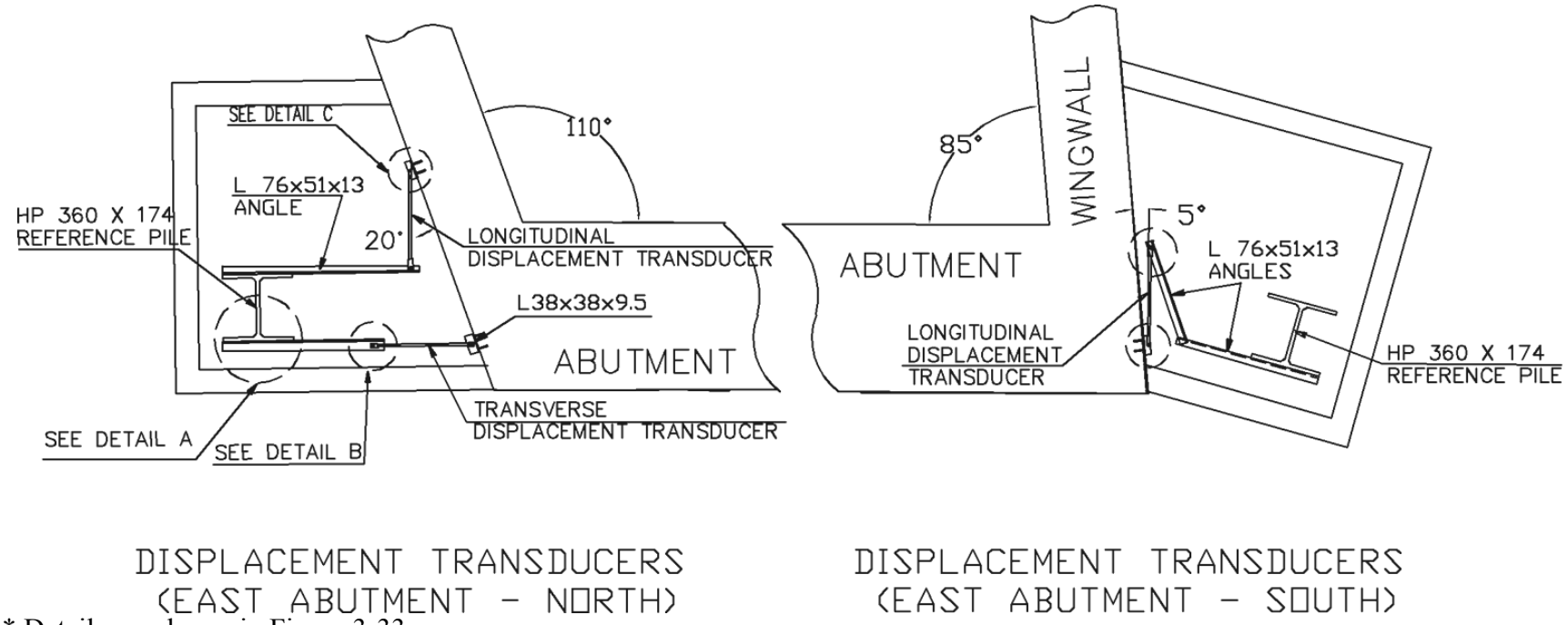

* Details are shown in Figure 3-33.

Figure 3-32: Displacement Transducers at the Stockbridge Bridge Abutment 2

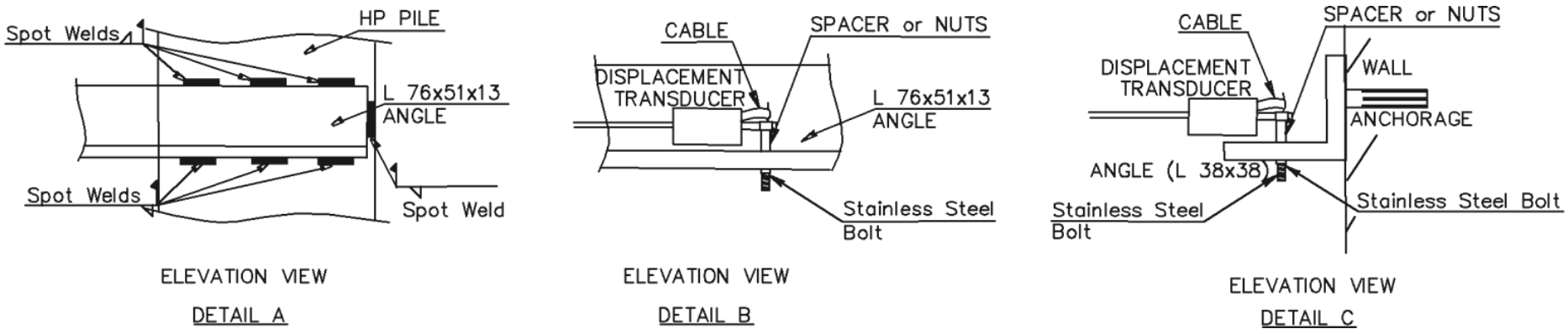

Figure 3-33: Connection Details for Displacement Transducers at the Stockbridge Bridge

3.5 Gage Installation

Instrumentation of the bridges includes nine different types of gages. Locations and number of gages were given in the previous sections. This section summarizes the installation procedure that was followed in the field for each gage type.

3.5.1 Strain Gages

Three types of strain gages were installed depending on the base material and instrumentation purpose – pile strain gages, girder strain gages and pier strain gages. The first two are steel-weldable gages whereas the last one is a concrete embedment gage. All strain gages are based on vibrating wire technology.

a) Pile Strain Gages

Pile strain gages (Geokon 4000) are mounted on the top region of abutment piles in order to determine pile strains caused by thermal bridge loading. These gages are typically used on steel structures such as piles and girders. Mounting blocks are welded on the steel element and the gages are secured onto the mounting blocks at instrumented sections.

The first set of gages was installed at the Stockbridge Bridge following recommended manufacturer procedures. Due to problems encountered during driving of the first set of piles, however, a modified gage installation procedure was developed and used for the remainder of the gages, as described in the following sections and shown in Figure 3-34. At the Middlesex and East Montpelier Bridges, the installation procedure was further modified. In these two bridges gages were installed after pile driving as described later in this section.

Gage mounting blocks were welded to the interior flanges of the piles. The manufacturer-provided spacer bar was used to correctly set the spacing between mounting blocks. Once the blocks were welded and the sections cooled, the gages were attached to the blocks. The gages consist of a steel tube that houses a vibrating wire and a plucking coil that has a groove on one side. Manufacturer instructions include a sequence of tightening set screws attaching one end of the gage tube to the mounting blocks, attaching the plucking coil to the gage tube with a manufacturer provided hose clamp, and then tightening the remaining set screws at the desired initial gage reading. Gage reading is obtained by monitoring the gage with a readout box while applying slight compression at the loose end of the gage tube.

During initial pile driving operations at the Stockbridge Bridge eleven strain gages at Abutment 2 malfunctioned (Figure 3-35). Careful inspection of gages during the pile driving

operation (Figure 3-36) noted that the attachment clamps provided with the gages were not sufficient to restrain the plucking coil from shifting on the gage enclosure. In addition, some set screws were loosened and a few vibrating wires fractured during the pile driving process. To avoid construction delays not all of the malfunctioning strain gages were replaced. Thereafter a more robust strain gage attachment method was implemented. The revised method, used on all subsequent gages, is as follows. Epoxy putty was placed around and in the groove of the plucking coil to prevent slippage relative to the gage tube. A PEX clamp was then tightened around the plucking coil and epoxy putty in order to fully engage the gage tube and the plucking coil and prevent any slippage. Once the clamp was tightened, Loc-tite adhesive was placed on the set screws in the mounting blocks to prevent loosening. These screws were tightened while gages were set at the desired initial gage reading. All gages were fully functional in this abutment and the revised installation method is recommended.

At the Middlesex and East Montpelier bridges, the installation procedure was further modified. In these two bridges, soil was excavated around the top region of the piles after driving to expose the pile area where gages were to be installed. Installation of gages was performed after piles were driven to required depth so pile driving would not cause gage installation problems. The exposed sections of the piles were backfilled after gages were installed and protected using protective steel cover angles. Major advantages of this procedure are ease of gage installation and avoidance of transferring pile driving forces to the gages. However, soil variability in typical construction is no longer maintained due to the introduction of non-virgin soil around the pile near the abutment.

After gage installation, signal cables were tied together and directed to the top of the piles. Gages and cabling were covered with non-flammable insulation sheets and protective angles were welded on the flanges to protect each gage. Protective angles were cut to lengths of 0.6 m (2 ft) to avoid significantly altering the pile axial stiffness. At the Stockbridge Bridge, initially, protective angles were first cut to length. The contractor opted to weld 0.6 m (2 ft) sections of protective angle to the piles, feed the gages through for installation, and then complete the protective angles by installing the intermediate 0.6 m (2 ft) sections. At the Middlesex and East Montpelier Bridges, protective angles were welded after gage installation was completed. No damage occurred to gages and cables due to welding operations.

Figure 3-37 and Figure 3-38 show the installation steps in East Montpelier and Stockbridge Bridges, respectively.

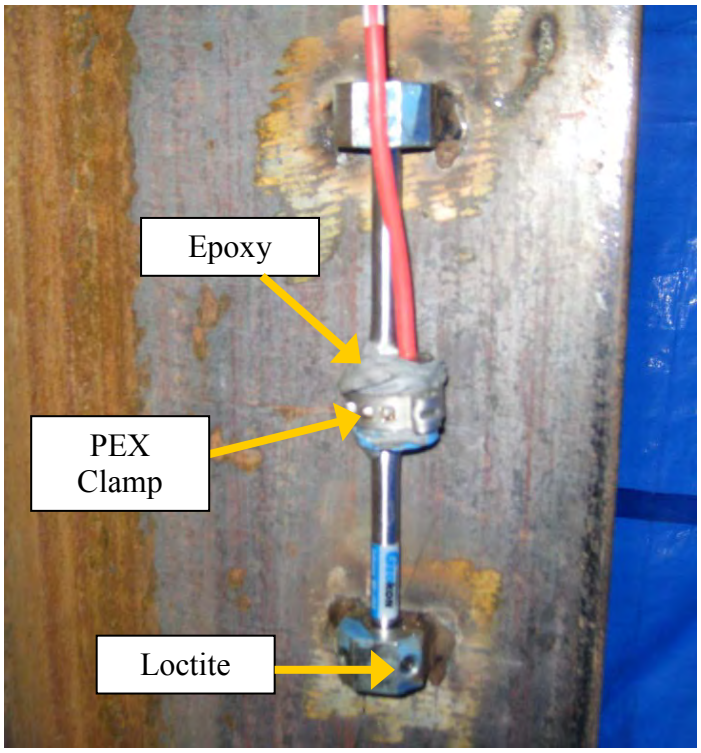

Figure 3-34: Modified Gage Installation

(a) (b)

Figure 3-35: Pile Driving at Stockbridge Bridge (a) Driven Piles (b) Vibrated Piles

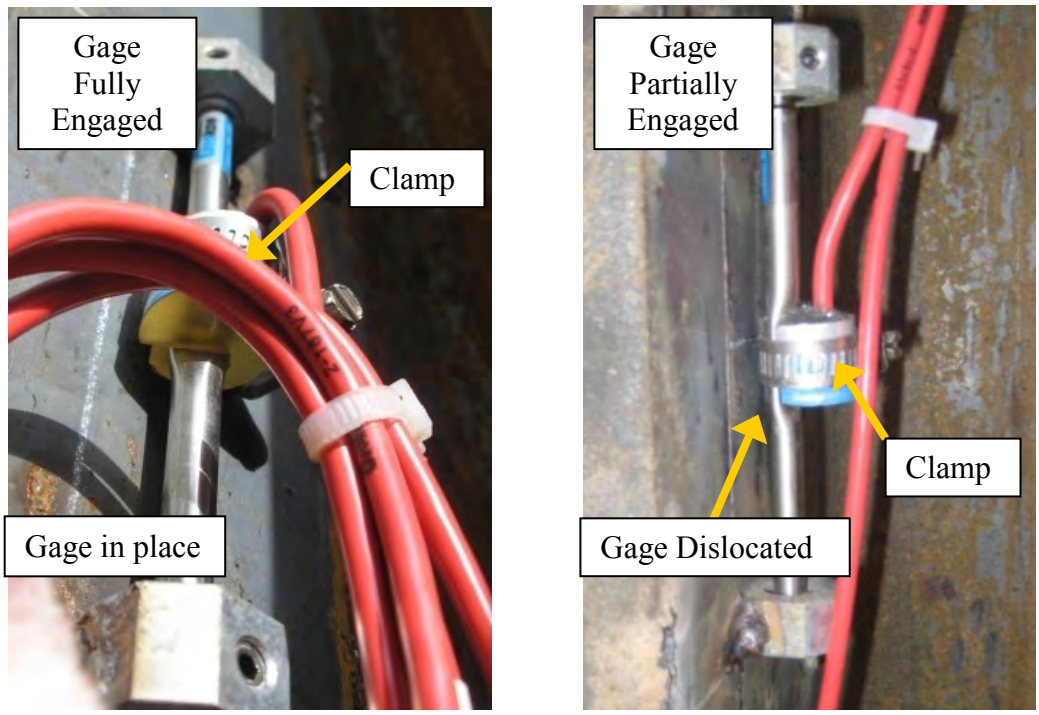

(a) (b)

Figure 3-36: Gage Slippage Using Original Clamps (a) Correct Position of Plucking Coil and (b) Plucking Coil Shift due to Pile Driving Vibrations (Prior to Implementing Modified Installation Procedures)

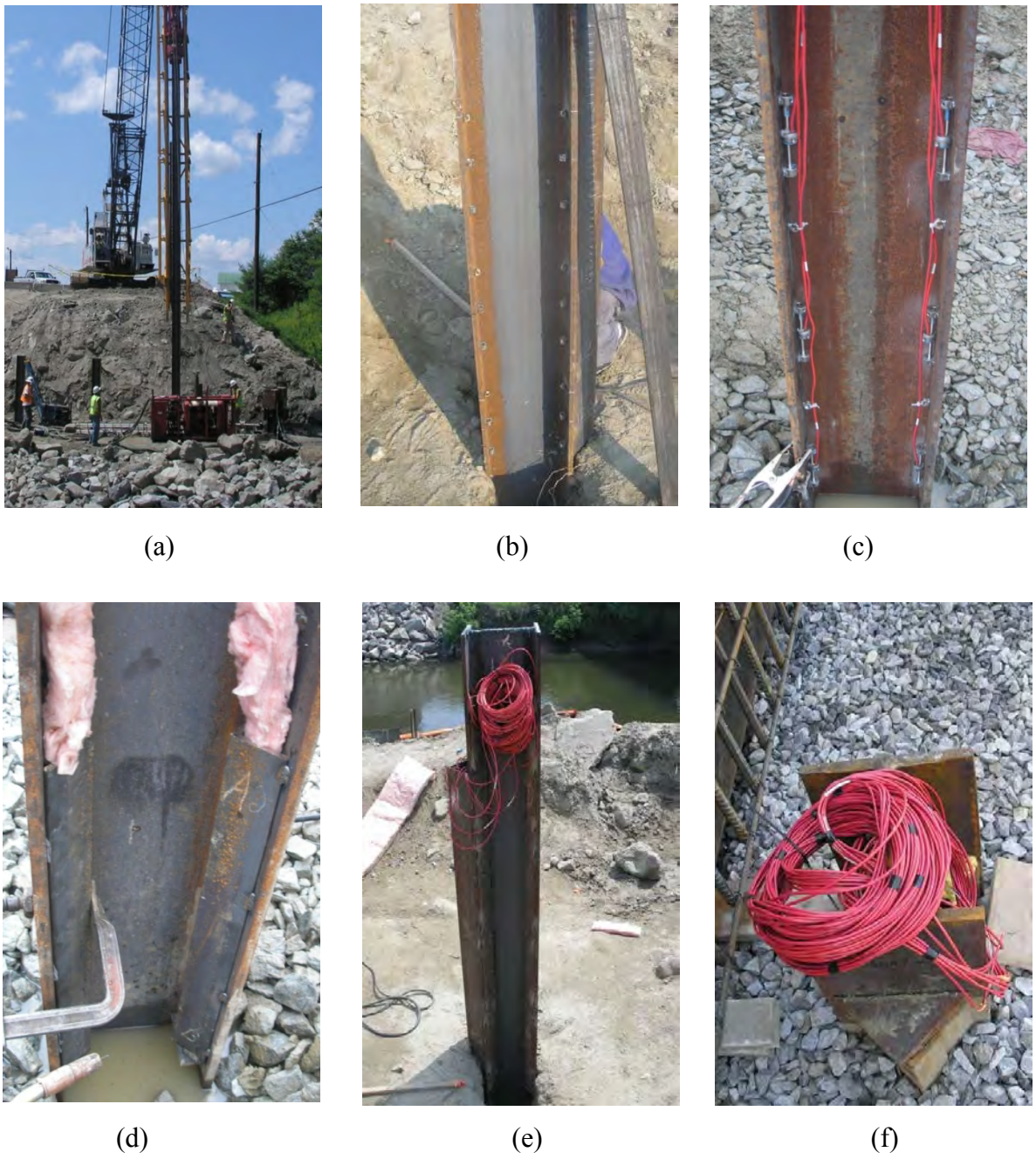

(a) (b) (c)

(d) (e) (f)

Figure 3-37: Pile Strain Gage Installation in East Montpelier Bridge: (a) Pile Driving; (b) End Blocks Welded on Exposed Pile Region; (c) Gages Mounted on End Blocks, (d) Insulation Placed and Welding of Protective Angles, (e) Top of Pile Prior to Backfilling; and (f) Top of Pile After Backfilling

Figure 3-38: Pile Strain Gage Installation in Stockbridge Bridge: (a) Gage End Blocks Installed; (b) Strain Gage Installation Showing Tightening of PEX Clamp; (c) View of Installed Gage; (d) Gages Covered with Protective Angles and Insulation; and (e) Vibrating Piles to Required Depth

b) Girder Strain Gages

Geokon 4050 strain gages were selected to monitor strains on girders. These 30.5 cm (12 in) vibrating wire gages are longer than pile strain gages and are used for measuring strain over a larger gage distance.

The girder strain gage installation procedure is similar to pile strain gage installation, though the plucking coil is located within the gage which simplifies the process. For the girders the gage end blocks (weldable fixtures) were welded at the fabrication shop since field welding on girders was not allowed by VTrans. Some end block set screws showed signs of rust and were difficult to remove and replace by the time of construction since the girders were stored for a significant period of time (a full season at the Stockbridge Bridge).

For the Middlesex and Stockbridge Bridges, girder strain gages were installed after girder erection. At the East Montpelier Bridge, gages were installed prior to placement of girders. The latter option simplified the gage installation process by allowing easy access to the gage locations but included the risk of damaging gages during girder placement. No gage damage resulted from either method.

Strain gages were attached to end blocks in the field by tightening the set screws once the desired initial reading was obtained (approximately the mid-range value of each gage). Loc-tite epoxy was applied to all set screws. Once set screws were tightened, the flange surfaces around the gages were wire-brushed and cleaned in order to mount protective angles. These 0.6 m (2 ft) angles were attached using epoxy over the gages as field welding to girders was not allowed by VTrans. Several protective angles were dislodged during construction, though it is noted that potential damage to gages after construction is not likely. Gage cables were secured in either flexible metal or PVC conduit and routed to the multiplexer boxes located on the abutment walls.

Figure 3-39 illustrates girder strain gage installation procedures. Figure 3-40 shows a gage pair at the Stockbridge Bridge after protective angles were attached to the girders.

At the East Montpelier Bridge the deck construction was modified due to issues with the cross bracing. This required removal of a portion of the completed deck as noted previously. During this process one strain gage was damaged and needed to be replaced. In addition, several cables showed some visual damage, though gage readings were unaffected. Due to access issues these cables were left in place and continue to function acceptably.

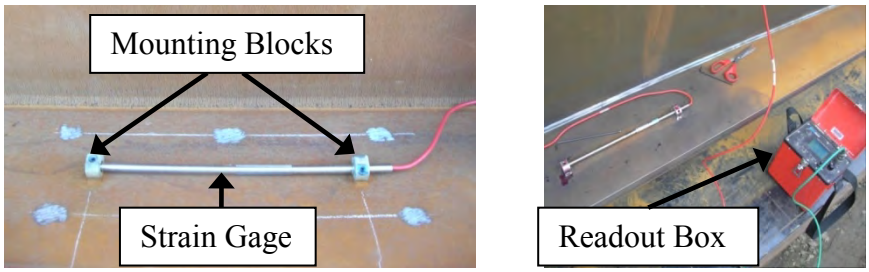

(a) (b)

Figure 3-39: Girder Strain Gage Installation: (a) Girder strain gage and (b) Gage and readout box to ensure proper signal from gage

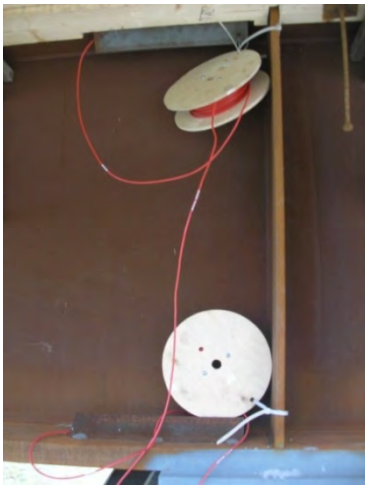

Figure 3-40: Girder Strain Gages on Top and Bottom Flanges with Protective Angles

c) Pier Strain Gages

Pier strain gages (Geokon 4200) were used to measure strains occurring in the concrete interior pier column at the Stockbridge Bridge. The gages were installed prior to concrete placement and embedded into the concrete. Installation of these gages consisted of securing the gages to the reinforcing bars within the pier using tie wires to maintain the intended orientation and position of the gages during concrete placement. Figure 3-41 shows the installation of the gages and close-up view of the gage attached to the reinforcing bar.

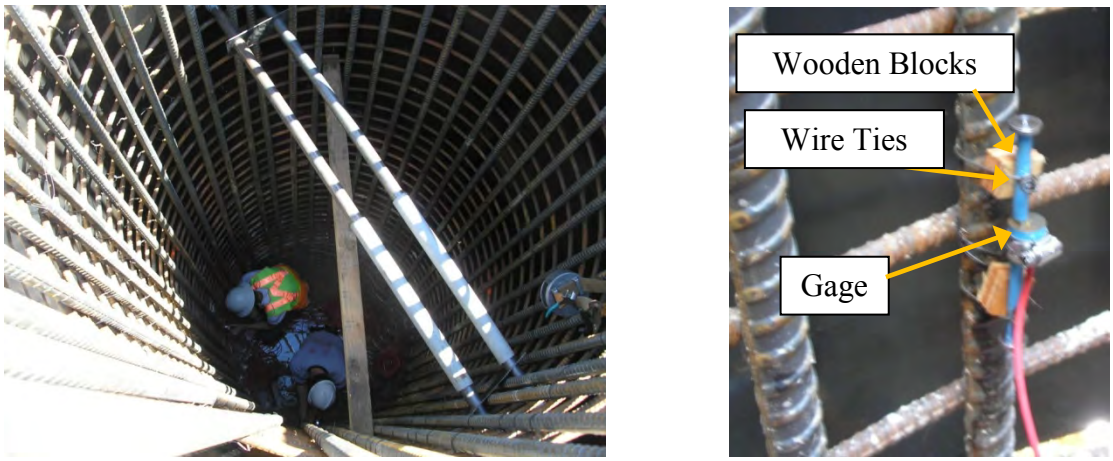

(a) (b)

Figure 3-41: Pier Column Strain Gage at Stockbridge Bridge: (a) Gage Installation; and (b) Gage Attached to Reinforcing Bars

3.5.2 Earth Pressure Cells

Earth pressure cells (Geokon 4810 and Geokon 4815) were selected to measure the soil pressures generated on abutments and wingwalls as a result of thermal movements of bridge substructures. Each gage is composed of two parts, the transducer housing and a pressure cell. The transducer housing includes a vibrating wire and is bent slightly to keep it away from the abutment surface. The pressure cell is circular in shape and was nailed directly to the formwork to provide a flush face directly in contact with the soil after removal of the formwork and backfilling. Gage installation was often difficult due to reinforcement congestion and dimensions of the abutment and wingwalls.

Two different types of pressure cells are used in the projects - Geokon 4810 and Geokon 4815. The difference between these cells is the design of the cell. Geokon 4810 pressure cells measure the pressure through a single thin pressure sensitive plate that rests against the formwork (exposed face of the gage). This type of gage is suitable for monitoring the pressures on fine-grained soil. Geokon 4815 pressure cells have a thick plate on both faces of the instrument and are recommended to measure stresses in coarse-grained soils. In the Middlesex and East Montpelier bridges, Geokon 4815 gages were used to monitor the pressures on bridge substructures. Both types of pressure cells (Geokon 4810 and Geokon 4815) were used at the Stockbridge Bridge. Geokon 4810 gages were installed to measure pressures behind the abutment in locations where GeoFoam was placed. Figure 3-42, Figure 3-43 and Figure 3-44 show the details of earth pressure cells and their location on the abutment backwall.

In order to secure the reference pressure cell that is embedded below one approach slab in each bridge, a concrete block was cast with the pressure cell positioned flush on one face of the

block. A reference pressure cell before and after pouring the concrete block is shown in Figure 3-45. In Stockbridge, the reference pressure cell cable was damaged following the installation. This cell was replaced by the contractor and placed at the Abutment 1 embarkment.

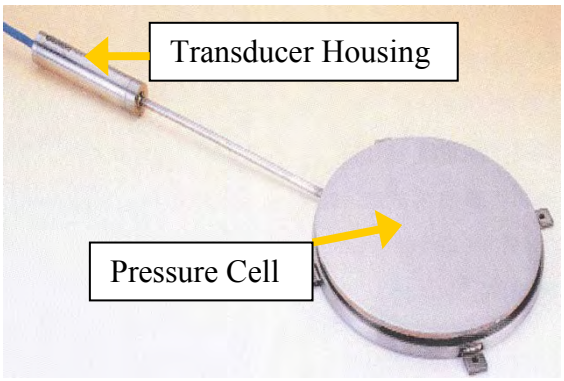

Figure 3-42: Earth Pressure Cell (Geokon 4810, used by Permission)

Figure 3-43: Earth Pressure Cell Installation

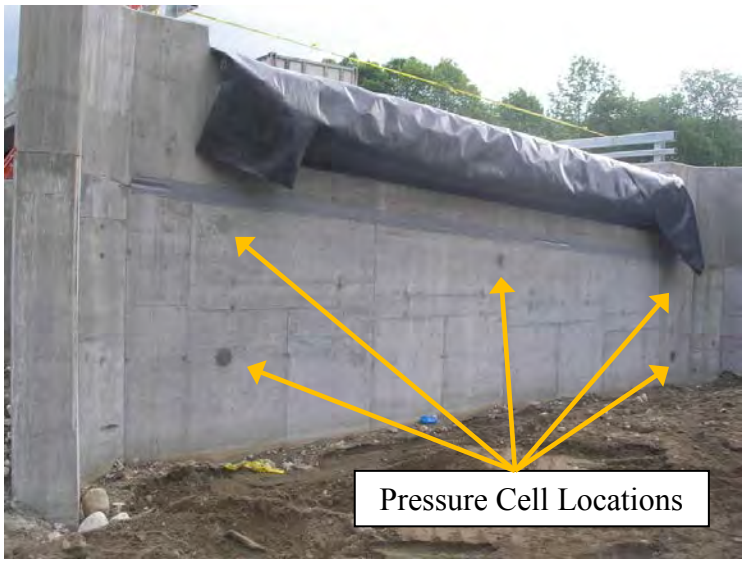

Figure 3-44: Abutment Pressure Cell during Backfilling at Stockbridge Bridge (Top Two Rows of Cells)

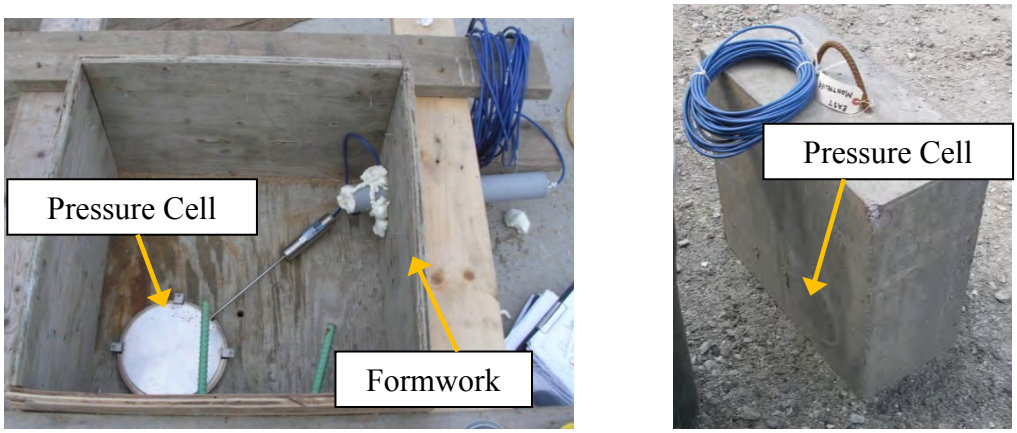

(a) (b)

Figure 3-45: Reference Pressure Cell Installation (a) Formwork for Concrete Block at the Middlesex Bridge (b) Reference Pressure Cell Concrete Block at the East Montpelier Bridge)

3.5.3 Displacement Transducers

Displacement transducers (Geokon 4420) were chosen to measure longitudinal (parallel to the roadway) and transverse (perpendicular to the roadway) displacements of the abutments. Several options were considered for monitoring abutment deflections, all with potential shortcomings related to the position of the reference point for data. Ultimately the selected

system consisted of displacement transducers on the sides of the abutments at each end of the bridge attached to reference piles located near the abutment walls.

Transducers were positioned to measure the displacements of the abutment relative to a reference pile. One end of the instrument was attached to a steel angle attached to the abutment wall with expansion anchors. The other end of the instrument was attached to an extension angle welded to the top of the reference pile. All the extension angles except the ones at the Middlesex Bridge were welded to the reference piles flanges. In the Middlesex Bridge, because of space constraints, angles were attached to the top of the reference pile. During installation the instrument position was adjusted to have the initial reading position within the mid-range of displacements that can be recorded by the transducers to be able to read displacements in positive or negative directions (construction temperatures were approximately mid-range of expected fluctuations). The gages were carefully oriented perpendicular and parallel to the abutments (or at a known angle if necessary) and their final elevation recorded with respect to the construction joint on abutments. Locations and orientation of gages installed are shown in the previous sections. Figure 3-46 shows the location of concrete enclosure. Figure 3-47, Figure 3-48 and Figure 3-49 shows example displacement transducers from Middlesex, East Montpelier and Stockbridge bridges, respectively.

Figure 3-46: Displacement Transducer Enclosure

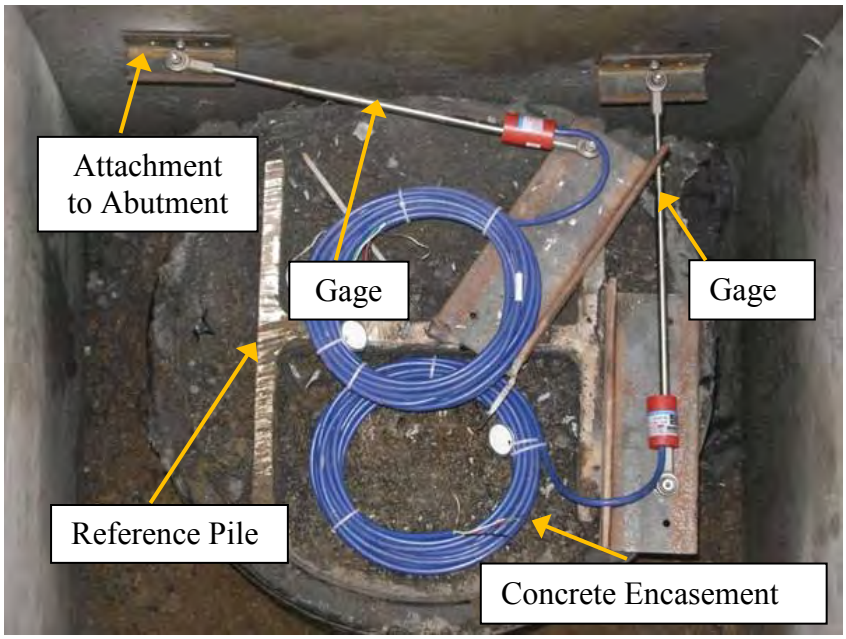

Figure 3-47: Displacement Transducers at Middlesex Bridge

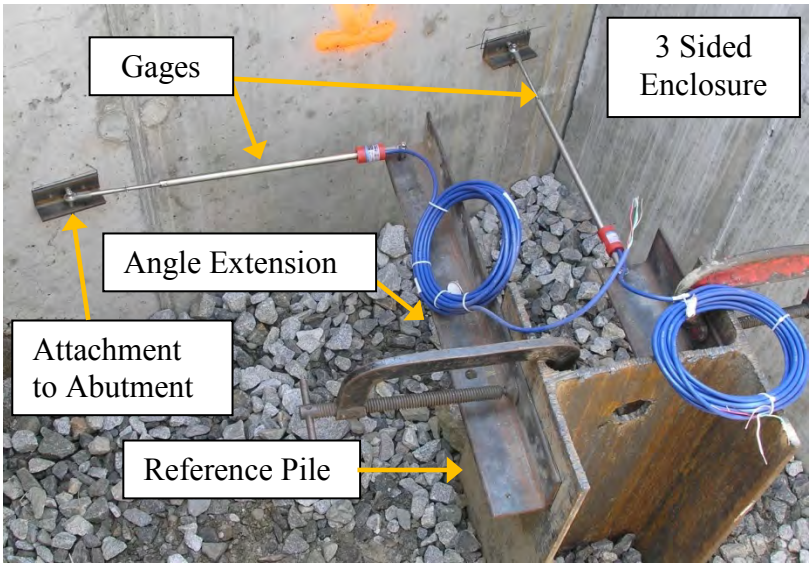

Figure 3-48: Displacement Transducers at East Montpelier Bridge

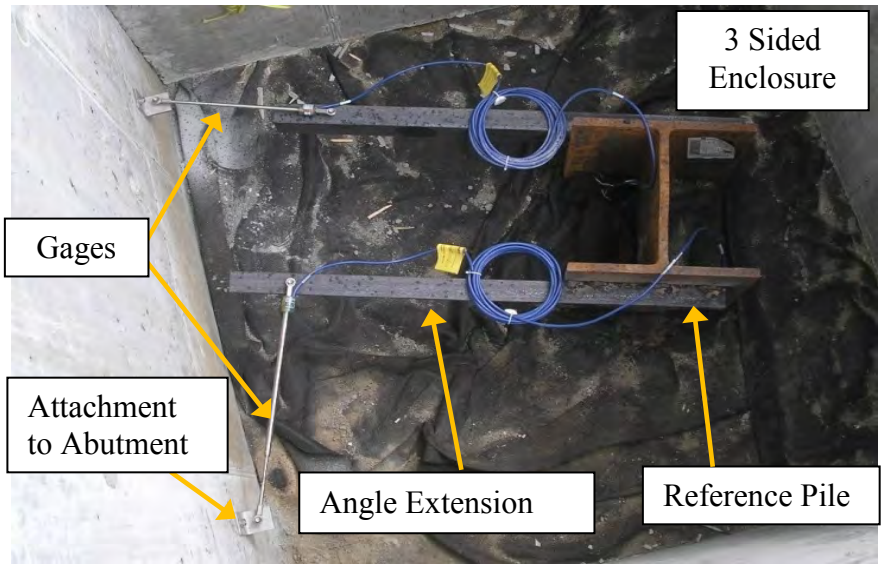

Figure 3-49: Displacement Transducers at Stockbridge Bridge

3.5.4 Tiltmeters

Tiltmeters are attached to the face of the abutment to measure abutment rotation. Two types of tiltmeters were used for instrumentation – a Geokon 6160 (biaxial) and a Geokon 6350 (uniaxial). Biaxial units are MEMS, while uniaxial models are vibrating wire instruments. Biaxial tiltmeters are capable of measuring the abutment rotations about axes oriented parallel and perpendicular to the roadway alignment. Uniaxial tiltmeters were positioned to record rotations about an axis perpendicular to roadway alignment. Middlesex and East Montpelier bridges have uniaxial tiltmeters whereas the Stockbridge Bridge has biaxial gages.

Gage geometry and the installation process were similar for both tiltmeter types. Gages were held in the vertical position and supported on mounting brackets that were anchored into the abutment concrete through expansion anchors. During installation, high strength Loc-tite was used to fix cap screws and bolts. Once gages were attached to the abutment wall, they were secured by a protective steel angle fitted with end plates. Tiltmeter cables were routed to the multiplexer boxes through PVC conduit. Figure 3-50 shows the location of a typical tiltmeter and Figure 3-51 shows a tiltmeter before and after placing the protective angle.

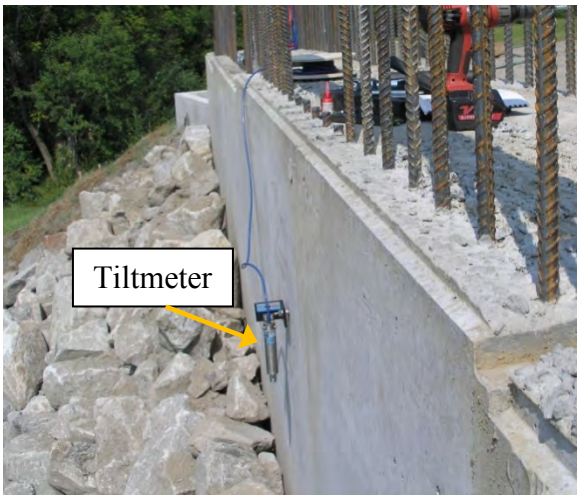

Figure 3-50: Tiltmeter Location Abutment at East Montpelier Bridge

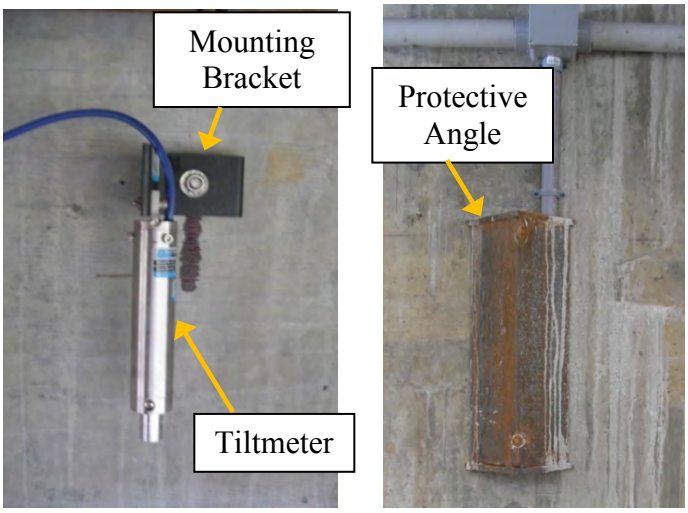

Figure 3-51: Tiltmeters Before and After Putting Protective Angles

3.5.5 Inclinometers

In-place inclinometers (Geokon 6150-Biaxial and Geokon 6350-Uniaxial) were used to determine rotations of selected piles within the instrumented region. These instruments consist of a string of tiltmeters that measure rotation within a set gage length. The string of the gages is positioned inside a PVC tube (Figure 3-52) secured to abutment piles. The tube is protected inside an angle welded to a flange of the instrumented pile. The space between the PVC tube and angle was filled with non-shrink grout. The continuous arrangement of gages allows for the determination of pile inclination as a function of depth. The inclinometer strings consist of tiltmeters mounted on steel tubing connected to wheel assemblies and separated from the next assembly by a universal joint. Steel tubing enables a rigid connection between two wheel

assemblies and defines the gage length and spacing between gages. Universal joints allow the gages to incline independently from the adjacent gages while maintaining constant spacing. The wheel assembly includes a loaded spring to maintain correct orientation inside the grooves of the PVC casing. The string of gages is hung from the top of the inclinometer casing with cabling that can be field adjusted to ensure the proper location of wheel assemblies.

In the field, inclinometer casings were placed in steel angle enclosures that were welded to the piles. Initially, at the Stockbridge Bridge the detail called for pipe steel sections welded to the inside of the web. Concerns of weld access led to several field modifications. During pile driving a series of weld failures led to significant revisions of subsequent details. There was limited time for troubleshooting, and in order to avoid construction delays two inclinometers planned for Abutment 2 were deleted from the instrumentation plan. The revised installation detail for Abutment 1 included inclinometer enclosures attached to the outer face of one flange in instrumented piles as shown in Figure 3-53. This detail was subsequently used in the Middlesex and East Montpelier bridges.

Inclinometer casings were made of PVC tubes glue-snapped to each other using ABS 771 cement. The bottom of the casing was covered by an end cap connected in the same manner. The joints between casing sections were additionally wrapped with duct tape. The grooves inside the casings were positioned perpendicular and parallel to the piles. The void space around the casing was grouted prior to placements of gages. During the grouting procedure, the casings were prevented from floating (due to buoyancy forces) by tying the PVC pipe to the reinforcing cage above and applying weights at the top of the casing. Inclinometer casings were carefully routed around final girder locations by securing the casings to formwork (Figure 3-54). The gages were installed temporarily during this process to verify gages could pass through the required curvature of the casing. Note that the East Montpelier inclinometer casing was terminated within the abutment and therefore was not routed around girders. This method was simpler, but does not allow for replacement or removal of any inclinometers in the future.

During gage installation, the whole gage string was assembled and then placed in the PVC enclosure. At the top of the assembly, a steel rope was attached to a hanger which seated on the top of the inclinometer casing. The length of this steel rope was field adjusted according to the length required to have the top wheel assembly at the bottom of the abutment. The hanger at the top rested on the top of the casing and is covered by the steel cover when it extended to the road surface, or sealed when embedded in the abutment. A security cable was attached to the bottom end of the gage assembly as a precaution in case the top cable detaches. In the Middlesex and East Montpelier bridges, the gage assembly was lifted by a crane and placed in the casing vertically. At the Stockbridge Bridge the gage assembly was placed by hand. Both methods worked equally well. The fixed wheel at the wheel assembly was always aligned towards the

river. Figure 3-55 and Figure 3-56 show gage installation stages at the Stockbridge and East Montpelier bridges.

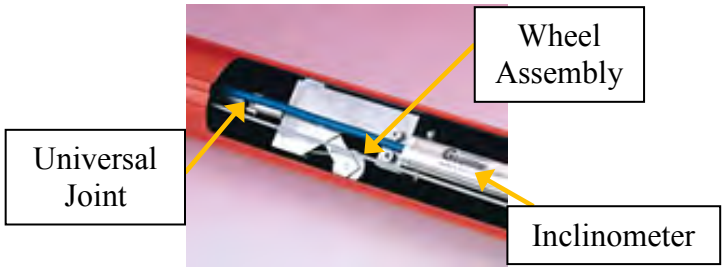

Figure 3-52: A Sectional View of a Single Inclinometer in Casing (Geokon, used by Permission)

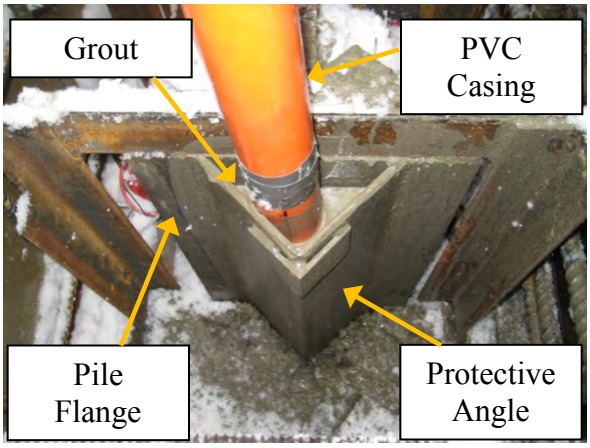

Figure 3-53: Inclinometer Casings Attached to the Pile Flanges

Figure 3-54: Inclinometer Casing Route around the Girders at the Top

(a)

(b)

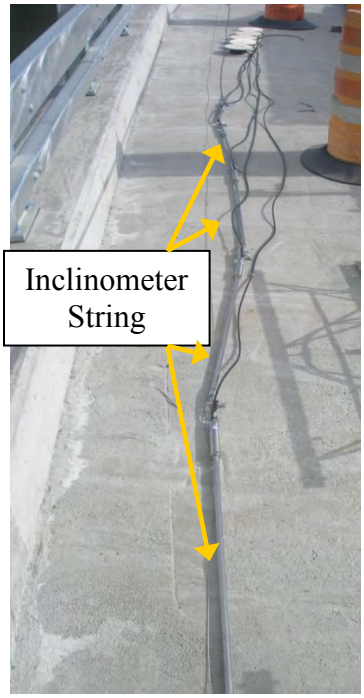

(c)

(d)

Figure 3-55: Installation of Inclinometers in Stockbridge Bridge: (a) During Grouting; (b) Gage in Casing within Abutment; (c) Inclinometer String Prior to Placement; and (d) Steel Cover on Roadway and Routing of Inclinometer Cables to Multiplexers

(a)

(b)

(c)

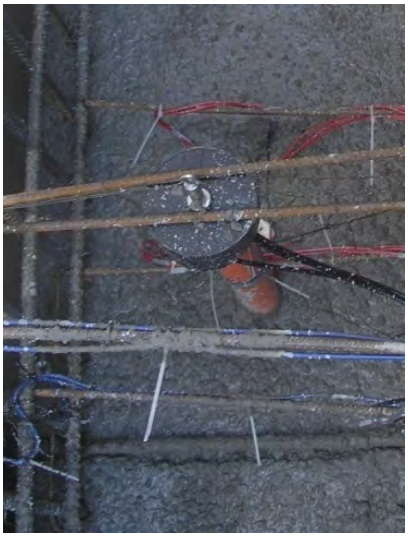

(d)

Figure 3-56: Installation of Inclinometers in East Montpelier Bridge: (a) Inclinometer String Prior to Placement; (b) Gage String Lifted for Placing in the Casing; (c) Casing Exiting Grouted Enclosure at Pile Top; and (d) Plan View of Inclinometer Gage and Casing during Abutment Concrete Placement

3.6 Summary

Instrumentation of East Montpelier Bridge and Stockbridge Bridge finished in November, 2009. Instrumentation Middlesex Bridge finished in December, 2009. A total of 83, 89 and 131 gages and accompanying data acquisition systems were installed at the Middlesex, East Montpelier and Stockbridge bridges, respectively. All the gages were installed according to the procedures provided in this chapter. Instruments that malfunctioned are listed in Table 3-3. The instrument channels used for the data acquisition system and corresponding gage locations are given in Appendix B.

Long-term monitoring of the three bridges initiated following completion of construction at each bridge. Monitoring of each bridge will continue for a minimum period of two years with data collected at least every 6 hours during this period.

Table 3-3: List of Gages Malfunctioned*

MIDDLESEX[1]	EAST MONTPELIER[1]	STOCKBRIDGE[2]
MUX_4 CH_10 (SGG-0M-TE)	MUX_3 CH_15 (SG-1S-3SE)	MUX_3 CH_3 (SG-1N-1SE)
MUX_6 CH_4 (SG-1E-3NW)		MUX_3 CH_5 (SG-1N-2NE)
		MUX_3 CH_8 (SG-1N-2SW)
		MUX_3 CH_9 (SG-1N-3NE)
		MUX_3 CH_15 (SG-1N-4SE)
		MUX_4 CH_1 (SG-1S-1NE)
		MUX_4 CH_5 (SG-1S-2NE)
		MUX_4 CH_7 (SG-1S-2SE)
		MUX_4 CH_9 (SG-1S-3NE)
		MUX_4 CH_13 (SG-1S-4NE)
		MUX_4 CH_16 (SG-1S-4SW)

*SG – Pile Strain Gage, SGG – Girder Strain Gage

[1]Gages failed during concrete deck pour.

[2] Gages failed during pile driving operations.

4 PRELIMINARY FINITE ELEMENT MODELING OF BRIDGES

A three dimensional Finite Element Model (FEM) of each structure will augment the field data. The models included all elements of the bridge superstructure (girders, cross diaphragms, concrete deck) and the bridge substructures (abutments, wingwalls, piles, pier, bent cap, and interior pier foundation). Soil backfill was modeled using nonlinear springs oriented perpendicular to the abutments and wingwalls. The soil surrounding abutment and pier piles was also modeled using nonlinear springs. Geometric nonlinearity was included in all analyses. Load cases considered to date are self weight, self weight combined with temperature increase and self weight combined with temperature decrease with temperature ranges defined by VTrans design guidelines and an assumed construction temperature.

The elastic and thermal material properties used in the FEMs are given in Table 4-1. Class A concrete was used for the concrete deck and for the segment of abutment above the construction joint located near the bottom of the steel girders. Class B concrete was used for all the other concrete elements in the bridge. Girders and HP-piles were modeled using steel section properties.

Table 4-1: Material Properties for Finite Element Models

	Strength [MPa (ksi)]	Elastic Modulus [MPa (ksi)]	Shear Modulus [MPa (ksi)]	Coeff. of Thermal Expansion [m/m/^{o}C (in./in./^{o}F)]	Poisson's Ratio	Unit Weight [kg/m^3 (lb/ft^3)]
Concrete (Class A)	28 (4.0)	25 (3605)	10 (1502)	9.9E-6 (5.5E-6)	0.2	2400 (150)
Concrete (Class B)	24 (3.5)	235 (3372)	10 (1405)	9.9E-6 (5.5E-6)	0.2	2400 (150)
Steel	345 (50.0)	200 (29000)	77 (11153)	11.7E-6 (6.5E-6)	0.3	7850 (490)

Concrete elements were modeled as 4-node shell elements with six degrees of freedom at each node and steel elements as two node frame elements with six degrees of freedom per node. Cracked section properties were assumed for all concrete elements (0.35 I_g for deck and 0.70 I_g for pier column). Steel girder properties were calculated at the center of the top flange using 2-node three dimensional frame elements with six degrees of freedom at each node. In order to simulate composite behavior of bridge superstructure, a body constraint (rigid link) was defined between each concrete deck nodes and the corresponding girder nodes. Rigid links were also used to simulate the depth of girders. Cross diaphragms were modeled using 2-node three dimensional frame elements with six degrees of freedom at each node. A schematic of the bridge superstructure showing cross section modeling is given in Figure 4-1.

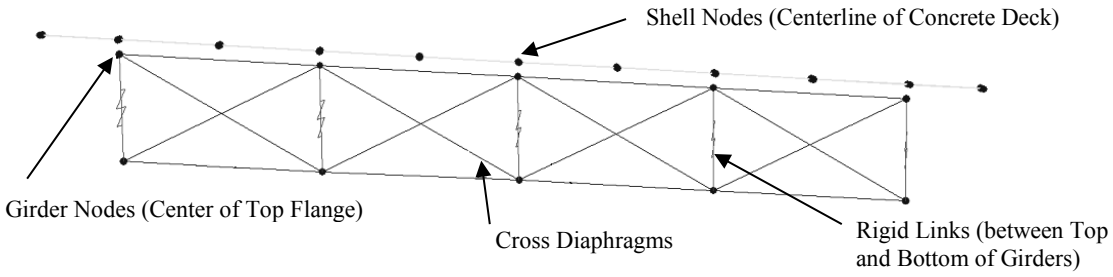

Figure 4-1: Node and Elements for Bridge Superstructure FEM Modeling (Cross Section)

Abutments and wingwalls were modeled using 4-node shell elements with six degrees of freedom at each node. Transfer of moments at bridge superstructure-abutment connection was enabled by making use of rigid links with all degrees of freedoms constrained. Using these rigid links, girders were attached to the abutments at three different nodes along their depth as shown in Figure 4-2

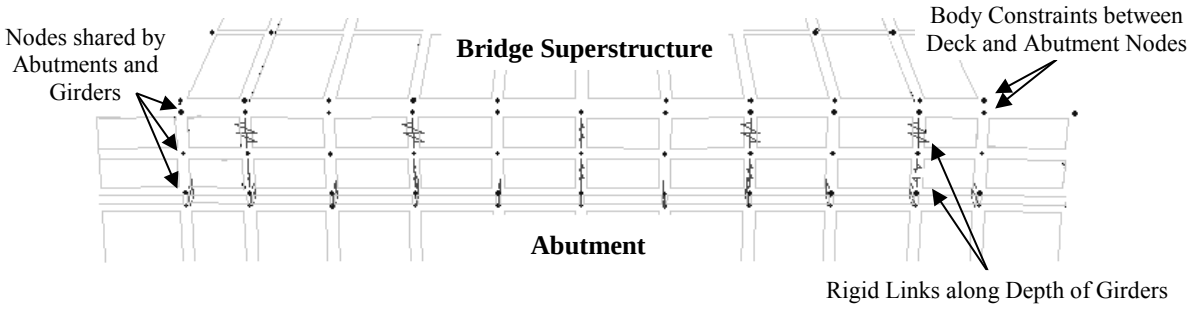

Figure 4-2: Bridge Superstructure – Abutment Connection Detail

Two-node frame elements with six degrees of freedom at each node were used to model the HP steel piles. Piles were modeled over the top 6.1 m (20.0 ft) depth and were assumed to be fixed at the base. This was done to decrease the size of the model after observing that moments in a full-depth pile model were negligible below this depth.

Nonlinear discrete Winkler springs were modeled to simulate soil-structure interaction behind the abutments and around the piles. For nonlinear spring behind the abutments, coefficients of lateral earth pressure were calculated for active and passive pressures following the report by Barker et al. (1991). Active pressures at the abutments were accounted for as an initial pressure with p-y curves offset accordingly. For nonlinear spring around the piles, p-y curves were defined using the hyperbolic tangent method described by API (1993) and the ultimate lateral soil resistance was found from Bogard & Matlock (1980) as described below.

Nonlinear discrete Winkler springs were attached at 30 cm (1 ft) intervals along the pile depth in both orthogonal directions to simulate lateral soil resistance around piles.

The initial modulus of subgrade reaction was determined from API (1993) based on the internal angle of friction. The pile lateral soil resistance-deflection (p-y) relationship for sand is approximated by Equations 4.1, 4.2 and 4.3.

$$P_{us}= (C_1 \times H \times C_2 \times D) \times \gamma \times H \quad \text{(Eq.4.1)}$$

$$P_{uD}=C_3 \times D \times \gamma \times H \quad \text{(Eq.4.2)}$$

Where,
γ= effective soil weight (lb/in^3)
H= depth, (in.)
φ= angle of internal friction of sand, (degrees)
C_1,C_2,C Coefficients determined from Figure 6.8.6-1 (API) as a function of φ
D= average pile diameter from surface to depth (in.)

$$P=A \times p_u \times tanh\left[\frac{k \times H}{A \times p_u} \times y\right] \quad \text{(Eq.4.3)}$$

Where,
P_u=min(p_{us},p_{uD})= ultimate bearing capacity at depth H, (lbs/in)
A= factor to account for cyclic or static loading condition

A= 0.9 for cyclic loading, A=$\left(3.0 - 0.8\frac{H}{D}\right) \geq 0.9$ for static loading.

k= initial modulus of subgrade reaction (lb/in^3)
y= lateral deflection, (in)

Figure 4-3 and Figure 4-4 show two different types of springs modeled in FEMs – abutment soil springs and pile soil springs. Medium dense sand properties were assumed for the soil surrounding all piles in the FEMs. This soil had a submerged unit weight of 925 kg/m^3 (57.6 lb/ft^3), a soil strength modulus of 960 kg/m^3 (60 lb/in^3), and an internal friction angle of 35^o.

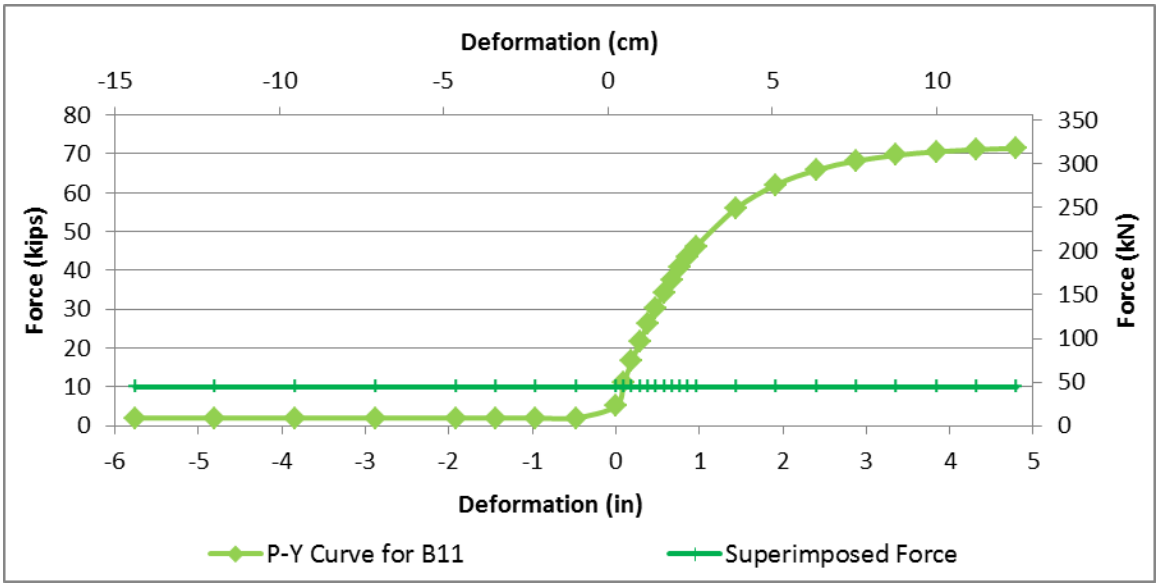

Figure 4-3: Modeled Abutment Force-Deformation Curve for Soil @ 2.1 m (6.9 ft) Depth (Stockbridge Bridge)

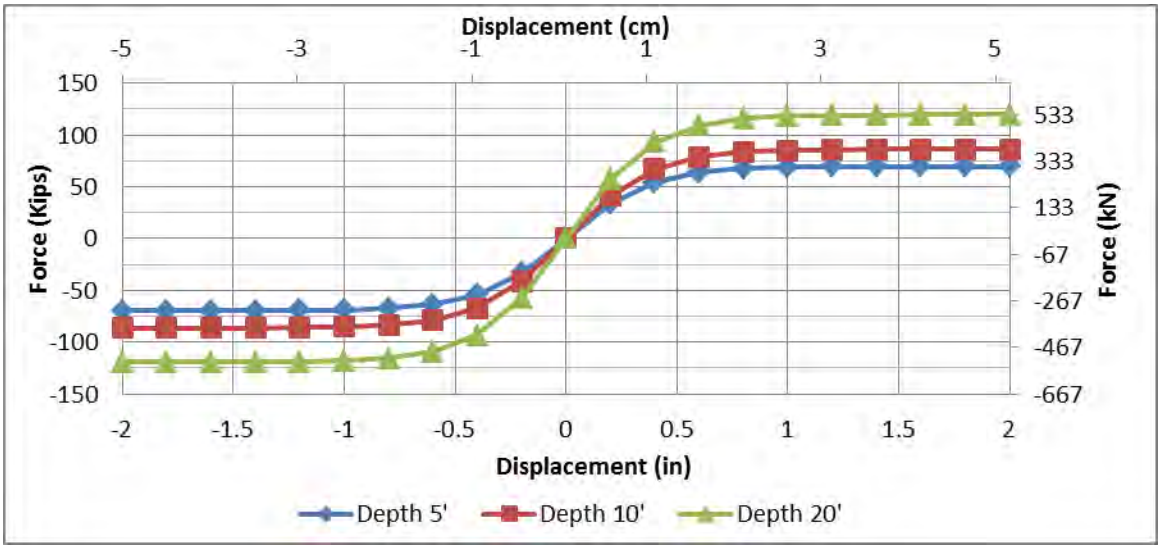

Figure 4-4: Force-Deformation Relationship for Soil Spring around Piles @ 1.5 m (5 ft), 3 m (10 ft) and 6.1m (20 ft) (Stockbridge Bridge)

The Stockbridge Bridge has an interior pier that is included in the FEMs. The pier cap beam was modeled using nonprismatic 2-node frame elements with six degrees of freedom at each node. Elastomeric bearing pads were idealized as two joint link elements (rigid links with appropriate degrees of freedom released). The interior pier was modeled using 2-node frame elements with six degrees of freedom at each node with a 2300 mm (90 in) top-end offset to account for the depth of the pier cap beam. The pile group was modeled as a single frame element with stiffness modifications to account for total lateral and vertical stiffnesses of all

sixteen piles in the group. Rotational and axial resistances of the pile group were represented by linear discrete Winkler springs with stiffnesses defined by NEHRP (2003). Rigid link elements were assigned between the bottom pier column element and the top pile group element to account for the presence of a rigid pile cap. Detail of the interior pier is given in Figure 4-5. Figure 4-6 and Figure 4-7 which shows screenshots from FEMs of the Middlesex Bridge and Stockbridge Bridge, respectively.

Field data will be used to verify FEM models. Finally, the models will be used to explain general structural behavior for comparison to current design procedures. The FEM models could also be used to extrapolate research results based on parametric analysis (changing curvature and skew angles).

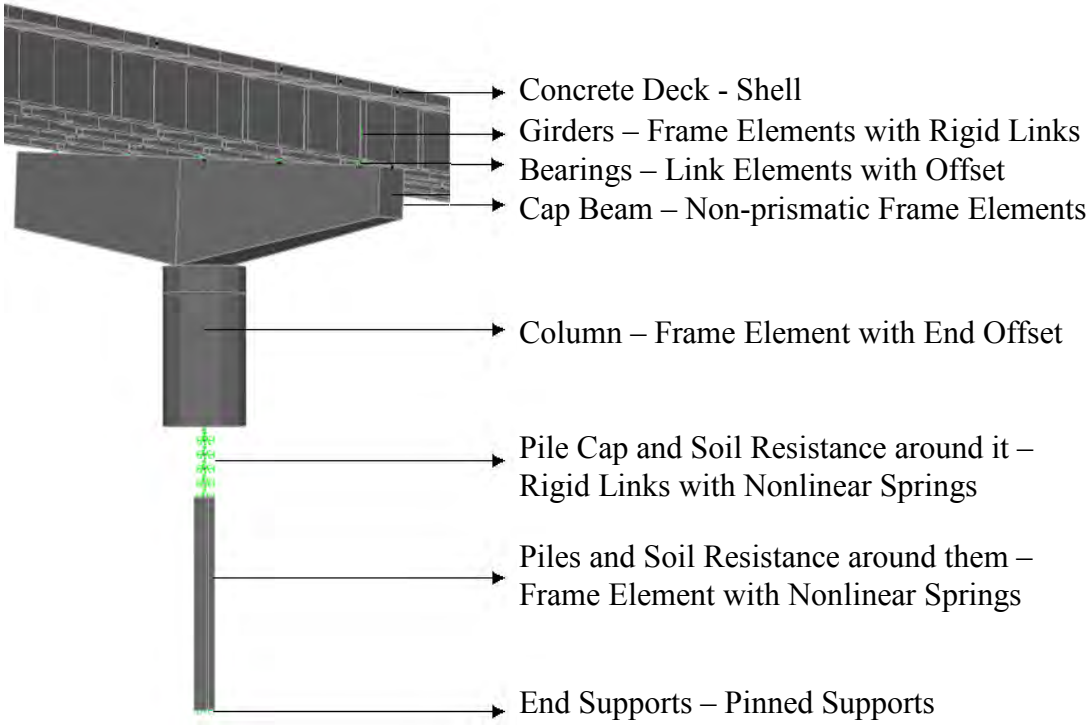

Figure 4-5: Finite Element Model of Interior Pier

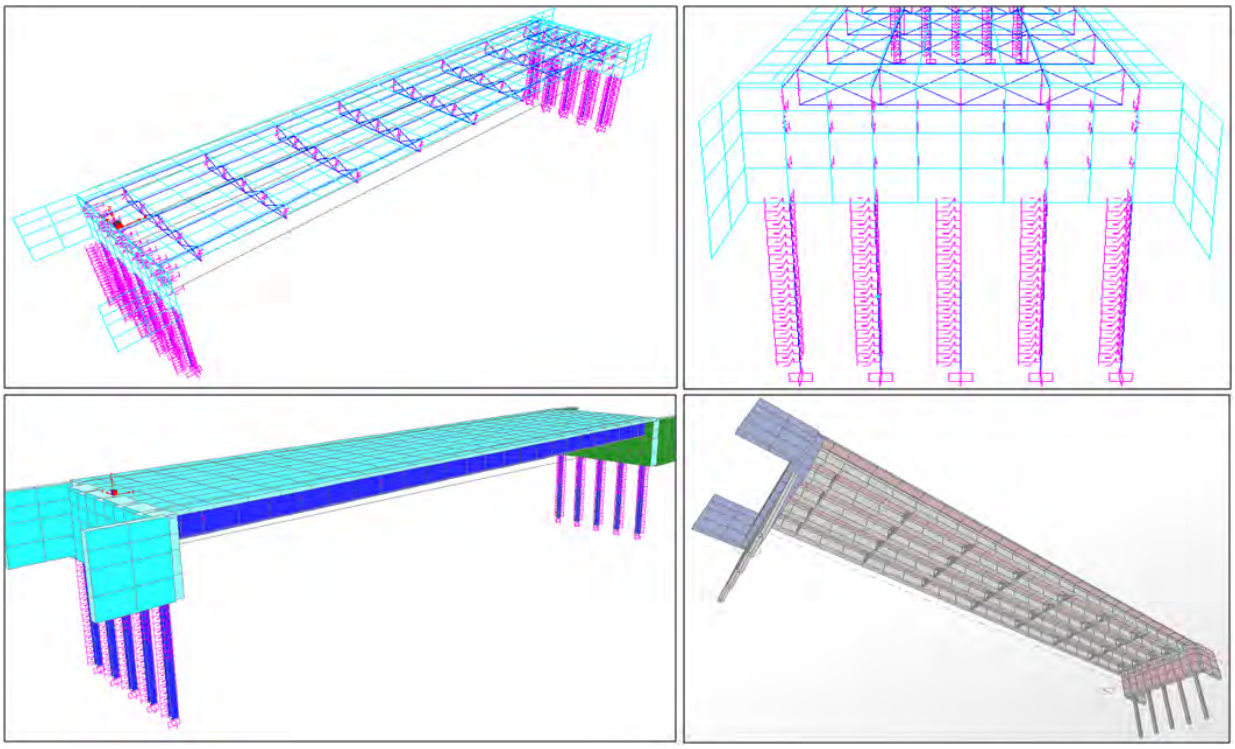

Figure 4-6: Finite Element Modeling of Middlesex Bridge

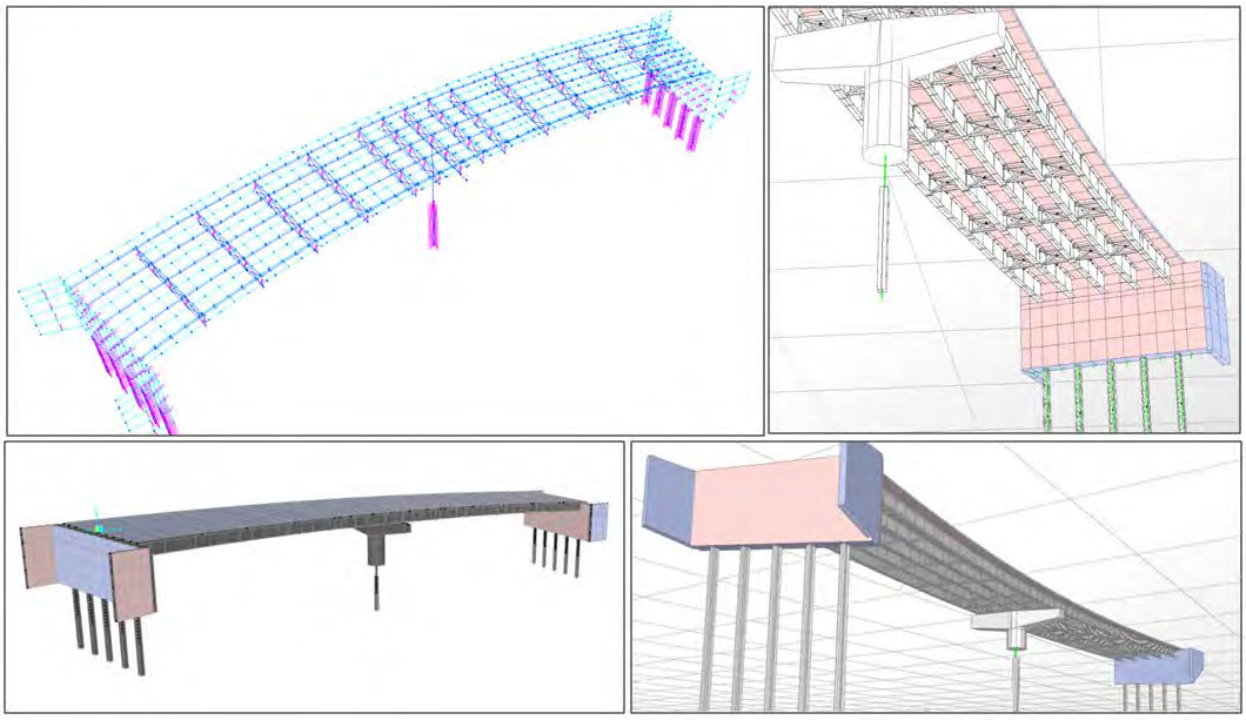

Figure 4-7: Finite Element Modeling of Stockbridge Bridge

5 LIVE LOAD TESTING OF BRIDGES

5.1 Introduction

The bridges were tested using loaded dump trucks stationed at various positions along the span to verify finite element models and evaluate the gravity load carrying characteristics of each bridge. The tests took place between December 17th and December 21th, 2009. For each bridge, three dump trucks were positioned at a number of locations along the bridge length to generate positive and negative moments in each lane and each travel direction. Permanent instrumentation installed for long term monitoring of the bridge was used to collect the readings. While the trucks were stationary at a specific station, a minimum of one set of readings was collected leading to waiting times of more than 6 minutes per location. Traffic was allowed on the bridge during data acquisition except when trucks were positioned transversely on the bridge deck.

Details of the tests at each bridge with truck locations are given in the following sections. Figure 5-1 illustrates the three dump trucks aligned longitudinally on one lane of the Stockbridge Bridge.

Figure 5-1: Load Testing of the Stockbridge Bridge

5.2 Live Load Testing of Middlesex Bridge

The Middlesex Bridge was tested on December 18th, 2009. The test started at 9:43 am and continued until 11:30 am. The lowest and highest ambient temperatures recorded during testing were -11.8°C (10.8°F) and -10.7°C (12.8°F), respectively. The truck wheel loads were measured by DMV's portable truck scales. The three trucks used in this bridge had axle weights as listed in Table 5-1. In 12 out of the 13 loading arrangements, the trucks were positioned longitudinally as shown in Figure 5-2. The approximate spacing of the trucks and truck axle locations are shown in Figure 5-3. For the last truck arrangement, the trucks were positioned transversely as shown in Figure 5-4.

The transverse positions of trucks for the upstream and downstream lanes are shown in Figure 5-5. A table listing the truck positions in the order in which the tests were conducted is given in Table 5-2. Each lane was loaded with trucks parked at three different positions along the bridge length in the forward and reverse travel directions, resulting in a total number of truck locations equal to 12. Figure 5-6 and Figure 5-7 show the truck locations in the order of testing. In addition to longitudinal truck arrangements, two of the trucks (T16056 and TK 03 16064) were simultaneously positioned in a transverse arrangement at bridge midspan. Figure 5-8 shows the truck locations for this last test.

Table 5-1: Truck Axle Loads

TRUCK ID	Axle	Left Wheel Load [kN (kips)]	Right Wheel Load [kN (kips)]	Total Axle Load [kN (kips)]	TRUCK WEIGHT [kN (kips)]
TK 03 16064 (Front Truck)	Front	31.1 (7.0)	42.2 (9.5)	73.4 (16.5)	236.6 (53.2)
	Middle	35.1 (7.9)	47.1 (10.6)	82.3 (18.5)	
	Rear	35.6 (8.0)	45.4 (10.2)	80.9 (18.2)	
TK 05 16075 (Middle-Truck)	Front	30.7 (6.9)	40.5 (9.1)	71.2 (16.0)	295.3 (66.4)
	Middle	60.0 (13.5)	52.9 (11.9)	113.0 (25.4)	
	Rear	46.7 (10.5)	64.5 (14.5)	111.2 (25.0)	
T16056 (Rear Truck)	Front	31.6 (7.1)	41.4 (9.3)	72.9 (16.4)	237.9 (53.5)
	Middle	36.5 (8.2)	45.8 (10.3)	82.3 (18.5)	
	Rear	36.5 (8.2)	46.3 (10.4)	82.7 (18.6)	

Figure 5-2: Middlesex Load Testing (Longitudinal Arrangement of Trucks)

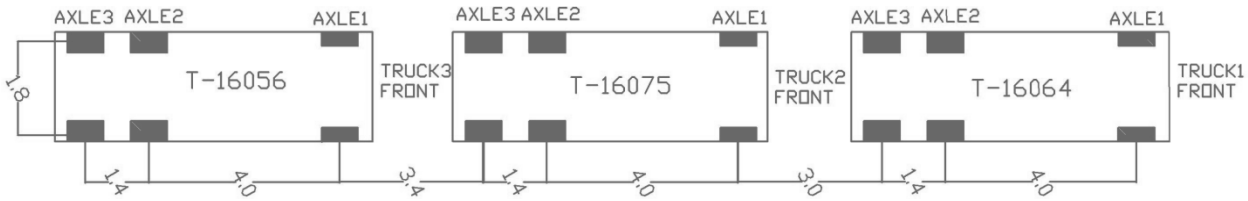

Figure 5-3: Plan View of Trucks

Figure 5-4: Middlesex Load Testing (Transverse Arrangement of Trucks)

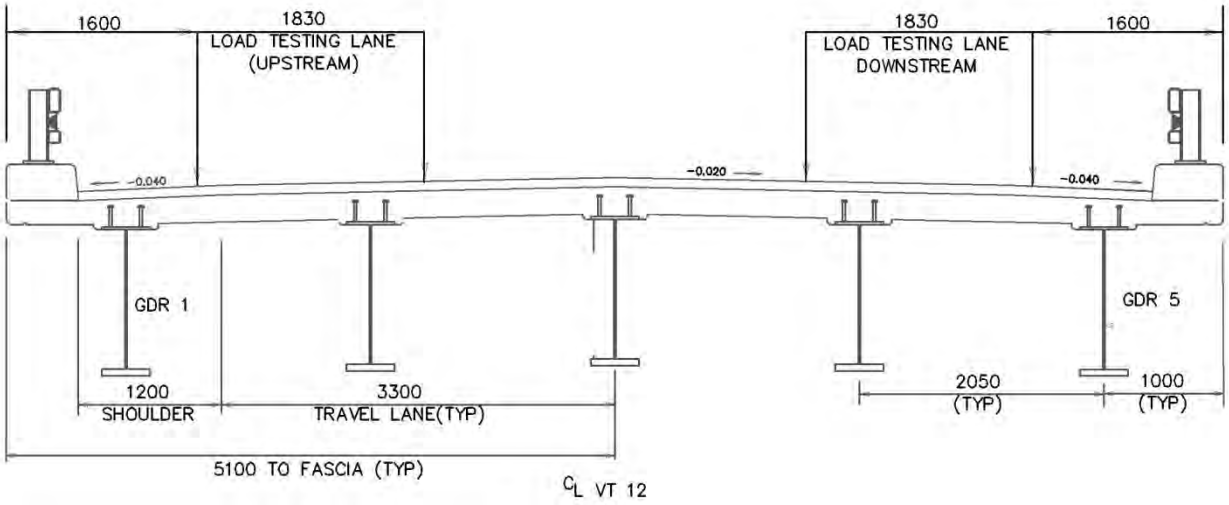

Figure 5-5: Lanes Loaded During Test

Table 5-2: Live Load Test Truck Record for Middlesex Bridge

Running Order	Run ID	Lane	Direction	Truck Location (Measured from Abutment 1)	
				Axle	Distance [m (ft)]
1	D-1	Downstream	Traffic	3rd Truck – 3rd Axle	0.0 (0.0)
2	D-2	Downstream	Traffic	3rd Truck – 3rd Axle	4.6 (15.0)
3	D-3	Downstream	Traffic	2nd Truck – 2nd Axle	22.0 (72.0)
4	UR-1	Upstream	Opposite Traffic	3rd Truck – 3rd Axle	0.0 (0.0)
5	UR-2	Upstream	Opposite Traffic	3rd Truck – 3rd Axle	4.6 (15.0)
6	UR-3	Upstream	Opposite Traffic	2nd Truck – 2nd Axle	22.0 (72.0)
7	U-1	Upstream	Traffic	3rd Truck – 3rd Axle	43.0 (141.0)
8	U-2	Upstream	Traffic	3rd Truck – 3rd Axle	38.4 (126.0)
9	U-3	Upstream	Traffic	2nd Truck – 2nd Axle	22.0 (72.0)
10	DR-1	Downstream	Opposite Traffic	3rd Truck – 3rd Axle	43.0 (141.0)
11	DR-2	Downstream	Opposite Traffic	3rd Truck – 3rd Axle	38.4 (126.0)
12	DR-3	Downstream	Opposite Traffic	2nd Truck – 2nd Axle	22.0 (72.0)
13	T (Transverse)	Both	Abutment 1	2nd Axle	22.0 (72.0)

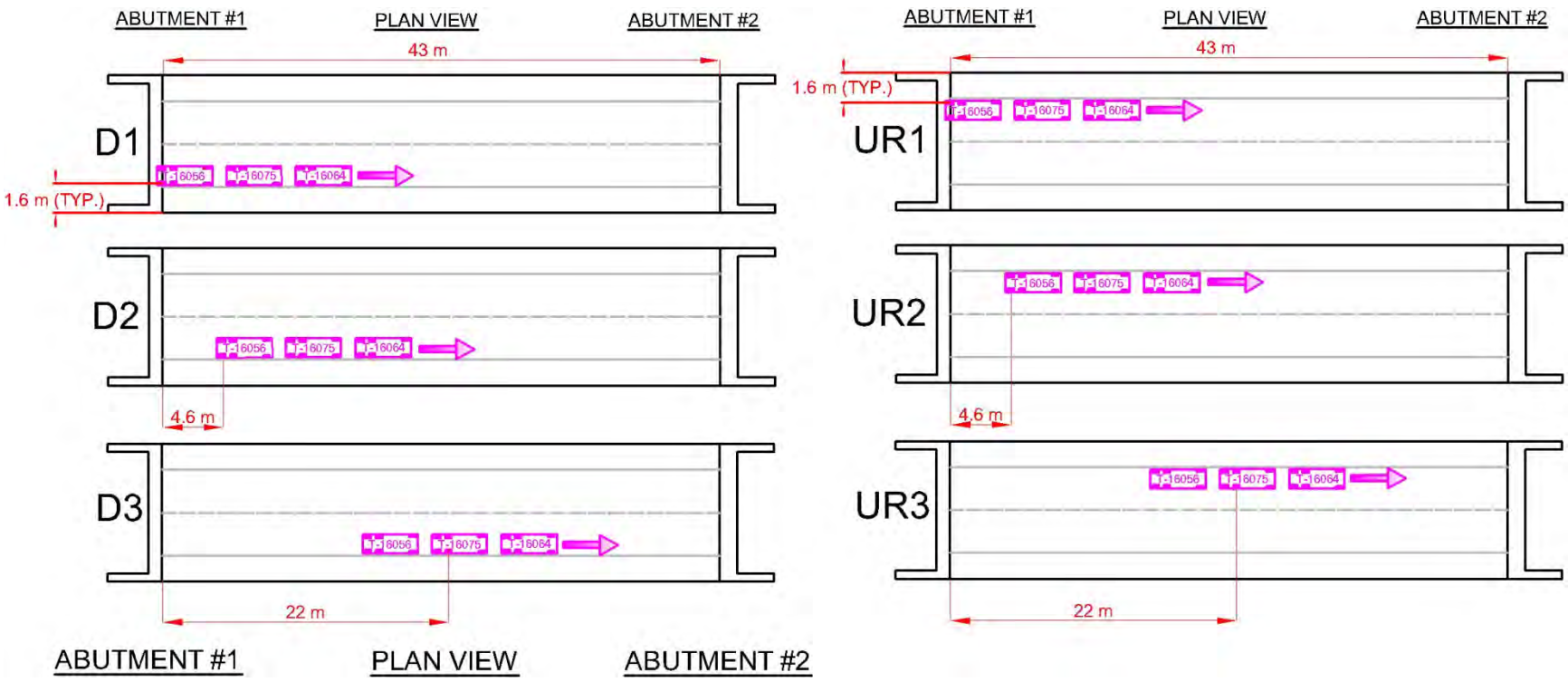

Figure 5-6: Middlesex Load Testing Truck Locations (Downstream Lane – Forward and Upstream – Reverse)

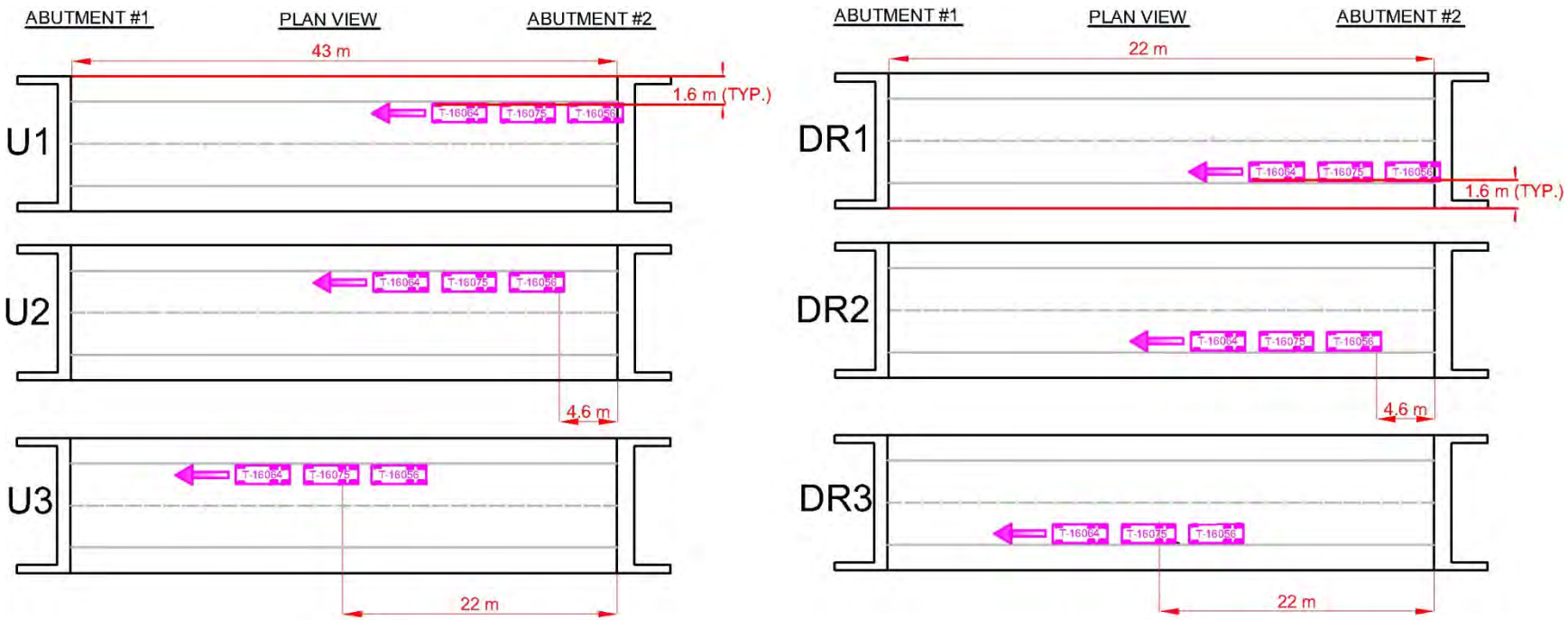

Figure 5-7: Middlesex Load Testing Truck Locations (Upstream Lane – Forward and Downstream – Reverse)

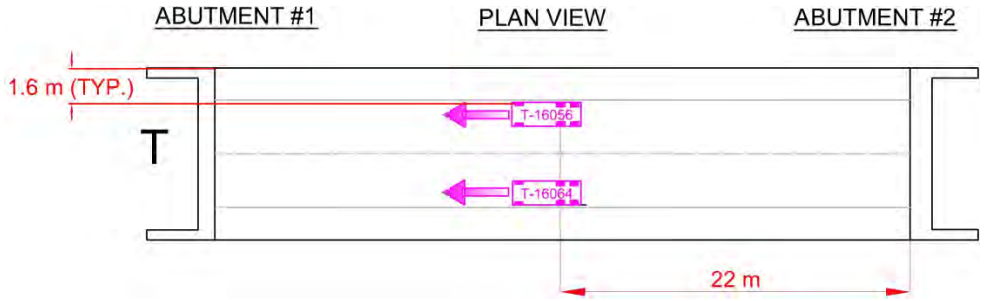

Figure 5-8: Middlesex Load Testing Truck Locations (Transverse Arrangement)

5.3 Live Load Testing of East Montpelier Bridge

The East Montpelier Bridge was tested on December 21th, 2009 between 9:37 am and 11:32 am. The lowest and highest ambient temperatures recorded during testing were -11.0°C (12.2°F) and -6.9°C (19.7°F), respectively. Figure 5-9 shows the data acquisition system located underneath the bridge. The bridge was loaded using three loaded dump trucks with axle loads as given in Table 5-3. In 12 out of the 13 loading positions, the trucks were arranged longitudinally as shown in Figure 5.10. The approximate spacing of the trucks and truck axle locations are shown in Figure 5-11. For the last truck arrangement, the trucks were positioned transversely as shown in Figure 5-12.

Figure 5-13 illustrates the truck placement within each of the loaded lanes. Table 5-4 gives details of the truck positions for each loading arrangement used during testing. In each lane trucks were placed at three different positions along the bridge length and measurements were taken with trucks facing the direction of travel or opposing the direction of travel. These arrangements were chosen to investigate symmetry in the response of the bridge. Figure 5-14 and Figure 5-15 show the truck locations in the order in which measurements were taken. In addition to longitudinal truck arrangements, the trucks were simultaneously positioned transversely at bridge midspan. Figure 5-16 shows the trucks placed for this final load test.

Figure 5-9: East Montpelier Load Testing (Data Acquisition during Testing)

Table 5-3: Truck Axle Loads

TRUCK ID	Axle	Left Wheel Load [kN (kips)]	Right Wheel Load [kN (kips)]	Total Axle Load [kN (kips)]	TRUCK WEIGHT [kN (kips)]
T 16075 (Front Truck)	Front	29.4 (6.6)	38.2 (8.6)	67.6 (15.2)	215.3 (48400)
	Second	28.9 (6.5)	44.5 (10.0)	73.4 (16.5)	
	Rear	32.0 (7.2)	42.2 (9.5)	74.3 (16.7)	
T 16056 (Mid Truck)	Front	31.1 (7.0)	42.7 (9.6)	73.8 (16.6)	241.0 (54200)
	Second	37.4 (8.4)	46.3 (10.4)	83.6 (18.8)	
	Rear	36.0 (8.1)	47.6 (10.7)	83.6 (18.8)	
T 16064 (Rear Truck)	Front	30.2 (6.8)	39.1 (8.8)	69.4 (15.6)	230.4 (51800)
	Second	37.4 (8.4)	44.0 (9.9)	81.4 (18.3)	
	Rear	36.0 (8.1)	43.6 (9.8)	79.6 (17.9)	

Figure 5-10: East Montpelier Load Testing (Longitudinal Arrangement of Trucks)

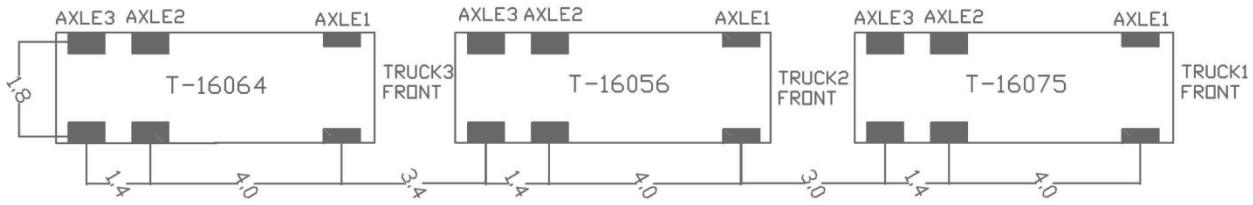

Figure 5-11: Plan View of Trucks

Figure 5-12: East Montpelier Load Testing (Transverse Arrangement of Trucks)

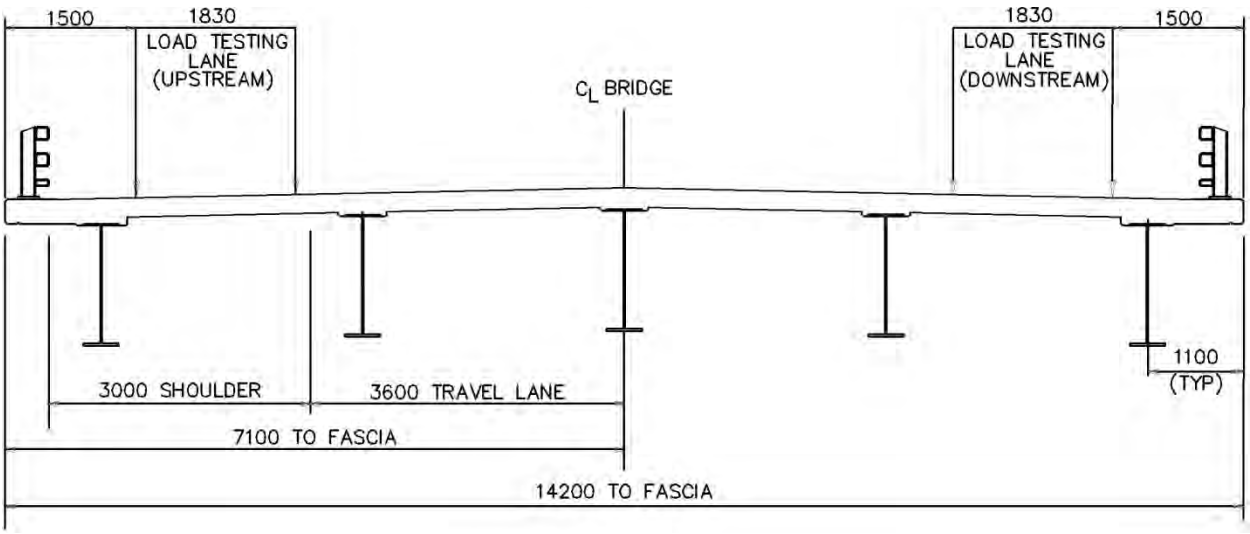

Figure 5-13: Load Test Truck Lanes

Table 5-4: Live Load Test Truck Record for East Montpelier Bridge

Running Order	Run ID	Lane	Direction	Truck Location (Measured from Abutment 1)	
				Axle	Distance [m (ft)]
1	U-1	Upstream	Traffic	3rd Truck – 3rd Axle	37.0 (122.0)
2	U-2	Upstream	Traffic	3rd Truck – 3rd Axle	32.4 (106.0)
3	U-3	Upstream	Traffic	2nd Truck – 2nd Axle	18.5 (61.0)
4	DR-1	Downstream	Opposite Traffic	3rd Truck – 3rd Axle	37.0 (122.0)
5	DR-2	Downstream	Opposite Traffic	3rd Truck – 3rd Axle	32.4 (106.0)
6	DR-3	Downstream	Opposite Traffic	2nd Truck – 2nd Axle	18.5 (61.0)
7	D-1	Downstream	Traffic	3rd Truck – 3rd Axle	0 (0.0)
8	D-2	Downstream	Traffic	3rd Truck – 3rd Axle	4.6 (15.0)
9	D-3	Downstream	Traffic	2nd Truck – 2nd Axle	18.5 (61.0)
10	UR-1	Upstream	Opposite Traffic	3rd Truck – 3rd Axle	0 (0.0)
11	UR-2	Upstream	Opposite Traffic	3rd Truck – 3rd Axle	4.6 (15.0)
12	UR-3	Upstream	Opposite Traffic	2nd Truck – 2nd Axle	18.5 (61.0)
13	T	Both	Abutment 2	2nd Axle	18.5 (61.0)

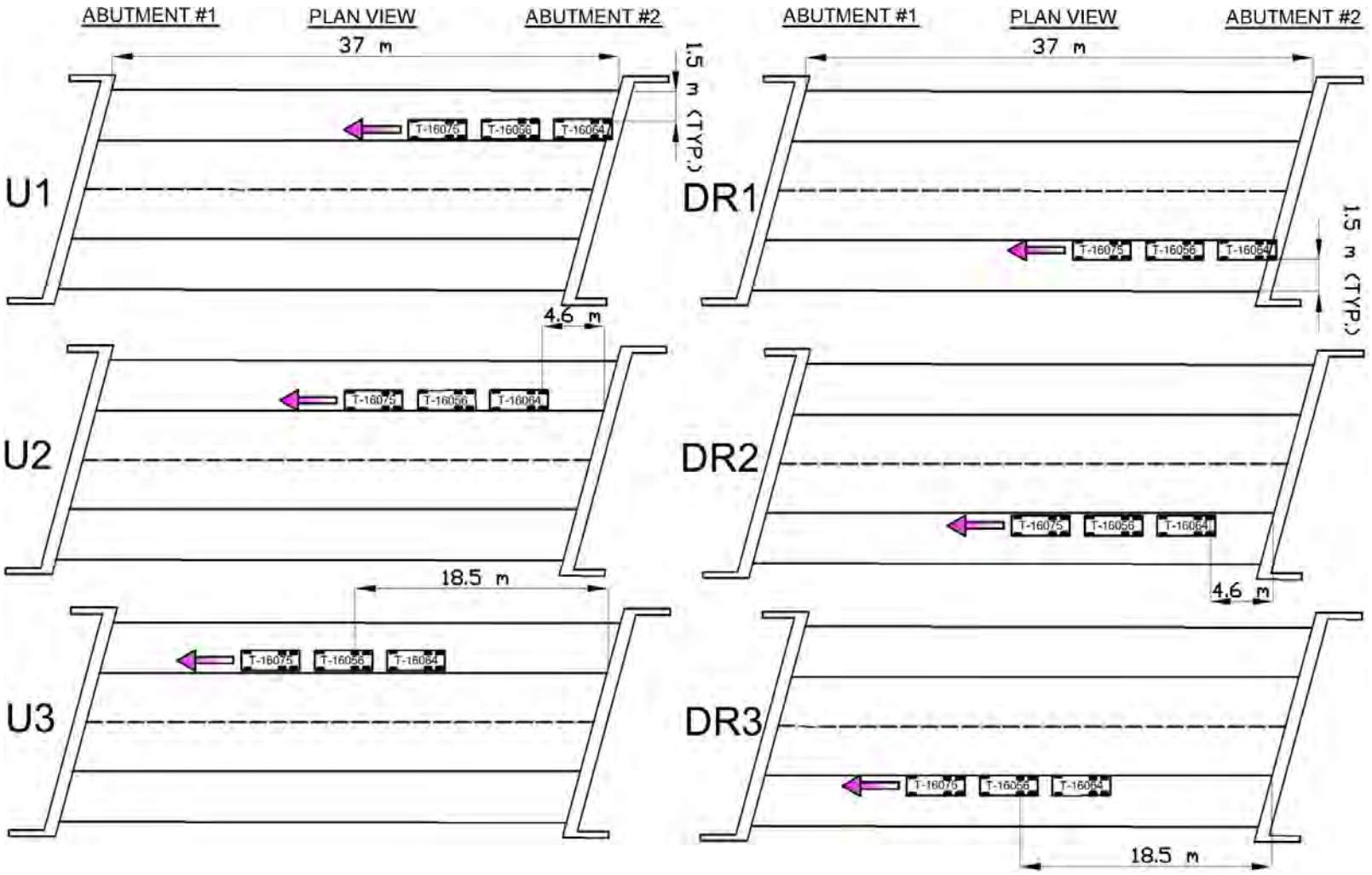

Figure 5-14: East Montpelier Load Testing Truck Locations (Upstream Lane – Forward and Downstream – Reverse)

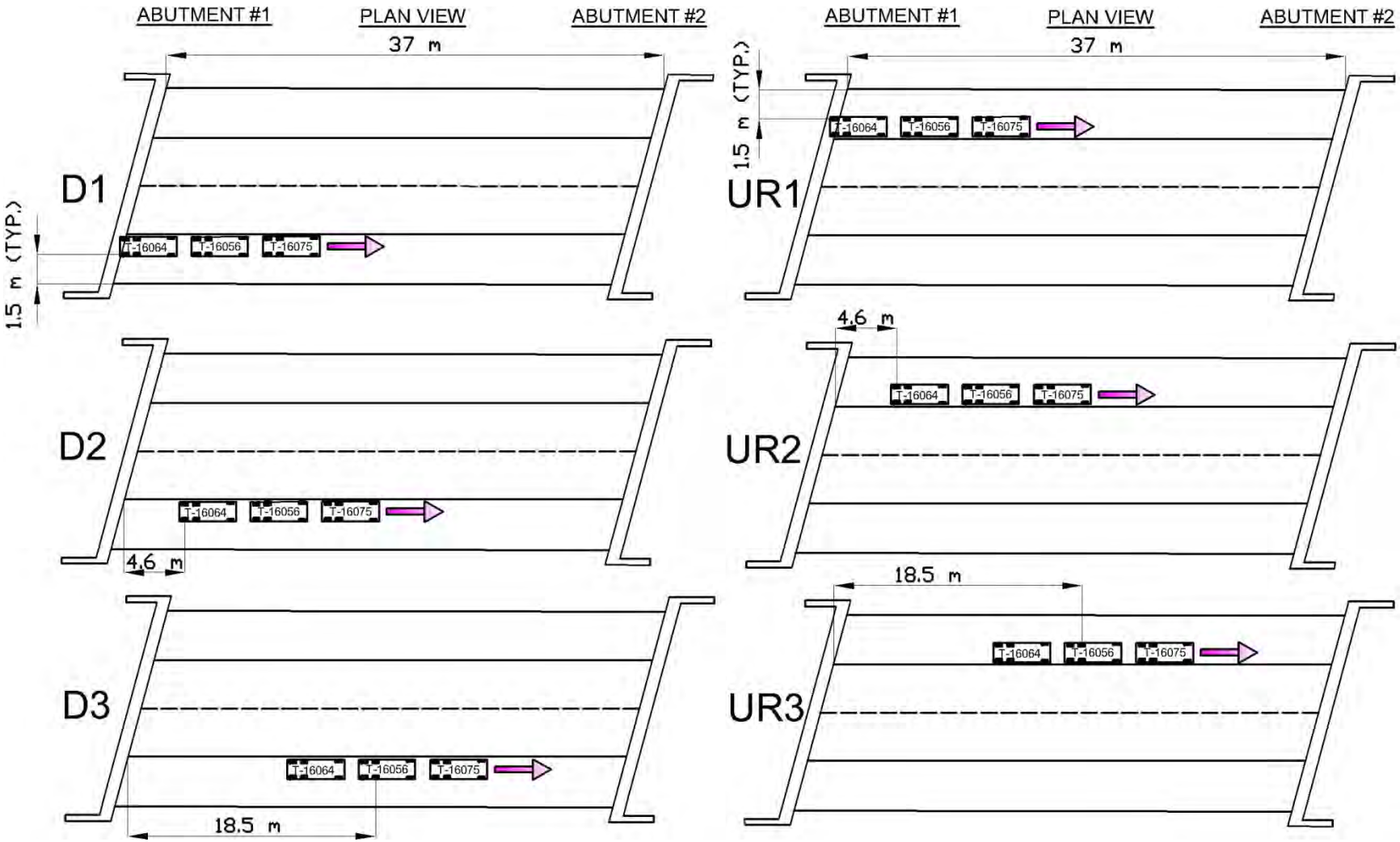

Figure 5-15: East Montpelier Load Testing Truck Locations (Downstream Lane – Forward and Upstream – Reverse)

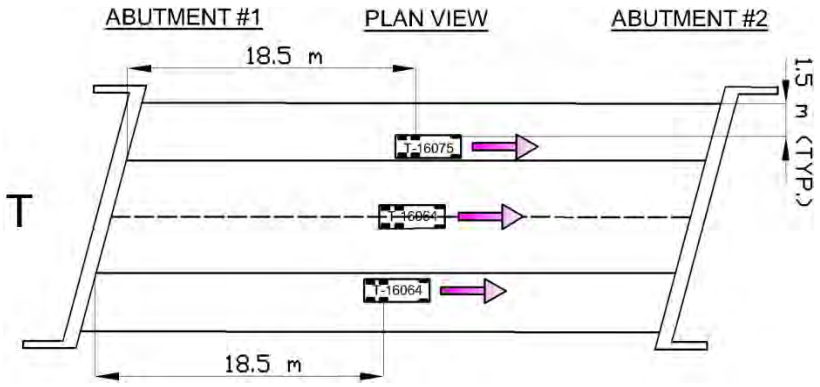

Figure 5-16: East Montpelier Load Testing Truck Locations (Transverse Arrangement)

5.4 Live Load Testing of Stockbridge Bridge

The Stockbridge Bridge was tested on December 17th, 2009 between 9.59 am and 12.38 pm. The lowest and highest temperature recorded during testing was -13.4°C (7.8 °F) and -12.8 °C (8.9°F), respectively. The bridge was loaded using three loaded dump trucks with axle loads as given in Table 5-5. Figure 5.17 shows the trucks positioned longitudinally. The approximate spacing of the trucks and truck axle locations are shown in Figure 5-18.

The truck placement within each of the loaded lanes is illustrated in Figure 5-19. Trucks were positioned in 12 different arrangements. Table 5-6 gives the truck arrangements in the order of testing. In each lane trucks were placed at four different positions along the bridge length and measurements were taken with trucks facing the direction of traffic. In addition, upstream lane was tested at four different locations in the opposing travel direction. Figure 5-20, Figure 5-21 and Figure 5-22 show the truck locations in the order in which measurements were taken.

Table 5-5: Truck Axle Loads

TRUCK ID	Axle	Left Wheel Load [kN (kips)]	Right Wheel Load [kN (kips)]	Total Axle Load [kN (kips)]	TRUCK WEIGHT [kN (kips)]
T16052 (Front Truck)	Front	31.1 (7.0)	40.7 (9.2)	71.8 (16.2)	262.4 (59.0)
	Second	40.5 (9.1)	56.0 (12.6)	96.5 (21.7)	
	Rear	37.4 (8.4)	56.7 (12.8)	94.1 (21.2)	
T16074 (Mid Truck)	Front	29.4 (6.6)	31.1 (7.0)	60.5 (13.6)	247.7 (55.7)
	Second	48.0 (10.8)	47.6 (10.7)	95.6 (21.5)	
	Rear	45.8 (10.3)	45.8 (10.3)	91.6 (20.6)	
T16082 (Rear Truck)	Front	27.8 (6.3)	31.1 (7.0)	58.9 (13.3)	243.9 (54.9)
	Second	45.4 (10.2)	48.5 (10.9)	93.8 (21.1)	
	Rear	43.1 (9.7)	48.0 (10.8)	91.2 (20.5)	

Figure 5-17: Stockbridge Bridge Load Testing

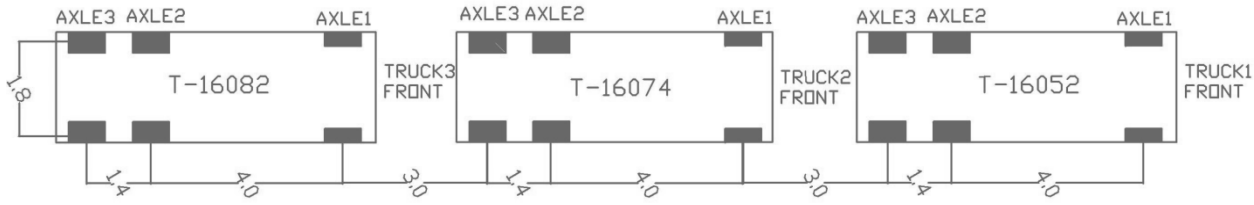

Figure 5-18: Plan View of Trucks

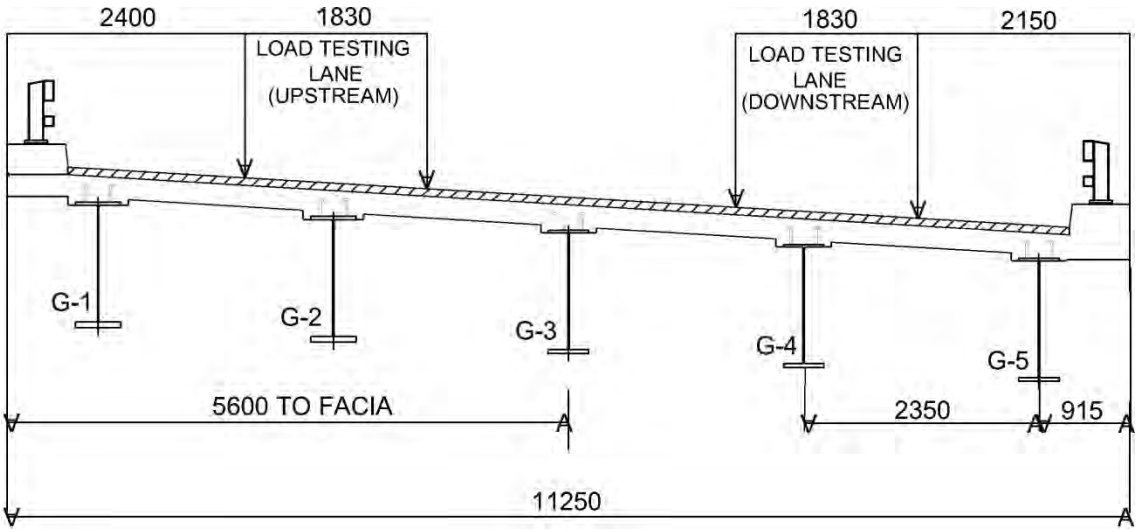

Figure 5-19: Load Test Truck Lanes

Table 5-6: Live Load Test Truck Record for Stockbridge Bridge

Running Order	Run ID	Lane	Direction	Truck Location (Measured from Abutment 1 – Chord Length)	
				Axle	Distance [m (ft)]
1	D-1	Downstream	Traffic	3rd Truck – 3rd Axle	0 (0.0)
2	D-2	Downstream	Traffic	2nd Truck – 2nd Axle	16.5 (54.0)
3	D-3	Downstream	Traffic	2nd Truck – 2nd Axle	33.0 (108.0)
4	D-4	Downstream	Traffic	2nd Truck – 2nd Axle	49.5 (162.0)
5	U-1	Upstream	Traffic	3rd Truck – 3rd Axle	68.0 (223.0)
6	U-2	Upstream	Traffic	2nd Truck – 2nd Axle	51.0 (167.0)
7	U-3	Upstream	Traffic	2nd Truck – 2nd Axle	34.0 (111.5)
8	U-4	Upstream	Traffic	2nd Truck – 2nd Axle	17.0 (55.5)
9	UR-1	Upstream	Opposite Traffic	3rd Truck – 3rd Axle	0 (0.0)
10	UR-2	Upstream	Opposite Traffic	2nd Truck – 2nd Axle	17.0 (55.5)
11	UR-3	Upstream	Opposite Traffic	2nd Truck – 2nd Axle	34.0 (111.5)
12	UR-4	Upstream	Opposite Traffic	2nd Truck – 2nd Axle	51.0 (167.0)

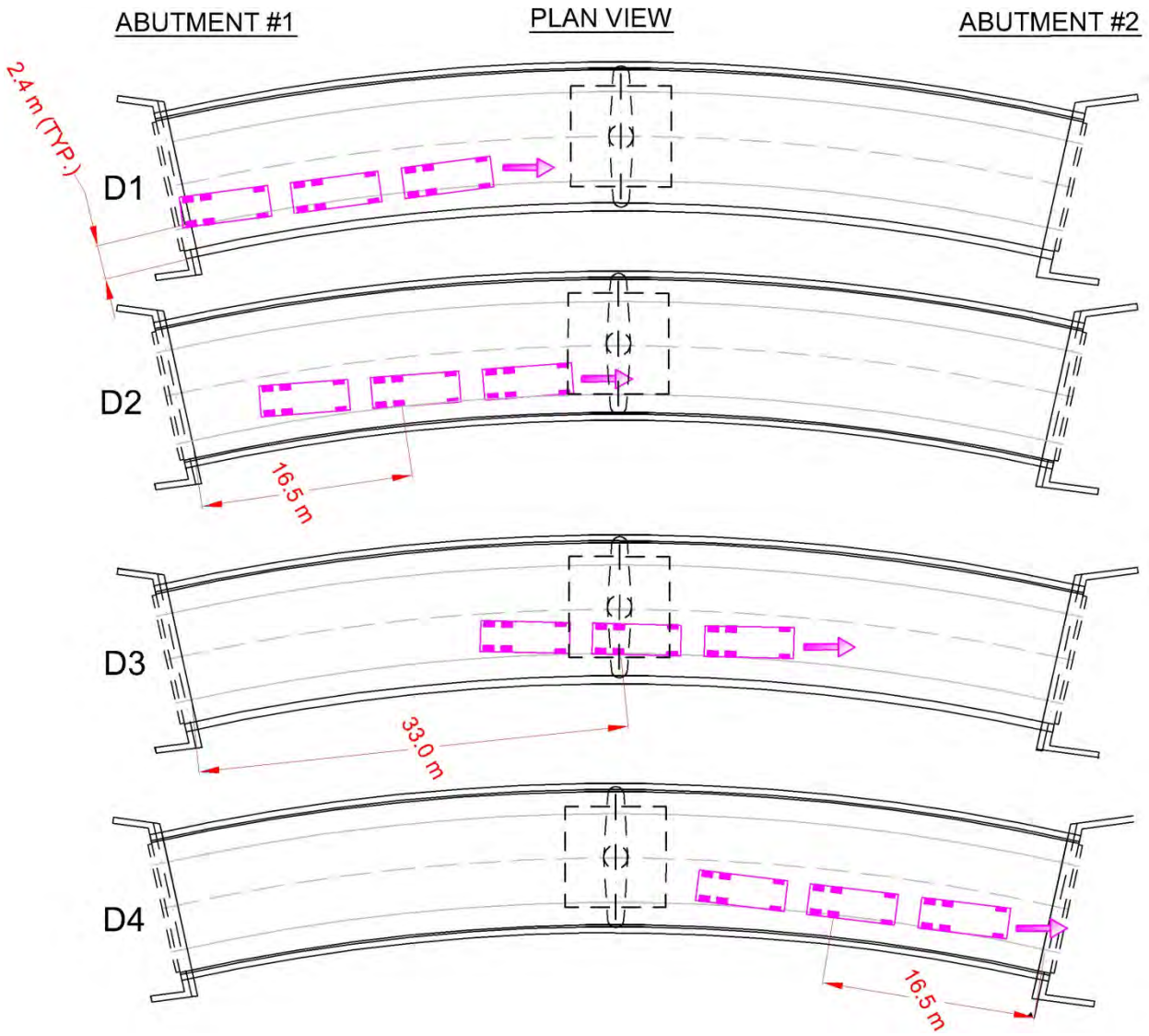

Figure 5-20: Stockbridge Load Testing Truck Locations (Downstream Lane – Forward)

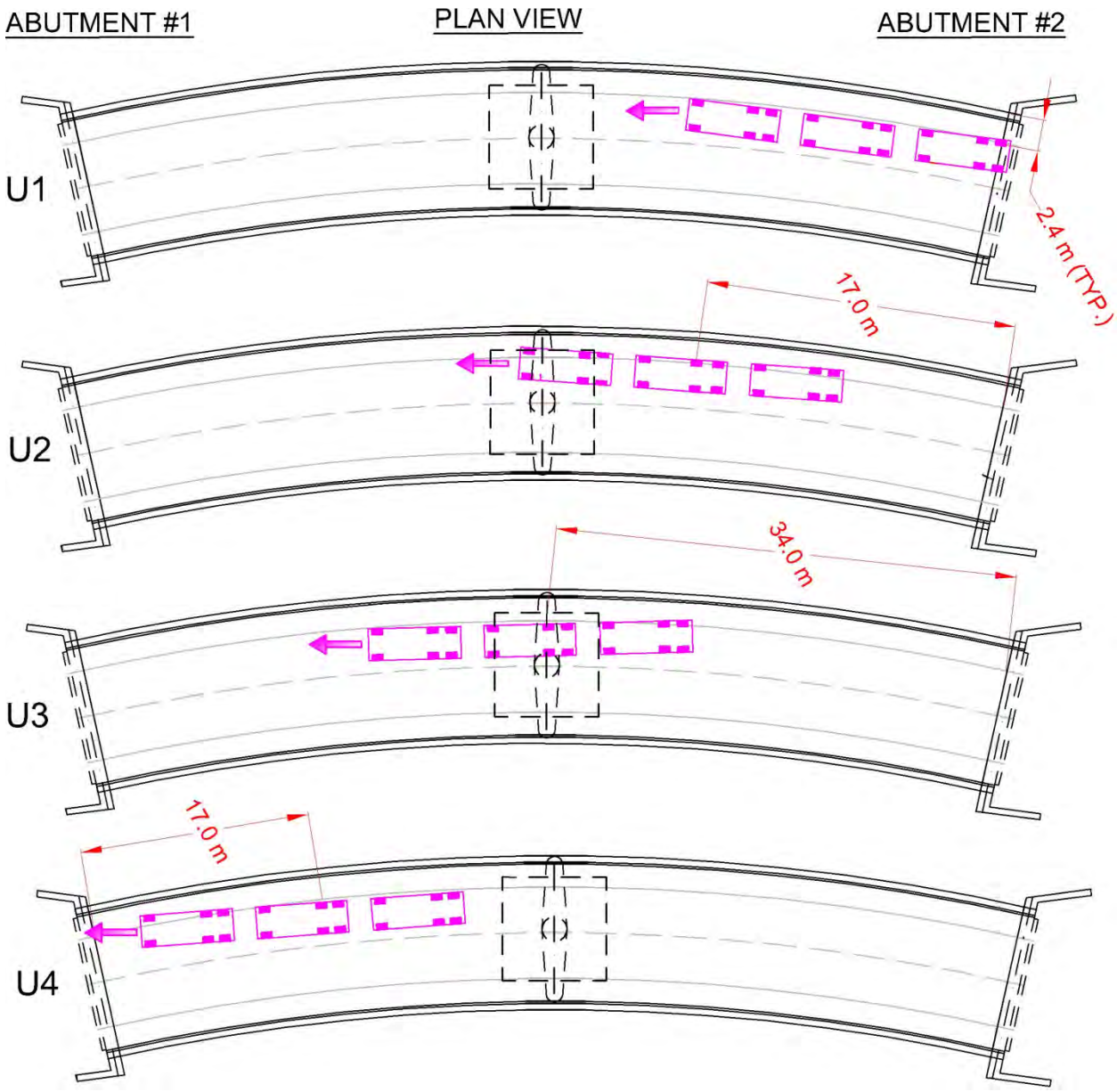

Figure 5-21: Stockbridge Load Testing Truck Locations (Upstream Lane – Forward)

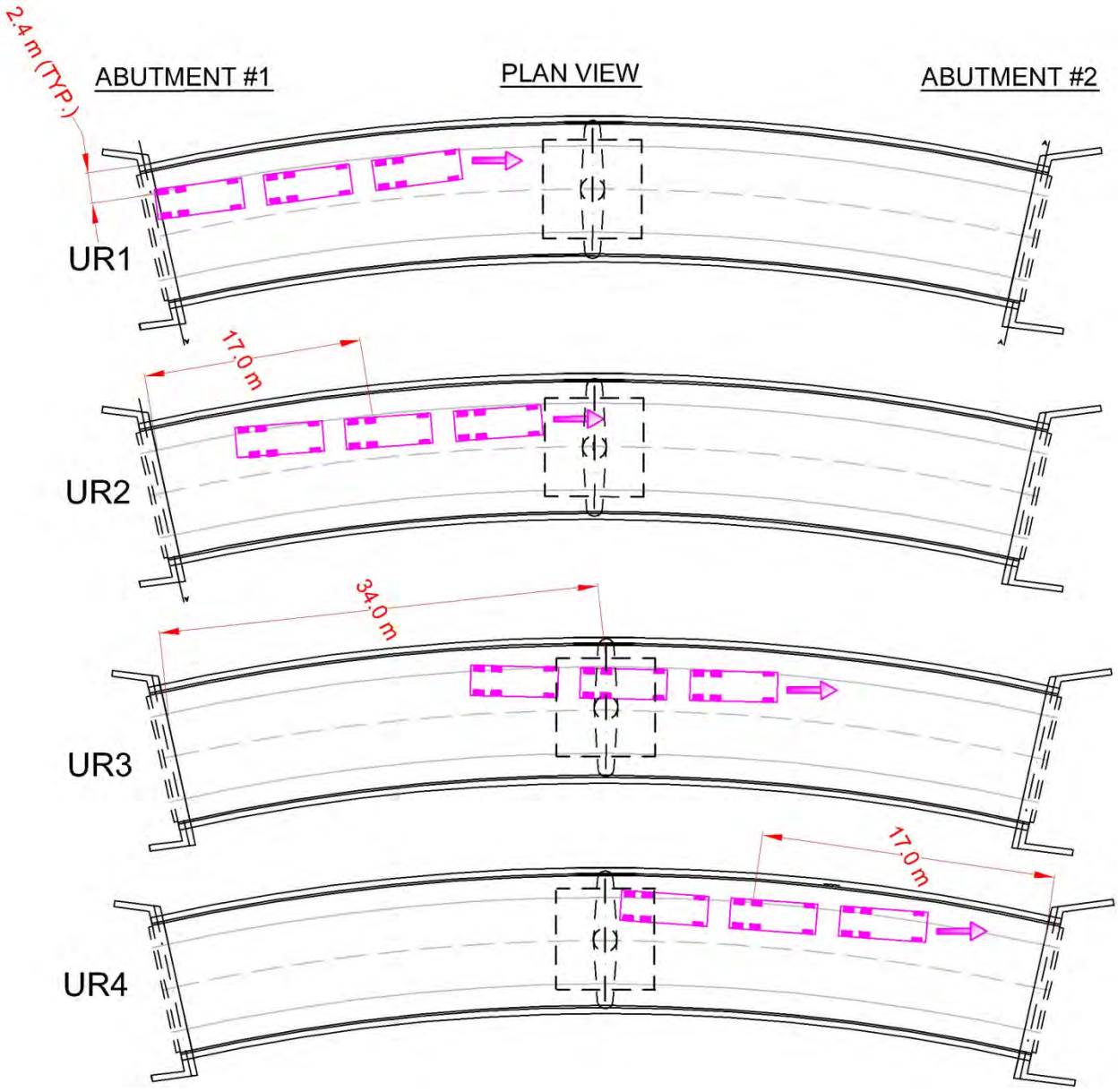

Figure 5-22: Stockbridge Load Testing Truck Locations (Upstream – Reverse)

6 INTERPRETATION OF LOAD TEST DATA AND COMPARISON WITH FINITE ELEMENT MODELS

6.1 Introduction

Computing live load effects on integral abutment bridges is a complex task due to continuity at abutments and resulting soil-structure interaction through the bridge substructure. The results presented in this report compare FEM predictions to measured field response recorded during load testing to calibrate the FEMs for live load and better understand the truck load distributions on bridge superstructure and substructure. Current U.S. bridge design guidelines do not consider the effects of integral abutments on the transverse distribution of truck load, though effects of integral abutments must be included for other types of load. However, for short and medium length single span IABs, live load can produce comparable forces and deformations to those caused by thermal loading. Literature on live load effects on integral abutment bridges is limited. Dagher et al.(1991) investigated the live loads effects on superstructures of integral abutment bridges by making use of analytical studies. Elgaaly et al. (1992) compared the analytical studies with field testing just for superstructure response whereas Mourad et al.(1998) reported the pile forces under live load using finite element modeling. Dicleli & Erhan (2008, 2009) investigated the effects of monolithic construction and soil-structure interaction on load distributions both on bridge superstructure and substructure for prestressed concrete integral bridges. These two papers also discussed the effect of bridge parameters such as soil type around piles, backfill pressures, pile sizes, presence of wingwalls on the bridge response.

In this report, comparison of measured data with FEM values of girder strains, pile strains and deflections, abutment displacements and rotations, and backfill pressures are presented. The field calibrated FEM can subsequently be used to estimate the live load response of bridges having different geometries (length, skew angle, etc.) and structural systems (deck cross section, abutment depth, etc.). These models can also be used in development of live load distribution factors specifically applicable to IABs.

6.2 Finite Element Modeling of Bridges and Truck Loading

The FEMs created for analysis of truck loads were identical with the FEMs created for long term monitoring of the bridges with some exceptions. The concrete sections were modeled as uncracked considering the presence of compressive forces in the deck and the proximity of the time between the completion of the bridge and load tests. The truck loads were modeled as concentrated forces acting at the exact axle location for all truck positions. A sample load

configuration for Middlesex Bridge is shown in Figure 6-1. A submeshing scheme was applied to the deck shell elements in order to facilitate a higher precision in transverse and longitudinal load transfer from location of concentrated forces and supporting girders.

Prior to testing the bridges, the bridges were assumed to be under a zero stress condition. Therefore, undeformed bridge geometry was used as an initial condition. However, the actual conditions in the field can vary with respect to the season in which the load test is conducted. The initial deformed shape likely affects the magnitude of backfill earth pressures, pile displacement and stresses resulting from load testing. In winter, the bridge will have contracted and active pressures would be acting behind the abutments. Therefore, during load testing, changes in backfill earth pressures would be minimal. However, in summer, expansion of the bridge superstructure due to temperature increase generates passive earth pressures behind the abutment. In the FEMs, in order to report results independent of the testing season, the initial bridge condition is assumed to be under no stress. Additional analyses related to the effect of season on bridge load testing results were conducted. Overall, the effects were minimal for the bridge superstructure response whereas the substructure response exhibited limited differences. However substructure response was dominated by seasonal thermal load and differences were therefore not significant under live load.

.

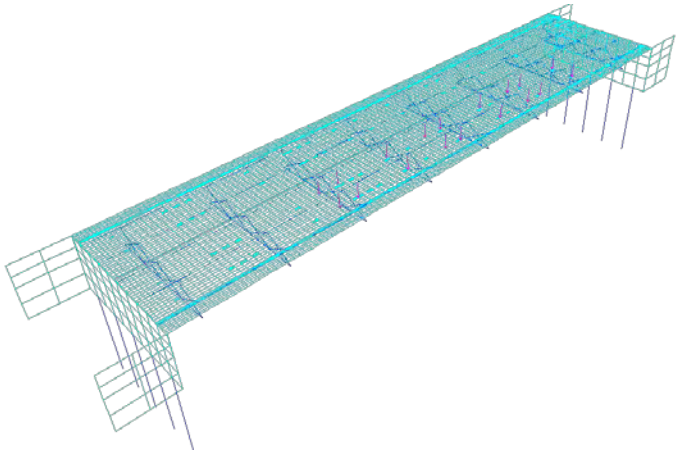

Figure 6-1: Truck Loading for D-3 Position

6.3 Analysis of Load Testing Data and FEM Predictions for Middlesex Bridge

6.3.1 Superstructure Response

The response computed using FEM was compared with measured field data for each corresponding truck loading location. Table 6.1 shows the maximum girder response parameters from the field testing and the FEMs. Throughout the day of testing, solar radiation generated temperature increase, which resulted in expansion of the bridge. Thermal variations affected the

value of individual gage readings and could not be precisely determined by conducting a global thermal analysis of the FEM models of the structure. Instead, a temperature correction of field data was used. This temperature correction was specific to each gage and dependent on the observed differential readings without truck load applied (differential readings immediately prior to and post load testing with no truck loading present). Once the difference between initial and final readings was determined, linear increase in ambient temperature assumption was used for temperature correction. All load test data were finally corrected according to the temperature correction. Figure 6-2 shows the stress profile of the downstream girder before and after temperature corrections. Subsequent to determination of stresses at the gage locations, steel girder moments were calculated with respect to neutral axis of composite section. Due to errors in calculating neutral axis locations from field data, especially in cases with very low measured strains, calculations were completed using the theoretical neutral axis of the composite section. The calculated steel girder moments from field data were then compared with the FEM girder element results (Figure 6-3) directly output from SAP. As shown in Figure 6-3, the effects of temperature correction were slight for initial load positions but increased towards the end of the load test. Figure 6-4 shows the moment distribution on the upstream girder along its length. These two comparisons evaluated the accuracy of the FEM models both for maximum positive and maximum negative moments.

For the Middlesex Bridge, the maximum positive moment recorded at midspan was about 30% higher than the maximum negative moment recorded by gages located near the bridge ends. The girders located near wheel loads exhibited the maximum moments, whereas the magnitude of moments on other girders varied between bridge cross sections. The bridge had a minimal moment at the far end of the bridge cross section when the trucks were located at the near end (Figure 6-5) except for the instrumented cross section located on Abutment 1. Here, maximum moments on the girder located at the far end of cross section were about 70% in absolute value of the maximum moment on girders in the proximity of truck wheel loads (Figure 6-6). Therefore, one can state that transverse moment distribution was wider for the ends of IABs compared to conventional bridges where the transverse moment distribution near the bridge ends is limited. The FEMs were generally successful in capturing the transverse moment distribution for girder at both cross sections. Figure 6-7 shows the girder moment at the bridge midspan when the trucks are located at both lanes. FEM results were also consistent with expected steel girder moment distribution when the trucks were positioned side-by-side.

Table 6-1: Summary of Superstructure Response for Middlesex Bridge

	Middlesex Bridge	
	Actual	FEM
Maximum Positive Girder Bending Moment	755 kN-m (6684 Kips-in)	800 kN-m (7083 Kips-in)
Maximum Negative Girder Bending Moment	530 kN-m (4690 Kips-in)	522 kN-m (4621 Kips-in)
Maximum Compressive Stress at Gage Locations (Girder Flanges)	18.90 MPa (2.33 ksi)	N/A
Maximum Tensile Stress at Gage Locations (Girder Flanges)	27.80 MPa (3.43 ksi)	N/A

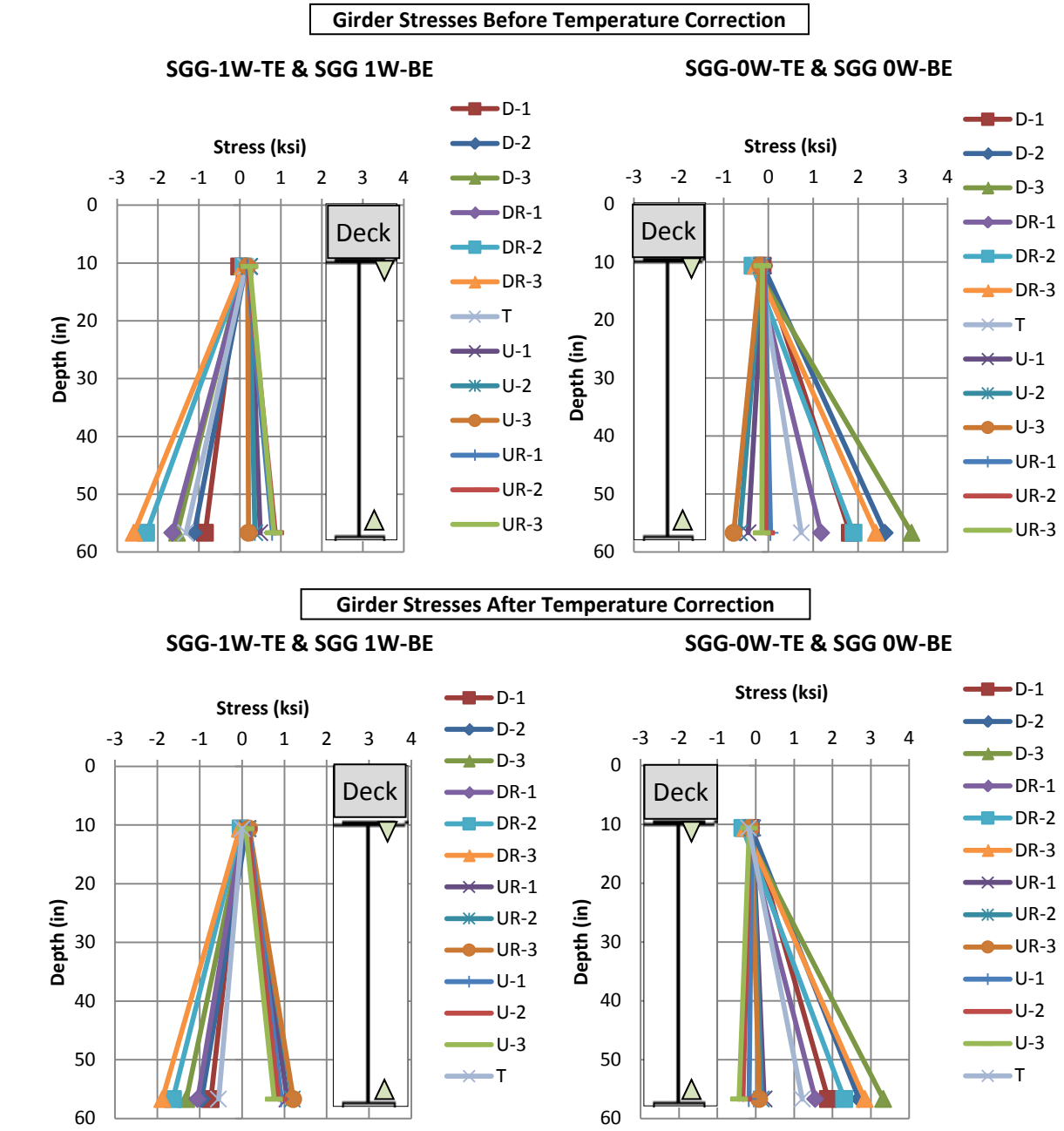

Figure 6-2: Stress Profiles SGG-1W and SGG-0W before and after Temperature Correction

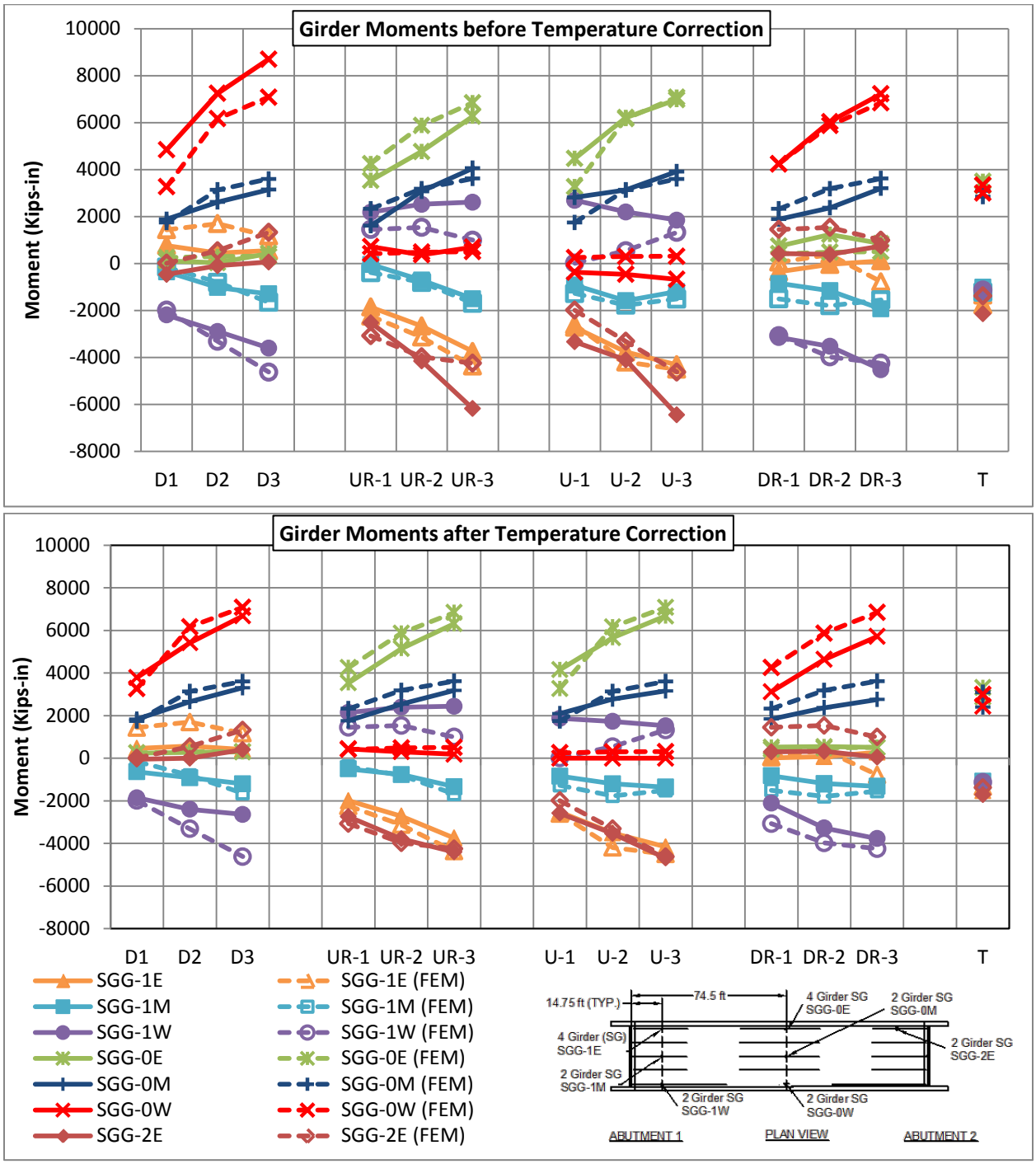

Figure 6-3: Girder Moments at the Middlesex Bridge (Field Data and FEMs)

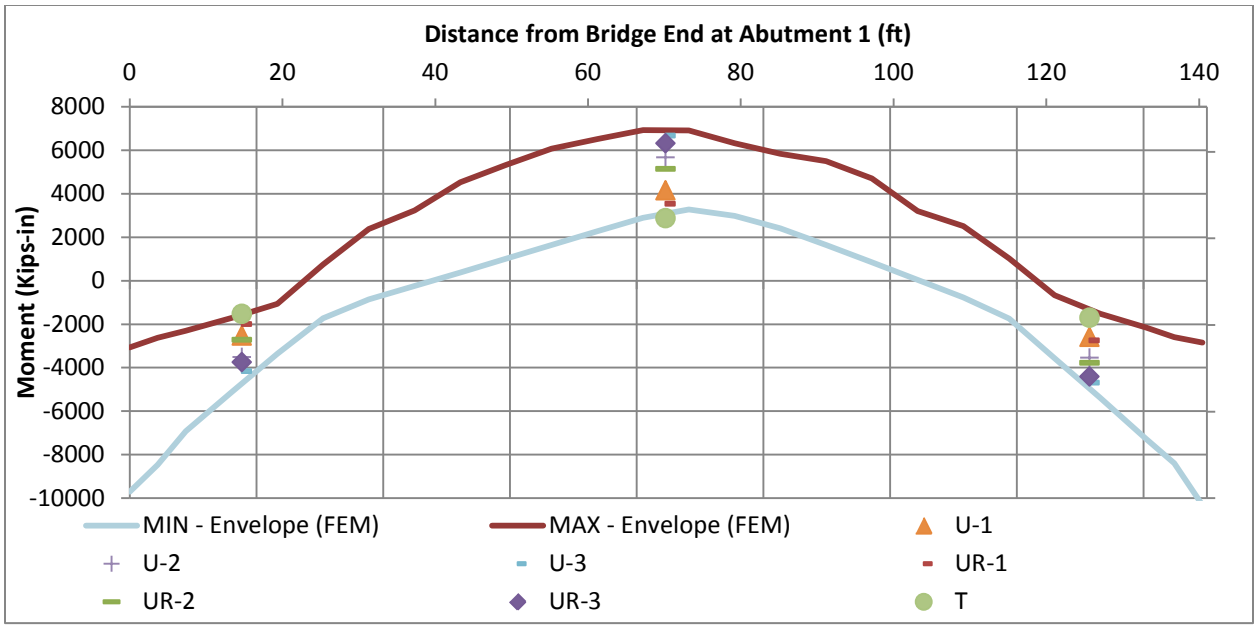

Figure 6-4: Girder Moments along Upstream Girder at the Middlesex Bridge (Field vs. FEM)

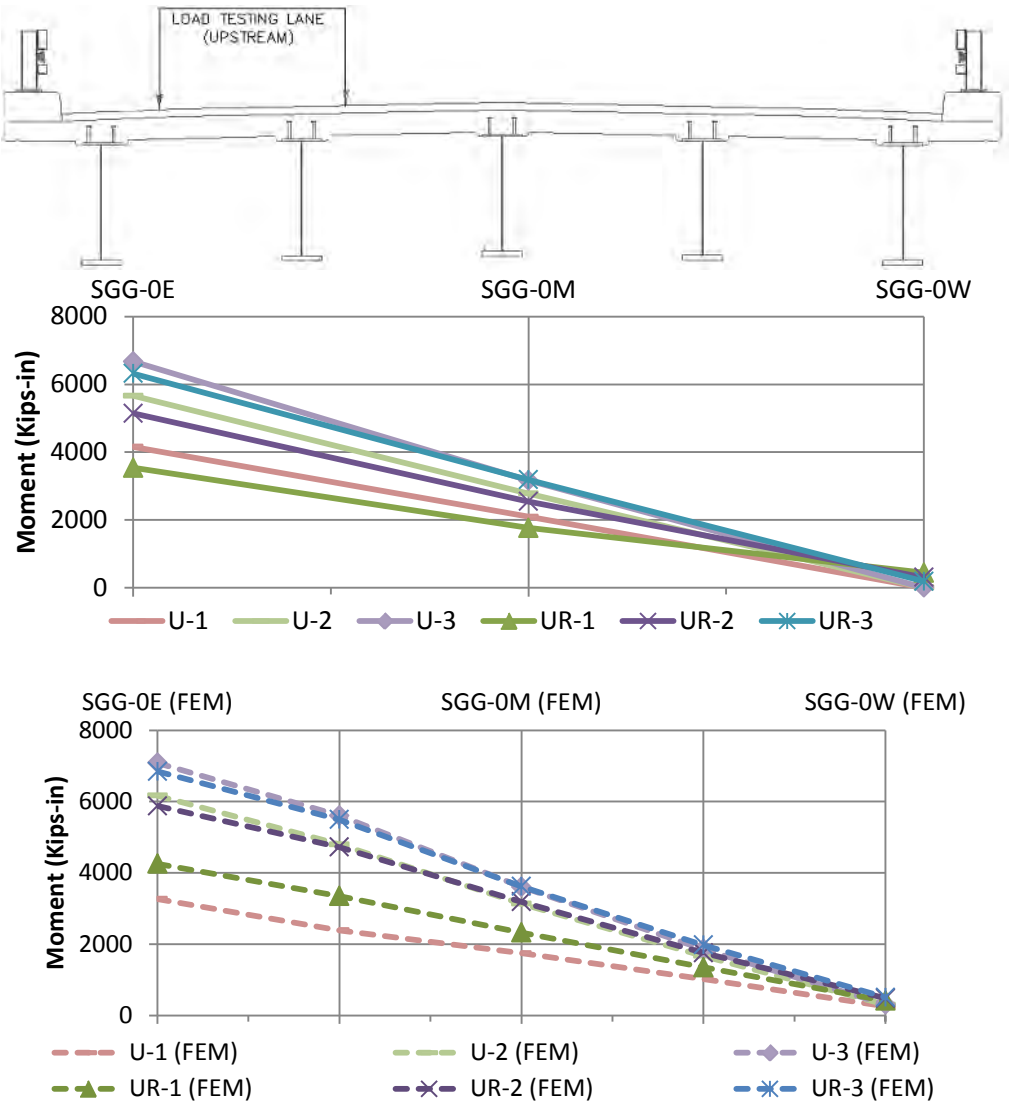

Figure 6-5: Girder Moments at the Bridge Midspan (Trucks at Upstream Lane)

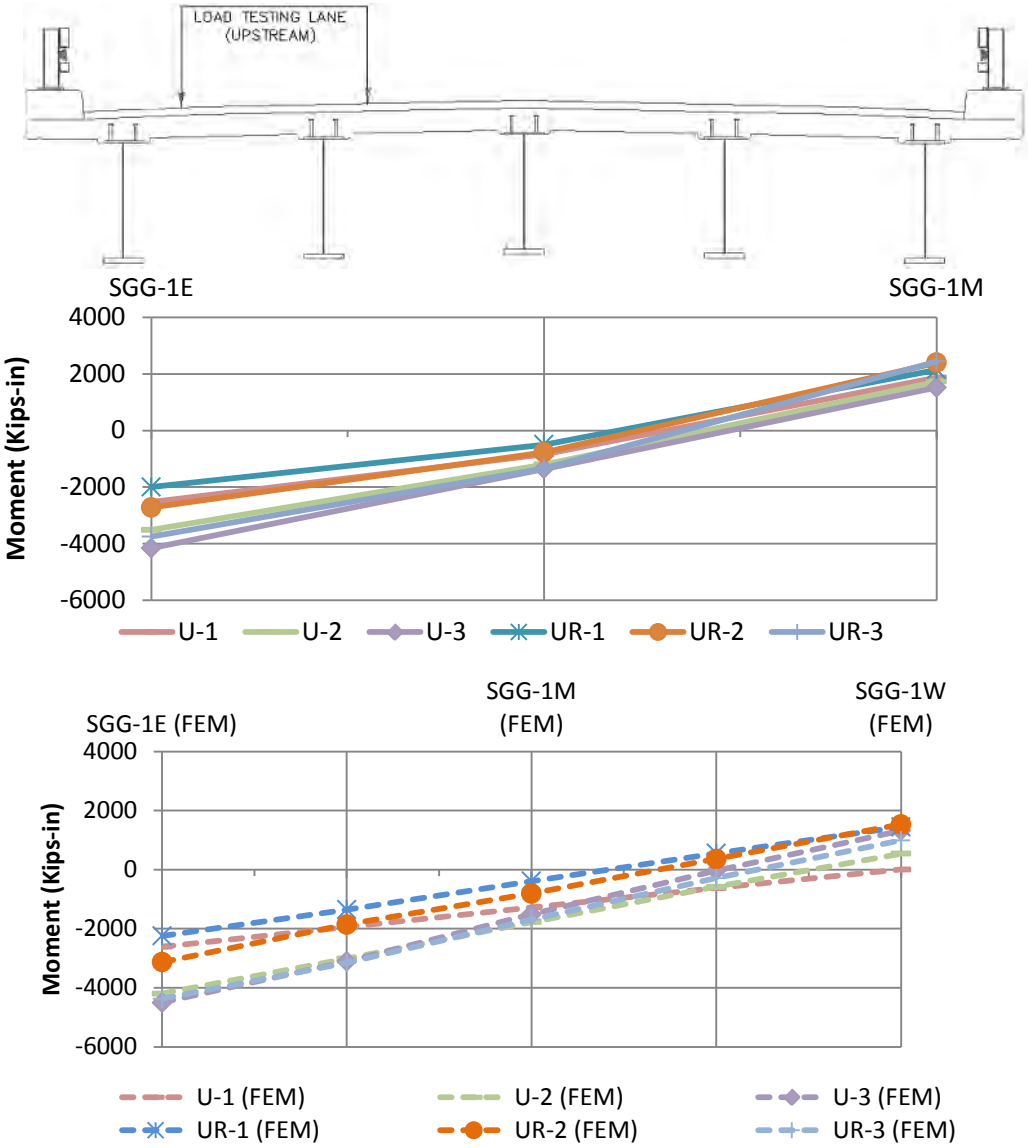

Figure 6-6: Girder Moments at Abutment 1 End of the Bridge (Trucks at Upstream Lane)

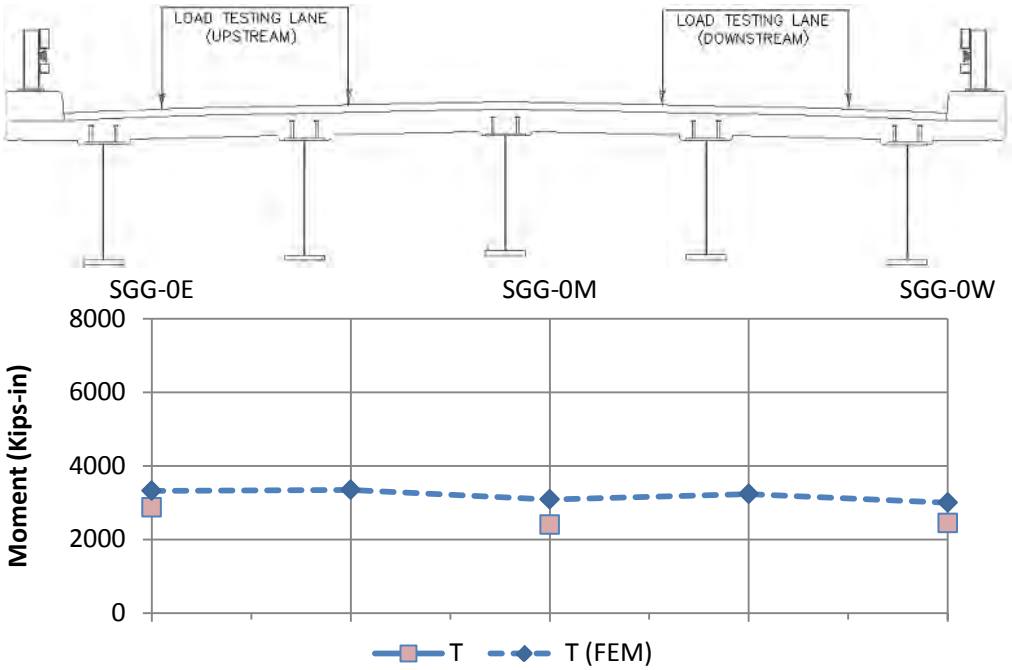

Figure 6-7: Girder Moments at the Bridge Midspan (Trucks at Both Lanes)

6.3.2 Substructure Response

Similar to girder strain gages, in order to separate the strain effects of truck loads from those induced by thermal changes during the test, two sets of readings immediately prior and subsequent to truck loading were used. Effects of temperature were assumed to be linear within the testing period (~2-3 hours) which was justified by data. The data corrected for temperature effects were then used to report abutment displacements, abutment rotations, backfill soil pressures, pile displacements and pile stresses.

In general, the field data suggested that pile displacements, abutment rotations and abutment displacements were minimal during load testing of the bridge. A complete displacement profile based on combining readings from 4 different inclinometers attached to the upstream pile, a displacement transducer and a tiltmeter attached to the abutment wall is shown in Figure 6-8.

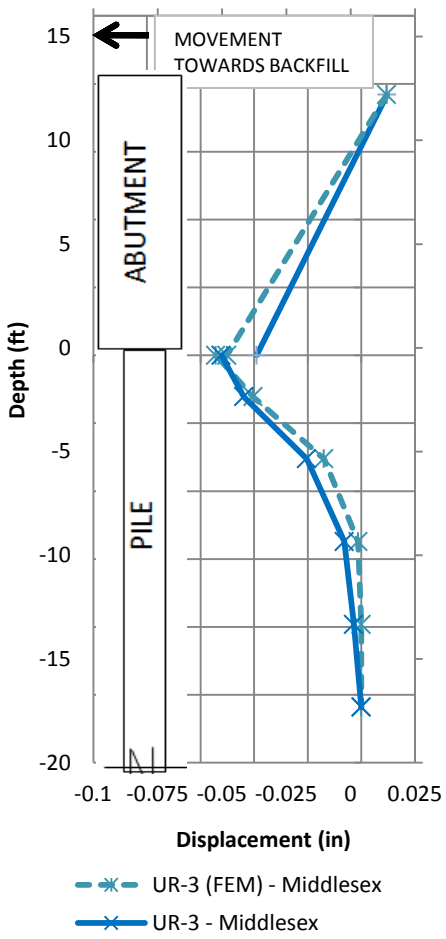

Figure 6-8: Maximum Substructure Displacement during Load Testing and FEM Predictions

Table 6-2 shows a summary of substructure response from field data and FEMs. The field values for abutment displacements were generally lower than FEM predictions which implied the presence of a more rigid substructure or a higher degree of soil-structure interaction in the field. These differences, however, are not considered substantial given the inherent variability in assumed soil properties and cracking of concrete members. Although FEM predictions were identical for both abutments, the field results showed that Abutment 1 was more flexible than Abutment 2. The bottoms of abutments were moving towards backfill while displacements at the top of abutments were towards the river. Transverse abutment movements were negligible with a maximum value of 0.15 mm (0.006 in).

The backfill pressures recorded by earth pressure cells including the pressures on wingwalls were minimal. In the field, maximum earth pressure on abutment wall was 2.1 KPa (0.3 psi). Wingwall earth pressures exhibited a maximum drop of 2.1 KPa (0.3 psi). Expected active pressure according to Rankine's theory was changing between 2.8 KPa (0.4 psi) to 9.7 KPa (1.4 psi) along the depth of abutment wall whereas the pressure values from the FEM were changing between 0.0 KPa (0.0 psi) and 12.1 KPa (1.76 psi). Low in-field pressure values

suggested that passive pressures weren't generated at the abutment wall. This meant that the backfill was initially under active pressure condition which was theoretically equal to the minimum earth pressure which was reasonable considering the cold temperatures present during the load tests.

For pile response, the FEM results were generally in good agreement with the field data, especially when the trucks were positioned on the adjacent lane to the piles that were instrumented. When the trucks were positioned at the far end of the bridge, FEMs predicted higher displacements at the piles that were located away from the trucks. Both field data and FEM results showed that the maximum pile stress and pile displacement occurred at the top of the piles. The accuracy of the FEM predictions for axial loads on piles was higher than the accuracy of the FEM predictions for weak axis bending of the piles. Generally, in the field, the weak axis bending moments were lower than FEM predictions. But overall, the magnitudes of weak axis stresses were limited. In order to determine the maximum pile stresses at the tip of flanges, field data were evaluated to determine the axial stresses and bending stresses separately. Then the resultant stresses at the tips of the pile flanges were calculated. With this calculation, maximum pile stress at the top gage location was 46.9 MPa (6.8 ksi) and 38.6 MPa (5.6 ksi) for Abutment 1 and Abutment 2, respectively (Figure 6-9). Calculated maximum stresses from FEMs at the same location was 56.5 MPa (8.1 ksi).

Table 6-2: Summary of Substructure Response of Middlesex Bridge

	Middlesex Bridge			
	Abutment 1		Abutment 2	
	Actual	FEM	Actual	FEM
Maximum Abutment Rotation	0.021 deg	0.030 deg 0.033 deg*	0.014 deg	0.030 deg 0.033 deg*
Maximum Longitudinal Abutment Displacement at the Top Flange of Girder	0.965 mm (0.038 in) (towards river)	0.635 mm (0.025 in) (towards river) 0.813 mm* (0.030 in)	0.914 mm (0.036 in) (towards river)	0.660 mm (0.026 in) (towards river) 0.813 mm* (0.030 in)
Maximum Longitudinal Abutment Displacement at the Bottom of Abutment	1.09 mm (0.04 in) (towards backfill)	1.27 mm (0.05 in) (towards backfill) 1.54 mm* (0.06 in)	0.56 mm (0.02 in) (towards backfill)	1.17 mm (0.05 in) (towards backfill) 1.54 mm* (0.06 in)
Maximum Pile Displacement at the Top of the Pile	1.300 mm (0.051 in) (towards backfill)	1.371 mm (0.054 in) (towards backfill) 1.54 mm* (0.06 in)	N/A	1.371 mm (0.054 in) (towards backfill) 1.54 mm* (0.06 in)
Maximum Pile Stress at Upstream Pile at the Gage Location	33.8 MPa (4.9 ksi) (compressive)	33.8 MPa (4.9 ksi) (compressive) 35.5 MPa* (5.2 ksi)	31. 0 MPa (4.5 ksi) (compressive)	34.5 MPa (5.0 ksi) (compressive) 35.5 MPa* (5.2 ksi)
Maximum Pile Stress at Middle Pile at the Gage Location	21.4 MPa (3.1 ksi) (compressive)	25.5 MPa (3.7 ksi) (compressive) 27.6 MPa* (4.0 ksi)	17.9 MPa (2.6 ksi) (compressive)	25.5 MPa (3.7 ksi) (compressive) 27.6 MPa* (4.0 ksi)
Depth at which Pile Displacement is Negligible	~ 4.0 m (13.0 ft)	~3.0 m (10 ft) ~4.3 m* (14.0 ft)	N/A	~3.0 m (10 ft) ~4.3 m* (14.0 ft)
Maximum Backfill Earth Pressure	2.1 KPa (0.3 psi)	12.1 KPa (1.76 psi) 0.00 KPa* (0.00 psi)	0.7 KPa (0.1 psi)	12.1 KPa (1.76 psi) 0.00 KPa* (0.00 psi)

* Neglecting passive pressures behind abutments.

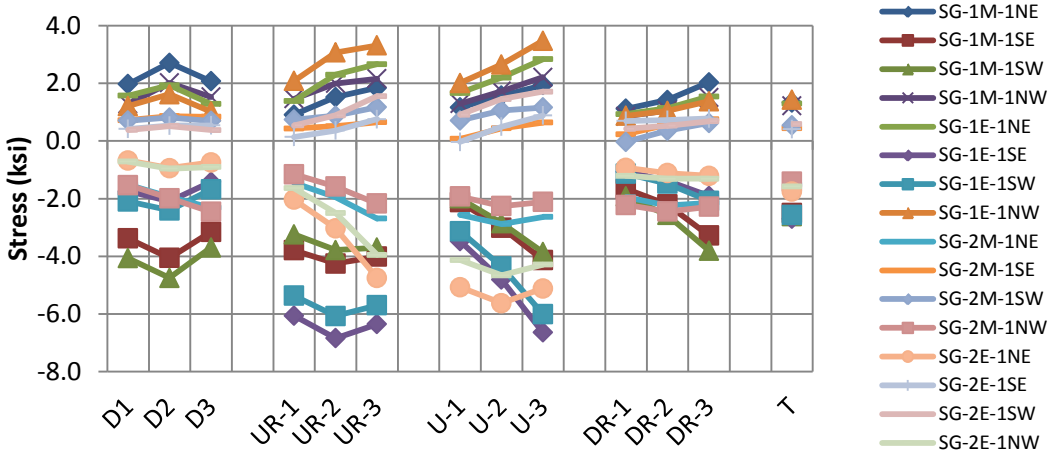

Figure 6-9: Resultant Stresses at the Piles

For Middlesex Bridge, a detailed analysis of bridge response was conducted as it is affected by the seasonal temperature. Since the load test was conducted during the cold season (December), the bridge was in a contracted state. Therefore, abutment displacements should be towards the river during the load tests which would eliminate development of passive pressures behind the abutments. This anticipated response was verified using the field data. Displacement and inclinations from pile and abutment gages showed that the bottom of the abutments were moving towards the backfill, however, at the same time, earth pressure readings demonstrated almost no pressure increase during load testing. In order to simulate this behavior in the FEMs, an additional FEM with only active backfill pressure was modeled to compare the field results with the FEM with respect to the passive pressures behind the abutments. Results (3% increase in maximum girder moment) showed that the superstructure response was not altered by the new modeling assumptions whereas the substructure response (20% increase in maximum weak axis pile moments, 30% increase in abutment displacements, etc.) showed significant differences though the values were still limited. The small change in superstructure response between the two models proved that the rotational resistance arising from the backfill soil pressure was small compared to the rotational restraint provided by the piles. Therefore, the backfill pressures specific to these bridges do not influence calculations for superstructure moments and load distributions.

6.4 Analysis of Load Testing Data and FEM Predictions for East Montpelier Bridge

6.4.1 Superstructure Response

For the East Montpelier Bridge, the interpretation of the steel girder response was done in a similar manner to the Middlesex Bridge. However, instead of linear temperature increase assumption, actual gage temperature readings at each truck position were used for temperature correction. Theoretical elastic neutral axis depth of the composite sections were used for girder moment calculations; these results corresponded better with FEM results than when neutral axis was calculated from strain readings for each individual run. Calculated and theoretical neutral axis values were generally similar, however using the theoretical neutral axis eliminated the error that could result from a sporadic bad gage reading, or when strain reading values were low. Temperature corrected gage readings (similar to the Middlesex Bridge) were used to calculate internal steel girder moments on each girder cross section. For East Montpelier Bridge, the data showed that the temperature correction was much more significant on the girders exposed to sun radiation (SGG-1S, SGG-0S and SGG-2S).

The girder moments from field data were compared with the FEM results in Figure 6-10. Figure 6-11 and Figure 6-12 show the moment distribution on the upstream girder and downstream girder along their lengths, respectively. The FEM model overestimated the maximum positive and negative girder moments; however generally FEM results were

comparable to field data. Maximum stresses at the girder flanges in the field were 22.5 MPa (3.3 ksi) in the tension region and 15.4 MPa (2.2 ksi) in the compression region. The maximum positive moment recorded at midspan was about 30% higher than the maximum negative moment at instrumented girder cross sections at the bridge ends. East Montpelier Bridge had a minimal moment at the far end of the bridge cross section when the trucks were located at the near end. The FEMs were successful in capturing the transverse load distribution when the trucks were positioned back-to-back and side-by-side (Figure 6-13 & Figure 6-14, respectively).

Table 6-3: Summary of Superstructure Response for East Montpelier Bridge

	East Montpelier Bridge	
	Actual	**FEM**
Maximum Positive Girder Bending Moment	693 kN-m (6134 Kips-in)	808 kN-m (7154 Kips-in)
Maximum Negative Girder Bending Moment	-475 kN-m (-4183 Kips-in)	-683 kN-m (-6042 Kips-in)
Maximum Compressive Stress at Gage Locations (Girder Flanges)	15.4 MPa (2.24 ksi)	N/A
Maximum Tensile Stress at Gage Locations (Girder Flanges)	22.5 MPa (3.27 ksi)	N/A

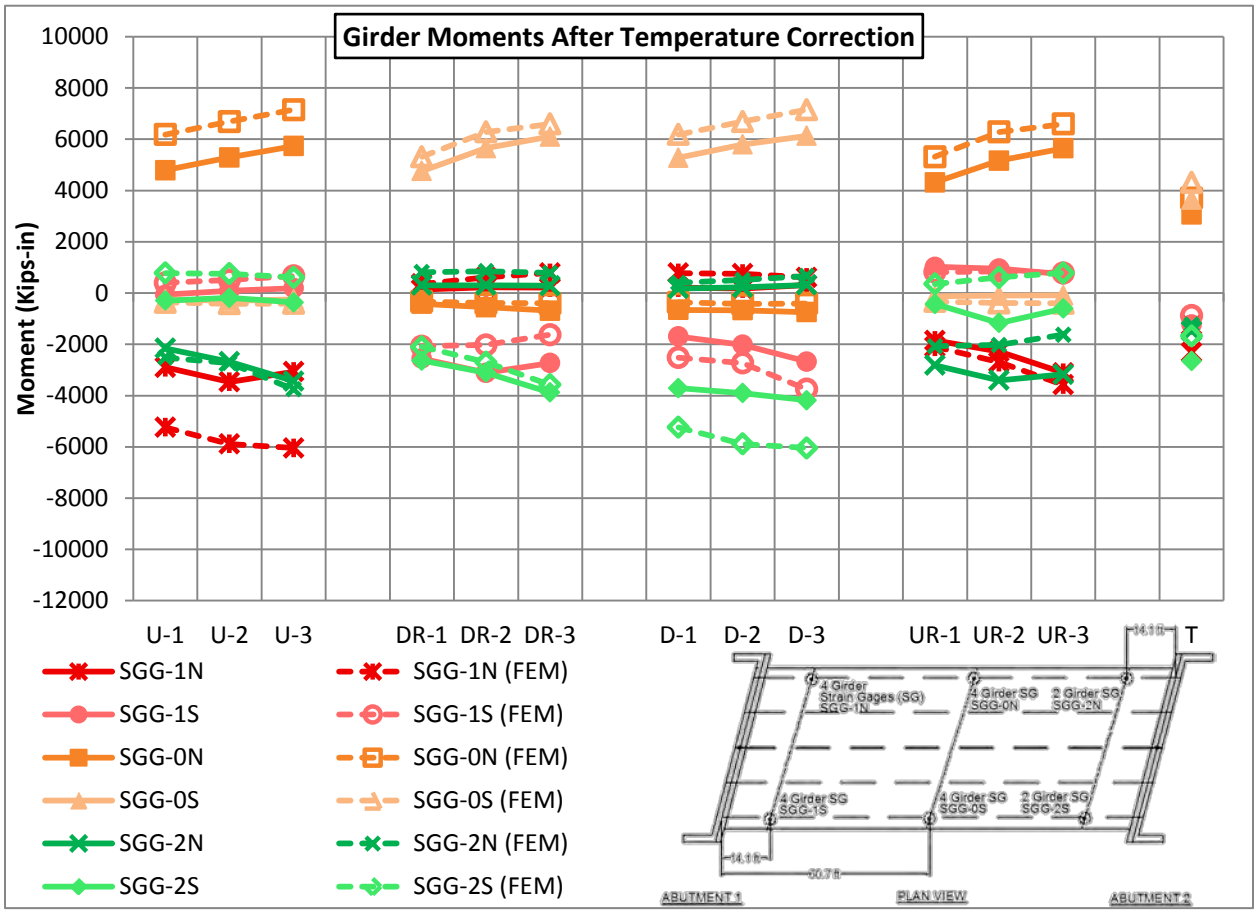

Figure 6-10: Girder Moments at East Montpelier Bridge (Field vs. FEM)

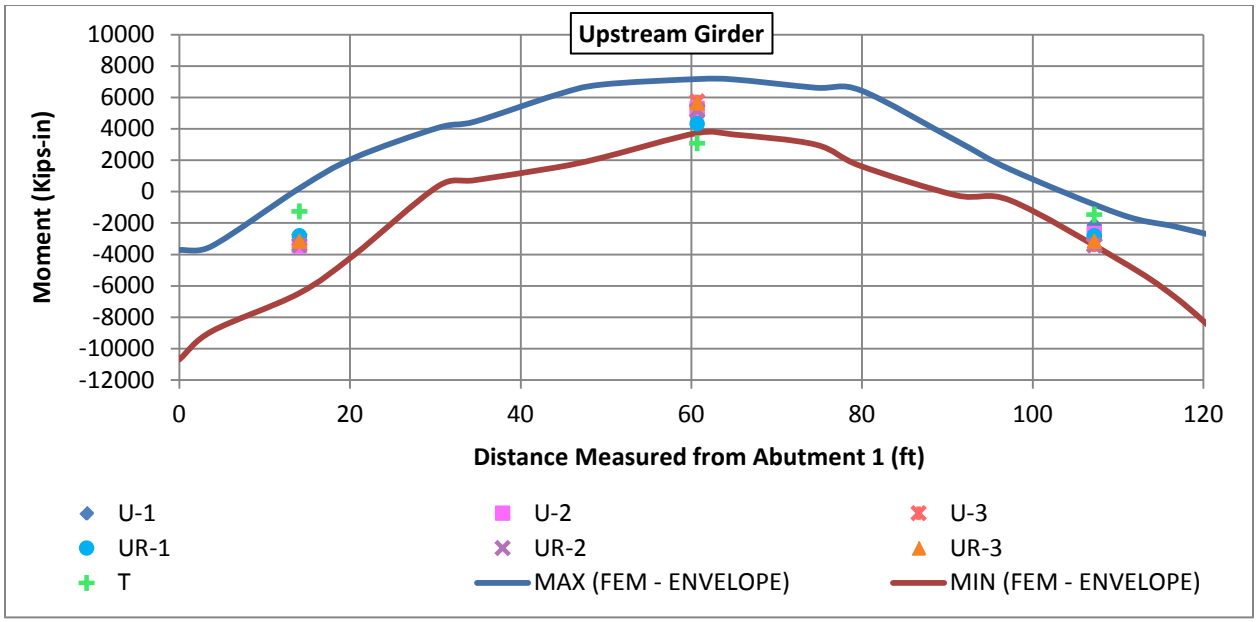

Figure 6-11: Girder Moments along Upstream Girder at the East Montpelier Bridge (Field vs. FEM)

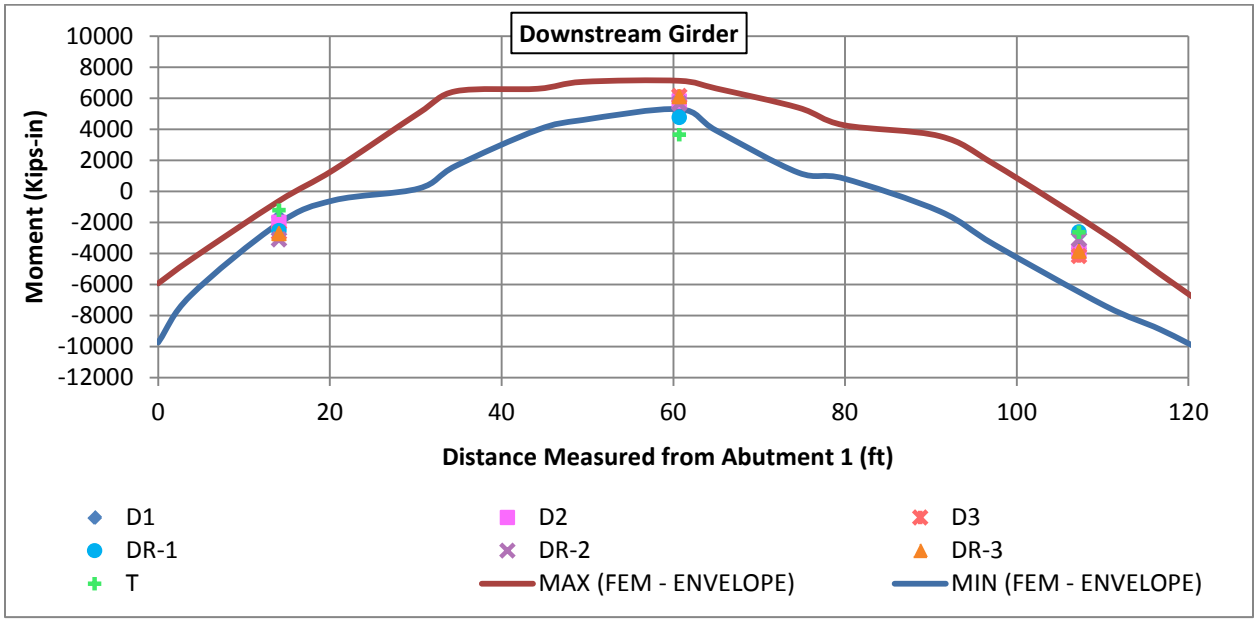

Figure 6-12: Girder Moments along Downstream Girder at the East Montpelier Bridge (Field vs. FEM)

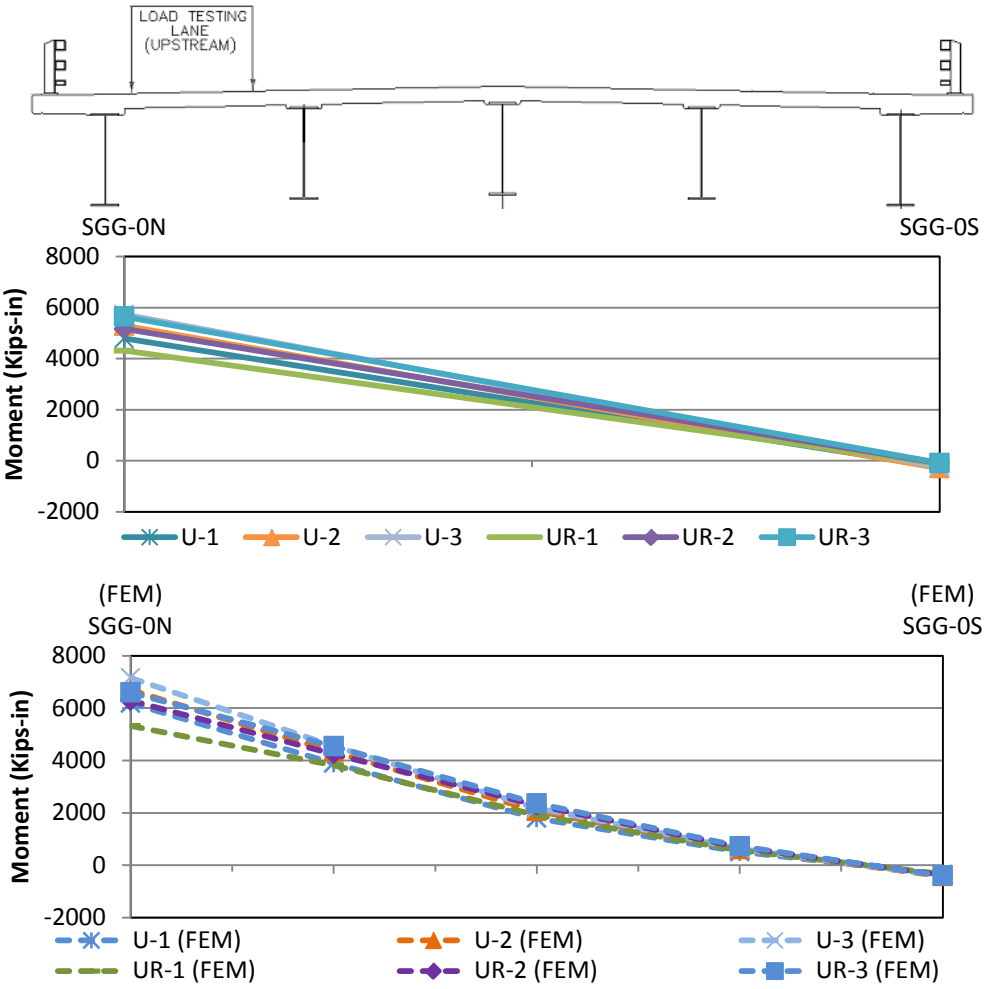

Figure 6-13: Moments on Instrumented Girder at Bridge Midspan (The trucks on Upstream Lane)

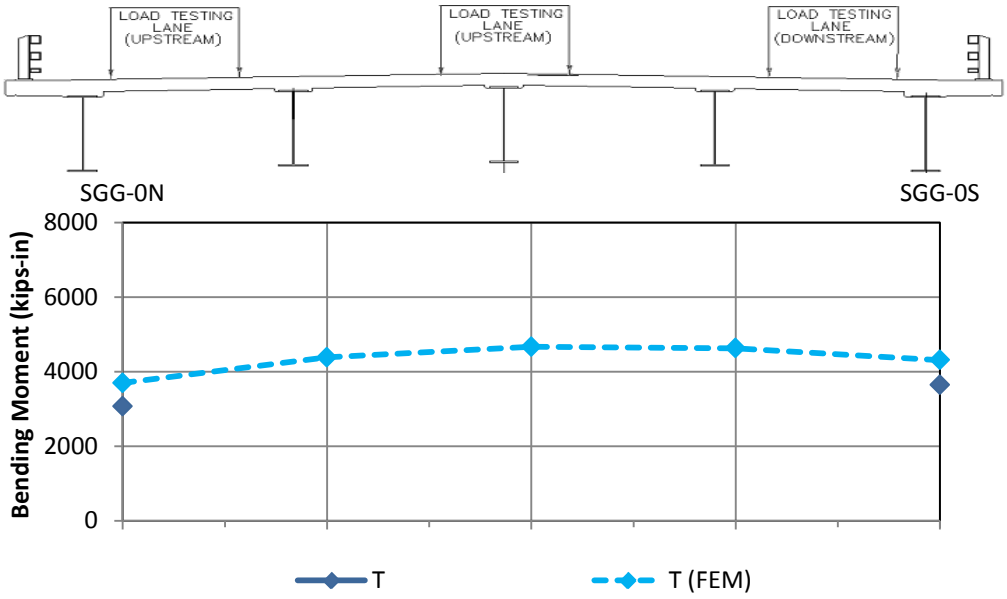

Figure 6-14: Girder Moments at Bridge Midspan (The trucks on Both Lanes)

6.4.2 Substructure Response

Abutments rotations during field testing were lower than FEM predictions. Values were limited with a maximum of 0.008 deg. Maximum longitudinal displacements were 0.69 mm (0.027 in) and 0.58 mm (0.023 in) for upstream (obtuse) and downstream (acute) corner of the Abutment 1, respectively. Abutment 2 displacements and rotations were following an unexpected pattern for truck locations as the values weren't consistent with either field data from Abutment 1 or FEM results. In many loading cases, the rotations were well below the expectations and even, in some cases, they had opposite signs. This behavior was also seen in analysis of field data during construction (Chapter 7). One should note that the abutment that gave erratic displacements and rotations was the abutment that had been poured before placing concrete deck in the revised deck placement schedule. Figure 6-15 shows the displacement profile of the bridge substructure including abutments and piles deflections.

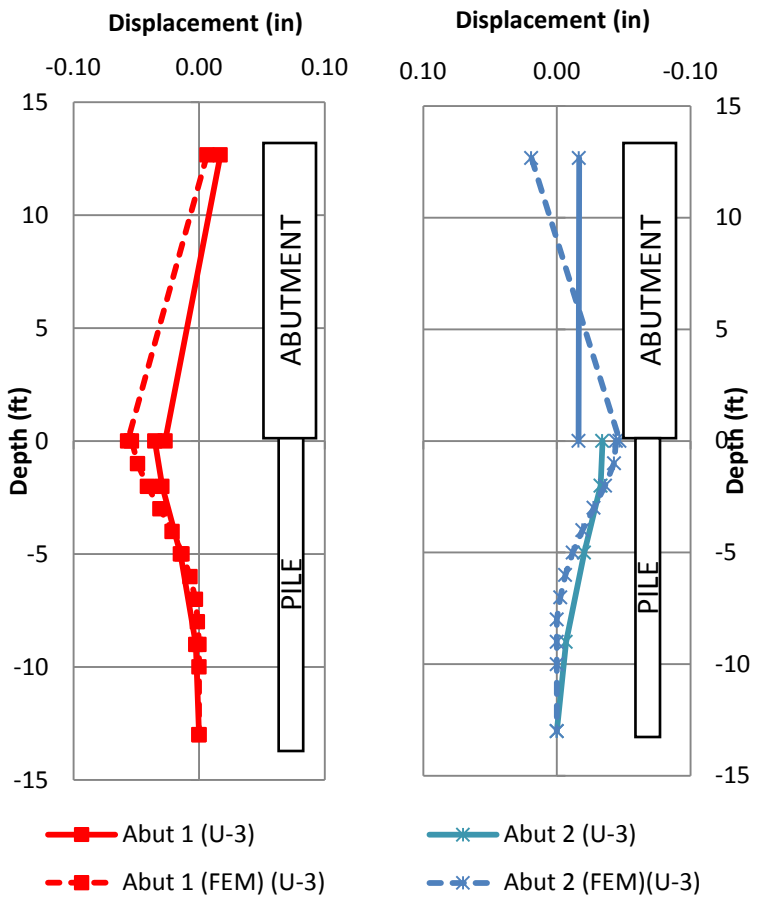

Figure 6-15: Substructure Displacement Profile (Field vs. FEM)

The backfill pressures recorded by earth pressure cells were minimal apart from the ones located at the obtuse corners. The increase in backfill pressure in obtuse corners of Abutment 1 were higher than estimated active pressures for some truck positions and also higher than the pressure at the acute corners. This indicated abutment rotation where one corner of the abutment was pushed towards the backfill while the other corner was pulled away. There was almost no pressure decrease when the acute abutment corner was pulled away from the backfill. This means that, the backfill was initially under active pressure condition which was theoretically equal to the minimum earth pressure. Similar to Middlesex Bridge, low in-field earth pressures in East Montpelier Bridge suggested that mainly active pressures presented behind the abutments. Generally, earth pressures on Abutment 1 were higher than earth pressures on Abutment 2 which was consistent with the limited rotation and displacement of Abutment 2 recorded by tiltmeters and displacement transducers.

Pile response from field data and FEM was compared for axial loads and bending moments, separately. The maximum axial stress from FEMs was approximately 200% of the

maximum stress from the field data, though maximum values were only 20.00 MPa (2.75 ksi). Noting that FEM results for axial loads and weak axis bending moment were generally consistent with field load testing of the Middlesex Bridge, different connection details for approach slab-bridge connection could be attributed as the reason for discrepancy in the East Montpelier data. At the East Montpelier Bridge, the bridge was directly attached to the approach slab with anchored rebars and no expansion plugs were present. Under gravity loads, the soil bearing below the approach slab could possibly decrease the axial force transmitted to the bridge substructure. Since the approach slab wasn't modeled in the FEMs, the results neglect the effects of this load transfer. Figure 6-17 shows axial loads for both the East Montpelier and Middlesex Bridges.

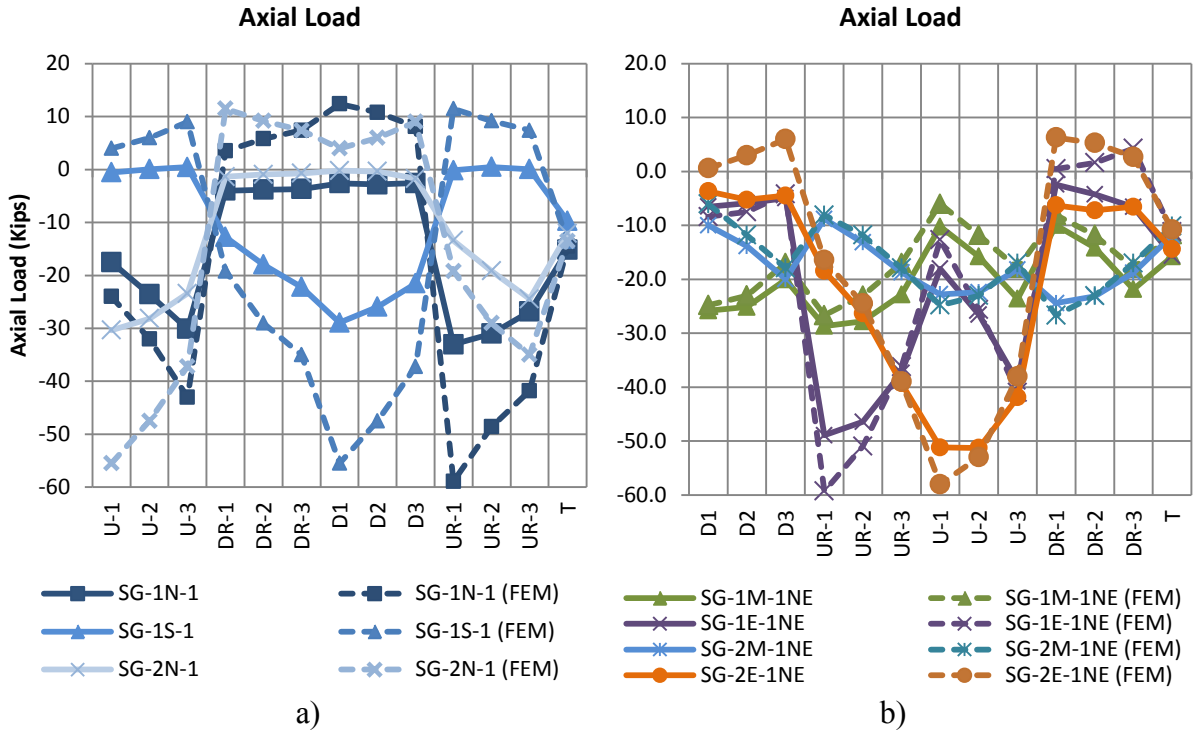

Figure 6-16: Axial Loads at the Top of Piles at a) the East Montpelier Bridge b) the Middlesex Bridge (Field Data vs. FEM)

High axial loads in FEMs also affected the resultant stresses on the piles and FEMs predictions were higher than stresses recorded during load testing. Maximum pile stresses for upstream and downstream piles were almost identical. Also, piles below Abutment 1 and Abutment 2 had a similar maximum stress. Figure 6-17 shows maximum calculated stresses at the tip of pile flanges. Maximum stress was 24.1, 22.1, 22.8 MPa (3.5 ksi, 3.2 ksi, 3.3 ksi) for upstream and downstream piles at Abutment 1 and upstream pile at Abutment 2, respectively. Table 6-2 summaries the substructure response of the East Montpelier Bridge.

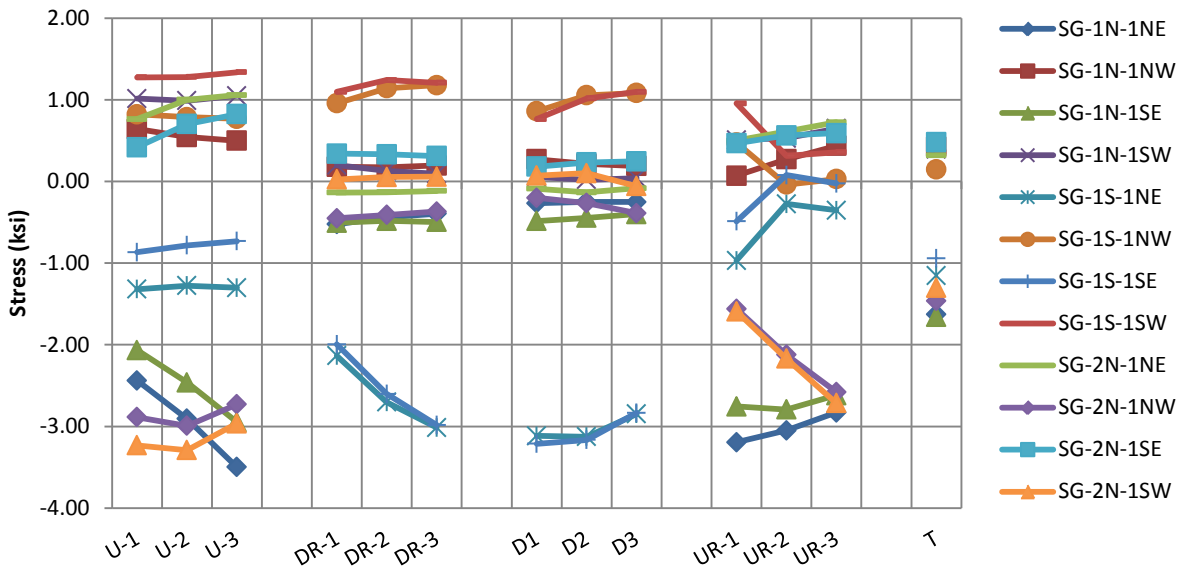

Figure 6-17: Resultant Stresses at the Piles (Field)

Table 6-4: Summary of Substructure Response of East Montpelier Bridge

	East Montpelier Bridge			
	Abutment 1		Abutment 2	
	Actual	FEM	Actual	FEM
Maximum Abutment Rotation	0.016 deg	0.016 deg	0.006 deg	0.016 deg
Maximum Longitudinal Abutment Displacement at the Top Flange of Girder	0.508 mm (0.020 in) (towards river)	0.635 mm (0.025 in) (towards river)	0.406 mm (0.016 in) (towards backfill)	0.635 mm (0.025 in) (towards river)
Maximum Longitudinal Abutment Displacement at the Bottom of Abutment	0.686 mm (0.027 in) (towards backfill)	1.524 mm (0.060 in) (towards backfill)	0.432 mm (0.017 in) (towards backfill)	1.270 mm (0.050 in) (towards backfill)
Maximum Pile Displacement at the Top of the Pile	1.016 mm (0.040 in) (towards backfill)	1.118 mm (0.044 in) (towards backfill)	0.914 mm (0.036 in) (towards backfill)	1.118 mm (0.044 in) (towards backfill)
Maximum Pile Stress at Upstream Pile at the Gage Location	19.3 MPa (2.8 ksi) (compressive)	36.5 MPa (5.3 ksi) (compressive)	18.6 MPa (2.7 ksi) (compressive)	29.6 MPa (4.3 ksi) (compressive)
Maximum Pile Stress at Downstream Pile at the Gage Location	18.6 MPa (2.7 ksi) (compressive)	34.5 MPa (5.0 ksi) (compressive)	N/A	N/A
Depth at which Pile Displacement is Negligible	~ 3 m (10.0 ft)	~2.4 m (8.0 ft)	~ 3.0 m (10.0 ft)	~2.4 m (8.0 ft)
Maximum Backfill Earth Pressure	10 KPa (1.45 psi)	14.4 KPa (2.09 psi)	3.2 KPa (0.46 psi)	14.4 KPa (2.09 psi)

6.5 Analysis of Load Testing Data for Stockbridge Bridge

6.5.1 Superstructure Response

Table 6-5 shows the maximum steel girder moments and stresses at the instrumented girder cross sections compared with FEM moment results. The temperature was approximately constant during load testing of the Stockbridge Bridge, which resulted in a negligible difference between readings before and after temperature correction. Instrumented girder section located at the top of pier exhibited negative moments for all truck positions. In general, the moments at this location were less than midspan moments recorded by the other strain gages. The truck positions U3, D3 and UR3 where the trucks were closely located to the interior pier generated the minimum stress at each girder cross section. Moment at midspan of each bridge span changed sign according to the positions of the truck. They mainly exhibited positive moment with tension at the bottom flange. However, when the trucks were located at the same lane of the further span, the gages recorded negative moments. The magnitudes of these negative moments were comparable with the positive moments recorded below the truck axle loads. Overall, while the trends of the bending moments were comparable between field and FEM, the FEM predicted greater positive bending moments, with this difference most notable on the upstream girder.

Maximum Girder moment at each instrumented girder cross section and FEM envelope vs field data are shown in Figure 6-18, Figure 6-19 and Figure 6-20. Girder moments when trucks are at the upstream lane are shown for the three cross sections along the bridge at Abutment 1 end, midspan, and Abutment 2 end in Figure 6-21, Figure 6-22, and Figure 6-23, respectively. The moment envelope for the upstream girder shows there is an 82% difference between maximum positive moments and a 40% difference in maximum negative moments. However, for the downstream girder the difference in maximum positive moments is 29% and the difference in maximum negative moments is 6%. The field results generally show a greater transverse distribution of bending moments than FEM results. For the cross sections instrumented within the spans, the FEM results predict the downstream girder moments will be nearly negligible when the upstream girder is loaded, while field data shows that the downstream girder has a moment approaching 225 kN-m (2000 kip-in).

Peak values of girder moments differ between FEM and field data and are more significant on the upstream girder than the downstream girder. A FEM assumption at this bridge was that the Geofoam behind the abutments reduced the backfill pressures to negligible values and were therefore neglected in the model. The FEM was also analyzed with a dense backfill for comparison, resulting in greater restraint to abutment movement. The resulting maximum positive girder moments were reduced by up to 113 kN-m (1000 kip-in). Therefore, some soil resistance may be present, but this does not account for the full discrepancy between maximum field data and FEM results. Another factor could be the location of the wheel loads in the FEM; the location of the wheel load has a very significant effect on the girder moments in sections

directly under the load. If the loads were applied closer to a girder than they were in the field, this would affect the magnitude of the moment in the FEM. Fixity conditions over the support pier or at abutments different from FEM assumptions could shift the two span moment diagram (magnitude and location of peak values). Moments at the pier (Figure 6-22) indicate that field data at the exterior girders was similar while FEM predicted different results. This could indicate different bearing conditions than assumed for these relatively low live loads. However, additional FEM analysis showed pier conditions to be of secondary importance to the peak moment results. Overall, the trends of the moment magnitudes for the various load cases were captured well by the FEM and the envelope gives a reasonable prediction of moments that could be expected in the field.

Table 6-5: Summary of Superstructure Response for Stockbridge Bridge

	Stockbridge Bridge	
	Actual	**FEM**
Maximum Positive Girder Bending Moment	426 kN-m (3774 Kips-in)	861 kN-m (7263 Kips-in)
Maximum Negative Girder Bending Moment	-507 kN-m (-4487 Kips-in)	-479 kN-m (-4240 Kips-in)
Maximum Compressive Stress at Gage Locations (Girder Flanges)	13.1 MPa (1.9 ksi)	N/A
Maximum Tensile Stress at Gage Locations (Girder Flanges)	18.6 MPa (2.7 ksi)	N/A

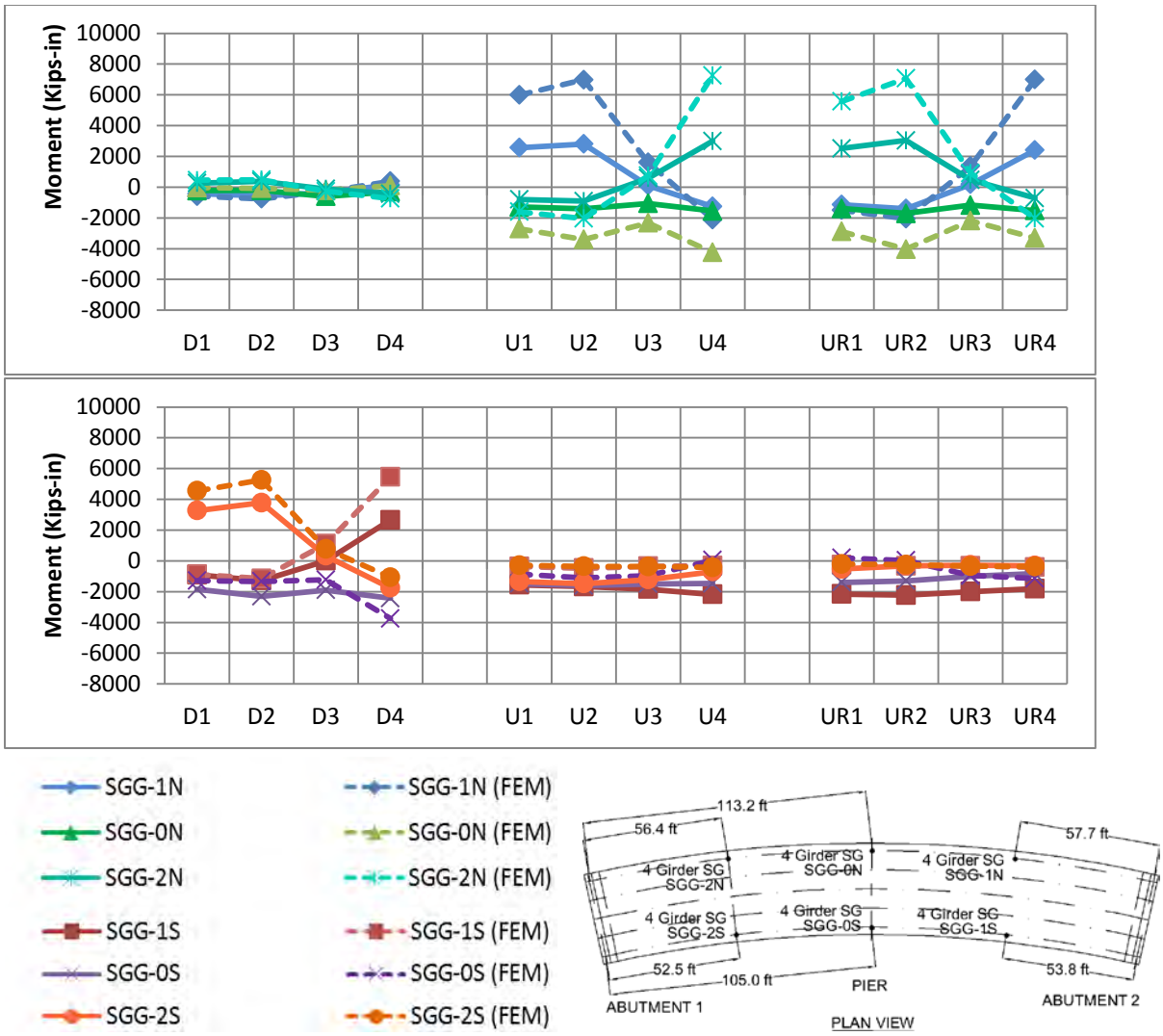

Figure 6-18 Girder Moments at Instrumented Girder Cross Sections (Field and FEM)

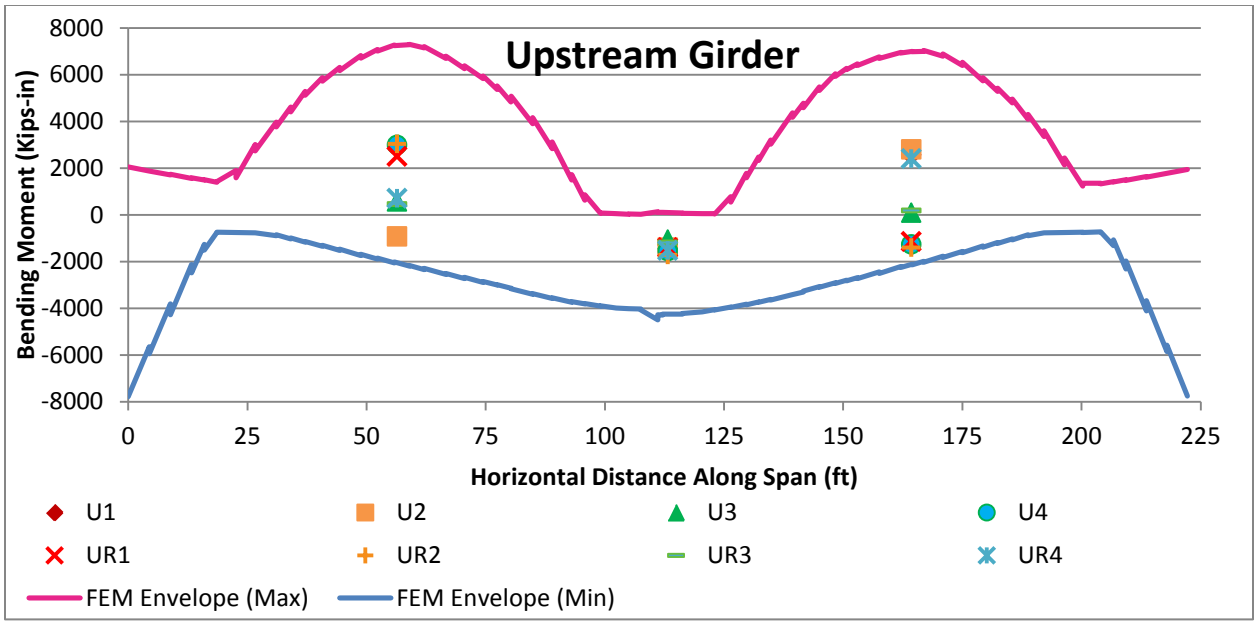

Figure 6-19 Girder Moments Along Upstream Girder at Stockbridge Bridge (Field and FEM)

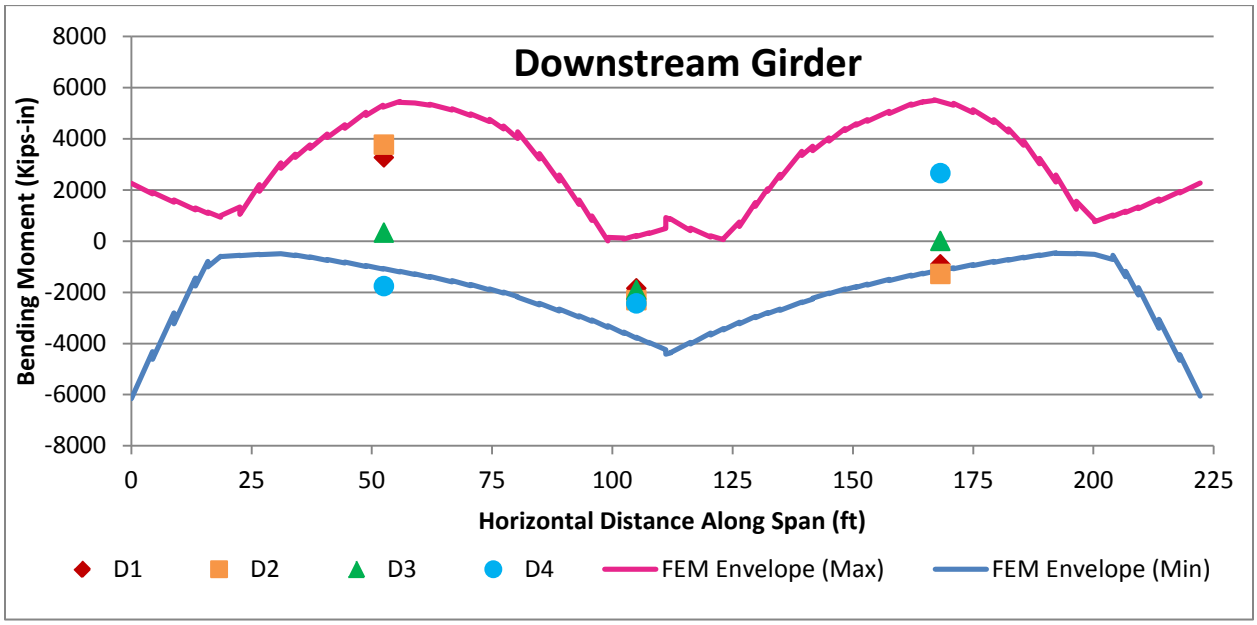

Figure 6-20 Girder Moments Along Downstream Girder at Stockbridge Bridge (Field and FEM)

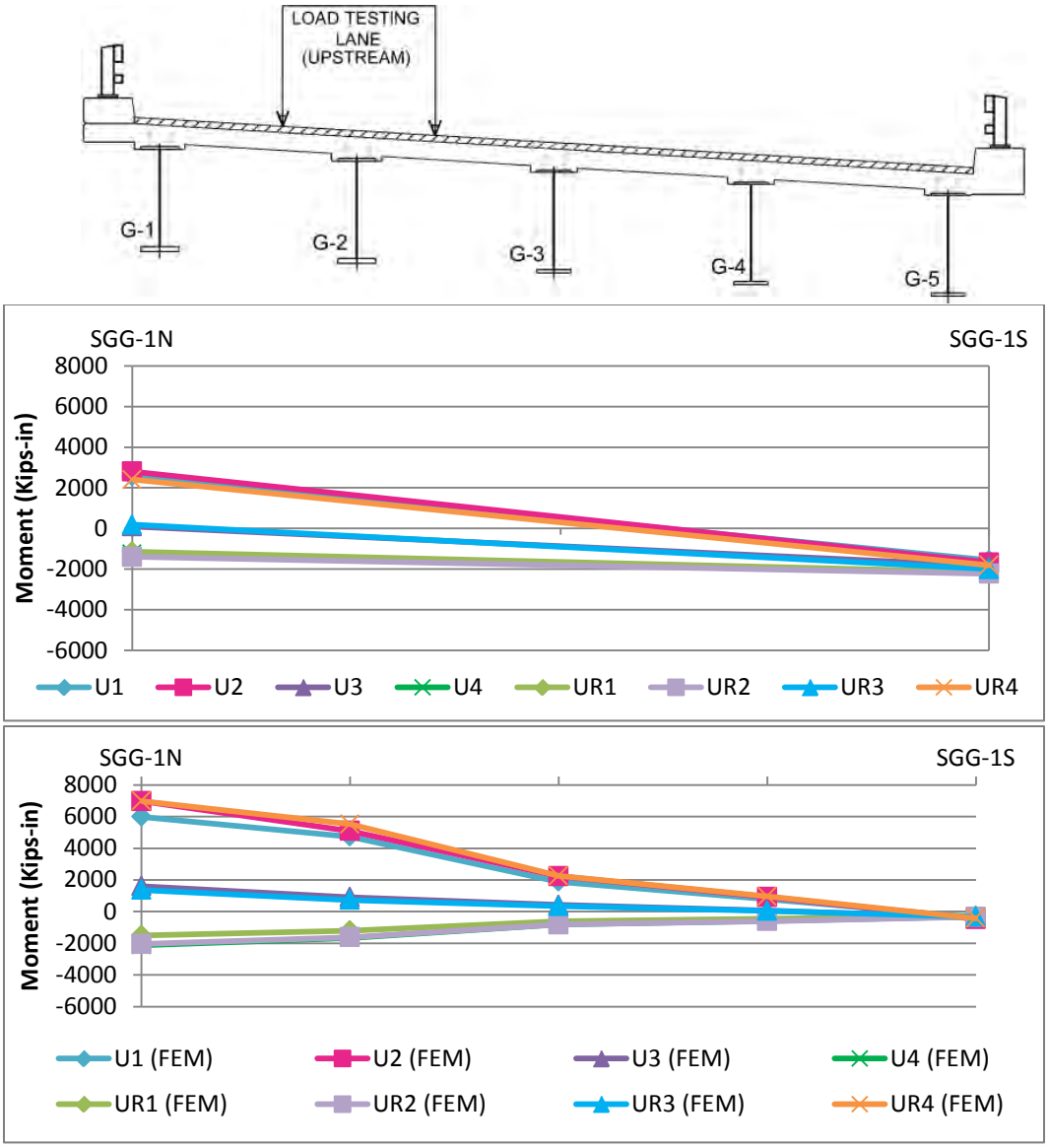

Figure 6-21 Girder Moments at Cross Section within Span nearest Abutment 1 (Trucks at Upstream Lane) Field and FEM

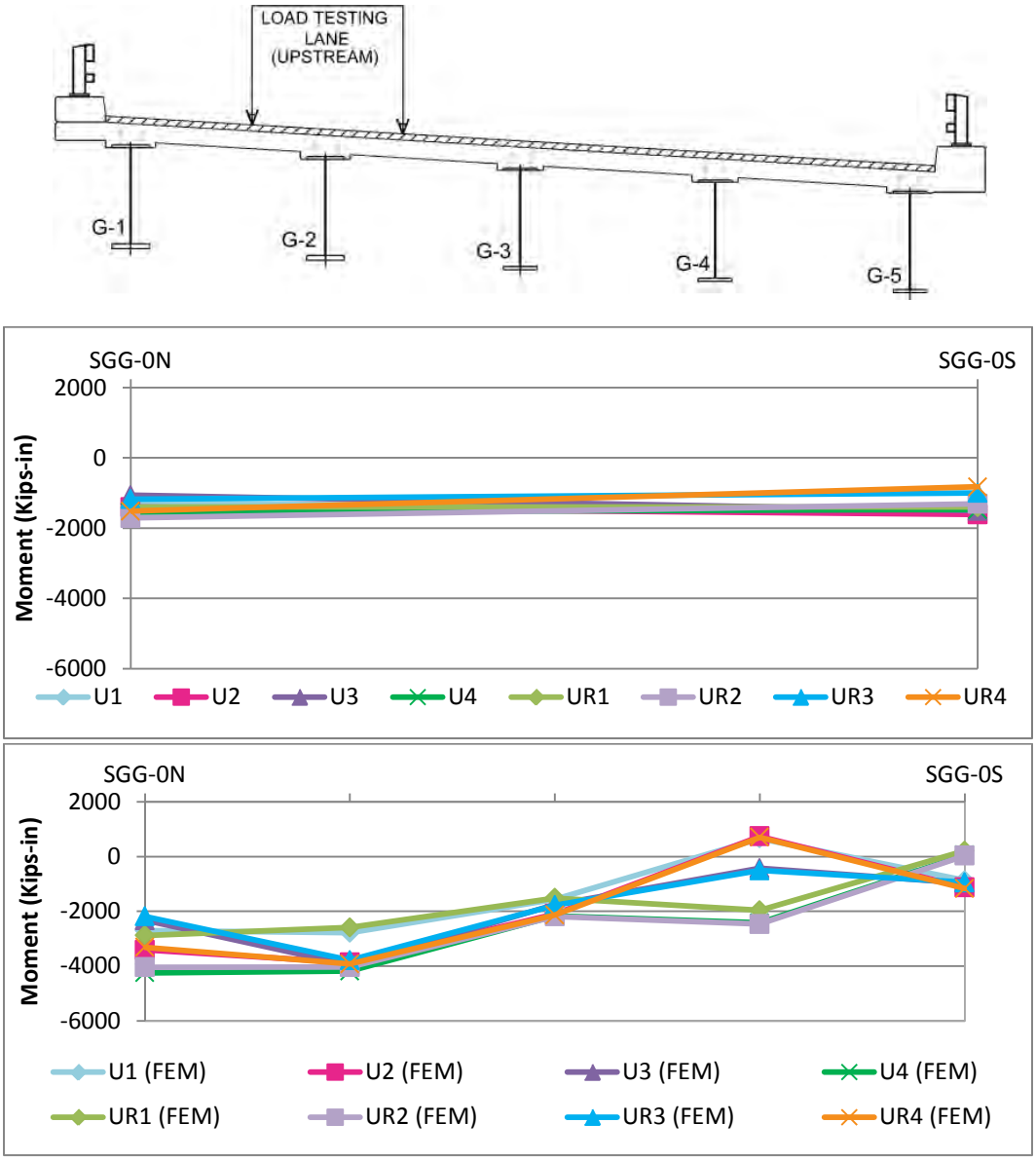

Figure 6-22 Girder Moments at Cross Section Over Center Pier (Trucks at Upstream Lane) Field and FEM

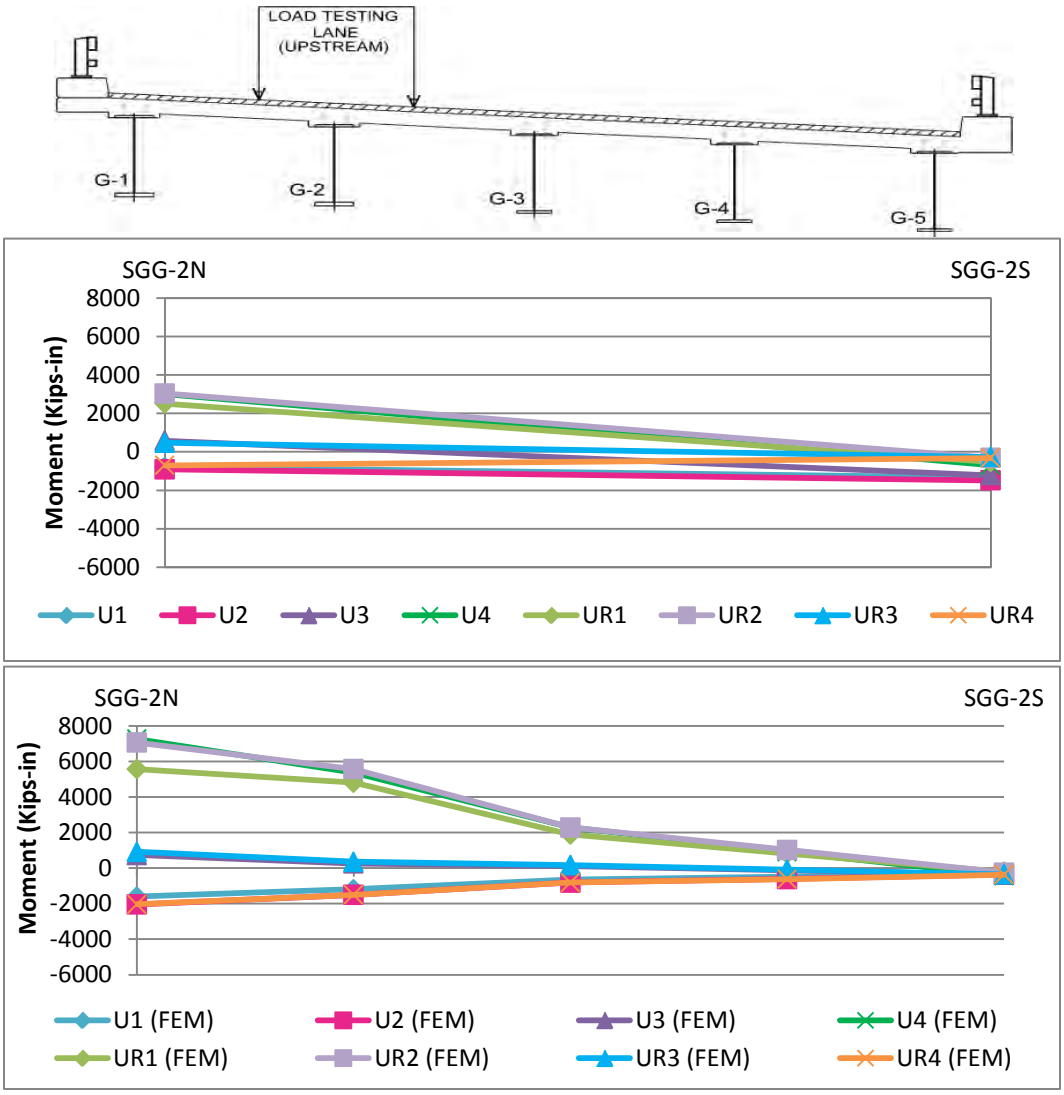

Figure 6-23: Girder Moments at Cross Section within Span Nearest Abutment 2 (Truck at Upstream Lane) Field and FEM

6.5.2 Substructure Response of Stockbridge Bridge

At the Stockbridge Bridge, abutment displacements and rotations were less than the other two bridges tested – Middlesex Bridge and East Montpelier Bridge. This is likely due to it being a two-span versus single span structure. Table 6-6 shows the summary of substructure response compared to FEM results.

Longitudinal abutment rotations shifted directions (towards river or towards backfill) depending on the truck location. Maximum abutment rotation in the transverse direction was 25% of maximum longitudinal abutment rotations. Pile deflections were only monitored at upstream and downstream piles below Abutment 1. Figure 6-24 shows the deflected shape of the bridge substructure for load cases that generated the maximum response and displays both field data and FEM results. Piles moved towards the backfill while the trucks were located on span adjacent to the piles. However, displacements were towards the span as the truck moved onto the further span. Displacements at the upstream pile were higher than downstream pile when the trucks were at the same relative location to the pile. Transverse pile displacements were minimal with a maximum of 0.127 mm (0.005 in). While the FEM predicted greater displacements than field data showed, the values were all low showing that substructure displacement is minimal during live load testing. Pile stresses were generally higher for upstream piles with a maximum pile stress of 21.7 MPa (3.1 ksi) which was recorded at the top of upstream pile below Abutment 2. Also the data showed that pile stresses at Abutment 2 were higher than those at Abutment 1. Figure 6-25 shows the resultant pile stresses for both sides of the bridge.

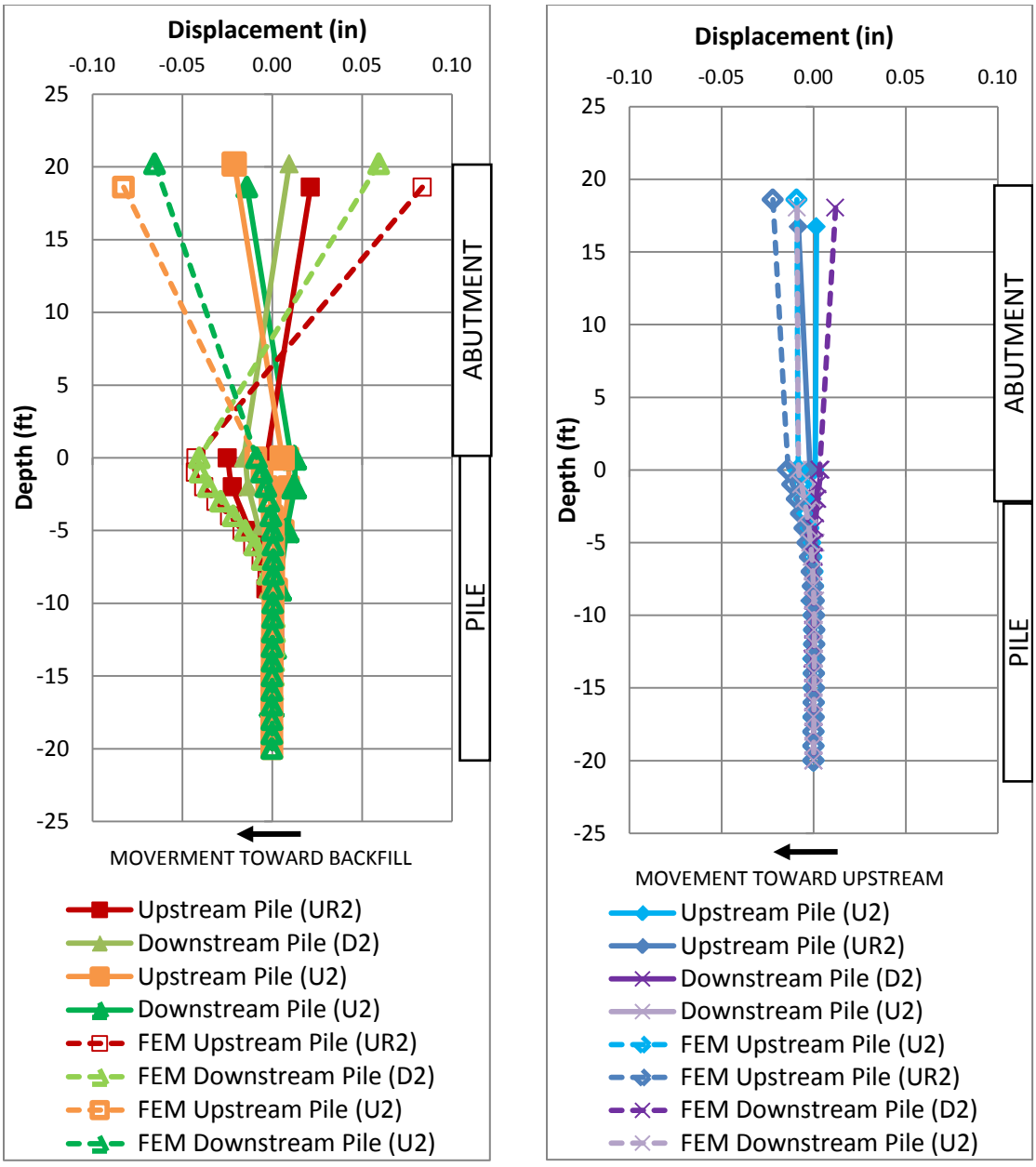

Figure 6-24: Substructure Displacement at Abutment 1, a) Longitudinal, b) Transverse

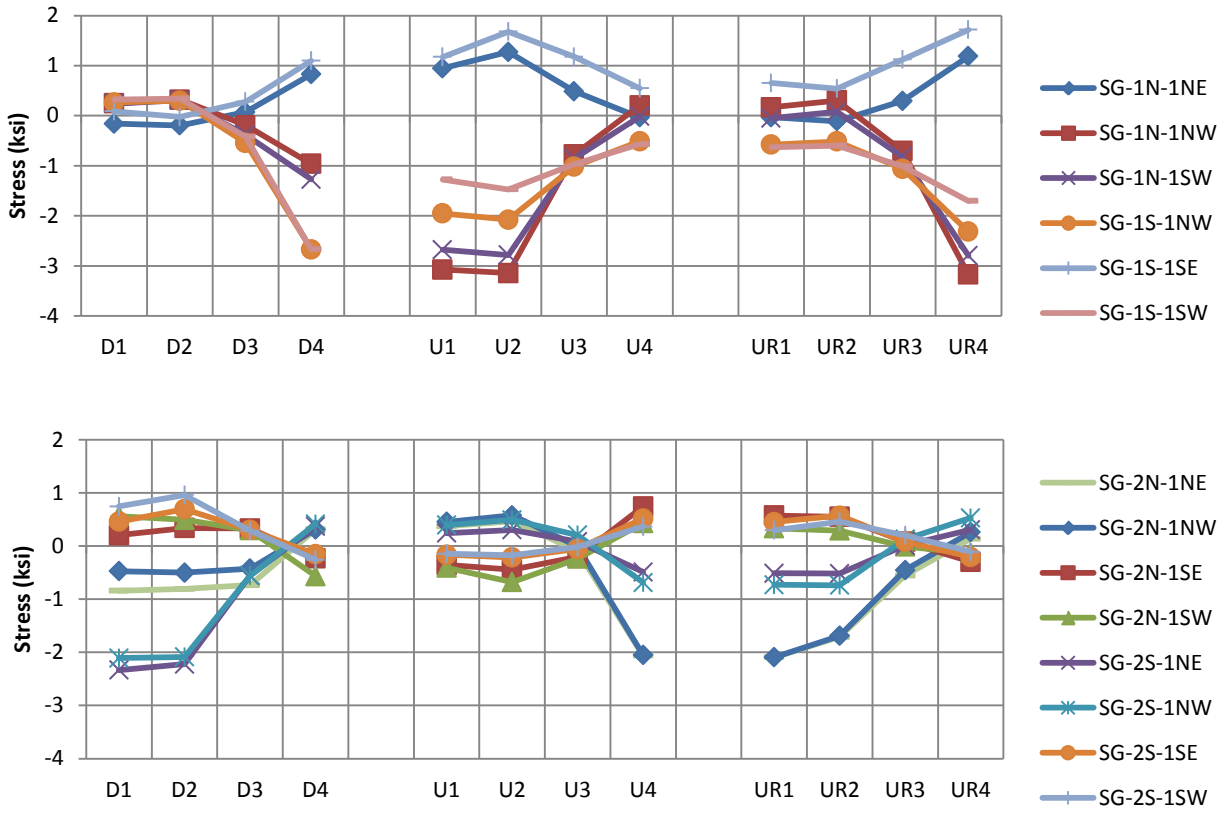

Figure 6-25: Resultant Stresses at Abutment 1 Piles and Abutment 2 Piles

The Stockbridge Bridge has a geofoam layer installed between the abutment wall and backfill. Earth pressure cells attached to the abutment walls are therefore covered with the geofoam material. During load testing, earth pressure readings in the field were small with a maximum pressure of 1.52 KPa (0.22 psi). However, the gages attached to the wingwalls recorded higher pressures. Maximum recorded earth pressures at wingwall were as high as 23.4 KPa (3.4 psi). The difference between earth pressure between abutments and wingwalls may be caused by transverse movement of abutments of the curved bridge. Maximum pressures behind the wingwalls were larger in field than FEM results, with a maximum difference of 8.27 KPa (1.2 psi).

Data from concrete embedded strain gages within the pier showed minimal pier strains with truck loading. The maximum stress increase was 6.9 MPa (1 ksi). This stress increase was caused by the combination of axial stress and bending stresses. Again, from the field test, the maximum axial stress acting on the bridge column was estimated as 1.72 MPa (0.25 ksi).

Table 6-6: Summary of Substructure Response for Stockbridge Bridge

	Stockbridge Bridge			
	Abutment 1[1]		Abutment 2[1]	
	Actual	FEM	Actual	FEM
Maximum Abutment Rotation (Longitudinal)	0.006 deg	0.022 deg	0.013 deg	0.017 deg
Maximum Abutment Rotation (Transverse)	-0.003 deg	-0.003 deg	-0.003 deg	-0.004 deg
Maximum Longitudinal Abutment Displacement at the Top Flange of Girder	0.721 mm (0.0284 in) (towards river)	2.110 mm (0.0832 in) (towards river)	0.975 mm (0.0384 in) (towards river)	1.702 mm (0.0671 in) (towards river)
Maximum Longitudinal Pile Displacement at the Top of the Pile	0.635 mm (0.025 in) (towards backfill) 0.356 mm (0.014 in) (towards river)	1.14 mm (0.045 in) (towards backfill) 0.762 mm (0.030 in) (towards river)	N/A	1.27 mm (0.050 in) (towards backfill)
Maximum Transverse Pile Displacement at the Top of the Pile	0.127 mm (0.005 in) (towards downstream) 0.051 mm (0.002 in) (towards upstream)	0.279 mm (0.011 in) (towards downstream) 0.0356 mm (0.014 in) (towards upstream)	N/A	0.330 mm (0.013 in) (towards downstream) 0.305 mm (0.012 in) (towards upstream)
Maximum Pile Stress at Upstream Pile at the Gage Location	14.5 MPa (2.1 ksi) (compressive)	N/A	22.1 MPa (3.2 ksi) (compressive)	N/A
Maximum Pile Stress at Downstream Pile at the Gage Location	18.6 MPa (2.7 ksi) (compressive)	N/A	17.9 MPa (2.6 ksi) (compressive)	N/A
Depth at which Pile Displacement is Negligible	~ 13 ft	~15 ft	N/A	~15 ft
Maximum Backfill Earth Pressure at Abutment Wall	1.38 KPa (0.20 psi)	N/A[2]	1.59 KPa (0.23 psi)	N/A[2]
Maximum Backfill Earth Pressure at Wing Wall	6.61 KPa (0.96 psi)	4.62 KPa (0.67 psi)	23.44 KPa (3.40 psi)	15.17 KPa (2.20 psi)

[1]According to labeling in the structural drawings.
[2]Abutment backfill was neglected in the FEM as Geofoam minimizes backfill pressures

6.6 Conclusion

The extensive monitoring carried out during the live load testing of these three IABs provided valuable information about integral abutment bridge response and has been used to calibrate FEM's of the Middlesex, East Montpelier, and Stockbridge Bridges. The superstructure exhibited negative bending moments at the ends (comparable to the maximum positive bending moments at the midspan). The girders located far from truck loading locations exhibited comparatively small bending stresses. The substructure displacement was minimal. Abutment backfill pressures were small because the bridges had contracted due to low seasonal temperatures. At the East Montpelier Bridge, the earth pressures and abutment displacements

were higher for obtuse corner of the abutment. However, the maximum values were still limited. At the Stockbridge Bridge, having 2-span structure with an interior pier resulted in a reduction in forces transferred to bridge abutments and piles. Therefore, bridge substructure displacements and stresses were less than the two other bridges tested. Unlike the Middlesex Bridge and East Montpelier Bridge, the data from Stockbridge Bridge showed that the geometry affected the distribution of forces (higher stresses and displacements at the upstream end of the bridge, higher earth pressure at wingwalls due to out-of plane movement of bridge, etc.). The accurate results that were obtained from FEM of the bridges compared with the measured field response provide confidence that these FEMs can be used to accurately predict behavior for other load positions needed to compute lateral load distribution factors. However, any analysis of field data that neglects the correction for temperature may contain significant errors. In particular, for the magnitude of stresses generated during load testing, the elimination of temperature effects is critical since temperature effects changed the top and bottom flange stresses a significant amount. If thermal correction had not been done and strain gage readings were used to calculate the neutral axis for each run, unrealistic neutral axis depths would be calculated.

7 ANALYSIS OF INTEGRAL ABUTMENT BRIDGES DURING CONSTRUCTION

7.1 Introduction

All three integral abutment bridges behaviors were evaluated during the construction process through field data and FEM. Field data and FEM results are compared to gain an understanding of embedded stresses in structural components during the construction process and after the bridges' completion. Correlation of measured data with FEM and hand calculation results of pile axial and biaxial bending stresses, girder stresses, backfill and form pressures, and abutment rotations are presented. Results are specific to integral abutment bridges of modest length, constructed with piles oriented for weak axis bending in the direction of traffic and with minimal continuity provided between the girders and substructure during construction until the upper abutments were placed.

The behavior of these IABs should respond similarly to a non-integral structure through all but the final stages of construction. This is due to the upper abutment being placed last in the construction sequence, resulting in the ends of the girders being restrained only by their seat supports until this final placement of concrete hardens. During final surfacing, curb placement and related work as well as subsequent to construction (live and thermal load) the superstructure acts integrally with the substructure. Therefore, there may be some built-in stresses that are specific to an IAB span. In addition, the substructure forces from construction become the initial state for integral behavior and may therefore limit forces that can be induced prior to yielding of piles.

7.2 Construction Sequence

All bridges were constructed similarly. The construction started with installation of piles for single span bridges (The Middlesex and East Montpelier Bridges) and with construction of the pier for 2-span Stockbridge Bridge. At the Middlesex and East Montpelier Bridges, the soil around the top 1.5 m (5.0 ft) of piles was excavated prior to driving piles. Subsequently, at the Middlesex Bridge, piles were driven to resistance (vibrated to depth prior to driving at East Montpelier) (Figure 7-1). Once the piles were in place, the top 1.5 m (5 ft) of the piles was filled with granular material. At the Stockbridge Bridge, piles below Abutment 2 were driven while the piles supporting Abutment 1 were vibrated to rock and then driven to the specified resistance. Subsequent to pile installation, the abutments were placed up to the construction joint just below the girder bottom flange. After curing the forms were removed and the bottoms of the abutments were backfilled. The girders were then placed (Figure 7-2), with a slight variation between the bridges. In the Middlesex Bridge, the girders were attached to the abutment with 52.4 mm ($2^{1}/_{16}$

in) diameter swedged, galvanized anchor bolts and 400 mm by 120 mm (thickness is equal to 14 mm) (15.75x4.7x0.55 in) steel leveling plates (nuts backed off to prevent moment transfer prior to concrete placement) while, in the East Montpelier Bridge, the girders simply sat on steel reinforced elastomeric bearing pads. At the Stockbridge Bridge, the girders rested on concrete pads at the ends of the bridge and on the guided bearings at the top of pier. Formwork for completion of the top of the abutment as well as the deck was then placed (Figure 7-3). At the Middlesex and Stockbridge Bridges, the slab was placed, followed by abutment-deck connection and abutments. At the East Montpelier Bridge, the construction was to progress from the east abutment to the deck to the west abutment. However, due to high lateral deformations of the girders during deck placement, construction was halted after approximately half of the deck was completed. After strengthening of the cross framing a portion of deck was removed such that approximately 16.5 percent of the slab was complete, which included Abutment 2 and 5.6 m (18.4 ft) of deck beyond the abutment. Five weeks after the initial placement the remaining slab and west abutment were completed. Due to this change in construction schedule different end conditions might be effective in the two abutments as the dead load was completed.

Figure 7-1: Pile Driving at the Middlesex Bridge

Figure 7-2: Girders Placed at the East Montpelier Bridge

Figure 7-3: Forms and Reinforcement Bars at the Middlesex Bridge

It is important to understand that composite action and integral abutment behavior are not realized during typical construction since the concrete deck and upper abutments encasing the girders are placed and reach strength during the final stages of construction. After the concrete cures and backfill is placed the behavior is that of a frame with rigidity between all superstructure and substructure components. Loads applied after this stage of construction include upper abutment backfill placement, dead load of topping slab, curb and guardrails, thermal fluctuations, creep and shrinkage. The construction schedules for bridges are provided in Table 7-1. Completed structures are shown in Figure 7-4.

Table 7-1: Construction Schedule for the East Montpelier Bridge

Activity	Middlesex Bridge		East Montpelier Bridge		Stockbridge Bridge	
	Start Date	End Date	Start Date	End Date	Start Date	End Date
Pile Placement	06-15-09	06-16-09	6-24-09	7-28-09	10-11-08	18-12-08
Conc. Placement of Lower Abut. 1	07-15-2009	07-15-2009	8-6-09	8-6-09	10-21-08	10-21-08
Conc. Placement of Lower Abut. 2	07-02-2009	07-02-2009	7-30-09	7-30-09	01-08-09	01-08-09
Backfill Lower Abutment 1	07-22-09	07-22-09	8-14-09	8-14-09	01-21-09	01-21-09
Backfill Lower Abutment 2	07-13-09	07-14-09	8-10-09	8-11-09	05-26-09	05-27-09
Placement of Girders	07-31-09	08-04-09	8-18-09	8-18-09	01-27-09	02-06-09
Placement of Deck Formwork	08-05-09	08-21-09	8-24-09	9-23-09	04-06-09	04-06-09
Deck Placement	08-27-09 6:50 AM	08-27-09 12:15 PM			05-06-09	05-06-09
1st Deck Placement			9-24-09	9-24-09		
Deck Removal			10-2-09	1-8-09		
2nd Deck Placement			10-29-09	10-29-09		
Conc. Placement of Upper Abut. 1	09-21-09 1:40 PM	09-21-09 3:40 PM	10-29-09	10-29-09	05-11-09	05-11-09
Conc. Placement of Upper Abut. 2	09-15-09 9:30 AM	09-15-09 11:45 AM	10-29-09	10-29-09	05-11-09	05-11-09
Removal of Deck Formwork	10-06-09	10-13-09	11-9-09	11-13-09	N/A	N/A
Backfill of Upper Abutment 1	10-07-09	10-07-09	10-21-09	11-23-09	08-10-09	08-12-09
Backfill of Upper Abutment 2	09-29-09	09-30-09	10-5-09	10-5-09	08-14-09	08-14-09
Curb pour	09-25-09	09-30-09			05-14-09	05-15-09
Paving (Temporary)	10-23-09	11-10-09				
Approach Slab Abut 1	10-09-09	10-09-09	N/A	N/A	N/A	N/A
Approach Slab Abut 2	10-05-09	10-05-09	N/A	N/A	N/A	N/A
Permanent Paving	05-10-10	05-20-10	11-3-09	11-4-09	08-31-09	09-08-09
Open for Traffic	10-27-09		11-19-09		01-08-09	

(a) (b)

(c)

Figure 7-4: Final Structures (a) the Middlesex Bridge (b) the East Montpelier Bridge (c) the Stockbridge Bridge

7.3 Temperature during Construction

Daily high and low temperatures during construction are shown in Figure 7-5, Figure 7-6 and Figure 7-7 for the weather stations closely located to the Middlesex, East Montpelier and Stockbridge Bridges, respectively. During construction the ambient temperature fluctuation was approximately 39 ^{o}C (70 ^{o}F) at the Middlesex and East Montpelier Bridges (between 32 ^{o}C [90 ^{o}F] and -7 ^{o}C [20 ^{o}F]). At the Stockbridge Bridge where the construction took more than a year, the temperature fluctuation was as high as 63^{o}C (113 ^{o}F) (between 33^{o}C [91 ^{o}F] and -30 ^{o}C [-22 ^{o}F.

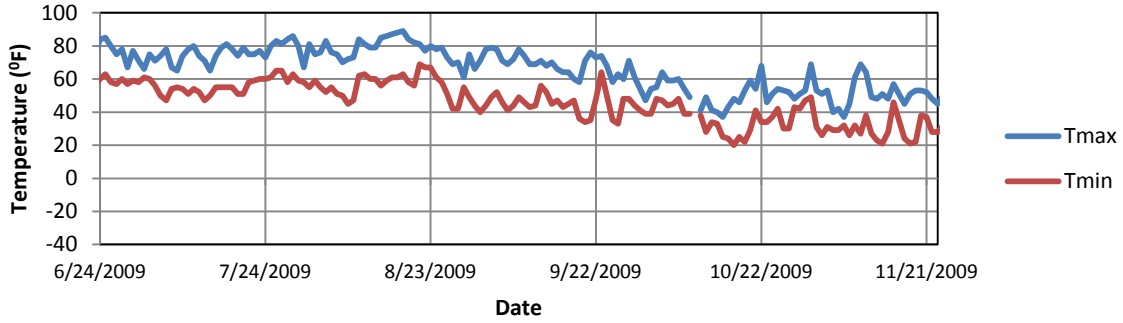

Figure 7-5: Montpelier Temperatures (Weather Station close to the Middlesex Bridge)

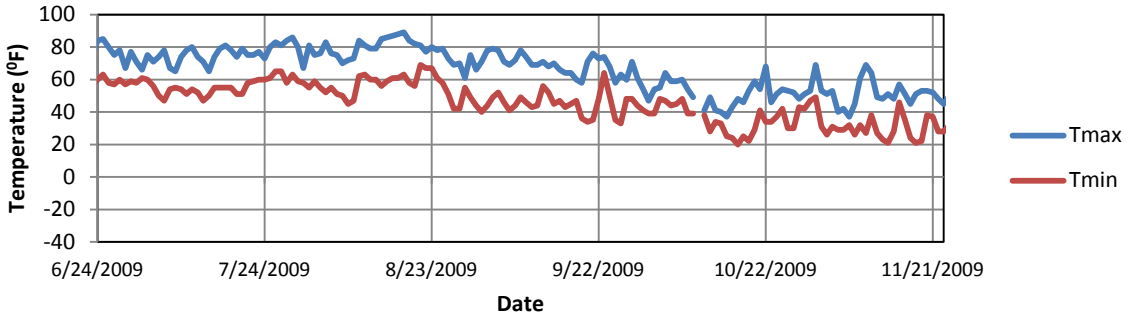

Figure 7-6: Montpelier-Barre Airport Temperatures (Weather Station close to the East Montpelier Bridge)

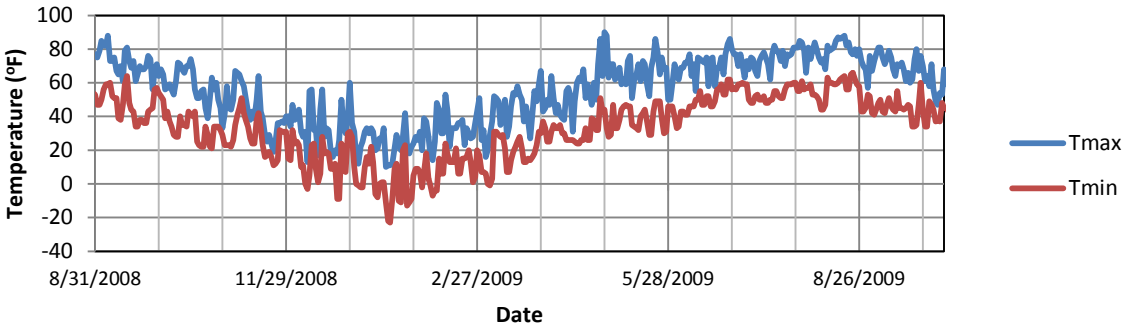

Figure 7-7: Rochester Temperatures (Weather Station close to the Stockbridge Bridge)

7.4 Analytical Modeling

The staged construction module of SAP2000 was utilized, although there were significant differences that needed to be considered between IAB and non-IAB structures. An IAB structure does not have any fixity at the girder ends until the entire dead load has been placed on the structure. After that point the abutment concrete has hardened and full continuity is realized between the girders, abutment and piles. The steps included in the finite element modeling of the Middlesex Bridge construction are shown in Figure 7-8. These steps do not directly correlate to the construction process, but the end of Step 3 corresponded to the completion of the construction. Step 1 includes the load from the wet concrete slab and girders, but only the plain steel girders resist these loads. This step will result in the girder stresses at the point when the deck has been completed. At the 2nd step, the temporary vertical support elements at the ends of the bridges at Step 1 are replaced by the bridge substructure. The forces and stresses generated at the end of Step 1 are manually applied to the structure at the Step 2. The Step 2 includes all substructure elements up to the construction joint, including the active soil pressures applied behind the completed abutment sections. Finally, the upper abutment is complete, fixity provided between the abutment and girders, and composite action introduced between the girders and deck. At this point the structure is completed including backfill (active pressures behind abutments) and would be the theoretical initial condition for evaluating seasonal thermal effects. At the East Montpelier Bridge, in order to simulate the revised deck placement (see Section 2.2), additional steps were modeled. These steps included the fixity between Abutment 2 and deck when the concrete deck was poured. In a linear elastic system the dead load response could be simply added to subsequent thermal effects. However, due to the potential non-linearity of soil structure interaction the construction process may affect the results.

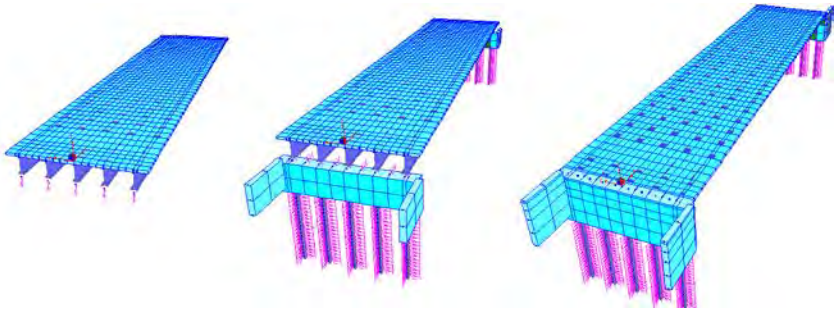

(a) Step 1 (b) Step 2 (c) Step 3

Figure 7-8: Stage Construction Model for the Middlesex Bridge

7.5 Construction Data

Due to construction sequencing, continuous data acquisition was not possible during bridge construction. Data was therefore collected manually at discrete points in time for each structure as shown in Table 7.2. The following sections address pile axial and bending stresses, girder axial stresses, backfill pressures, formwork pressures and abutment rotations at specific stages in the construction process.

Table 7-2: Dates for Field Data Collection

Middlesex Bridge								
Date	Pile Strain		Girder Strain	Pressure Cells		Inclinometers	Tiltmeters	Crackmeters
	Abut 1	Abut 2		Abut 1	Abut 2			
6/18/2009	X	X						
6/19/2009	X	X						
7/01/2009		X						
7/02/2009					X			
7/14/2009	X	X		X	X			
7/15/2009	X	X		X	X			
7/21/2009	X	X		X	X			
8/04/2009			X					
8/05/2009	X	X	X	X	X			
8/07/2009			X					
8/24/2009						X		X
9/08/2009	X	X		X	X	X	X	
10/05/2009				Ref only				
11/16/2009	X	X	X	X	X	X	X	X

East Montpelier Bridge								
Date	Pile Strain		Girder Strain	Pressure Cells		Inclinometers	Tiltmeters	Crackmeters
	Abut 1	Abut 2		Abut 1	Abut 2			
7/21/2009		X						
7/28/2009		X			X			
7/29/2009	X							
7/30/2009		X			X			
8/06/2009	X	X		X	X	X		
8/13/2009				X				
8/17/2009			X				X	
8/18/2009			X	Ref only			X	X
9/24/2009	X	X		X	X	X	X	X
10/05/2009	X	X	X			X	X	X
11/24/2009	X	X	X	X	X	X	X	X

Stockbridge Bridge									
Date	Pile Strain		Strain Gage		Pressure Cells		Inclinometers	Tiltmeters	Crackmeters
	Abut 1	Abut 2	Pier	Girder	Abut 1	Abut 2			
10/30/2008		X							
10/31/2008		X							
12/08/2008		X				X			
12/17/2008	X								
12/18/2008	X								
01/06/2009					X				
02/04/2009	X				X	X			
04/13/2009				X					
04/14/2009				X					
05/13/2009	X	X	X	X	X	X			
06/02/2009	X	X			X	X			
06/24/2009									X
07/15/2009					X	X			X
08/21/2008					Ref only				
09/15/2009	X	X	X	X	X	X	X	X	X

7.6 Pile Stresses during Construction

At the Middlesex Bridge and the East Montpelier Bridge, the pile strain gages were attached subsequent to pile driving, with soil backfilled and compacted around the top 1.5 m (5 ft) of the piles after gages were attached. At the Stockbridge Bridge, pile strain gages were attached as the pile was still above final grade, with data collected at this time and subsequent to driving to final pile resistance. The data collected in the top 3 m (10 ft) of Stockbridge piles during driving operations indicated that residual stresses in the pile due to pile driving were minimal. This is expected since the top of the pile is unconstrained along its length and soil friction in the upper sections of the pile is minimal due to low overburdened pressures. This would also be the case when piles are placed in pre-bored holes and backfilled. For subsequent construction data and long term thermal and live load performance the critical stresses occur near the top of the piles. Therefore it is reasonable to reference all pile strain gage data to the point subsequent to pile driving and this is used as the reference point for all of the following sections. Residual stresses due to the manufacturing process of the piles are not accounted for, though if yielding is indicated in the data it will be due to absolute stresses in the piles. Throughout the construction process and first year of temperature data there has been no indication of pile yielding in these structures. All pile results are referenced to the gage location 0.5 m (20 in), 0.5 m (20 in) and 0.3 m (11.8 in) below the bottom of the abutment for the Middlesex Bridge, the East Montpelier Bridge and the Stockbridge Bridge, respectively. FEM results were used to extrapolate values to the bottom of the abutment. A summary of pile response for each step of construction are given in Table 7-3 for all three bridges. Maximum pile stresses recorded at the gage locations were 90, 114, 95 MPa (13.0, 16.5 and 13.8 ksi) for the Middlesex, East Montpelier and Stockbridge Bridges, respectively. The breakdown of these resultant stresses into axial forces and weak/strong axis bending moments is summarized in the following sections.

Table 7-3: Pile Response during Construction

			MIDDLESEX BRIDGE			EAST MONTPELIER BRIDGE			STOCKBRIDGE BRIDGE	
Component	**Phase**		**Hand Calculations**	**FEM Results**	**Field Data**	**Calculations**	**FEM Results**	**Field Data**	**Hand Calculations**	**Field Data**
Pile Axial Load	Lower Abutment	Axial Force	135.2 KN (30.4 Kips)	142.3 KN (32 Kips)		153 K N (34.4 Kips)	485 KN (109 Kips)		112 KN (25 Kips) (0-24.5 KN [0 to 5.5 Kips] from WWs)	133-147 KN (1) (30-33 Kips)
		Axial Stress	8.3 MPa (1.2 ksi)	9.0 MPa (1.30ksi)	1.4 MPa (0.2 ksi) (1) 10.3 MPa (1.5 ksi) (2)	9.7 MPa (1.4 ksi)		6.9 MPa (1ksi) (2)	4.8 MPa (0.7 ksi)	5.5 - 6.2 MPa (1) (0.8-0.9 ksi)
	Girders Placed	Axial Force	238.4 KN (53.6 Kips)	433.7 KN (97.5 Kips)			80 KN (18 Kips) (1) 142-160 KN (32-36 Kips) (2)		169 KN (38 Kips) (0-24.5 KN [0 to 5.5 Kips] from WWs)	320-337 KN(1) (72-75 Kips)
		Axial Stress	15.2 MPa (2.2 ksi)	27.6 MPa (4.0 ksi) (includes slab weight)	16.5 MPa (2.4 ksi) (1) 20.7 MPa (3.0 ksi) (2)		5.1 MPa (0.7 ksi)(1) 9.0-10.2 MPa (1.3-1.5 ksi)(2)	23.4 MPa (3.4 ksi) (1) 37.9 MPa (5.5 ksi)(2)	7.6 MPa (1.1 ksi)	14.5 -15.2 MPa (1) (2.1-2.2 ksi)
	Upper Abutment	Axial Force	553.4 KN (124.4 Kips)			663 KN (149 Kips)				
		Axial Stress	35.2 MPa (5.1 ksi)		27.6 MPa (4.0 ksi) (1) 31.7 MPa (4.6 ksi) (2)	41.8 MPa (6.1 ksi)				
	Open for Traffic	Axial Force	707.3 KN (159.0 Kips)	566.7 KN (127.4 Kips)		714 KN (161 Kips)	685-645 KN (154-151 Kips) (1) 872- 695KN(196-146 Kips) (2)		743 KN (167 Kips) (0-37.8 KN [0-8.5 Kips]from WWs)	650-787 KN (146- 177 Kips)
		Axial Stress	44.8 MPa (6.5 ksi)	35.8 MPa (5.2 ksi)	48.3 MPa (7.0 ksi) (1) 59.3 MPa (8.6 ksi) (2)	45.0 MPa (6.5 ksi)	43.6-42.7 MPa (6.3-6.2 Ksi) (1) 55.4-41.3 MPa (8.0-6.0 ksi) (2)	27.6 MPa (4.0 ksi) (1) 45.5 MPa (6.6 ksi) (2)	33.8 MPa (4.9 ksi)	28.3 - 34.5 MPa (4.1-5.0 ksi) (1)
Pile Bending Moment	Lower Abutment	Weak Axis Bending Moment	0.0 to 56.7 KN-m (0 0 to 41.8 k-ft) (due to wingwall weight)		2.4 KN-m (1.8 k-ft) (1) (9.2 KN-m (6.8 k-ft) (2)	0.0 to 14.7 KN-m (0.0 to 10.8 k-ft) (due to wingwall weight)		24,7 KN-m (18.2 k-ft) (1) 12.1 KN-m (8.9 k-ft) (2)	0.0 to 67.8 KN-m (0.0 to 50.0 k-ft) (due to wingwall weight)	
		Strong Axis Bending Moment			-11.1 KN-m(-8.2 k-ft)(1) -8.4 KN-m (-6.2 k-ft) (2)					
	Girders Placed	Weak Axis Bending Moment	0.0 to 56.7 KN-m (0 0 to 41.8 k-ft) (due to wingwall weight)	15.6 KN-m (11.5 k-ft)	57.1 KN-m (42.1 k-ft) (1) 22.5 KN-m (16.6 k-ft) (2)	0.0 to 14.7 KN-m (0.0 to 10.8 k-ft) (due to wingwall weight)	6.8 KN-m (5.0 k-ft) (1) 6.8 KN-m (5.0 k-ft) (2)	11.9 KN-m (8.8 k-ft) (1) 23.5 KN-m (17.3 k-ft) (2)	0.0 to 67.8 KN-m (0.0 to 50.0 k-ft) (due to wingwall weight)	75 KN-m (55 k-ft) (1) 96 KN-m (71 k-ft) (2)
		Strong Axis Bending Moment		0.2 KN-m (0.15 k-ft)	3.3/-6.1KN-m (2.4/-4.5k-ft) (1) 8.5/-11.5 KN-m (6.3/-8.5 k-ft) (2)			-10.3/21.8 KN-m (-7.6/16.1k-ft) (1) 24.7 KN-m (18.2 k-ft) (2)		57 KN-m (42 k-ft)(1) 5.7 KN-m (4.2 k-ft)(2)
	Open for Traffic [ψ]	Weak Axis Bending Moment	0.0 to 98.4 KN-m (0.0 to 72.6 k-ft) (up to 1103 KN-m (814 k-ft) if piles were welded to girders)	14.6 KN-m (10.8 k-ft)	34.8 KN-m (25.7 k-ft) (1) 15.2 KN-m (11.2 k-ft) (2)	0.0 to 29.9 KN-m (0.0 to 22 k-ft) (due to wingwall weight)	5.4 KN-m (4.0 k-ft) (1) 5.4 KN-m (4.0 k-ft) (2)	47.0 KN-m (34.7 k-ft) (1) -26.2 KN-m (-19.3 k-ft) (2)	0.0 to 105.8 KN-m (0.0 to 78.0 k-ft)	56 KN-m (41 k-ft) (1) 48 KN-m (35 k-ft) (2)
		Strong Axis Bending Moment		0.3 KN-m (0.20 k-ft)	8.5 KN-m (6.3 k-ft) (1) -15.2 KN-m (-11.2 k-ft) (2)		3.0 KN-m (2.0k-ft) (1) 3.0 KN-m (2.0k-ft) (2)	-11.8 KN-m (-8.7 k-ft) (1) 0.3 KN-m (0.2k-ft) (2)		45 KN-m (33 k-ft)(1) 23 KN-m (17 k-ft)(2)

(1) Abutment 1, (2) Abutment 2, My – Weak Axis Bending Moment, Mx – Strong Axis Bending Moment, * If no fixity was modeled at Abutment 2- deck connection when the deck concrete was placed, [ψ] At the top of pile, includes effects of shrinkage, temperature between the dates of bridge completion and data collection.

7.6.1 Axial Stresses and Forces

Table 7-3 shows the force and stresses in the piles resulting from axial forces for each construction phase. Hand calculations were simply performed by assuming that abutments were supported directly by the piles centered on the abutment. Concrete density assumed to be 2320 kg/m^3 (145 pcf) and lower/upper abutment defined by dimensions in the construction drawings. Wing walls were assumed to cantilever from the abutment after construction to obtain a maximum pile moment, though this moment would be nonexistent if the wing walls were directly supported by soil. At the Middlesex Bridge, the wingwalls were placed directly against the ground, while at the East Montpelier and Stockbridge Bridges wingwalls were formed tapering upwards from the soil. Total abutment weights and moments were divided by the number of piles under each abutment (5) assuming a fully rigid abutment. At the East Montpelier and Stockbridge Bridges, moment induced out of plane by the wingwalls (strong axis pile bending direction) would be expected to induce compression and tension stresses in individual piles rather than moment due to abutment rigidity. A linear distribution of force in each pile was assumed (maximum in outer piles) and these stresses were found to be minimal due to the distance between outer piles. Girder weights were calculated from cross sections and an additional 10 percent weight addition for miscellaneous materials such as braces and gusset plates. Girder weights were applied as pure axial load on the piles. Deck and upper abutment weights were applied similarly, assuming that the wet concrete load was distributed prior to reaching strength and therefore pinned connections between superstructure and substructure were maintained. Axial loads from ½ of the approach slab, topping slab and curbs were divided equally among piles.

At the Stockbridge Bridge, in order to calculate the axial loads on piles, a 2-span, single-supported, straight frame model was used. Effect of curvature on weight calculation was considered but the values were averaged while considering the effective loads on piles. This simple hand calculation showed that only approximately 37.5 percent of superstructure weight should be carried equally by the piles below both abutments while the remaining 62.5 percent is carried by the interior pier.

FEM results were taken directly from the models described previously, and account for fixity in the final construction stage. Field data interpretation assumed linear distributions of strain in the piles. While there was no indication of yielding (all observed strains here and in the first year of data show no divergence from linearity at each gage location), possible non-linearity of strain distributions across the sections could introduce some errors in bending data interpretation. These would be highest in construction when skin friction is still likely, but minimal for readings subsequent to construction. Axial strains are averages of all gages at a given pile depth.

During initial stages of loading it was found that axial pile strains varied with depth and were often much lower than expected. With time axial stresses stabilized and were reasonably close to predictions throughout the measured depths. The cause of this is likely initial support of the abutment by the underlying soil. Soil resistance diminishes under sustained loading and movements of the abutment and piles. Higher axial loads occurred in piles at the abutment with lower elevation, which was predicted by FEM (20 percent increase at lower abutment in the model) but not included in hand calculations. All pile axial forces at the end of construction were higher than predicted, within 5 percent at the East Montpelier and Stockbridge Bridges, but as much as 33 percent higher at the Middlesex Bridge. Possible explanations are variations in the material densities and construction tolerances in the bridge (such as deck and topping slab thickness), or non-linear strain distributions along the pile flanges even under low stress changes (linear distributions were assumed in analysis of field data). At the Stockbridge Bridge, axial loads on upstream piles were slightly higher than loads on downstream piles which were expected considering uneven distribution of self weight on the bridge superstructure resulting from curvature and different girder sizes for upstream and downstream ends of the bridge.

Overall, for all three bridges, the maximum axial stresses recorded ranged between 34.5-62.0 MPa (5.0-9.0 ksi). The average pile axial stresses at the end of construction were well predicted by simple hand calculations.

7.6.2 Weak Axis Bending

Weak axis bending moment at different stages of construction is given in Table 7-2. Field data weak axis moments were calculated through averaging opposing flange strain gage readings (Equation 7.1). Positive weak axis moment in piles was defined as having tension on the river side and compression on the approach span side of the piles.

$$M = \frac{E*\varepsilon*I_x}{y} \qquad \text{(Eq.7.1)}$$

where M = bending moment in the piles, E = modulus of elasticity of steel, ε = strain readings from field data, y = the distance between gage location and neutral axis of the steel cross section, I_x = moment of inertia of the cross section around weak axis.

Bending in piles was expected to be positive (toward backfill) in early stages of construction due to wing wall cantilevered weights. Moments from topping slab and curbs would counteract wing wall moments, but were neglected in the hand calculations since the degree of fixity was not directly established. Calculated values should be realized once forms were removed from the tapered walls at the East Montpelier and the Stockbridge Bridges, but would be an upper bound if soil under the wing wall provided any vertical support at the Middlesex Bridge.

Field data showed very low pile moments at the Middlesex Bridge when forms were removed from abutments, but values increased to the calculated value at one abutment when girders were placed. An interesting result at the abutment where the wing wall moment was not obtained is that, for the single data point during backfilling operations, pile moments increased slightly rather than decreasing as would be expected. It appears that compacting backfill near the wing walls may have relieved vertical soil support under the wall which had more influence on pile moments than the counteracting active soil pressures against the abutment. Pile moments were relatively unchanged when the cantilevered upper abutment was added, indicating that additional load was initially supported on the subsoil. Addition of the topping slab, curbs and guardrails once the structure was integral counteracted the wing wall induced moments. The reduction in moment was more significant in the abutment with less soil resistance below the wingwall as would be expected.

At the East Montpelier Bridge, field data showed the moments were approximately 20 percent lower than calculated. The tapered wingwalls reduced the expected pile moments. Pile moments as the bridge was open for traffic showed an unexpected change that indicated the bridge was deflecting towards Abutment 2 rather than exhibiting simple frame action (see Figure 7-11). This was also noted in load testing of this structure (reported elsewhere) in which live load resulted in apparent movement towards Abutment 2.

At the Stockbridge Bridge, the maximum weak axis bending moment was recorded prior to deck placement. This moment was generated by the cantilever wingwalls, backfilling and girder setting. It was approximately 40 percent higher than the calculated moment at this construction phase. However, for the subsequent construction phases, the weak axis bending moments decreased and reached to about one half of the calculated moments at the end of construction. Generally, the downstream piles exhibited slightly higher weak axis bending moments than the upstream piles (~7 KN-m (5 k-ft)).

Pile moments at the end of construction differed from FEM predictions for the Middlesex and East Montpelier Bridges. The maximum moment was 14.6 KN-m (10.8 k-ft) at the Middlesex Bridge (compared to maximum of 34.8 KN-m (25.7 k-ft) from the field data) whereas it was 5.4 KN-m (4.0 k-ft) at the East Montpelier Bridge (compared to a maximum of 47.0 KN-m (34.7 k-ft) from the field data). At the East Montpelier Bridge, if fixity was modeled between Abutment 2 and the end of deck while the remaining concrete deck was poured, higher moments will be obtained from FEMs. Figure 7-9 shows a deflected shape of an IAB with and without end fixity during construction.

Overall, for all cases, stresses from weak axis bending moment during construction was under 50.9, 55.1 and 70.4 MPa (7.4, 8.0 and 10.2 ksi), respectively for the Middlesex, East Montpelier and Stockbridge Bridges.

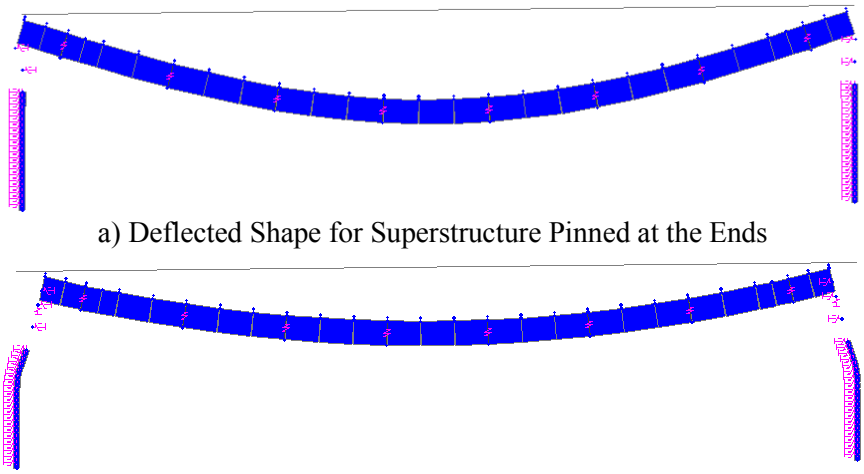

a) Deflected Shape for Superstructure Pinned at the Ends

b) Deflected Shape with Fixity between Superstructure and Substructure

Figure 7-9: Effects of Fixity between Girder and Pile during Construction

7.6.3 Strong Axis Bending

Field data weak axis moments were calculated through averaging opposing flange strain gage readings (Equation 7.2). Positive strong axis moment in piles was defined as having tension on the upstream side and compression on the downstream flange of the piles.

$$M = \frac{E*\varepsilon*I_y}{y} \qquad \text{(Eq.7.2)}$$

where M = bending moment in the piles, E = modulus of elasticity of steel, ε = strain readings from field data, y = the distance between gage location and neutral axis of the steel cross section, I_y = moment of inertia of the cross section around strong axis.

Strong axis moments should be negligible at the Middlesex Bridge due to the bridge symmetry. Field data indicated that strong axis bending of 15.2 kN-m (11.2 k-ft), which corresponds to a fairly low stress of 6.9 MPa (1.0 ksi) which occurred after pouring abutment concrete and backfilling. Strong axis moments were not consistent between piles, indicating P-delta effects of axial load acting through slight vertical offsets in the upper pile region due to construction tolerances. At the end of construction there was a shift in strong axis readings which corresponded to slight movement of the bridge abutment in the upstream direction.

At the East Montpelier Bridge, strong axis bending stresses in the piles reached values as high as 19.3 MPa (2.8 ksi) during partial deck placement, but were all less than 6.9 MPa (1.0 ksi) at the end of construction. Due to slight rotation and displacement of the abutment due to skew angle under dead and thermal loads the strong axis pile moments are difficult to predict but within expected ranges. This corresponds to simple calculation assumptions that strong axis

moments would be resolved as axial forces rather than bending moments on individual piles due to abutment rigidity.

At the Stockbridge Bridge, the strong axis bending moments differed between piles below different abutments and piles at the upstream end and downstream end. At selected locations such as upstream pile of Abutment 1, the maximum strong axis bending stress was 17.9 MPa (2.6 ksi) which corresponds to 57 KN-m (42 k-ft) though at most all other piles the values were much lower. This moment occurred before pouring the abutment concrete and decreased for the subsequent construction phases. The maximum strong axis bending moment on downstream piles was only 24 KN-m (18 k-ft). The difference between strong axis bending moments of upstream and downstream piles could be a result of the different wingwall geometries.

Overall, for all cases, stresses from strong axis bending moment was under 6.9, 19.3 and 18.0 MPa (1.0, 2.8 and 2.6 ksi), respectively for the Middlesex, East Montpelier and Stockbridge Bridges.

7.7 Backfill Pressures during Construction

Pressure cells were included in the abutment and wingwall and were referenced to the pressure reading when formwork was removed. At the Stockbridge Bridge, the reference point was initial installation of gages due to lack of data before the backfilling process. However, data from other bridges showed that the pressure generated during abutment concrete pour and formwork installation is somewhat relieved when the formwork is removed. It is important to note that pressure readings can fluctuate significantly due to thermal variations in the cell fluid and that this is not accounted for in manufacturer temperature correction factors. These effects have been accounted for by the inclusion of a reference pressure cell at each site placed in comparable backfill materials and monitored for one year. Long term monitoring results from reference earth pressure cells are shown in Figure 7-10. Corrections have been made to all pressure cells to match this reference cell data. No correction was necessary prior to backfilling against the earth pressure cells.

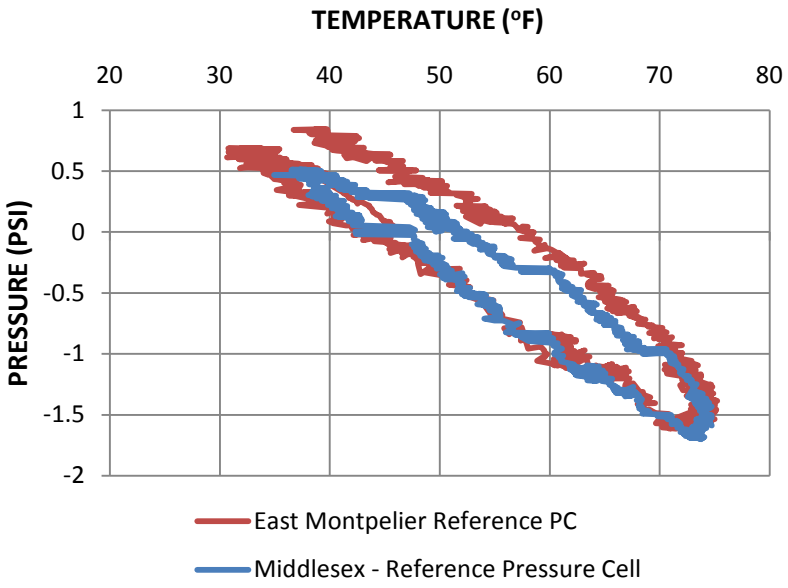

Figure 7-10: Long-term Monitoring Data for Reference Pressure Cells

In the field, pressures were measured only over the lower abutment placement. During backfill operations there is some variability in the pressure induced against the abutments. Maximum earth pressure immediately after backfilling to the construction joint elevation was 10.4 and 17.9 KPa (1.5 psi and 2.6 psi), respectively at the Middlesex and East Montpelier Bridges. At this point of the construction, the estimated at-rest pressures (based on k_o=0.40) at the top, center and bottom gage locations were approximately 1.4, 8.3 and 15.2 KPa (0.2, 1.20 and 2.20 psi) and 2.8, 8.3, 11.7 KPa (0.4, 1.2 and 1.7 psi), respectively at the Middlesex and East Montpelier Bridges. The Stockbridge Bridge didn't have a recorded data at this point of construction phase. For the subsequent final phase of construction, maximum earth pressures recorded on abutments were 28.3, 22.8 and 36.6 KPa (4.1, 3.3 and 5.3 psi) at the Middlesex, East Montpelier and Stockbridge Bridges, respectively. It should be noted that these pressures resulted from both the construction activity (backfilling the upper abutment, deck placement, etc.) and also the changes in ambient temperatures after the abutments and decks had been placed.

At the Middlesex and East Montpelier Bridges, the maximum pressures on wingwalls during backfilling and at the end of construction were 0.7 and 9.0 KPa (0.1 and 1.3 psi), respectively. However, at the Stockbridge Bridge, maximum pressures on wingwalls ranged from 78 to 200 KPa (11 to 29 psi) at the end of construction. All pressures include a combination of construction load and temperature effects, the latter being much greater at Stockbridge due to the ambient temperatures when deck was cast. Even the high pressure on the wingwall was a small percentage of passive earth pressures (based on k_p=5.8) which would be as high as 760 KPa (110 psi) at the bottom gage locations.

The temperature correction was a significant component of the results changing pressures from raw data by approximately 11.7, 14.5 and 20.7 KPa (1.7, 2.1 and 3.0 psi) at the Middlesex, East Montpelier and Stockbridge Bridges. In the following 12 months of Vermont bridge field data, earth pressure fluctuations on the abutment were in the range of 55, 83 and 48 KPa (8 psi, 12 psi and 7 psi) at the Middlesex, East Montpelier and Stockbridge Bridges. The earth pressure on wingwalls for the same time interval fluctuated by a maximum of 28, 35 and 152 KPa (4,5 and 22 psi), respectively for the Middlesex, East Montpelier and Stockbridge Bridges. Therefore, even though construction pressures were less than earth pressures generated in the long term, the studies that do not account for initial construction pressures can underestimate the pressures applied to the abutment.

For the Middlesex and East Montpelier Bridges, FEM results considering construction sequence resulted in only active pressures behind the abutments with maximum value of maximum 38.6 KPa (5.6 psi) at the bottom of abutments when the abutments were backfilled completely.

7.8 Abutment Rotation during Construction

The tiltmeters at the Middlesex Bridge were installed after the deck pour. The maximum abutment rotation at this bridge was 0.01 degrees at Abutment 1 and 0.04 degrees at Abutment 2 toward the river from the end of the deck pour until the bridge was open for traffic. These rotations were a combination of dead load applied after deck concrete was set (topping slab, curb and guardrails) as well as the net superstructure shrinkage and contraction due to temperature decrease.

At the East Montpelier Bridge, the tiltmeters were installed prior to deck placement but after setting girders. Therefore, readings included the effects of initial and final deck placement but not the backfilling of lower abutments and setting girders. The field readings showed unexpected abutment rotations, but confirmed results reported on weak axis pile moments and live load testing. The initial deck pour (half pour that had been removed in order to strength the superstructure) resulted in 0.05 degree rotation towards the river at the Abutment 2, while Abutment 1 rotation was constant. Subsequent dead (complete deck pour) and thermal load through opening for traffic switched Abutment 2 rotation toward the approach slab (up to 0.22 degrees) while Abutment 1 rotated toward the river as expected (up to 0.17 degrees) (see Figure 7-11). The results indicated that construction tolerances may play a role. If Abutment 2 piles had initial top deflections or misalignment toward the approach slab (as indicated previously due to wing wall moment and weak axis moment data), P-Δ effects from dead load could result in rotation in this direction under additional gravity load. This highlights the difficulty of accurately

predicting precise construction induced stresses in piles due to the influence of construction tolerances in pile placement.

At the Stockbridge Bridge, the tiltmeters were installed after the bridge construction was completed; therefore, there were no readings available to observe the abutment rotations during different construction stages.

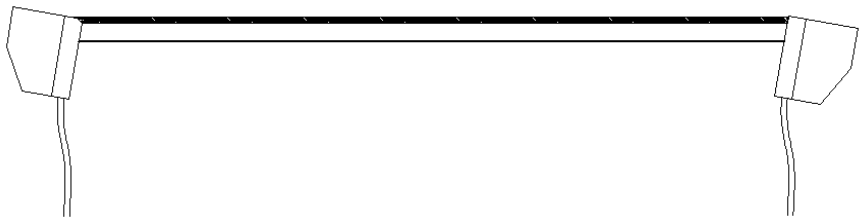

Figure 7-11: Shift of the East Montpelier Bridge towards Abutment 2 for Vertical Loads

7.9 Girder Strains during Construction

During construction, girder strains were monitored in order to estimate the stresses induced at the girder flanges. At the Middlesex and East Montpelier Bridges, field readings were available during installation of girder strain gages and at the completion of construction. The Stockbridge Bridge had an additional reading following the deck placement but prior to abutment backfilling.

In this study, the analysis of girders focused on the resultant stresses instead of axial loads and weak axis bending moments. An accurate estimation of the axial loads and weak axis bending moments from the field data wasn't possible since axial loads and weak/strong axis bending moments were coupled to both temperature and dead loads effects.

At the Middlesex Bridge, the maximum girder stresses were 170.3 MPa (24.7 ksi) (compressive – top flange) and 69.0 MPa (10.0 ksi) (tensile – bottom flange) at the midspan. At the bridge ends, maximum stresses were 69.0 MPa (10.0 ksi) (compressive – top flange) and 15.9 MPa (2.3 ksi) (tensile – bottom flange). The maximum stress values include stresses from the combination of axial loads as well as weak and strong axis bending moments, which cannot be separated in the data. The calculations for maximum stress were referenced to the initial reading following the gage installation which took place after girders were set at abutments and, therefore, didn't account for the stresses resulted from self weight of the girders. The FEM results for bridge midspan showed a maximum compressive bending stress of 51.0 MPa (7.4 ksi) and 172.5 MPa (25.0 ksi) after setting girders and concrete deck placement (includes the girder weight), respectively.

At the East Montpelier Bridge, the maximum stresses were as high as 183.4 MPa (26.6 ksi) (compressive – top flange) and 112.0 MPa (16.2 ksi) (tensile – bottom flange) at the midspan whereas it was 39.3 MPa (5.7 ksi) (compressive – top flange) and 29.0 MPa (4.2 ksi) (tensile – bottom flange) at the bridge ends. Since the gages at the East Montpelier Bridge were installed before the girders were set at the abutments, the resultant stresses included the girder weight as well. It is interesting to note that the East Montpelier Bridge showed a limited degree of fixity at the abutment that was cast prior to stoppage of construction when the remaining deck was placed. The stresses recorded by gages on this side of the bridge were slightly higher (at most 20.7 MPa [3 ksi]) than the stresses recorded at the far end of the bridge (Abutment 1). The FEM results showed a maximum compressive bending stress of 39.8 MPa (5.8 ksi) and 177.7 MPa (25.8 ksi) after girder setting and concrete deck placement (includes the girder weight), respectively.

At the Stockbridge Bridge, gages were installed after the girders were set on the abutments. Maximum girder stresses recorded at the top of pier were 89.7 MPa (13.0 ksi) (compressive - bottom flange) and 62.1 MPa (9.0 ksi) (tensile – top flange). At the midspan of bridge spans, they were 83.4 MPa (12.1 ksi) (compressive – top flange) and 26.2 MPa (3.8 ksi) (tensile – top flange). The maximum stresses following the deck and abutment placement were 68.9 MPa (10.0 ksi) (compressive - bottom flange) and 62.0 MPa (9.0 ksi) (compressive – top flange) for the same locations. Thus, it can be concluded that the stresses resulting from backfilling, paving the roadway, installation guardrails and temperature difference between 05/13/2009 and 09/15/2009 were on the order of 20.7 MPa (3.0 ksi) or less (compressive).

In all three bridges, girders were set after the placement of the lower abutment concrete. Girders were pin ended at this stage of construction (assuming anchor rods at the Middlesex Bridge and elastomeric bearing pads at the East Montpelier Bridge allowed free rotation). This allows for simple hand calculations of the bending moments along the span. Generally, hand calculations were consistent with the FEM results. The calculated moments and FEM results didn't include the superimposed dead loads such as curbs, paving or guardrails. Table 7-4 shows the maximum moment values from hand calculations and FEM models.

Table 7-4: Strong Axis Bending Moments from Hand Calculations and FEM Results

		Middlesex Bridge		East Montpelier Bridge	
Component	Construction Phase	Hand Calculations (2D assumptions)	FEM Results (3D)	Hand Calculations (2D assumptions)	FEM Results (3D)
Girder Strong Axis Bending Moment	Girders Placed	1013 kN-m (747.0 k-ft)	1006 kN-m (742.0 k-ft)	673 kN-m* (496 k-ft)	791 kN-m* (583 k-ft)
	Deck and Upper Abutment Placement	3421 kN-m (2523 k-ft)	3404 kN-m (2511 k-ft)	3268 kN-m* (2410 k-ft)	2267 kN-m$^{\alpha}$ (2601 k-ft)

* Includes the weight of additional cross bracings between girders

$^{\alpha}$ Doesn't account for continuity at Abutment 2 during deck placement.

Finally, it should be noted that, in the field, both temperature loads and dead loads acted on the girders once they were set on the abutments. FEM results that accounted for dead loads only showed negligible axial loads on the girders (15.2 kN [3.9 kips] at the Middlesex Bridge and 17.4 kN [3.4 kips] at the East Montpelier Bridge).

7.10 Formwork Pressures during Construction

The inclusion of pressure cells embedded in the formwork provided some information regarding formwork pressures during the placement of the abutment concrete. At the Middlesex Bridge abutments had individual placement depths of 2.3 m (7.55 ft) and 1.7 m (5.6 ft) for the bottom and top abutment placement, respectively. At the East Montpelier Bridge depths were 1.9 m (6.2 ft) and 2.0 m (6.6 ft). In both bridges, pressure cells were only placed in the lower abutment. ACI347-04 Equation 2.2 would predict maximum formwork pressures ranging from 17.9 to 26.2 KPa (2.6 psi to 3.8 psi) depending on placement rate and concrete temperature variability at the abutments. Static head from ACI 347-04 Equation 2.1 would result in expected based on 2320 kg/m^3 (145 psf) times depth is 9.0, 27.6, 45.5 KPa (1.3, 4.0, 6.6 psi) for top, middle and bottom cells respectively during placement of the bottom section of abutment. Data (4.9-9.0 KPa [0.7-1.3 psi], 9.0-17.9 KPa [1.3-2.6 psi], 11.7-33.1 KPa [1.7-4.8 psi]) shows variability, likely due to partial setting of initial layers at the time of placement of the final concrete. Peak localized pressure at two gages were greater than calculated values, but well within the safety factor used in form work design and well below static pressure at the bottom gages. Thermal changes during construction were 7.5 ^{o}C (13.5 ^{o} F) within the formwork. At the East Montpelier Bridge expected static head based on 2320 kg/m^3 (145 psf) times depth is 6.9, 20.7, 34.5 KPa (1.0, 3.0, 5.0 psi) for top, middle and bottom cells respectively. Data (12.4-17.9 KPa [1.8-2.6 psi], 14.5-27.6 KPa [2.1-4.0 psi], 17.3-53.1 KPa [2.5-7.7 psi]) shows variability and lower pressures than static pressures would indicate. Thermal changes during construction were 7.5 ^{o}C (13.5 ^{o} F) in Abutment 2 but 13.0 ^{o}C (23.4 ^{o}F) at Abutment 1 within the formwork. It is interesting to note that the higher form pressures were all in Abutment 1 which had higher heat during placement. No reading was taken during concrete pours at the Stockbridge Bridge.

7.11 Conclusions

This study made use of field monitoring, FEM and hand calculations to estimate the stresses and forces generated on different parts of integral abutment bridges during construction. The results presented here are specific to integral abutment bridges of modest length, constructed with piles oriented for weak axis bending in the direction of traffic and with minimal continuity provided between the girders and substructure during construction until the upper abutments were placed.

The maximum pile stresses recorded at the gage locations were 90, 114, 95 MPa (13.0, 16.5 and 13.8 ksi) for the Middlesex, East Montpelier and Stockbridge Bridges, respectively. These stresses primarily resulted from weak axis bending moments and axial forces. Pile strong axis moments appear to be influenced by construction tolerances and bridge geometries, but ultimately resulted in maximum stresses of 7, 21 and 18 MPa (1.0, 3.0 and 2.6 ksi) in the Middlesex, East Montpelier and Stockbridge piles, respectively. Although accuracy between the hand calculations, FEM models and field results were poor for initial construction stages, the difference in results were within reasonable limits by the end of construction. This appears to be due to dissipation of soil pressures with time and/or re-loading. In a few instances, the field data showed unexpected results. For instance, at the Middlesex Bridge, pile weak axis moments differ significantly at the two ends of the bridges at the end of construction, and this would be very difficult to predict in the design process. Instead, upper and lower bounds of construction stresses when checking pile yielding could be considered. When long U shaped wingwalls are used, high pile moments from construction loads could be mitigated and construction forces estimated more accurately if wingwalls are isolated from the abutment or provided in-line with the abutment.

The earth pressures at the abutments and wingwalls were limited (on the order of at-rest earth pressures or slightly higher) except from the earth pressures at the Stockbridge Bridge's wingwalls which had pressures as high as 200 KPa (29 psi).

Until the concrete deck hardened, there was no rotational fixity between superstructure and abutment. This construction method limited the abutment rotations during construction. At the East Montpelier Bridge, the abutment rotations and weak axis pile moments indicated an unexpected movement of the bridge towards Abutment 2. This may be due to P-Δ effects resulting from pile construction tolerances. While these effects did not significantly change construction stresses, they do point out the difficulty in making accurate predictions of pile stresses during construction.

The girder stresses were monitored before the deck placement and after completion of bridges. The maximum compressive stresses recorded were 170.3, 183.4 and 89.7 MPa (24.7 ksi, 26.6 ksi and 13.0 ksi) respectively for the Middlesex, East Montpelier and Stockbridge Bridges. Due to difference in installation scheduling, the East Montpelier reading included the self weight of the girders whereas the others did not. These results were compared to hand calculations and FEM results.

For construction methods used in these IAB's thermal effects are only accounted for in the post construction thermal load design. However, if girder and pile connectivity is introduced prior to abutment placements the dead load thermal effects during construction should be explicitly considered in the design process. As an example, it should be noted that, based on the FEM results of these bridges, girders rigidly attach to the piles during construction would induce

very large pile bending moments when dead load is applied (beyond the pile yield stresses for the simple span structures). The degree of anchor bolt tightening when the deck is poured could affect this. It is interesting to note that in past construction some states have welded the girder directly to the pile, while others specify that anchor bolts should be loosened prior to applying additional dead load. There does not appear to be any significant differences in design procedures to account for this potentially significant change in construction load distribution.

8 SUMMARY

Three IABs in Vermont, US have been instrumented during construction and are currently being monitored with results compared to FEM models. Monitoring of the bridges focused primarily on the seasonal response induced by thermal loading of the bridges. However, the data was also collected during stages of construction to evaluate the forces and stresses developed in the bridges. In addition, static live-load testing of the bridges was conducted to gain information on the live-load carrying characteristics of these bridges.

The bridges instrumented and monitored are the Middlesex Bridge (a straight bridge with 43 m-141 ft- span), the East Montpelier Bridge (a 15 degree skew bridge with 37 m - 121 ft -span), and the Stockbridge Bridge (a 68 m (221 ft) two span curved bridge with 11.25 degrees of curvature). The bridges are instrumented with 83, 89, and 131 gages, respectively. Each bridge was constructed to replace an existing aging jointed structure. Abutments are supported using deep pile foundations for the three bridges. In addition, the Stockbridge Bridge has an interior pier at the center of the bridge. The bridges have a concrete deck supported on 5 straight or curved steel girders depending on the bridge alignment. The deep foundations consist of HP steel piles orientated with their weak axis perpendicular to the roadway alignment.

The permanent field monitoring system includes gages that were installed during construction, automated data acquisition system (dataloggers, multiplexers) and remote access for downloading data. Data is currently being collected by the automated monitoring system from each gage at 6 hour intervals. Although the bridge design philosophy is similar for all three bridges (steel composite superstructure, monolithic abutment-deck connection, single row of HP pile foundation, etc.), the bridges are distinct by virtue of their geometry – straight, skewed and curved alignment. During instrumentation planning, the bridge alignment was one of the criteria that defined the gage locations and instrumentation plans. Other criteria were significance/criticality of the response monitored and degree of redundancy required for verifying readings and to account for the possibility of some gages malfunctioning. Bridge instrumentation was primarily planned to measure the bridge substructure response, but girder stresses at selected locations along the superstructure were also of interest. The types of gages installed include earth pressure cells, inclinometers, tiltmeters, displacement transducers, thermistors and strain gages at three different locations (pile, girder, and concrete pier column). Passive and active earth pressures behind abutments and wingwalls, strains in piles and girders, abutment movements (longitudinal, transverse and rotational) and deformations in the piles are monitored by means of these instruments.

The analytical models of the bridges have been generated concurrently with the instrumentation and monitoring of the bridges. Three-dimensional nonlinear FEM were developed to analyze the bridges using SAP2000. The models included all relevant elements of the bridge superstructure (girders, cross diaphragms, concrete deck) and the bridge substructures

(abutments, wingwalls, pier and its foundation, piles). Soil backfill was modeled using nonlinear springs. Also, the soil surrounding piles was modeled using nonlinear springs. Geometric nonlinearity and material nonlinearity (when required) was included in all analyses.

Bridge behavior during construction was investigated by taking discrete readings right after the gage installation and at the later stages. The field monitoring results were generally in good agreement with simple hand calculations and FEM results. The overall bridge response was influenced by construction method, construction tolerances and bridge geometries. The construction method (No rotational fixity between superstructure and abutment until concrete deck hardened) limited the forces transferred to bridge substructure. Field data showed a few unexpected results such as movement of East Montpelier Bridge towards Abutment 2 and asymmetric abutment response at the Middlesex Bridge, but in general was estimated well from simple calculations. However, discrepancies pointed out the difficulty in making accurate predictions of forces and stresses during construction. Therefore, upper and lower bounds of construction stresses when checking pile yielding should be considered.

Following construction of the bridges, live-load tests were conducted using loaded dump trucks in order to understand bridge response under static truck loads. Three loaded dump trucks were located at several different positions on each lane of the bridges to record the significant response of the bridge components. A set of readings was collected for each truck position. The data was subsequently used to calibrate FEM's of the Middlesex and East Montpelier Bridges. The superstructure response showed signs of rotational fixity at the ends of bridges and the results were in line with the FEM predictions. The accuracy of the analysis for superstructure response was dependent on methods of temperature correction and neutral axis depth calculation specific for all girder cross sections and for all truck positions. The substructure response under live load was minimal. The timing of the test influenced the bridge substructure response. Since the load tests were conducted during the cold season (December, 2009), the bridges were in a contracted state compared to their initial condition during construction. The accuracy of results obtained from FEMs and field data gave the confidence that these FEMs can be used to predict the behavior for other truck load positions needed to compute lateral load distribution factors.

A final report will be prepared after the monitoring phase of the project is completed. This final report will include the evaluation of long term seasonal data.

APPENDIX A. GAGE LABELING

Gage labeling is not directly related to abutment numbers for a couple of logistical reasons. First, instrumentation planning took place prior to development of structural drawings for two bridges. Therefore, final labeling of Abutment 1 and Abutment 2 was not determined, nor were compass directions (North-South-East-West) known by the research team. Gage labels starting with "1" indicated the abutment nearest the datalogger, which was typically the more heavily instrumented abutment to minimize cable lengths. Second, during construction a few gages were interchanged due to contractor preference for multiplexer locations. This avoided the need for splicing of predetermined cable lengths for these gages. For these reasons labeling of gages are not always consistent with the directions and numbering indicated in the structural drawings. This section describes the final as-built locations of gages for each bridge. Gages are labeled according to directions and abutment numbering shown in Figure A-0-1, Figure A-0-2 and Figure A-0-3. Differences from structural drawing callouts are noted. Gage labels are described per structural drawing position in Appendix B, along with channel locations in each multiplexer and datalogger.

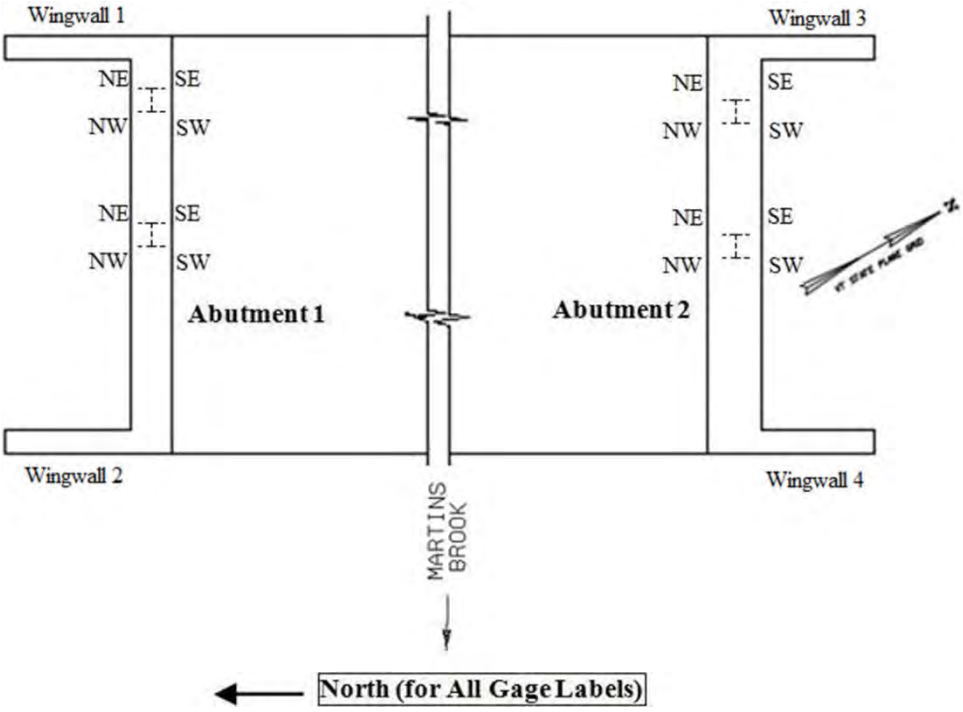

*Abutment numbering is consistent with structural drawings

Figure A-0-1: Gage Labeling for Middlesex Bridge

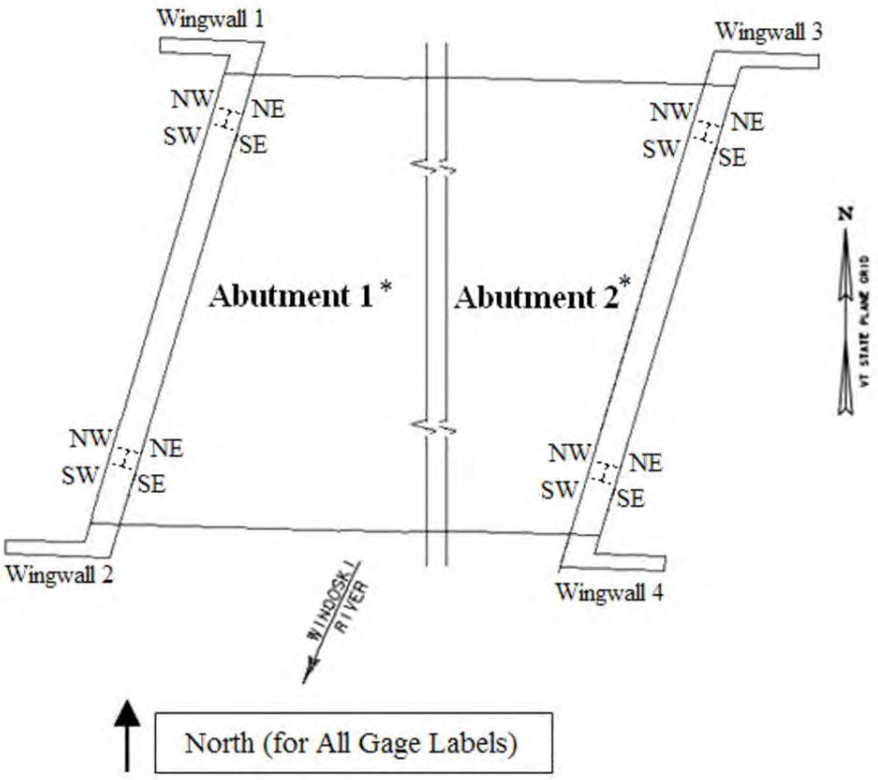

*Abutment numbering is consistent with structural drawings

Figure A-0-2: Gage Labeling for East Montpelier Bridge

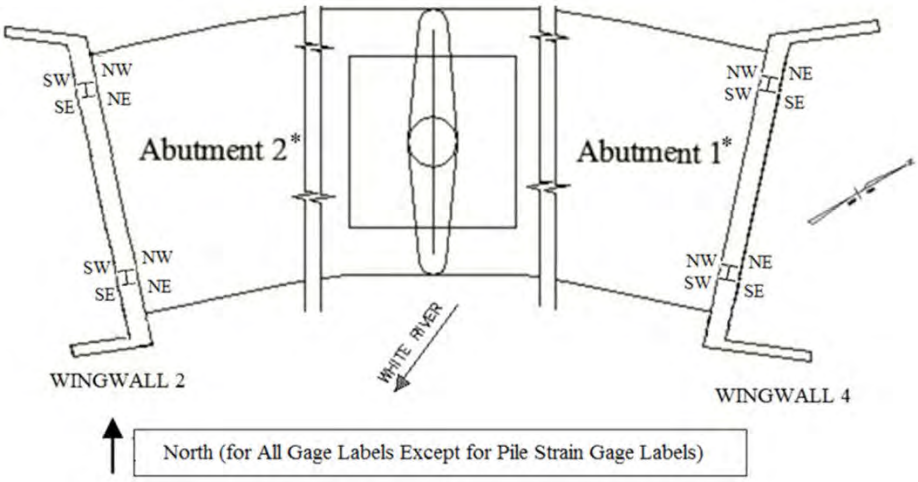

*Abutment numbering is NOT consistent with structural drawings

Figure A-0-3: Gage Labeling for Stockbridge Bridge

APPENDIX B. INSTRUMENTATION CHANNEL LISTS & GAGE LOCATIONS

As noted in Appendix A, gage labeling is not always consistent with bridge orientation and structural drawing callouts. This section describes the final as-built locations of gages for each bridge. Gages are labeled according to directions and abutment numbering presented in Appendix A. Gage labels are fully described by data acquisition multiplexer channel number and descriptive location related to structural drawings.

Data acquisition system is composing of 16-channel multiplexers and 6-channel dataloggers. Each VW gage is connected to a single multiplexer channel while each MEMS gage (biaxial gage) is connected to two different channels.

a) Middlesex Bridge

As-built gage information for the Middlesex Bridge is given in Table B-1 and Table B-2 for Abutment 1and Abutment 2 multiplexers, respectively. Figures showing gage locations without labeling are found in Section 3.2.

Table B-1: Abutment 1 Multiplexer Channel List and Gage Locations

Mux	Channel	Gage Label	Gage Type	Model	Location
1	1	CM-1ET	Displacement Transducer	4420	Abutment 1, Upstream, Transverse, 1.95 m (6.43 ft) below construction joint
1	2	CM-1E	Displacement Transducer	4420	Abutment 1, Upstream, Longitudinal, 1.95 (6.43 ft) below construction joint
1	3	P-1CT	Earth Pressure Cell	4815	Abutment 1, Center of Abutment, 1.9 m (6.2 ft) above the bottom of abutment,
1	4	P-1CM	Earth Pressure Cell	4815	Abutment 1, Center of Abutment, 1.1 m (3.6 ft) above the bottom of abutment,
1	5	P-1CB	Earth Pressure Cell	4815	Abutment 1, Center of Abutment, 0.3 m (1.0 ft) above the bottom of abutment,
1	6	P-1EM*	Earth Pressure Cell	4815	Abutment 1, Downstream, 1.1 m (3.6 ft) above the bottom of abutment, 0.8 m (2.6 ft) away from abutment-wingwall connection
1	7	P-1EB1*	Earth Pressure Cell	4815	Abutment 1, Downstream, 0.3 m (1.0 ft) above the bottom of abutment, 0.8 m (2.6 ft) away from abutment-wingwall connection
1	8	P-1WM1*	Earth Pressure Cell	4815	Abutment 1, Upstream, 1.1 m (3.6 ft) above the bottom of abutment, 0.8 m (2.6 ft) away from abutment-wingwall connection
1	9	P-1WB1*	Earth Pressure Cell	4815	Abutment 1, Upstream, 0.3 m (1.0 ft) above the bottom of abutment, 1.0 m (3.3 ft) away from abutment-wingwall connection
1	10	SGG-1E-TE	Girder Strain Gage	4050	Upstream Girder, Upstream-Top Flange, 4.5 m (14.75 ft) from the end of steel girder section at Abutment 1.
1	11	SGG-1E-BE	Girder Strain Gage	4050	Upstream Girder, Upstream-Bottom Flange, 4.5 m (14.75 ft) from the end of steel girder section at Abutment 1.
1	12	SGG-1E-TW	Girder Strain Gage	4050	Upstream Girder, Downstream-Top Flange, 4.5 m (14.75 ft) from the end of steel girder section at Abutment 1.
1	13	SGG-1E-BW	Girder Strain Gage	4050	Upstream Girder, Downstream-Bottom Flange, 4.5 m (14.75 ft) from the end of steel girder section at Abutment 1.
1	14	SGG-1M-TE	Girder Strain Gage	4050	Interior Girder, Upstream-Top Flange, 4.5 m (14.75 ft) from the end of steel girder section at Abutment 1.
1	15	SGG-1M-BE	Girder Strain Gage	4050	Interior Girder, Upstream-Bottom Flange, 4.5 m (14.75 ft) from the end of steel girder section at Abutment 1.
1	16	SGG-1W-TE	Girder Strain Gage	4050	Downstream Girder, Upstream-Top Flange, 4.5 m (14.75 ft) from the end of steel girder section at Abutment 1.

* Gage label is not consistent with other callouts. Gage locations switched to match cable length with actual multiplexer location.

Table B-1: Abutment 1 Multiplexer Channel List and Gage Locations (cont.)

Mux	Channel	Gage Label	Gage Type	Model	Location
2	1	SGG-1W-BE	Girder Strain Gage	4050	Downstream Girder, Upstream-Bottom Flange, 4.5 m (1.6 ft) from the end of steel girder section at Abutment 1.
2	2	SGG-0E-TE	Girder Strain Gage	4050	Upstream Girder, Upstream-Top Flange, 22.7 m (74.5 ft) from the end of steel girder section at Abutment 1.
2	3	SGG-0E-BE	Girder Strain Gage	4050	Upstream Girder, Upstream-Bottom Flange, 22.7 m (74.5 ft) from the end of steel girder section at Abutment 1.
2	4	SGG-0E-TW	Girder Strain Gage	4050	Upstream Girder, Downstream-Top Flange, 22.7 m (74.5 ft) from the end of steel girder section at Abutment 1.
2	5	SGG-0E-BW	Girder Strain Gage	4050	Upstream Girder, Downstream-Bottom Flange, 22.7 m (74.5 ft) from the end of steel girder section at Abutment 1.
2	6	TM-1M	Tiltmeter (Uniaxial)	6300	Abutment 1, Center of Abutment, 0.5 m (1.6 ft) from the bottom of middle girder.
2	7	IN-1E-1	Inclinometer (Uniaxial)	6300	Abutment 1, Pile below Girder 2, Flange facing towards the centerline of the roadway, 0.0-0.6 m (0-2 ft) below the bottom of Abutment 1.
2	8	IN-1E-2	Inclinometer (Uniaxial)	6300	Abutment 1, Pile below Girder 2, Flange facing towards the centerline of the roadway, 0.6-1.5 m (2-5 ft) below the bottom of Abutment 1.
2	9	IN-1E-3	Inclinometer (Uniaxial)	6300	Abutment 1, Pile below Girder 2, Flange facing towards the centerline of the roadway, 1.5-2.7 m (5-9 ft) below the bottom of Abutment 1.
2	10	IN-1E-4	Inclinometer (Uniaxial)	6300	Abutment 1, Pile below Girder 2, Flange facing towards the centerline of the roadway, 2.7-4.0 m (9-13 ft) below the bottom of Abutment 1.
2	11	IN-1E-5	Inclinometer (Uniaxial)	6300	Abutment 1, Pile below Girder 2, Flange facing towards the centerline of the roadway, 4.0-5.2 m (13-17 ft) below the bottom of Abutment 1.
2	12	IN-1W-1	Inclinometer (Uniaxial)	6300	Abutment 1, Pile below Girder 4, Flange facing towards the centerline of the roadway, 0.0-0.6 m (0-2 ft) below the bottom of Abutment 1.
2	13	IN-1W-2	Inclinometer (Uniaxial)	6300	Abutment 1, Pile below Girder 4, Flange facing towards the centerline of the roadway, 0.6-1.5 m (2-5 ft) below the bottom of Abutment 1.
2	14	IN-1W-3	Inclinometer (Uniaxial)	6300	Abutment 1, Pile below Girder 4, Flange facing towards the centerline of the roadway, 1.5-2.7 m (5-9 ft) below the bottom of Abutment 1.
2	15	IN-1W-4	Inclinometer (Uniaxial)	6300	Abutment 1, Pile below Girder 4, Flange facing towards the centerline of the roadway, 2.7-4.0 m (9-13 ft) below the bottom of Abutment 1.
2	16	P-R	Reference Pressure Cell	4815	Under Approach Slab on Abutment 1 side, Facing towards the centerline of the roadway, 6 m (19.7 ft) away from the bridge end, 3.3 m (10.8 ft) away the centerline of roadway (towards upstream), 1.0 m (3.0 ft) below approach slab,

Table B-1: Abutment 1 Multiplexer Channel List and Gage Locations (cont.)

Mux	Channel	Gage Label	Gage Type	Model	Location
3	1	SG-1M-1NE	Pile Strain Gage	4000	Middle Pile (below Girder 3), 0.5 m (1.6 ft) from bottom of Abutment 1 77 mm (3.0 in) from the edge of flange.
3	2	SG-1M-1SE	Pile Strain Gage	4000	Middle Pile (below Girder 3), 0.5 m (1.6 ft) from bottom of Abutment 1 77 mm (3.0 in) from the edge of flange.
3	3	SG-1M-1SW	Pile Strain Gage	4000	Middle Pile (below Girder 3), 0.5 m (1.6 ft) from bottom of Abutment 1 77 mm (3.0 in) from the edge of flange.
3	4	SG-1M-1NW	Pile Strain Gage	4000	Middle Pile (below Girder 3), 0.5 m (1.6 ft) from bottom of Abutment 1 77 mm (3.0 in) from the edge of flange.
3	5	SG-1M-3NE	Pile Strain Gage	4000	Middle Pile (below Girder 3), 1.5 m (4.9 ft) from bottom of Abutment 1 77 mm (3.0 in) from the edge of flange.
3	6	SG-1M-3SE	Pile Strain Gage	4000	Middle Pile (below Girder 3), 1.5 m (4.9 ft) from bottom of Abutment 1 77 mm (3.0 in) from the edge of flange.
3	7	SG-1M-3SW	Pile Strain Gage	4000	Middle Pile (below Girder 3), 1.5 m (4.9 ft) from bottom of Abutment 1 77 mm (3.0 in) from the edge of flange.
3	8	SG-1M-3NW	Pile Strain Gage	4000	Middle Pile (below Girder 3), 1.5 m (4.9 ft) from bottom of Abutment 1 77 mm (3.0 in) from the edge of flange.
3	9	SG-1E-1NE	Pile Strain Gage	4000	Upstream Pile (below Girder 1), 0.5 m (1.6 ft) from bottom of Abutment 1 77 mm (3.0 in) from the edge of flange.
3	10	SG-1E-1SE	Pile Strain Gage	4000	Upstream Pile (below Girder 1), 0.5 m (1.6 ft) from bottom of Abutment 1 77 mm (3.0 in) from the edge of flange.
3	11	SG-1E-1SW	Pile Strain Gage	4000	Upstream Pile (below Girder 1), 0.5 m (1.6 ft) from bottom of Abutment 1 77 mm (3.0 in) from the edge of flange.
3	12	SG-1E-1NW	Pile Strain Gage	4000	Upstream Pile (below Girder 1), 0.5 m (1.6 ft) from bottom of Abutment 1 77 mm (3.0 in) from the edge of flange.
3	13	SG-1E-2NE	Pile Strain Gage	4000	Upstream Pile (below Girder 1), 1.0 m (3.3 ft) from bottom of Abutment 1 77 mm (3.0 in) from the edge of flange.
3	14	SG-1E-2SE	Pile Strain Gage	4000	Upstream Pile (below Girder 1), 1.0 m (3.3 ft) from bottom of Abutment 1 77 mm (3.0 in) from the edge of flange.
3	15	SG-1E-2SW	Pile Strain Gage	4000	Upstream Pile (below Girder 1), 1.0 m (3.3 ft) from bottom of Abutment 1 77 mm (3.0 in) from the edge of flange.
3	16	SG-1E-2NW	Pile Strain Gage	4000	Upstream Pile (below Girder 1), 1.0 m (3.3 ft) from bottom of Abutment 1 77 mm (3.0 in) from the edge of flange.

Table B-1: Abutment 1 Multiplexer Channel List and Gage Locations (cont.)

Mux	Channel	Gage Label	Gage Type	Model	Location
6	1	SG-1E-3NE	Pile Strain Gage	4000	Upstream Pile (below Girder 1), 1.5 m (4.9 ft) from bottom of Abutment 1 77 mm (3.0 in) from the edge of flange.
6	2	SG-1E-3SE	Pile Strain Gage	4000	Upstream Pile (below Girder 1), 1.5 m (4.9 ft) from bottom of Abutment 1 77 mm (3.0 in) from the edge of flange.
6	3	SG-1E-3SW	Pile Strain Gage	4000	Upstream Pile (below Girder 1), 1.5 m (4.9 ft) from bottom of Abutment 1 77 mm (3.0 in) from the edge of flange.
6	4	SG-1E-3NW	Pile Strain Gage	4000	Upstream Pile (below Girder 1), 1.5 m (4.9 ft) from bottom of Abutment 1 77 mm (3.0 in) from the edge of flange.

Table B-2: Abutment 2 Multiplexer Channel List and Gage Locations

Mux	Channel	Gage Label	Gage Type	Model	Location
4	1	CM-2ET	Displacement Transducer	4420	Abutment 2, Upstream, Transverse, 1.95 m (6.43 ft) below construction joint
4	2	CM-2E	Displacement Transducer	4420	Abutment 2, Upstream, Longitudinal, 1.95 (6.43 ft) below construction joint
4	3	P-2CT	Earth Pressure Cell	4815	Abutment 2, Center of Abutment, 1.9 m (6.2 ft) above the bottom of abutment, 0.8 m (2.6 ft) away from abutment-wingwall connection
4	4	P-2CB	Earth Pressure Cell	4815	Abutment 2, Center of Abutment, 0.3 m (1.0 ft) above the bottom of abutment, 0.8 m (2.6 ft) away from abutment-wingwall connection
4	5	P-2EB	Earth Pressure Cell	4815	Abutment 2, Upstream, 0.3 m (1.0 ft) above the bottom of abutment, 0.8 m (2.6 ft) away from abutment-wingwall connection
4	6	P-2WB	Earth Pressure Cell	4815	Abutment 2, Downstream, 0.3 m (1.0 ft) above the bottom of abutment, 0.8 m (2.6 ft) away from abutment-wingwall connection
4	7	PW-1E	Earth Pressure Cell	4815	Wingwall 3 (Abutment 2, Upstream), 1.2 m (3.9 ft) above the bottom of wingwall, 1 m (3 ft) away from abutment-wingwall connection
4	8	SGG-2E-TW	Girder Strain Gage	4050	Upstream Girder, Downstream-Top Flange, 4.5 m (14.75 ft) from the end of steel girder section at Abutment 2.
4	9	SGG-2E-BW	Girder Strain Gage	4050	Upstream Girder, Downstream-Top Flange, 4.5 m (14.75 ft) from the end of steel girder section at Abutment 2.
4	10	SGG-0M-TE	Girder Strain Gage	4050	Center Girder, Upstream-Top Flange, 22.7 m (74.5 ft) from the end of steel girder section at Abutment 1.
4	11	SGG-0M-BE	Girder Strain Gage	4050	Center Girder, Upstream-Top Flange, 22.7 m (74.5 ft) from the end of steel girder section at Abutment 1.
4	12	SGG-0W-TE	Girder Strain Gage	4050	Downstream Girder, Upstream-Top Flange, 22.7 m (74.5 ft) from the end of steel girder section at Abutment 1.
4	13	SGG-0W-BE	Girder Strain Gage	4050	Downstream Girder, Upstream-Bottom Flange, 22.7 m (74.5 ft) from the end of steel girder section at Abutment 1.
4	14	SG-2M-1NE	Pile Strain Gage	4000	Middle Pile (below Girder 3), 0.5 m (1.6 ft) from bottom of Abutment 2 77 mm (3.0 in) from the edge of flange.
4	15	SG-2M-1SE	Pile Strain Gage	4000	Middle Pile (below Girder 3), 0.5 m (1.6 ft) from bottom of Abutment 2 77 mm (3.0 in) from the edge of flange.

Table B-2: Abutment 2 Multiplexer Channel List and Gage Locations (cont.)

Mux	Channel	Gage Label	Gage Type	Model	Location
5	1	SG-2M-1SW	Pile Strain Gage	4000	Middle Pile (below Girder 3), 0.5 m (1.6 ft) from bottom of Abutment 2, 77 mm (3.0 in) from the edge of flange.
5	2	SG-2M-1NW	Pile Strain Gage	4000	Middle Pile (below Girder 3), 0.5 m (1.6 ft) from bottom of Abutment 2, 77 mm (3.0 in) from the edge of flange.
5	3	SG-2M-3NE	Pile Strain Gage	4000	Middle Pile (below Girder 3), 1.5 m (4.9 ft) from bottom of Abutment 2, 77 mm (3.0 in) from the edge of flange.
5	4	SG-2M-3SE	Pile Strain Gage	4000	Middle Pile (below Girder 3), 1.5 m (4.9 ft) from bottom of Abutment 2, 77 mm (3.0 in) from the edge of flange.
5	5	SG-2M-3SW	Pile Strain Gage	4000	Middle Pile (below Girder 3), 1.5 m (4.9 ft) from bottom of Abutment 2, 77 mm (3.0 in) from the edge of flange.
5	6	SG-2E-1NE	Pile Strain Gage	4000	Upstream Pile (below Girder 1), 0.5 m (1.6 ft) from bottom of Abutment 2 77 mm (3.0 in) from the edge of flange.
5	7	SG-2E-1SE	Pile Strain Gage	4000	Upstream Pile (below Girder 1), 0.5 m (1.6 ft) from bottom of Abutment 2 77 mm (3.0 in) from the edge of flange.
5	8	SG-2E-1SW	Pile Strain Gage	4000	Upstream Pile (below Girder 1), 0.5 m (1.6 ft) from bottom of Abutment 2 77 mm (3.0 in) from the edge of flange.
5	9	SG-2E-1NW	Pile Strain Gage	4000	Upstream Pile (below Girder 1), 0.5 m (1.6 ft) from bottom of Abutment 2 77 mm (3.0 in) from the edge of flange.
5	10	SG-2E-2NE	Pile Strain Gage	4000	Upstream Pile (below Girder 1), 1.0 m (3.3 ft) from bottom of Abutment 2 77 mm (3.0 in) from the edge of flange.
5	11	SG-2E-2SE	Pile Strain Gage	4000	Upstream Pile (below Girder 1), 1.0 m (3.3 ft) from bottom of Abutment 2 77 mm (3.0 in) from the edge of flange.
5	12	SG-2E-2SW	Pile Strain Gage	4000	Upstream Pile (below Girder 1), 1.0 m (3.3 ft) from bottom of Abutment 2 77 mm (3.0 in) from the edge of flange.
5	13	SG-2E-3NE	Pile Strain Gage	4000	Upstream Pile (below Girder 1), 1.5 m (4.9 ft) from bottom of Abutment 2 77 mm (3.0 in) from the edge of flange.
5	14	SG-2E-3SE	Pile Strain Gage	4000	Upstream Pile (below Girder 1), 1.5 m (4.9 ft) from bottom of Abutment 2 77 mm (3.0 in) from the edge of flange.
5	15	SG-2E-3SW	Pile Strain Gage	4000	Upstream Pile (below Girder 1), 1.5 m (4.9 ft) from bottom of Abutment 2 77 mm (3.0 in) from the edge of flange.
5	16	TM-2M	Tiltmeter (Uniaxial)	6350	Abutment 2, Center of Abutment, 0.5 m (1.6 ft) from the bottom of middle girder.

b) East Montpelier Bridge

As-built gage information for the East Montpelier Bridge is given in Table B-3 and Table B-4 for Abutment 1 and Abutment 2 multiplexers, respectively. Figures showing gage locations without labeling are found in Section 3.3.

Table B-3: Abutment 1 Multiplexer Channel List and Gage Locations

Mux	Channel	Gage Label	Gage Type	Model	Location
1	1	CM-1NT	Displacement Transducer	4420	Abutment 1, Upstream, Transverse, 1.7 m (5.6 ft) below construction joint.
1	2	CM-1N	Displacement Transducer	4420	Abutment 1, Upstream, Longitudinal, 1.7 m (5.6 ft) below construction joint.
1	3	CM-1S	Displacement Transducer	4420	Abutment 1, Downstream, Longitudinal, 1.7 m (5.6 ft) below construction joint.
1	4	P-1NT	Earth Pressure Cell	4815	Abutment 1, Upstream, 1.6 m (5.2 ft) above the bottom of abutment, 2.12 m (6.96 ft) away from abutment-wingwall connection.
1	5	P-1NM	Earth Pressure Cell	4815	Abutment 1, Upstream, 1.0 m (3.3 ft) above the bottom of abutment, 2.12 m (6.96 ft) away from abutment-wingwall connection.
1	6	P-1NB	Earth Pressure Cell	4815	Abutment 1, Upstream, 0.4 m (1.3 ft) above the bottom of abutment, 2.12 m (6.96 ft) away from abutment-wingwall connection.
1	7	P-1CM	Earth Pressure Cell	4815	Abutment 1, Center of Abutment, 1.0 m (3.3 ft) above the bottom of abutment.
1	8	P-1CB	Earth Pressure Cell	4815	Abutment 1, Center of Abutment, 0.4 m (1.3 ft) above the bottom of abutment.
1	9	P-1ST	Earth Pressure Cell	4815	Abutment 1, Downstream, 1.6 m (5.2 ft) above the bottom of abutment, 2.12 m (6.96 ft) away from abutment-wingwall connection.
1	10	P-1SM	Earth Pressure Cell	4815	Abutment 1, Downstream, 1.0 m (3.3 ft) above the bottom of abutment, 2.12 m (6.96 ft) away from abutment-wingwall connection
1	11	P-1SB	Earth Pressure Cell	4815	Abutment 1, Downstream, 0.4 m (1.3 ft) above the bottom of abutment, 2.12 m (6.96 ft) away from abutment-wingwall connection.
1	12	PW-1N	Earth Pressure Cell	4815	Wingwall 1 (Abutment 1, Upstream), 1.2 m (3.9 ft) above the bottom of abutment, 1 m (3 ft) away from abutment-wingwall connection.
1	13	TM-1M	Tiltmeter (Uniaxial)	6350	Abutment 1, Center of Abutment, 0.5 m (1.6 ft) from the bottom of middle girder.
1	14	P-R	Earth Pressure Cell	4815	Under Approach Slab on Abutment 1 side, Facing towards the abutment.

Table B-3: Abutment 1 Multiplexer Channel List and Gage Locations (cont.)

Mux	Channel	Gage Label	Gage Type	Model	Location
2	1	SGG-1N-TE*	Girder Strain Gage	4050	Upstream Girder, Downstream-Top Flange, 4.35 m (14.30 ft) from the end of steel girder section at Abutment 1.
2	2	SGG-1N-BE*	Girder Strain Gage	4050	Upstream Girder, Downstream-Bottom Flange, 4.35 m (14.30 ft) from the end of steel girder section at Abutment 1.
2	3	SGG-1N-TW*	Girder Strain Gage	4050	Upstream Girder, Upstream-Top Flange, 4.35 m (14.30 ft) from the end of steel girder section at Abutment 1.
2	4	SGG-1N-BW*	Girder Strain Gage	4050	Upstream Girder, Upstream-Bottom Flange, 4.35 m (14.30 ft) from the end of steel girder section at Abutment 1.
2	5	SGG-1S-TE*	Girder Strain Gage	4050	Downstream Girder, Downstream-Top Flange, 4.35 m (14.30 ft) from the end of steel girder section at Abutment 1.
2	6	SGG-1S-BE*	Girder Strain Gage	4050	Downstream Girder, Downstream-Bottom Flange, 4.35 m (14.30 ft) from the end of steel girder section at Abutment 1.
2	7	SGG-1S-TW*	Girder Strain Gage	4050	Downstream Girder, Upstream-Top Flange, 4.35 m (14.30 ft) from the end of steel girder section at Abutment 1.
2	8	SGG-1S-BW*	Girder Strain Gage	4050	Downstream Girder, Upstream-Bottom Flange, 4.35 m (14.30 ft) from the end of steel girder section at Abutment 1.
2	9	SG-1N-1NE	Pile Strain Gage	4000	Upstream Pile, 0.5 m (1.6 ft) from bottom of Abutment 1 51 mm (2.0 in) from the edge of flange.
2	10	SG-1N-1NW	Pile Strain Gage	4000	Upstream Pile, 0.5 m (1.6 ft) from bottom of Abutment 1 51 mm (2.0 in) from the edge of flange.
2	11	SG-1N-1SE	Pile Strain Gage	4000	Upstream Pile, 0.5 m (1.6 ft) from bottom of Abutment 1 51 mm (2.0 in) from the edge of flange.
2	12	SG-1N-1SW	Pile Strain Gage	4000	Upstream Pile, 0.5 m (1.6 ft) from bottom of Abutment 1 51 mm (2.0 in) from the edge of flange.
2	13	SG-1N-2NE	Pile Strain Gage	4000	Upstream Pile, 1.0 m (3.3 ft) from bottom of Abutment 1 51 mm (2.0 in) from the edge of flange.
2	14	SG-1N-2NW	Pile Strain Gage	4000	Upstream Pile, 1.0 m (3.3 ft) from bottom of Abutment 1 51 mm (2.0 in) from the edge of flange.
2	15	SG-1N-2SE	Pile Strain Gage	4000	Upstream Pile, 1.0 m (3.3 ft) from bottom of Abutment 1 51 mm (2.0 in) from the edge of flange.
2	16	SG-1N-2SW	Pile Strain Gage	4000	Upstream Pile, 1.0 m (3.3 ft) from bottom of Abutment 1 51 mm (2.0 in) from the edge of flange.

* W and E in gage labels correspond to upstream (north) and downstream (south) flanges of the girders, respectively.

Table B-3: Abutment 1 Multiplexer Channel List and Gage Locations (cont.)

Mux	Channel	Gage Label	Gage Type	Model	Location
3	1	SG-1N-3NE	Pile Strain Gage	4000	Upstream Pile, 1.5 m (4.9 ft) from bottom of Abutment 1 51 mm (2.0 in) from the edge of flange.
3	2	SG-1N-3NW	Pile Strain Gage	4000	Upstream Pile, 1.5 m (4.9 ft) from bottom of Abutment 1 51 mm (2.0 in) from the edge of flange.
3	3	SG-1N-3SE	Pile Strain Gage	4000	Upstream Pile, 1.5 m (4.9 ft) from bottom of Abutment 1 51 mm (2.0 in) from the edge of flange.
3	4	SG-1N-3SW	Pile Strain Gage	4000	Upstream Pile, 1.5 m (4.9 ft) from bottom of Abutment 1 51 mm (2.0 in) from the edge of flange.
3	5	SG-1S-1NE	Pile Strain Gage	4000	Downstream Pile, 0.5 m (1.6 ft) from bottom of Abutment 1 51 mm (2.0 in) from the edge of flange.
3	6	SG-1S-1NW	Pile Strain Gage	4000	Downstream Pile, 0.5 m (1.6 ft) from bottom of Abutment 1 51 mm (2.0 in) from the edge of flange.
3	7	SG-1S-1SE	Pile Strain Gage	4000	Downstream Pile, 0.5 m (1.6 ft) from bottom of Abutment 1 51 mm (2.0 in) from the edge of flange.
3	8	SG-1S-1SW	Pile Strain Gage	4000	Downstream Pile, 0.5 m (1.6 ft) from bottom of Abutment 1 51 mm (2.0 in) from the edge of flange.
3	9	SG-1S-2NE	Pile Strain Gage	4000	Downstream Pile, 1.0 m (3.3 ft) from bottom of Abutment 1 51 mm (2.0 in) from the edge of flange.
3	10	SG-1S-2NW	Pile Strain Gage	4000	Downstream Pile, 1.0 m (3.3 ft) from bottom of Abutment 1 51 mm (2.0 in) from the edge of flange.
3	11	SG-1S-2SE	Pile Strain Gage	4000	Downstream Pile, 1.0 m (3.3 ft) from bottom of Abutment 1 51 mm (2.0 in) from the edge of flange.
3	12	SG-1S-2SW	Pile Strain Gage	4000	Downstream Pile, 1.0 m (3.3 ft) from bottom of Abutment 1 51 mm (2.0 in) from the edge of flange.
3	13	SG-1S-3NE	Pile Strain Gage	4000	Downstream Pile, 1.5 m (4.9 ft) from bottom of Abutment 1 51 mm (2.0 in) from the edge of flange.
3	14	SG-1S-3NW	Pile Strain Gage	4000	Downstream Pile, 1.5 m (4.9 ft) from bottom of Abutment 1 51 mm (2.0 in) from the edge of flange.
3	15	SG-1S-3SE	Pile Strain Gage	4000	Downstream Pile, 1.5 m (4.9 ft) from bottom of Abutment 1 51 mm (2.0 in) from the edge of flange.
3	16	SG-1S-3SW	Pile Strain Gage	4000	Downstream Pile, 1.5 m (4.9 ft) from bottom of Abutment 1 51 mm (2.0 in) from the edge of flange.

Table B-3: Abutment 1 Multiplexer Channel List and Gage Locations (cont.)

Mux	Channel	Gage Label	Gage Type	Model	Location
6	1	IN-1N-1	Inclinometer (Biaxial) - Ch-1 (Longitudinal)	6150	Abutment 1, Upstream Pile, Flange facing the fascia of the bridge, 0.0-0.6 m (0-2 ft) below the bottom of Abutment 1.
6	2	IN-1N-1	Inclinometer (Biaxial) - Ch-2 (Transverse)	6150	Abutment 1, Upstream Pile, Flange facing the fascia of the bridge, 0.0-0.6 m (0-2 ft) below the bottom of Abutment 1.
6	3	IN-1N-2	Inclinometer (Biaxial) - Ch-1 (Longitudinal)	6150	Abutment 1, Upstream Pile, Flange facing the fascia of the bridge, 0.6-1.5 m (2-5 ft) below the bottom of Abutment 1.
6	4	IN-1N-2	Inclinometer (Biaxial) - Ch-2 (Transverse)	6150	Abutment 1, Upstream Pile, Flange facing the fascia of the bridge, 0.6-1.5 m (2-5 ft) below the bottom of Abutment 1.
6	5	IN-1N-3	Inclinometer (Biaxial) - Ch-1 (Longitudinal)	6150	Abutment 1, Upstream Pile, Flange facing the fascia of the bridge, 1.5-2.7 m (5-9 ft) below the bottom of Abutment 1.
6	6	IN-1N-3	Inclinometer (Biaxial) - Ch-2 (Transverse)	6150	Abutment 1, Upstream Pile, Flange facing the fascia of the bridge, 1.5-2.7 m (5-9 ft) below the bottom of Abutment 1.
6	7	IN-1N-4	Inclinometer (Biaxial) - Ch-1 (Longitudinal)	6150	Abutment 1, Upstream Pile, Flange facing the fascia of the bridge, 2.7-4.0 m (9-13 ft) below the bottom of Abutment 1.
6	8	IN-1N-4	Inclinometer (Biaxial) - Ch-2 (Transverse)	6150	Abutment 1, Upstream Pile, Flange facing the fascia of the bridge, 2.7-4.0 m (9-13 ft) below the bottom of Abutment 1.
6	9	IN-1S-1	Inclinometer (Biaxial) - Ch-1 (Longitudinal)	6150	Abutment 1, Downstream Pile, Flange facing the fascia of the bridge, 0.0-0.6 m (0-2 ft) below the bottom of Abutment 1.
6	10	IN-1S-1	Inclinometer (Biaxial) - Ch-2 (Transverse)	6150	Abutment 1, Downstream Pile, Flange facing the fascia of the bridge, 0.0-0.6 m (0-2 ft) below the bottom of Abutment 1.
6	11	IN-1S-2	Inclinometer (Biaxial) - Ch-1 (Longitudinal)	6150	Abutment 1, Downstream Pile, Flange facing the fascia of the bridge, 0.6-1.5 m (2-5 ft) below the bottom of Abutment 1.
6	12	IN-1S-2	Inclinometer (Biaxial) - Ch-2 (Transverse)	6150	Abutment 1, Downstream Pile, Flange facing the fascia of the bridge, 0.6-1.5 m (2-5 ft) below the bottom of Abutment 1.
6	13	IN-1S-3	Inclinometer (Biaxial) - Ch-1 (Longitudinal)	6150	Abutment 1, Downstream Pile, Flange facing the fascia of the bridge, 1.5-2.7 m (5-9 ft) below the bottom of Abutment 1.
6	14	IN-1S-3	Inclinometer (Biaxial) - Ch-2 (Transverse)	6150	Abutment 1, Downstream Pile, Flange facing the fascia of the bridge, 1.5-2.7 m (5-9 ft) below the bottom of Abutment 1.
6	15	IN-1S-4	Inclinometer (Biaxial) - Ch-1 (Longitudinal)	6150	Abutment 1, Downstream Pile, Flange facing the fascia of the bridge, 2.7-4.0 m (9-13 ft) below the bottom of Abutment 1.
6	16	IN-1S-4	Inclinometer (Biaxial) - Ch-2 (Transverse)	6150	Abutment 1, Downstream Pile, Flange facing the fascia of the bridge, 2.7-4.0 m (9-13 ft) below the bottom of Abutment 1.

Table B-4: Abutment 2 Multiplexer Channel List and Gage Locations

Mux	Channel	Gage Label	Gage Type	Model	Location
4	1	CM-2NT	Displacement Transducer	4420	Abutment 2, Upstream, Transverse, 1.58 m (5.18 ft) below construction joint
4	2	CM-2N	Displacement Transducer	4420	Abutment 2, Upstream, Longitudinal 1.58 m (5.18 ft) below construction joint
4	3	P-2NT	Earth Pressure Cell	4815	Abutment 2, Upstream, 1.6 m (5.2 ft) above the bottom of abutment, 2.12 m (6.96 ft) away from abutment-wingwall connection.
4	4	P-2NB	Earth Pressure Cell	4815	Abutment 1, Upstream, 0.4 m (1.3 ft) above the bottom of abutment, 2.12 m (6.96 ft) away from abutment-wingwall connection.
4	5	P-2ST	Earth Pressure Cell	4815	Abutment 2, Downstream, 1.6 m (5.2 ft) above the bottom of abutment, 2.12 m (6.96 ft) away from abutment-wingwall connection.
4	6	P-2SB	Earth Pressure Cell	4815	Abutment 1, Downstream, 0.4 m (1.3 ft) above the bottom of abutment, 2.12 m (6.96 ft) away from abutment-wingwall connection.
4	7	SGG-2N-TW	Girder Strain Gage	4050	Upstream Girder, Upstream-Top Flange, 4.35 m (14.30 ft) from the end of steel girder section at Abutment 2.
4	8	SGG-2N-BW	Girder Strain Gage	4050	Upstream Girder, Upstream-Bottom Flange, 4.35 m (14.30 ft) from the end of steel girder section at Abutment 2.
4	9	SGG-2S-TW	Girder Strain Gage	4050	Downstream Girder, Downstream-Top Flange, 4.35 m (14.30 ft) from the end of steel girder section at Abutment 2.
4	10	SGG-2S-BW	Girder Strain Gage	4050	Downstream Girder, Downstream-Bottom Flange, 4.35 m (14.30 ft) from the end of steel girder section at Abutment 1.
4	11	TM-2M	Tiltmeter (Uniaxial)	6350	Abutment 2, Center of Abutment, 0.5 m (1.6 ft) from the bottom of middle girder.

Table B-4: Abutment 2 Multiplexer Channel List and Gage Locations (cont.)

Mux	Channel	Gage Label	Gage Type	Model	Location
5	1	SGG-0N-TE	Girder Strain Gage	4050	Upstream Girder, Downstream-Top Flange, 18.5 m (61 ft) from the end of steel girder section at Abutment 1.
5	2	SGG-0N-BE	Girder Strain Gage	4050	Upstream Girder, Downstream-Bottom Flange, 18.5 m (61 ft) from the end of steel girder section at Abutment 1.
5	3	SGG-0N-TW	Girder Strain Gage	4050	Upstream Girder, Upstream-Top Flange, 18.5 m (61 ft) from the end of steel girder section at Abutment 1.
5	4	SGG-0N-BW	Girder Strain Gage	4050	Upstream Girder, Upstream-Bottom Flange, 18.5 m (61 ft) from the end of steel girder section at Abutment 1.
5	5	SGG-0S-TE	Girder Strain Gage	4050	Downstream Girder, Downstream-Top Flange, 18.5 m (61 ft) from the end of steel girder section at Abutment 1.
5	6	SGG-0S-BE	Girder Strain Gage	4050	Downstream Girder, Downstream-Bottom Flange, 18.5 m (61 ft) from the end of steel girder section at Abutment 1.
5	7	SGG-0S-TW	Girder Strain Gage	4050	Downstream Girder, Upstream-Top Flange, 18.5 m (61 ft) from the end of steel girder section at Abutment 1.
5	8	SGG-0S-BW	Girder Strain Gage	4050	Downstream Girder, Upstream-Bottom Flange, 18.5 m (61 ft) from the end of steel girder section at Abutment 1.
5	9	SG-2N-1NE	Pile Strain Gage	4000	Upstream Pile, 0.5 m (1.6 ft) from bottom of Abutment 2. 51 mm (2.0 in) from the edge of flange.
5	10	SG-2N-1NW	Pile Strain Gage	4000	Upstream Pile, 0.5 m (1.6 ft) from bottom of Abutment 2. 51 mm (2.0 in) from the edge of flange.
5	11	SG-2N-1SE	Pile Strain Gage	4000	Upstream Pile, 0.5 m (1.6 ft) from bottom of Abutment 2. 51 mm (2.0 in) from the edge of flange.
5	12	SG-2N-1SW	Pile Strain Gage	4000	Upstream Pile, 0.5 m (1.6 ft) from bottom of Abutment 2. 51 mm (2.0 in) from the edge of flange.
5	13	SG-2N-3NE	Pile Strain Gage	4000	Upstream Pile, 1.5 m (4.9 ft) from bottom of Abutment 2. 51 mm (2.0 in) from the edge of flange.
5	14	SG-2N-3NW	Pile Strain Gage	4000	Upstream Pile, 1.5 m (4.9 ft) from bottom of Abutment 2. 51 mm (2.0 in) from the edge of flange.
5	15	SG-2N-3SE	Pile Strain Gage	4000	Upstream Pile, 1.5 m (4.9 ft) from bottom of Abutment 2. 51 mm (2.0 in) from the edge of flange.
5	16	SG-2N-3SW	Pile Strain Gage	4000	Upstream Pile, 1.5 m (4.9 ft) from bottom of Abutment 2. 51 mm (2.0 in) from the edge of flange.

Table B-4: Abutment 2 Multiplexer Channel List and Gage Locations (cont.)

Mux	Channel	Gage Label	Gage Type	Model	Location
7	1	1N-1*	Inclinometer (Biaxial) - Ch-1 (Longitudinal)	6150	Abutment 2, Upstream Pile, Flange facing the centerline of the roadway, 0.0-0.6 m (0-2 ft) below the bottom of Abutment 2.
7	2	1N-1*	Inclinometer (Biaxial) - Ch-2 (Transverse)	6150	Abutment 2, Upstream Pile, Flange facing the centerline of the roadway, 0.0-0.6 m (0-2 ft) below the bottom of Abutment 2.
7	3	1N-2*	Inclinometer (Biaxial) - Ch-1 (Longitudinal)	6150	Abutment 2, Upstream Pile, Flange facing the centerline of the roadway, 0.6-1.5 m (2-5 ft) below the bottom of Abutment 2.
7	4	1N-2*	Inclinometer (Biaxial) - Ch-2 (Transverse)	6150	Abutment 2, Upstream Pile, Flange facing the centerline of the roadway, 0.6-1.5 m (2-5 ft) below the bottom of Abutment 2.
7	5	1N-3*	Inclinometer (Biaxial) - Ch-1 (Longitudinal)	6150	Abutment 2, Upstream Pile, Flange facing the centerline of the roadway, 1.5-2.7 m (5-9 ft) below the bottom of Abutment 2.
7	6	1N-3*	Inclinometer (Biaxial) - Ch-2 (Transverse)	6150	Abutment 2, Upstream Pile, Flange facing the centerline of the roadway, 1.5-2.7 m (5-9 ft) below the bottom of Abutment 2.
7	7	1N-4*	Inclinometer (Biaxial) - Ch-1 (Longitudinal)	6150	Abutment 2, Upstream Pile, Flange facing the centerline of the roadway, 2.7-4.0 m (9-13 ft) below the bottom of Abutment 2.
7	8	1N-4*	Inclinometer (Biaxial) - Ch-2 (Transverse)	6150	Abutment 2, Upstream Pile, Flange facing the centerline of the roadway, 2.7-4.0 m (9-13 ft) below the bottom of Abutment 2.
7	9	1S-1*	Inclinometer (Biaxial) - Ch-1 (Longitudinal)	6150	Abutment 2, Downstream Pile, Flange facing the centerline of the roadway, 0.0-0.6 m (0-2 ft) below the bottom of Abutment 2.
7	10	1S-1*	Inclinometer (Biaxial) - Ch-2 (Transverse)	6150	Abutment 2, Downstream Pile, Flange facing the centerline of the roadway, 0.0-0.6 m (0-2 ft) below the bottom of Abutment 2.
7	11	1S-2*	Inclinometer (Biaxial) - Ch-1 (Longitudinal)	6150	Abutment 2, Downstream Pile, Flange facing the centerline of the roadway, 0.6-1.5 m (2-5 ft) below the bottom of Abutment 2.
7	12	1S-2*	Inclinometer (Biaxial) - Ch-2 (Transverse)	6150	Abutment 2, Downstream Pile, Flange facing the centerline of the roadway, 0.6-1.5 m (2-5 ft) below the bottom of Abutment 2.
7	13	1S-3*	Inclinometer (Biaxial) - Ch-1 (Longitudinal)	6150	Abutment 2, Downstream Pile, Flange facing the centerline of the roadway, 1.5-2.7 m (5-9 ft) below the bottom of Abutment 2.
7	14	1S-3*	Inclinometer (Biaxial) - Ch-2 (Transverse)	6150	Abutment 2, Downstream Pile, Flange facing the centerline of the roadway, 1.5-2.7 m (5-9 ft) below the bottom of Abutment 2.
7	15	1S-4*	Inclinometer (Biaxial) - Ch-1 (Longitudinal)	6150	Abutment 2, Downstream Pile, Flange facing the centerline of the roadway, 2.7-3.7 m (9-12 ft) below the bottom of Abutment 2.
7	16	1S-4*	Inclinometer (Biaxial) - Ch-2 (Transverse)	6150	Abutment 2, Downstream Pile, Flange facing the centerline of the roadway, 2.7-3.7 m (9-12 ft) below the bottom of Abutment 2.

* Originally intended for use at Stockbridge. Abutment numbers on gage labels don't correspond to East Montpelier callout.

c) Stockbridge Bridge

As-built gage information for the Stockbridge Bridge is given in Table B-5 and Table B-6 for Abutment 1 and Abutment 2 (as determined by structural drawings) multiplexers, respectively. Figures showing gage locations without labeling are found in Section 3.4.

Table B-5: Abutment 1 (per Structural Drawings) Multiplexer Channel Allocation and Gage Locations

Mux	Channel	Gage Label	Gage Type	Model	Location
6	1	CM-2NT	Displacement Transducer	4420-50mm	Abutment 1, Upstream, Transverse, 1.28 m (4.18 ft) below construction joint
6	2	CM-2N	Displacement Transducer	4420-100mm	Abutment 1, Upstream, Longitudinal, 1.28 m (4.18 ft) below construction joint
6	3	CM-2S	Displacement Transducer	4420-100mm	Abutment 1, Downstream, Longitudinal, 3.55 m (11.65 ft) below construction joint
6	4	P-2NT	Earth Pressure Cell	4810	Abutment 1, Upstream, 3.6 m (12.0 ft) above the bottom of abutment, 1 m (3 ft) away from abutment-wingwall connection
6	5	P-2NM	Earth Pressure Cell	4810	Abutment 1, Upstream, 2.1 m (7.0 ft) above the bottom of abutment, 1 m (3 ft) away from abutment-wingwall connection
6	6	P-2NB	Earth Pressure Cell	4810	Abutment 1, Upstream, 0.6 m (2.0 ft) above the bottom of abutment, 1 m (3 ft) away from abutment-wingwall connection
6	7	P-2CT	Earth Pressure Cell	4810	Abutment 1, Center of Abutment, 3.6 m (12.0 ft) above the bottom of abutment,
6	8	P-2CB	Earth Pressure Cell	4810	Abutment 1, Center of Abutment, 0.6 m (2.0 ft) above the bottom of abutment,
6	9	P-2ST	Earth Pressure Cell	4810	Abutment 1, Downstream, 3.6 m (12.0 ft) above the bottom of abutment, 1 m (3 ft) away from abutment-wingwall connection
6	10	P-2SM	Earth Pressure Cell	4810	Abutment 1, Downstream, 2.1 m (7.0 ft) above the bottom of abutment, 1 m (3 ft) away from abutment-wingwall connection
6	11	P-2SB	Earth Pressure Cell	4810	Abutment 1, Downstream, 0.6 m (2.0 ft) above the bottom of abutment, 1 m (3 ft) away from abutment-wingwall connection
6	12	PW-2N	Earth Pressure Cell	4815	Wingwall 1, 1.2 m (4.0 ft) above the bottom of wingwall, 1 m (3 ft) away from abutment-wingwall connection
6	13	PW-2S	Earth Pressure Cell	4815	Wingwall 2, 1.2 m (4.0 ft) above the bottom of wingwall, 1 m (3 ft) away from abutment-wingwall connection
6	14	P-R	Earth Pressure Cell	4810	Under Approach Slab on Abutment 1 Side, 1.5 m (4.9 ft) away from the bridge end, At the centerline of roadway, 1.0 m (3.0 ft) below approach slab

Table B-5: Abutment 1 (per Structural Drawings) Multiplexer Channel Allocation and Gage Locations (cont.)

Mux	Channel	Gage Label	Gage Type	Model	Location
7	1	SGG-2N-TN	Girder Strain Gage	4050	Upstream Girder, Upstream-Top Flange, 17.2 m (56.4 ft) from the end of steel girder section at Abutment 1.
7	2	SGG-2N-TS	Girder Strain Gage	4050	Upstream Girder, Downstream-Top Flange, 17.2 m (56.4 ft) from the end of steel girder section at Abutment 1.
7	3	SGG-2N-BN	Girder Strain Gage	4050	Upstream Girder, Upstream-Bottom Flange, 17.2 m (56.4 ft) from the end of steel girder section at Abutment 1.
7	4	SGG-2N-BS	Girder Strain Gage	4050	Upstream Girder, Downstream-Bottom Flange, 17.2 m (56.4 ft) from the end of steel girder section at Abutment 1.
7	5	SGG-2S-TN	Girder Strain Gage	4050	Downstream Girder, Upstream-Top Flange, 16.0 m (52.5 ft) from the end of steel girder section at Abutment 1.
7	6	SGG-2S-TS	Girder Strain Gage	4050	Downstream Girder, Downstream-Top Flange, 16.0 m (52.5 ft) from the end of steel girder section at Abutment 1.
7	7	SGG-2S-BN	Girder Strain Gage	4050	Downstream Girder, Upstream-Bottom Flange, 16.0 m (52.5 ft) from the end of steel girder section at Abutment 1.
7	8	SGG-2S-BS	Girder Strain Gage	4050	Downstream Girder, Downstream-Bottom Flange, 16.0 m (52.5 ft) from the end of steel girder section at Abutment 1.

Table B-5: Abutment 1 (per Structural Drawings) Multiplexer Channel Allocation and Gage Locations (cont.)

Mux	Channel	Gage Label	Gage Type	Model	Location
8	1	SG-2N-1NE	Pile Strain Gage	4000	Upstream Pile, 0.3 m (1.0 ft) from bottom of Abutment 1 64 mm (2.5 in) from the edge of flange.
8	2	SG-2N-1NW	Pile Strain Gage	4000	Upstream Pile, 0.3 m (1.0 ft) from bottom of Abutment 1 64 mm (2.5 in) from the edge of flange.
8	3	SG-2N-1SE	Pile Strain Gage	4000	Upstream Pile, 0.3 m (1.0 ft) from bottom of Abutment 1 64 mm (2.5 in) from the edge of flange.
8	4	SG-2N-1SW	Pile Strain Gage	4000	Upstream Pile, 0.3 m (1.0 ft) from bottom of Abutment 1 64 mm (2.5 in) from the edge of flange.
8	5	SG-2N-2NE	Pile Strain Gage	4000	Upstream Pile, 1.2 m (4.0 ft) from bottom of Abutment 1 64 mm (2.5 in) from the edge of flange.
8	6	SG-2N-2NW	Pile Strain Gage	4000	Upstream Pile, 1.2 m (4.0 ft) from bottom of Abutment 1 64 mm (2.5 in) from the edge of flange.
8	7	SG-2N-2SE	Pile Strain Gage	4000	Upstream Pile, 1.2 m (4.0 ft) from bottom of Abutment 1 64 mm (2.5 in) from the edge of flange.
8	8	SG-2N-2SW	Pile Strain Gage	4000	Upstream Pile, 1.2 m (4.0 ft) from bottom of Abutment 1 64 mm (2.5 in) from the edge of flange.
8	9	SG-2N-3NE	Pile Strain Gage	4000	Upstream Pile, 2.1 m (7.0 ft) from bottom of Abutment 1 64 mm (2.5 in) from the edge of flange.
8	10	SG-2N-3NW	Pile Strain Gage	4000	Upstream Pile, 2.1 m (7.0 ft) from bottom of Abutment 1 64 mm (2.5 in) from the edge of flange.
8	11	SG-2N-3SW	Pile Strain Gage	4000	Upstream Pile, 2.1 m (7.0 ft) from bottom of Abutment 1 64 mm (2.5 in) from the edge of flange.
8	12	SG-2N-4NE	Pile Strain Gage	4000	Upstream Pile, 3.0 m (10.0 ft) from bottom of Abutment 1 64 mm (2.5 in) from the edge of flange.
8	13	SG-2N-4NW	Pile Strain Gage	4000	Upstream Pile, 3.0 m (10.0 ft) from bottom of Abutment 1 64 mm (2.5 in) from the edge of flange.
8	14	SG-2N-4SW	Pile Strain Gage	4000	Upstream Pile, 3.0 m (10.0 ft) from bottom of Abutment 1 64 mm (2.5 in) from the edge of flange.

Table B-5: Abutment 1 (per Structural Drawings) Multiplexer Channel Allocation and Gage Locations (cont.)

Mux	Channel	Gage Label	Gage Type	Model	Location
9	1	SG-2S-1NE	Pile Strain Gage	4000	Downstream Pile, 0.3 m (1.0 ft) from bottom of Abutment 1 64 mm (2.5 in) from the edge of flange.
9	2	SG-2S-1NW	Pile Strain Gage	4000	Downstream Pile, 0.3 m (1.0 ft) from bottom of Abutment 1 64 mm (2.5 in) from the edge of flange.
9	3	SG-2S-1SE	Pile Strain Gage	4000	Downstream Pile, 0.3 m (1.0 ft) from bottom of Abutment 1 64 mm (2.5 in) from the edge of flange.
9	4	SG-2S-1SW	Pile Strain Gage	4000	Downstream Pile, 0.3 m (1.0 ft) from bottom of Abutment 1 64 mm (2.5 in) from the edge of flange.
9	5	SG-2S-2NE	Pile Strain Gage	4000	Downstream Pile, 1.2 m (4.0 ft) from bottom of Abutment 1 64 mm (2.5 in) from the edge of flange.
9	6	SG-2S-2NW	Pile Strain Gage	4000	Downstream Pile, 1.2 m (4.0 ft) from bottom of Abutment 1 64 mm (2.5 in) from the edge of flange.
9	7	SG-2S-2SE	Pile Strain Gage	4000	Downstream Pile, 1.2 m (4.0 ft) from bottom of Abutment 1 64 mm (2.5 in) from the edge of flange.
9	8	SG-2S-2SW	Pile Strain Gage	4000	Downstream Pile, 1.2 m (4.0 ft) from bottom of Abutment 1 64 mm (2.5 in) from the edge of flange.
9	9	SG-2S-3NE	Pile Strain Gage	4000	Downstream Pile, 2.1 m (7.0 ft) from bottom of Abutment 1 64 mm (2.5 in) from the edge of flange.
9	10	SG-2S-3NW	Pile Strain Gage	4000	Downstream Pile, 2.1 m (7.0 ft) from bottom of Abutment 1 64 mm (2.5 in) from the edge of flange.
9	11	SG-2S-3SW	Pile Strain Gage	4000	Downstream Pile, 2.1 m (7.0 ft) from bottom of Abutment 1 64 mm (2.5 in) from the edge of flange.
9	12	SG-2S-4NE	Pile Strain Gage	4000	Downstream Pile, 3.0 m (10.0 ft) from bottom of Abutment 1 64 mm (2.5 in) from the edge of flange.
9	13	SG-2S-4NW	Pile Strain Gage	4000	Downstream Pile, 3.0 m (10.0 ft) from bottom of Abutment 1 64 mm (2.5 in) from the edge of flange.
9	14	SG-2S-4SW	Pile Strain Gage	4000	Downstream Pile, 3.0 m (10.0 ft) from bottom of Abutment 1 64 mm (2.5 in) from the edge of flange.

Table B-5: Abutment 1 (per Structural Drawings) Multiplexer Channel Allocation and Gage Locations

Mux	Channel	Gage Label	Gage Type	Model	Location
11	1	TM-2M	Tiltmeter (Biaxial) - Ch-1 (Longitudinal)	6160	Abutment 1, Center of Abutment, 1.0 m (3.0ft) below the bottom of middle girder
11	2	TM-2M	Tiltmeter (Biaxial) - Ch-2 (Transverse)	6160	Abutment 1, Center of Abutment, 1.0 m (3.0ft) below the bottom of middle girder
11	3	IN-2N-1	Inclinometer (Biaxial) - Ch-1 (Longitudinal)	6150	Abutment 1, Upstream Pile, Flange facing the roadway 0.0-0.6 m (0-2 ft) below the bottom of Abutment 1
11	4	IN-2N-1	Inclinometer (Biaxial) - Ch-2 (Transverse)	6150	Abutment 1, Upstream Pile, Flange facing the roadway 0.0-0.6 m (0-2 ft) below the bottom of Abutment 1
11	5	IN-2N-2	Inclinometer (Biaxial) - Ch-1 (Longitudinal)	6150	Abutment 1, Upstream Pile, Flange facing the roadway 0.6-1.5 m (2-5 ft) below the bottom of Abutment 1
11	6	IN-2N-2	Inclinometer (Biaxial) - Ch-2 (Transverse)	6150	Abutment 1, Upstream Pile, Flange facing the roadway 0.6-1.5 m (2-5 ft) below the bottom of Abutment 1
11	7	IN-2N-3	Inclinometer (Biaxial) - Ch-1 (Longitudinal)	6150	Abutment 1, Upstream Pile, Flange facing the roadway 1.5-2.7 m (5-9 ft) below the bottom of Abutment 1
11	8	IN-2N-3	Inclinometer (Biaxial) - Ch-2 (Transverse)	6150	Abutment 1, Upstream Pile, Flange facing the roadway 1.5-2.7 m (5-9 ft) below the bottom of Abutment 1
11	9	IN-2N-4	Inclinometer (Biaxial) - Ch-1 (Longitudinal)	6150	Abutment 1, Upstream Pile, Flange facing the roadway 2.7-4.0 m (9-13 ft) below the bottom of Abutment 1
11	10	IN-2N-4	Inclinometer (Biaxial) - Ch-2 (Transverse)	6150	Abutment 1, Upstream Pile, Flange facing the roadway 2.7-4.0 m (9-13 ft) below the bottom of Abutment 1
11	11	IN-2N-5	Inclinometer (Biaxial) - Ch-1 (Longitudinal)	6150	Abutment 1, Upstream Pile, Flange facing the roadway 4.0-5.2 m (13-17 ft) below the bottom of Abutment 1
11	12	IN-2N-5	Inclinometer (Biaxial) - Ch-2 (Transverse)	6150	Abutment 1, Upstream Pile, Flange facing the roadway 4.0-5.2 m (13-17 ft) below the bottom of Abutment 1

Table B-5: Abutment 1 (per Structural Drawings) Multiplexer Channel Allocation and Gage Locations (cont.)

Mux	Channel	Gage Label	Gage Type	Model	Location
12	1	IN-2S-1	Inclinometer (Biaxial) - Ch-1 (Longitudinal)	6150	Abutment 1, Downstream Pile, Flange facing the roadway 0.0-0.6 m (0-2 ft) below the bottom of Abutment 1
12	2	IN-2S-1	Inclinometer (Biaxial) - Ch-2 (Transverse)	6150	Abutment 1, Downstream Pile, Flange facing the roadway 0.0-0.6 m (0-2 ft) below the bottom of Abutment 1
12	3	IN-2S-2	Inclinometer (Biaxial) - Ch-1 (Longitudinal)	6150	Abutment 1, Downstream Pile, Flange facing the roadway 0.6-1.5 m (2-5 ft) below the bottom of Abutment 1
12	4	IN-2S-2	Inclinometer (Biaxial) - Ch-2 (Transverse)	6150	Abutment 1, Downstream Pile, Flange facing the roadway 0.6-1.5 m (2-5 ft) below the bottom of Abutment 1
12	5	IN-2S-3	Inclinometer (Biaxial) - Ch-1 (Longitudinal)	6150	Abutment 1, Downstream Pile, Flange facing the roadway 1.5-2.7 m (5-9 ft) below the bottom of Abutment 1
12	6	IN-2S-3	Inclinometer (Biaxial) - Ch-2 (Transverse)	6150	Abutment 1, Downstream Pile, Flange facing the roadway 1.5-2.7 m (5-9 ft) below the bottom of Abutment 1
12	7	IN-2S-4	Inclinometer (Biaxial) - Ch-1 (Longitudinal)	6150	Abutment 1, Downstream Pile, Flange facing the roadway 2.7-4.0 m (9-13 ft) below the bottom of Abutment 1
12	8	IN-2S-4	Inclinometer (Biaxial) - Ch-2 (Transverse)	6150	Abutment 1, Downstream Pile, Flange facing the roadway 2.7-4.0 m (9-13 ft) below the bottom of Abutment 1.
12	9	IN-2S-5	Inclinometer (Biaxial) - Ch-1 (Longitudinal)	6150	Abutment 1, Downstream Pile, Flange facing the roadway 4.0-5.2 m (13-17 ft) below the bottom of Abutment 1
12	10	IN-2S-5	Inclinometer (Biaxial) - Ch-2 (Transverse)	6150	Abutment 1, Downstream Pile, Flange facing the roadway 4.05.2 m (13-17 ft) below the bottom of Abutment 1

Table B-6: Abutment 2 (per Structural Drawings) Multiplexer Channel Allocation and Gage Locations

Mux	Channel	Gage Label	Gage Type	Model	Location
1	1	CM-1NT	Displacement Transducer	4420-50mm	Abutment 2, Upstream, Transverse, 2.68 m (8.78 ft) below construction joint.
1	2	CM-1N	Displacement Transducer	4420-100mm	Abutment 2, Upstream, Longitudinal, 2.68 m (8.78 ft) below construction joint.
1	3	CM-1S	Displacement Transducer	4420-100mm	Abutment 2, Downstream, Longitudinal, 1.58 m (5.17 ft) below construction joint.
1	4	P-1NT	Earth Pressure Cell	4810	Abutment 2, Upstream, 3.6 m (12.0 ft) above the bottom of abutment, 1 m (3 ft) away from abutment-wingwall connection.
1	5	P-1NM	Earth Pressure Cell	4810	Abutment 2, Upstream, 2.1 m (7.0 ft) above the bottom of abutment, 1 m (3 ft) away from abutment-wingwall connection.
1	6	P-1NB	Earth Pressure Cell	4810	Abutment 2, Upstream, 0.6 m (2.0 ft) above the bottom of abutment, 1 m (3 ft) away from abutment-wingwall connection.
1	7	P-1CT	Earth Pressure Cell	4810	Abutment 2, Center of Abutment 3.6 m (12.0 ft) above the bottom of abutment.
1	8	P-1CB	Earth Pressure Cell	4810	Abutment 2, Center of Abutment 0.6 m (2.0 ft) above the bottom of abutment.
1	9	P-1ST	Earth Pressure Cell	4810	Abutment 2, Downstream, 3.6 m (12.0 ft) above the bottom of abutment, 1 m (3 ft) away from abutment-wingwall connection.
1	10	P-1SM	Earth Pressure Cell	4810	Abutment 2, Downstream, 2.1 m (7.0 ft) above the bottom of abutment, 1 m (3 ft) away from abutment-wingwall connection.
1	11	P-1SB	Earth Pressure Cell	4810	Abutment 2, Downstream, 0.6 m (2.0 ft) above the bottom of abutment, 1 m (3 ft) away from abutment-wingwall connection.
1	12	Empty Channel			
1	13	PW-1N	Earth Pressure Cell	4815	Wingwall 3, 1.2 m (4.0 ft) above the bottom of wingwall, 1 m (3 ft) away from abutment-wingwall connection.
1	14	PW-1S	Earth Pressure Cell	4815	Wingwall 4, 1.8 m (6.0 ft) above the bottom of wingwall, 1 m (3 ft) away from abutment-wingwall connection.

Table B-6: Abutment 2 (per Structural Drawings) Multiplexer Channel Allocation and Gage Locations (cont.)

Mux	Channel	Gage Label	Gage Type	Model	Location
2	1	SGG-1N-TN	Girder Strain Gage	4050	Upstream Girder, Upstream-Top Flange, 17.6 m (57.7 ft) from the end of steel girder section at Abutment 2.
2	2	SGG-1N-TS	Girder Strain Gage	4050	Upstream Girder, Downstream-Top Flange, 17.6 m (57.7 ft) from the end of steel girder section at Abutment 2.
2	3	SGG-1N-BN	Girder Strain Gage	4050	Upstream Girder, Upstream-Bottom Flange, 17.6 m (57.7 ft) from the end of steel girder section at Abutment 2.
2	4	SGG-1N-BS	Girder Strain Gage	4050	Upstream Girder, Downstream-Bottom Flange, 17.6 m (57.7 ft) from the end of steel girder section at Abutment 2.
2	5	SGG-1S-TN	Girder Strain Gage	4050	Downstream Girder, Upstream-Top Flange, 16.4 m (53.8 ft) from the end of steel girder section at Abutment 2.
2	6	SGG-1S-TS	Girder Strain Gage	4050	Downstream Girder, Downstream-Top Flange, 16.4 m (53.8 ft) from the end of steel girder section at Abutment 2.
2	7	SGG-1S-BN	Girder Strain Gage	4050	Downstream Girder, Upstream-Bottom Flange, 16.4 m (53.8 ft) from the end of steel girder section at Abutment 2.
2	8	SGG-1S-BS	Girder Strain Gage	4050	Downstream Girder, Downstream-Bottom Flange, 16.4 m (53.8 ft) from the end of steel girder section at Abutment 2.
2	9	SGG-0N-TN	Girder Strain Gage	4050	Upstream Girder, Upstream-Top Flange, 34.5 m (113.2 ft) from the end of steel girder section at Abutment 1.
2	10	SGG-0N-TS	Girder Strain Gage	4050	Upstream Girder, Downstream-Top Flange, 34.5 m (113.2 ft) from the end of steel girder section at Abutment 1.
2	11	SGG-0N-BN	Girder Strain Gage	4050	Upstream Girder, Upstream-Bottom Flange, 34.5 m (113.2 ft) from the end of steel girder section at Abutment 1.
2	12	SGG-0N-BS	Girder Strain Gage	4050	Upstream Girder, Downstream-Bottom Flange, 34.5 m (113.2 ft) from the end of steel girder section at Abutment 1.
2	13	SGG-0S-TN	Girder Strain Gage	4050	Downstream Girder, Upstream-Top Flange, 32.0 m (105.0 ft) from the end of steel girder section at Abutment 1.
2	14	SGG-0S-TS	Girder Strain Gage	4050	Downstream Girder, Downstream-Top Flange, 32.0 m (105.0 ft) from the end of steel girder section at Abutment 1.
2	15	SGG-0S-BN	Girder Strain Gage	4050	Downstream Girder, Upstream-Bottom Flange, 32.0 m (105.0 ft) from the end of steel girder section at Abutment 1.
2	16	SGG-0S-BS	Girder Strain Gage	4050	Downstream Girder, Downstream-Bottom Flange, 32.0 m (105.0 ft) from the end of steel girder section at Abutment 1.

Table B-6: Abutment 2 (per Structural Drawings) Multiplexer Channel Allocation and Gage Locations (cont.)

Mux	Channel	Gage Label	Gage Type	Model	Location
3	1	SG-1N-1NE	Pile Strain Gage	4000	Upstream Pile, 0.3 m (1.0 ft) from bottom of Abutment 2 64 mm (2.5 in) from the edge of flange.
3	2	SG-1N-1NW	Pile Strain Gage	4000	Upstream Pile, 0.3 m (1.0 ft) from bottom of Abutment 2 64 mm (2.5 in) from the edge of flange.
3	3	SG-1N-1SE	Pile Strain Gage	4000	Upstream Pile, 0.3 m (1.0 ft) from bottom of Abutment 2 64 mm (2.5 in) from the edge of flange.
3	4	SG-1N-1SW	Pile Strain Gage	4000	Upstream Pile, 0.3 m (1.0 ft) from bottom of Abutment 2 64 mm (2.5 in) from the edge of flange.
3	5	SG-1N-2NE	Pile Strain Gage	4000	Upstream Pile, 1.2 m (4.0 ft) from bottom of Abutment 2 64 mm (2.5 in) from the edge of flange.
3	6	SG-1N-2NW	Pile Strain Gage	4000	Upstream Pile, 1.2 m (4.0 ft) from bottom of Abutment 2 64 mm (2.5 in) from the edge of flange.
3	7	SG-1N-2SE	Pile Strain Gage	4000	Upstream Pile, 1.2 m (4.0 ft) from bottom of Abutment 2 64 mm (2.5 in) from the edge of flange.
3	8	SG-1N-2SW	Pile Strain Gage	4000	Upstream Pile, 1.2 m (4.0 ft) from bottom of Abutment 2 64 mm (2.5 in) from the edge of flange.
3	9	SG-1N-3NE	Pile Strain Gage	4000	Upstream Pile, 2.1 m (7.0 ft) from bottom of Abutment 2 64 mm (2.5 in) from the edge of flange.
3	10	SG-1N-3NW	Pile Strain Gage	4000	Upstream Pile, 2.1 m (7.0 ft) from bottom of Abutment 2 64 mm (2.5 in) from the edge of flange.
3	11	SG-1N-3SE	Pile Strain Gage	4000	Upstream Pile, 2.1 m (7.0 ft) from bottom of Abutment 2 64 mm (2.5 in) from the edge of flange.
3	12	SG-1N-3SW	Pile Strain Gage	4000	Upstream Pile, 2.1 m (7.0 ft) from bottom of Abutment 2 64 mm (2.5 in) from the edge of flange.
3	13	SG-1N-4NE	Pile Strain Gage	4000	Upstream Pile, 3.0 m (10.0 ft) from bottom of Abutment 2 64 mm (2.5 in) from the edge of flange.
3	14	SG-1N-4NW	Pile Strain Gage	4000	Upstream Pile, 3.0 m (10.0 ft) from bottom of Abutment 2 64 mm (2.5 in) from the edge of flange.
3	15	SG-1N-4SE	Pile Strain Gage	4000	Upstream Pile, 3.0 m (10.0 ft) from bottom of Abutment 2 64 mm (2.5 in) from the edge of flange.
3	16	SG-1N-4SW	Pile Strain Gage	4000	Upstream Pile, 3.0 m (10.0 ft) from bottom of Abutment 2 64 mm (2.5 in) from the edge of flange.

Table B-6: Abutment 2 (per Structural Drawings) Multiplexer Channel Allocation and Gage Locations (cont.)

Mux	Channel	Gage Label	Gage Type	Model	Location
4	1	SG-1S-1NE	Pile Strain Gage	4000	Downstream Pile, 0.3 m (1.0 ft) from bottom of Abutment 2 64 mm (2.5 in) from the edge of flange.
4	2	SG-1S-1NW	Pile Strain Gage	4000	Downstream Pile, 0.3 m (1.0 ft) from bottom of Abutment 2 64 mm (2.5 in) from the edge of flange.
4	3	SG-1S-1SE	Pile Strain Gage	4000	Downstream Pile, 0.3 m (1.0 ft) from bottom of Abutment 2 64 mm (2.5 in) from the edge of flange.
4	4	SG-1S-1SW	Pile Strain Gage	4000	Downstream Pile, 0.3 m (1.0 ft) from bottom of Abutment 2 64 mm (2.5 in) from the edge of flange.
4	5	SG-1S-2NE	Pile Strain Gage	4000	Downstream Pile, 1.2 m (4.0 ft) from bottom of Abutment 2 64 mm (2.5 in) from the edge of flange.
4	6	SG-1S-2NW	Pile Strain Gage	4000	Downstream Pile, 1.2 m (4.0 ft) from bottom of Abutment 2 64 mm (2.5 in) from the edge of flange.
4	7	SG-1S-2SE	Pile Strain Gage	4000	Downstream Pile, 1.2 m (4.0 ft) from bottom of Abutment 2 64 mm (2.5 in) from the edge of flange.
4	8	SG-1S-2SW	Pile Strain Gage	4000	Downstream Pile, 1.2 m (4.0 ft) from bottom of Abutment 2 64 mm (2.5 in) from the edge of flange.
4	9	SG-1S-3NE	Pile Strain Gage	4000	Downstream Pile, 2.1 m (7.0 ft) from bottom of Abutment 2 64 mm (2.5 in) from the edge of flange.
4	10	SG-1S-3NW	Pile Strain Gage	4000	Downstream Pile, 2.1 m (7.0 ft) from bottom of Abutment 2 64 mm (2.5 in) from the edge of flange.
4	11	SG-1S-3SE	Pile Strain Gage	4000	Downstream Pile, 2.1 m (7.0 ft) from bottom of Abutment 2 64 mm (2.5 in) from the edge of flange.
4	12	SG-1S-3SW	Pile Strain Gage	4000	Downstream Pile, 2.1 m (7.0 ft) from bottom of Abutment 2 64 mm (2.5 in) from the edge of flange.
4	13	SG-1S-4NE	Pile Strain Gage	4000	Downstream Pile, 3.0 m (10.0 ft) from bottom of Abutment 2 64 mm (2.5 in) from the edge of flange.
4	14	SG-1S-4NW	Pile Strain Gage	4000	Downstream Pile, 3.0 m (10.0 ft) from bottom of Abutment 2 64 mm (2.5 in) from the edge of flange.
4	15	SG-1S-4SE	Pile Strain Gage	4000	Downstream Pile, 3.0 m (10.0 ft) from bottom of Abutment 2 64 mm (2.5 in) from the edge of flange.
4	16	SG-1S-4SW	Pile Strain Gage	4000	Upstream Pile, 3.0 m (10.0 ft) from bottom of Abutment 2 64 mm (2.5 in) from the edge of flange.

Table B-62: Abutment 2 (per Structural Drawings) Multiplexer Channel Allocation and Gage Locations (cont.)

Mux	Channel	Gage Label	Gage Type	Model	Location
5	1	SGP-TN	Pier Strain Gage	4200	0.3 m (1 ft) below top of interior pier column, upstream
5	2	SGP-TS	Pier Strain Gage	4200	0.3 m (1 ft) below top of interior pier column, downstream
5	3	SGP-TE	Pier Strain Gage	4200	0.3 m (1 ft) below top of interior pier column, towards Abutment 2
5	4	SGP-TW	Pier Strain Gage	4200	0.3 m (1 ft) below top of interior pier column, towards Abutment 1
5	5	SGP-BN	Pier Strain Gage	4200	0.3 m (1 ft) above bottom of interior pier column, upstream
5	6	SGP-BS	Pier Strain Gage	4200	0.3 m (1 ft) above bottom of interior pier column, downstream
5	7	SGP-BE	Pier Strain Gage	4200	0.3 m (1 ft) above bottom of interior pier column, towards Abutment 2
5	8	SGP-BW	Pier Strain Gage	4200	0.3 m (1 ft) above bottom of interior pier column, towards Abutment 1

Table B-6: Abutment 2 (per Structural Drawings) Multiplexer Channel Allocation and Gage Locations (cont.)**[*]**

Mux	Channel	Gage Label	Gage Type	Model	Location
10	1	TM-1M	Tiltmeter (Biaxial) - Ch-1 (Longitudinal)	6160	Abutment 2, Center of Abutment, 1.0 m (3.0ft) below the bottom of middle girder
10	2	TM-1M	Tiltmeter (Biaxial) - Ch-2 (Transverse)	6160	Abutment 2, Center of Abutment, 1.0 m (3.0ft) below the bottom of middle girder

[*] Inclinometers planned to be connected to Mux 10 were not installed due to construction issues noted in Section 3.5.5.

APPENDIX C. PICTURES FROM CONSTRUCTION

a) Middlesex Bridge

Figure C-0-4: Middlesex Bridge Construction

b) East Montpelier Bridge

Figure C-0-5: East Montpelier Bridge Construction

c) Stockbridge Bridge

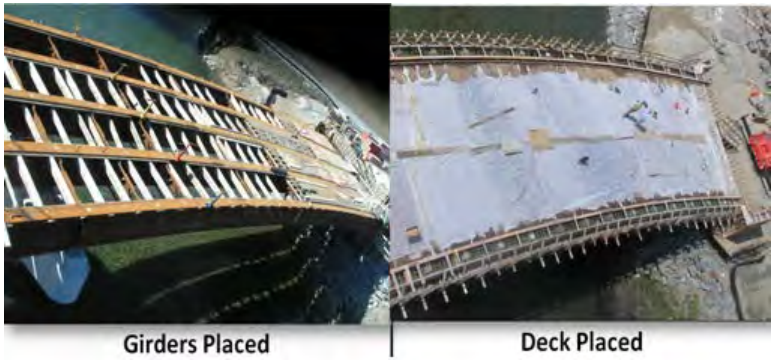

Figure C-0-6: Stockbridge Construction

BIBLIOGRAPHY

API. *Recommended Practice for Planning, Designing and Constructing Fixed Offshore Platforms - Working Stress Design.* Washington, DC: American Petroleum Institute, 1993.

Barker, R.M., Duncan, J.M., Rojiani, K.B., Ooi, P.S.K., Tan, C.K., Kim, S.G. *National Cooperative Highway Research Program (NCHRP) Manuals for the Design of Bridge Foundations.* Washington: Transportation Research Board, 1991.

Barr, P.J., Yanadori, N., Halling, M.W., Wormack, K.C. "Live-Load Analysis of Curved I-Girder Bridge." *Journal of Bridge Engineering*, July/August 2007: 477-484.

Bogard, D., Matlock, H. *Simplified Calculation of p-y Curves for Laterally Loaded Piles.* Unpublished Report, Ertec Inc., 1980.

Bonczar, C., Civjan, S., Brena, S., DeJong, J. *Behavior of Integral Abutment Bridges: Field Data and Computer Modeling.* Boston: EOT Office of Transportation Planning, 2005.

Burke, M. P. "The Design of Integral Concrete Bridges." *Concrete International* 15, no. 6 (1993): 37-42.

Burke, M. P. *Integral Bridges.* Transportation Research Board, National Research Council, 1990.

Conboy, D., Stoothoff, E., "Integral Abutment Design and Construction: The New England Experience." *Proceedings of the 2005 FHWA Conference: Integral Abutment and Jointless Bridges.* Baltimore, Maryland, 2005. 50-60.

Daigle, L. "Temperature Influence on Earth Pressure Cell Readings." *Geotechnical News* 23, no. 4 (2005): 32-36.

Fennema J.L., Laman J.A., Linzell, D.G. "Predicted and Measured Response of an Integral Abutment Bridge." *Journal of Bridge Engineering* 10, no. 6 (2005): 666-677.

Greimann, L F, Wolde-Tinsae, A M Amde, and P S Yang. "Nonlinear Analysis of Integral Abutment Bridges." *Journal of Structural Engineering* (ASCE) 112, no. 10 (1986): 2263-2280.

Iles, D. "Integral Bridges in UK." *International Workshop on IAB's – Lulea University of Technology.* 2006.

Kunin, J., Alampalli, S. "Integral Abutment Bridges: Current Practice in United States and Canada." *Journal of Performance of Constructed Facilities* (ASCE) 14, no. 3 (2000): 104-111.

Lawver, A., French, C., Shield, C.K. "Field Performance of Integral Abutment Bridge." *Journal of the Transportation Research Board* (Transportation Research Record) 1740 (2000): 108-117.

Maruri, R., Petro, S. "Integral Abutments and Jointless Bridges (IAJB) 2004 Survey Summary." *The 2005 FHWA Conference (Integral Abutments and Jointless Bridges).* Baltimore, Maryland, 2005.

Mistry, Vasant C. "Integral Abutment and Jointless Bridges." *The 2005 FWTA Conference.* Baltimore, Maryland, 2005.

Moorty, S., Roeder, C.W. "Temperature-Dependent Bridge Movements." *Journal of Structural Engineering* (ASCE), 1992: 1090-1105.

NEHRP. *Recommended Provisions for Seismic Regulations for New Buildings and Other Structures (FEMA 450).* Building Seismic Safety Council for the FEMA Agency, 2003.

O'Neill, M.W., Murchison, J. M. *An Evaluation of p-y Relationship in Sands.* Res. Rept. GT-DF02-83 to American Petroleum Institute, Houston, Texas: Univ. of Houston, 1983.

Pugasap, K., Kim, W., Laman, A. "Long-Term Response Prediction of Integral Abutment Bridges." *Journal of Bridge Engineering* 14, no. 2 (2009): 129-139.

Roeder, C.W., Moorty. S. "Thermal Movements in Bridges." *Transportation Research Record.* Vol. 1290, Washington, D.C.: Transportation Research Board, National research Council, 1990. 135-143.

Soltani, A.A., Kukreti., A. R. "Performance Evaluation of Integral Abutment Bridges." *Transportation Research Record 1371.* Washington, D.C.: TRB, National Research Council, 1992. 17-25.

Ting, J.M, Faraji, S. *Streamlined Analysis and Design of Integral Abutment Bridges.* Department of Civil and Environmental Engineering, University of Massachusetts Lowell, University of Massachusetts Amherst Transportation Center, 1998.

VTrans. *Structures Manual*. State of Vermont, Agency of Transportation, 2004.

Wiss, Janney, Elstner Associates, Inc. *Synthesis of Technical Information for Jointless Bridge Construction.* State of Vermont, Agency of Transportation, 2002.

PERFORMANCE MONITORING OF JOINTLESS BRIDGES

PHASE III

Report 2014 – 07

PART II

Table of Contents

List of Tables

Table of Figures

1 Introduction

Integral abutment bridges (IABs) have been constructed by State Departments of Transportation for years, serving as a cost-effective alternative to jointed bridges. However, common design guidelines for these bridges are lacking and limitations on IAB design are imposed by State agencies. The Vermont Agency of Transportation (VTrans) initiated a program of field instrumentation and analysis to evaluate the performance of three IABs beginning at bridge construction, and monitored over four years. The bridges are of increasing complexity, a straight girder non-skew bridge, a straight girder 15 degree skew bridge, and a curved girder two-span continuous structure with 11.25 degrees of curvature. The construction, instrumentation, and live load analysis are addressed separately in the Part I report of the project. This report covers Part II of the project, the long term behavior and analysis of these bridges. Finite Element Models (FEMs) of the three bridges were created using SAP2000 and used for comparison to field data. Details of these models are described in the Part I report of the project. Data presented in this report focus on the thermally induced response of the bridges including girder stresses, longitudinal and transverse bridge movement, abutment rotations, abutment and wingwall pressures, substructure displacements, and pile bending moments. All gages used on the bridges include internal thermistors which are used to record the temperature at the gage at each reading. For data analysis, the temperature used for the ambient bridge temperature is the average of the temperature recorded by the shaded bottom flange gages on the bridge girders.

First, this report will give a brief description of the three bridges (which are also addressed in the Part I report). Next, the long term response of each bridge will be detailed and compared to FEM results, with each bridge addressed in a separate chapter. Finally, a comprehensive conclusion will summarize and compare results from the three bridges. Gage labeling and location of gages for each bridge can be found in the appendix.

1.1 Details of Middlesex Bridge

The Middlesex Bridge is located over Martin's Brook on VT12 in Middlesex, Vermont. The bridge is a straight girder non-skewed single span IAB with a bearing to bearing length of 141.0 ft (43.0 m) and a width of 33.5 ft (10.2 m) to outside of fascia. Five plate girders support an 8.7 in (220 mm) concrete deck. Each girder has a 46.1x0.6 in (1170x14 mm) web, with top and bottom flange plates of 20.1x1.0 in (510x25 mm) and 20.1x2.1 in (510x54 mm), respectively. Girders start at 3.28 ft (1.00 m) from fascia and are evenly spaced at 6.70 ft (2.05 m).The abutment is 3.28 ft (1.00 m) thick with a height of 13.12 ft (4.00 m) and 13.78 ft (4.20 m) from bottom of abutment to top of concrete at the fascia and center of roadway, respectively. Wingwalls are integral with the abutment with a thickness of 1.48 ft (0.45 m) and extend 9.84 ft (3.00 m) orthogonal to the abutment. Five HP12x84 (HP310x125) steel piles support each abutment wall; the piles are embedded 3.28 ft (1.00 m) into the bottom of the abutment and extend approximately 29.53 ft (9.00 m) below the abutment. The plan and elevation views of the bridge are shown in Figure 1-1.

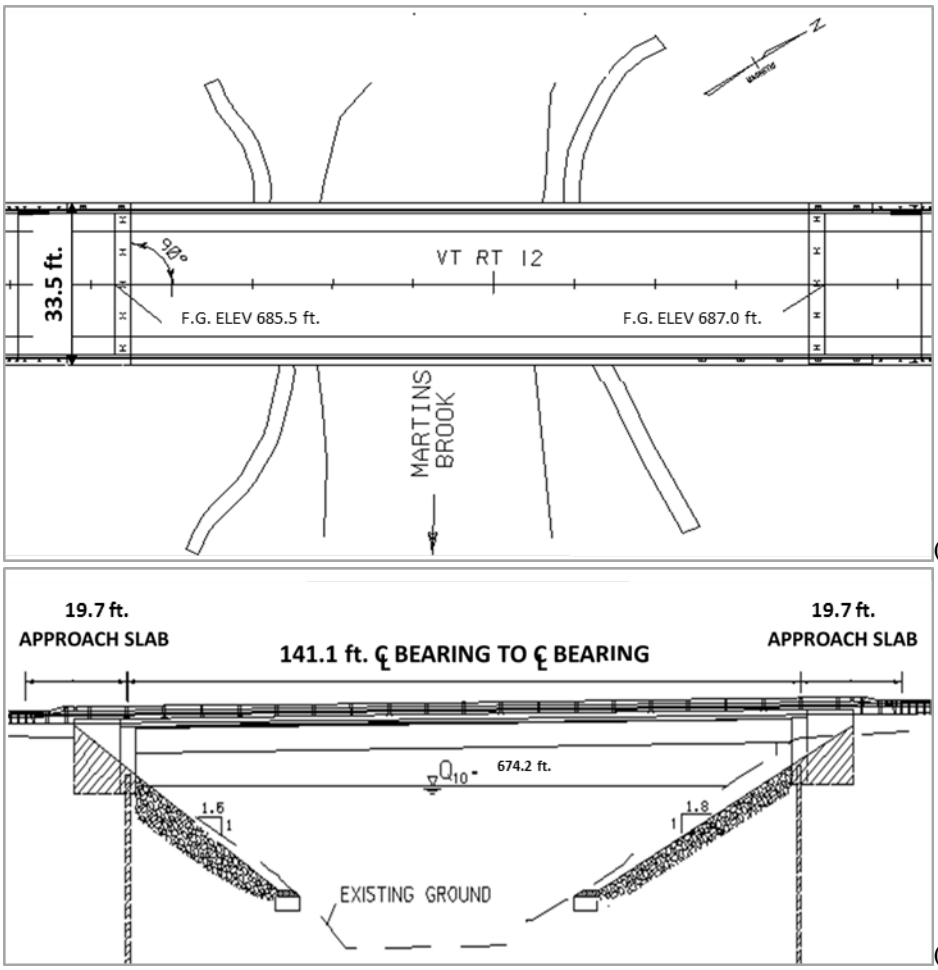

Figure 1-1 Middlesex Bridge (a) plan view (b) elevation view

1.2 Details of East Montpelier Bridge

The East Montpelier Bridge is located over the Winooski River on US2 in East Montpelier, Vermont. The bridge is a straight girder IAB with a 15 degree bridge skew. The bearing to bearing length is 121.4 ft (37.0 m) and the width is 46.6 ft (14.2 m) to outside of fascia. Five plate girders support an 8.7 in (220 m) concrete deck. Each girder web is 53x0.6 in (1346x16 mm) with top and bottom flange plates of 18x0.87 in (457x22 mm) and 18x1.6 in (457x41 mm), respectively. Starting 3.61 ft (1.10 m) from each fascia, the girders are evenly spaced at 8.84 ft (3.00 m) across the bridge. The abutment is 2.95 ft (0.90 m) thick with a height of 12.80 ft (3.90 m) and 13.3 ft (4.10 m) from the bottom of abutment to top of concrete at the fascia and center of roadway, respectively. Wing walls are integral with the abutment, with a thickness of 1.48 ft (0.45 m) and extend 9.19 ft (2.80 m) from the centerline of the abutment at a 15 degree skew. Five HP12x84 (HP310x125) steel piles support each abutment; the piles are embedded 1.97 ft (0.60 m) into the bottom of the abutment and extend approximately 125 ft (38 m) below the abutment. The plan and elevation views are shown in Figure 1-2.

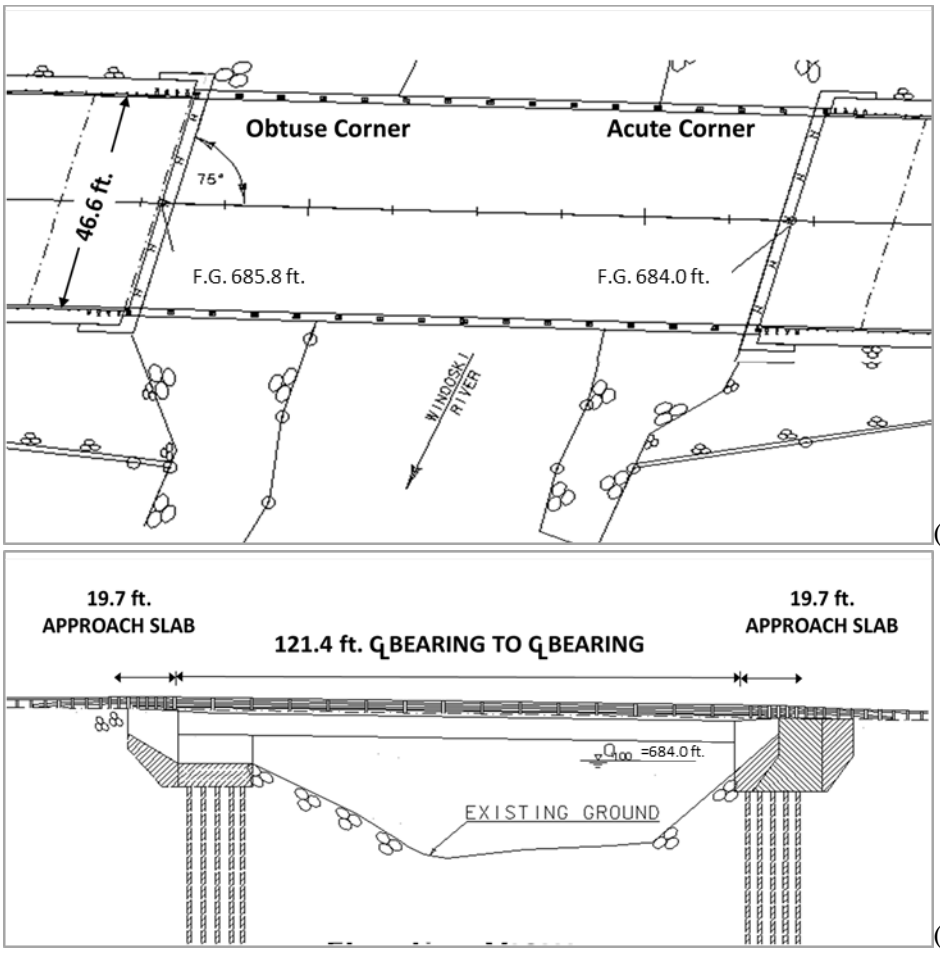

Figure 1-2 East Montpelier Bridge (a) plan view (b) elevation view

1.3 Details of Stockbridge Bridge

The Stockbridge Bridge is a curved girder IAB located on VT Route 100, crossing the White River in Stockbridge, Vermont. The bridge length is 222.0 ft (67.6 m) along its curved centerline, with an 11.25 degree of curvature along the bridge alignment, and a width of 37.1 ft (11.3 m) to the fascia. This two-span bridge includes a center pier with guided bearings on top of the pier cap positioned to support each steel girder. There is a superelevation of 6 percent at road level and a vertical elevation difference of 4.3 ft (1.3 m) between start and end of the bridge. The bridge is composite with an 8 in (203 mm) thick reinforced concrete and five built-up steel plate girders. The girders are spaced at 6.70 ft (2.36 m) supporting the deck. The girder web dimensions are constant at 46x0.6 in (1170x16mm). Flange dimensions differ among girders and vary along the span (cross sections are presented in Part I). Abutments are 3.00 ft (0.90 m) thick with an average depth of 20.70 ft (6.30 m) Wing walls have a thickness of 1.50 ft (0.45 m) and extend 10.00 ft (3.00 m) and 14.00 ft (4.30 m) from the centerline of Abutment 1 and Abutment 2, respectively. The wing walls are oriented at 85 degrees and 110 degrees from the abutment and have a tapered bottom face. The abutments are supported on five HP 14x117 (HP 360x174) steel piles that are embedded 2.00 ft (0.60 m) into the bottom of the abutment and extend approximately 75.5 ft (23.0 m) below the abutment. Geofoam material was applied at the abutment backwalls prior to backfilling to reduce earth pressures on abutments. The bridge plan and elevation views are shown in Figure 1-3.

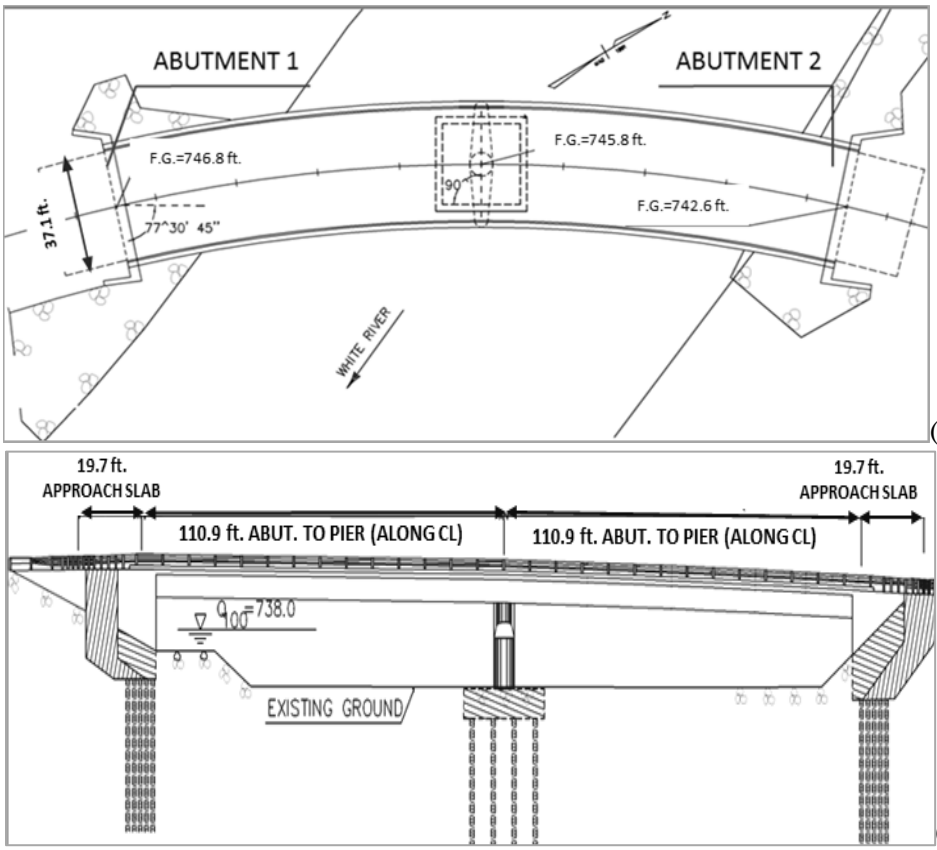

Figure 1-3 Stockbridge Bridge (a) plan view (b) elevation view

2 Long Term Response of the Middlesex Bridge

The long term monitoring of the Middlesex Bridge began when construction was completed on December 04, 2009. This section documents the long term response of this IAB from December 04, 2009 through December 31, 2013. The ambient bridge temperature over the monitoring period is shown in Figure 2-1.

A three-dimensional finite element model (FEM) was created for the bridge using SAP2000. Soil is modeled using non-linear Winkler springs. The original model used for comparison to field data contained soil springs based on the soil boring logs reported at bridge construction (medium-dense soil around the piles and dense backfill). The model was then calibrated to match conditions seen in field data to compare values. This will be discussed in greater detail in later sections of the chapter.

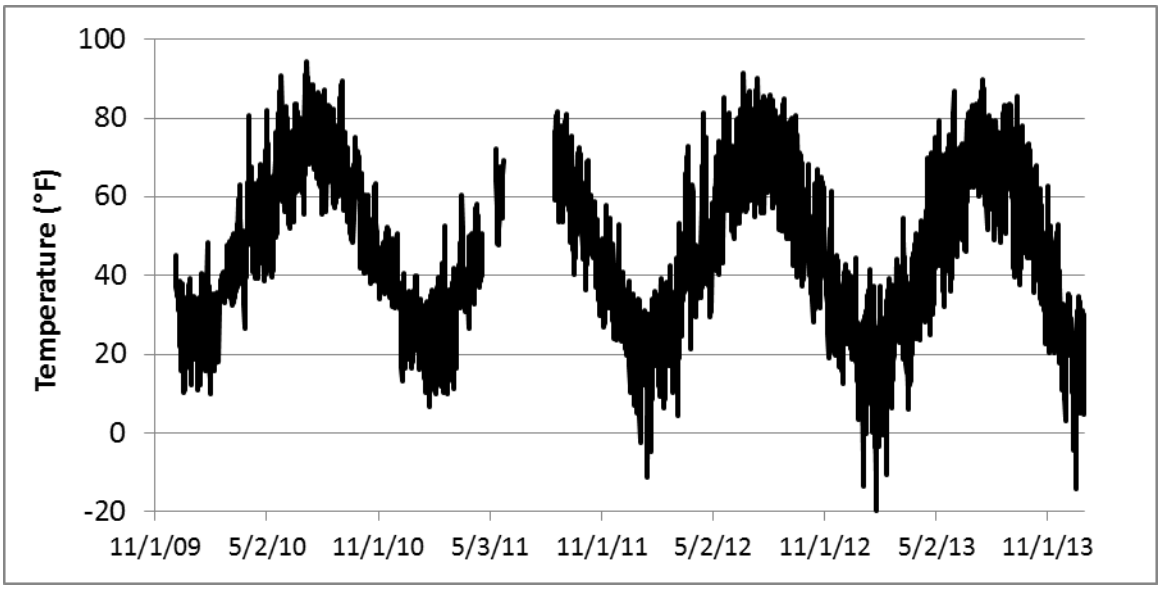

Figure 2-1 Average Bridge Deck Temperature

2.1 Girder Stresses

All stress values presented in this section correspond to those induced by thermal effects only. Girder stresses are presented in Figure 2-2, Figure 2-3, and Figure 2-4. First, the flange stresses are presented with temperature, and then shown over time. A negative value indicates compressive stress and a positive value indicates tensile stress. Bottom flange stresses are consistently greater than top flange stresses due to the elastic neutral axis located near the slab/girder interface. Girder top flange stresses range between -2.1 ksi (-14.5 MPa) and 1.7 ksi (11.7 MPa) while bottom flange stresses range between -6.4 ksi (-44.1 MPa) and 4.3 ksi (29.6 MPa). Temperature has little effect on top flange stresses which indicates that the girders act compositely for both positive and negative bending. Girder stresses across the abutment are consistent; the upstream, middle, and downstream girder have comparable stress values at any given point in time as seen for the Abutment 1 end in Figure 2-3 and Figure 2-4. These stresses are also comparable at midspan of the bridge and at the Abutment 2 end, demonstrating the constant induced girder moment along the bridge for a given thermal change, as expected from FEA.

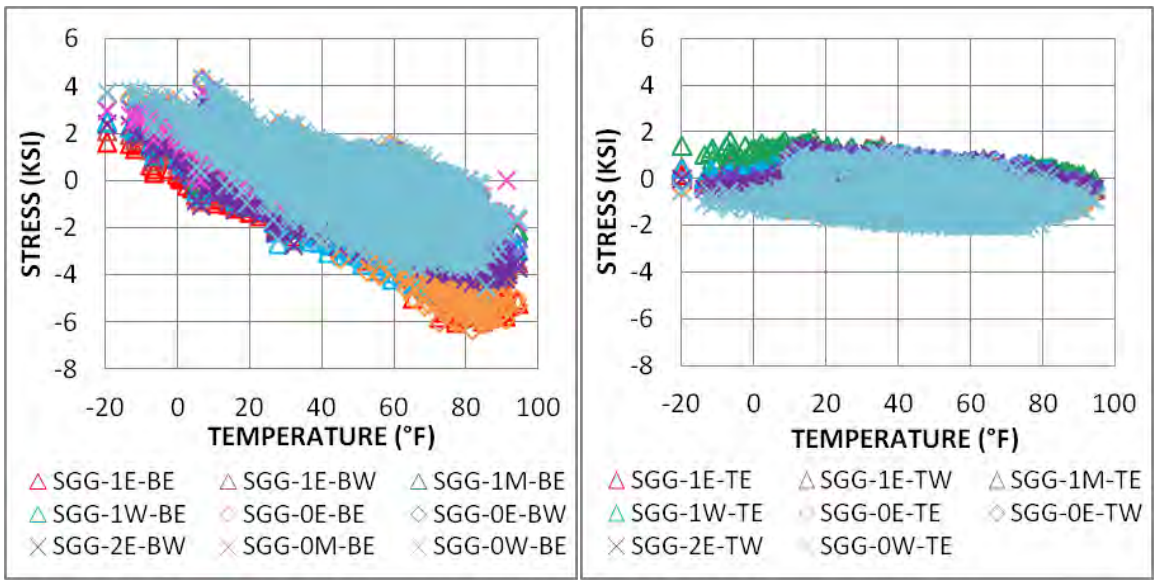

(a) (b)

Figure 2-2 Girder Stresses with Temperature (a) bottom flange gages (b) top flange gages

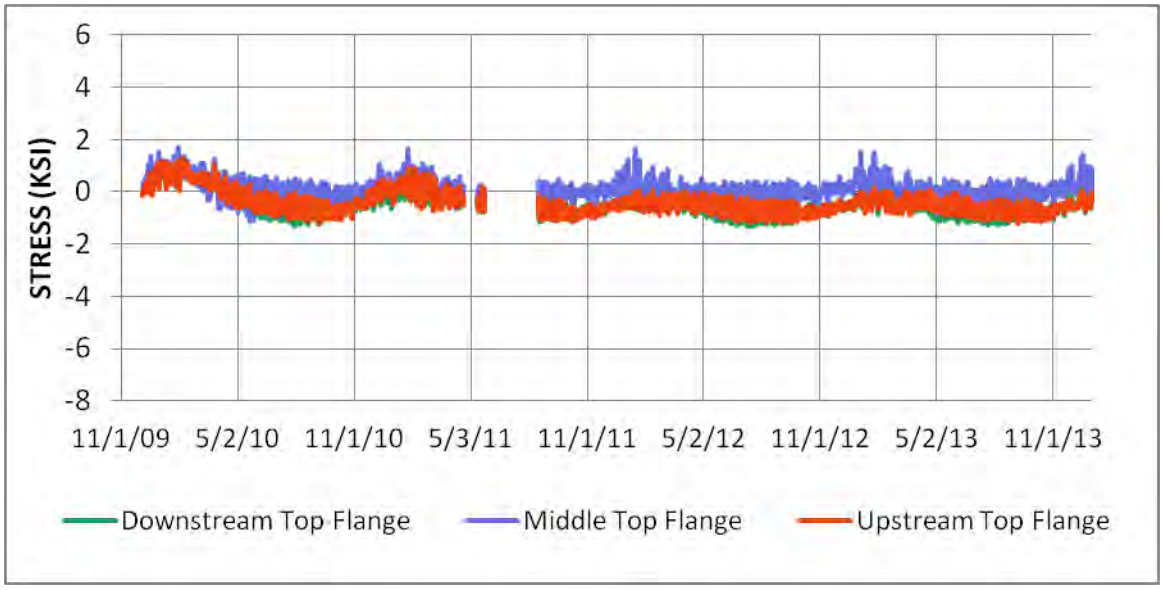

Figure 2-3 Top Flange Girder Stresses at Abutment 1

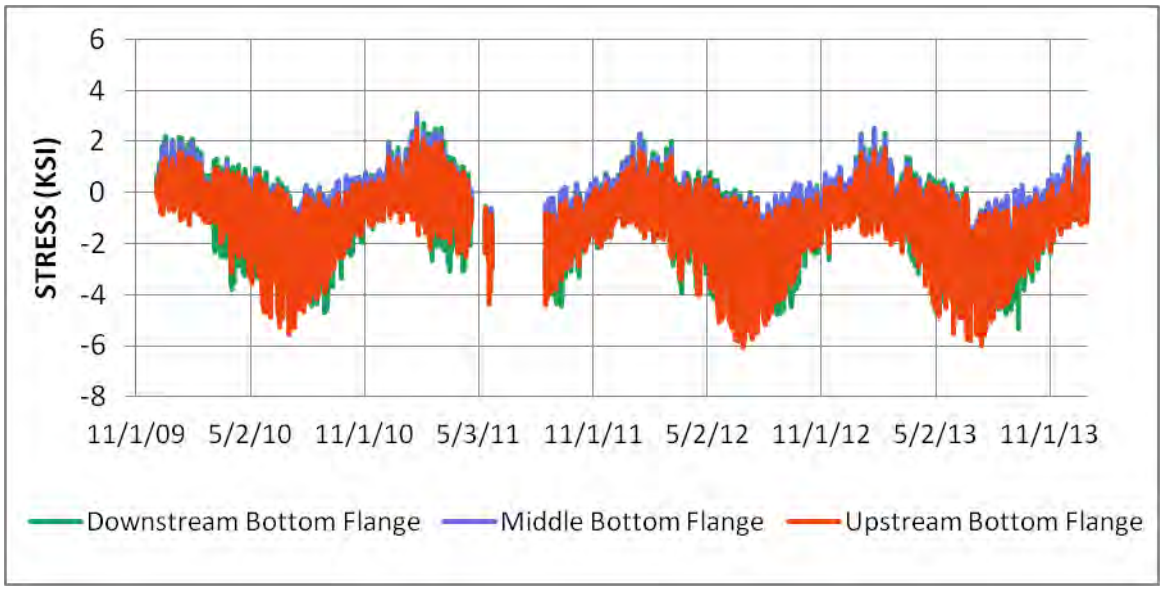

Figure 2-4 Bottom Flange Girder Stresses at Abutment 1

2.2 Displacement

Displacements presented in this section are those caused by thermal effects (they do not include displacements that occurred during construction). Longitudinal abutment displacements are presented in Figure 2-5 and Figure 2-6, for tops and bottoms of abutments, respectively. Top of abutment displacement refers to the displacement at the top of the girder top flange. For Abutment 1, a positive displacement indicates movement towards the river while a negative displacement indicates movement towards the backfill. For Abutment 2, the opposite sign convention is used (positive displacement for bridge expansion and negative displacement for bridge contraction). The figures also include FEM results for maximum and minimum yearly temperatures. Using the equation for unrestrained thermal expansion

$\delta=\alpha L\Delta T$, (Equation 1)

where L = span length; α = coefficient of thermal expansion of superstructure 6.5×10^{-6}°F, and ΔT = temperature change, estimated displacements due to thermal loading were calculated. The total expected longitudinal displacement (sum of both abutment movements) due to thermal fluctuation from yearly minimum to maximum temperature is compared to field data as well as FEM results in Table 2-1 and Table 2-2, for top and bottom of abutment displacements, respectively.

Both abutment displacements increased over time towards their backfill, however displacements have stabilized in 2012 and 2013. In 2011, Abutment 1 showed a significant shift towards the backfill after electrical storms and Hurricane Irene (August 28-29, 2011) that was not seen at Abutment 2. When the shift occurred, the displacement at Abutment 1 was approximately 33% greater than at Abutment 2. Seasonal movements of the abutments remained similar after the shift occurred; peak to peak displacements after 2011 were comparable to those before the severe weather noted above. Bottom of abutment displacements were significantly lower than the tops of the abutments due to abutment rotation.

The FEM results were a good match to field data for both abutments until the shift in Abutment 1, after which FEM results were still a comparable match for Abutment 2 but do not match Abutment 1 as the model would not predict this shift in displacement of the symmetric bridge. For the bottom of

the abutments, FEM results underestimated displacements showing that there is less restraint to movement at the top of the pile than is assumed in the FEM (which is based on soil borings from the site and reported backfill conditions). The equation of thermal expansion, which is based on unrestrained conditions, also does not match the displacements at the bottom of the abutments because the abutment movement is a combination of translation and rotation which results in significantly lower displacements at the bottom of the abutments.

Table 2-1 and Table 2-2 show the net thermal abutment displacement from minimum to maximum temperature from 2010 through 2013. FEM results were almost exactly the same as the net expansion predicted by the thermal expansion equation for the top of the abutment. Aside from 2011, peak to peak displacements were comparable to FEM and thermal expansion equation results. Overall, both FEM and the equation of thermal expansion could be good estimates in predicting thermally induced net superstructure response. The thermal expansion equation is not representative of bottom of abutment displacements due to abutment rotation. The FEM results were an underestimate of bottom of abutment displacement under bridge expansion for all four years showing that the backfill was looser than the original dense soil conditions reported at the site. For bridge contraction, the FEM results were closer in the first two years while in the latter two years it was not a good match due in part to the lag in pile recovery from its expanded deflected shape (this will be addressed in greater detail in the substructure displacement section).

After the severe weather in summer 2011, field data shows unsymmetrical behavior between the two abutments that would not be expected for this symmetric straight-girder non-skew bridge nor predicted by any of the mentioned methods. However, the peak to peak abutment displacements after the shift in Abutment 1 were still close to the results from both FEM and the equation for thermal expansion (at the top of the abutments) and also show that the bridge has stabilized in the latter years. Therefore, these methods can be a good estimate of long term bridge response.

The seasonal relation between displacement at the top of the abutment and displacement at the bottom of the abutment is shown in Figure 2-7 for both abutments. Winter to summer corresponds with the beginning of October through the end of March, and summer to winter corresponds with the beginning of April through the end of September. These displacement relations show the variability in behavior of the abutments in the beginning of monitoring, especially during the shift that occurred during 2011 which resulted in greater displacements at the top and bottom of Abutment 1 while Abutment 2 seasonal displacements were more consistent year to year. The last two years of monitoring show the stabilized behavior at both abutments.

Transverse abutment displacements are shown in Figure 2-8. The transverse displacements have increased over time; however the maximum peak to peak transverse displacement is 0.07 in (1.8 mm) occurring in 2013, this is well below the 0.29 in (7.4 mm) predicted by the thermal expansion equation for this change in temperature. Overall, transverse displacements are minimal and are within the bounds of expected displacements due to thermal expansion.

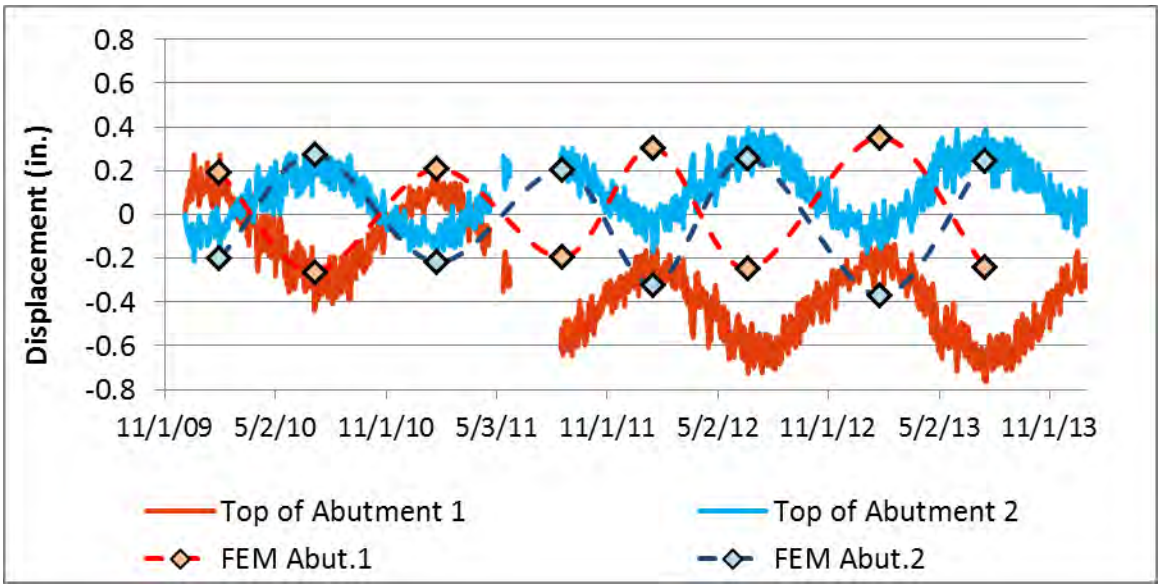

Figure 2-5 Longitudinal Top of Abutment Displacements (field data and FEM)

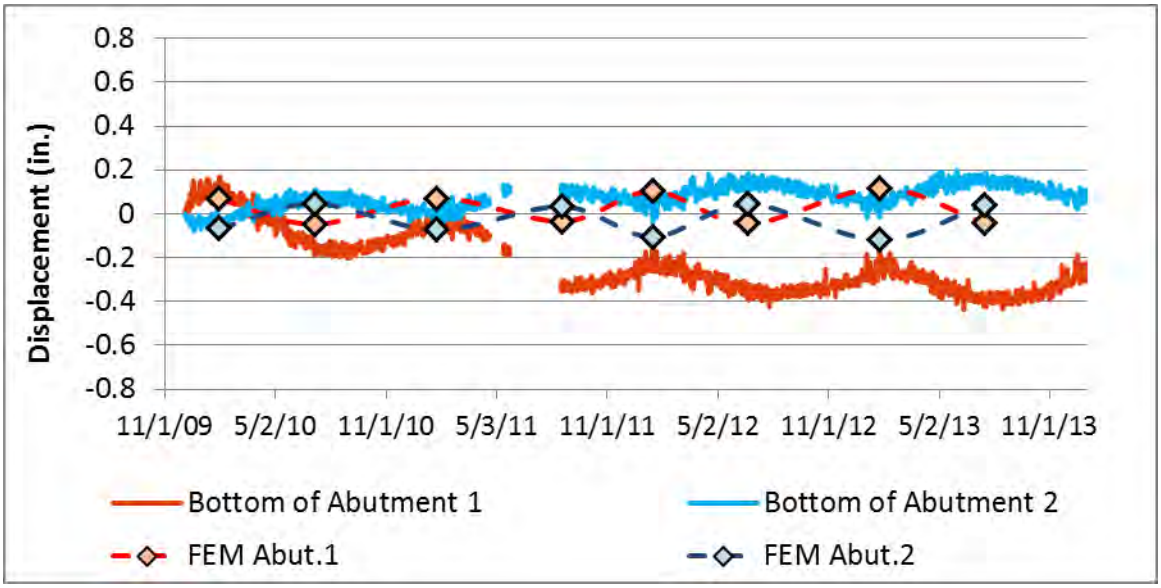

Figure 2-6 Longitudinal Bottom of Abutment Displacements (field data and FEM)

Table 2-1 Peak to Peak Top of Abutment Displacements

Year	DT (°F)	Field Data Sum of Abutment Displacements (in.) (Abut.1+Abut.2)	FEM Sum of Abutment Displacements (in.)	Thermal Expansion Eq. (in)
2010	84.2	0.67+0.47=1.14	0.46+0.47=0.93	0.93
2011	75.1	0.86+0.53=1.39	0.40+0.42=0.82	0.83
2012	102.8	0.59+0.56=1.15	0.55+0.58=1.13	1.13
2013	109.5	0.64+0.53=1.17	0.59+0.62=1.20	1.20

Table 2-2 Peak to Peak Bottom of Abutment Displacements

Year	DT (°F)	Field Data Sum of Abutment Displacements (in.) (Abut.1+Abut.2)	FEM Sum of Abutment Displacements (in.)	Thermal Expansion Equation (in.)
2010	84.2	0.35+0.18=0.52	0.11+0.11=0.22	0.93
2011	75.1	0.41+0.19=0.60	0.11+0.11=0.22	0.83
2012	102.8	0.25+0.21=0.46	0.15+0.15=0.30	1.13
2013	109.5	0.27+0.20=0.47	0.16+0.16=0.32	1.20

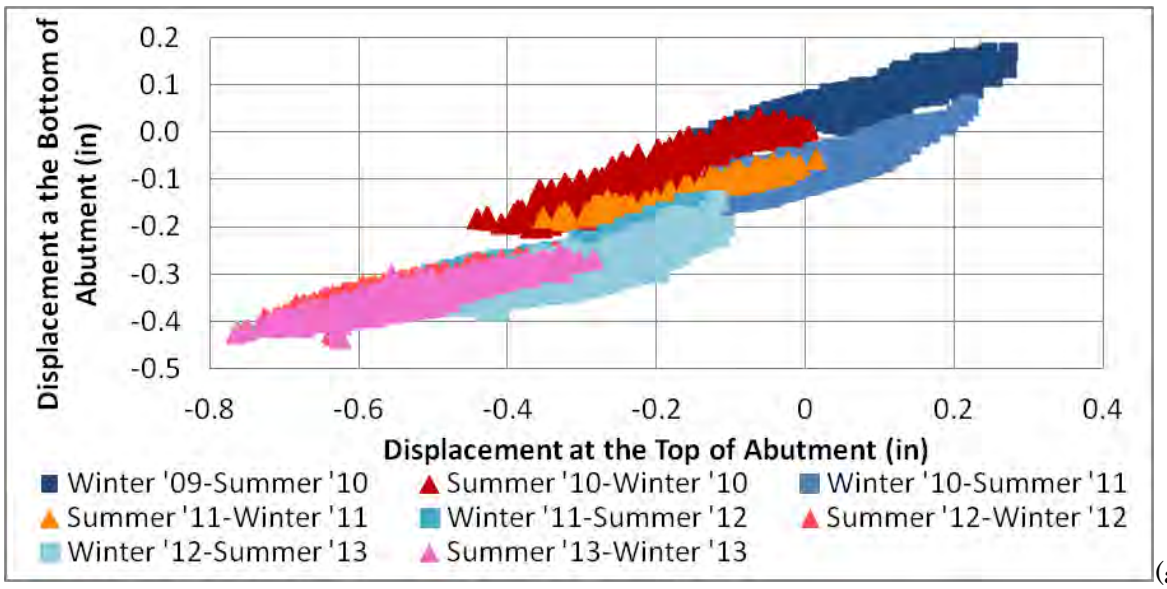

(a)

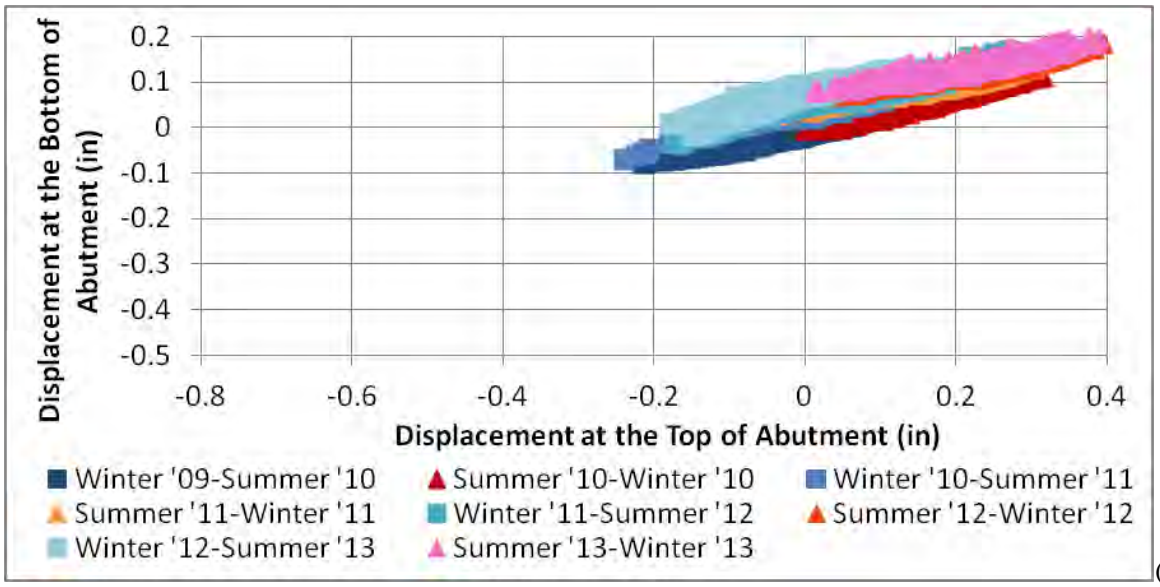

(b)

Figure 2-7 Seasonal Displacements at the top and bottom of (a) Abutment 1 (b) Abutment 2

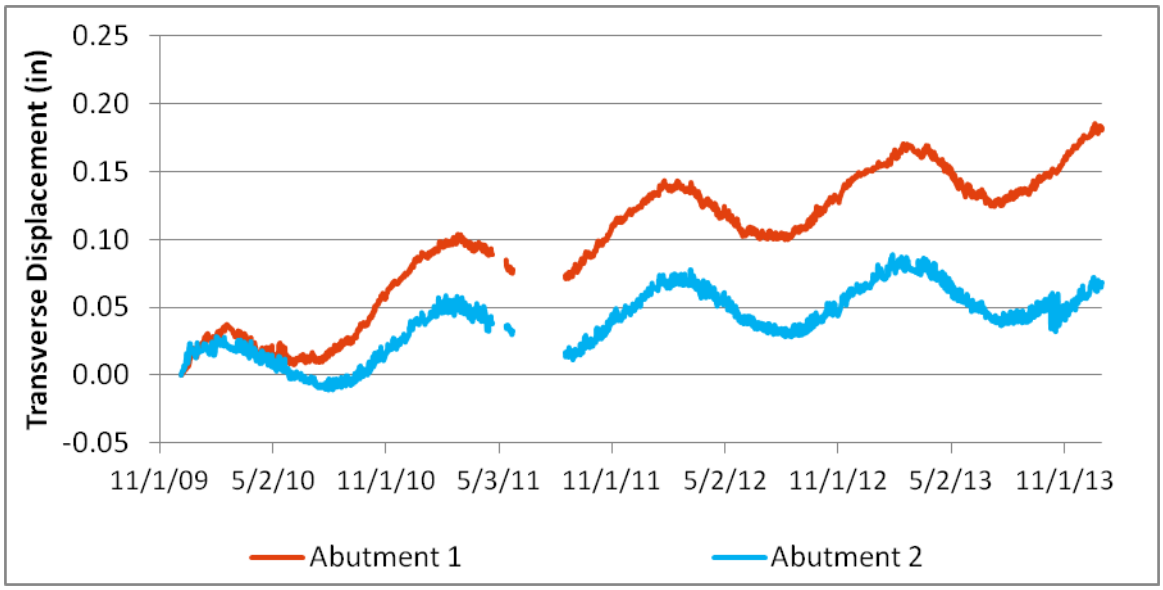

Figure 2-8 Transverse Abutment Displacements

2.3 Abutment Rotation

Abutment rotations presented in this section are the rotations resulting from thermal effects. Abutment rotations are presented in Figure 2-9 and Figure 2-10. A positive rotation value indicated rotation towards the river (bridge contraction) while a negative rotation value indicates rotation towards the backfill (bridge expansion) for both abutments. Abutment rotation has increased over time as can be seen in Figure 2-9, with a slightly greater rotation at Abutment 1 after 2011 which is consistent with the shift in displacement towards the backfill of the abutment.

In Figure 2-10, the first year of abutment rotations is distinguished from the later years with a darker shade of color. This figure shows that although FEM results do not match as well for later years of monitoring, they actually match the first year quite well. Even though the rotation values do not match in the later years, the peak to peak rotations from the FEM are very close to peak to peak rotations from field data for all four years (except, again, Abutment 1 in 2011). These values are presented in Table 2-3 and show the stabilization of peak to peak rotations.

IABs are often designed assuming the displacement at the top of the abutment is constant throughout the height of the abutment thereby neglecting abutment rotation; this field data suggests that this design assumption is overly conservative. Even though the FEM static thermal analysis does not capture the increase in rotations as the abutments shift towards their backfills, the model captures net rotations quite well and this could be useful to use in considering design of this type of IAB.

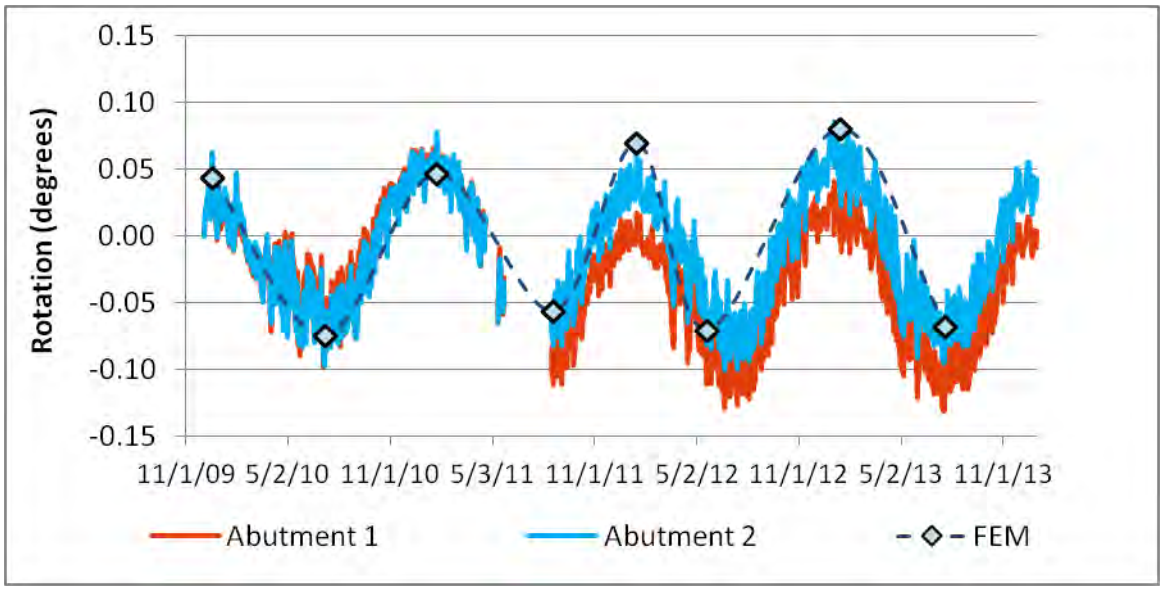

Figure 2-9 Abutment Rotation

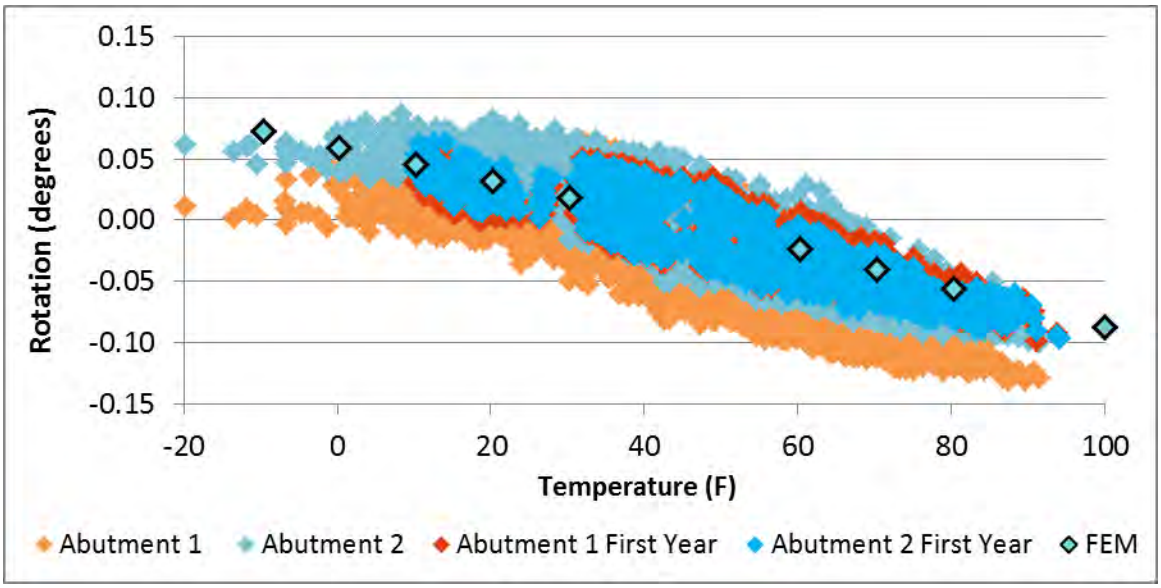

Figure 2-10 Abutment Rotation with Temperature (field data and FEM)

Table 2-3 Peak to Peak Abutment Rotations (field data and FEM)

Year	Field Data Rotation (degrees)		FEM Rotation (degrees)	
	Abutment 1	Abutment 2	Abutment 1	Abutment 2
2010	0.13	0.14	0.12	0.12
2011	0.17	0.16	0.10	0.11
2012	0.14	0.16	0.14	0.15
2013	0.14	0.15	0.15	0.16

2.4 Earth Pressure

Pressures presented in this section are the changes in pressure since construction due to thermal loading Earth pressures are presented over time in Figure 2-11, Figure 2-12, and Figure 2-13 for top, middle, and bottom rows of pressure cells (exact locations are provided in the appendix). The pressures were greatest at the middle row of pressure cells (3.6 ft (1.1 m) above bottom of abutment). The maximum pressure was 5.5 psi (37.9 KPa), and the maximum average pressure of pressure cells at this depth was 5.4 psi (37.2 KPa) showing the consistency in pressures across the abutment. Pressures were also comparable between the two abutments which are seen in the figures (Abutment 2 instrumentation was more limited and did not have middle pressure cells).

Figure 2-14 shows that pressure tends to increase for increasing displacements during a given season. However, when the same displacement is reached in subsequent seasons, the corresponding pressure is less than the first time this displacement occurred. This behavior shows that soil ratcheting is not occurring in the backfill at this bridge.

At the completion of bridge construction, the pressure at the middle depth of pressure cells was 3.1 psi (21.4 KPa); therefore the maximum cumulative earth pressure the bridge has experienced is 8.6 psi (59.3 KPa). The assumed fully passive pressure at this depth is 30.6 psi (211.0 KPa). Therefore, this bridge has experienced 28% of the assumed fully passive pressure at the depth where the maximum instrumented pressure occurred.

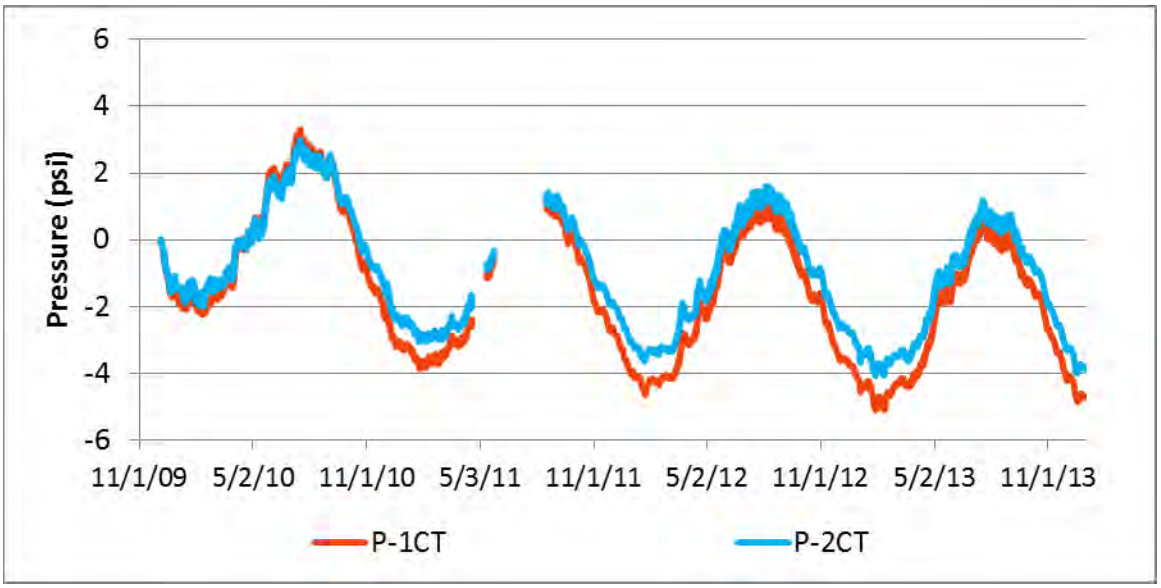

Figure 2-11 Earth Pressure in Top Row of Pressure Cells

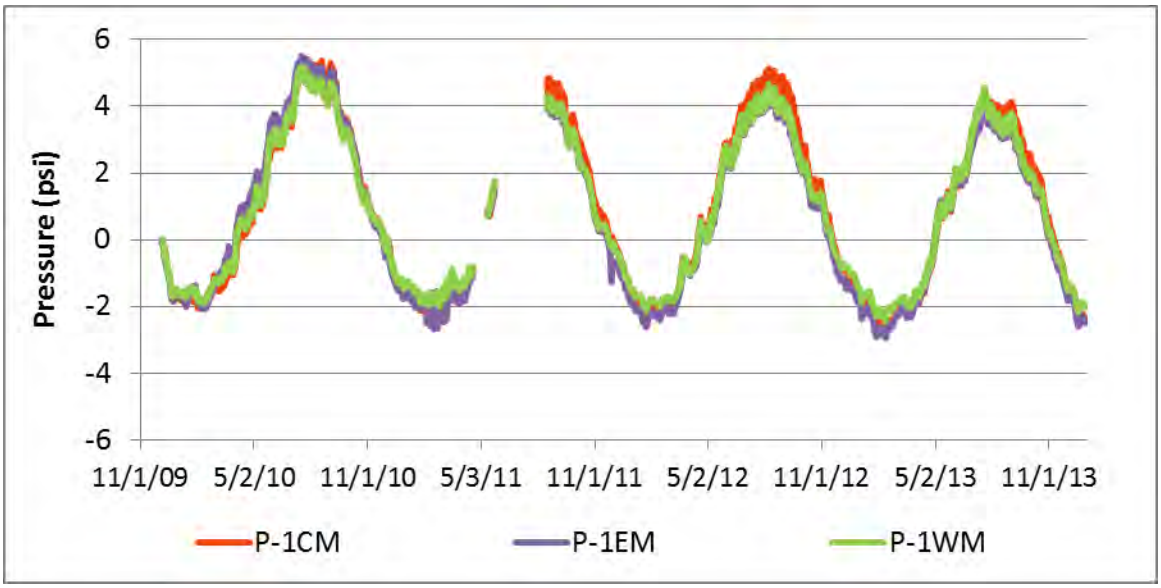

Figure 2-12 Earth Pressure in Middle Row of Pressure Cells

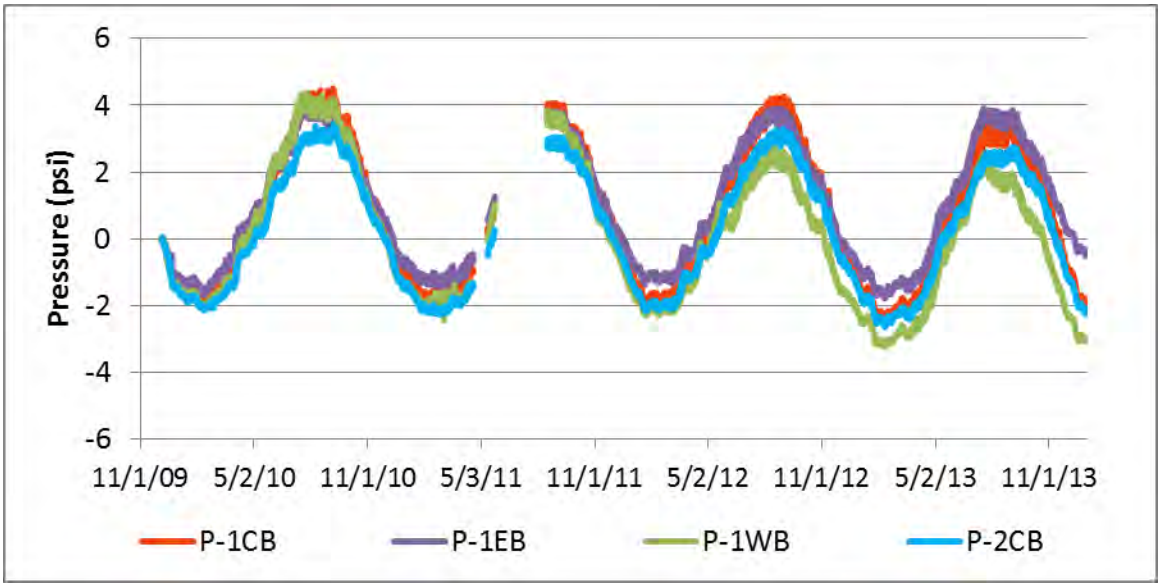

Figure 2-13 Earth Pressure in Bottom Row of Pressure Cells

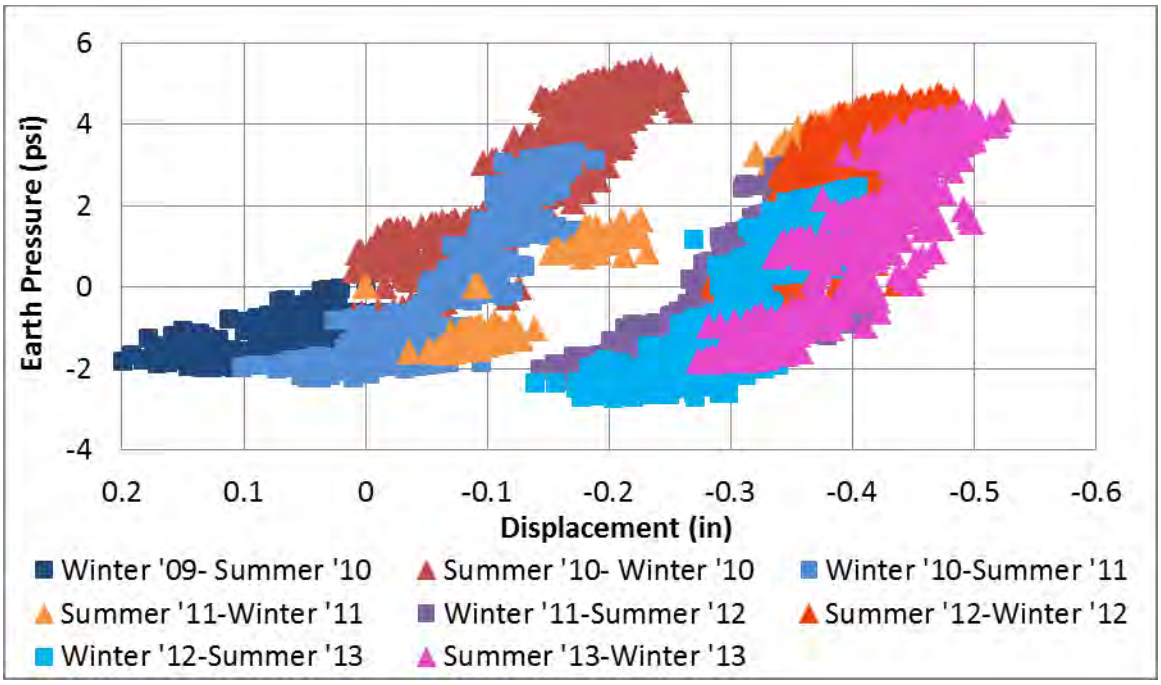

Figure 2-14 Average Earth Pressure in Middle Row of Pressure Cells vs. Corresponding Displacement

2.5 Substructure Displacement at Maximum and Minimum Temperatures

The substructure displacements presented in this section are those resulting from thermal effects only. Response of IABs to thermal fluctuation is an important factor to consider in design since the integral connection of superstructure to substructure means that thermal expansion and contraction is directly resisted by the substructure. Field data shows that many factors are involved in the thermally induced substructure response of the bridge including the time of year that a given temperature occurs, and complex non-linear soil behavior. These factors make it difficult to predict the substructure behavior of an IAB under thermal loading using a static FEM. Field data shows that there is a lag in recovery of the pile from its expanded deflected shape; this can be seen in Figure 2-15 and was also mentioned in Section 2.2 regarding bottom of abutment displacement being underestimated.

Figure 2-15 shows substructure displacement from field data for the maximum and minimum temperature that occurred each year, as well as a similar warm or cold temperature that occurred at the beginning and end of that season. The deflected shapes clearly show that temperature is not the only factor involved in the substructure response. At the beginning of the season the bridge expands as it experiences the first warm temperature, then when the maximum temperature occurs it expands to its maximum deflected shape of that season (as would be expected from a thermal expansion equation or FEM), however at the end of the season while the top of the abutment begins to contract the top of the pile maintains its deflected shape resulting in concentrated curvature at the pile-abutment interface. While substructure displacement under bridge contraction shows a more elastic response, after 2011 the pile never fully recovers from its expanded deflected shape even under the minimum temperature of the year. Figure 2-16 shows the maximum and minimum temperatures that occurred each year, as well as FEM results for the same temperature using soil conditions reported from soil boring logs when the bridge was constructed. These plots show that for

warm temperatures the FEM with the original soil conditions does not match the field behavior for any year, and for the cold temperatures while the model is a decent match for the first two years, the minimum temperature deflected shape does not agree in the latter years. This could be due to a number of factors such as soil properties changing upon repeated thermal loading, cracks forming in the deck, and the lag in pile recovery seen in field data that is not captured in a static thermal analysis.

For all of the reasons mentioned above, analyzing the FEM for a thermal load matching the temperature in the field with the same soil conditions for every year will not accurately capture bridge behavior. To be able to compare field data to the FEM, the model was calibrated to match the displacement at the top of the abutment (by increasing or decreasing thermal loading as necessary) and then adjusting the soil conditions in the model to replicate the field behavior. By doing this, field results such as pile bending moments can be compared to the matched FEM results as well as to FEM using nominal soil properties. Figure 2-17 and Figure 2-18 show the deflected shape resulting from calibrating the FEM, as well as the soil conditions used to match the field data. Soil properties used in FEMs can be found in Table 2-4.

As was stated previously, the original soil conditions at the site were reported as medium-dense soil around the piles and dense backfill. The bridge was constructed in cold weather and long term monitoring began in the winter months. FEM Matched results show that the first time the bridge reached its expanded shape the backfill was already acting as a loose soil, and the soil around the top 10.0 ft (3.0 m) of the pile was loose as well. In subsequent years, the backfill condition remained the same but the soil loosened slightly more. For bridge contraction, the soil acted as loose for the first two years, but in 2012 and 2013 when the bridge contracts it is as if there is effectively no soil around the top 8.0 ft (2.4 m) of the pile as a result of the pile holding its expanded deflected shape. These “FEM Matched” model results will be discussed further in Section 2.6.

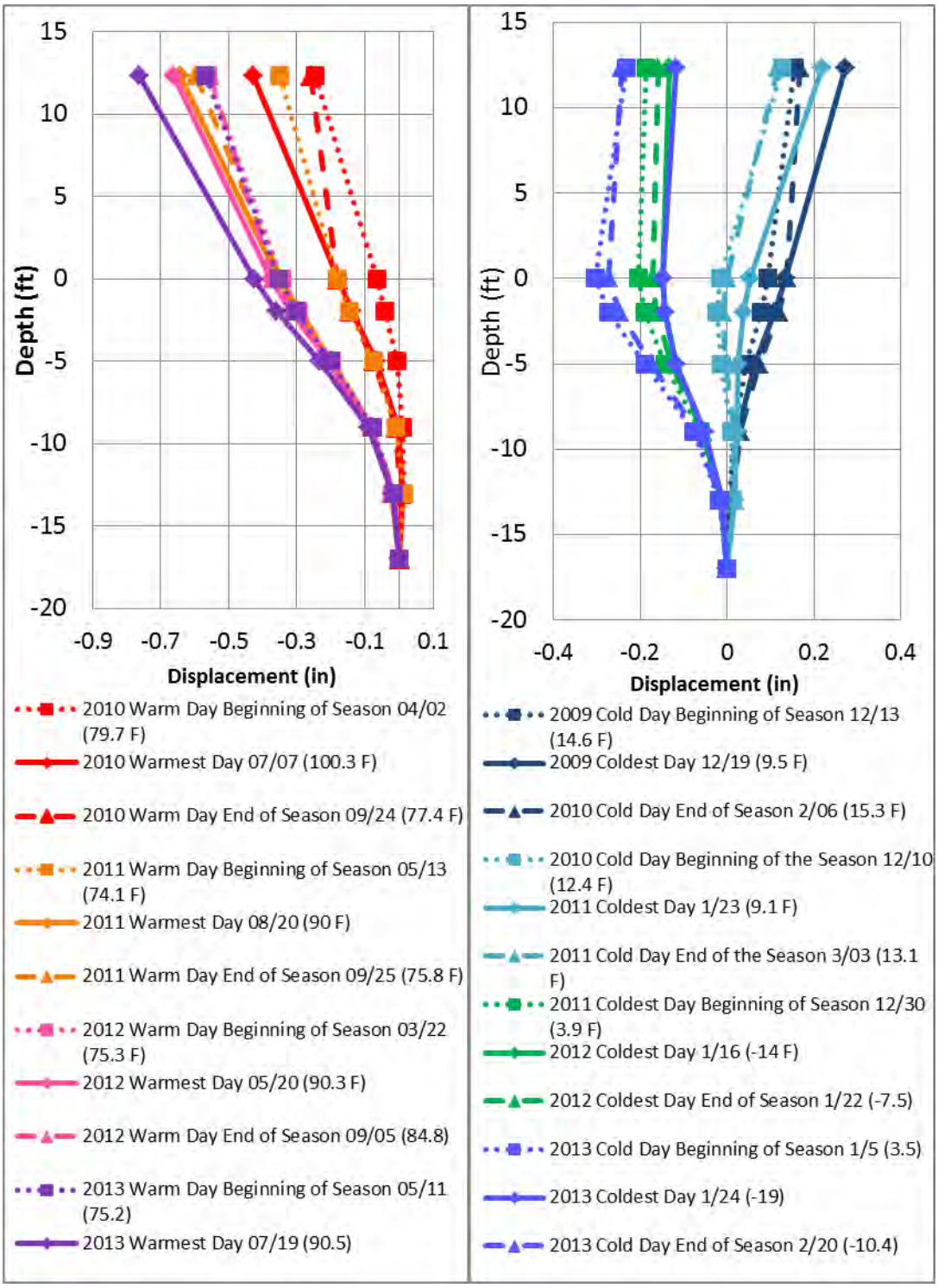

Figure 2-15 Seasonal substructure displacement for warm temperatures (left) and cold temperatures (right)

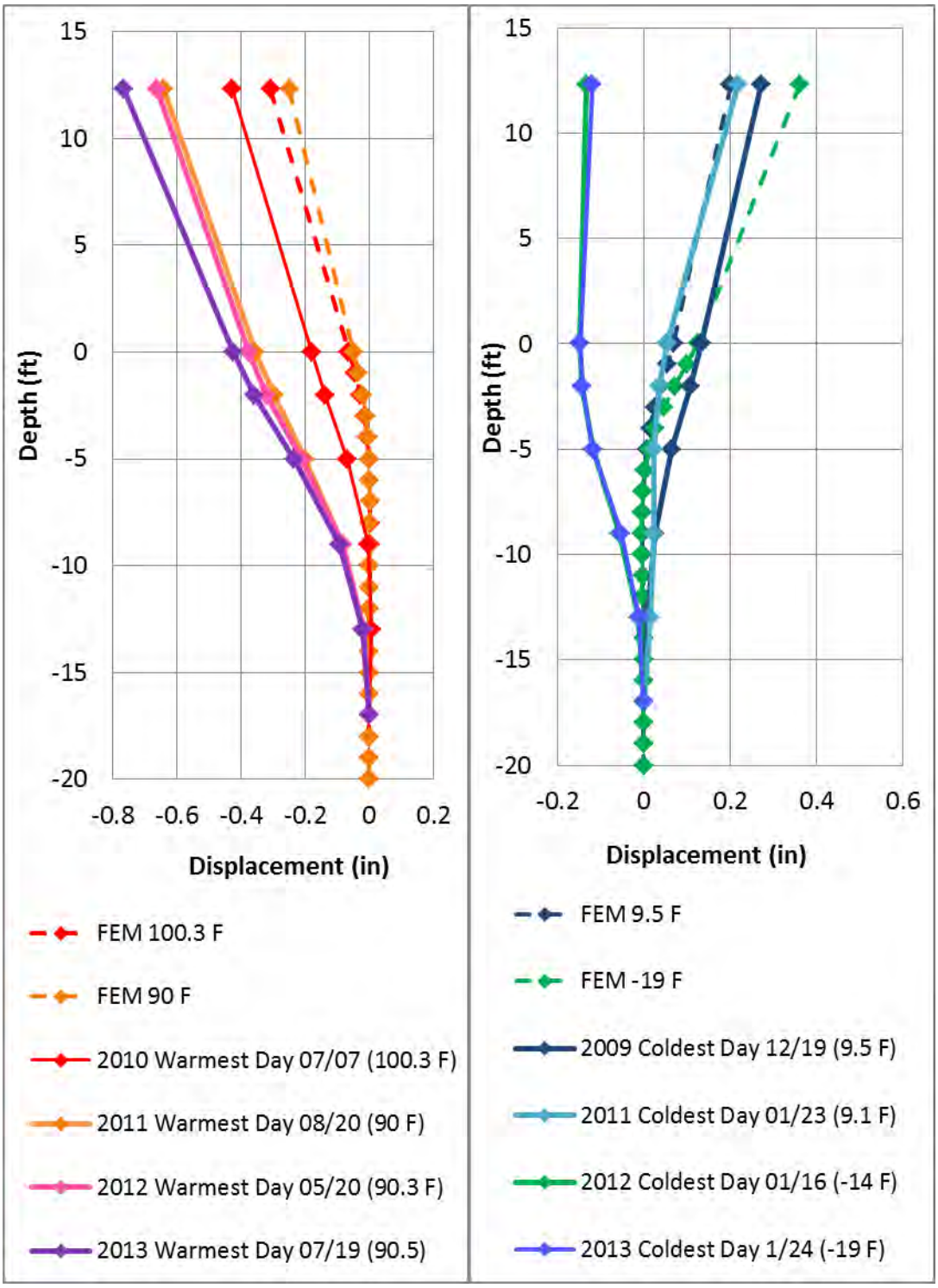

Figure 2-16 Substructure displacement for maximum (left) and minimum (right) yearly temperatures with FEM (using original soil conditions from site)

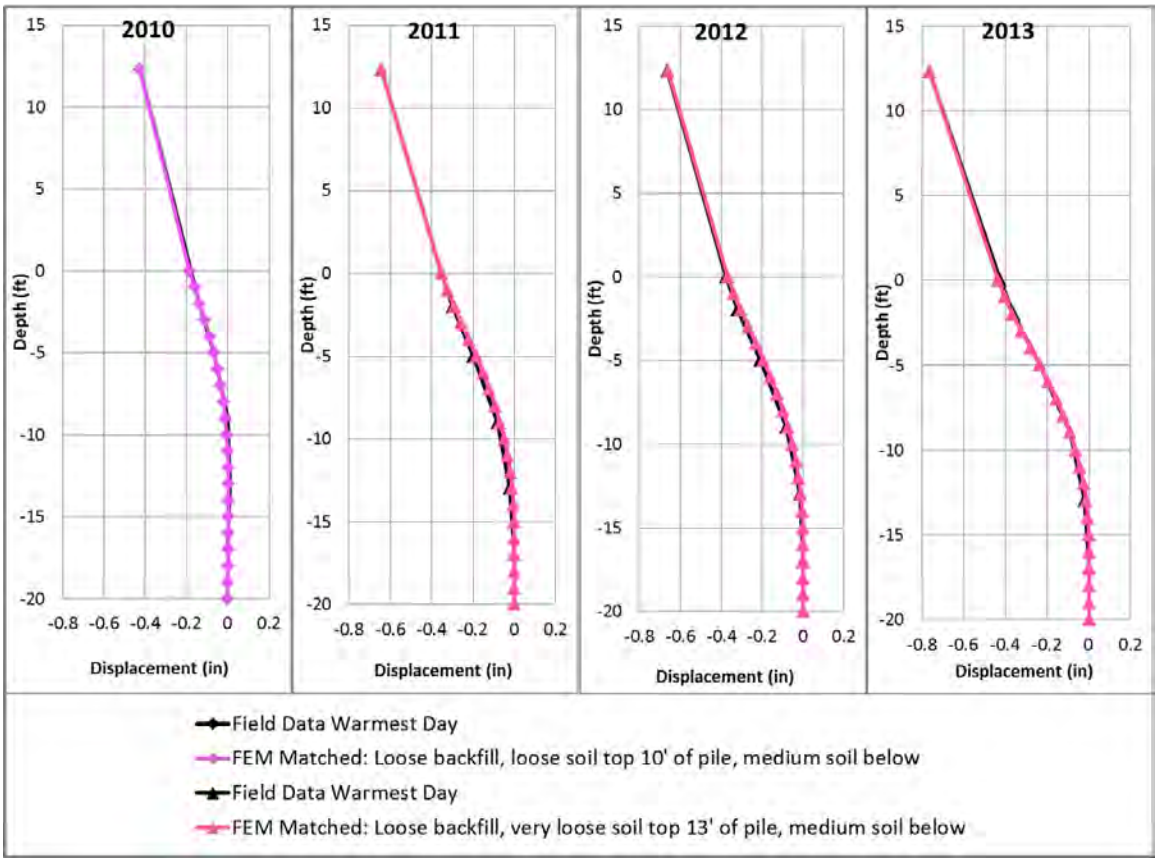

Figure 2-17 Maximum yearly temperatures with FEM Matched deflected shapes

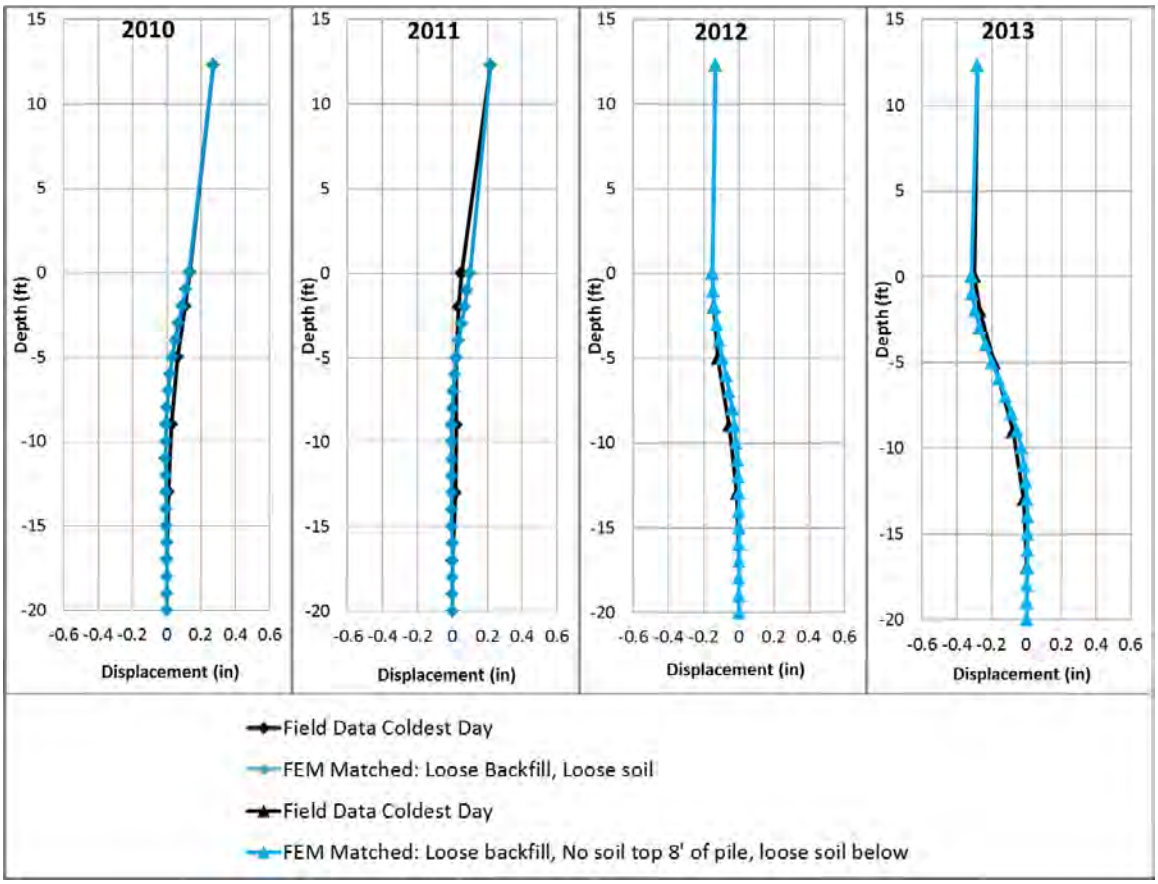

Figure 2-18 Minimum yearly temperatures with matched FEM deflected shapes

Table 2-4 Soil Properties Used in FEMs

Soil Classification	Friction Angle φ	Saturated Soil Density (pcf) g
Dense (backfill)	45	145
Medium Dense (piles)	35	135
Loose (backfill)	28	100
Loose (piles)	25	75
Very Loose (piles)	20	70

2.6 Pile Bending Moments with FEM Results

Bending moments presented in this section are those resulting from thermally induced loads only. Gage notation and exact locations are provided in APPENDIX A and APPENDIX B. Pile bending moments are calculated from strain gages on the pile flanges. A positive bending moment indicates bending towards river while a negative bending moment indicates bending toward backfill for both abutments. Bending moments from field data are presented from the top instrumented section located 1.60 ft (0.49 m) from the top of the pile. Figure 2-19 shows the weak axis bending moments

as well as the maximum bending moment from the FEM Matched results (which were presented in Figure 2-17 and Figure 2-18). The reason maximum bending moments are presented from the FEM Matched is because in some cases, the point of inflection of the pile occurs close to the instrumented section and therefore field data is not actually capturing the maximum moment that the pile experiences.

Figure 2-20 shows a comparison of the pile bending moment diagrams using the FEM with original soil conditions and field temperature (FEM Nominal), as well as pile bending moment for the FEM Matched conditions along with respective maximum bending moments. It can be seen that the permanent offset in the pile significantly changes the moment diagram in the pile FEM results, though values are still small. When dense backfill is assumed in the model, the pile does not experience reverse curvature under bridge expansion, while with loose backfill the pile does experience reverse curvature and the resulting pile moments differ.

Figure 2-21 shows the pile bending moment diagrams for FEM Nominal and FEM Matched results for 2013. This figure shows how the FEM Nominal would not predict accurate moments in subsequent years; the pile does not recover from its expanded deflected shape (seen in Figure 2-17 and Figure 2-18) therefore the maximum moment due to bridge contraction is a negative value (contrary to a positive bending moment observed when the pile contracts towards the river). This is compounded by the looser soil conditions. The moments are also greater for the FEM Matched conditions. For example, considering 2013 data, the FEM Nominal had a maximum moment of 37.4 kip-ft (50.7 KN-m) for bridge contraction and the FEM Matched maximum moment of -45.6 kip-ft (-61.8 KN-m). For bridge expansion the FEM Nominal had a maximum moment of 11.1 kip-ft (15.04 KN-m) and FEM Matched had a maximum moment of -30.1 kip-ft (-40.8 KN-m).

Table 2-5 shows the moment recorded at the gage location in the field data, the moment at this depth in the FEM Matched model, the point of inflection from the FEM, and the maximum bending moment in the FEM Matched. Since the pile goes through reverse curvature, both positive and negative maximum bending moments are reported. This table is useful because it shows that field data at the instrumented location was generally comparable to the corresponding location in the FEM Matched; however depending on how close the point of inflection is to the gage location this may be significantly lower than the actual maximum moment the pile experiences.

Since field data may not be representative of actual maximum pile moments, maximum moments from the Matched FEM should be considered. The maximum weak axis moments predicted from the FEM Matched model for all years of monitoring range from -50.4 kip-ft (-68.4 KN-m) to 33.1 kip-ft (44.9 KN-m). Figure 2-22 shows the strong axis bending moments; for this straight-girder non-skew symmetric bridge, strong axis bending was minimal. Field data for bending moment about the strong axis ranged from -15.4 kip-ft (-20.9 KN-m) to 7.1 kip-ft (9.7 KN-m). The yield moment about the weak axis of the piles is 144.2 kip-ft (195.5 KN-m) and the yield moment about the strong axis is 441.7 kip-ft (598.9 KN-m).

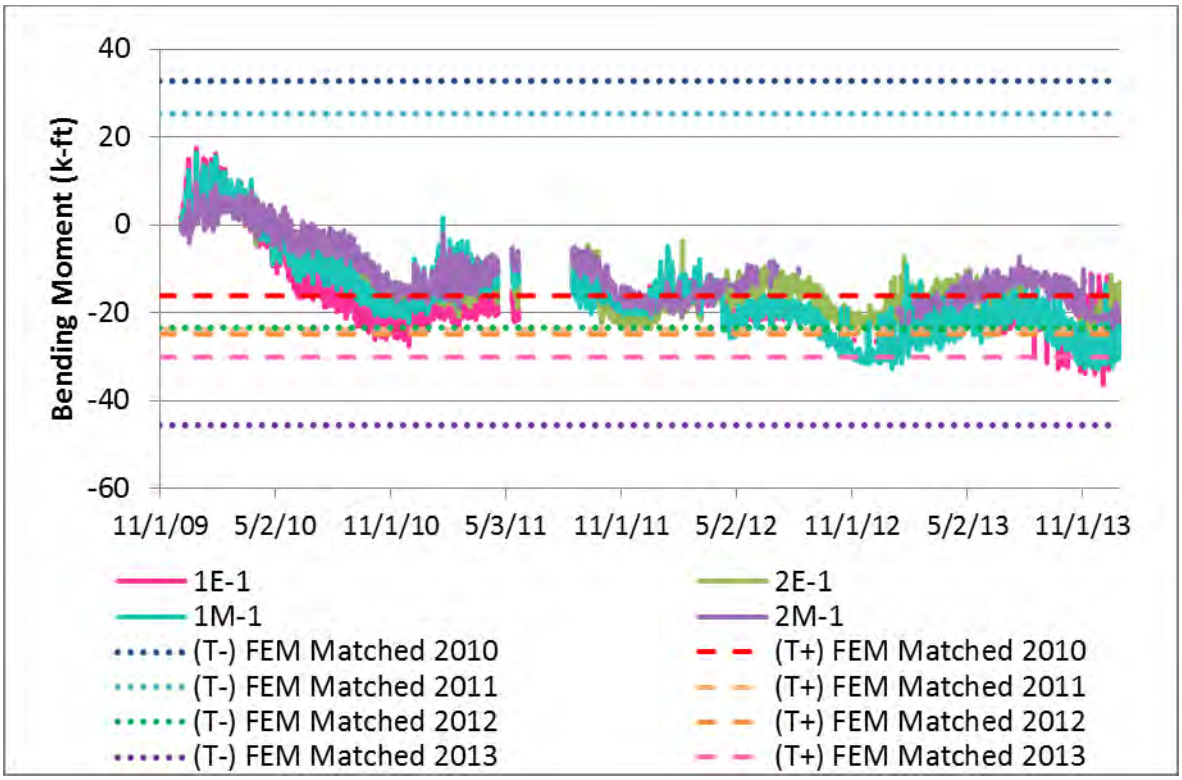

Figure 2-19 Pile weak axis bending moments at top instrumented location and Matched FEM maximum bending moments

*FEM Matched moments shown in figure are presented in Table 2-5.

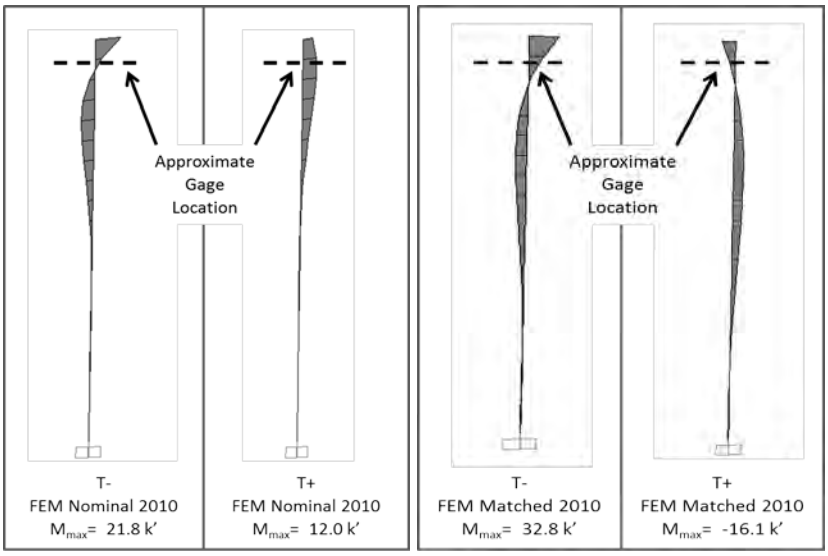

Figure 2-20 2010 Maximum Bending Moment from FEM Nominal (left) and FEM Matched (right)

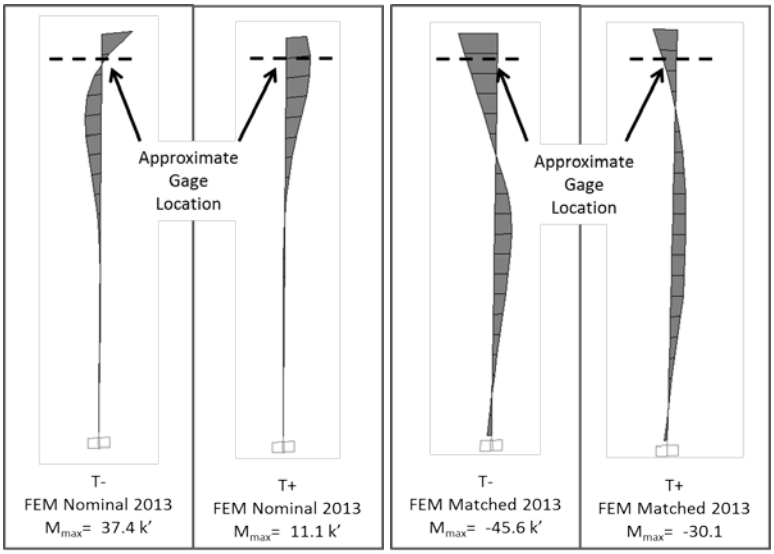

Figure 2-21 2013 Maximum bending moment from FEM Nominal (left) and FEM Matched (right)

Table 2-5 Pile Bending Moment Results for Maximum and Minimum Temperatures (field data and FEM)

Date	Temp. (°F)	Moment at Gage Location (1.6 ft below top of pile) (k-ft)		Point of Inflection (FEM) (ft)	FEM Maximum Moment (k-ft)	
		FIELD DATA	FEM		M^+	M^-
12/19/09	9.5	12.6	10.9	2.9	32.8	-11.9
7/7/10	100.3	-2.3	-2.4	1.9	11.0	-16.3
1/23/11	9.1	-2.6	-1.7	1.5	25.3	-9.7
8/20/11	90.0	-11.1	-11.0	3.5	13.1	-23.8
1/16/12	-14.0	N/A	-16.6	5.7	9.9	-23.4
5/20/12	90.3	-18.9	-12.4	3.6	13.7	-24.5
1/24/13	-19.0	N/A	-33.0	5.7	19.4	-45.6
7/19/13	90.5	-18.8	-16.0	3.8	16.2	-30.1

* M_{yy}=144.2 kip-ft, M_{py}=221.7 kip-ft (HP12x84) weak axis yield moment and plastic moment, respectively

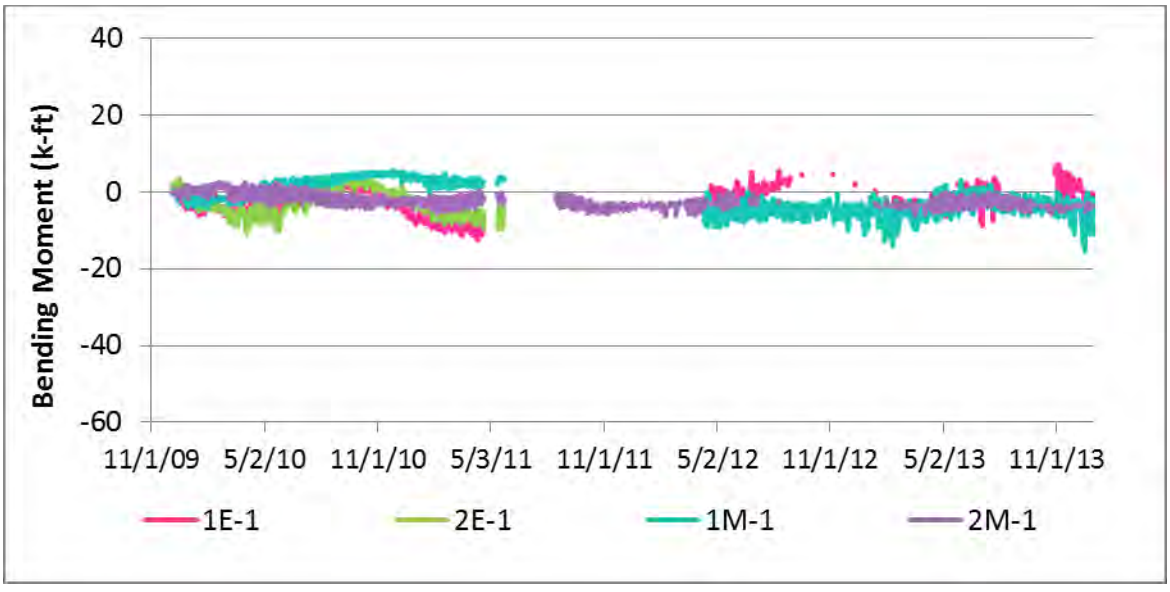

Figure 2-22 Pile strong axis bending moments at top instrumented location

3 East Montpelier Bridge

The long term monitoring of the East Montpelier Bridge began when construction was completed on November 24, 2009. This section documents the long term response of this skewed IAB from November 24, 2009 through December 31, 2013. The bridge temperature over the monitoring period is shown in Figure 3-1.

A three-dimensional finite element model (FEM) was created for the bridge using SAP2000. Soil is modeled using non-linear Winkler springs. The original model used for comparison to field data contained soil springs based on the soil boring logs reported at bridge construction (medium-dense soil around the piles and dense backfill). The model was then calibrated to match conditions seen in field data to compare values. This will be discussed in greater detail in later sections of the chapter.

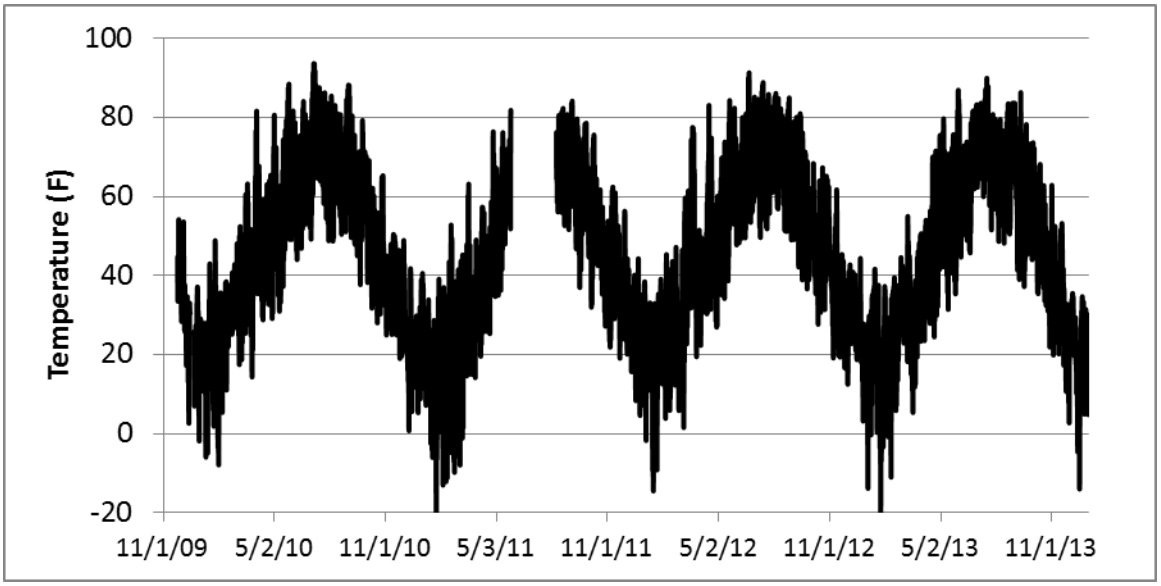

Figure 3-1 Ambient Bridge Temperature

3.1 Girder Stresses

All stress values presented in this section correspond to those induced by thermal effects only. The girder stresses are presented in Figure 3-2 and Figure 3-3. A positive value indicates a tensile stress while a negative value indicates a compressive stress. Temperature had little effect on top flange stresses. Stress values varied between gages due to the neutral axis location of each gage. The maximum top flange compressive stress was 5.2 ksi (35.9 MPa) and maximum tensile stress was 2.8 ksi (19.3 MPa). An increase in temperature caused an increase in compressive stresses on the bottom flanges. For the bottom flanges, the maximum compressive stress was 6.4 ksi (44.1 MPa) and the maximum tensile stress was 5.5 ksi (37.9 MPa). Stresses were consistent at the Abutment 1 girder end, midspan of the bridge, and Abutment 2 girder end and were consistent from year to year; this is consistent with FEM results that show constant moments along the bridge span due to abutment constraints. The neutral axis remains near the top of the cross section for both positive and negative bending moment; therefore the girders are composite even for negative bending. The cumulative maximum stress on a girder flange (stress at end of construction including dead load plus maximum stress over long term monitoring) was 25.9 ksi (178.6 MPa) which is approximately half of the yield stress of 50 ksi (344.7 MPa). Thermally induced girder stresses are small compared to dead load and construction induced effects.

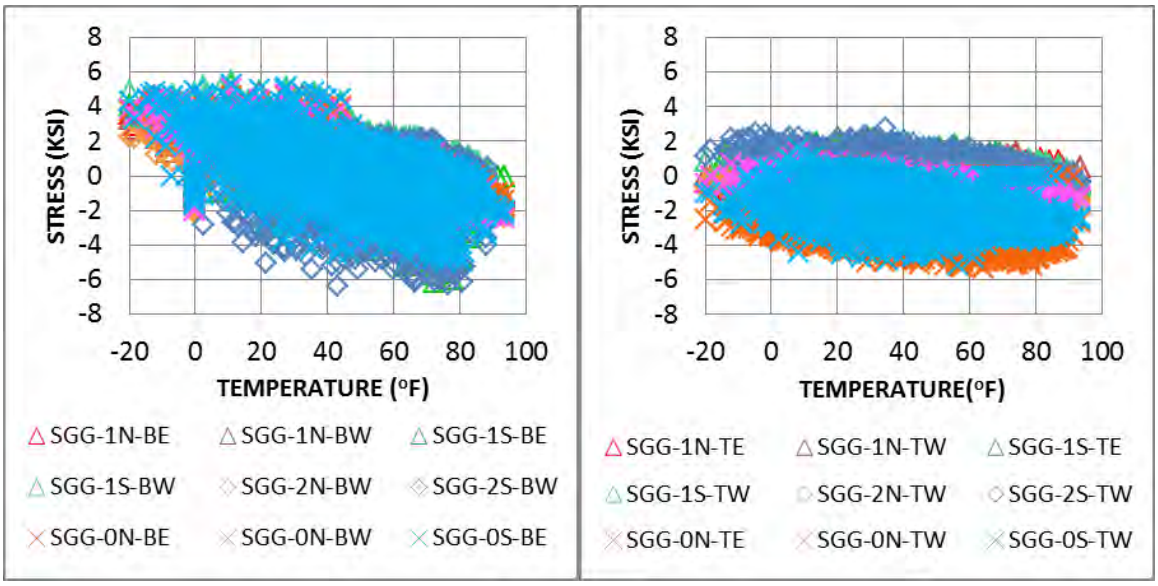

(a) (b)

Figure 3-2 Girder Stresses (a) bottom flange (b) top flange

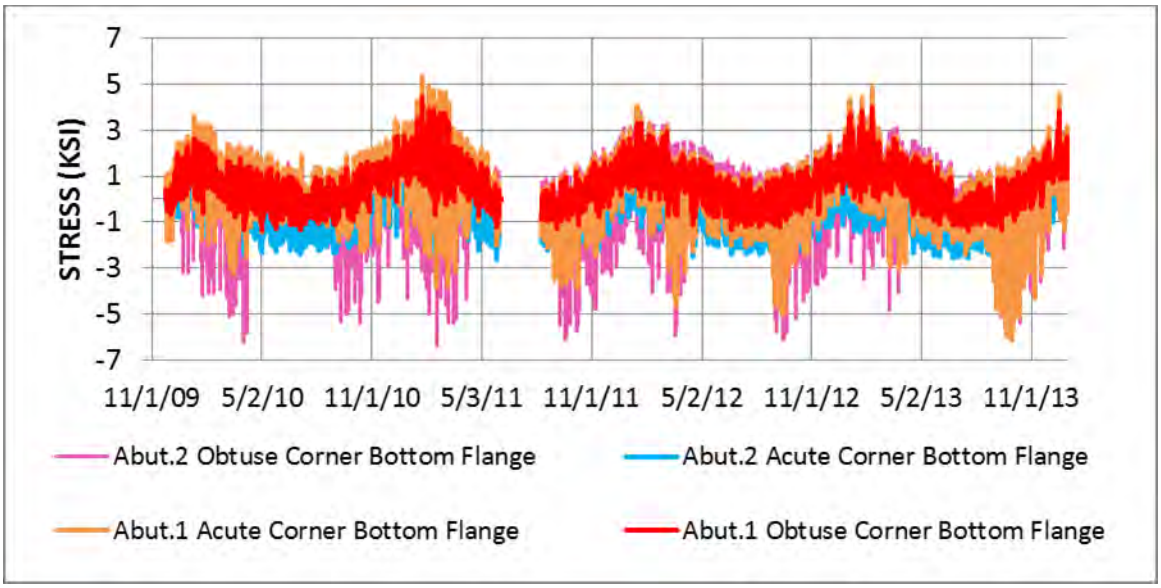

(a)

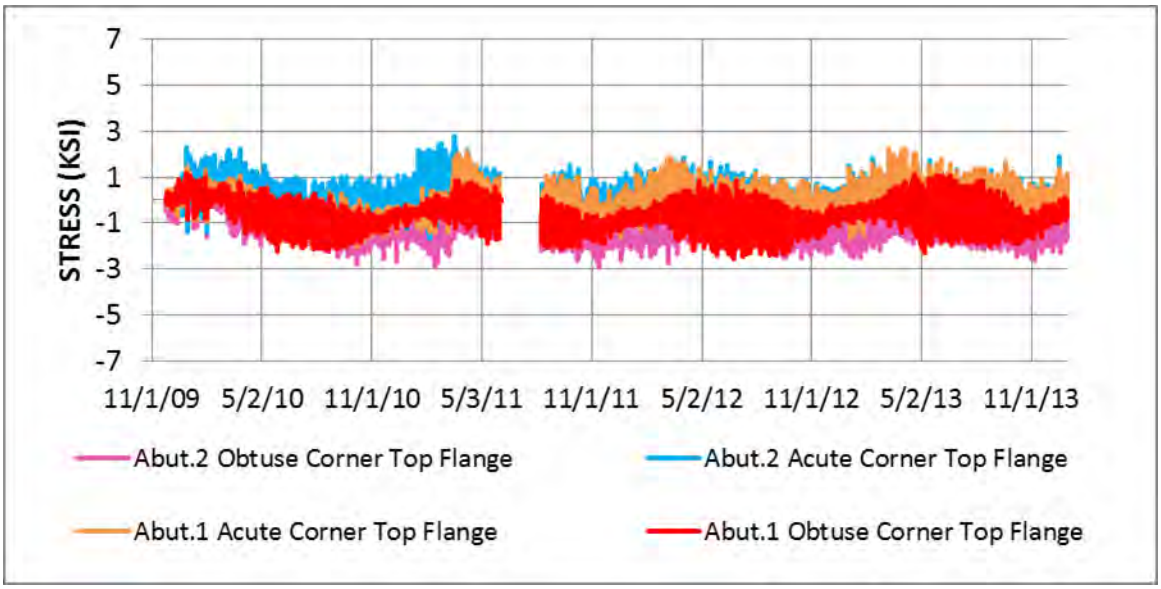

(b)

Figure 3-3 Girder Stresses at Obtuse and Acute Corner Girder Ends (a) Bottom Flange Gages (b) Top Flange Gages

3.2 Displacement

Displacements presented in this section are those occurring from thermally induced loads only. Displacements reported for the top of the abutment refer to displacement at the girder top flange. Measured longitudinal displacements at the top and bottom of three corners and bottom of one corner of the skewed bridge are presented in Figure 3-4 and Figure 3-5. For Abutment 1, negative displacements indicate movement toward the backfill while positive displacements indicate movement towards the river. For Abutment 2, negative displacements indicate movement toward the river while positive displacements indicate movement towards the backfill. For the figures of longitudinal displacements over time, maximum and minimum yearly temperatures were analyzed as a thermal loading in SAP2000 and the results are presented as markers on the date corresponding to that temperature. Transverse displacements are shown in Figure 3-6. For

Abutment 1, positive displacement indicates movement toward downstream and the opposite orientation is used for Abutment 2. Expected displacements due to thermal loading were calculated using the equation for thermal expansion

$$\delta=\alpha L\Delta T$$

where L = span length; α = coefficient of thermal expansion of superstructure $6.5x10^{-6}$/°F, and ΔT = temperature change. For example, the total longitudinal displacement (sum of both abutment movements) due to thermal fluctuation for 100°F is expected to be 1.0 in (25.4 mm). Transverse displacements due to this thermal fluctuation are expected to be 0.36 in (9.1 mm).

The longitudinal displacement at the acute and obtuse corner of each abutment experienced similar displacements showing that the 15° skew does not affect longitudinal thermal bridge movement for this bridge.

Table 3-1 presents the peak to peak top of abutment displacement (total displacement from minimum to maximum yearly temperature) at the upstream side of each abutment as well as the net displacement at the top of the bridge (sum of both abutments) due to the thermal change. Note that skew appears to have negligible effect on longitudinal displacements; data is presented for upstream side because there is no data for downstream side of top of Abutment 2 (obtuse corner). The maximum net displacement was 1.45 in (36.8 mm) at the top of the bridge in 2011. Both abutments have increased displacements over time showing a shift toward their backfill resulting in net bridge expansion; however this trend appears to be stabilizing.

Table 3-2 and Table 3-3 show comparison of net abutment displacement from field data with displacement predicted by thermal expansion equation and FEM results for top and bottom of abutment displacement values, respectively. Again, these values are presented for the upstream side to compare to field data reported at this side of the bridge; however displacements are comparable to the downstream side of the bridge. Bottom of abutment displacements are significantly lower than those at the top of the abutments due to abutment rotation. The maximum peak to peak displacement at the bottom of the abutments was 0.49 in (12.4 mm).

For the top of abutment displacements, the thermal expansion equation results were a reasonable approximation of values recorded from field data. However, since abutment thermal movement is not only translational but also rotational, the equation results significantly overestimated bottom of abutment.

Transverse displacements at the top of the pile at each corner of the bridge are presented in Figure 3-6. Transverse displacements are dependent upon the geometry of the skewed bridge, with the acute corners consistently experiencing higher displacements than the obtuse corners. The sum of the average of the transverse displacements (average of the acute and obtuse corner displacement at each abutment) is 0.25 in (6.35 mm) which is below that predicted by the thermal expansion equation, likely due to restraint of the piles. The bridge shows a twisting behavior as it expands and contracts, with the acute corners experiencing the greatest displacements. A schematic of this seasonal twisting of the bridge is shown in Figure 3-7 for contraction and expansion.

The 15° skew angle of this bridge had negligible effect on the longitudinal thermal displacement of this bridge and therefore a two-dimensional analysis would likely be adequate for approximating global longitudinal superstructure movement due to thermal fluctuation. However, the transverse thermal bridge movement introduces strong axis bending moments on the piles that would not be captured in a two-dimensional analysis and these would need to be otherwise accounted for.

The seasonal relation between top and bottom of abutment longitudinal displacements are presented in Figure 3-8. This figure shows the stabilization of the bridge in recent seasons with far less variation in displacement relations than in the early years of monitoring. The maximum positive

rotation (bridge contraction) occurred in winter 2009 while the maximum negative rotation (bridge expansion) occurred in summer 2013.

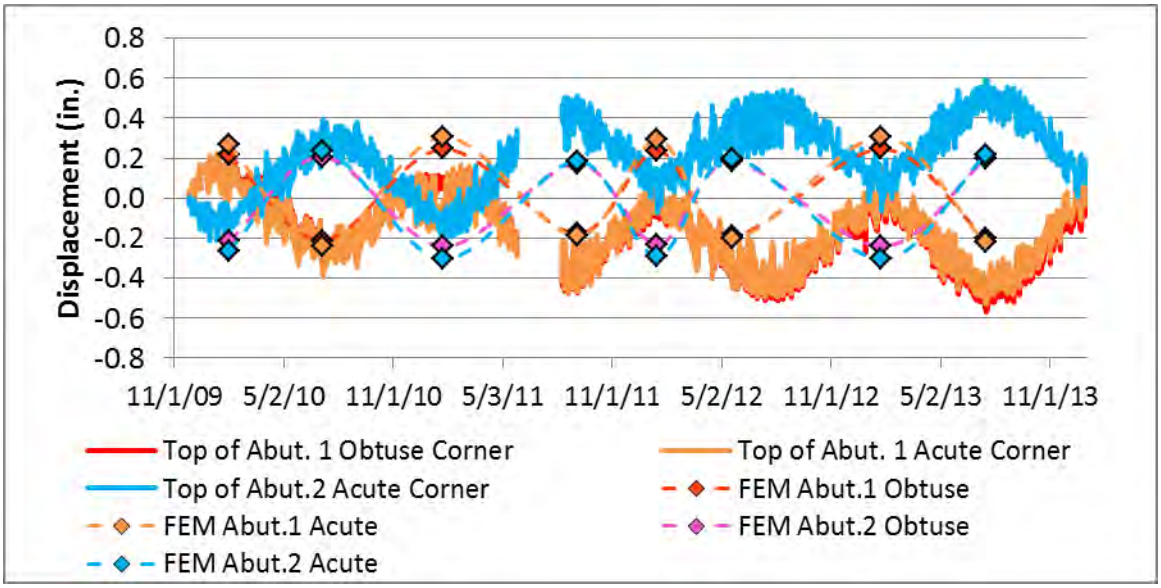

Figure 3-4 Longitudinal Top of Abutment Displacements (field data and FEM)

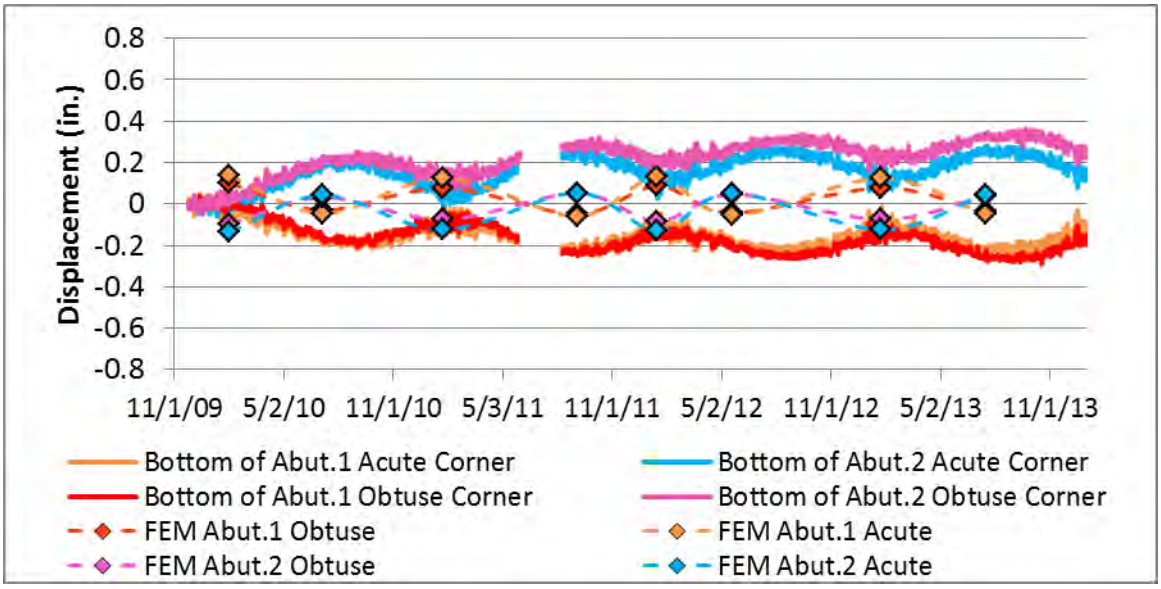

Figure 3-5 Longitudinal Bottom of Abutment Displacements (field data and FEM)

Table 3-1 Peak to Peak Top of Abutment Displacements

Year	ΔT (°F)	Abutment 1 Obtuse Corner (in.)	Abutment 2 Acute Corner (in.)	Sum of Abutment Displacements (upstream) (in.)
2010	100.6	0.61	0.63	1.24
2011	99.4	0.72	0.73	1.45
2012	98.4	0.56	0.52	1.08
2013	108.7	0.69	0.67	1.35

Table 3-2 Peak to Peak Top of Abutment Longitudinal Displacements (field data and FEM)

Year	ΔT (°F)	Sum of Abutment Displacements (in.)	Thermal Expansion Equation (in.)	FEM* Sum of Abutment Displacements (in.)
2010	100.6	1.24	0.95	0.92
2011	99.4	1.45	0.94	0.91
2012	98.4	1.08	0.93	0.91
2013	108.7	1.35	1.03	0.97

*FEM reported for upstream side of bridge (Abut.1 obtuse corner and Abut.2 acute corner) (same as field data)

Table 3-3 Peak to Peak Bottom of Abutment Longitudinal Displacements (field data and FEM)

Year	ΔT (°F)	Sum of Abutment Displacements (in.)	Thermal Expansion Equation (in.)	FEM Sum of Abutment Displacements (in.)
2010	100.6	0.49	0.95	0.31
2011	99.4	0.49	0.94	0.30
2012	98.4	0.37	0.93	0.31
2013	108.7	0.47	1.03	0.28

*FEM reported for upstream side of bridge (Abut.1 obtuse corner and Abut.2 acute corner) (same as field data)

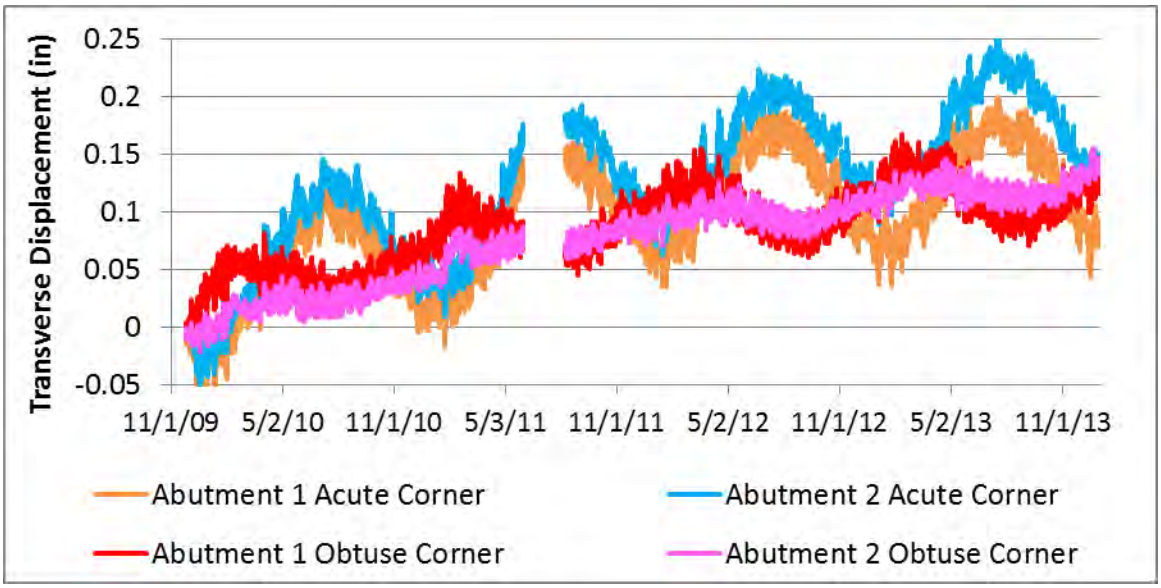

Figure 3-6 Transverse Abutment Displacements

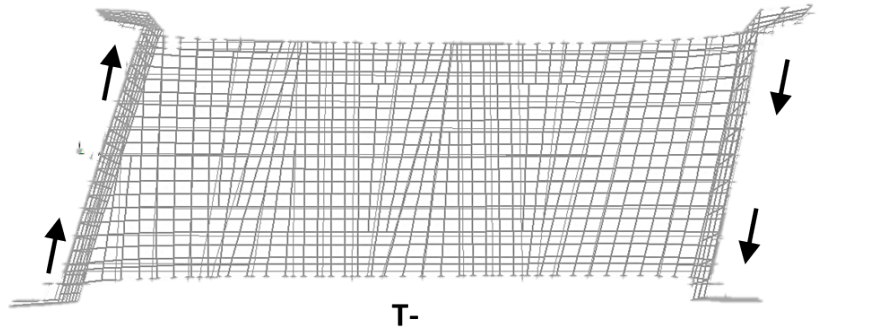

(a)

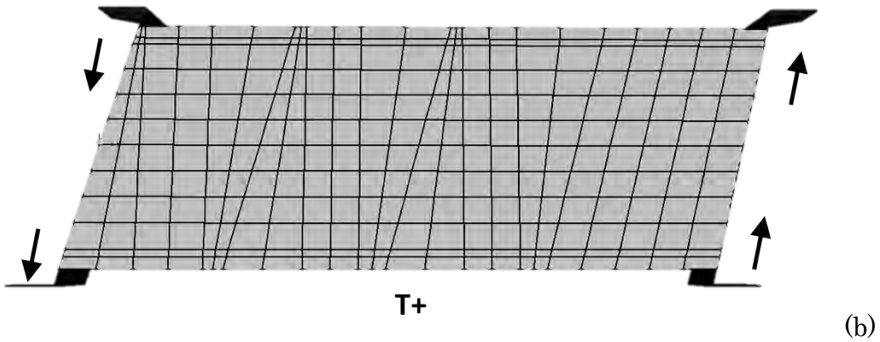

(b)

Figure 3-7 Seasonal Twisting of Bridge during (a) Contraction and (b) Expansion

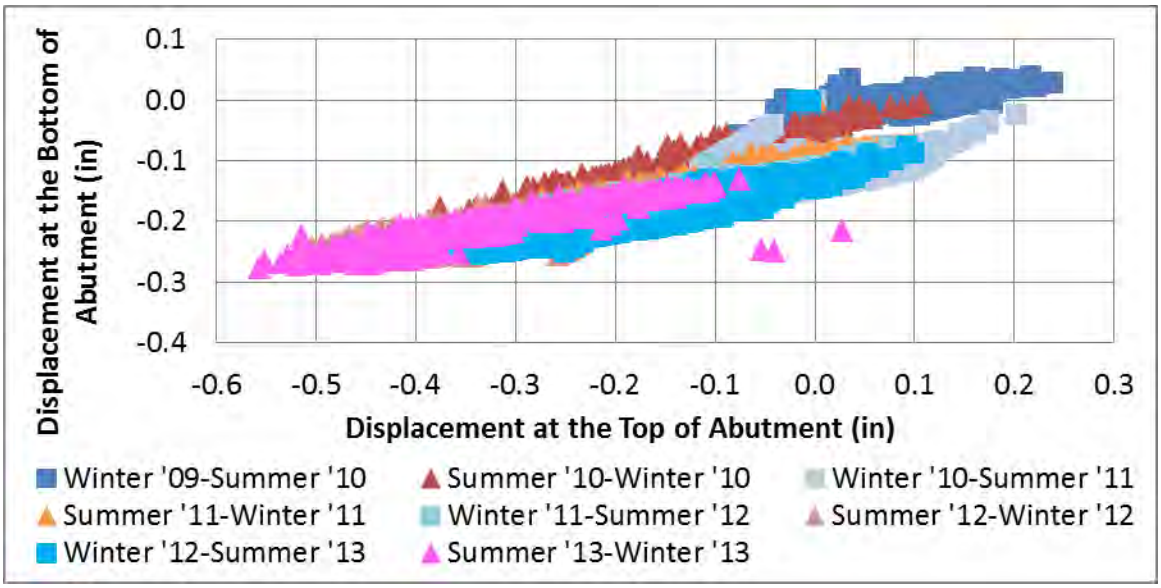

Figure 3-8 Seasonal Displacements at Top and Bottom of Abutment 1

3.3 Abutment Rotation

Abutment rotations presented in this section are those resulting from thermal effects only. For both abutments, rotation towards river is indicated by a positive value while rotation towards the backfill is indicated by a negative value. Abutment rotation is presented over time in Figure 3-9 and seasonal rotation at Abutment 1 is presented with temperature in Figure 3-10. This figure shows that abutment rotations have increased over time but appear to be stabilizing which is consistent with the stabilization of the top and bottom of abutment displacement relations presented previously. Abutment rotations are important to consider in design, as they reduce the deformation demands on the piles. A common IAB design practice is to assume the top of abutment displacement is consistent throughout the height of the abutment therefore neglecting abutment rotation. Abutment rotations are essentially identical at each end of the structure, although Abutment 2 appears to have slightly higher abutment rotations.

FEM results are compared to field data for maximum and minimum yearly temperatures in Table 3-4 for Abutment 1 and Abutment 2. Table 3-5 presents peak to peak rotation values (from minimum to maximum temperature each year) for both abutments and FEM results. There are many factors that could account for the difference between field results and FEM results. For instance, the FEM does not account for the yearly shift of the abutments towards their backfill. The FEM also does not capture changing soil conditions that have been observed in the field. Seasonal rotations are shown in Figure 3-10 which shows the increase in rotation from season to season as abutments shift towards their backfills. The rotations range from 0.078 to -0.11 degrees, while maximum peak to peak rotation was 0.17 degrees at Abutment 1 and 0.18 degrees at Abutment 2.

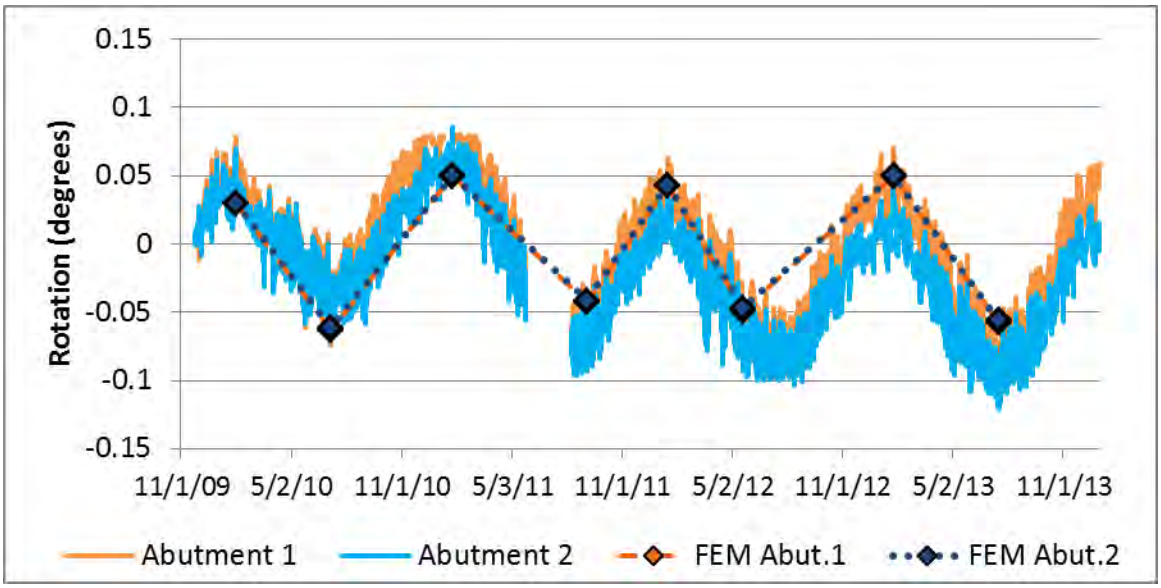

Figure 3-9 Abutment Rotation Over Time (field data and FEM)

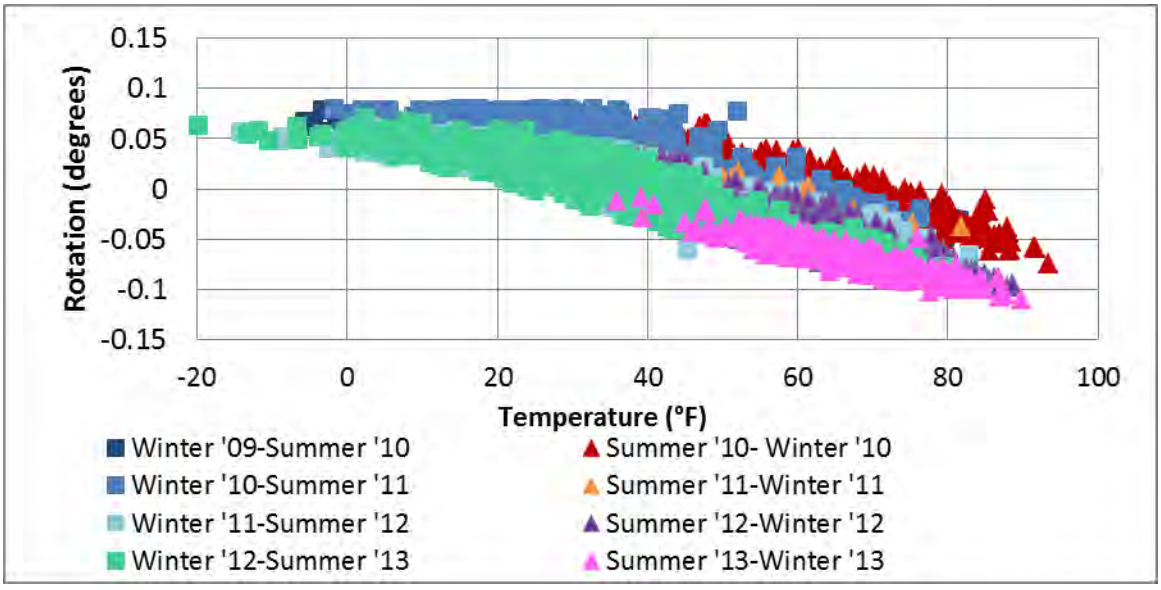

Figure 3-10 Abutment 1 Seasonal Rotation vs. Temperature

Table 3-4 Abutment Rotation at Yearly Maximum/Minimum Temperatures (field data and FEM)

Date	Temp. (°F)	Abutment 1 Rotation (degrees)		Abutment 2 Rotation (degrees)	
		Field Data	FEM	Field Data	FEM
1/31/10	-7.2	0.07	0.04	0.07	0.04
7/7/10	93.4	-0.05	-0.06	-0.07	-0.06
1/24/11	-19	N/A	0.06	0.09	0.06
9/4/11	80.4	-0.08	-0.04	-0.09	-0.04
1/16/12	-14.3	0.06	0.05	0.04	0.05
5/20/12	84.1	-0.09	-0.05	-0.09	-0.05
7/17/13	-19	0.06	0.06	0.04	0.06
1/24/13	89.7	-0.11	-0.06	-0.12	-0.06

Table 3-5 Peak to Peak Abutment Rotation (field data and FEM)

Year	D Temp. (°F)	Abutment 1 Rotation (degrees)		Abutment 2 Rotation (degrees)	
		Field Data	FEM	Field Data	FEM
2010	100.6	0.12	0.10	0.14	0.10
2011	99.4	N/A	0.10	0.18	0.10
2012	98.4	0.15	0.10	0.13	0.10
2013	108.7	0.17	0.12	0.16	0.12

3.4 Earth Pressures

Pressures presented in this section are the changes in pressure since construction due to thermal loading. Gage locations are provided in detail in the appendix; North gages are at the obtuse corner of Abutment 1 and the acute corner of Abutment 2, and south gages are at the acute corner of Abutment 1 and obtuse corner of Abutment 2. The greatest pressure at this bridge occurred in the top row of pressure cells at the obtuse corner of Abutment 1 (5.2 ft (1.6 m) above the bottom of the abutment). The maximum pressure had a value of 15.3 psi (105.5 KPa), while the maximum average pressure of all pressure cells at this depth on Abutment 1 was 7.7 psi (53.1 KPa) demonstrating the significant variation of pressures across the abutments.

Figure 3-11, Figure 3-12 and Figure 3-13 show abutment pressures over time in the top, middle, and bottom row of pressure cells for both abutments (except for middle pressure cells which were only installed at Abutment 1). These plots demonstrate the variability of pressure distribution not only across Abutment 1 but also between Abutment 1 and Abutment 2. All pressures at Abutment 2 were very low, as well as pressures at the acute corner of Abutment 1. The highest pressures and only location where pressures increase from year to year is at the top pressure cell at Abutment 1 obtuse corner. Readings at all other corners of the bridge exhibited stable pressures over time.

Perhaps more meaningful for design are the average pressures at a row of pressure cells, such as that plotted with their corresponding displacement (at the same top depth as the pressure cells that had the highest individual readings) in Figure 3-14. Pressures increase for increased displacement the first time it occurs, but when the same displacement occurs in subsequent seasons the pressure is less showing the soil ratcheting does not occur.

At the East Montpelier Bridge, increasing transverse displacements were noted each year (similar to Middlesex) but wingwall pressures remained constant. The instrumented wingwall happened to be

in the location where the bridge was moving toward the backfill so should have the highest wingwall pressures. However, the instrumented location had very low overall pressures with a maximum of about 4.0 psi (27.6 KPa) and showed no signs of soil ratcheting.

While the maximum pressure experienced at any instrumented location on this bridge over long term monitoring is 15.3 psi (53.1 KPa), the cumulative maximum pressure (pressure from construction plus pressure from thermal fluctuations throughout long term monitoring) is 20.4 psi (140.7 KPa) which is about 47% of the 43.5 psi (299.9 KPa) assumed fully passive pressure at the gage depth. The slight increases in soil pressure at one gage and stable readings at other gages do not indicate any need for the design for full passive pressures in the backfill of bridges of similar span and skew.

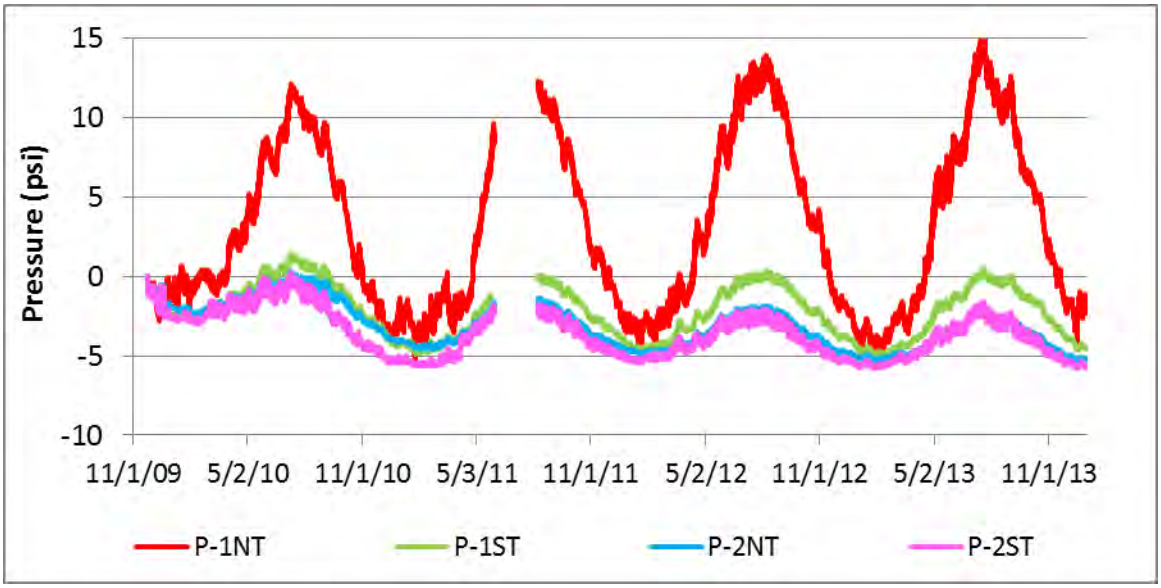

Figure 3-11 Earth Pressures in Top Row of Pressure Cells (Both Abutments)

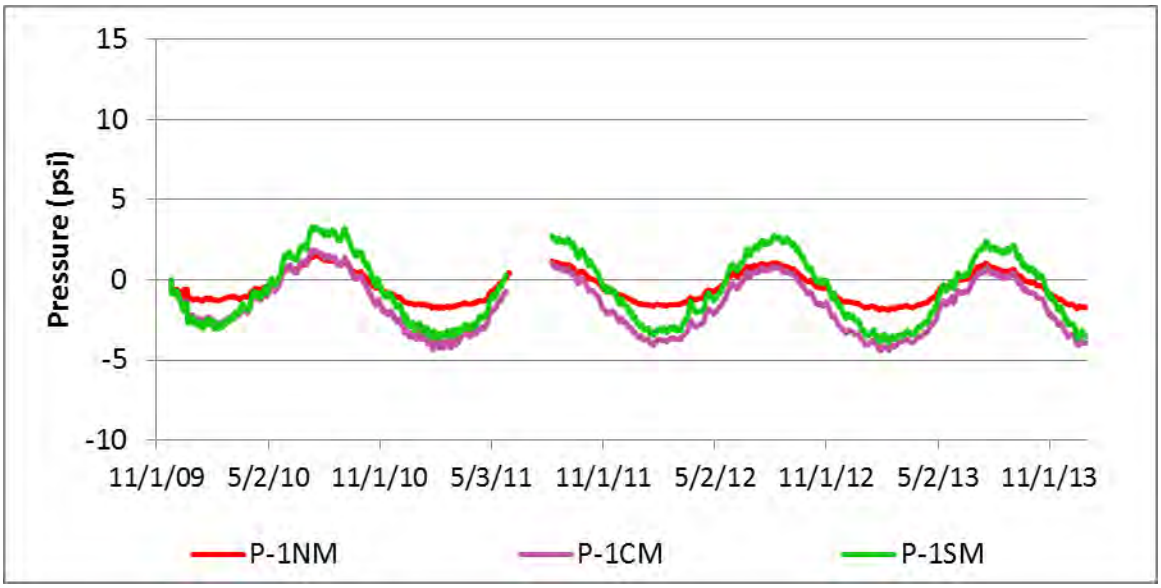

Figure 3-12 Earth Pressures in Middle Row of Pressure Cells (Abutment 1 Only)

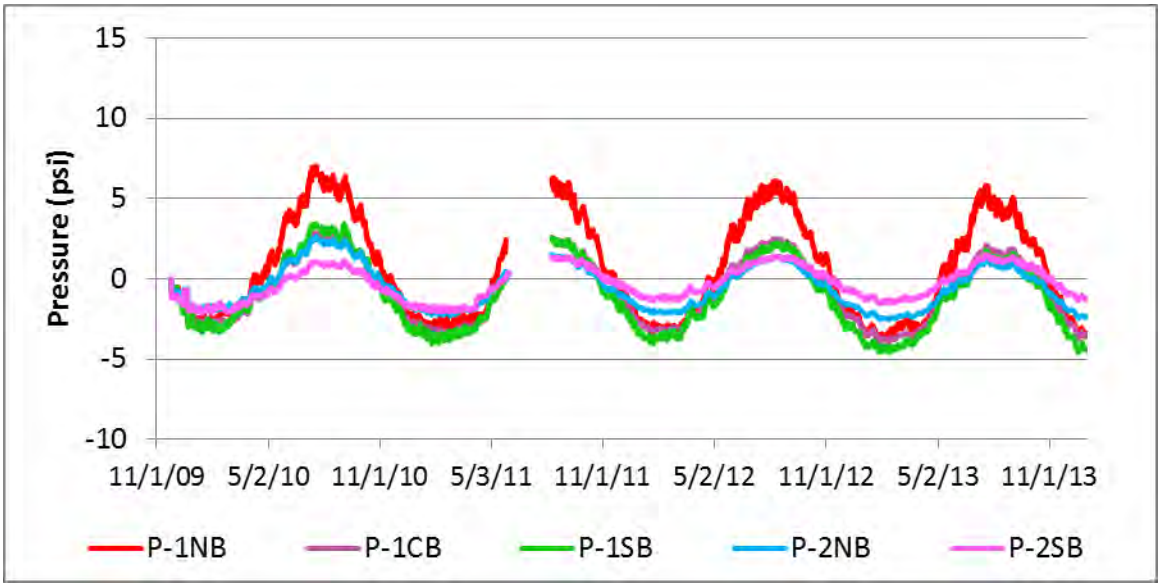

Figure 3-13 Earth Pressures in Bottom Row of Pressure Cells (Both Abutments)

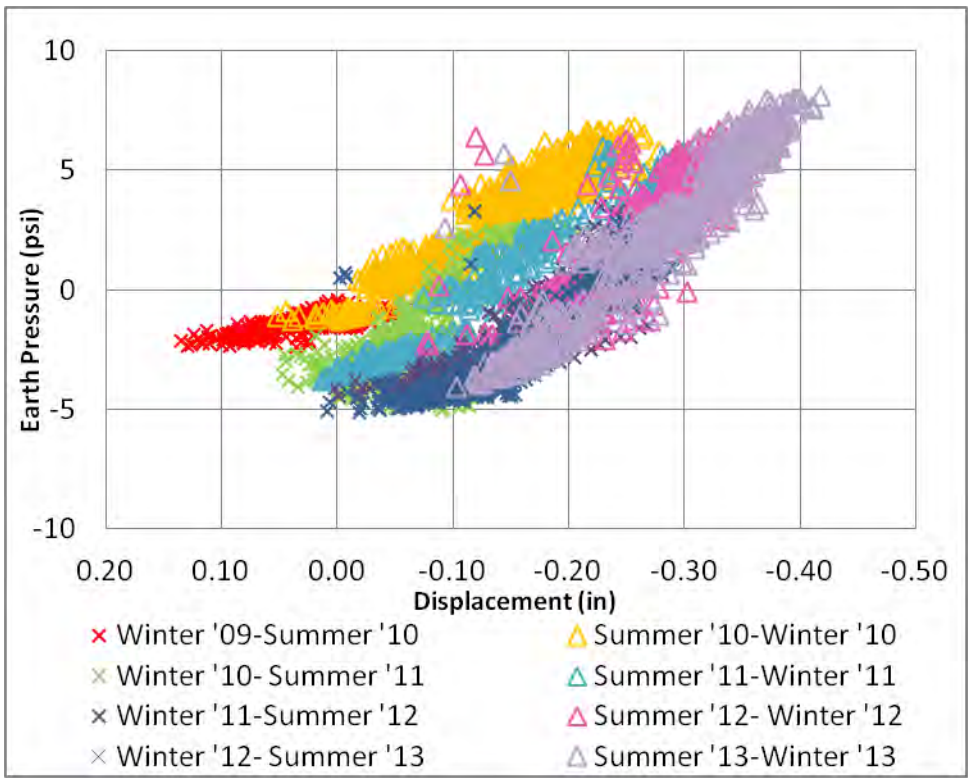

Figure 3-14 Average Earth Pressures vs. Corresponding Displacement (Top Pressure Cells at Abutment 1)

3.5 Substructure Displacement at Maximum and Minimum Temperatures

Substructure displacements presented in this section are those induced by thermal loads only. As was discussed in Section 2.5, predicting substructure response to thermal load is quite complicated because response is not solely dependent on temperature. In the case of the East Montpelier Bridge, FEM results using nominal soil properties for displacement at top of the abutment only matched field displacement at this location for the very first minimum temperature, and in this case the rest of the substructure response was not a close match to field data. After this point in time, similar to the response at the Middlesex Bridge described in Section 2.5, the soil behind the abutments became much looser than the original dense soil assumed as nominal soil properties. The soil around the piles also acted as a significantly looser soil upon bridge expansion, whereas original soil boring logs showed medium dense soil. Furthermore, the field data shows that there is a lag in recovery of the pile from its deflected expanded shape. This is seen year to year in Figure 3-15. This figure shows the warmest (and coldest) day of the year, as well as comparable warm (or cold) temperatures that occur at the beginning and end of the season. When the first warm temperature occurs the bridge expands, and then on the warmest day it expands further as would be expected; however, upon the warm day at the end of the season while the top of abutment contracts the pile holds its deflected expanded shape. This lag in pile recovery is in turn seen in the cold weather plot which shows that after the first year of cold temperatures, the pile never fully contracts. In 2012 and 2013, when bridge behavior has stabilized, the pile shows a deflected shape that does not recover.

For all of these reasons, a static thermal FEM cannot capture this complex combination of factors. Figure 3-16 shows the results of the FEM using the nominal soil conditions reported at the site, analyzed using the minimum and maximum temperature that occurred each year. These plots clearly show that this model does not capture the behavior seen in the field data. If the FEM with these conditions were used to compare values to field data, it may not be an accurate representation. In order to compare field values to FEM results, the FEM was modified to match the substructure deflected shape from the field and therefore values such as bending moments can be compared with greater confidence in their accuracy.

FEM Matched results refer to the results using the model that was calibrated to match field data. This was done by first adjusting the temperature load to match the top of abutment displacement. Then, the soil spring properties were modified to match substructure deflected shape. The matched substructure displacements for warm and cold temperatures are shown in Figure 3-17 and Figure 3-18, respectively. For this bridge, under bridge expansion matched FEM backfill was a loose soil and there was effectively no soil acting around the top 7.0 ft (2.1 m) of the pile. This soil condition was consistent for all four years. For cold temperatures, the static FEM was unable to capture the deflected shape very well due to the model not accounting for the significant lag in pile response. Top of abutment displacement from field data was calculated from pile inclinometers and a tiltmeter on the abutment; this data was also verified by displacement transducers at the bridge therefore any error in deformations from not capturing the pile point of fixity with inclinometers is expected to be minimal. Figure 3-18 shows the FEM Matched results using both the original soil conditions as well as a "rigid soil" which is presented to show that even modeling an extremely rigid soil condition around the piles this only restrains them from contracting but no soil condition can replicate the pile holding its expanded deflected shape without forcing pile deformation in the model. For this reason, FEM Matched using original soil conditions will be used for comparison to field data. The result of these FEM Matched models will be discussed further in Section 3.6.

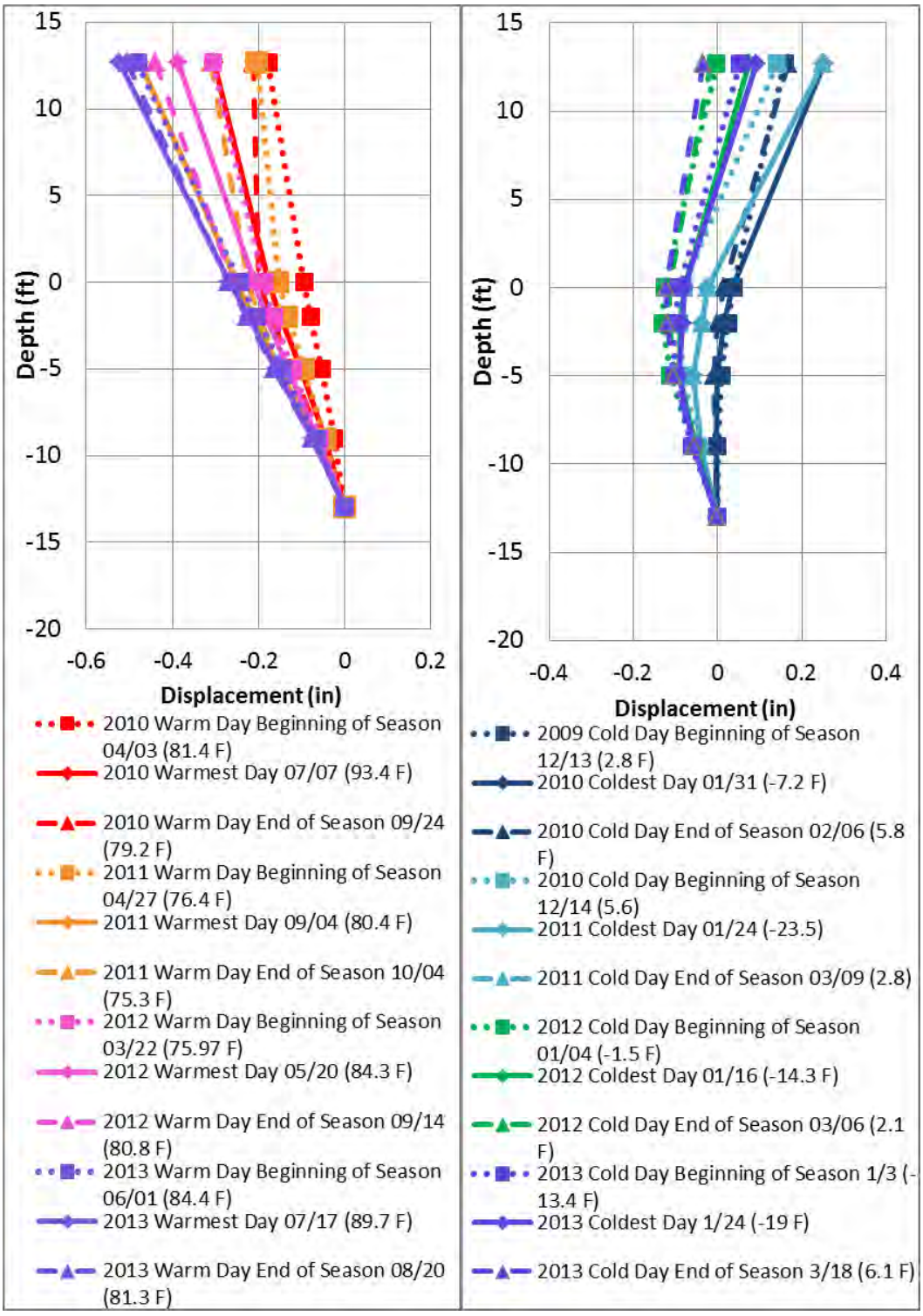

Figure 3-15 Seasonal Substructure Displacement for Warm Temperatures (left) and Cold Temperatures (right)

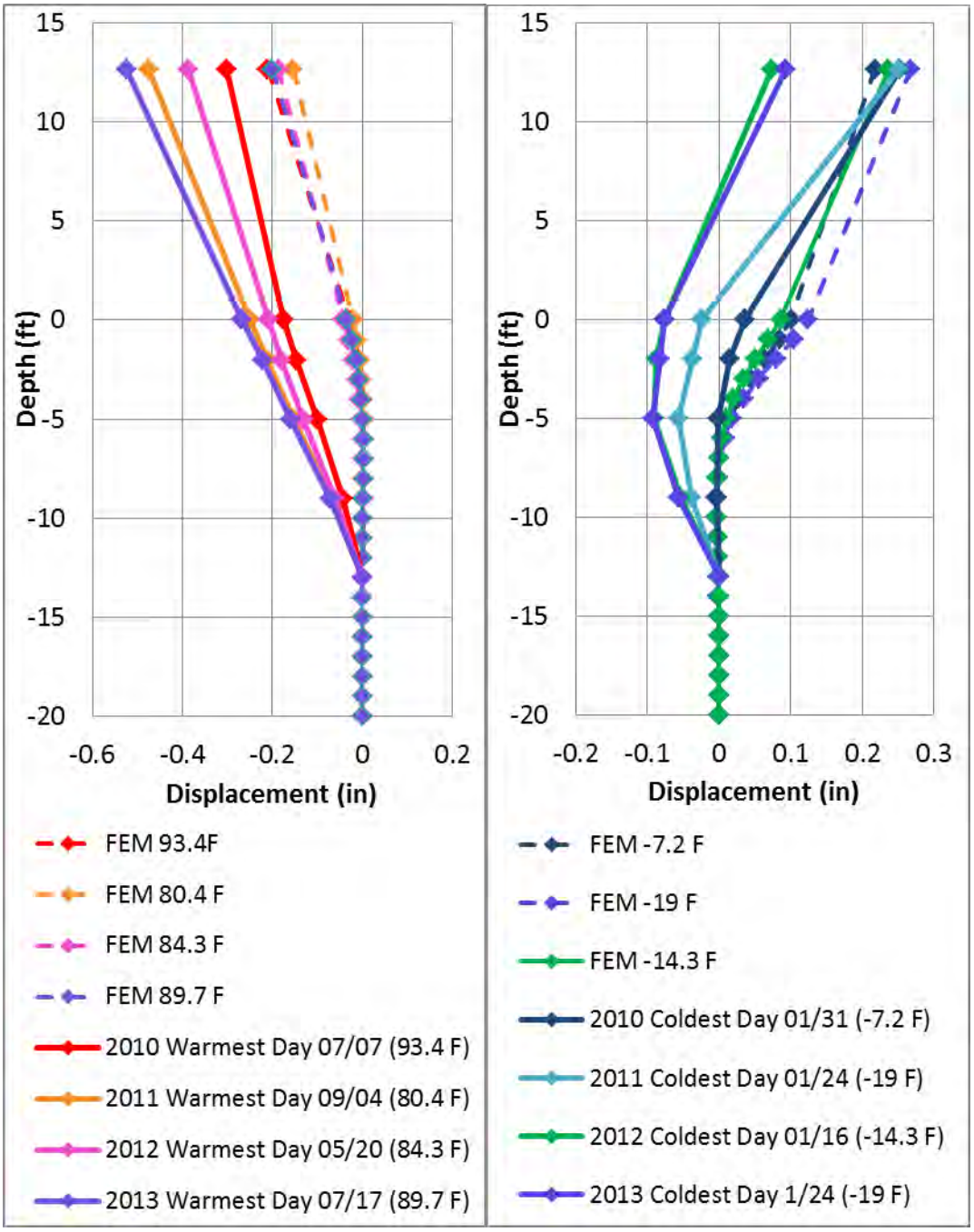

Figure 3-16 Substructure Displacement for Maximum (left) and Minimum (right) Yearly Temperatures with FEM (using original soil conditions from site)

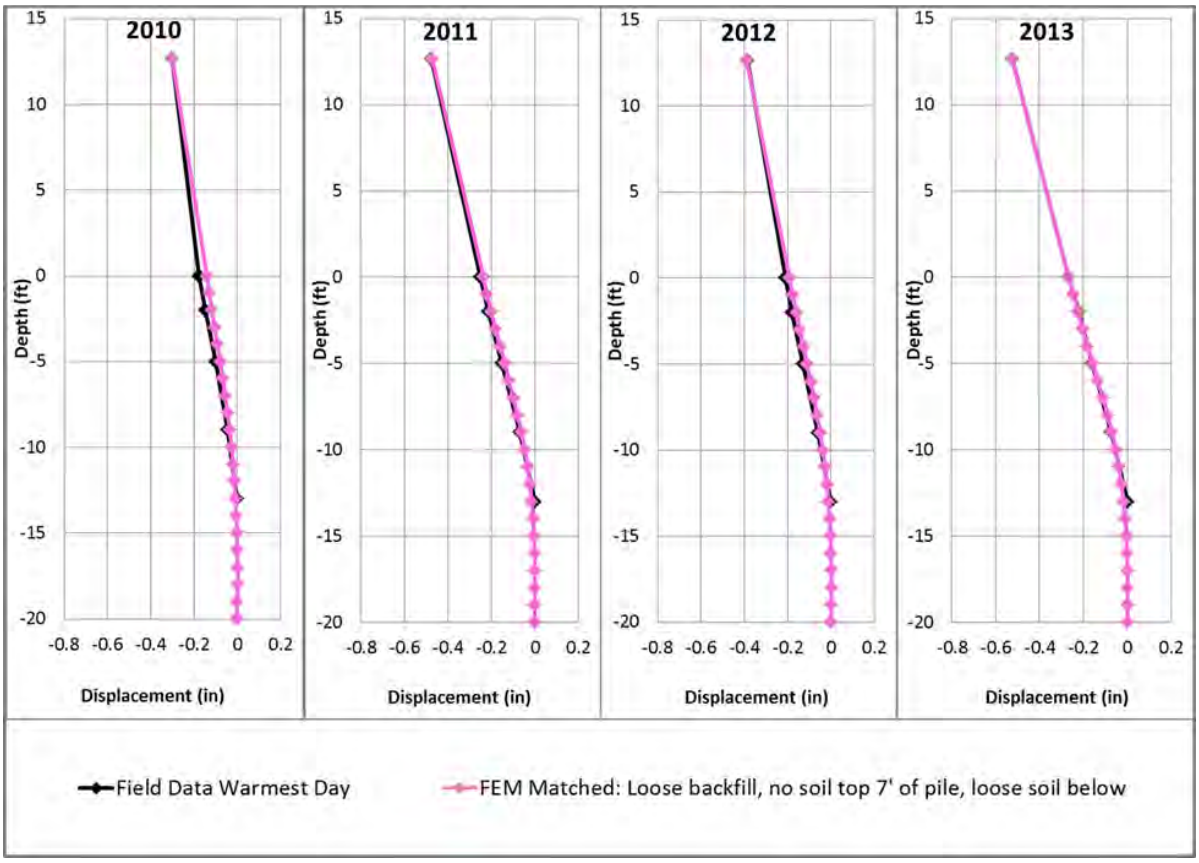

Figure 3-17 FEM Matched results for maximum yearly temperatures

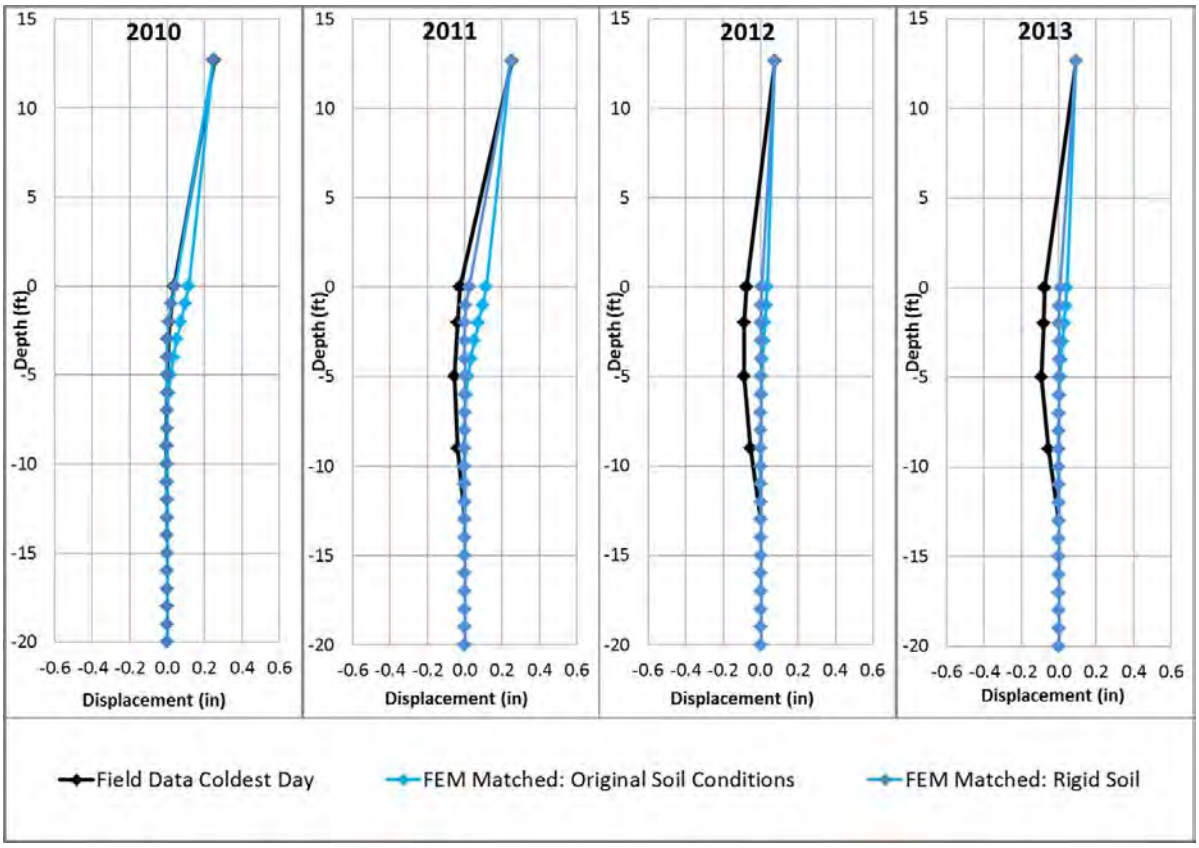

Figure 3-18 FEM Matched results for yearly minimum temperatures

Table 3-6 Soil Properties Used in FEMs

Soil Classification	Friction Angle φ	Saturated Soil Density (pcf) g
Dense (backfill)	45	145
Medium Dense (piles)	35	135
Loose (backfill)	28	100
Loose (piles)	25	75

3.6 Pile Bending Moments

Pile bending moments presented in this section are those due to thermal effects only. Gage notation and locations can be found in APPENDIX A and APPENDIX B. A positive bending moment indicates bending toward the river while a negative bending moment indicates bending toward the backfill, for both abutments. Pile bending moments are calculated from strain gages on the pile flanges. As will be discussed further, field data is not collected at the location of maximum pile moments and therefore the FEM results bounding the data are better predictions of maximum pile moments. Figure 3-19 and Figure 3-20 show field data bending moments with FEM Matched results for bending about the weak axis and strong axis, respectively. FEM Matched conditions predict that

maximum bending moments will range between -22.1 kip-ft (-30.0 KN-m) to71.9 kip-ft (97.5 KN-m) about the weak axis, and -46.7 kip-ft (-63.3 KN-m) to 38.6 kip-ft (52.3 KN-m) about the strong axis. The FEM and field data both show that bending moments about the weak and strong axis can be similar in value. Bending moments occur about the strong axis due to the seasonal rotation of the bridge in plan view and higher stiffness of piles when bending about their strong axis. The yield moment about the weak axis of the piles is 144.2 kip-ft (195.5 KN-m) and the yield moment about the strong axis is 441.7 kip-ft (598.9 KN-m).

Figure 3-21 shows the pile weak axis bending moment diagram for minimum and maximum temperature using the original soil conditions per soil boring logs ("FEM Nominal") as well as the bending moment diagrams using FEM Matched conditions. Figure 3-22 shows the same temperatures and soil conditions for strong axis bending moments. These figures are presented to show the variation in the location of the point of inflection of the pile as a result of changing soil properties. It can be seen that the permanent offset in the pile significantly changes the moment diagram in the pile FEM results. These figures also show that nominal and FEM Matched results were comparable in value, slightly underestimating moments due to bridge contraction and overestimating moments due to bridge expansion. In later years, bending moments were underestimated by the FEM Nominal by up to 21 kip-ft. However, overall the values are all below the yield moment of the piles about the weak and strong axes.

Table 3-7 and Table 3-8 present results for weak axis and strong axis bending moments, respectively. The tables include the field data moments at the gage location for maximum and minimum yearly temperatures, the corresponding moment at the same depth in the FEM Matched, the maximum moment expected from FEM Matched, and the point of inflection of the pile from FEM Matched. Moments reported for the top of the pile in the field are calculated from strain gages located 1.60 ft (0.49 m) below the top of the pile. The point of inflection is referenced in the tables to point out that in cases where the point of inflection is close to the gage location, the field data bending moment is not representative of the actual maximum moment occurring.

In the field data the maximum strong axis bending moments always occurred at the acute corners of the bridge (Abutment 1 South and Abutment 2 North), however the FEM results predict that the obtuse corners will experience the greatest bending moments about the strong axis. Abutment 1 obtuse corner is the corner that experienced high pressures compared to the rest of the bridge which could suggest that there is greater restraint to pile movement at the obtuse corner of the bridge in the field which was not captured by the FEM.

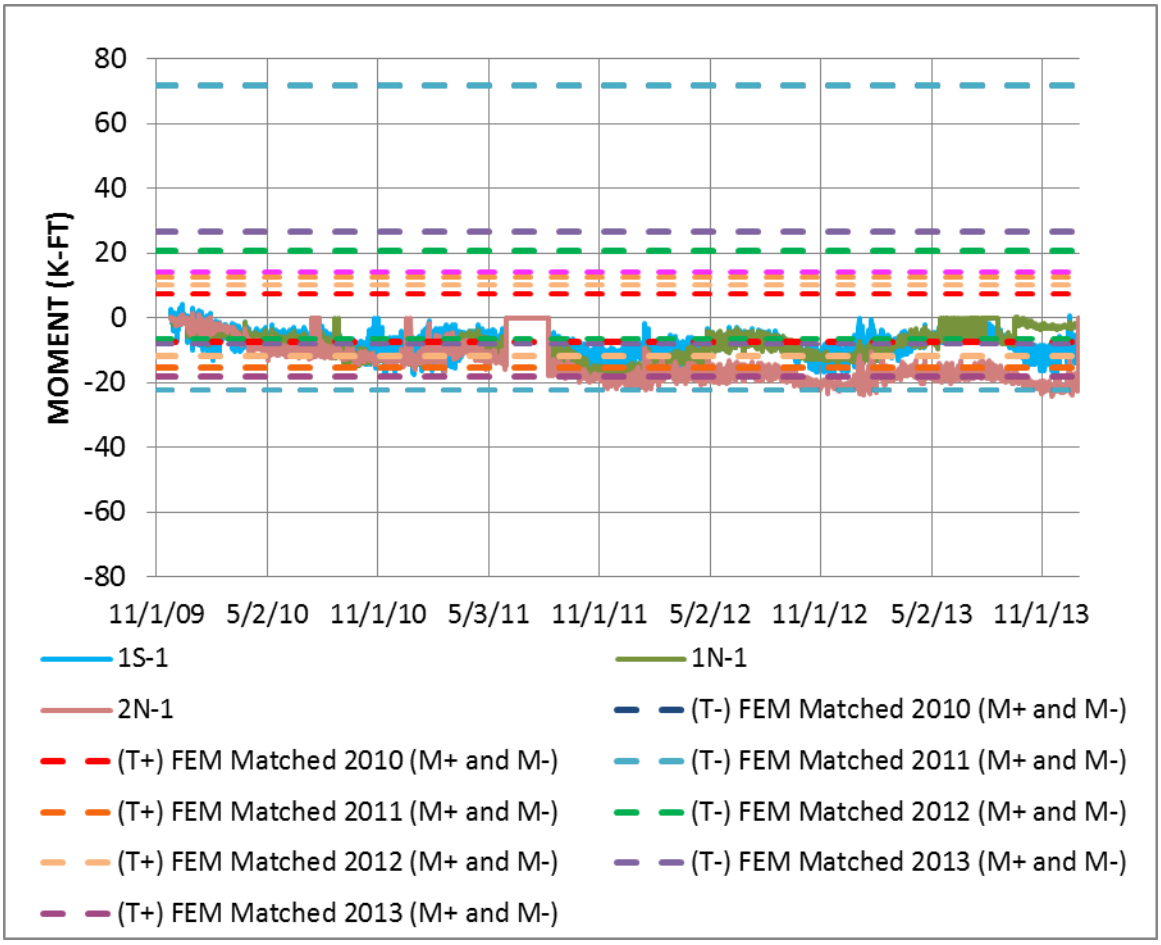

Figure 3-19 Pile weak axis bending moments (field data and FEM Matched)

*FEM Matched values shown in figure are presented in Table 3-7

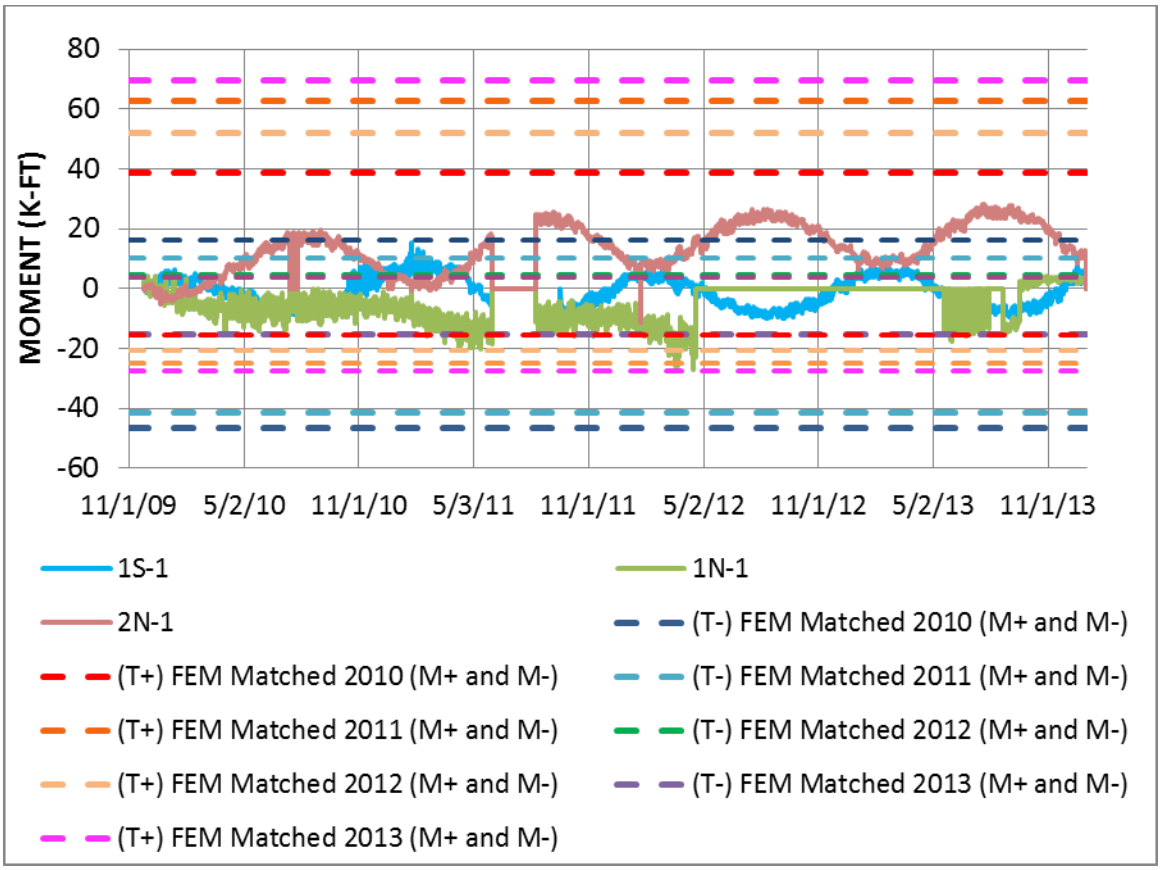

Figure 3-20 Pile strong axis bending moments (field data and FEM Matched)
***FEM Matched values shown in figure are presented in Table 3-8**

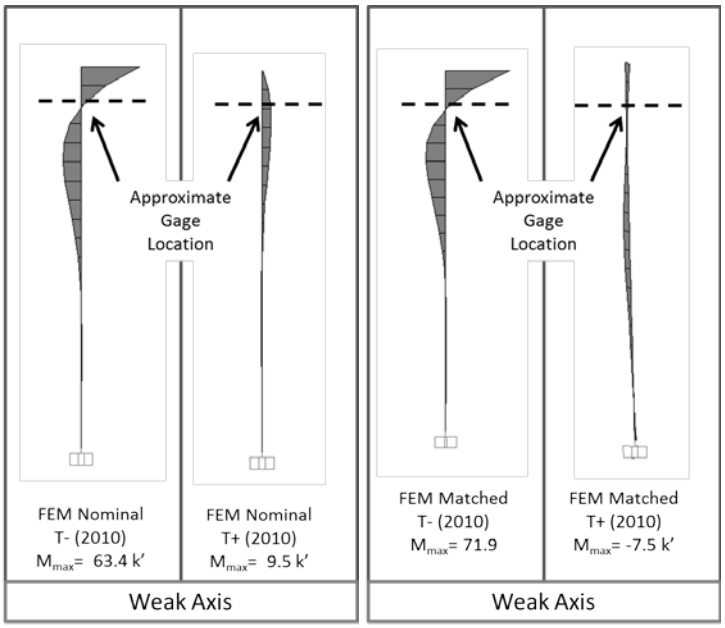

Figure 3-21 Weak Axis Pile Bending Moment Diagram for FEM with Original Soil Conditions (left) and FEM Matched (right)

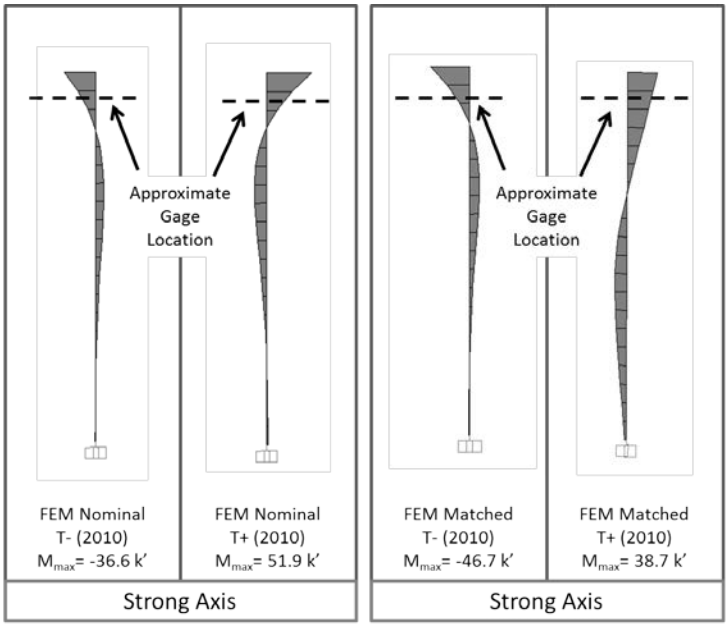

Figure 3-22 Strong Axis Pile Bending Moment Diagram for FEM with Original Soil Conditions (left) and FEM Matched (right)

Table 3-7 Weak Axis Pile Bending Moments (field data and FEM Matched)

Date	Temp. (°F)	Moment at Gage Location (1.6' below top of pile) (kip-ft)		Point of Inflection (FEM) (ft)	FEM Maximum Moment (k-ft)	
		FIELD DATA	FEM		M+	M-
1/31/10	-7.2	-13.0	-11.7	2.2	71.9	-22.1
7/7/10	93.4	-6.4	-4.6	4.2	7.4	-7.5
1/24/11	-19	-16.2	-11.7	2.2	71.8	-22.1
9/4/11	80.4	-11.0	-9.9	4.7	12.5	-15.5
1/16/12	-14.3	-3.3	3.3	2.1	20.6	-6.3
5/20/12	84.3	-5.5	-7.3	4.5	10.0	-11.6
1/24/13	-19	-9.6	-4.3	2.2	26.5	-8.2
7/17/13	89.7	-5.7	-11.6	4.7	14.1	-18.0

* M_{yy}=144.2 kip-ft, M_{py}=221.7 kip-ft (HP12x84) weak axis yield moment and plastic moment, respectively

Table 3-8 Strong Axis Pile Bending Moments (field data and FEM Matched)

Date	Temp. (°F)	Moment at Gage Location (1.6' below top of pile) (kip-ft)		Point of Inflection (FEM) (ft)	FEM Maximum Moment (k-ft)	
		FIELD DATA	FEM		M+	M-
1/31/10	-7.2	0.60	1.9	2.0	16.2	-46.7
7/7/10	93.4	15.5	16.2	5.7	38.7	-15.3
1/24/11	-19	0.6	1.9	2.0	10.2	-41.5
9/4/11	80.4	23.5	24.7	5.7	62.8	-24.8
1/16/12	-14.3	4.7	0.7	1.9	4.6	-13.3
5/20/12	84.3	18.1	20.5	5.7	52.0	-20.6
1/24/13	-19	8.0	0.7	2.0	3.8	-15.4
7/17/13	89.7	26.7	27.3	5.7	69.7	-27.5

* M_{yy}=441.7 kip-ft, M_{py}=500.0 kip-ft (HP12x84) strong axis yield moment and plastic moment, respectively

4 Stockbridge Bridge

The long term monitoring of the Stockbridge Bridge began on November 2, 2009. This section presents the data collected from the beginning of long term monitoring through December 31, 2013. The bridge temperature over the monitoring period is shown in Figure 4-1.

A three-dimensional FEM was created for the bridge using SAP2000. Soil is modeled using non-linear Winkler springs. The original model used for comparison to field data contained soil springs based on the soil boring logs reported at bridge construction (medium-dense soil around the piles), and backfill was neglected in this model due to the presence of Geofoam behind the abutments which minimizes backfill pressure. The model was later calibrated to match conditions seen in field data to compare values which will be discussed in greater detail in the last two sections of this chapter.

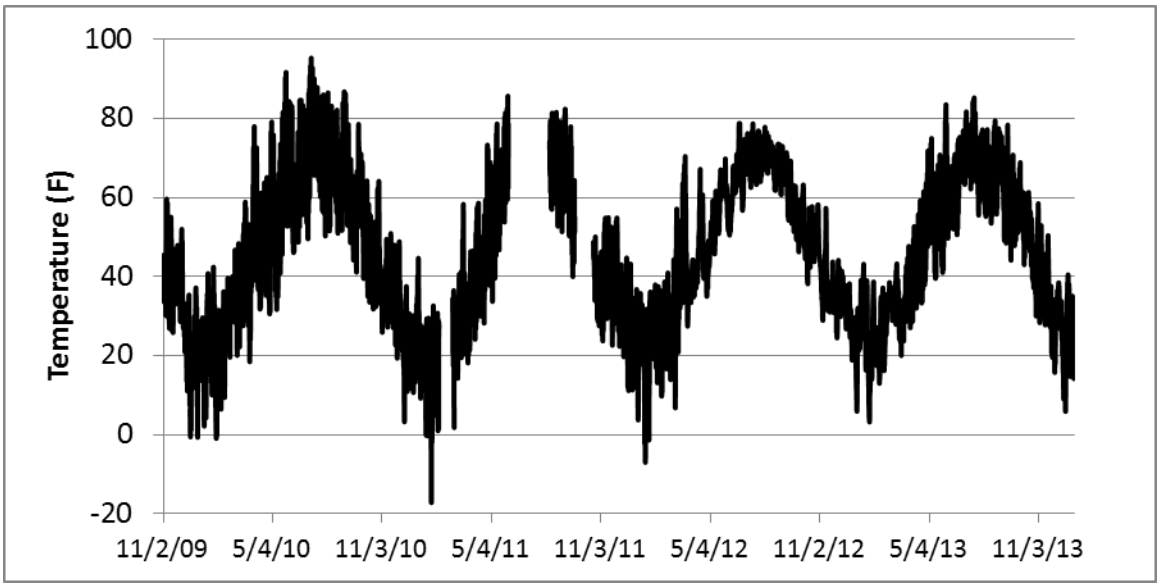

Figure 4-1 Ambient Bridge Temperature

4.1 Girder Stresses

All stress values presented in this section correspond to those induced by thermal effects only. Girder stresses over time are presented for top flange gages and bottom flange gages in Figure 4-2. A positive stress value indicates tensile stress and a negative stress value indicates compressive stress. The bottom flange stresses are consistently greater than top flange stresses due to the elastic neutral axis being located near the slab/girder interface. The top flange stresses range from -2.9 ksi (-20.0 MPa) to 2.7 ksi (18.6 MPa), while the bottom flange stresses range from -6.5 ksi (44.8 MPa) to 4.9 ksi (33.8 MPa). Girder stresses are presented with corresponding temperature in Figure 4-3, these are shown for the three instrumented segments (Abutment 1 girder ends, midspan, and Abutment 2 girder ends), and are also split up into top and bottom flange gages. Midspan gages are located 113.2 ft (34.5 m) and 105.0 ft (32.0 m) from Abutment 1 for upstream and downstream girder, respectively.

The FEM results for the girder moments induced by temperature increase and temperature decrease are presented in Figure 4-4. For a decrease in temperature, mid-span moments should be negative while the ends of the bridge experience positive moments. For an increase in temperature the ends of the bridge have negative bending moments while the mid-span of the bridge has positive moments. For the FEM, maximum and minimum temperatures of 95°F and -0.7°F, respectively, were analyzed which corresponds to the maximum and minimum temperatures experienced in the first year of monitoring. In the case of temperature increase, the girder moments at the ends ranged from -380

kip-ft (-515.2 KN-m) to -394 kip-ft (-534.2 KN-m) while mid-span girder moments ranged from 140 kip-ft (189.8 KN-m) to 388 kip-ft (526.1 KN-m). In the case of temperature decrease, the girder moments at the ends ranged from 209 kip-ft (283.4 KN-m) to 274 kip-ft (371.5 KN-m) and the girder moments at mid-span ranged from -135 kip-ft (-183.0 KN-m) to -203 kip-ft (-275.2 KN-m). In both the temperature increase and temperature decrease cases, the greater bending moment occurred on the upstream girder on the outer radius of the bridge.

At the completion of construction, the maximum girder stress was a compressive stress of 13.0 ksi (89.6 MPa). Therefore, the cumulative maximum girder stress from construction and thermally induced loads is 19.5 ksi (134.4 MPa). Both top and bottom flange girder stresses have been consistent from year to year.

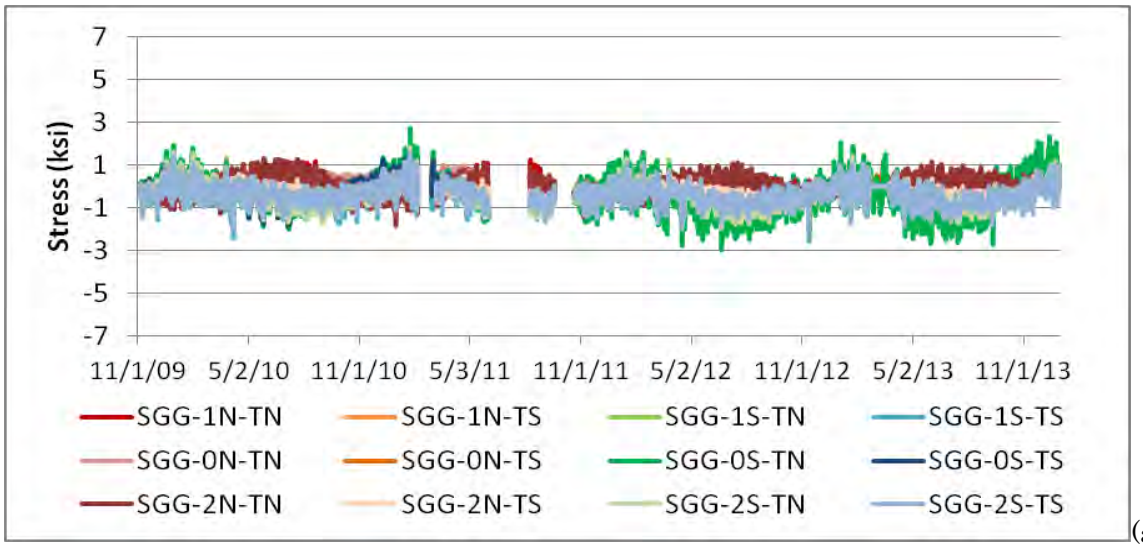

(a)

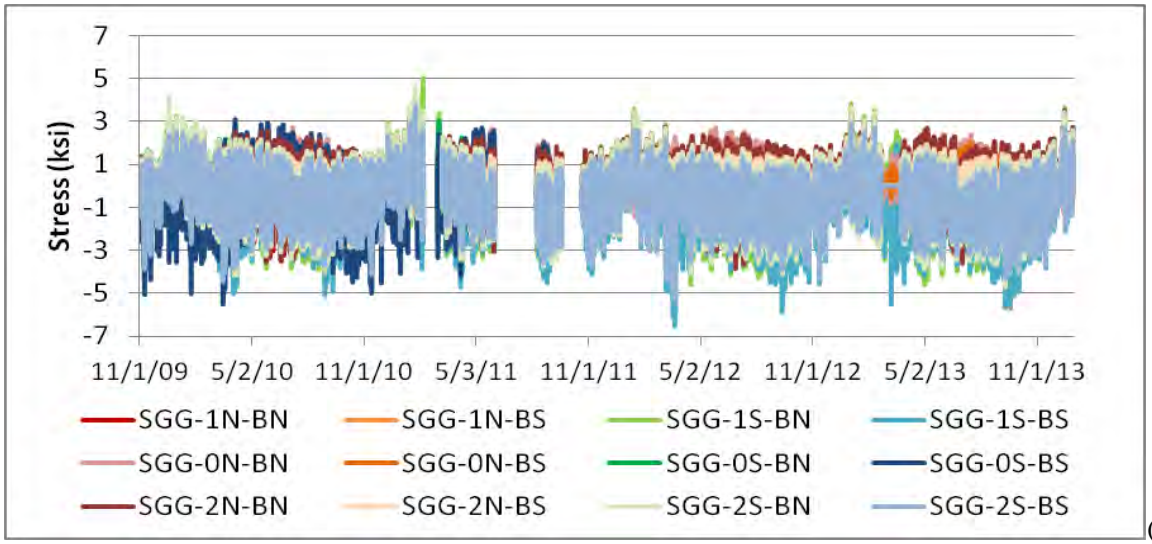

(b)

Figure 4-2 Girder Stresses (a) Top Flange Gages (b) Bottom Flange Gages

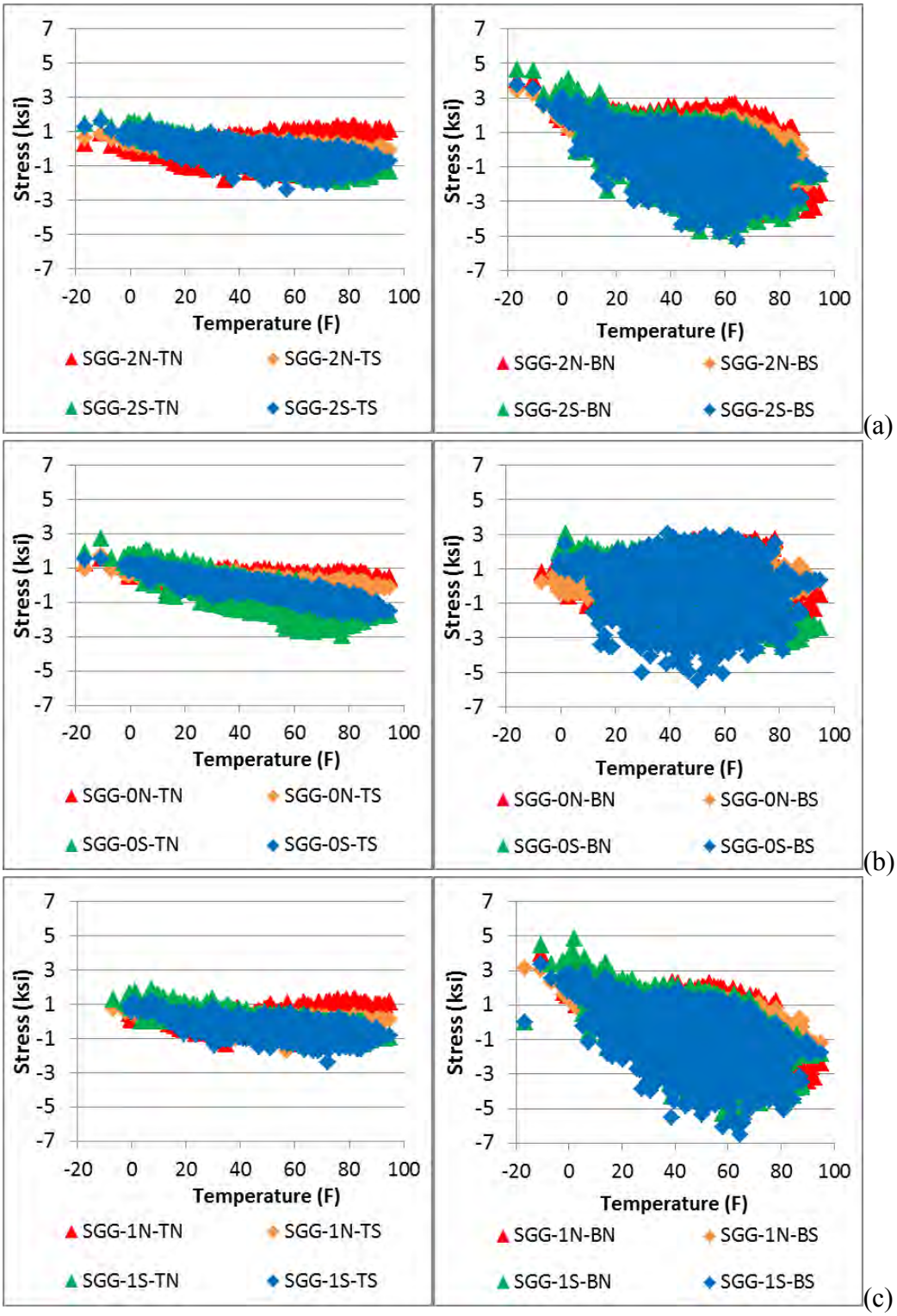

Figure 4-3 Girder Stresses vs. Temperature – (left) Top Flange Gages (right) Bottom Flange Gages -- (a) Abutment 1 (b) midspan and (c) Abutment 2

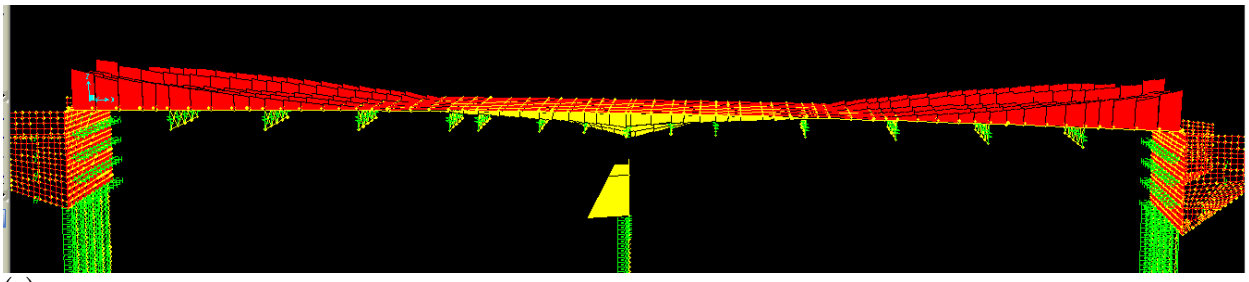

(a)

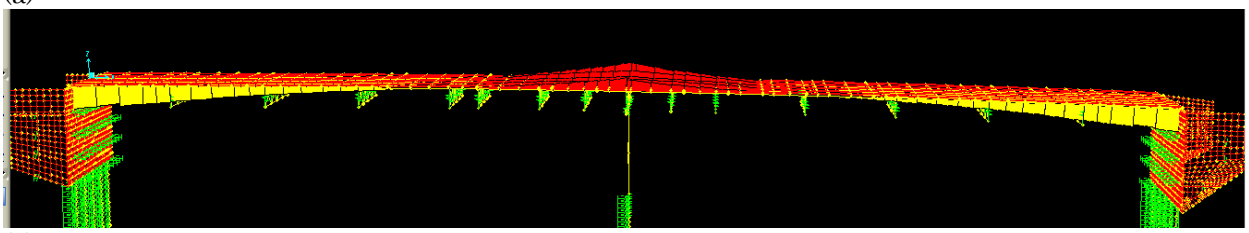

(b)

Figure 4-4 Girder Moment Diagram from SAP2000 (a) Temperature Increase (b) Temperature Decrease

4.2 Displacements

Displacements presented in this section are those occurring from thermally induced loads only. Longitudinal and transverse displacements at the top and bottom of the abutments are presented in the following section. Top of abutment displacements refer to displacements at the girder top flange. For Abutment 1 longitudinal displacements, positive displacement value indicates movement towards the river (bridge contraction) while a negative displacement value indicates movement towards the backfill (bridge expansion). For Abutment 2 longitudinal displacements, the opposite sign convention is used (positive value for expansion and negative value for contraction). For the figures of longitudinal displacements over time, maximum and minimum yearly temperatures were analyzed as a thermal loading in SAP2000 and the results are presented as markers on the date corresponding to that temperature.

Expected displacements due to thermal loading were calculated using the equation for thermal expansion

$$\delta=\alpha L\Delta T$$

where L= span length, α = coefficient for thermal expansion of superstructure $6.5\text{x}10^{-6}$/°F, and ΔT = temperature change. Table 4-1 lists the peak to peak top of abutment displacements for the four corners of the bridge, as well at the change in temperature that occurred from minimum to maximum temperature. These temperature changes were used for the thermal expansion equation prediction; Table 4-2 presents the net average top of abutment displacements and compares those values with the thermal expansion equation and FEM results.

Longitudinal abutment displacements are shown with time in Figure 4-5 and Figure 4-6, for top and bottom of abutments respectively. Top of abutment displacements are significantly greater than bottom of abutment displacements as a result of abutment rotation. Many IABs are designed assuming constant displacement along the depth of the abutment, and these results show that this is an overly conservative design assumption.

For top of abutment displacements, the greatest net bridge displacement occurred in 2013 with a displacement of 1.95 in (49.53 mm) (total value from contracted to expanded position). In the first two years, the field results for top of abutment displacement were closer to the values predicted

using the thermal expansion equation and FEM than in the latter years. The upstream side of Abutment 2 shows that it is tending to increase in displacements over time, while the upstream and downstream sides of Abutment 1 are have consistently similar displacements. Even with the increase in displacements at the Abutment 2 upstream side, the average displacement of the two corners of the abutment is below the average displacements at Abutment 1.

For the bottom of abutment displacements, the FEM values underestimated displacements due to bridge expansion and overestimated the values due to bridge contraction. The bottom of Abutment 2 upstream has been shifting towards the backfill at the abutment which is consistent with the top of abutment behavior at this location, while Abutment 2 downstream shows minimal movement over time. The peak to peak displacements at Abutment 2 are lower than those at Abutment 1. The maximum peak to peak bottom of abutment displacement (sum of both abutments) was 0.48 in (25.4 mm). The bottom of abutment displacements show that there is a lag in recovery of displacement at the top of the pile as it holds its deflected shape while the top of abutment contracts away.

Seasonal displacement relations between top and bottom of abutment displacements are presented in Figure 4-7 for Abutment 1 and Abutment 2. For Abutment 1, the relation between top and bottom of abutment displacements is very consistent over time. The top of abutment displacement is very similar from year to year while the corresponding bottom of abutment displacement gradually increases which could be a result of the lag in recovery of bottom of abutment displacements causing a slight build up and shift towards the backfill. However, Abutment 2 seasonal changes show not only a shift towards the backfill at the bottom of the abutment but also at the top of the abutment.

Transverse displacements at the top of the abutment are shown with time in Figure 4-8. For Abutment 1, a positive value indicates displacement towards upstream. For Abutment 2, a positive value indicates displacement towards downstream. Abutment 1 upstream shows a slight shift towards downstream over time during temperature increase, while Abutment 2 upstream shows a shift towards upstream. Maximum peak to peak transverse displacement was in 2011 with a displacement of 0.28 in (7.1 mm) which is below the 0.30 in (7.6 mm) predicted by the equation of thermal expansion.

Table 4-1 Abutment Displacements from Minimum to Maximum Temperature 2010-2013

Year	ΔT (°F)	Abutment 1 (in.)			Abutment 2 (in.)		
		Upstream	Downstream	Average	Upstream	Downstream	Average
2010	95.70	1.11	1.09	1.10	0.86	0.64	0.75
2011	102.10	0.91	0.87	0.89	0.73	0.54	0.64
2012	85.50	1.02	1.01	1.02	0.90	0.73	0.81
2013	81.90	1.11	1.09	1.10	0.92	0.76	0.84

Table 4-2 Comparison of Peak to Peak Displacement from Field Data, Thermal Expansion Eq., and FEM Results

Year	ΔT (°F)	Sum of Average Abutment Displacements (in)	Thermal Expansion Prediction	Sum of Abut. Displacements from FEM
2010	95.70	1.87	1.66	1.48
2011	102.10	1.55	1.77	1.51
2012	85.50	1.84	1.48	1.43
2013	81.90	1.95	1.42	1.42

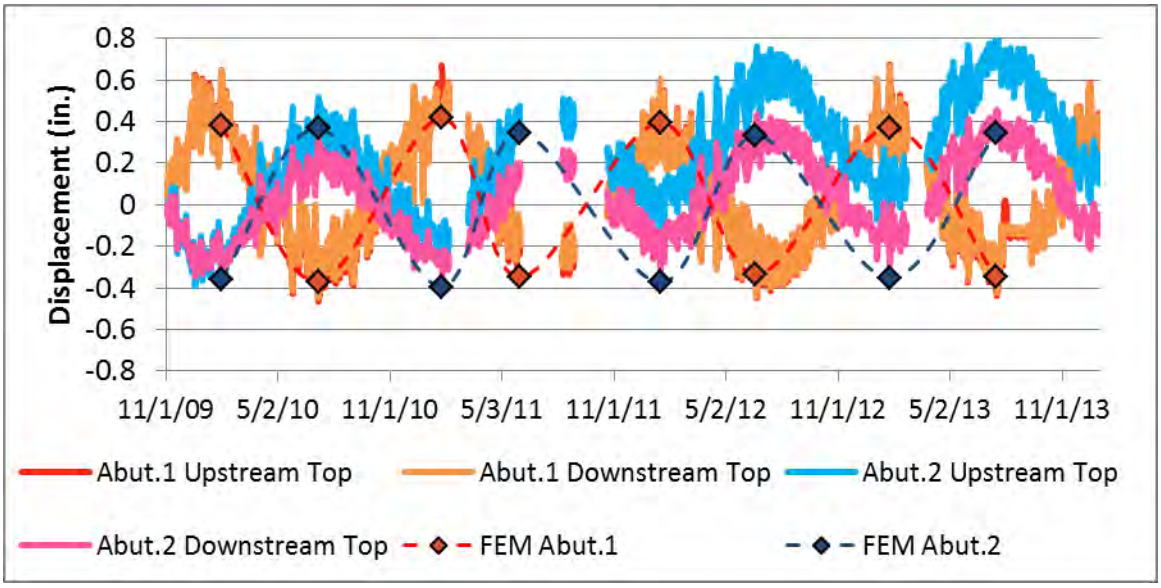

Figure 4-5 Top of Abutment Displacement (field and FEM)

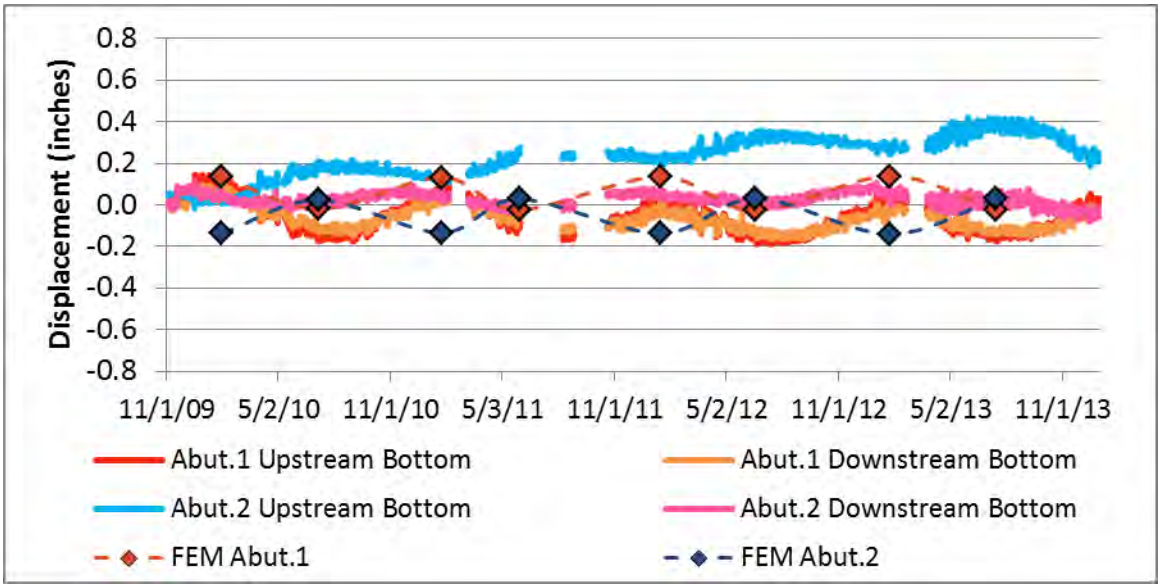

Figure 4-6 Bottom of Abutment Displacements

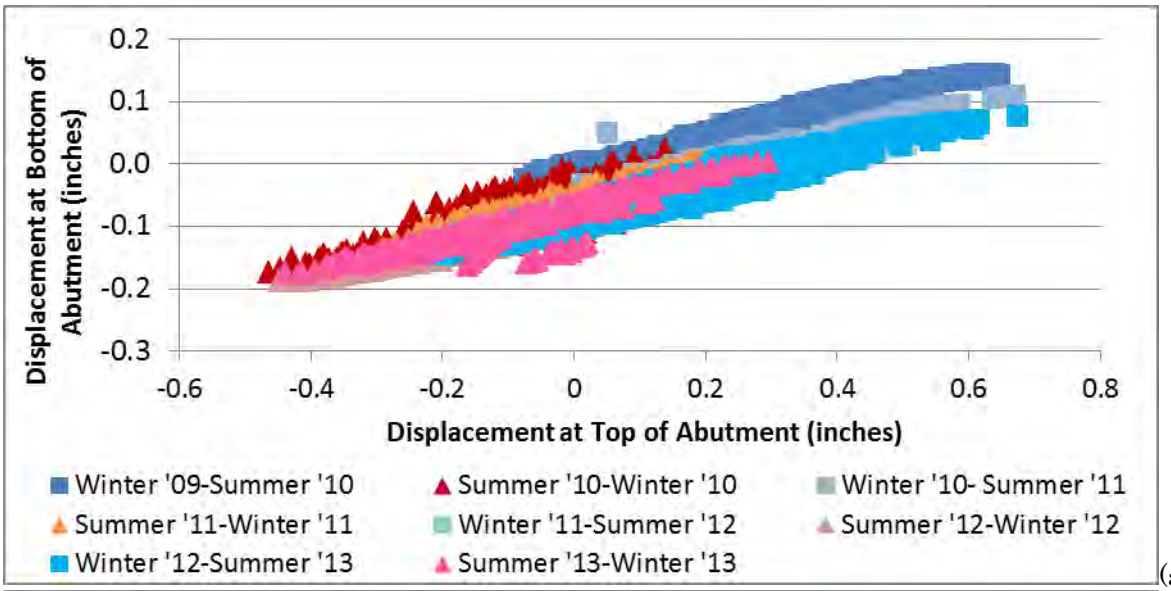

(a)

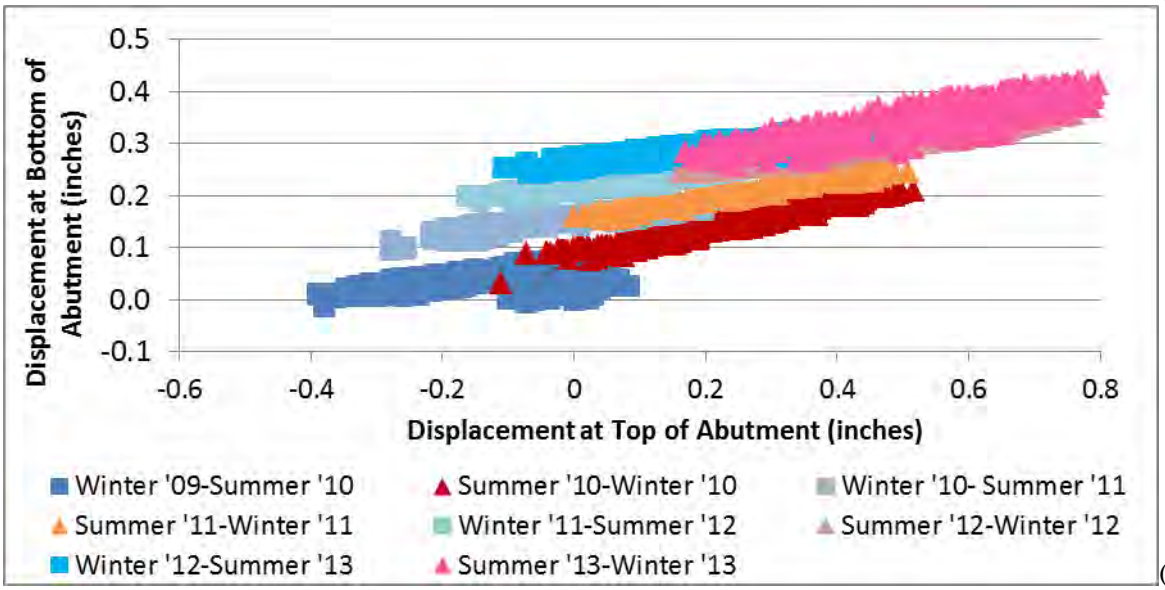

(b)

Figure 4-7 Seasonal Displacements at Top and Bottom of (a) Abutment 1 (b) Abutment 2

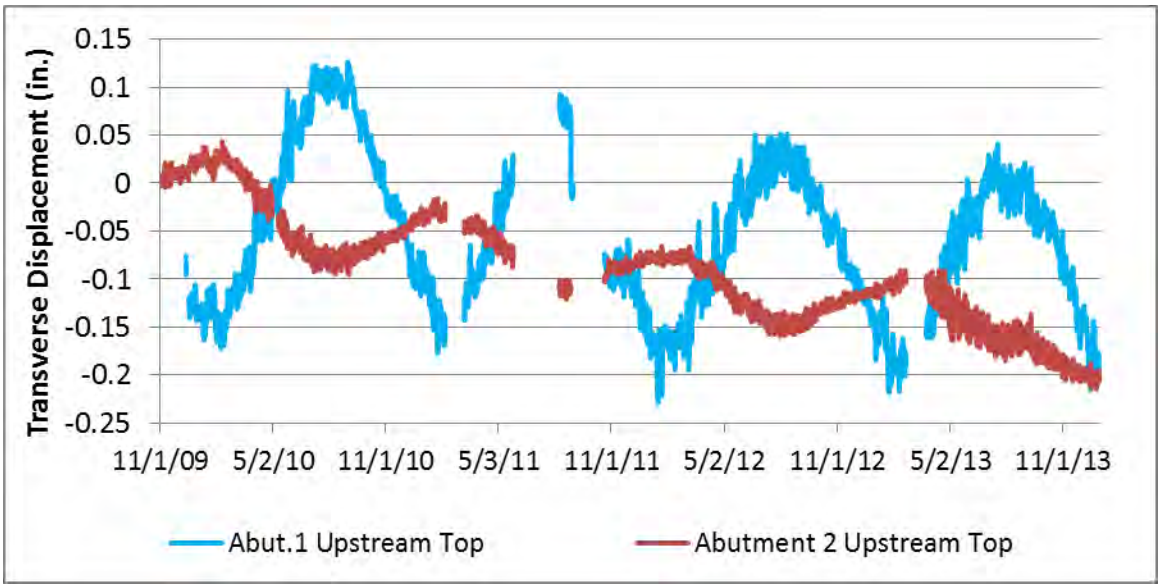

Figure 4-8 Transverse Displacement at Top of Abutment 1

4.3 Abutment Rotation

Abutment rotations presented in this section are those resulting from thermal effects only. Abutment rotations are presented in Figure 4-9 and Figure 4-10. For both abutments, a positive rotation value indicates rotation towards the river and a negative rotation value indicates rotation towards the backfill. The FEM results predicted nearly the same rotation value at both abutments. The abutment rotations were very similar in the first year of monitoring; however Abutment 2 does begin having slightly greater negative rotations beginning in the middle of 2010. The shift in rotation at Abutment 2 is not too significant due to the fact that the top and bottom of abutment are both experiencing a permanent shift towards the backfill therefore the relation (angle of rotation) between the two is similar year to year. FEM results are generally a good match for bridge expansion, while they underestimate rotation under bridge contraction. This could again be due to the lag in recovery of bottom of abutment displacement. The peak to peak rotation values (from minimum to maximum yearly temperature) are presented with FEM results in Table 4-3. The maximum peak to peak rotation occurred at Abutment 2 in 2013 with a value of 0.21 degrees.

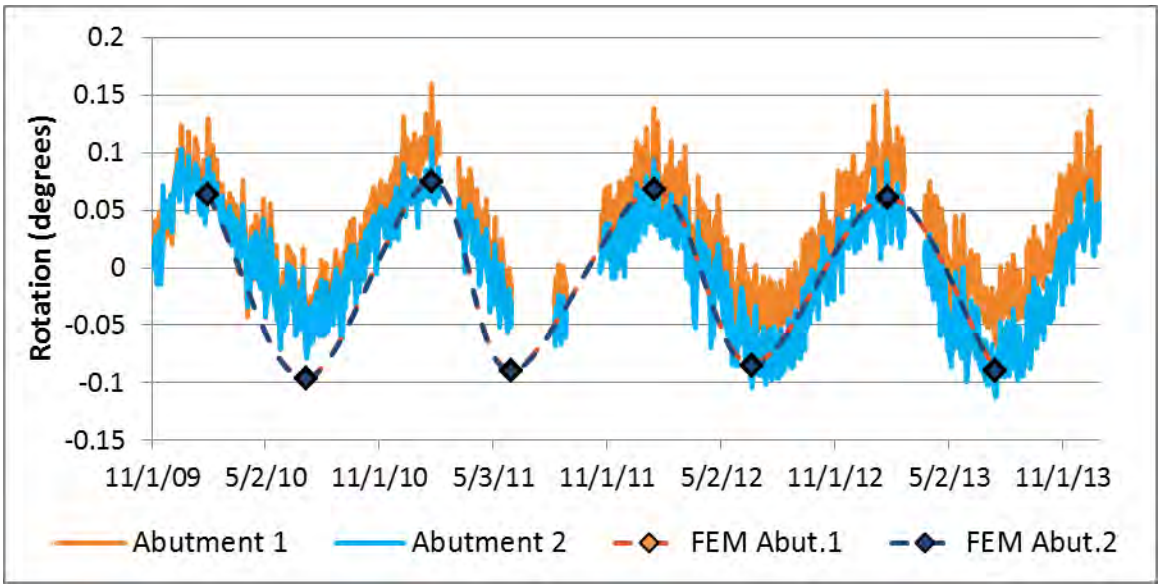

Figure 4-9 Abutment Rotation (field data and FEM)

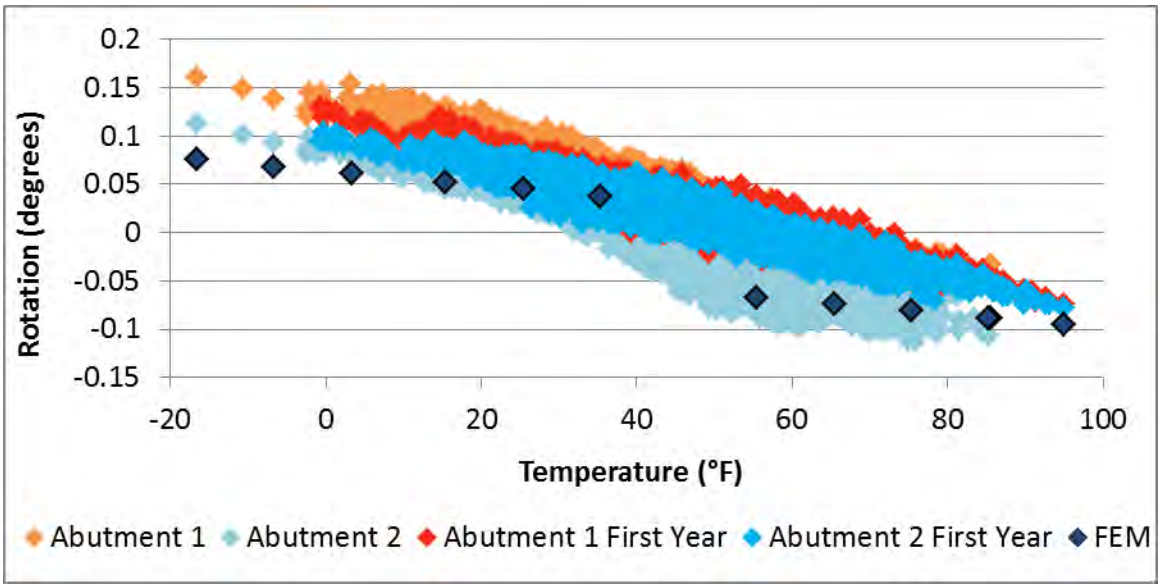

Figure 4-10 Abutment Rotation vs. Temperature (field data and FEM)

Table 4-3 Peak to Peak Abutment Rotation (field data and FEM)

Year	D Temp. (°F)	Abutment 1 Rotation (degrees)		Abutment 2 Rotation (degrees)	
		Field Data	FEM	Field Data	FEM
2010	95.7	0.17	0.16	0.20	0.16
2011	102.1	0.16	0.17	0.19	0.17
2012	85.5	0.16	0.15	0.17	0.16
2013	88.5	0.20	0.15	0.21	0.15

4.4 Earth Pressures

Pressures presented in this section are the changes in pressure since construction due to thermal loading. The abutment walls were constructed with geofoam material behind the walls before they were backfilled. This geofoam was included with the intention of reducing the earth pressures on the abutment wall. The wing walls do not have the geofoam material behind them. The greatest earth pressures at the Stockbridge Bridge occurred behind the wing walls, as shown in Figure 4-11. The maximum wing wall pressure occurred behind the upstream wing wall at Abutment 1 with a pressure of 13.9 psi (95.8 KPa).

The earth pressures at the top, middle, and bottom of abutments are presented in Figure 4-12, Figure 4-13, and Figure 4-14, respectively. The greatest pressure behind the abutments occurred in the top row of pressure cells at Abutment 1 in the center of the abutment. The maximum pressure at this location was 2.9 psi (20.0 KPa), while the pressures in the top row of pressure cells in other locations were comparable. The maximum pressure does not occur when the maximum temperature occurs; it takes some time after the maximum temperature occurs for pressures to build up to their maximum value. The geofoam material provided behind the abutments not only appears to be effective at reducing earth pressures on the abutment wall, but also on keeping the pressures consistent year to year.

At the end of construction, the maximum wingwall pressure was 29.0 psi (144.1 KPa), while the maximum abutment pressure was 5.3 psi (36.5 KPa). Therefore, cumulative maximum pressures at this bridge are 42.9 psi (295.8 KPa) behind the wing wall, and 8.2 psi (56.5 KPa) behind the abutment. The passive earth pressure (based on the coefficient of passive earth pressure K_p=5.8) behind the wing wall is estimated to be 110.0 psi (758.4 KPa) at the gage location, therefore the cumulative maximum pressure behind the wing wall is approximately 39% of the estimated passive pressure.

Figure 4-15 shows the average earth pressure in the top row of pressure cells at Abutment 1 vs. the corresponding displacement at that depth, split up by seasons where “Winter-Summer” indicates October through the beginning of April, and “Summer-Winter” indicates April through the end of September. This plot clearly shows that when a displacement is reached in subsequent seasons, the pressure is less than the first time that displacement occurred. This shows that increase in soil pressure from season to season, the phenomenon known as soil ratcheting, does not occur at this bridge.

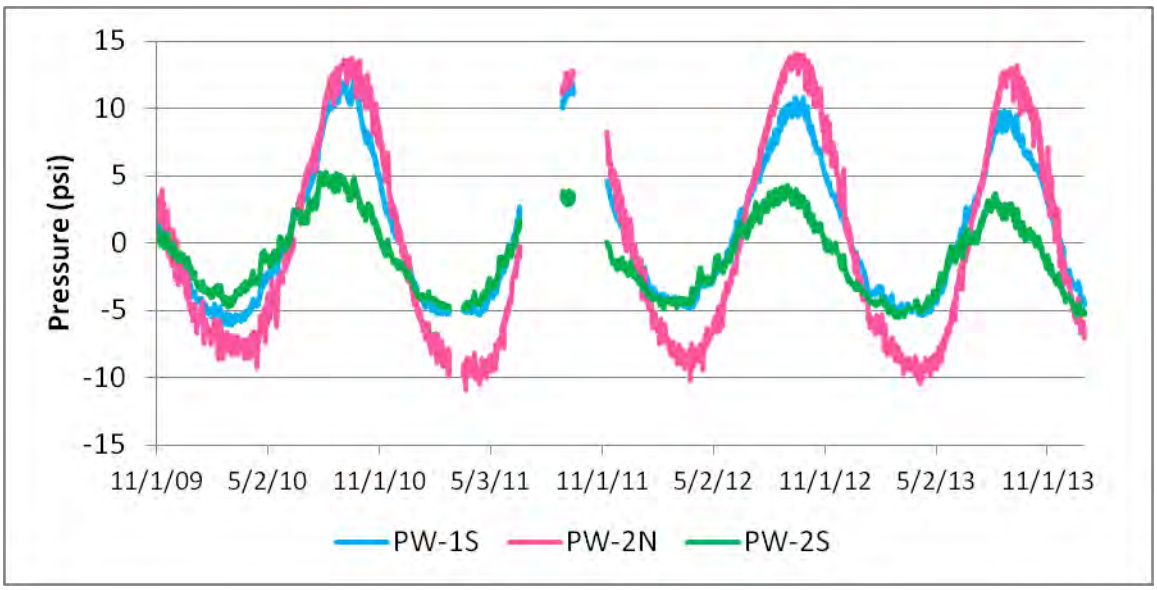

Figure 4-11 Earth Pressure Behind Wing Walls

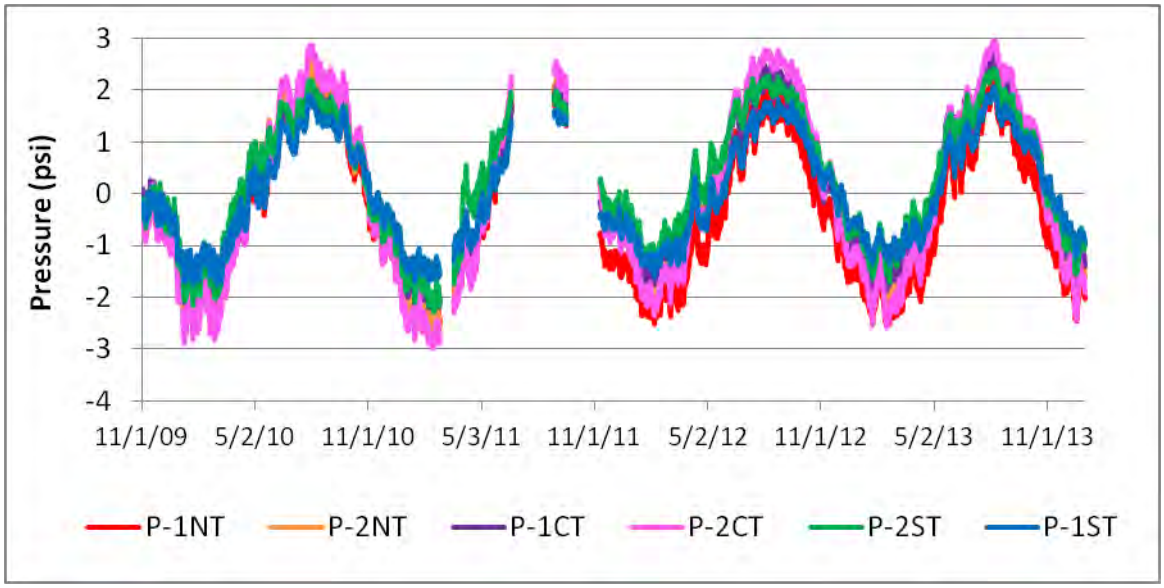

Figure 4-12 Pressures in Top Row of Pressure Cells Behind Abutments

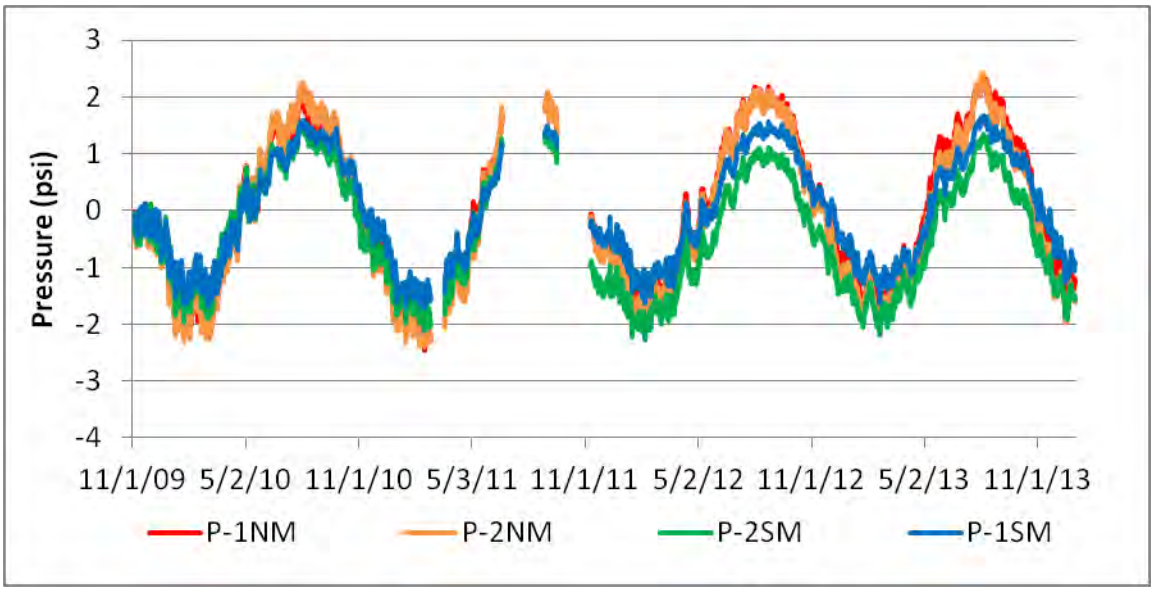

Figure 4-13 Pressure in Middle Row of Pressure Cells Behind Both Abutments

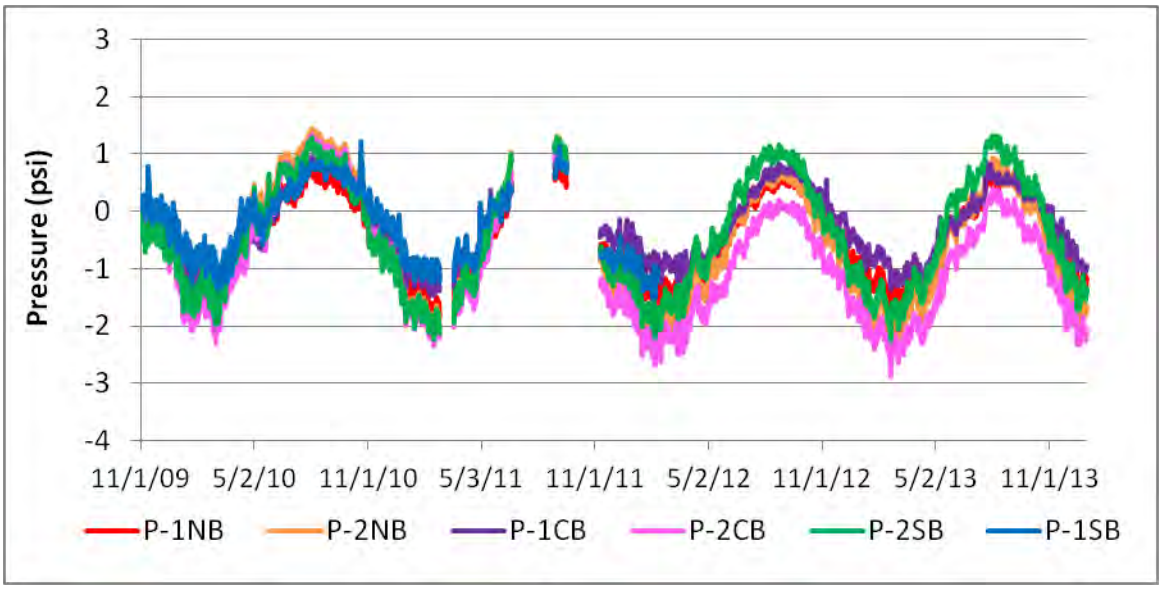

Figure 4-14 Pressure in Bottom Row of Pressure Cells Behind Both Abutments

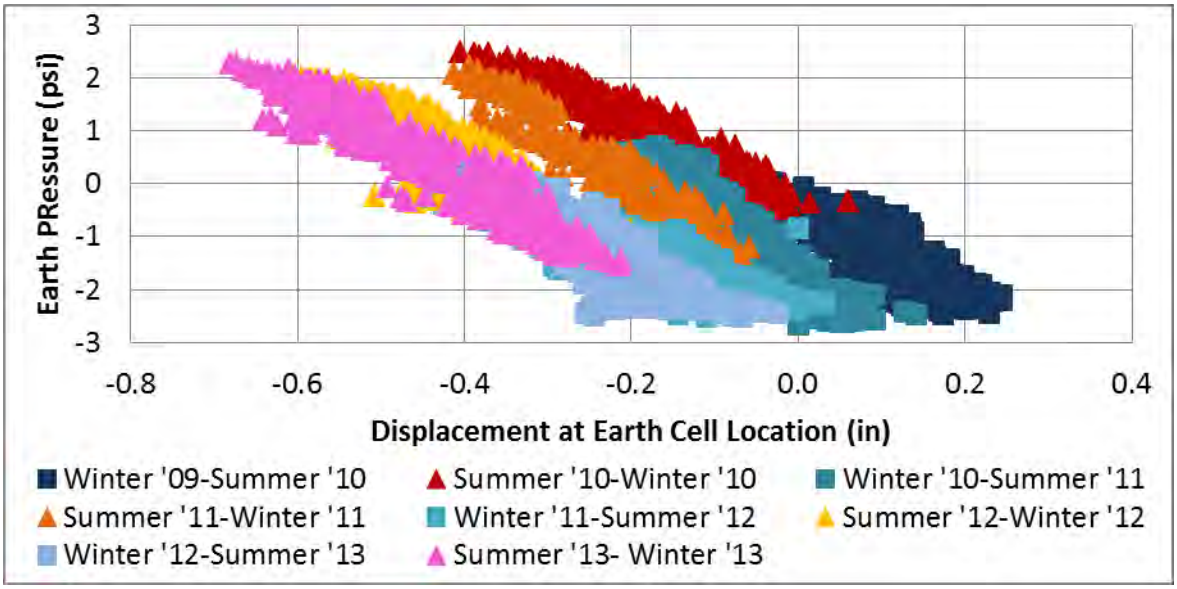

Figure 4-15 Average Earth Pressure vs. Displacement at Top of Abutment 1

4.5 Substructure Displacement at Maximum and Minimum Temperatures

Substructure displacements presented in this section are those due to thermal effects only. Seasonal substructure behavior under warm and cold temperatures is shown in Figure 4-16 for Abutment 1 upstream. These plots show that for the warm temperature at the end of the season, the pile holds its deflected shape in the backfill with nearly the same magnitude as it had on the warmest day of the year while the top of the abutment contracts back close to where it was when the warm temperature occurred at the beginning of the season. The offset in pile displacements is accommodated by localized rotation at the top of the pile. The offset in the piles can also be seen in the cold temperature plots, although the cold temperature response shows more elastic behavior. The initial bridge contraction is the greatest displacement towards the river that the pile sees over time, even though the top of abutment displacement in 2013 is greater than the coldest day in 2010. The pile does still contract and return past its zero position, however the lag in pile recovery seen in bridge expansion causes a cumulative offset towards the backfill in subsequent cold seasons. This lag in response is due to cyclic thermal loading and is something that the FEM thermal model does not capture. The overall repeatability of results within each season is much more consistent at Stockbridge than in the other two bridges, likely due to the Geofoam behind the abutment and/or the modifications to pile placement in the other two bridges where soil was initially excavated to accommodate pile strain gage placements.

The FEM Nominal for this bridge used medium dense soil around the piles per soil borings reported from the bridge site. Backfill pressures at the bridge are minimal (likely due to the geofoam material behind the abutment wall), therefore backfill soil springs were not included in the modeling. When backfill springs were included, FEM results showed far less displacement and did not match field data.

The FEM Nominal (using the original soil assumptions) was analyzed for maximum and minimum temperatures and compared with field data, the results are presented in Figure 4-17. These plots show that for bridge expansion, the FEM underestimates the pile displacement. The FEM results at the top of the abutment are a reasonable match for the maximum temperatures aside from 2011. For

bridge contraction, the top of abutment displacement is underestimated while the pile displacement is overestimated. These results show that modeling substructure displacements with FEMs require further analysis due to the changing soil conditions upon repeated cyclic loading that is not captured in a static thermal analysis.

In order to compare field data to FEM results, the FEM was calibrated to match the substructure displacement seen in the field. This was done by first adjusting the thermal loading in order to match the displacement at the top of the abutment, and then soil properties were adjusted until the results from the FEM matched the substructure displacement in the field. These results are reported as "FEM Matched". Figure 4-18 and Figure 4-19 show the FEM Matched results for yearly maximum and minimum temperatures, respectively. These plots also show the soil conditions used to match field data. Soil conditions used in FEMs are presented in Table 4-4. Once the FEM Matched soil properties were adjusted to match the first year of data, these conditions matched for all four years, showing the more consistent behavior at Stockbridge compared to the other two bridges. For warm temperatures the soil was loose around the top 10.0 ft of the pile and medium dense below that. For cold temperatures, the soil in the FEM was required to be very dense around the top 2 ft of the pile and loose below. The dense soil shows that there was some restraint to bridge contraction around the top of the pile which mimics the lag in recovery of pile displacement from its expanded deflected shape. These FEM Matched results will be discussed further in Section 4.6.

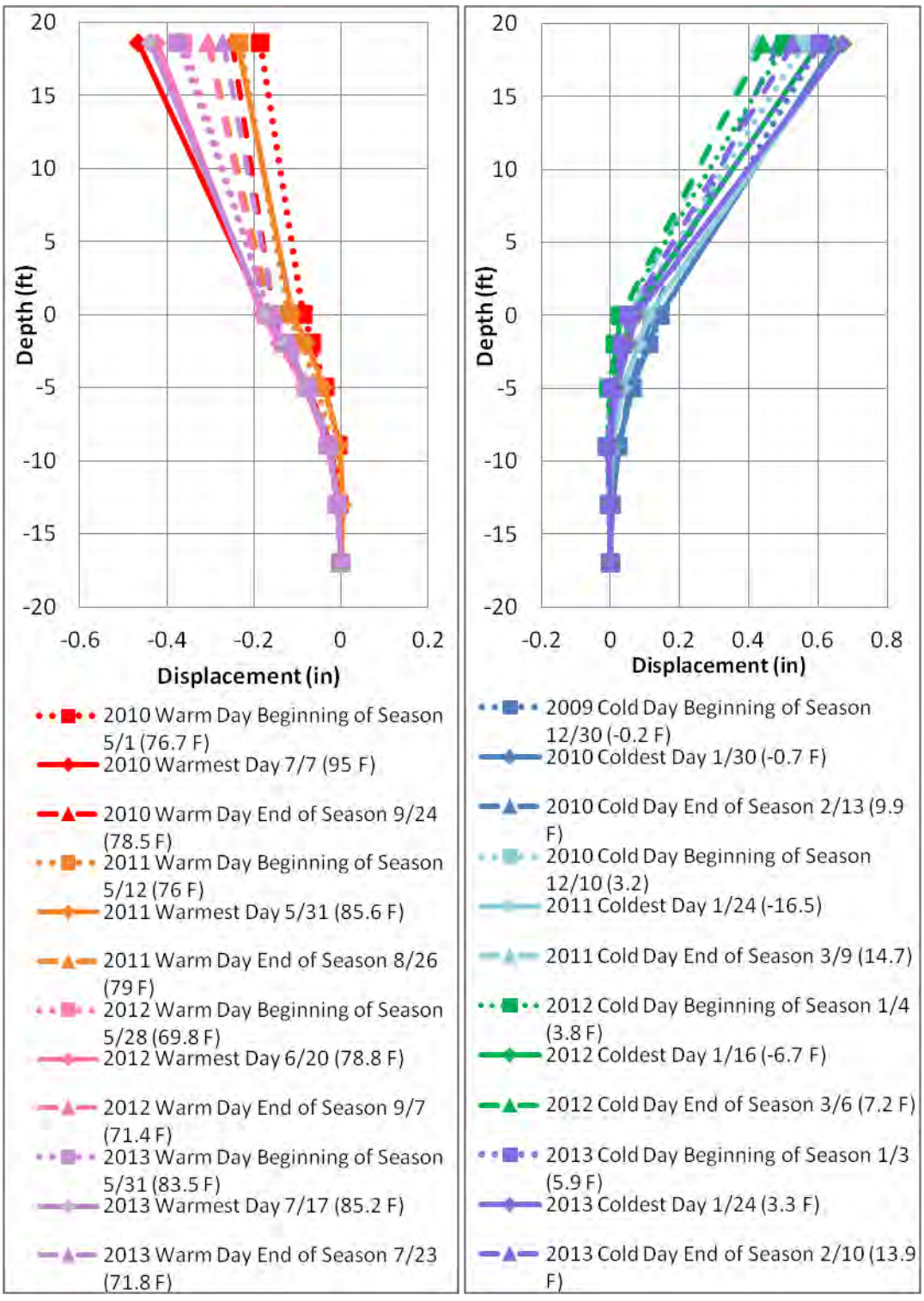

Figure 4-16 Seasonal Substructure Displacement for Warm Temperatures (left) and Cold Temperatures (right)

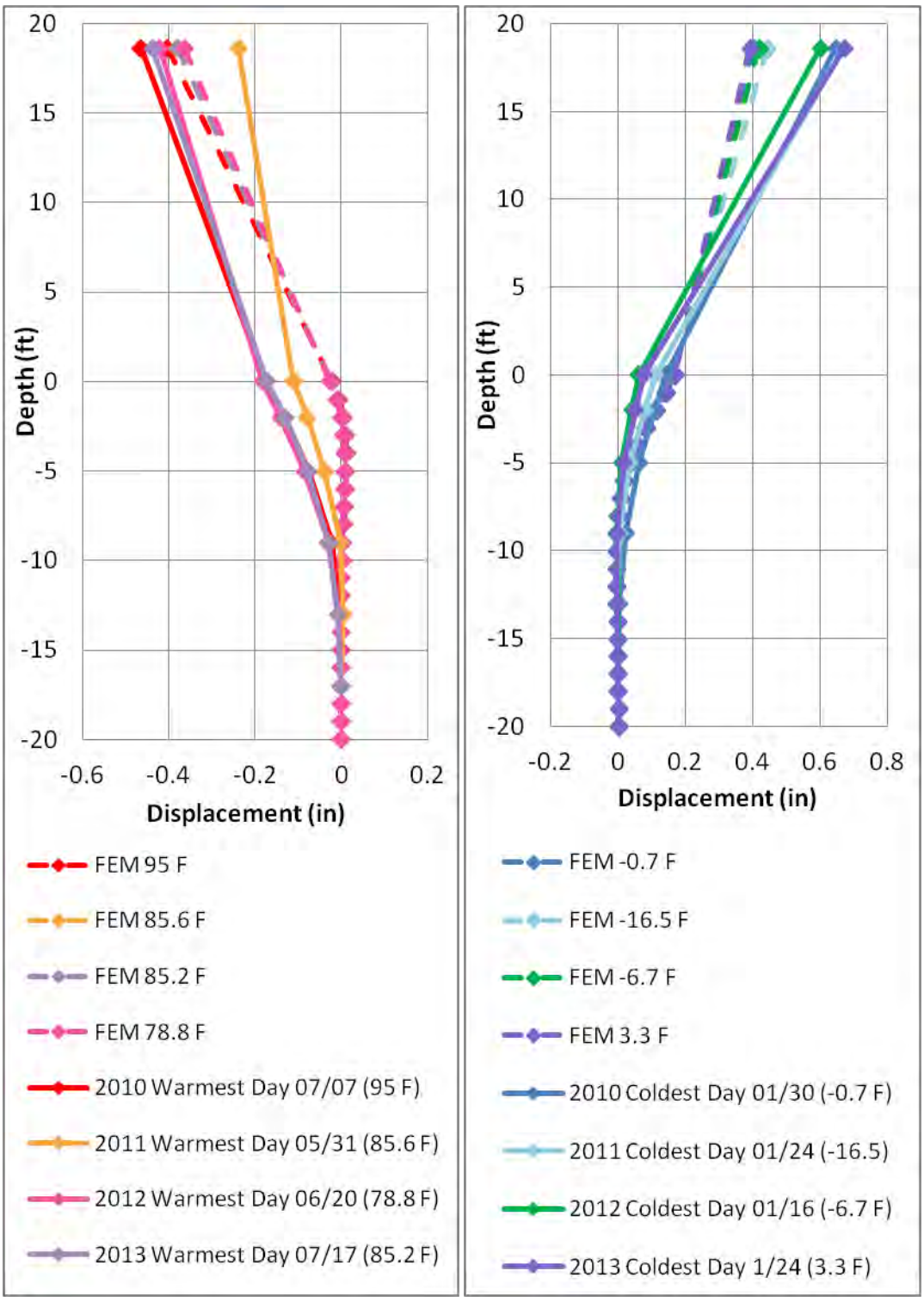

Figure 4-17 Substructure Displacement for Maximum (left) and Minimum (right) Yearly Temperatures with FEM (using original soil conditions from site)

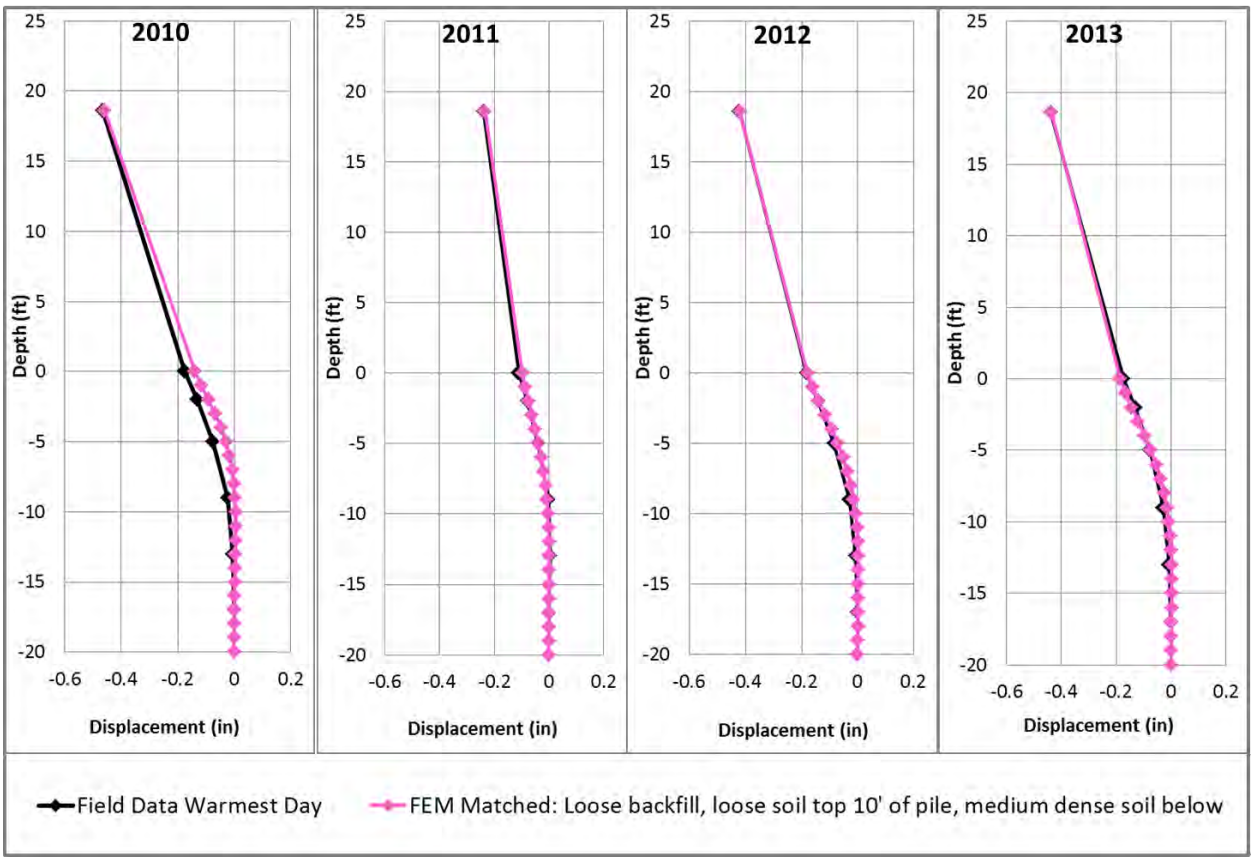

Figure 4-18 FEM Matched Results for Maximum Yearly Temperatures

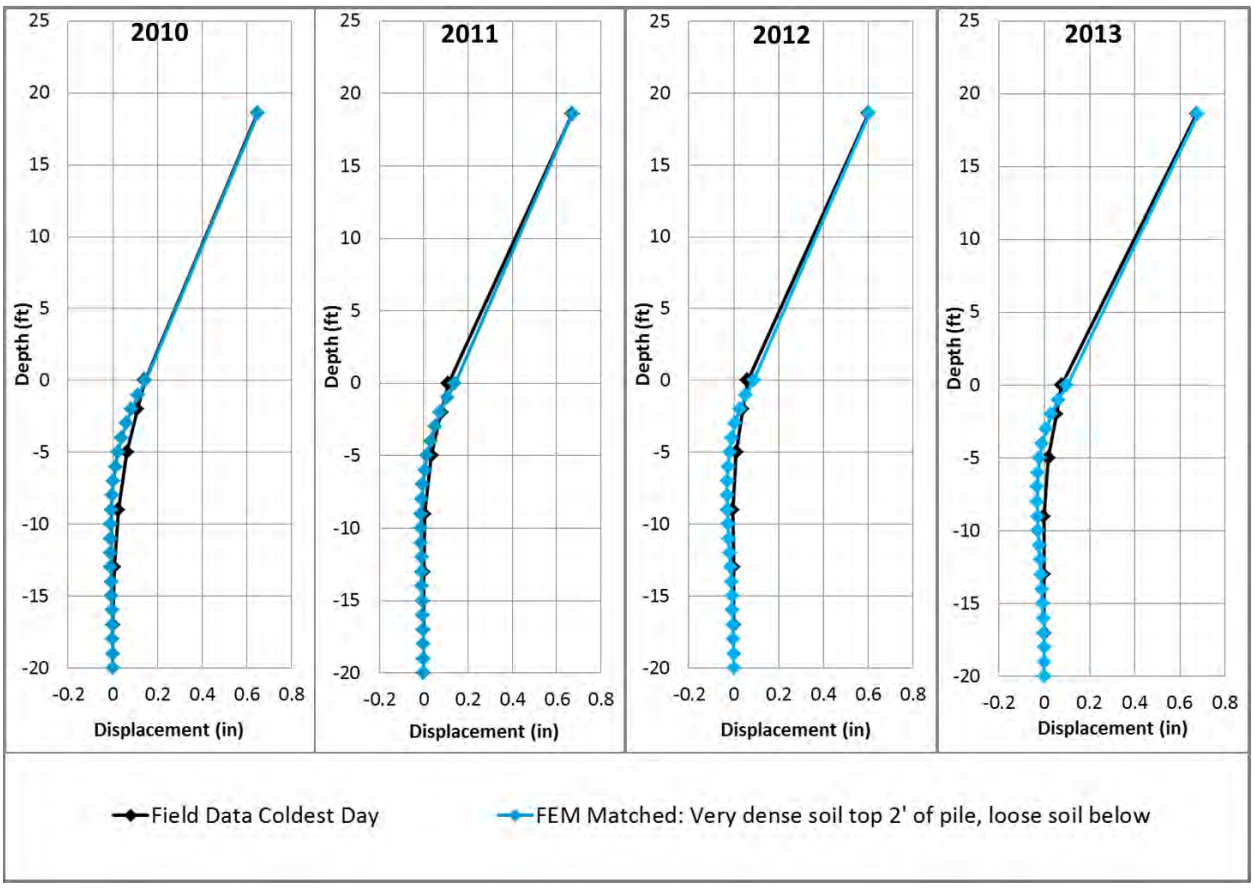

Figure 4-19 FEM Matched Results for Minimum Yearly Temperatures

Table 4-4 Soil Properties Used in FEMS

Soil Classification	Friction Angle φ	Saturated Soil Density (pcf) g
Very Dense (piles)	45	150
Medium Dense (piles)	35	135
Loose (piles)	25	75

4.6 Pile Stresses

Pile stresses presented in this section are those due to thermal effects only. A positive bending moment indicates bending toward the river while a negative bending moment indicates bending toward the backfill, for both abutments. Pile bending moments are calculated from strain gages on the pile flanges. As will be discussed further, field data is not collected at the location of maximum pile moments and therefore the FEM results bounding the data are better predictions of maximum pile moments. Gage notation and locations can be found in APPENDIX A and APPENDIX B. The piles stresses are greatest at the gages at the tops of the piles (located 1.6 ft (0.49 m) below top of pile). It was selected to place gages away from the geometry change at the top of pile and instrument

a location of expected linear strain distribution due to St. Venant's Principle. These stresses are shown in Figure 4-20 and Figure 4-21 for Abutment 1 piles and Abutment 2 piles, respectively. The pile stresses at Abutment 2 are greater than those at Abutment 1 and tend to be increasing over time. This is likely a result of the shift in displacement at Abutment 2 shown in Section 4.2. The maximum pile stress at Abutment 2 is 5.8 ksi (40.0 MPa) (tension) on the downstream pile, and 4.3 ksi (29.6 MPa) (compression) on the upstream pile. At Abutment 1, the maximum stress is 3.5 ksi (24.1 MPa) (tension) on the downstream pile and 4.2 ksi (29.0 MPa) (compression) on the upstream pile. At the completion of construction, the maximum pile stress on the bridge due to thermal effects was 5.0 ksi (34.5 MPa).

Bending moments could not be calculated as strain gages at some locations were damaged and there are not enough to calculate moments. However, the maximum weak and strong axis bending moments from the FEM Matched analyses are provided in Table 4-5. For pile bending about the weak axis, maximum bending moments ranged from -51.8 kip-ft (-70.2 KN-m) to 60.1 kip-ft (81.5 KN-m). Strong axis bending moments ranged from -14.2 kip-ft (-19.3 KN-m) to 17.6 kip-ft (-23.9 KN-m). The yield moment of the pile about the weak axis is 247.9 kip-ft (336.1 KN-m) and yield moment about the strong axis is 716.7 kip-ft (971.7 KN-m).

Figure 4-22 and Figure 4-23 show bending moment diagrams for maximum and minimum temperatures from both FEM Nominal and FEM Matched. The FEM Nominal weak axis bending moment results in this case were comparable to FEM Matched for the first year of monitoring. For strong axis bending moments, FEM Nominal values were about half that of FEM Matched, however these values were all minimal. Over time, the maximum values from FEM Matched (-51.8 k-ft (-70.2 KN-m) and 60.1 kip-ft (81.5 KN-m)) were comparable to FEM Nominal values of -49.3 kip-ft (-66.8 KN-m) and 45.8 kip-ft (62.1 KN-m). While the FEM Nominal underestimated strong axis bending moments, these values were minimal even in the FEM Matched condition.

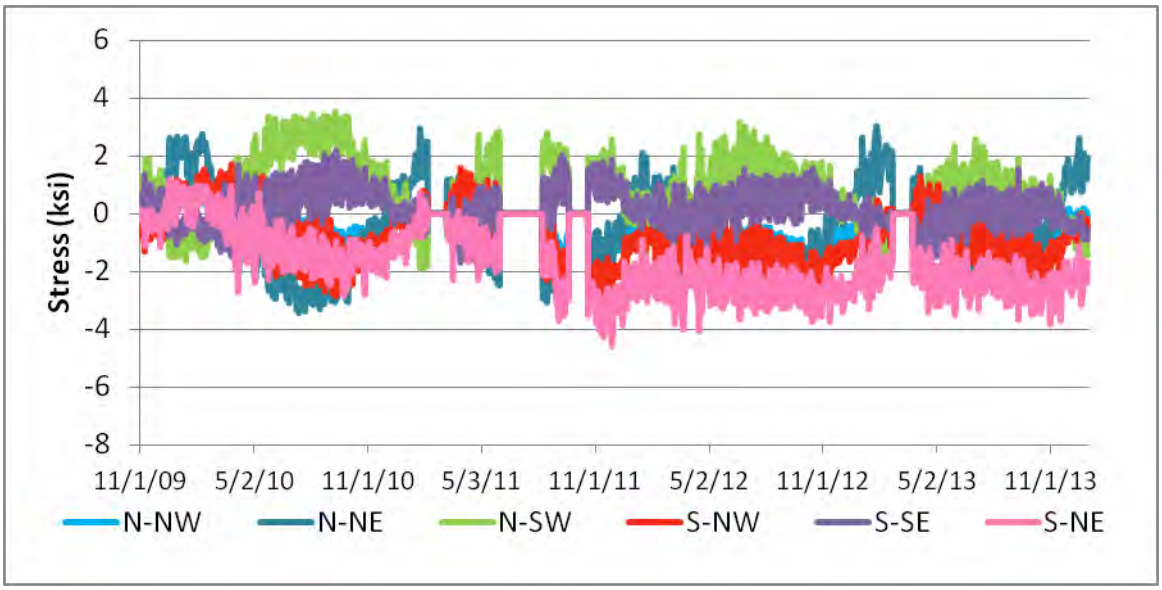

Figure 4-20 Stresses at Top of Upstream and Downstream Pile at Abutment 1

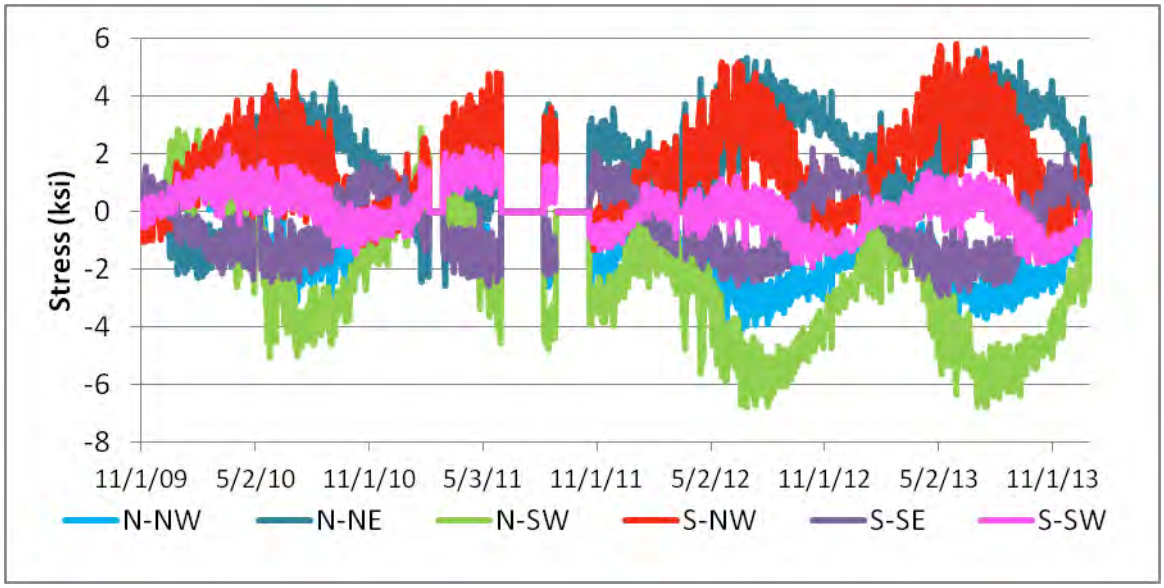

Figure 4-21 Stress at Top of Upstream and Downstream Pile of Abutment 2

Table 4-5 FEM Matched Maximum Weak and Strong Axis Pile Bending Moments

Date	Temp. (°F)	FEM Matched Maximum Bending Moment (k-ft)*	
		Weak Axis**	Strong Axis***
1/30/10	-0.7	56.7	10.7
7/7/10	95	-46.8	-14.2
1/24/11	-16.5	59.6	17.5
5/31/11	85.6	-26.5	-7.1
1/16/12	-6.7	53.1	15.7
6/20/12	78.8	-49.7	-12.5
1/16/13	3.3	60.1	17.6
7/7/13	85.2	-51.8	-13.0

* 1 kip-ft=1.36 kN-m
** M_{yy}=247.9 kip-ft, M_{py}=380.8 kip-ft (HP14x117) weak axis yield moment and plastic moment, respectively
*** M_{yy}=716.7 kip-ft, M_{py}=808.3 kip-ft (HP14x117) strong axis yield moment and plastic moment, respectively

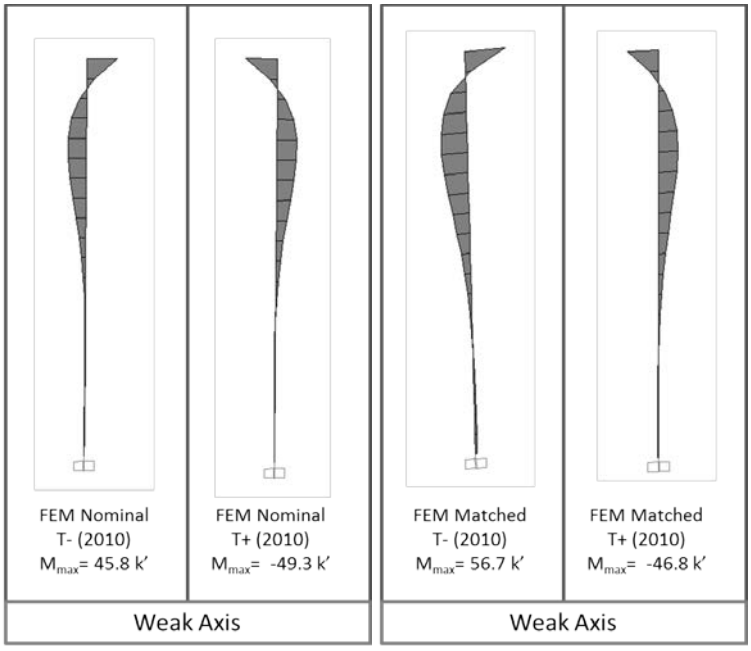

Figure 4-22 Weak Axis Bending Moment Diagrams for FEM Nominal (left) and FEM Matched (right)

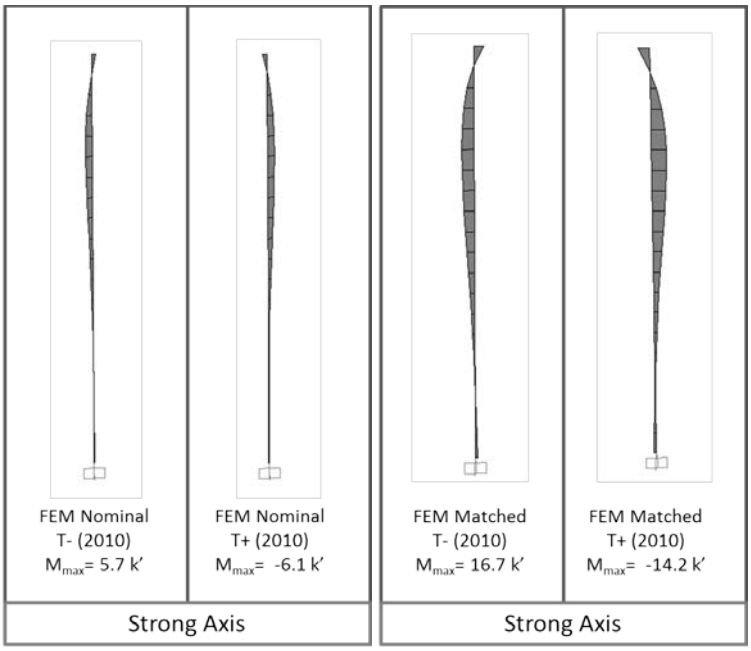

Figure 4-23 Strong Axis Bending Moment Diagrams for FEM Nominal (left) and FEM Matched (right)

5 Conclusions

The Vermont Agency of Transportation (VTrans) initiated a program of field instrumentation and analysis to evaluate the performance of three IABs beginning at bridge construction, and monitored over four years. The bridges are of increasing complexity, a straight girder non-skew bridge, a straight girder 15 degree skew bridge, and a curved girder two-span continuous structure with 11.25 degrees of curvature. The Part I Report covers construction, instrumentation, and live load testing. This Part II report focuses on the long term thermally induced response of the bridges over the four years of long term monitoring.

Overall, after four years of monitoring, all three bridges have performed well and no yielding of piles or girders has been observed. The approach slabs at all bridges are also in good condition with no observed settlement. Most behavior was comparable between the straight-girder non-skew Middlesex Bridge, the straight-girder 15° skewed East Montpelier Bridge, and the curved-girder 11.25 degrees curved Stockbridge Bridge. It was determined that two-dimensional analysis would be adequate for predicting net peak to peak longitudinal displacement at the top of the abutments for all bridges. The notable differences in response occurred in the East Montpelier Bridge where seasonal rotation of the bridge in plan view resulted in strong axis pile bending moments of comparable magnitude to those about the weak axis. There were also greater pressures behind the abutment at this skewed bridge and greater variability in pressure distribution. However, these pressures were still well below assumed full passive pressure values.

Differences in behavior were noted between the two abutments of each bridge, even in the symmetric and straight Middlesex Bridge. This is expected due to initial tolerances in construction, variation in materials and the practicality of backfilling one abutment at a time. Further variability was reported due to shifts in bridge movements and changes in effective soil properties in subsequent years. These differences in response between abutments and from year to year were generally more significant than the effects of the 15 degree skew and11.25 degree of curvature studied.

The Geofoam material provided behind the abutments at the curved Stockbridge Bridge proved effective at minimizing abutment pressures. This bridge also had the most consistent substructure displacement from year to year. Designers should consider these benefits of Geofoam and investigate the impact on design of abutments and piles. While the Geofoam would add some cost, it may result in a lower overall cost of the structure due to reduced thickness of abutment and/or less abutment reinforcement if designers account for the reduced backfill pressures. This project monitored the bridges for four years, so did not verify Geofoam performance over the bridge life-cycle. Designers should consider the consistency of performance and potential cost benefit of Geofoam.

Results presented in this report focus on girder stresses, abutment longitudinal and transverse displacements, abutment rotation, earth pressures behind abutments and wing walls, substructure displacement at maximum and minimum temperatures, and pile bending moments. Results from field data were compared with FEM results. A brief conclusion summarizing each of these measured responses will be covered in the following sections.

All results presented in this report are those induced by thermal effects only, they do not include effects from construction.

5.1 Girder Stresses

Thermally induced girder stresses were minimal. For all bridges, the bottom flange stresses were greater than top flange stresses due to the elastic neutral axis being located near the girder/slab interface. Temperature had minimal influence on top flange stresses indicating that girders act compositely for both positive and negative bending. Stresses were comparable between the three bridges; the 15° skew of the East Montpelier Bridge and the 11.25 degree curvature of the Stockbridge Bridge had negligible effect on girder stresses due to seasonal thermal fluctuations.

5.2 Abutment Displacement

Longitudinal displacements were comparable at all bridges. The maximum net (sum of both abutments) peak to peak displacement at the top of the abutments (from yearly minimum to maximum temperature) was 1.95 in (49.5 mm) at the curved Stockbridge Bridge, 1.45 in (36.8 mm) at the skewed East Montpelier Bridge, and 1.39 in (35.3 mm) at the Middlesex Bridge.

All bridges experienced some net shift toward their backfill over time, as well as changing soil properties that were not captured by the original FEM (based on field reporting of soil properties and measured thermal changes) used for each bridge. However, net peak to peak displacements at the top of the abutments were still a fairly good match to FEM and thermal expansion equation predictions for all three bridges.

Bottom of abutment displacements were significantly less than top of abutment displacements at all bridges due to abutment rotation. Overall, bottom of abutment longitudinal displacements after the first year of monitoring were not captured well by the FEM with original soil conditions as a result of changing soil properties over time. The equation of thermal expansion was not a good estimate either since this is based on unrestrained conditions and assumes pure translation of the abutment while field data shows there is a combination of abutment translation and rotation. Maximum net peak to peak bottom of abutment displacement was 0.60 in (15.2 mm) at the Middlesex Bridge, 0.49 in (12.4 mm) at the East Montpelier Bridge and 0.48 in (12.2 mm) at the Stockbridge Bridge.

Transverse displacements were small at the Middlesex Bridge and the Stockbridge Bridge though they did both display a slight transverse shift over time. At the East Montpelier Bridge, the bridge exhibited seasonal rotation in plan with the majority of the transverse displacement occurring at the acute corners of the bridge.

Overall, two-dimensional analysis would be adequate for predicting net longitudinal displacement at the top of the abutments. However, as the seasonal twisting of the skewed bridge is concentrated at the acute corners of the bridge this results in strong axis bending moments that would not be captured in a two-dimensional analysis and may need to be considered separately.

5.3 Abutment Rotation

Abutment rotations are important to consider in design, as they can reduce the deformation demands on the piles. Field data confirms that the abutment behavior is a combination of translation and rotation which results in significantly lower displacements at the bottom of the abutments.

Rotation results were similar between the three bridges. The maximum peak to peak abutment rotation was 0.17 degrees at the Middlesex Bridge, 0.18 degrees at the East Montpelier Bridge, and 0.21 degrees at the Stockbridge Bridge.

5.4 Earth Pressure

The Stockbridge Bridge had the lowest maximum pressure with a value of 2.1 psi (14.5 KPa) in the top row of pressure cells. The Middlesex Bridge had a maximum pressure of 5.5 psi (37.9 KPa) occurring in the middle row of pressure cells; pressures were consistent along the abutment and between the two abutments. The East Montpelier Bridge had the greatest maximum pressure of 15.3 psi (105.5 KPa) which occurred in the top row of pressure cells behind the obtuse corner of Abutment 1, pressures were minimal at all other locations across the abutment and at Abutment 2 showing the variability in pressure distribution.

The Stockbridge Bridge was the only bridge to have Geofoam installed behind the abutments prior to backfilling. Geofoam was not only effective at minimizing abutment pressures but also resulted in

the most consistent pressures year to year. The skewed East Montpelier Bridge is the only bridge that had significant variation in pressures at the same depth across the abutment, with highest pressure concentrated at the obtuse corner.

At all three bridges, pressures increased with increasing displacements but were lower when the same displacement was reached in subsequent seasons showing that soil ratcheting did not occur at any of the bridges.

5.5 Seasonal Substructure Displacement

All three bridges demonstrated a lag in the recovery of the pile from its expanded deflected shape. The maximum displacement occurred at the maximum temperature, however after this temperature occurred and the top of abutment contracts the pile holds its deflected shape. The Middlesex Bridge and East Montpelier Bridge had dense backfill in the original FEMs based on soil boring logs from the bridge sites. However, FEM results indicate that as the long term monitoring of both bridges began in winter months, after the first bridge contraction the backfill was significantly looser than originally assumed at both the straight and skewed bridges (which are also seen in the minimal earth pressures behind the abutments). The original Stockbridge Model neglected backfill soil since Geofoam was present and minimized backfill pressures.

Due to the complex, non-linear behavior of soil and the lag in recovery of the pile from its expanded deflected shape, FEMs using original soil conditions did not capture substructure displacement after the first year or even after the first bridge contraction. To compare FEM results to field data, the FEMs were calibrated to match the substructure deflected shape seen in the field. This was done by adjusting temperatures to match displacement at the top of the abutment, and then adjusting soil conditions.

The Stockbridge Bridge had the most consistent response year to year, and more elastic response under bridge contraction. However, in all three bridges FEM results indicate that soil properties changed over time and pile lag was noted. Under bridge expansion all three bridges exhibited looser soil around the piles that was originally reported per soil boring logs. For bridge contraction, soil conditions varied to match field data, which in part is due to the inability of a static FEM to capture the lag in pile response from its expanded deflected shape. A static thermal FEM with original soil conditions is incapable of capturing bridge response, especially in later years. This merits further study.

The FEM Matched modeling used in this report is site specific; it could not be done without field data and is not a modeling technique that would be used in design. This modeling method was used to compare the response of the bridge at displacements that were recorded in the field and were not captured by thermal analysis alone. The specific soil conditions and temperatures used to match field data differed from bridge to bridge. One consistent result was the softening of backfill over time at the two bridges (East Montpelier and Middlesex) where dense backfill was originally assumed. Again, these results were only possible because of the availability of field data to compare to FEM results. Further study is merited to predict the behavior of IABs, such as shifting of substructure and hysteretic soil response, resulting from cyclic thermal loading.

5.6 Pile Bending Moments

Bending moments presented in this report are those due to thermal effects only, and do not include those induced during construction. FEM results show that depending on soil conditions and temperature, the point of inflection of the pile may be very close to the gage location on the pile. As a result, bending moments calculated from field data are not always an accurate representation of the actual maximum bending moment. Therefore, maximum bending moments are reported from the FEM Matched model that matched substructure displacement in the field. FEM Matched results are difficult to predict, however maximum bending moments from FEM Matched are still relatively low

compared to yield moments. Further, design moment is independent of 3-dimensional FEM; design is often controlled by other effects such as scour.

Maximum weak axis pile bending moments based on FEM Matched results were similar between all three bridges with a maximum of 50.4 kip-ft (68.5 KN-m) at the Middlesex Bridge, 71.9 kip-ft (97.5 KN-m) at the East Montpelier Bridge, and 60.1 kip-ft (81.5 KN-m) at the Stockbridge Bridge. The yield moment about the weak axis is 144.2 kip-ft (196.1 KN-m) at the Middlesex and East Montpelier Bridge, and 247.9 kip-ft (337.1 KN-m) at the Stockbridge Bridge.

Maximum strong axis pile bending moments were minimal at the Middlesex Bridge and the Stockbridge Bridge. The Middlesex Bridge had a maximum of 15.4 kip-ft (20.9 KN-m) and the Stockbridge Bridge had a maximum of 17.6 kip-ft (23.9 KN-m) showing that the 11.25 degree curvature had negligible effect on strong axis bending moments and was comparable to the straight-girder non-skew Middlesex Bridge.

The East Montpelier Bridge pile strong axis bending moment maximum values were generally comparable to those about the weak axis. The maximum strong axis bending moment based on FEM Matched results was 46.7 kip-ft (63.3 KN-m). Even though there are significant moments that occur due to transverse movements at this 15 skewed bridge, the strong axis of the pile is oriented to resist this with a yield moment of 500.0 kip-ft (680.0 KN-m) therefore yielding is not expected, even under combined force conditions of axial load, strong and weak axis bending moments.

APPENDIX A GAGE LABELING

Gage labeling is not directly related to abutment numbers for a couple of logistical reasons. First, instrumentation planning took place prior to development of structural drawings for two bridges. Therefore, final labeling of Abutment 1 and Abutment 2 was not determined, nor were compass directions (North-South-East-West) known by the research team. Gage labels starting with "1" indicated the abutment nearest the datalogger, which was typically the more heavily instrumented abutment to minimize cable lengths. Second, during construction a few gages were interchanged due to contractor preference for multiplexer locations. This avoided the need for splicing of predetermined cable lengths for these gages. For these reasons labeling of gages are not always consistent with the directions and numbering indicated in the structural drawings. This section describes the final as-built locations of gages for each bridge. Gages are labeled according to directions and abutment numbering shown in Figure A-1, Figure A-2 and Figure A-3. Differences from structural drawing callouts are noted. Gage labels are described per structural drawing position in Appendix B, along with channel locations in each multiplexer and datalogger.

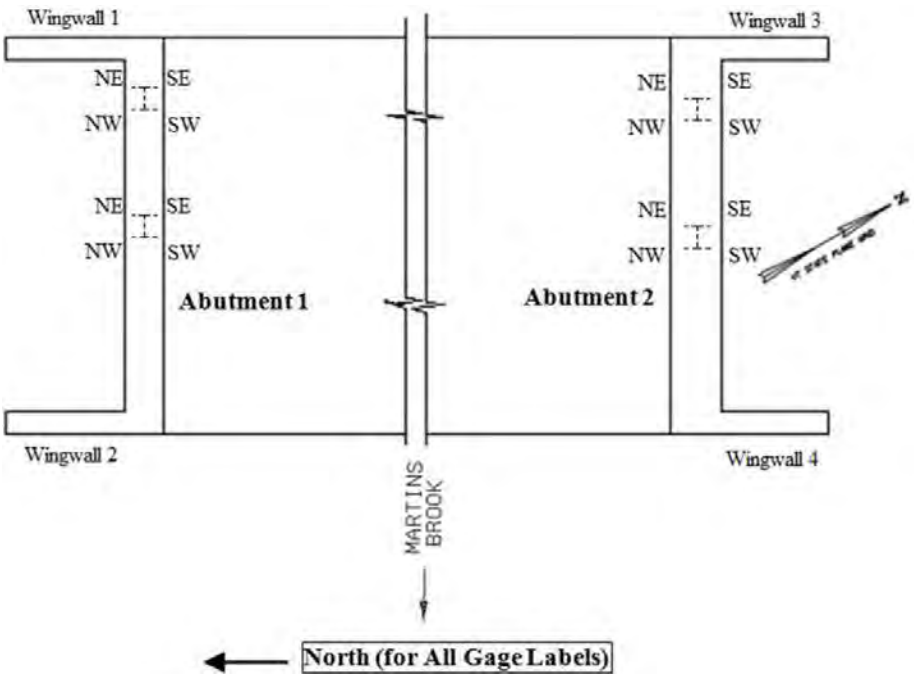

*Abutment numbering is consistent with structural drawings

Figure A-1 Gage Labeling for Middlesex Bridge

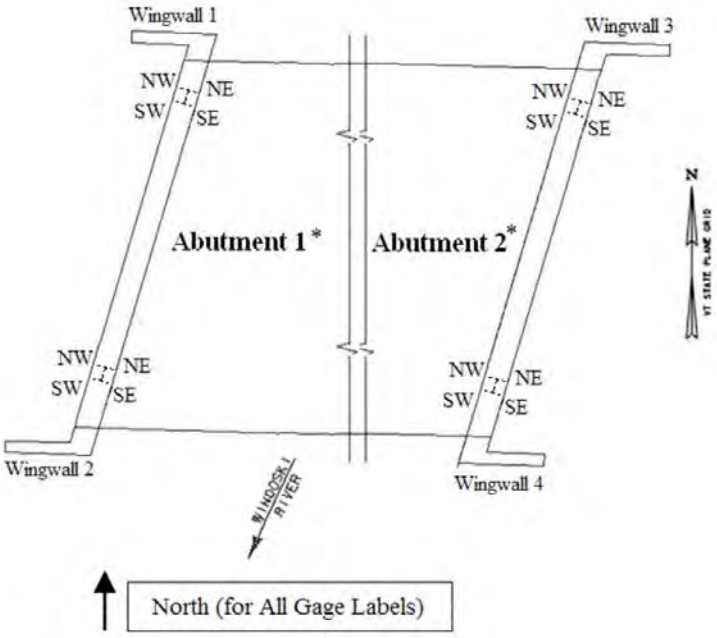

*Abutment numbering is consistent with structural drawings

Figure A-2 Gage Labeling for East Montpelier Bridge

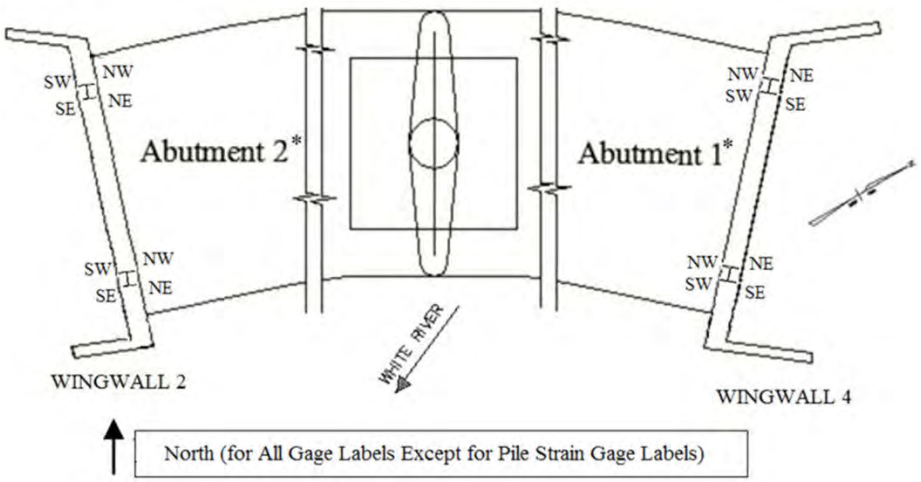

*Abutment numbering is NOT consistent with structural drawings

Figure A-3 Gage Labeling for Stockbridge Bridge

APPENDIX B INSTRUMENTATION CHANNEL LISTS & GAGE LOCATIONS

As noted in Appendix A, gage labeling is not always consistent with bridge orientation and structural drawing callouts. This section describes the final as-built locations of gages for each bridge. Gages are labeled according to directions and abutment numbering presented in Appendix A. Gage labels are fully described by data acquisition multiplexer channel number and descriptive location related to structural drawings.

Data acquisition system is composing of 16-channel multiplexers and 6-channel dataloggers. Each VW gage is connected to a single multiplexer channel while each MEMS gage (biaxial gage) is connected to two different channels.

a) The Middlesex Bridge

As-built gage information for the Middlesex Bridge is given in Table B-1 and Table B-2 for Abutment 1and Abutment 2 multiplexers, respectively. Figures showing gage locations without labeling are found in Section 3.2.

Table B-1: Abutment 1 Multiplexer Channel List and Gage Locations

Mux	Channel	Gage Label	Gage Type	Model	Location
1	1	CM-1ET	Disp. Transducer	4420	Abutment 1, Upstream, Transverse, 1.95 m (6.43 ft) below construction joint
1	2	CM-1E	Disp. Transducer	4420	Abutment 1, Upstream, Longitudinal, 1.95 (6.43 ft) below construction joint
1	3	P-1CT	Earth Pressure Cell	4815	Abutment 1, Center of Abutment, 1.9 m (6.2 ft) above the bottom of abutment,
1	4	P-1CM	Earth Pressure Cell	4815	Abutment 1, Center of Abutment, 1.1 m (3.6 ft) above the bottom of abutment,
1	5	P-1CB	Earth Pressure Cell	4815	Abutment 1, Center of Abutment, 0.3 m (1.0 ft) above the bottom of abutment,
1	6	P-1EM[1]	Earth Pressure Cell	4815	Abutment 1, Downstream, 1.1 m (3.6 ft) above the bottom of abutment, 0.8 m (2.6 ft) away from abutment-wingwall connection
1	7	P-1EB1*	Earth Pressure Cell	4815	Abutment 1, Downstream, 0.3 m (1.0 ft) above the bottom of abutment, 0.8 m (2.6 ft) away from abutment-wingwall connection
1	8	P-1WM1*	Earth Pressure Cell	4815	Abutment 1, Upstream, 1.1 m (3.6 ft) above the bottom of abutment, 0.8 m (2.6 ft) away from abutment-wingwall connection
1	9	P-1WB1*	Earth Pressure Cell	4815	Abutment 1, Upstream, 0.3 m (1.0 ft) above the bottom of abutment, 1.0 m (3.3 ft) away from abutment-wingwall connection
1	10	SGG-1E-TE	Girder Strain Gage	4050	Upstream Girder, Upstream-Top Flange, 4.5 m (14.75 ft) from the end of steel girder section at Abutment 1.
1	11	SGG-1E-BE	Girder Strain Gage	4050	Upstream Girder, Upstream-Bottom Flange, 4.5 m (14.75 ft) from the end of steel girder section at Abutment 1.
1	12	SGG-1E-TW	Girder Strain Gage	4050	Upstream Girder, Downstream-Top Flange, 4.5 m (14.75 ft) from the end of steel girder section at Abutment 1.
1	13	SGG-1E-BW	Girder Strain Gage	4050	Upstream Girder, Downstream-Bottom Flange, 4.5 m (14.75 ft) from the end of steel girder section at Abutment 1.
1	14	SGG-1M-TE	Girder Strain Gage	4050	Interior Girder, Upstream-Top Flange, 4.5 m (14.75 ft) from the end of steel girder section at Abutment 1.
1	15	SGG-1M-BE	Girder Strain Gage	4050	Interior Girder, Upstream-Bottom Flange, 4.5 m (14.75 ft) from the end of steel girder section at Abutment 1.
1	16	SGG-1W-TE	Girder Strain Gage	4050	Downstream Girder, Upstream-Top Flange, 4.5 m (14.75 ft) from the end of steel girder section at Abutment 1.

[1] Gage label is not consistent with other callouts. Gage locations switched to match cable length with actual multiplexer location.

Table B-1: Abutment 1 Multiplexer Channel List and Gage Locations (cont.)

Mux	Channel	Gage Label	Gage Type	Model	Location
2	1	SGG-1W-BE	Girder Strain Gage	4050	Downstream Girder, Upstream-Bottom Flange, 4.5 m (1.6 ft) from the end of steel girder section at Abutment 1.
2	2	SGG-0E-TE	Girder Strain Gage	4050	Upstream Girder, Upstream-Top Flange, 22.7 m (74.5 ft) from the end of steel girder section at Abutment 1.
2	3	SGG-0E-BE	Girder Strain Gage	4050	Upstream Girder, Upstream-Bottom Flange, 22.7 m (74.5 ft) from the end of steel girder section at Abutment 1.
2	4	SGG-0E-TW	Girder Strain Gage	4050	Upstream Girder, Downstream-Top Flange,22.7 m (74.5 ft) from the end of steel girder section at Abutment 1.
2	5	SGG-0E-BW	Girder Strain Gage	4050	Upstream Girder, Downstream-Bottom Flange, 22.7 m (74.5 ft) from the end of steel girder section at Abutment 1.
2	6	TM-1M	Tiltmeter (Uniaxial)	6300	Abutment 1, Center of Abutment, 0.5 m (1.6 ft) from the bottom of middle girder.
2	7	IN-1E-1	Inclinometer (Uniaxial)	6300	Abutment 1, Pile below Girder 2, Flange facing towards the centerline of the roadway, 0.0-0.6 m (0-2 ft) below the bottom of Abutment 1.
2	8	IN-1E-2	Inclinometer (Uniaxial)	6300	Abutment 1, Pile below Girder 2, Flange facing towards the centerline of the roadway, 0.6-1.5 m (2-5 ft) below the bottom of Abutment 1.
2	9	IN-1E-3	Inclinometer (Uniaxial)	6300	Abutment 1, Pile below Girder 2, Flange facing towards the centerline of the roadway, 1.5-2.7 m (5-9 ft) below the bottom of Abutment 1.
2	10	IN-1E-4	Inclinometer (Uniaxial)	6300	Abutment 1, Pile below Girder 2, Flange facing towards the centerline of the roadway, 2.7-4.0 m (9-13 ft) below the bottom of Abutment 1.
2	11	IN-1E-5	Inclinometer (Uniaxial)	6300	Abutment 1, Pile below Girder 2, Flange facing towards the centerline of the roadway, 4.0-5.2 m (13-17 ft) below the bottom of Abutment 1.
2	12	IN-1W-1	Inclinometer (Uniaxial)	6300	Abutment 1, Pile below Girder 4, Flange facing towards the centerline of the roadway, 0.0-0.6 m (0-2 ft) below the bottom of Abutment 1.
2	13	IN-1W-2	Inclinometer (Uniaxial)	6300	Abutment 1, Pile below Girder 4, Flange facing towards the centerline of the roadway, 0.6-1.5 m (2-5 ft) below the bottom of Abutment 1.
2	14	IN-1W-3	Inclinometer (Uniaxial)	6300	Abutment 1, Pile below Girder 4, Flange facing towards the centerline of the roadway, 1.5-2.7 m (5-9 ft) below the bottom of Abutment 1.
2	15	IN-1W-4	Inclinometer (Uniaxial)	6300	Abutment 1, Pile below Girder 4, Flange facing towards the centerline of the roadway, 2.7-4.0 m (9-13 ft) below the bottom of Abutment 1.
2	16	P-R	Reference Pressure Cell	4815	Under Approach Slab on Abutment 1 side, Facing towards the centerline of the roadway, 6 m (19.7 ft) away from the bridge end, 3.3 m (10.8 ft) away the centerline of roadway (towards upstream), 1.0 m (3.0 ft) below approach slab,

Table B-1: Abutment 1 Multiplexer Channel List and Gage Locations (cont.)

Mux	Channel	Gage Label	Gage Type	Model	Location
3	1	SG-1M-1NE	Pile Strain Gage	4000	Middle Pile (below Girder 3), 0.5 m (1.6 ft) from bottom of Abutment 1, 77 mm (3.0 in) from the edge of flange.
3	2	SG-1M-1SE	Pile Strain Gage	4000	Middle Pile (below Girder 3), 0.5 m (1.6 ft) from bottom of Abutment 1, 77 mm (3.0 in) from the edge of flange.
3	3	SG-1M-1SW	Pile Strain Gage	4000	Middle Pile (below Girder 3), 0.5 m (1.6 ft) from bottom of Abutment 1, 77 mm (3.0 in) from the edge of flange.
3	4	SG-1M-1NW	Pile Strain Gage	4000	Middle Pile (below Girder 3), 0.5 m (1.6 ft) from bottom of Abutment 1, 77 mm (3.0 in) from the edge of flange.
3	5	SG-1M-3NE	Pile Strain Gage	4000	Middle Pile (below Girder 3), 1.5 m (4.9 ft) from bottom of Abutment 1, 77 mm (3.0 in) from the edge of flange.
3	6	SG-1M-3SE	Pile Strain Gage	4000	Middle Pile (below Girder 3), 1.5 m (4.9 ft) from bottom of Abutment 1, 77 mm (3.0 in) from the edge of flange.
3	7	SG-1M-3SW	Pile Strain Gage	4000	Middle Pile (below Girder 3), 1.5 m (4.9 ft) from bottom of Abutment 1, 77 mm (3.0 in) from the edge of flange.
3	8	SG-1M-3NW	Pile Strain Gage	4000	Middle Pile (below Girder 3), 1.5 m (4.9 ft) from bottom of Abutment 1, 77 mm (3.0 in) from the edge of flange.
3	9	SG-1E-1NE	Pile Strain Gage	4000	Upstream Pile (below Girder 1), 0.5 m (1.6 ft) from bottom of Abutment 1, 77 mm (3.0 in) from the edge of flange.
3	10	SG-1E-1SE	Pile Strain Gage	4000	Upstream Pile (below Girder 1), 0.5 m (1.6 ft) from bottom of Abutment 1, 77 mm (3.0 in) from the edge of flange.
3	11	SG-1E-1SW	Pile Strain Gage	4000	Upstream Pile (below Girder 1), 0.5 m (1.6 ft) from bottom of Abutment 1, 77 mm (3.0 in) from the edge of flange.
3	12	SG-1E-1NW	Pile Strain Gage	4000	Upstream Pile (below Girder 1), 0.5 m (1.6 ft) from bottom of Abutment 1, 77 mm (3.0 in) from the edge of flange.
3	13	SG-1E-2NE	Pile Strain Gage	4000	Upstream Pile (below Girder 1), 1.0 m (3.3 ft) from bottom of Abutment 1, 77 mm (3.0 in) from the edge of flange.
3	14	SG-1E-2SE	Pile Strain Gage	4000	Upstream Pile (below Girder 1), 1.0 m (3.3 ft) from bottom of Abutment 1, 77 mm (3.0 in) from the edge of flange.
3	15	SG-1E-2SW	Pile Strain Gage	4000	Upstream Pile (below Girder 1), 1.0 m (3.3 ft) from bottom of Abutment 1, 77 mm (3.0 in) from the edge of flange.
3	16	SG-1E-2NW	Pile Strain Gage	4000	Upstream Pile (below Girder 1), 1.0 m (3.3 ft) from bottom of Abutment 1, 77 mm (3.0 in) from the edge of flange.

Table B-1: Abutment 1 Multiplexer Channel List and Gage Locations (cont.)

Mux	Channel	Gage Label	Gage Type	Model	Location
6	1	SG-1E-3NE	Pile Strain Gage	4000	Upstream Pile (below Girder 1), 1.5 m (4.9 ft) from bottom of Abutment 1, 77 mm (3.0 in) from the edge of flange.
6	2	SG-1E-3SE	Pile Strain Gage	4000	Upstream Pile (below Girder 1), 1.5 m (4.9 ft) from bottom of Abutment 1, 77 mm (3.0 in) from the edge of flange.
6	3	SG-1E-3SW	Pile Strain Gage	4000	Upstream Pile (below Girder 1), 1.5 m (4.9 ft) from bottom of Abutment 1, 77 mm (3.0 in) from the edge of flange.
6	4	SG-1E-3NW	Pile Strain Gage	4000	Upstream Pile (below Girder 1), 1.5 m (4.9 ft) from bottom of Abutment 1, 77 mm (3.0 in) from the edge of flange.

Table B-2: Abutment 2 Multiplexer Channel List and Gage Locations

Mux	Channel	Gage Label	Gage Type	Model	Location
4	1	CM-2ET	Displacement Transducer	4420	Abutment 2, Upstream, Transverse, 1.95 m (6.43 ft) below construction joint
4	2	CM-2E	Displacement Transducer	4420	Abutment 2, Upstream, Longitudinal, 1.95 (6.43 ft) below construction joint
4	3	P-2CT	Earth Pressure Cell	4815	Abutment 2, Center of Abutment, 1.9 m (6.2 ft) above the bottom of abutment, 0.8 m (2.6 ft) away from abutment-wingwall connection
4	4	P-2CB	Earth Pressure Cell	4815	Abutment 2, Center of Abutment, 0.3 m (1.0 ft) above the bottom of abutment, 0.8 m (2.6 ft) away from abutment-wingwall connection
4	5	P-2EB	Earth Pressure Cell	4815	Abutment 2, Upstream, 0.3 m (1.0 ft) above the bottom of abutment, 0.8 m (2.6 ft) away from abutment-wingwall connection
4	6	P-2WB	Earth Pressure Cell	4815	Abutment 2, Downstream, 0.3 m (1.0 ft) above the bottom of abutment, 0.8 m (2.6 ft) away from abutment-wingwall connection
4	7	PW-1E	Earth Pressure Cell	4815	Wingwall 3 (Abutment 2, Upstream), 1.2 m (3.9 ft) above the bottom of wingwall, 1 m (3 ft) away from abutment-wingwall connection
4	8	SGG-2E-TW	Girder Strain Gage	4050	Upstream Girder, Downstream-Top Flange, 4.5 m (14.75 ft) from the end of steel girder section at Abutment 2.
4	9	SGG-2E-BW	Girder Strain Gage	4050	Upstream Girder, Downstream-Top Flange, 4.5 m (14.75 ft) from the end of steel girder section at Abutment 2.
4	10	SGG-0M-TE	Girder Strain Gage	4050	Center Girder, Upstream-Top Flange 22.7 m (74.5 ft) from the end of steel girder section at Abutment 1.
4	11	SGG-0M-BE	Girder Strain Gage	4050	Center Girder, Upstream-Top Flange 22.7 m (74.5 ft) from the end of steel girder section at Abutment 1.
4	12	SGG-0W-TE	Girder Strain Gage	4050	Downstream Girder, Upstream-Top Flange, 22.7 m (74.5 ft) from the end of steel girder section at Abutment 1.
4	13	SGG-0W-BE	Girder Strain Gage	4050	Downstream Girder, Upstream-Bottom Flange, 22.7 m (74.5 ft) from the end of steel girder section at Abutment 1.
4	14	SG-2M-1NE	Pile Strain Gage	4000	Middle Pile (below Girder 3), 0.5 m (1.6 ft) from bottom of Abutment 2, 77 mm (3.0 in) from the edge of flange.
4	15	SG-2M-1SE	Pile Strain Gage	4000	Middle Pile (below Girder 3), 0.5 m (1.6 ft) from bottom of Abutment 2, 77 mm (3.0 in) from the edge of flange.

Table B-2: Abutment 2 Multiplexer Channel List and Gage Locations (cont.)

Mux	Channel	Gage Label	Gage Type	Model	Location
5	1	SG-2M-1SW	Pile Strain Gage	4000	Middle Pile (below Girder 3), 0.5 m (1.6 ft) from bottom of Abutment 2, 77 mm (3.0 in) from the edge of flange.
5	2	SG-2M-1NW	Pile Strain Gage	4000	Middle Pile (below Girder 3), 0.5 m (1.6 ft) from bottom of Abutment 2, 77 mm (3.0 in) from the edge of flange.
5	3	SG-2M-3NE	Pile Strain Gage	4000	Middle Pile (below Girder 3), 1.5 m (4.9 ft) from bottom of Abutment 2, 77 mm (3.0 in) from the edge of flange.
5	4	SG-2M-3SE	Pile Strain Gage	4000	Middle Pile (below Girder 3), 1.5 m (4.9 ft) from bottom of Abutment 2, 77 mm (3.0 in) from the edge of flange.
5	5	SG-2M-3SW	Pile Strain Gage	4000	Middle Pile (below Girder 3), 1.5 m (4.9 ft) from bottom of Abutment 2, 77 mm (3.0 in) from the edge of flange.
5	6	SG-2E-1NE	Pile Strain Gage	4000	Upstream Pile (below Girder 1), 0.5 m (1.6 ft) from bottom of Abutment 2, 77 mm (3.0 in) from the edge of flange.
5	7	SG-2E-1SE	Pile Strain Gage	4000	Upstream Pile (below Girder 1), 0.5 m (1.6 ft) from bottom of Abutment 2, 77 mm (3.0 in) from the edge of flange.
5	8	SG-2E-1SW	Pile Strain Gage	4000	Upstream Pile (below Girder 1), 0.5 m (1.6 ft) from bottom of Abutment 2, 77 mm (3.0 in) from the edge of flange.
5	9	SG-2E-1NW	Pile Strain Gage	4000	Upstream Pile (below Girder 1), 0.5 m (1.6 ft) from bottom of Abutment 2, 77 mm (3.0 in) from the edge of flange.
5	10	SG-2E-2NE	Pile Strain Gage	4000	Upstream Pile (below Girder 1), 1.0 m (3.3 ft) from bottom of Abutment 2, 77 mm (3.0 in) from the edge of flange.
5	11	SG-2E-2SE	Pile Strain Gage	4000	Upstream Pile (below Girder 1), 1.0 m (3.3 ft) from bottom of Abutment 2, 77 mm (3.0 in) from the edge of flange.
5	12	SG-2E-2SW	Pile Strain Gage	4000	Upstream Pile (below Girder 1), 1.0 m (3.3 ft) from bottom of Abutment 2, 77 mm (3.0 in) from the edge of flange.
5	13	SG-2E-3NE	Pile Strain Gage	4000	Upstream Pile (below Girder 1), 1.5 m (4.9 ft) from bottom of Abutment 2, 77 mm (3.0 in) from the edge of flange.
5	14	SG-2E-3SE	Pile Strain Gage	4000	Upstream Pile (below Girder 1), 1.5 m (4.9 ft) from bottom of Abutment 2, 77 mm (3.0 in) from the edge of flange.
5	15	SG-2E-3SW	Pile Strain Gage	4000	Upstream Pile (below Girder 1), 1.5 m (4.9 ft) from bottom of Abutment 2, 77 mm (3.0 in) from the edge of flange.
5	16	TM-2M	Tiltmeter (Uniaxial)	6350	Abutment 2, Center of Abutment, 0.5 m (1.6 ft) from the bottom of middle girder.

b) The East Montpelier Bridge

As-built gage information for the East Montpelier Bridge is given in Table B-3 and Table B-4 for Abutment 1 and Abutment 2 multiplexers, respectively. Figures showing gage locations without labeling are found in Section 3.3.

Table B-3: Abutment 1 Multiplexer Channel List and Gage Locations

Mux	Channel	Gage Label	Gage Type	Model	Location
1	1	CM-1NT	Displacement Transducer	4420	Abutment 1, Upstream, Transverse, 1.7 m (5.6 ft) below construction joint.
1	2	CM-1N	Displacement Transducer	4420	Abutment 1, Upstream, Longitudinal, 1.7 m (5.6 ft) below construction joint.
1	3	CM-1S	Displacement Transducer	4420	Abutment 1, Downstream, Longitudinal, 1.7 m (5.6 ft) below construction joint.
1	4	P-1NT	Earth Pressure Cell	4815	Abutment 1, Upstream, 1.6 m (5.2 ft) above the bottom of abutment, 2.12 m (6.96 ft) away from abutment-wingwall connection.
1	5	P-1NM	Earth Pressure Cell	4815	Abutment 1, Upstream, 1.0 m (3.3 ft) above the bottom of abutment, 2.12 m (6.96 ft) away from abutment-wingwall connection.
1	6	P-1NB	Earth Pressure Cell	4815	Abutment 1, Upstream, 0.4 m (1.3 ft) above the bottom of abutment, 2.12 m (6.96 ft) away from abutment-wingwall connection.
1	7	P-1CM	Earth Pressure Cell	4815	Abutment 1, Center of Abutment, 1.0 m (3.3 ft) above the bottom of abutment.
1	8	P-1CB	Earth Pressure Cell	4815	Abutment 1, Center of Abutment, 0.4 m (1.3 ft) above the bottom of abutment.
1	9	P-1ST	Earth Pressure Cell	4815	Abutment 1, Downstream, 1.6 m (5.2 ft) above the bottom of abutment, 2.12 m (6.96 ft) away from abutment-wingwall connection.
1	10	P-1SM	Earth Pressure Cell	4815	Abutment 1, Downstream, 1.0 m (3.3 ft) above the bottom of abutment, 2.12 m (6.96 ft) away from abutment-wingwall connection
1	11	P-1SB	Earth Pressure Cell	4815	Abutment 1, Downstream, 0.4 m (1.3 ft) above the bottom of abutment, 2.12 m (6.96 ft) away from abutment-wingwall connection.
1	12	PW-1N	Earth Pressure Cell	4815	Wingwall 1 (Abutment 1, Upstream), 1.2 m (3.9 ft) above the bottom of abutment, 1 m (3 ft) away from abutment-wingwall connection.
1	13	TM-1M	Tiltmeter (Uniaxial)	6350	Abutment 1, Center of Abutment, 0.5 m (1.6 ft) from the bottom of middle girder.
1	14	P-R	Earth Pressure Cell	4815	Under Approach Slab on Abutment 1 side, Facing towards the abutment.

Table B-3: Abutment 1 Multiplexer Channel List and Gage Locations (cont.)

Mux	Channel	Gage Label	Gage Type	Model	Location
2	1	SGG-1N-TE2	Girder Strain Gage	4050	Upstream Girder, Downstream-Top Flange, 4.35 m (14.30 ft) from the end of steel girder section at Abutment 1.
2	2	SGG-1N-BE*	Girder Strain Gage	4050	Upstream Girder, Downstream-Bottom Flange, 4.35 m (14.30 ft) from the end of steel girder section at Abutment 1.
2	3	SGG-1N-TW*	Girder Strain Gage	4050	Upstream Girder, Upstream-Top Flange, 4.35 m (14.30 ft) from the end of steel girder section at Abutment 1.
2	4	SGG-1N-BW*	Girder Strain Gage	4050	Upstream Girder, Upstream-Bottom Flange, 4.35 m (14.30 ft) from the end of steel girder section at Abutment 1.
2	5	SGG-1S-TE*	Girder Strain Gage	4050	Downstream Girder, Downstream-Top Flange, 4.35 m (14.30 ft) from the end of steel girder section at Abutment 1.
2	6	SGG-1S-BE*	Girder Strain Gage	4050	Downstream Girder, Downstream-Bottom Flange, 4.35 m (14.30 ft) from the end of steel girder section at Abutment 1.
2	7	SGG-1S-TW*	Girder Strain Gage	4050	Downstream Girder, Upstream-Top Flange, 4.35 m (14.30 ft) from the end of steel girder section at Abutment 1.
2	8	SGG-1S-BW*	Girder Strain Gage	4050	Downstream Girder, Upstream-Bottom Flange, 4.35 m (14.30 ft) from the end of steel girder section at Abutment 1.
2	9	SG-1N-1NE	Pile Strain Gage	4000	Upstream Pile, 0.5 m (1.6 ft) from bottom of Abutment 1 51 mm (2.0 in) from the edge of flange.
2	10	SG-1N-1NW	Pile Strain Gage	4000	Upstream Pile, 0.5 m (1.6 ft) from bottom of Abutment 1 51 mm (2.0 in) from the edge of flange.
2	11	SG-1N-1SE	Pile Strain Gage	4000	Upstream Pile, 0.5 m (1.6 ft) from bottom of Abutment 1 51 mm (2.0 in) from the edge of flange.
2	12	SG-1N-1SW	Pile Strain Gage	4000	Upstream Pile, 0.5 m (1.6 ft) from bottom of Abutment 1 51 mm (2.0 in) from the edge of flange.
2	13	SG-1N-2NE	Pile Strain Gage	4000	Upstream Pile, 1.0 m (3.3 ft) from bottom of Abutment 1 51 mm (2.0 in) from the edge of flange.
2	14	SG-1N-2NW	Pile Strain Gage	4000	Upstream Pile, 1.0 m (3.3 ft) from bottom of Abutment 1 51 mm (2.0 in) from the edge of flange.
2	15	SG-1N-2SE	Pile Strain Gage	4000	Upstream Pile, 1.0 m (3.3 ft) from bottom of Abutment 1 51 mm (2.0 in) from the edge of flange.
2	16	SG-1N-2SW	Pile Strain Gage	4000	Upstream Pile, 1.0 m (3.3 ft) from bottom of Abutment 1 51 mm (2.0 in) from the edge of flange.

[2] W and E in gage labels correspond to upstream (north) and downstream (south) flanges of the girders, respectively.

Table B-3: Abutment 1 Multiplexer Channel List and Gage Locations (cont.)

Mux	Channel	Gage Label	Gage Type	Model	Location
3	1	SG-1N-3NE	Pile Strain Gage	4000	Upstream Pile, 1.5 m (4.9 ft) from bottom of Abutment 1 51 mm (2.0 in) from the edge of flange.
3	2	SG-1N-3NW	Pile Strain Gage	4000	Upstream Pile, 1.5 m (4.9 ft) from bottom of Abutment 1 51 mm (2.0 in) from the edge of flange.
3	3	SG-1N-3SE	Pile Strain Gage	4000	Upstream Pile, 1.5 m (4.9 ft) from bottom of Abutment 1 51 mm (2.0 in) from the edge of flange.
3	4	SG-1N-3SW	Pile Strain Gage	4000	Upstream Pile, 1.5 m (4.9 ft) from bottom of Abutment 1 51 mm (2.0 in) from the edge of flange.
3	5	SG-1S-1NE	Pile Strain Gage	4000	Downstream Pile, 0.5 m (1.6 ft) from bottom of Abutment 1 51 mm (2.0 in) from the edge of flange.
3	6	SG-1S-1NW	Pile Strain Gage	4000	Downstream Pile, 0.5 m (1.6 ft) from bottom of Abutment 1 51 mm (2.0 in) from the edge of flange.
3	7	SG-1S-1SE	Pile Strain Gage	4000	Downstream Pile, 0.5 m (1.6 ft) from bottom of Abutment 1 51 mm (2.0 in) from the edge of flange.
3	8	SG-1S-1SW	Pile Strain Gage	4000	Downstream Pile, 0.5 m (1.6 ft) from bottom of Abutment 1 51 mm (2.0 in) from the edge of flange.
3	9	SG-1S-2NE	Pile Strain Gage	4000	Downstream Pile, 1.0 m (3.3 ft) from bottom of Abutment 1 51 mm (2.0 in) from the edge of flange.
3	10	SG-1S-2NW	Pile Strain Gage	4000	Downstream Pile, 1.0 m (3.3 ft) from bottom of Abutment 1 51 mm (2.0 in) from the edge of flange.
3	11	SG-1S-2SE	Pile Strain Gage	4000	Downstream Pile, 1.0 m (3.3 ft) from bottom of Abutment 1 51 mm (2.0 in) from the edge of flange.
3	12	SG-1S-2SW	Pile Strain Gage	4000	Downstream Pile, 1.0 m (3.3 ft) from bottom of Abutment 1 51 mm (2.0 in) from the edge of flange.
3	13	SG-1S-3NE	Pile Strain Gage	4000	Downstream Pile, 1.5 m (4.9 ft) from bottom of Abutment 1 51 mm (2.0 in) from the edge of flange.
3	14	SG-1S-3NW	Pile Strain Gage	4000	Downstream Pile, 1.5 m (4.9 ft) from bottom of Abutment 1 51 mm (2.0 in) from the edge of flange.
3	15	SG-1S-3SE	Pile Strain Gage	4000	Downstream Pile, 1.5 m (4.9 ft) from bottom of Abutment 1 51 mm (2.0 in) from the edge of flange.
3	16	SG-1S-3SW	Pile Strain Gage	4000	Downstream Pile, 1.5 m (4.9 ft) from bottom of Abutment 1 51 mm (2.0 in) from the edge of flange.

Table B-3: Abutment 1 Multiplexer Channel List and Gage Locations (cont.)

Mux	Channel	Gage Label	Gage Type	Model	Location
6	1	IN-1N-1	Inclinometer (Biaxial) - Ch-1 (Longitudinal)	6150	Abutment 1, Upstream Pile, Flange facing the fascia of the bridge, 0.0-0.6 m (0-2 ft) below the bottom of Abutment 1.
6	2	IN-1N-1	Inclinometer (Biaxial) - Ch-2 (Transverse)	6150	Abutment 1, Upstream Pile, Flange facing the fascia of the bridge, 0.0-0.6 m (0-2 ft) below the bottom of Abutment 1.
6	3	IN-1N-2	Inclinometer (Biaxial) - Ch-1 (Longitudinal)	6150	Abutment 1, Upstream Pile, Flange facing the fascia of the bridge, 0.6-1.5 m (2-5 ft) below the bottom of Abutment 1.
6	4	IN-1N-2	Inclinometer (Biaxial) - Ch-2 (Transverse)	6150	Abutment 1, Upstream Pile, Flange facing the fascia of the bridge, 0.6-1.5 m (2-5 ft) below the bottom of Abutment 1.
6	5	IN-1N-3	Inclinometer (Biaxial) - Ch-1 (Longitudinal)	6150	Abutment 1, Upstream Pile, Flange facing the fascia of the bridge, 1.5-2.7 m (5-9 ft) below the bottom of Abutment 1.
6	6	IN-1N-3	Inclinometer (Biaxial) - Ch-2 (Transverse)	6150	Abutment 1, Upstream Pile, Flange facing the fascia of the bridge, 1.5-2.7 m (5-9 ft) below the bottom of Abutment 1.
6	7	IN-1N-4	Inclinometer (Biaxial) - Ch-1 (Longitudinal)	6150	Abutment 1, Upstream Pile, Flange facing the fascia of the bridge, 2.7-4.0 m (9-13 ft) below the bottom of Abutment 1.
6	8	IN-1N-4	Inclinometer (Biaxial) - Ch-2 (Transverse)	6150	Abutment 1, Upstream Pile, Flange facing the fascia of the bridge, 2.7-4.0 m (9-13 ft) below the bottom of Abutment 1.
6	9	IN-1S-1	Inclinometer (Biaxial) - Ch-1 (Longitudinal)	6150	Abutment 1, Downstream Pile, Flange facing the fascia of the bridge, 0.0-0.6 m (0-2 ft) below the bottom of Abutment 1.
6	10	IN-1S-1	Inclinometer (Biaxial) - Ch-2 (Transverse)	6150	Abutment 1, Downstream Pile, Flange facing the fascia of the bridge, 0.0-0.6 m (0-2 ft) below the bottom of Abutment 1.
6	11	IN-1S-2	Inclinometer (Biaxial) - Ch-1 (Longitudinal)	6150	Abutment 1, Downstream Pile, Flange facing the fascia of the bridge, 0.6-1.5 m (2-5 ft) below the bottom of Abutment 1.
6	12	IN-1S-2	Inclinometer (Biaxial) - Ch-2 (Transverse)	6150	Abutment 1, Downstream Pile, Flange facing the fascia of the bridge, 0.6-1.5 m (2-5 ft) below the bottom of Abutment 1.
6	13	IN-1S-3	Inclinometer (Biaxial) - Ch-1 (Longitudinal)	6150	Abutment 1, Downstream Pile, Flange facing the fascia of the bridge, 1.5-2.7 m (5-9 ft) below the bottom of Abutment 1.
6	14	IN-1S-3	Inclinometer (Biaxial) - Ch-2 (Transverse)	6150	Abutment 1, Downstream Pile, Flange facing the fascia of the bridge, 1.5-2.7 m (5-9 ft) below the bottom of Abutment 1.
6	15	IN-1S-4	Inclinometer (Biaxial) - Ch-1 (Longitudinal)	6150	Abutment 1, Downstream Pile, Flange facing the fascia of the bridge, 2.7-4.0 m (9-13 ft) below the bottom of Abutment 1.

6	16	IN-1S-4	Inclinometer (Biaxial) - Ch-2 (Transverse)	6150	Abutment 1, Downstream Pile, Flange facing the fascia of the bridge, 2.7-4.0 m (9-13 ft) below the bottom of Abutment 1.

Table B-4: Abutment 2 Multiplexer Channel List and Gage Locations

Mux	Channel	Gage Label	Gage Type	Model	Location
4	1	CM-2NT	Displacement Transducer	4420	Abutment 2, Upstream, Transverse, 1.58 m (5.18 ft) below construction joint
4	2	CM-2N	Displacement Transducer	4420	Abutment 2, Upstream, Longitudinal1.58 m (5.18 ft) below construction joint
4	3	P-2NT	Earth Pressure Cell	4815	Abutment 2, Upstream, 1.6 m (5.2 ft) above the bottom of abutment, 2.12 m (6.96 ft) away from abutment-wingwall connection.
4	4	P-2NB	Earth Pressure Cell	4815	Abutment 1, Upstream, 0.4 m (1.3 ft) above the bottom of abutment, 2.12 m (6.96 ft) away from abutment-wingwall connection.
4	5	P-2ST	Earth Pressure Cell	4815	Abutment 2, Downstream, 1.6 m (5.2 ft) above the bottom of abutment,2.12 m (6.96 ft) away from abutment-wingwall connection.
4	6	P-2SB	Earth Pressure Cell	4815	Abutment 1, Downstream, 0.4 m (1.3 ft) above the bottom of abutment, 2.12 m (6.96 ft) away from abutment-wingwall connection.
4	7	SGG-2N-TW	Girder Strain Gage	4050	Upstream Girder, Upstream-Top Flange, 4.35 m (14.30 ft) from the end of steel girder section at Abutment 2.
4	8	SGG-2N-BW	Girder Strain Gage	4050	Upstream Girder, Upstream-Bottom Flange, 4.35 m (14.30 ft) from the end of steel girder section at Abutment 2.
4	9	SGG-2S-TW	Girder Strain Gage	4050	Downstream Girder, Downstream-Top Flange, 4.35 m (14.30 ft) from the end of steel girder section at Abutment 2.
4	10	SGG-2S-BW	Girder Strain Gage	4050	Downstream Girder, Downstream-Bottom Flange, 4.35 m (14.30 ft) from the end of steel girder section at Abutment 1.
4	11	TM-2M	Tiltmeter (Uniaxial)	6350	Abutment 2, Center of Abutment, 0.5 m (1.6 ft) from the bottom of middle girder.

Table B-4: Abutment 2 Multiplexer Channel List and Gage Locations (cont.)

Mux	Channel	Gage Label	Gage Type	Model	Location
5	1	SGG-0N-TE	Girder Strain Gage	4050	Upstream Girder, Downstream-Top Flange, 18.5 m (61 ft) from the end of steel girder section at Abutment 1.
5	2	SGG-0N-BE	Girder Strain Gage	4050	Upstream Girder, Downstream-Bottom Flange, 18.5 m (61 ft) from the end of steel girder section at Abutment 1.
5	3	SGG-0N-TW	Girder Strain Gage	4050	Upstream Girder, Upstream-Top Flange, 18.5 m (61 ft) from the end of steel girder section at Abutment 1.
5	4	SGG-0N-BW	Girder Strain Gage	4050	Upstream Girder, Upstream-Bottom Flange, 18.5 m (61 ft) from the end of steel girder section at Abutment 1.
5	5	SGG-0S-TE	Girder Strain Gage	4050	Downstream Girder, Downstream-Top Flange, 18.5 m (61 ft) from the end of steel girder section at Abutment 1.
5	6	SGG-0S-BE	Girder Strain Gage	4050	Downstream Girder, Downstream-Bottom Flange, 18.5 m (61 ft) from the end of steel girder section at Abutment 1.
5	7	SGG-0S-TW	Girder Strain Gage	4050	Downstream Girder, Upstream-Top Flange, 18.5 m (61 ft) from the end of steel girder section at Abutment 1.
5	8	SGG-0S-BW	Girder Strain Gage	4050	Downstream Girder, Upstream-Bottom Flange, 18.5 m (61 ft) from the end of steel girder section at Abutment 1.
5	9	SG-2N-1NE	Pile Strain Gage	4000	Upstream Pile, 0.5 m (1.6 ft) from bottom of Abutment 2.51 mm (2.0 in) from the edge of flange.
5	10	SG-2N-1NW	Pile Strain Gage	4000	Upstream Pile, 0.5 m (1.6 ft) from bottom of Abutment 2. 51 mm (2.0 in) from the edge of flange.
5	11	SG-2N-1SE	Pile Strain Gage	4000	Upstream Pile, 0.5 m (1.6 ft) from bottom of Abutment 2. 51 mm (2.0 in) from the edge of flange.
5	12	SG-2N-1SW	Pile Strain Gage	4000	Upstream Pile, 0.5 m (1.6 ft) from bottom of Abutment 2. 51 mm (2.0 in) from the edge of flange.
5	13	SG-2N-3NE	Pile Strain Gage	4000	Upstream Pile, 1.5 m (4.9 ft) from bottom of Abutment 2. 51 mm (2.0 in) from the edge of flange.
5	14	SG-2N-3NW	Pile Strain Gage	4000	Upstream Pile, 1.5 m (4.9 ft) from bottom of Abutment 2. 51 mm (2.0 in) from the edge of flange.
5	15	SG-2N-3SE	Pile Strain Gage	4000	Upstream Pile, 1.5 m (4.9 ft) from bottom of Abutment 2. 51 mm (2.0 in) from the edge of flange.
5	16	SG-2N-3SW	Pile Strain Gage	4000	Upstream Pile, 1.5 m (4.9 ft) from bottom of Abutment 2. 51 mm (2.0 in) from the edge of flange.

Table B-4: Abutment 2 Multiplexer Channel List and Gage Locations (cont.)

Mux	Channel	Gage Label	Gage Type	Model	Location
7	1	1N-1[3]	Inclinometer (Biaxial) - Ch-1 (Longitudinal)	6150	Abutment 2, Upstream Pile, Flange facing the centerline of the roadway, 0.0-0.6 m (0-2 ft) below the bottom of Abutment 2.
7	2	1N-1*	Inclinometer (Biaxial) - Ch-2 (Transverse)	6150	Abutment 2, Upstream Pile, Flange facing the centerline of the roadway, 0.0-0.6 m (0-2 ft) below the bottom of Abutment 2.
7	3	1N-2*	Inclinometer (Biaxial) - Ch-1 (Longitudinal)	6150	Abutment 2, Upstream Pile, Flange facing the centerline of the roadway, 0.6-1.5 m (2-5 ft) below the bottom of Abutment 2.
7	4	1N-2*	Inclinometer (Biaxial) - Ch-2 (Transverse)	6150	Abutment 2, Upstream Pile, Flange facing the centerline of the roadway, 0.6-1.5 m (2-5 ft) below the bottom of Abutment 2.
7	5	1N-3*	Inclinometer (Biaxial) - Ch-1 (Longitudinal)	6150	Abutment 2, Upstream Pile, Flange facing the centerline of the roadway, 1.5-2.7 m (5-9 ft) below the bottom of Abutment 2.
7	6	1N-3*	Inclinometer (Biaxial) - Ch-2 (Transverse)	6150	Abutment 2, Upstream Pile, Flange facing the centerline of the roadway, 1.5-2.7 m (5-9 ft) below the bottom of Abutment 2.
7	7	1N-4*	Inclinometer (Biaxial) - Ch-1 (Longitudinal)	6150	Abutment 2, Upstream Pile, Flange facing the centerline of the roadway, 2.7-4.0 m (9-13 ft) below the bottom of Abutment 2.
7	8	1N-4*	Inclinometer (Biaxial) - Ch-2 (Transverse)	6150	Abutment 2, Upstream Pile, Flange facing the centerline of the roadway, 2.7-4.0 m (9-13 ft) below the bottom of Abutment 2.
7	9	1S-1*	Inclinometer (Biaxial) - Ch-1 (Longitudinal)	6150	Abutment 2, Downstream Pile, Flange facing the centerline of the roadway, 0.0-0.6 m (0-2 ft) below the bottom of Abutment 2.
7	10	1S-1*	Inclinometer (Biaxial) - Ch-2 (Transverse)	6150	Abutment 2, Downstream Pile, Flange facing the centerline of the roadway, 0.0-0.6 m (0-2 ft) below the bottom of Abutment 2.
7	11	1S-2*	Inclinometer (Biaxial) - Ch-1 (Longitudinal)	6150	Abutment 2, Downstream Pile, Flange facing the centerline of the roadway, 0.6-1.5 m (2-5 ft) below the bottom of Abutment 2.
7	12	1S-2*	Inclinometer (Biaxial) - Ch-2 (Transverse)	6150	Abutment 2, Downstream Pile, Flange facing the centerline of the roadway, 0.6-1.5 m (2-5 ft) below the bottom of Abutment 2.
7	13	1S-3*	Inclinometer (Biaxial) - Ch-1 (Longitudinal)	6150	Abutment 2, Downstream Pile, Flange facing the centerline of the roadway, 1.5-2.7 m (5-9 ft) below the bottom of Abutment 2.

[3] Originally intended for use at Stockbridge. Abutment numbers on gage labels don't correspond to East Montpelier callout.

7	14	1S-3*	Inclinometer (Biaxial) - Ch-2 (Transverse)	6150	Abutment 2, Downstream Pile, Flange facing the centerline of the roadway, 1.5-2.7 m (5-9 ft) below the bottom of Abutment 2.
7	15	1S-4*	Inclinometer (Biaxial) - Ch-1 (Longitudinal)	6150	Abutment 2, Downstream Pile, Flange facing the centerline of the roadway, 2.7-3.7 m (9-12 ft) below the bottom of Abutment 2.
7	16	1S-4*	Inclinometer (Biaxial) - Ch-2 (Transverse)	6150	Abutment 2, Downstream Pile, Flange facing the centerline of the roadway, 2.7-3.7 m (9-12 ft) below the bottom of Abutment 2.

c) The Stockbridge Bridge

As-built gage information for the Stockbridge Bridge is given in Table B-5 and Table B-6 for Abutment 1 and Abutment 2 (as determined by structural drawings) multiplexers, respectively.

Table B-5: Abutment 1 (per Structural Drawings) Multiplexer Channel Allocation and Gage Locations

Mux	Channel	Gage Label	Gage Type	Model	Location
6	1	CM-2NT	Displacement Transducer	4420-50mm	Abutment 1, Upstream, Transverse, 1.28 m (4.18 ft) below construction joint
6	2	CM-2N	Displacement Transducer	4420-100mm	Abutment 1, Upstream, Longitudinal, 1.28 m (4.18 ft) below construction joint
6	3	CM-2S	Displacement Transducer	4420-100mm	Abutment 1, Downstream, Longitudinal, 3.55 m (11.65 ft) below construction joint
6	4	P-2NT	Earth Pressure Cell	4810	Abutment 1, Upstream, 3.6 m (12.0 ft) above the bottom of abutment,1 m (3 ft) away from abutment-wingwall connection
6	5	P-2NM	Earth Pressure Cell	4810	Abutment 1, Upstream, 2.1 m (7.0 ft) above the bottom of abutment,1 m (3 ft) away from abutment-wingwall connection
6	6	P-2NB	Earth Pressure Cell	4810	Abutment 1, Upstream, 0.6 m (2.0 ft) above the bottom of abutment,1 m (3 ft) away from abutment-wingwall connection
6	7	P-2CT	Earth Pressure Cell	4810	Abutment 1, Center of Abutment, 3.6 m (12.0 ft) above the bottom of abutment,
6	8	P-2CB	Earth Pressure Cell	4810	Abutment 1, Center of Abutment, 0.6 m (2.0 ft) above the bottom of abutment,
6	9	P-2ST	Earth Pressure Cell	4810	Abutment 1, Downstream, 3.6 m (12.0 ft) above the bottom of abutment,1 m (3 ft) away from abutment-wingwall connection
6	10	P-2SM	Earth Pressure Cell	4810	Abutment 1, Downstream, 2.1 m (7.0 ft) above the bottom of abutment,1 m (3 ft) away from abutment-wingwall connection
6	11	P-2SB	Earth Pressure Cell	4810	Abutment 1, Downstream, 0.6 m (2.0 ft) above the bottom of abutment,1 m (3 ft) away from abutment-wingwall connection
6	12	PW-2N	Earth Pressure Cell	4815	Wingwall 1, 1.2 m (4.0 ft) above the bottom of wingwall,1 m (3 ft) away from abutment-wingwall connection
6	13	PW-2S	Earth Pressure Cell	4815	Wingwall 2, 1.2 m (4.0 ft) above the bottom of wingwall,1 m (3 ft) away from abutment-wingwall connection
6	14	P-R	Earth Pressure Cell	4810	Under Approach Slab on Abutment 1 Side,1.5 m (4.9 ft) away from the bridge end, At the centerline of roadway, 1.0 m (3.0 ft) below approach slab

Table B-5: Abutment 1 (per Structural Drawings) Multiplexer Channel Allocation and Gage Locations (cont.)

Mux	Channel	Gage Label	Gage Type	Model	Location
7	1	SGG-2N-TN	Girder Strain Gage	4050	Upstream Girder, Upstream-Top Flange, 17.2 m (56.4 ft) from the end of steel girder section at Abutment 1.
7	2	SGG-2N-TS	Girder Strain Gage	4050	Upstream Girder, Downstream-Top Flange, 17.2 m (56.4 ft) from the end of steel girder section at Abutment 1.
7	3	SGG-2N-BN	Girder Strain Gage	4050	Upstream Girder, Upstream-Bottom Flange, 17.2 m (56.4 ft) from the end of steel girder section at Abutment 1.
7	4	SGG-2N-BS	Girder Strain Gage	4050	Upstream Girder, Downstream-Bottom Flange, 17.2 m (56.4 ft) from the end of steel girder section at Abutment 1.
7	5	SGG-2S-TN	Girder Strain Gage	4050	Downstream Girder, Upstream-Top Flange, 16.0 m (52.5 ft) from the end of steel girder section at Abutment 1.
7	6	SGG-2S-TS	Girder Strain Gage	4050	Downstream Girder, Downstream-Top Flange, 16.0 m (52.5 ft) from the end of steel girder section at Abutment 1.
7	7	SGG-2S-BN	Girder Strain Gage	4050	Downstream Girder, Upstream-Bottom Flange, 16.0 m (52.5 ft) from the end of steel girder section at Abutment 1.
7	8	SGG-2S-BS	Girder Strain Gage	4050	Downstream Girder, Downstream-Bottom Flange, 16.0 m (52.5 ft) from the end of steel girder section at Abutment 1.

Table B-5: Abutment 1 (per Structural Drawings) Multiplexer Channel Allocation and Gage Locations (cont.)

Mux	Channel	Gage Label	Gage Type	Model	Location
8	1	SG-2N-1NE	Pile Strain Gage	4000	Upstream Pile, 0.3 m (1.0 ft) from bottom of Abutment 1 64 mm (2.5 in) from the edge of flange.
8	2	SG-2N-1NW	Pile Strain Gage	4000	Upstream Pile, 0.3 m (1.0 ft) from bottom of Abutment 1 64 mm (2.5 in) from the edge of flange.
8	3	SG-2N-1SE	Pile Strain Gage	4000	Upstream Pile, 0.3 m (1.0 ft) from bottom of Abutment 1 64 mm (2.5 in) from the edge of flange.
8	4	SG-2N-1SW	Pile Strain Gage	4000	Upstream Pile, 0.3 m (1.0 ft) from bottom of Abutment 1 64 mm (2.5 in) from the edge of flange.
8	5	SG-2N-2NE	Pile Strain Gage	4000	Upstream Pile, 1.2 m (4.0 ft) from bottom of Abutment 1 64 mm (2.5 in) from the edge of flange.
8	6	SG-2N-2NW	Pile Strain Gage	4000	Upstream Pile, 1.2 m (4.0 ft) from bottom of Abutment 1 64 mm (2.5 in) from the edge of flange.
8	7	SG-2N-2SE	Pile Strain Gage	4000	Upstream Pile, 1.2 m (4.0 ft) from bottom of Abutment 1 64 mm (2.5 in) from the edge of flange.
8	8	SG-2N-2SW	Pile Strain Gage	4000	Upstream Pile, 1.2 m (4.0 ft) from bottom of Abutment 1 64 mm (2.5 in) from the edge of flange.
8	9	SG-2N-3NE	Pile Strain Gage	4000	Upstream Pile, 2.1 m (7.0 ft) from bottom of Abutment 1 64 mm (2.5 in) from the edge of flange.
8	10	SG-2N-3NW	Pile Strain Gage	4000	Upstream Pile, 2.1 m (7.0 ft) from bottom of Abutment 1 64 mm (2.5 in) from the edge of flange.
8	11	SG-2N-3SW	Pile Strain Gage	4000	Upstream Pile, 2.1 m (7.0 ft) from bottom of Abutment 1 64 mm (2.5 in) from the edge of flange.
8	12	SG-2N-4NE	Pile Strain Gage	4000	Upstream Pile, 3.0 m (10.0 ft) from bottom of Abutment 1 64 mm (2.5 in) from the edge of flange.
8	13	SG-2N-4NW	Pile Strain Gage	4000	Upstream Pile, 3.0 m (10.0 ft) from bottom of Abutment 1 64 mm (2.5 in) from the edge of flange.
8	14	SG-2N-4SW	Pile Strain Gage	4000	Upstream Pile, 3.0 m (10.0 ft) from bottom of Abutment 1 64 mm (2.5 in) from the edge of flange.

Table B-5: Abutment 1 (per Structural Drawings) Multiplexer Channel Allocation and Gage Locations (cont.)

Mux	Channel	Gage Label	Gage Type	Model	Location
9	1	SG-2S-1NE	Pile Strain Gage	4000	Downstream Pile, 0.3 m (1.0 ft) from bottom of Abutment 1 64 mm (2.5 in) from the edge of flange.
9	2	SG-2S-1NW	Pile Strain Gage	4000	Downstream Pile, 0.3 m (1.0 ft) from bottom of Abutment 1 64 mm (2.5 in) from the edge of flange.
9	3	SG-2S-1SE	Pile Strain Gage	4000	Downstream Pile, 0.3 m (1.0 ft) from bottom of Abutment 1 64 mm (2.5 in) from the edge of flange.
9	4	SG-2S-1SW	Pile Strain Gage	4000	Downstream Pile, 0.3 m (1.0 ft) from bottom of Abutment 1 64 mm (2.5 in) from the edge of flange.
9	5	SG-2S-2NE	Pile Strain Gage	4000	Downstream Pile, 1.2 m (4.0 ft) from bottom of Abutment 1 64 mm (2.5 in) from the edge of flange.
9	6	SG-2S-2NW	Pile Strain Gage	4000	Downstream Pile, 1.2 m (4.0 ft) from bottom of Abutment 1 64 mm (2.5 in) from the edge of flange.
9	7	SG-2S-2SE	Pile Strain Gage	4000	Downstream Pile, 1.2 m (4.0 ft) from bottom of Abutment 1 64 mm (2.5 in) from the edge of flange.
9	8	SG-2S-2SW	Pile Strain Gage	4000	Downstream Pile, 1.2 m (4.0 ft) from bottom of Abutment 1 64 mm (2.5 in) from the edge of flange.
9	9	SG-2S-3NE	Pile Strain Gage	4000	Downstream Pile, 2.1 m (7.0 ft) from bottom of Abutment 1 64 mm (2.5 in) from the edge of flange.
9	10	SG-2S-3NW	Pile Strain Gage	4000	Downstream Pile, 2.1 m (7.0 ft) from bottom of Abutment 1 64 mm (2.5 in) from the edge of flange.
9	11	SG-2S-3SW	Pile Strain Gage	4000	Downstream Pile, 2.1 m (7.0 ft) from bottom of Abutment 1 64 mm (2.5 in) from the edge of flange.
9	12	SG-2S-4NE	Pile Strain Gage	4000	Downstream Pile, 3.0 m (10.0 ft) from bottom of Abutment 1 64 mm (2.5 in) from the edge of flange.
9	13	SG-2S-4NW	Pile Strain Gage	4000	Downstream Pile, 3.0 m (10.0 ft) from bottom of Abutment 1 64 mm (2.5 in) from the edge of flange.
9	14	SG-2S-4SW	Pile Strain Gage	4000	Downstream Pile, 3.0 m (10.0 ft) from bottom of Abutment 1 64 mm (2.5 in) from the edge of flange.

Table B-5: Abutment 1 (per Structural Drawings) Multiplexer Channel Allocation and Gage Locations (cont.)

Mux	Channel	Gage Label	Gage Type	Model	Location
11	1	TM-2M	Tiltmeter (Biaxial) - Ch-1 (Longitudinal)	6160	Abutment 1, Center of Abutment, 1.0 m (3.0ft) below the bottom of middle girder
11	2	TM-2M	Tiltmeter (Biaxial) - Ch-2 (Transverse)	6160	Abutment 1, Center of Abutment, 1.0 m (3.0ft) below the bottom of middle girder
11	3	IN-2N-1	Inclinometer (Biaxial) - Ch-1 (Longitudinal)	6150	Abutment 1, Upstream Pile, Flange facing the roadway 0.0-0.6 m (0-2 ft) below the bottom of Abutment 1
11	4	IN-2N-1	Inclinometer (Biaxial) - Ch-2 (Transverse)	6150	Abutment 1, Upstream Pile, Flange facing the roadway 0.0-0.6 m (0-2 ft) below the bottom of Abutment 1
11	5	IN-2N-2	Inclinometer (Biaxial) - Ch-1 (Longitudinal)	6150	Abutment 1, Upstream Pile, Flange facing the roadway 0.6-1.5 m (2-5 ft) below the bottom of Abutment 1
11	6	IN-2N-2	Inclinometer (Biaxial) - Ch-2 (Transverse)	6150	Abutment 1, Upstream Pile, Flange facing the roadway 0.6-1.5 m (2-5 ft) below the bottom of Abutment 1
11	7	IN-2N-3	Inclinometer (Biaxial) - Ch-1 (Longitudinal)	6150	Abutment 1, Upstream Pile, Flange facing the roadway 1.5-2.7 m (5-9 ft) below the bottom of Abutment 1
11	8	IN-2N-3	Inclinometer (Biaxial) - Ch-2 (Transverse)	6150	Abutment 1, Upstream Pile, Flange facing the roadway 1.5-2.7 m (5-9 ft) below the bottom of Abutment 1
11	9	IN-2N-4	Inclinometer (Biaxial) - Ch-1 (Longitudinal)	6150	Abutment 1, Upstream Pile, Flange facing the roadway 2.7-4.0 m (9-13 ft) below the bottom of Abutment 1
11	10	IN-2N-4	Inclinometer (Biaxial) - Ch-2 (Transverse)	6150	Abutment 1, Upstream Pile, Flange facing the roadway 2.7-4.0 m (9-13 ft) below the bottom of Abutment 1
11	11	IN-2N-5	Inclinometer (Biaxial) - Ch-1 (Longitudinal)	6150	Abutment 1, Upstream Pile, Flange facing the roadway 4.0-5.2 m (13-17 ft) below the bottom of Abutment 1
11	12	IN-2N-5	Inclinometer (Biaxial) - Ch-2 (Transverse)	6150	Abutment 1, Upstream Pile, Flange facing the roadway 4.0-5.2 m (13-17 ft) below the bottom of Abutment 1

Table B-5: Abutment 1 (per Structural Drawings) Multiplexer Channel Allocation and Gage Locations (cont.)

Mux	Channel	Gage Label	Gage Type	Model	Location
12	1	IN-2S-1	Inclinometer (Biaxial) - Ch-1 (Longitudinal)	6150	Abutment 1, Downstream Pile, Flange facing the roadway 0.0-0.6 m (0-2 ft) below the bottom of Abutment 1
12	2	IN-2S-1	Inclinometer (Biaxial) - Ch-2 (Transverse)	6150	Abutment 1, Downstream Pile, Flange facing the roadway 0.0-0.6 m (0-2 ft) below the bottom of Abutment 1
12	3	IN-2S-2	Inclinometer (Biaxial) - Ch-1 (Longitudinal)	6150	Abutment 1, Downstream Pile, Flange facing the roadway 0.6-1.5 m (2-5 ft) below the bottom of Abutment 1
12	4	IN-2S-2	Inclinometer (Biaxial) - Ch-2 (Transverse)	6150	Abutment 1, Downstream Pile, Flange facing the roadway 0.6-1.5 m (2-5 ft) below the bottom of Abutment 1
12	5	IN-2S-3	Inclinometer (Biaxial) - Ch-1 (Longitudinal)	6150	Abutment 1, Downstream Pile, Flange facing the roadway 1.5-2.7 m (5-9 ft) below the bottom of Abutment 1
12	6	IN-2S-3	Inclinometer (Biaxial) - Ch-2 (Transverse)	6150	Abutment 1, Downstream Pile, Flange facing the roadway 1.5-2.7 m (5-9 ft) below the bottom of Abutment 1
12	7	IN-2S-4	Inclinometer (Biaxial) - Ch-1 (Longitudinal)	6150	Abutment 1, Downstream Pile, Flange facing the roadway 2.7-4.0 m (9-13 ft) below the bottom of Abutment 1
12	8	IN-2S-4	Inclinometer (Biaxial) - Ch-2 (Transverse)	6150	Abutment 1, Downstream Pile, Flange facing the roadway 2.7-4.0 m (9-13 ft) below the bottom of Abutment 1.
12	9	IN-2S-5	Inclinometer (Biaxial) - Ch-1 (Longitudinal)	6150	Abutment 1, Downstream Pile, Flange facing the roadway 4.0-5.2 m (13-17 ft) below the bottom of Abutment 1
12	10	IN-2S-5	Inclinometer (Biaxial) - Ch-2 (Transverse)	6150	Abutment 1, Downstream Pile, Flange facing the roadway 4.05.2 m (13-17 ft) below the bottom of Abutment 1

Table B-6: Abutment 2 (per Structural Drawings) Multiplexer Channel Allocation and Gage Locations

Mux	Channel	Gage Label	Gage Type	Model	Location
1	1	CM-1NT	Displacement Transducer	4420-50mm	Abutment 2, Upstream, Transverse, 2.68 m (8.78 ft) below construction joint.
1	2	CM-1N	Displacement Transducer	4420-100mm	Abutment 2, Upstream, Longitudinal, 2.68 m (8.78 ft) below construction joint.
1	3	CM-1S	Displacement Transducer	4420-100mm	Abutment 2, Downstream, Longitudinal, 1.58 m (5.17 ft) below construction joint.
1	4	P-1NT	Earth Pressure Cell	4810	Abutment 2, Upstream, 3.6 m (12.0 ft) above the bottom of abutment, 1 m (3 ft) away from abutment-wingwall connection.
1	5	P-1NM	Earth Pressure Cell	4810	Abutment 2, Upstream, 2.1 m (7.0 ft) above the bottom of abutment, 1 m (3 ft) away from abutment-wingwall connection.
1	6	P-1NB	Earth Pressure Cell	4810	Abutment 2, Upstream, 0.6 m (2.0 ft) above the bottom of abutment, 1 m (3 ft) away from abutment-wingwall connection.
1	7	P-1CT	Earth Pressure Cell	4810	Abutment 2, Center of Abutment 3.6 m (12.0 ft) above the bottom of abutment.
1	8	P-1CB	Earth Pressure Cell	4810	Abutment 2, Center of Abutment 0.6 m (2.0 ft) above the bottom of abutment.
1	9	P-1ST	Earth Pressure Cell	4810	Abutment 2, Downstream, 3.6 m (12.0 ft) above the bottom of abutment, 1 m (3 ft) away from abutment-wingwall connection.
1	10	P-1SM	Earth Pressure Cell	4810	Abutment 2, Downstream, 2.1 m (7.0 ft) above the bottom of abutment, 1 m (3 ft) away from abutment-wingwall connection.
1	11	P-1SB	Earth Pressure Cell	4810	Abutment 2, Downstream, 0.6 m (2.0 ft) above the bottom of abutment, 1 m (3 ft) away from abutment-wingwall connection.
1	12	Empty Channel			
1	13	PW-1N	Earth Pressure Cell	4815	Wingwall 3, 1.2 m (4.0 ft) above the bottom of wingwall, 1 m (3 ft) away from abutment-wingwall connection.
1	14	PW-1S	Earth Pressure Cell	4815	Wingwall 4, 1.8 m (6.0 ft) above the bottom of wingwall, 1 m (3 ft) away from abutment-wingwall connection.

Table B-6: Abutment 2 (per Structural Drawings) Multiplexer Channel Allocation and Gage Locations (cont.)

Mux	Channel	Gage Label	Gage Type	Model	Location
2	1	SGG-1N-TN	Girder Strain Gage	4050	Upstream Girder, Upstream-Top Flange, 17.6 m (57.7 ft) from the end of steel girder section at Abutment 2.
2	2	SGG-1N-TS	Girder Strain Gage	4050	Upstream Girder, Downstream-Top Flange, 17.6 m (57.7 ft) from the end of steel girder section at Abutment 2.
2	3	SGG-1N-BN	Girder Strain Gage	4050	Upstream Girder, Upstream-Bottom Flange, 17.6 m (57.7 ft) from the end of steel girder section at Abutment 2.
2	4	SGG-1N-BS	Girder Strain Gage	4050	Upstream Girder, Downstream-Bottom Flange, 17.6 m (57.7 ft) from the end of steel girder section at Abutment 2.
2	5	SGG-1S-TN	Girder Strain Gage	4050	Downstream Girder, Upstream-Top Flange, 16.4 m (53.8 ft) from the end of steel girder section at Abutment 2.
2	6	SGG-1S-TS	Girder Strain Gage	4050	Downstream Girder, Downstream-Top Flange, 16.4 m (53.8 ft) from the end of steel girder section at Abutment 2.
2	7	SGG-1S-BN	Girder Strain Gage	4050	Downstream Girder, Upstream-Bottom Flange, 16.4 m (53.8 ft) from the end of steel girder section at Abutment 2.
2	8	SGG-1S-BS	Girder Strain Gage	4050	Downstream Girder, Downstream-Bottom Flange, 16.4 m (53.8 ft) from the end of steel girder section at Abutment 2.
2	9	SGG-0N-TN	Girder Strain Gage	4050	Upstream Girder, Upstream-Top Flange, 34.5 m (113.2 ft) from the end of steel girder section at Abutment 1.
2	10	SGG-0N-TS	Girder Strain Gage	4050	Upstream Girder, Downstream-Top Flange, 34.5 m (113.2 ft) from the end of steel girder section at Abutment 1.
2	11	SGG-0N-BN	Girder Strain Gage	4050	Upstream Girder, Upstream-Bottom Flange, 34.5 m (113.2 ft) from the end of steel girder section at Abutment 1.
2	12	SGG-0N-BS	Girder Strain Gage	4050	Upstream Girder, Downstream-Bottom Flange, 34.5 m (113.2 ft) from the end of steel girder section at Abutment 1.
2	13	SGG-0S-TN	Girder Strain Gage	4050	Downstream Girder, Upstream-Top Flange, 32.0 m (105.0 ft) from the end of steel girder section at Abutment 1.
2	14	SGG-0S-TS	Girder Strain Gage	4050	Downstream Girder, Downstream-Top Flange, 32.0 m (105.0 ft) from the end of steel girder section at Abutment 1.
2	15	SGG-0S-BN	Girder Strain Gage	4050	Downstream Girder, Upstream-Bottom Flange, 32.0 m (105.0 ft) from the end of steel girder section at Abutment 1.
2	16	SGG-0S-BS	Girder Strain Gage	4050	Downstream Girder, Downstream-Bottom Flange, 32.0 m (105.0 ft) from the end of steel girder section at Abutment 1.

Table B-6: Abutment 2 (per Structural Drawings) Multiplexer Channel Allocation and Gage Locations (cont.)

Mux	Channel	Gage Label	Gage Type	Model	Location
3	1	SG-1N-1NE	Pile Strain Gage	4000	Upstream Pile, 0.3 m (1.0 ft) from bottom of Abutment 2 64 mm (2.5 in) from the edge of flange.
3	2	SG-1N-1NW	Pile Strain Gage	4000	Upstream Pile, 0.3 m (1.0 ft) from bottom of Abutment 2 64 mm (2.5 in) from the edge of flange.
3	3	SG-1N-1SE	Pile Strain Gage	4000	Upstream Pile, 0.3 m (1.0 ft) from bottom of Abutment 2 64 mm (2.5 in) from the edge of flange.
3	4	SG-1N-1SW	Pile Strain Gage	4000	Upstream Pile, 0.3 m (1.0 ft) from bottom of Abutment 2 64 mm (2.5 in) from the edge of flange.
3	5	SG-1N-2NE	Pile Strain Gage	4000	Upstream Pile, 1.2 m (4.0 ft) from bottom of Abutment 2 64 mm (2.5 in) from the edge of flange.
3	6	SG-1N-2NW	Pile Strain Gage	4000	Upstream Pile, 1.2 m (4.0 ft) from bottom of Abutment 2 64 mm (2.5 in) from the edge of flange.
3	7	SG-1N-2SE	Pile Strain Gage	4000	Upstream Pile, 1.2 m (4.0 ft) from bottom of Abutment 2 64 mm (2.5 in) from the edge of flange.
3	8	SG-1N-2SW	Pile Strain Gage	4000	Upstream Pile, 1.2 m (4.0 ft) from bottom of Abutment 2 64 mm (2.5 in) from the edge of flange.
3	9	SG-1N-3NE	Pile Strain Gage	4000	Upstream Pile, 2.1 m (7.0 ft) from bottom of Abutment 2 64 mm (2.5 in) from the edge of flange.
3	10	SG-1N-3NW	Pile Strain Gage	4000	Upstream Pile, 2.1 m (7.0 ft) from bottom of Abutment 2 64 mm (2.5 in) from the edge of flange.
3	11	SG-1N-3SE	Pile Strain Gage	4000	Upstream Pile, 2.1 m (7.0 ft) from bottom of Abutment 2 64 mm (2.5 in) from the edge of flange.
3	12	SG-1N-3SW	Pile Strain Gage	4000	Upstream Pile, 2.1 m (7.0 ft) from bottom of Abutment 2 64 mm (2.5 in) from the edge of flange.
3	13	SG-1N-4NE	Pile Strain Gage	4000	Upstream Pile, 3.0 m (10.0 ft) from bottom of Abutment 2 64 mm (2.5 in) from the edge of flange.
3	14	SG-1N-4NW	Pile Strain Gage	4000	Upstream Pile, 3.0 m (10.0 ft) from bottom of Abutment 2 64 mm (2.5 in) from the edge of flange.
3	15	SG-1N-4SE	Pile Strain Gage	4000	Upstream Pile, 3.0 m (10.0 ft) from bottom of Abutment 2 64 mm (2.5 in) from the edge of flange.
3	16	SG-1N-4SW	Pile Strain Gage	4000	Upstream Pile, 3.0 m (10.0 ft) from bottom of Abutment 2 64 mm (2.5 in) from the edge of flange.

Table B-6: Abutment 2 (per Structural Drawings) Multiplexer Channel Allocation and Gage Locations (cont.)

Mux	Channel	Gage Label	Gage Type	Model	Location
4	1	SG-1S-1NE	Pile Strain Gage	4000	Downstream Pile, 0.3 m (1.0 ft) from bottom of Abutment 2 64 mm (2.5 in) from the edge of flange.
4	2	SG-1S-1NW	Pile Strain Gage	4000	Downstream Pile, 0.3 m (1.0 ft) from bottom of Abutment 2 64 mm (2.5 in) from the edge of flange.
4	3	SG-1S-1SE	Pile Strain Gage	4000	Downstream Pile, 0.3 m (1.0 ft) from bottom of Abutment 64 mm (2.5 in) from the edge of flange.
4	4	SG-1S-1SW	Pile Strain Gage	4000	Downstream Pile, 0.3 m (1.0 ft) from bottom of Abutment 2 64 mm (2.5 in) from the edge of flange.
4	5	SG-1S-2NE	Pile Strain Gage	4000	Downstream Pile, 1.2 m (4.0 ft) from bottom of Abutment 2 64 mm (2.5 in) from the edge of flange.
4	6	SG-1S-2NW	Pile Strain Gage	4000	Downstream Pile, 1.2 m (4.0 ft) from bottom of Abutment 2 64 mm (2.5 in) from the edge of flange.
4	7	SG-1S-2SE	Pile Strain Gage	4000	Downstream Pile, 1.2 m (4.0 ft) from bottom of Abutment 64 mm (2.5 in) from the edge of flange.
4	8	SG-1S-2SW	Pile Strain Gage	4000	Downstream Pile, 1.2 m (4.0 ft) from bottom of Abutment 64 mm (2.5 in) from the edge of flange.
4	9	SG-1S-3NE	Pile Strain Gage	4000	Downstream Pile, 2.1 m (7.0 ft) from bottom of Abutment 64 mm (2.5 in) from the edge of flange.
4	10	SG-1S-3NW	Pile Strain Gage	4000	Downstream Pile, 2.1 m (7.0 ft) from bottom of Abutment 64 mm (2.5 in) from the edge of flange.
4	11	SG-1S-3SE	Pile Strain Gage	4000	Downstream Pile, 2.1 m (7.0 ft) from bottom of Abutment 2 64 mm (2.5 in) from the edge of flange.
4	12	SG-1S-3SW	Pile Strain Gage	4000	Downstream Pile, 2.1 m (7.0 ft) from bottom of Abutment 2 64 mm (2.5 in) from the edge of flange.
4	13	SG-1S-4NE	Pile Strain Gage	4000	Downstream Pile, 3.0 m (10.0 ft) from bottom of Abutment 64 mm (2.5 in) from the edge of flange.
4	14	SG-1S-4NW	Pile Strain Gage	4000	Downstream Pile, 3.0 m (10.0 ft) from bottom of Abutment 64 mm (2.5 in) from the edge of flange.
4	15	SG-1S-4SE	Pile Strain Gage	4000	Downstream Pile, 3.0 m (10.0 ft) from bottom of Abutment 64 mm (2.5 in) from the edge of flange.
4	16	SG-1S-4SW	Pile Strain Gage	4000	Upstream Pile, 3.0 m (10.0 ft) from bottom of Abutment 64 mm (2.5 in) from the edge of flange.

Table B-6: Abutment 2 (per Structural Drawings) Multiplexer Channel Allocation and Gage Locations (cont.)

Mux	Channel	Gage Label	Gage Type	Model	Location
5	1	SGP-TN	Pier Strain Gage	4200	0.3 m (1 ft) below top of interior pier column, upstream
5	2	SGP-TS	Pier Strain Gage	4200	0.3 m (1 ft) below top of interior pier column, downstream
5	3	SGP-TE	Pier Strain Gage	4200	0.3 m (1 ft) below top of interior pier column, towards Abutment 2
5	4	SGP-TW	Pier Strain Gage	4200	0.3 m (1 ft) below top of interior pier column, towards Abutment 1
5	5	SGP-BN	Pier Strain Gage	4200	0.3 m (1 ft) above bottom of interior pier column, upstream
5	6	SGP-BS	Pier Strain Gage	4200	0.3 m (1 ft) above bottom of interior pier column, downstream
5	7	SGP-BE	Pier Strain Gage	4200	0.3 m (1 ft) above bottom of interior pier column, towards Abutment 2
5	8	SGP-BW	Pier Strain Gage	4200	0.3 m (1 ft) above bottom of interior pier column, towards Abutment 1

APPENDIX C LONG TERM MONITORING PLOTS FOR IABs

a) Long Term Monitoring of the Middlesex Bridge

DATES: 12-04-2009/12-31-2013

NOTES:

- All values are relative to the readings from 12-04-2009 at 6.00 pm.
- Temperature on the Bridge Deck during initial reading is 46.1 ^{o}F.
- Highest temperature within the period (on the Bridge Deck): 102.5 ^{o}F (08/26/2012).
- Lowest temperature within the period (on the Bridge Deck): -11.3 ^{o}F (01/16/2012).

Report a-1 Max Earth Pressure vs. Time

Report a-2 Max Earth Pressure vs. Abutment Displacement

WINTER 2009-SUMMER 2010

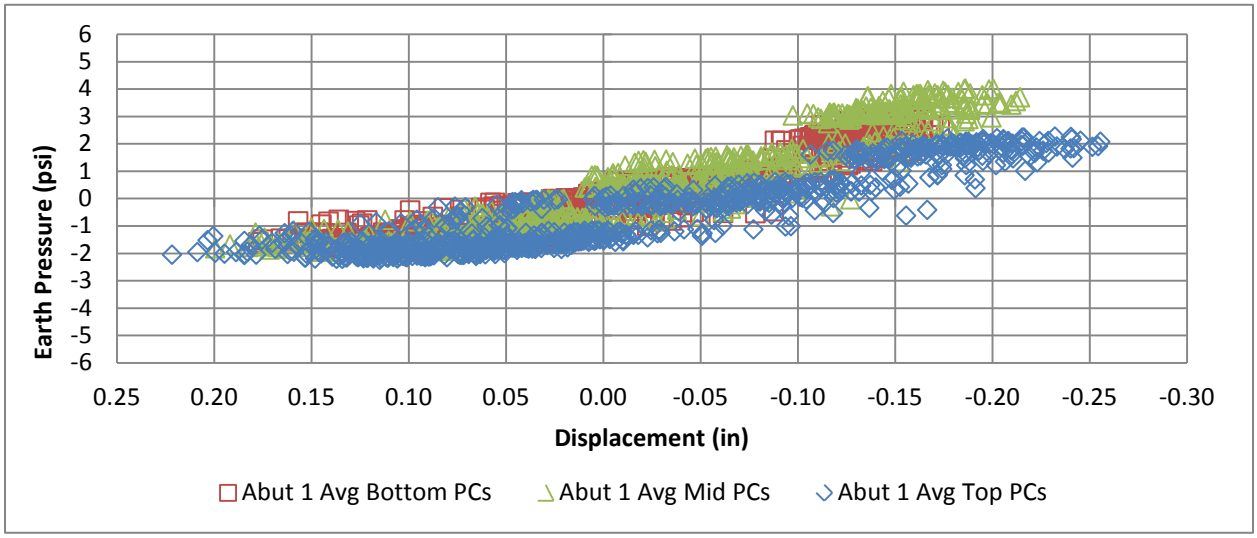

SUMMER 2010-WINTER 2011

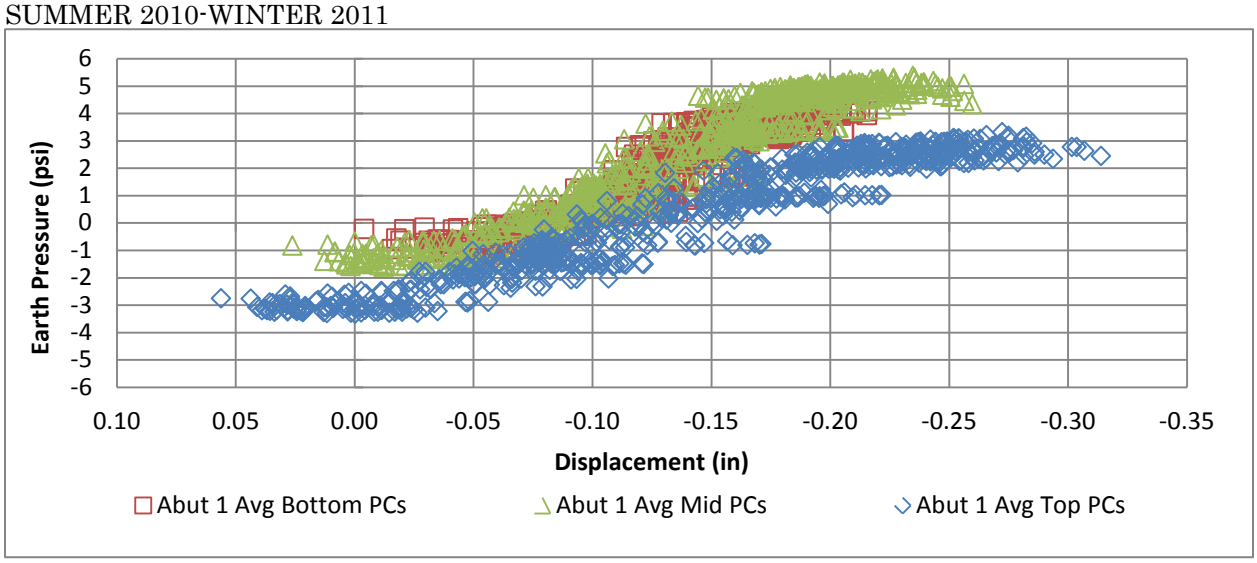

WINTER 2011-SUMMER 2011

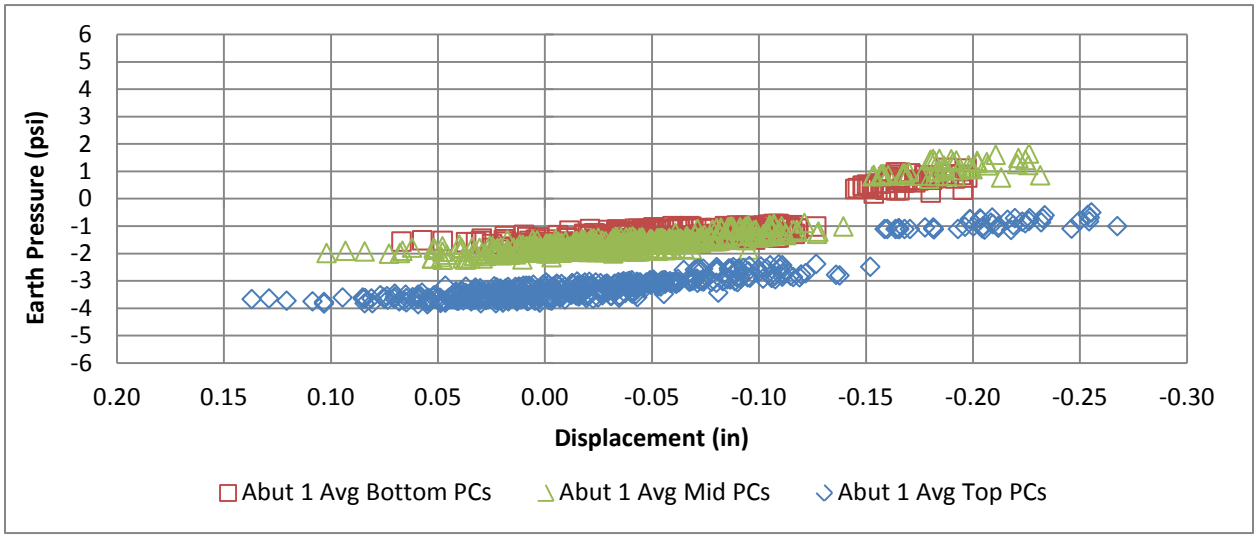

SUMMER 2011-WINTER 2012

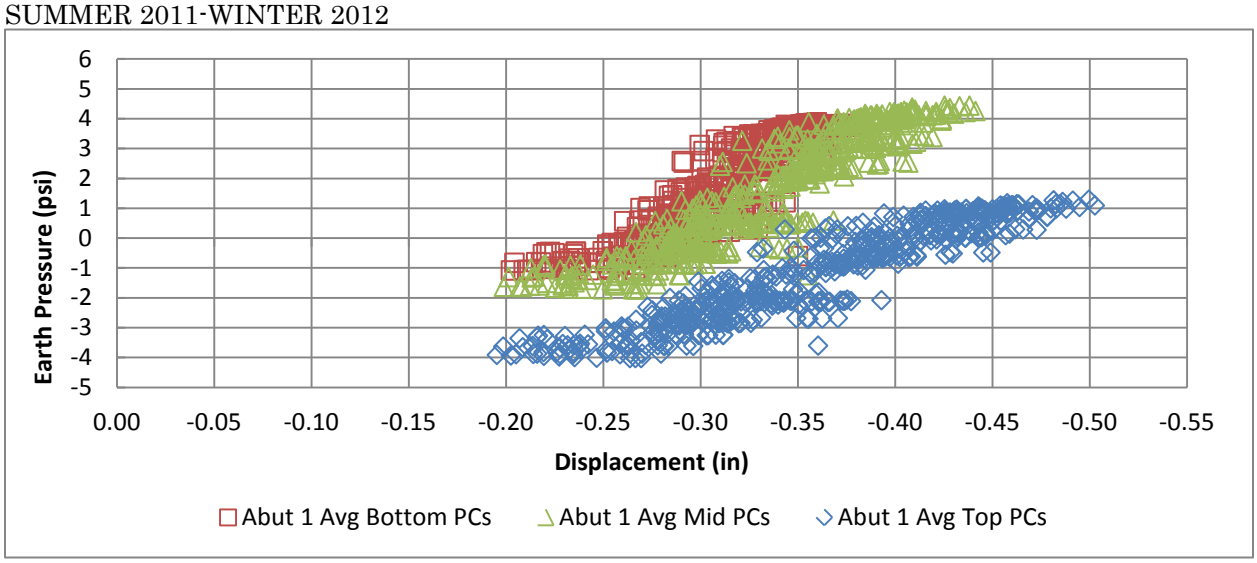

WINTER 2012-SUMMER 2012

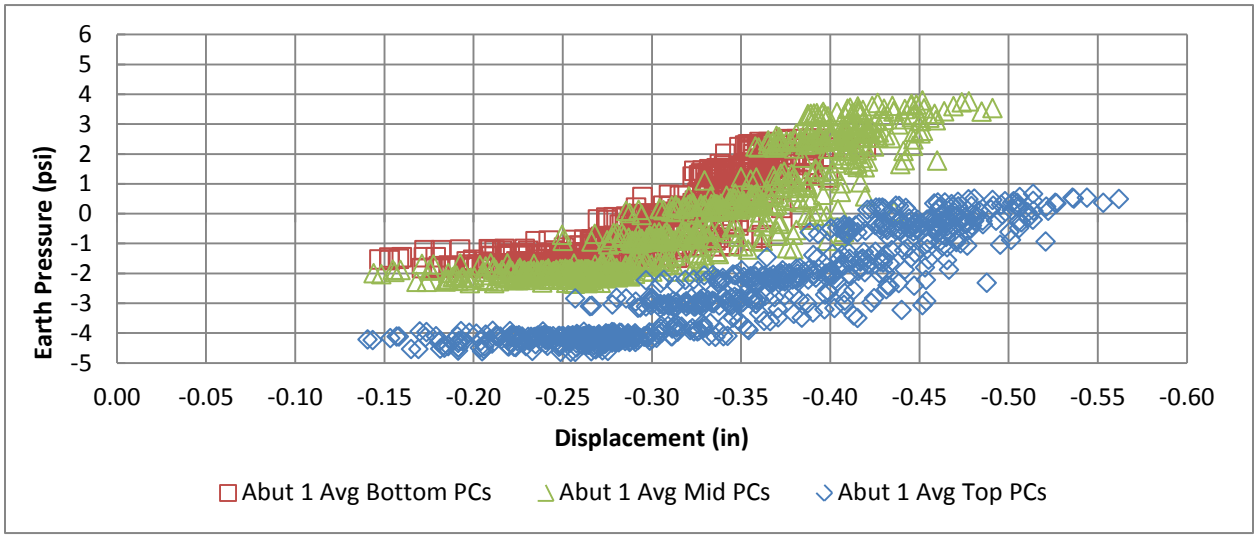

SUMMER 2012-WINTER 2013

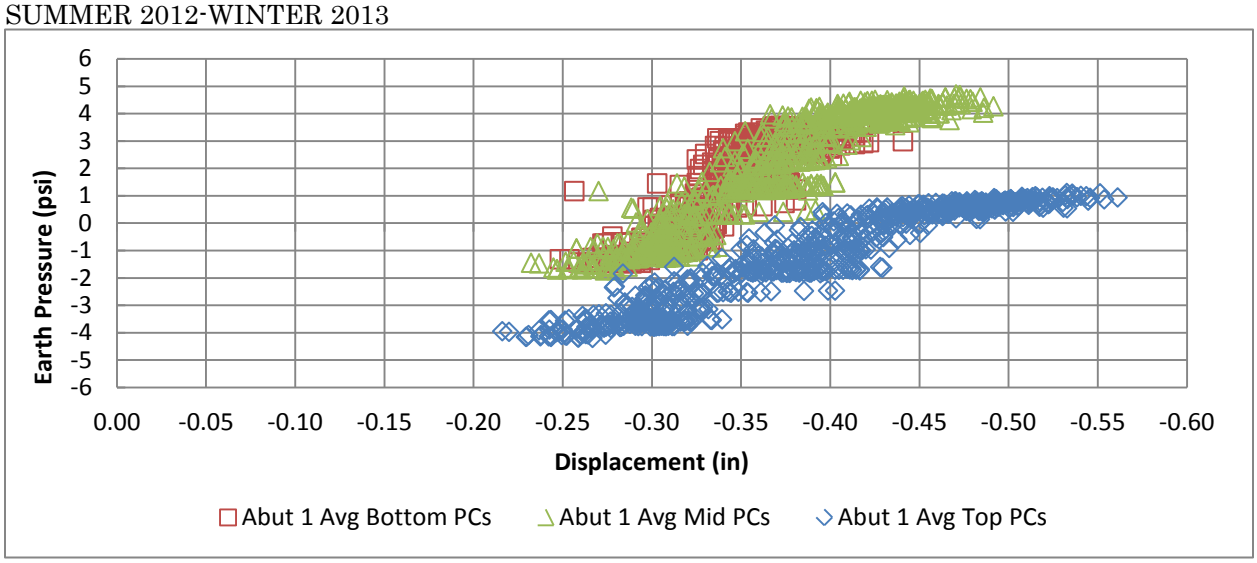

WINTER 2013-SUMMER 2013

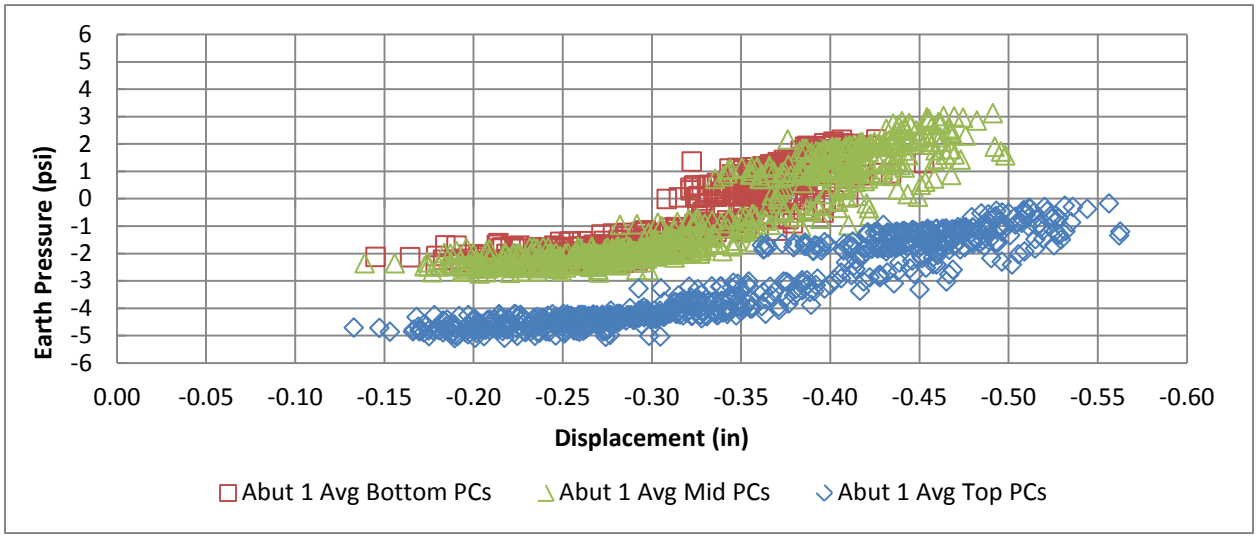

SUMMER 2013-WINTER 2014

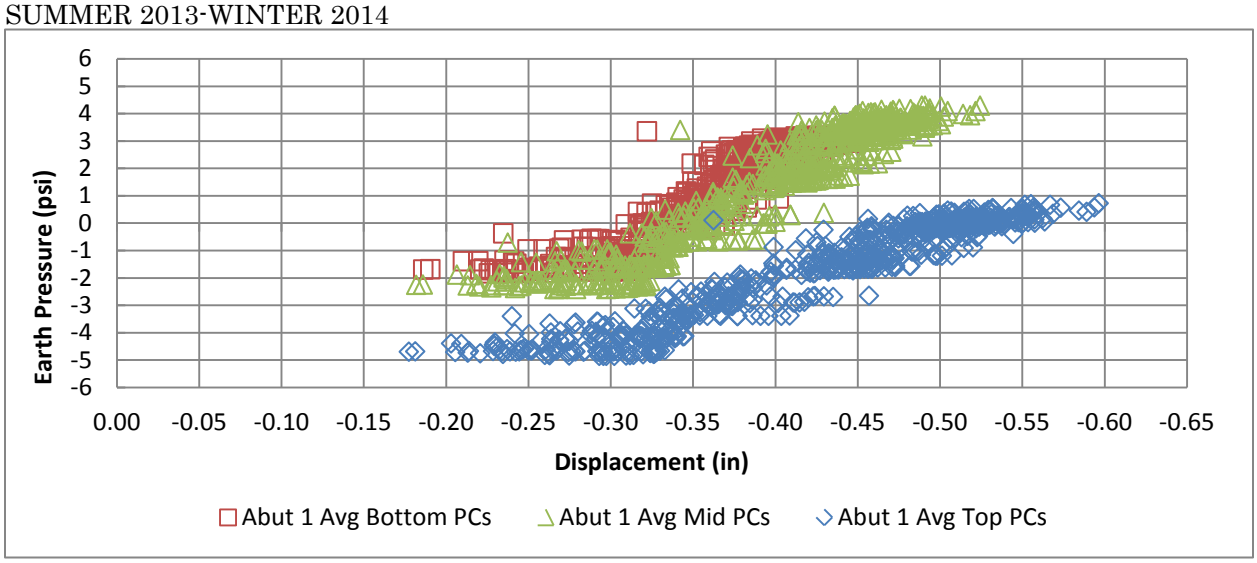

Report a-3 Displacement at the Top of Pile vs. Time

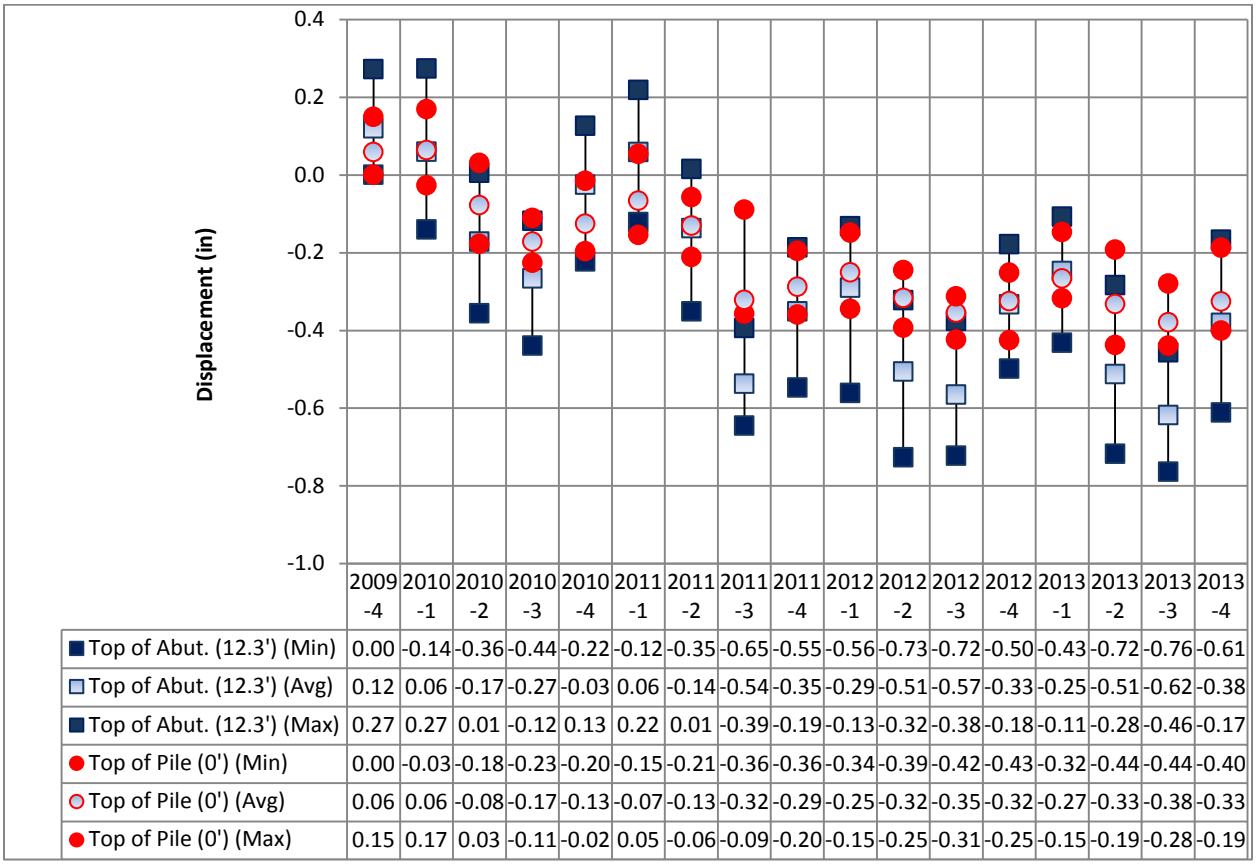

	2009 -4	2010 -1	2010 -2	2010 -3	2010 -4	2011 -1	2011 -2	2011 -3	2011 -4	2012 -1	2012 -2	2012 -3	2012 -4	2013 -1	2013 -2	2013 -3	2013 -4
Top of Abut. (12.3') (Min)	0.00	-0.14	-0.36	-0.44	-0.22	-0.12	-0.35	-0.65	-0.55	-0.56	-0.73	-0.72	-0.50	-0.43	-0.72	-0.76	-0.61
Top of Abut. (12.3') (Avg)	0.12	0.06	-0.17	-0.27	-0.03	0.06	-0.14	-0.54	-0.35	-0.29	-0.51	-0.57	-0.33	-0.25	-0.51	-0.62	-0.38
Top of Abut. (12.3') (Max)	0.27	0.27	0.01	-0.12	0.13	0.22	0.01	-0.39	-0.19	-0.13	-0.32	-0.38	-0.18	-0.11	-0.28	-0.46	-0.17
Top of Pile (0') (Min)	0.00	-0.03	-0.18	-0.23	-0.20	-0.15	-0.21	-0.36	-0.36	-0.34	-0.39	-0.42	-0.43	-0.32	-0.44	-0.44	-0.40
Top of Pile (0') (Avg)	0.06	0.06	-0.08	-0.17	-0.13	-0.07	-0.13	-0.32	-0.29	-0.25	-0.32	-0.35	-0.32	-0.27	-0.33	-0.38	-0.33
Top of Pile (0') (Max)	0.15	0.17	0.03	-0.11	-0.02	0.05	-0.06	-0.09	-0.20	-0.15	-0.25	-0.31	-0.25	-0.15	-0.19	-0.28	-0.19

Report a-4 Displacement at the Top of Pile vs. Temperature

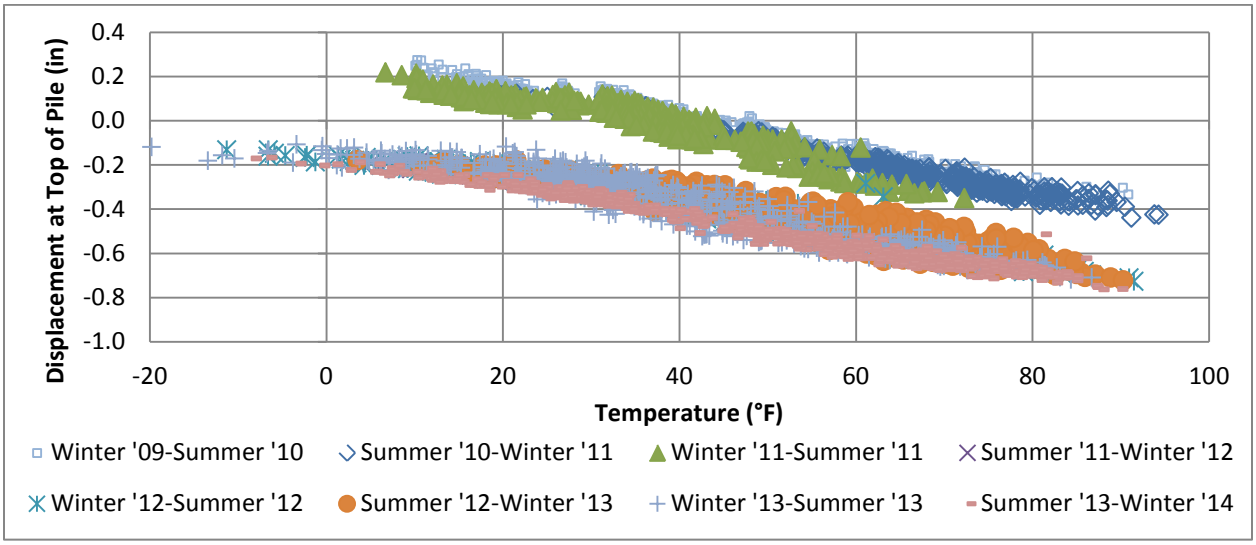

Report a-5 Abutment Rotation vs. Time

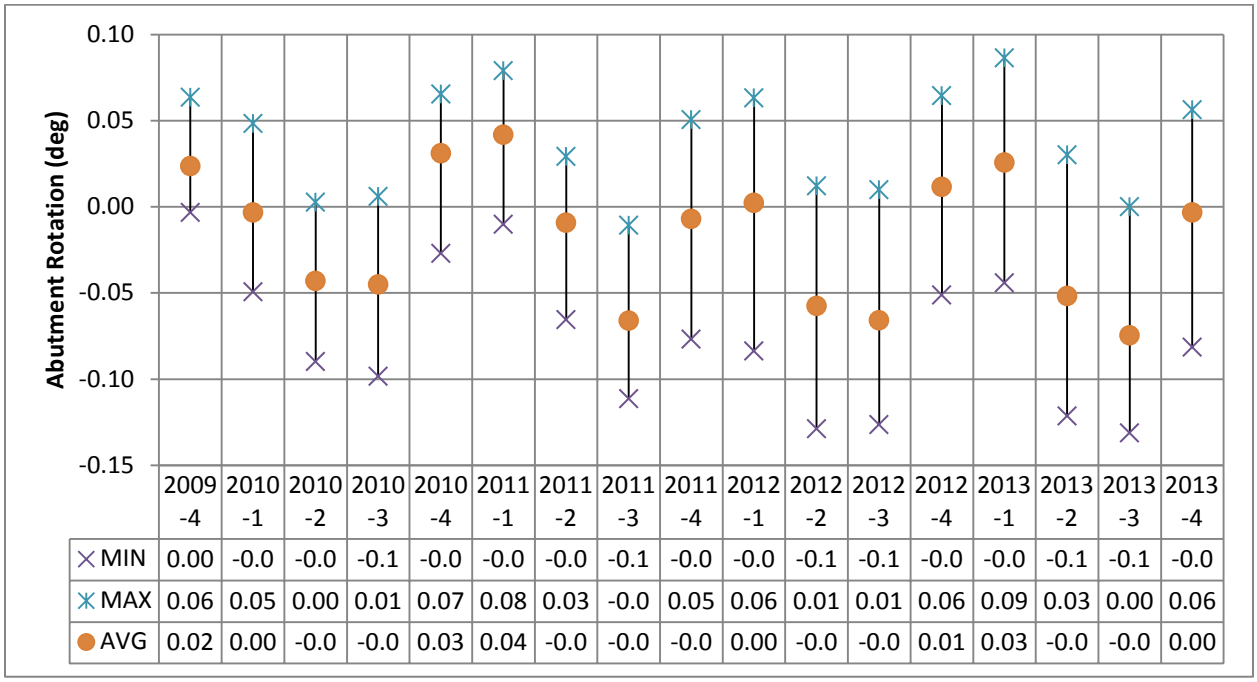

	2009-4	2010-1	2010-2	2010-3	2010-4	2011-1	2011-2	2011-3	2011-4	2012-1	2012-2	2012-3	2012-4	2013-1	2013-2	2013-3	2013-4
MIN	0.00	-0.0	-0.0	-0.1	-0.0	-0.0	-0.0	-0.1	-0.0	-0.0	-0.1	-0.1	-0.0	-0.0	-0.1	-0.1	-0.0
MAX	0.06	0.05	0.00	0.01	0.07	0.08	0.03	-0.0	0.05	0.06	0.01	0.01	0.06	0.09	0.03	0.00	0.06
AVG	0.02	0.00	-0.0	-0.0	0.03	0.04	-0.0	-0.0	-0.0	0.00	-0.0	-0.0	0.01	0.03	-0.0	-0.0	0.00

Report a-6 Flange Stresses vs. Time

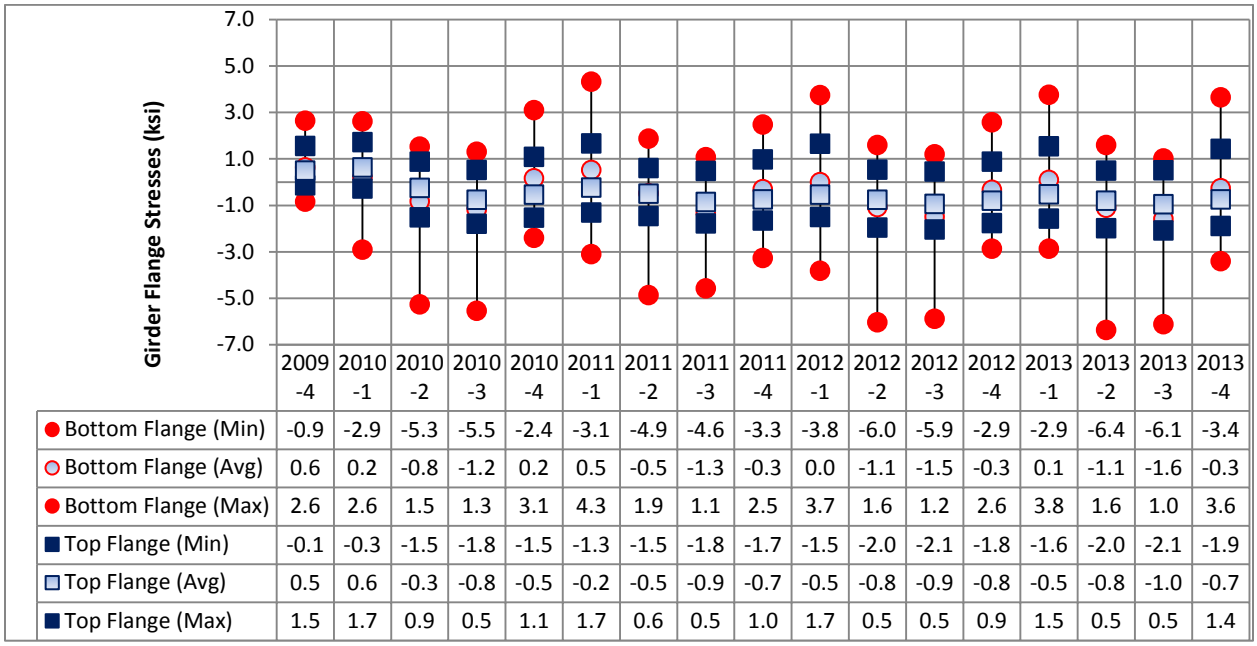

	2009-4	2010-1	2010-2	2010-3	2010-4	2011-1	2011-2	2011-3	2011-4	2012-1	2012-2	2012-3	2012-4	2013-1	2013-2	2013-3	2013-4
Bottom Flange (Min)	-0.9	-2.9	-5.3	-5.5	-2.4	-3.1	-4.9	-4.6	-3.3	-3.8	-6.0	-5.9	-2.9	-2.9	-6.4	-6.1	-3.4
Bottom Flange (Avg)	0.6	0.2	-0.8	-1.2	0.2	0.5	-0.5	-1.3	-0.3	0.0	-1.1	-1.5	-0.3	0.1	-1.1	-1.6	-0.3
Bottom Flange (Max)	2.6	2.6	1.5	1.3	3.1	4.3	1.9	1.1	2.5	3.7	1.6	1.2	2.6	3.8	1.6	1.0	3.6
Top Flange (Min)	-0.1	-0.3	-1.5	-1.8	-1.5	-1.3	-1.5	-1.8	-1.7	-1.5	-2.0	-2.1	-1.8	-1.6	-2.0	-2.1	-1.9
Top Flange (Avg)	0.5	0.6	-0.3	-0.8	-0.5	-0.2	-0.5	-0.9	-0.7	-0.5	-0.8	-0.9	-0.8	-0.5	-0.8	-1.0	-0.7
Top Flange (Max)	1.5	1.7	0.9	0.5	1.1	1.7	0.6	0.5	1.0	1.7	0.5	0.5	0.9	1.5	0.5	0.5	1.4

Report a-7 Abutment Displacement (Bottom) vs. Abutment Displacement (Top)

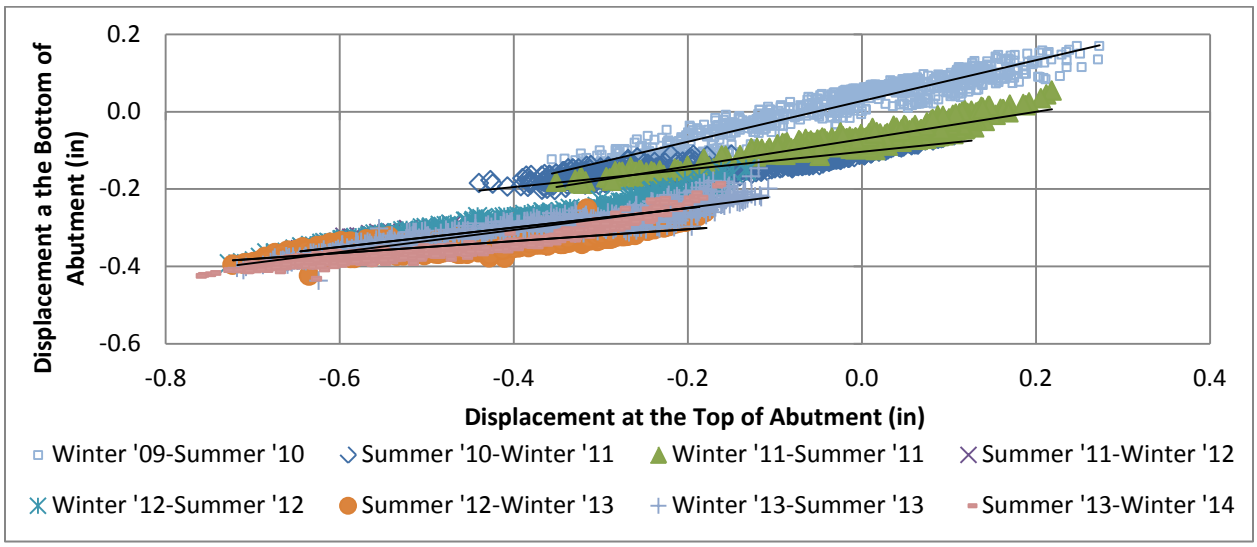

Report a-8 Max Pile Stress at Different Layers vs. Displacement at Top of Abutment (2009-2013)

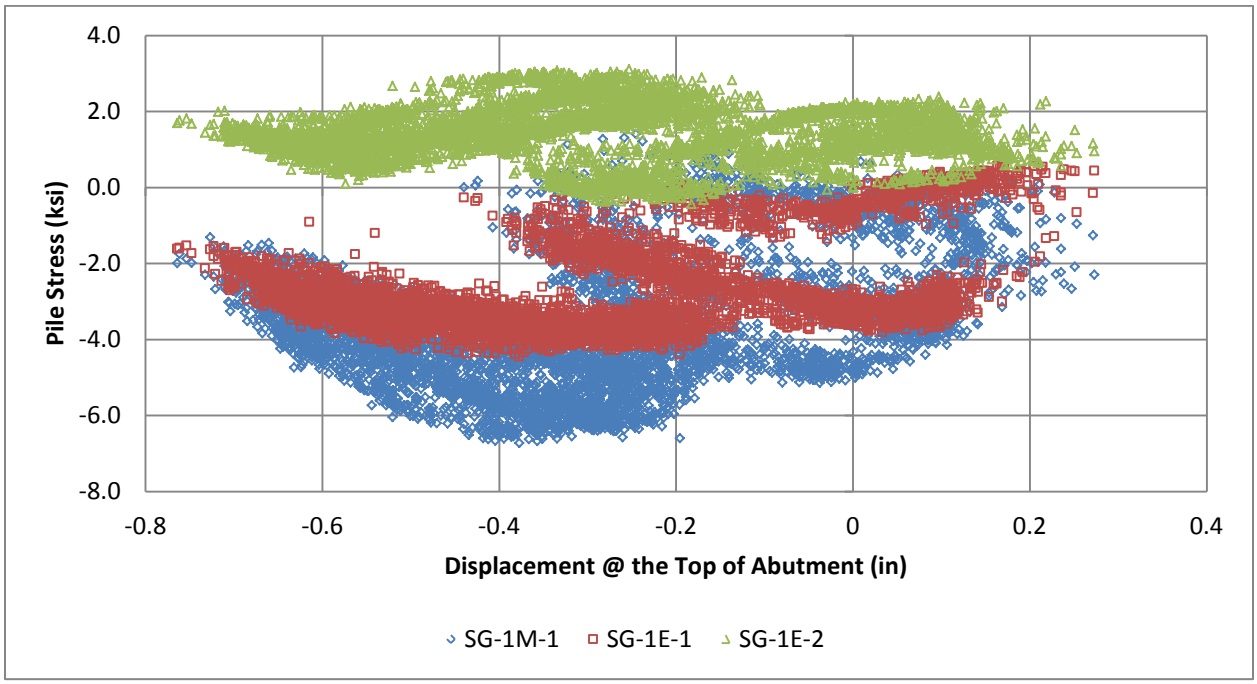

Report a-9 Pile Stress at Gage Location vs. Time

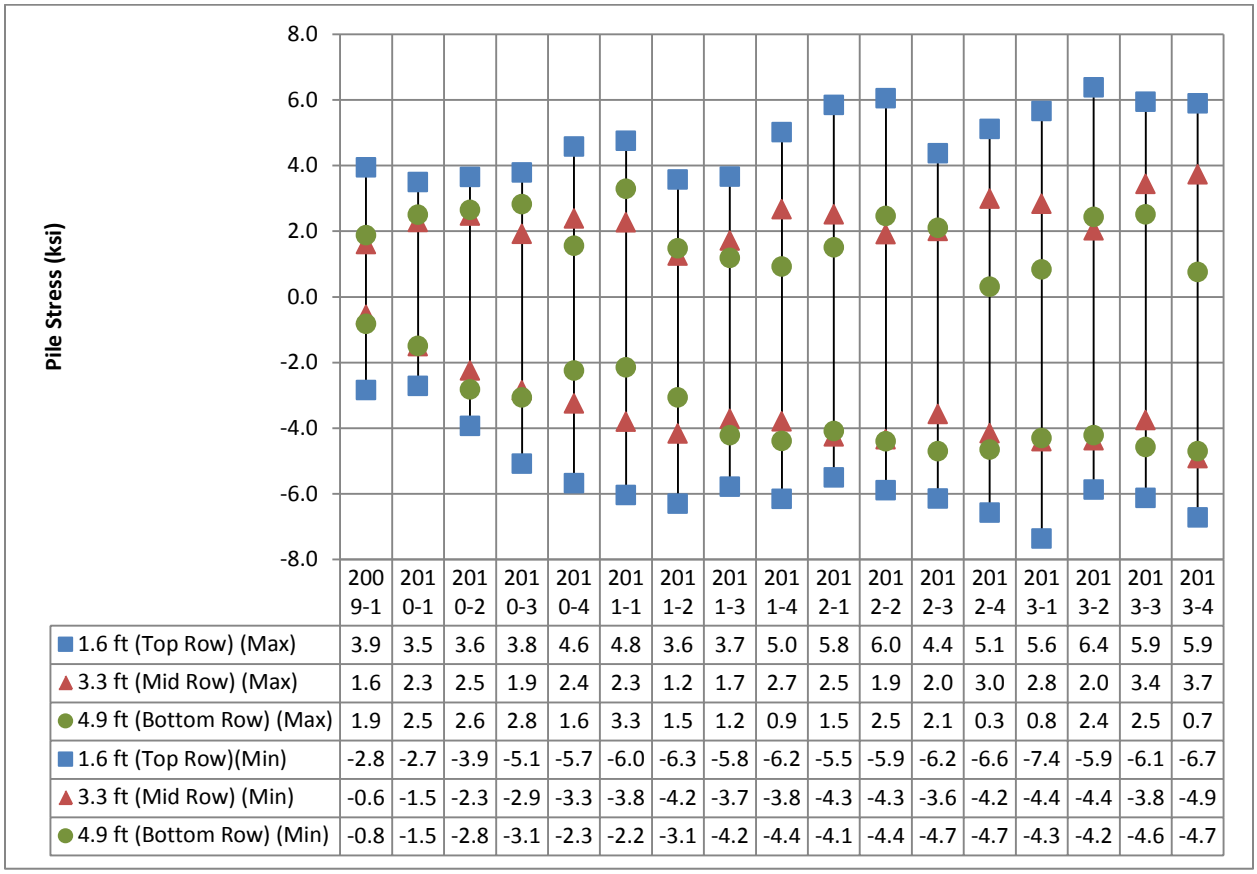

	2009-1	2010-1	2010-2	2010-3	2010-4	2011-1	2011-2	2011-3	2011-4	2012-1	2012-2	2012-3	2012-4	2013-1	2013-2	2013-3	2013-4
1.6 ft (Top Row) (Max)	3.9	3.5	3.6	3.8	4.6	4.8	3.6	3.7	5.0	5.8	6.0	4.4	5.1	5.6	6.4	5.9	5.9
3.3 ft (Mid Row) (Max)	1.6	2.3	2.5	1.9	2.4	2.3	1.2	1.7	2.7	2.5	1.9	2.0	3.0	2.8	2.0	3.4	3.7
4.9 ft (Bottom Row) (Max)	1.9	2.5	2.6	2.8	1.6	3.3	1.5	1.2	0.9	1.5	2.5	2.1	0.3	0.8	2.4	2.5	0.7
1.6 ft (Top Row)(Min)	-2.8	-2.7	-3.9	-5.1	-5.7	-6.0	-6.3	-5.8	-6.2	-5.5	-5.9	-6.2	-6.6	-7.4	-5.9	-6.1	-6.7
3.3 ft (Mid Row) (Min)	-0.6	-1.5	-2.3	-2.9	-3.3	-3.8	-4.2	-3.7	-3.8	-4.3	-4.3	-3.6	-4.2	-4.4	-4.4	-3.8	-4.9
4.9 ft (Bottom Row) (Min)	-0.8	-1.5	-2.8	-3.1	-2.3	-2.2	-3.1	-4.2	-4.4	-4.1	-4.4	-4.7	-4.7	-4.3	-4.2	-4.6	-4.7

Report a-10 Pile Displacement vs. Depth vs. Cap Displacement (2009-2013)

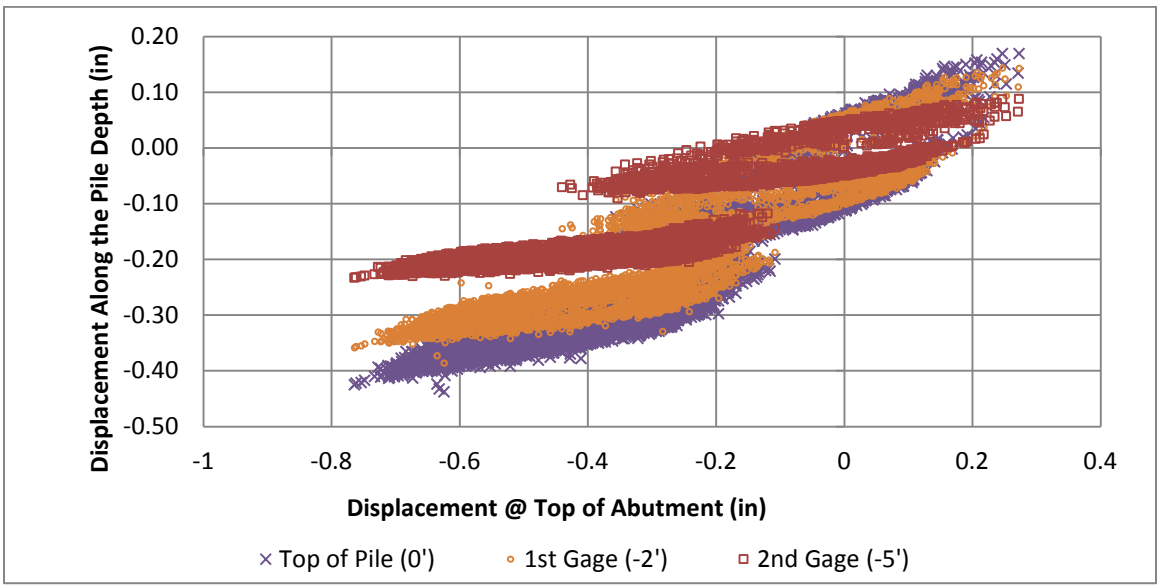

b) Long Term Monitoring of the East Montpelier Bridge

DATES: 11-24-2009/12-31-2013

NOTES:

- All values are relative to the readings from 11-24-2009 at 6.00 pm.
- Temperature on the Bridge Deck during initial reading is 44.8 ^{o}F.
- Highest temperature within the period (on the Bridge Deck): 93.4 ^{o}F (07/07/2010).
- Lowest temperature within the period (on the Bridge Deck): -19 ^{o}F (01/24/2011).

Report b-1 Max Earth Pressure vs. Time

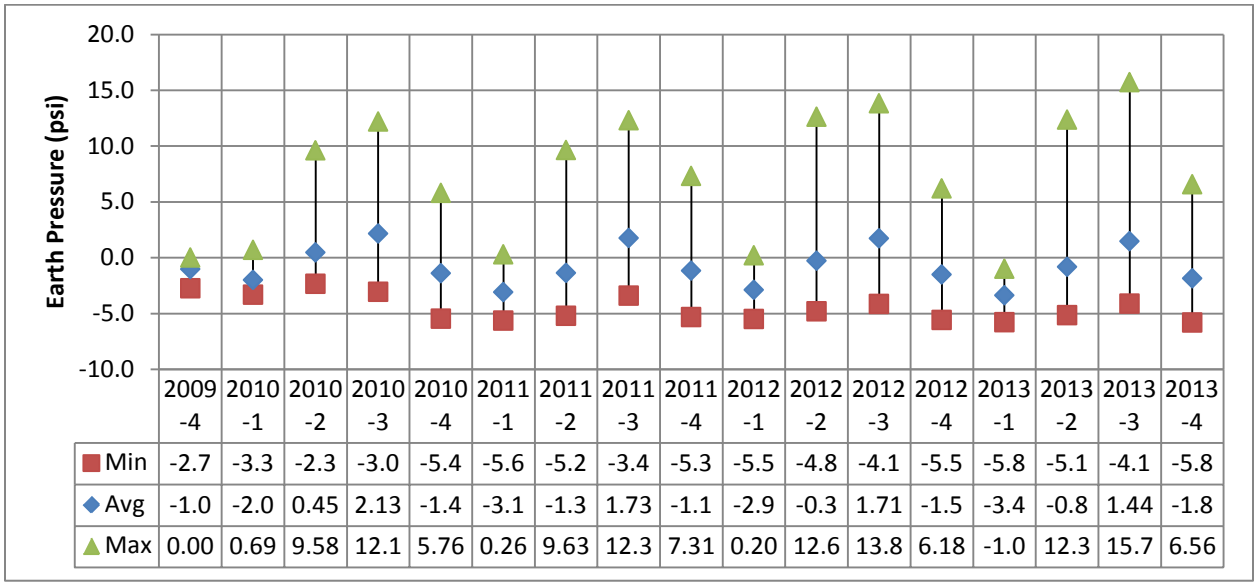

	2009-4	2010-1	2010-2	2010-3	2010-4	2011-1	2011-2	2011-3	2011-4	2012-1	2012-2	2012-3	2012-4	2013-1	2013-2	2013-3	2013-4
Min	-2.7	-3.3	-2.3	-3.0	-5.4	-5.6	-5.2	-3.4	-5.3	-5.5	-4.8	-4.1	-5.5	-5.8	-5.1	-4.1	-5.8
Avg	-1.0	-2.0	0.45	2.13	-1.4	-3.1	-1.3	1.73	-1.1	-2.9	-0.3	1.71	-1.5	-3.4	-0.8	1.44	-1.8
Max	0.00	0.69	9.58	12.1	5.76	0.26	9.63	12.3	7.31	0.20	12.6	13.8	6.18	-1.0	12.3	15.7	6.56

Report b-2 Max Earth Pressure vs. Abutment Displacement

WINTER 2009-SUMMER 2010

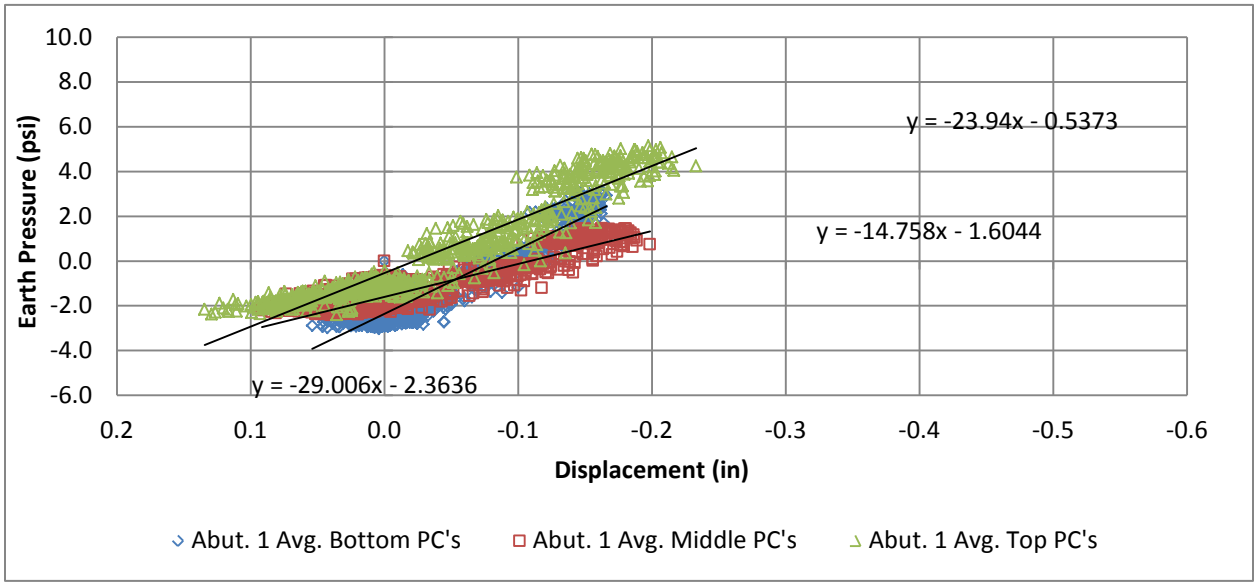

SUMMER 2010-WINTER 2011

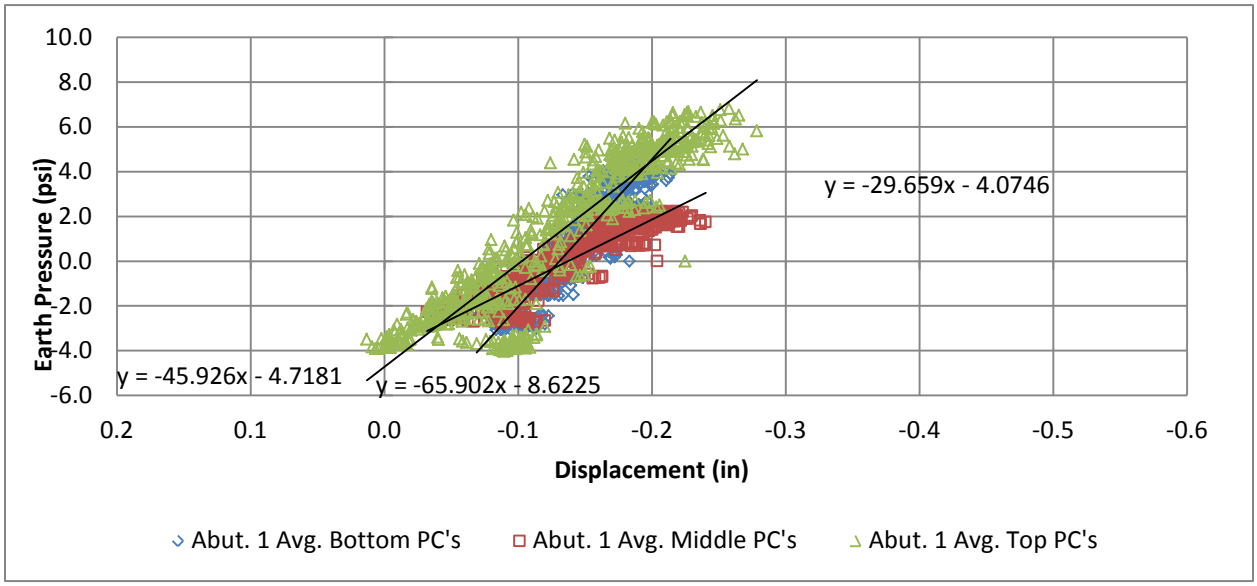

WINTER 2011-SUMMER 2011

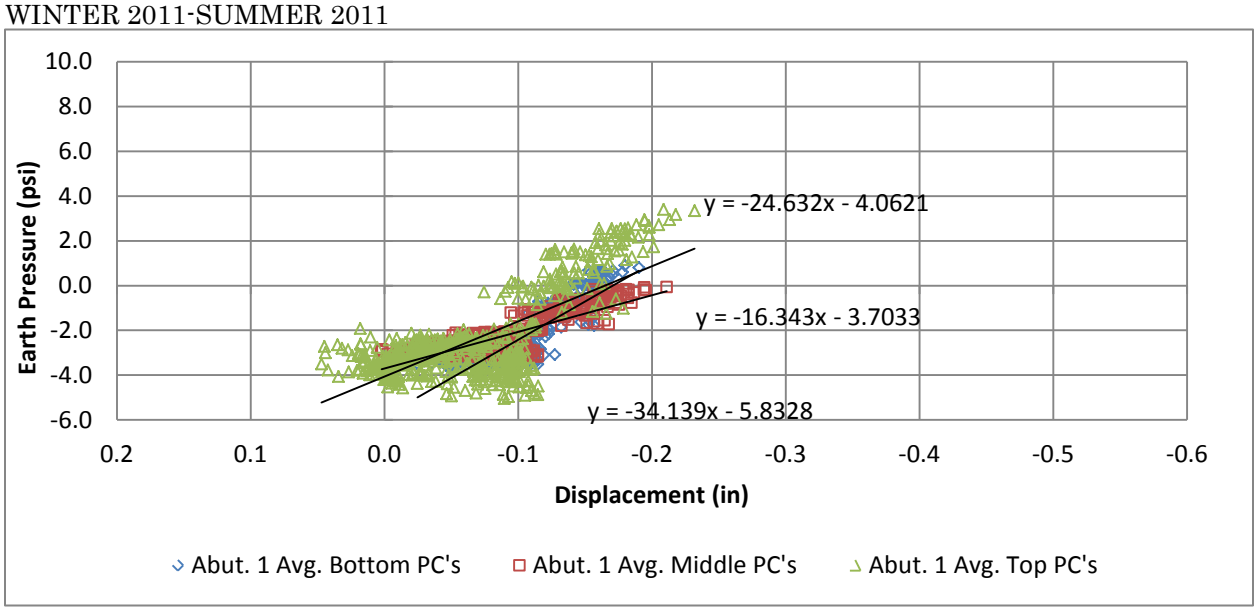

SUMMER 2011-WINTER 2012

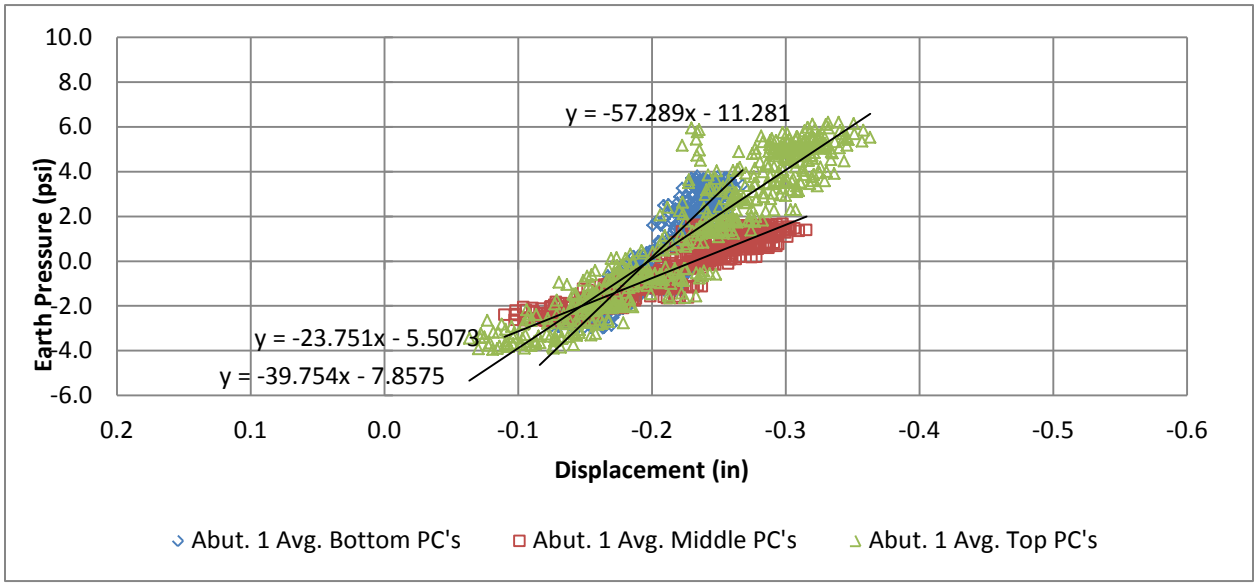

WINTER 2012-SUMMER 2012

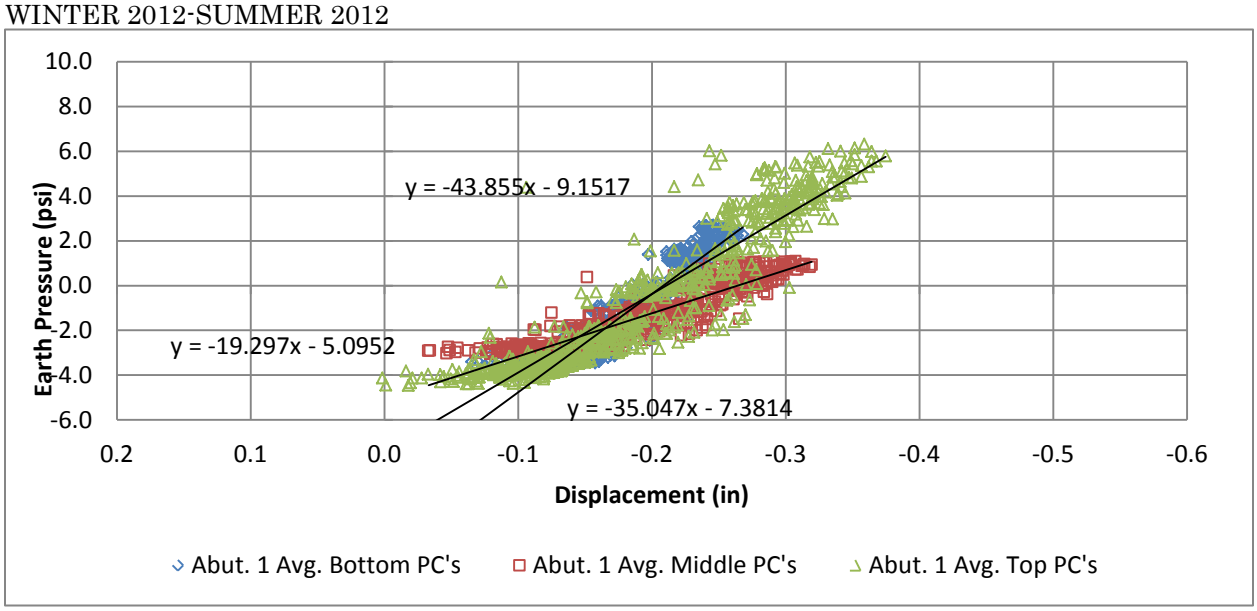

SUMMER 2012-WINTER 2013

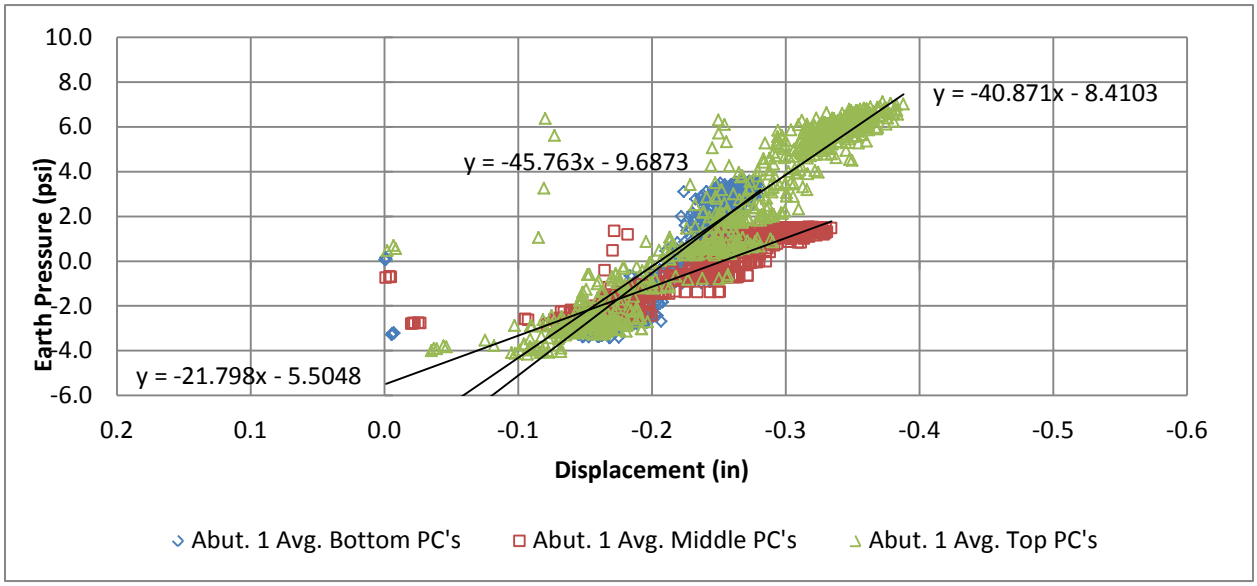

WINTER 2013-SUMMER 2013

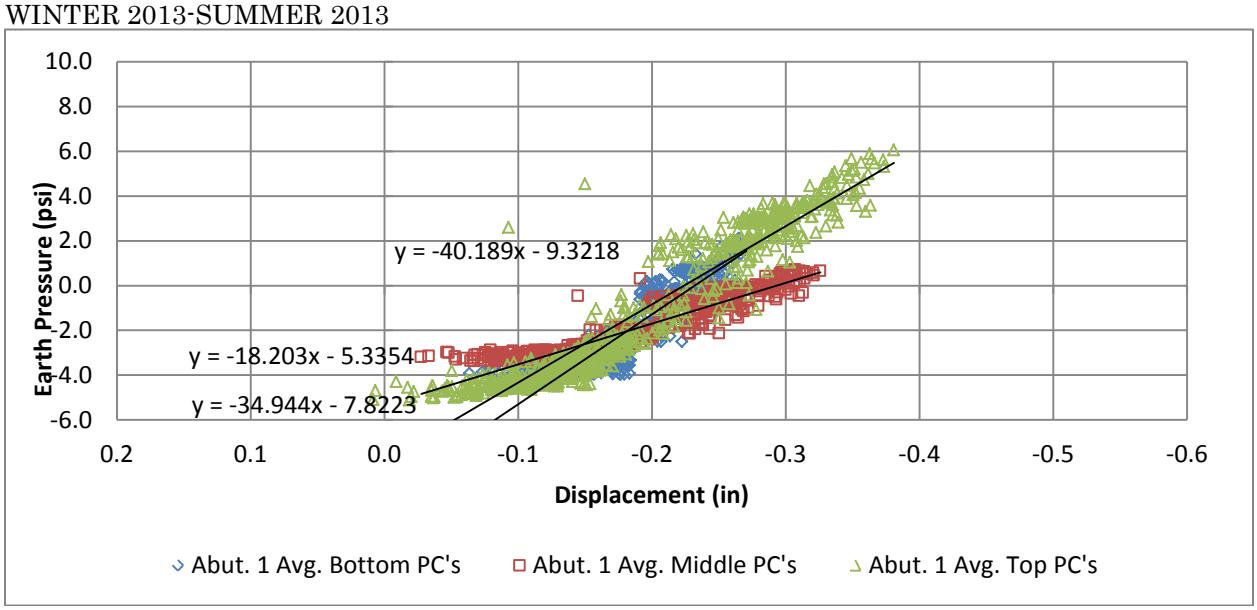

SUMMER 2013-WINTER 2014

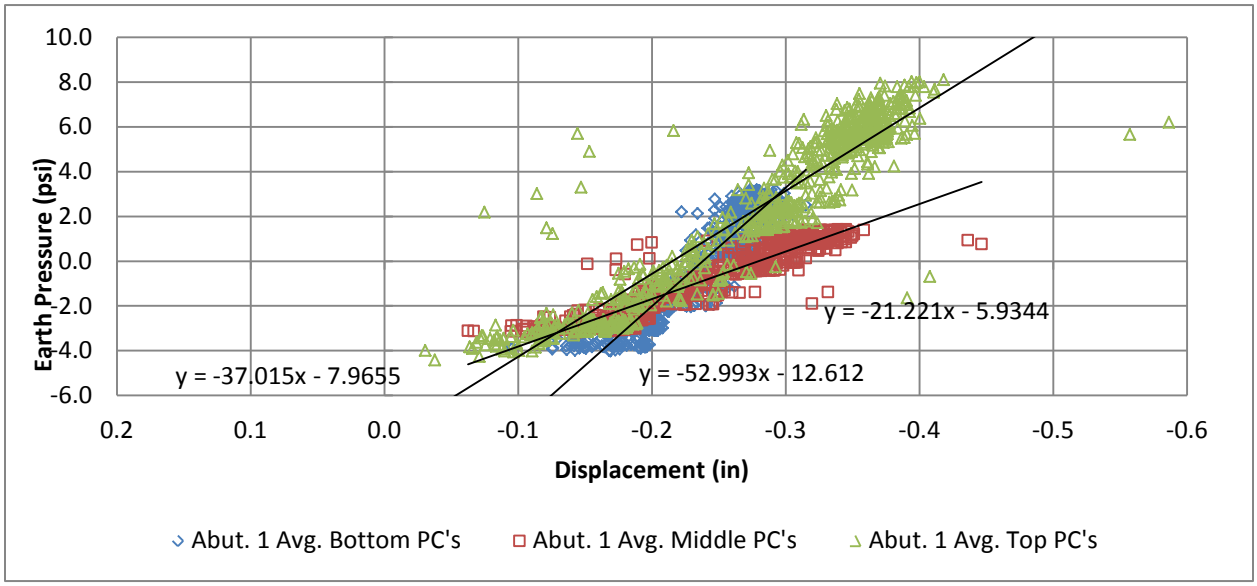

Report b-3 Displacement at the Top of Pile vs. Time

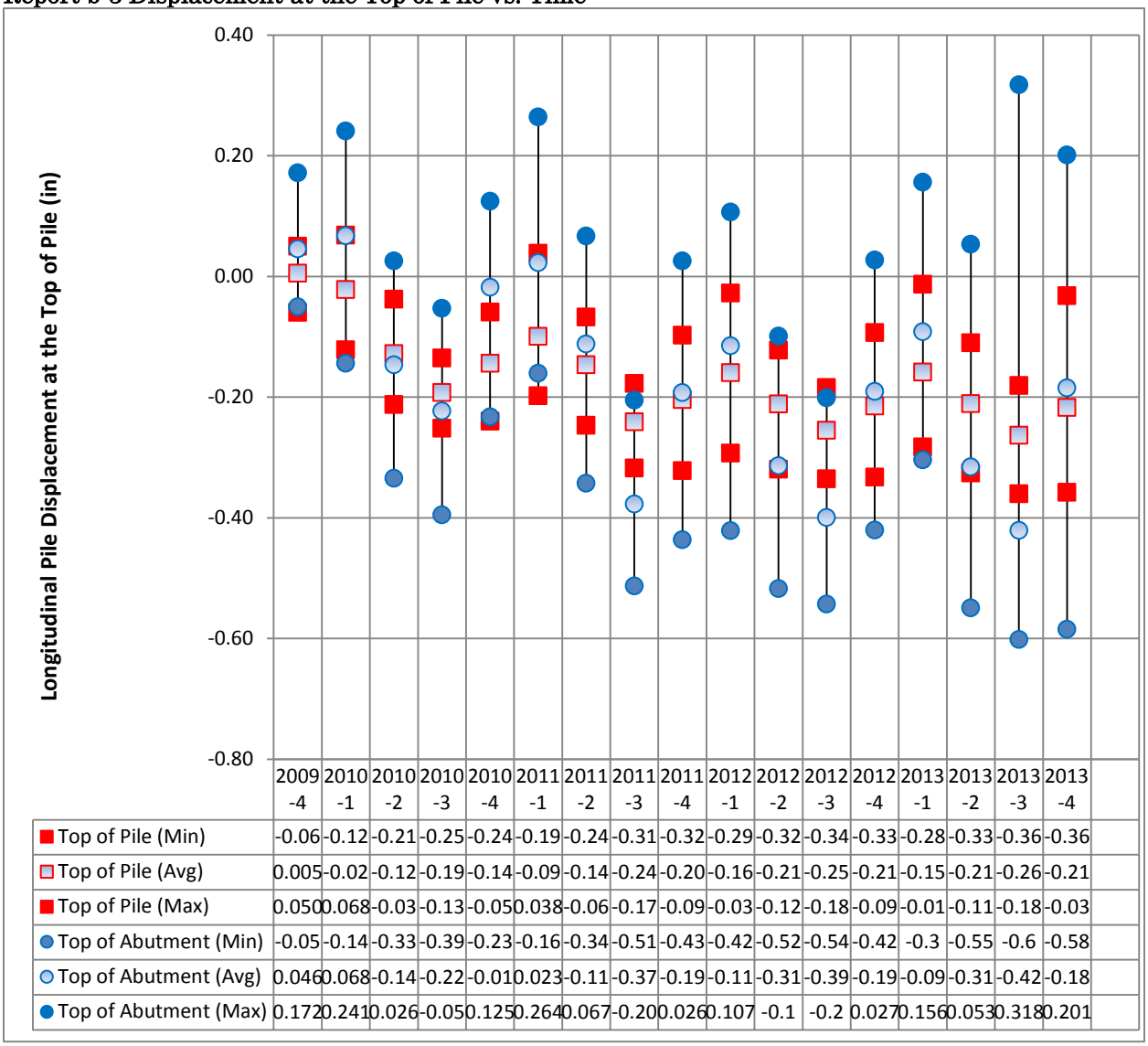

	2009-4	2010-1	2010-2	2010-3	2010-4	2011-1	2011-2	2011-3	2011-4	2012-1	2012-2	2012-3	2012-4	2013-1	2013-2	2013-3	2013-4
Top of Pile (Min)	-0.06	-0.12	-0.21	-0.25	-0.24	-0.19	-0.24	-0.31	-0.32	-0.29	-0.32	-0.34	-0.33	-0.28	-0.33	-0.36	-0.36
Top of Pile (Avg)	0.005	-0.02	-0.12	-0.19	-0.14	-0.09	-0.14	-0.24	-0.20	-0.16	-0.21	-0.25	-0.21	-0.15	-0.21	-0.26	-0.21
Top of Pile (Max)	0.050	0.068	-0.03	-0.13	-0.05	0.038	-0.06	-0.17	-0.09	-0.03	-0.12	-0.18	-0.09	-0.01	-0.11	-0.18	-0.03
Top of Abutment (Min)	-0.05	-0.14	-0.33	-0.39	-0.23	-0.16	-0.34	-0.51	-0.43	-0.42	-0.52	-0.54	-0.42	-0.3	-0.55	-0.6	-0.58
Top of Abutment (Avg)	0.046	0.068	-0.14	-0.22	-0.01	0.023	-0.11	-0.37	-0.19	-0.11	-0.31	-0.39	-0.19	-0.09	-0.31	-0.42	-0.18
Top of Abutment (Max)	0.172	0.241	0.026	-0.05	0.125	0.264	0.067	-0.20	0.026	0.107	-0.1	-0.2	0.027	0.156	0.053	0.318	0.201

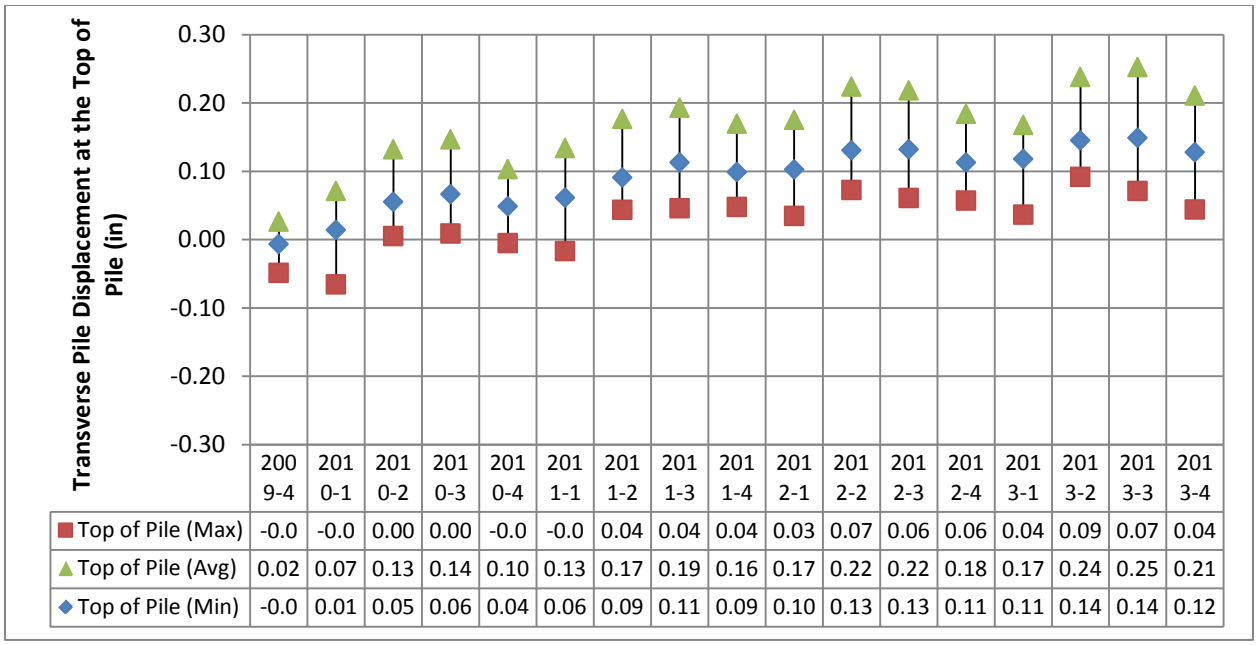

	2009-4	2010-1	2010-2	2010-3	2010-4	2011-1	2011-2	2011-3	2011-4	2012-1	2012-2	2012-3	2012-4	2013-1	2013-2	2013-3	2013-4
Top of Pile (Max)	-0.0	-0.0	0.00	0.00	-0.0	-0.0	0.04	0.04	0.04	0.03	0.07	0.06	0.06	0.04	0.09	0.07	0.04
Top of Pile (Avg)	0.02	0.07	0.13	0.14	0.10	0.13	0.17	0.19	0.16	0.17	0.22	0.22	0.18	0.17	0.24	0.25	0.21
Top of Pile (Min)	-0.0	0.01	0.05	0.06	0.04	0.06	0.09	0.11	0.09	0.10	0.13	0.13	0.11	0.11	0.14	0.14	0.12

Report b-4 Displacement at the Top of Pile vs. Temperature

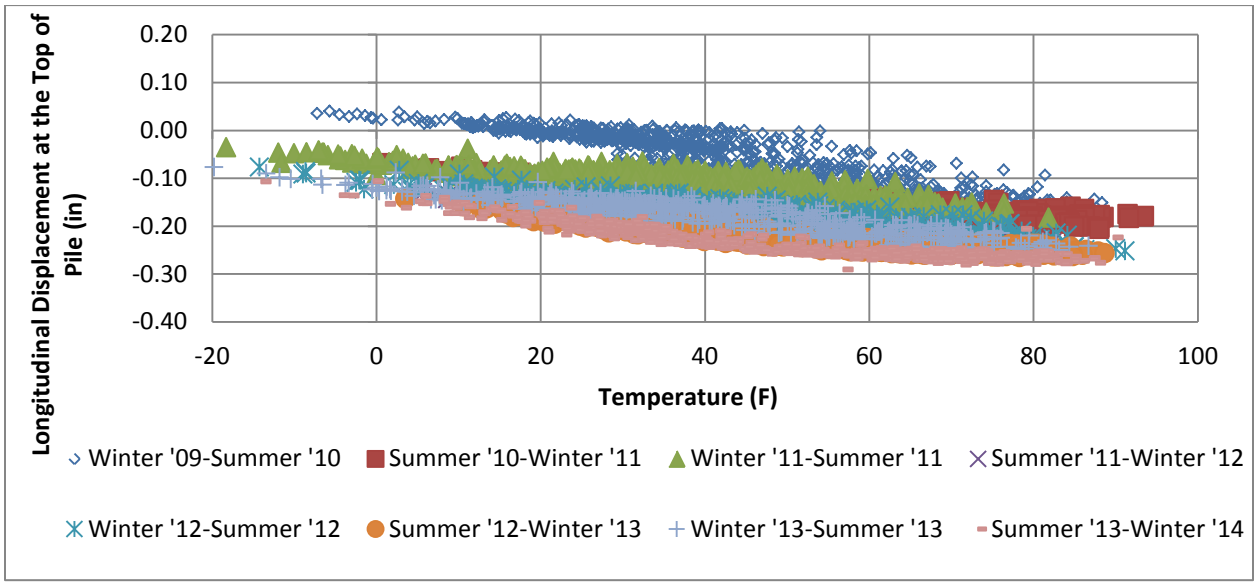

Report b-5 Abutment Rotation vs. Time

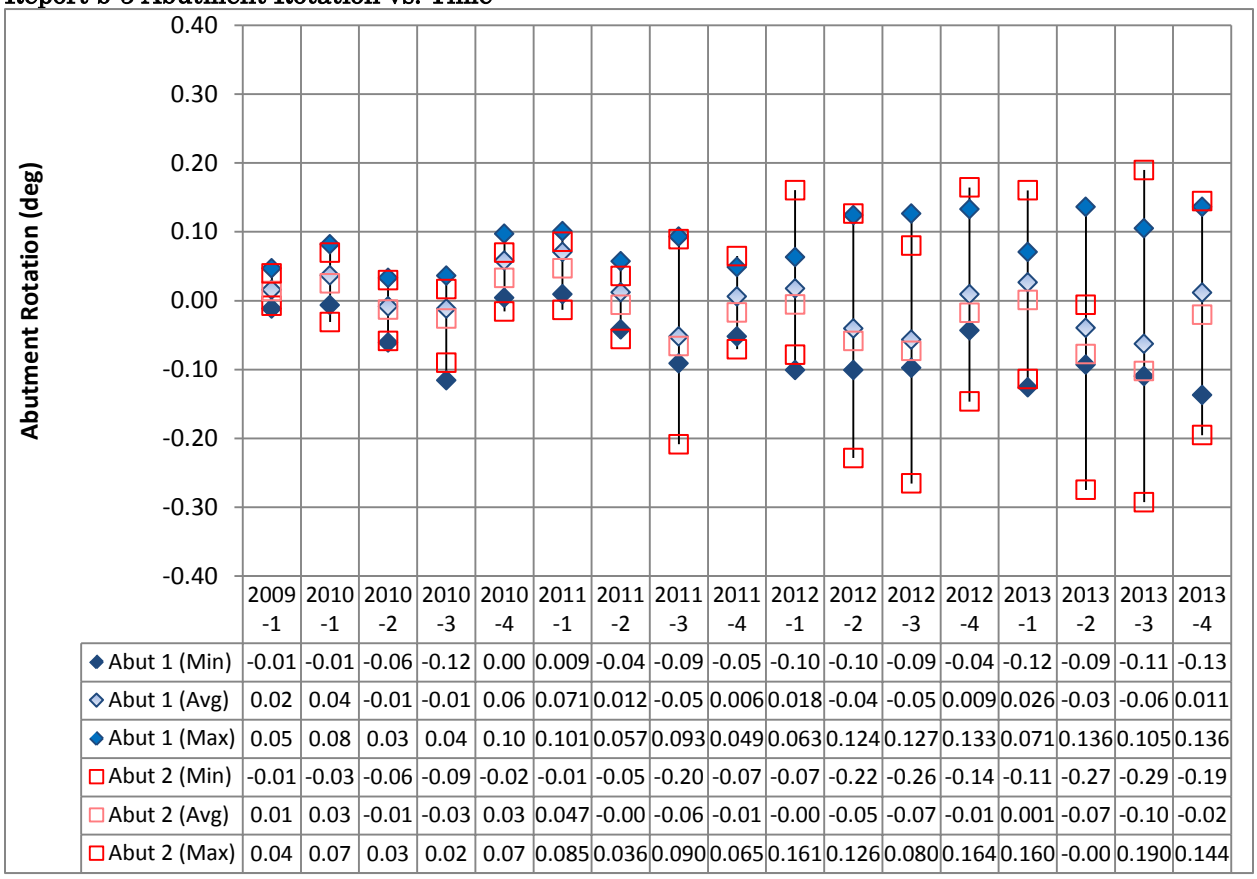

	2009-1	2010-1	2010-2	2010-3	2010-4	2011-1	2011-2	2011-3	2011-4	2012-1	2012-2	2012-3	2012-4	2013-1	2013-2	2013-3	2013-4
Abut 1 (Min)	-0.01	-0.01	-0.06	-0.12	0.00	0.009	-0.04	-0.09	-0.05	-0.10	-0.10	-0.09	-0.04	-0.12	-0.09	-0.11	-0.13
Abut 1 (Avg)	0.02	0.04	-0.01	-0.01	0.06	0.071	0.012	-0.05	0.006	0.018	-0.04	-0.05	0.009	0.026	-0.03	-0.06	0.011
Abut 1 (Max)	0.05	0.08	0.03	0.04	0.10	0.101	0.057	0.093	0.049	0.063	0.124	0.127	0.133	0.071	0.136	0.105	0.136
Abut 2 (Min)	-0.01	-0.03	-0.06	-0.09	-0.02	-0.01	-0.05	-0.20	-0.07	-0.07	-0.22	-0.26	-0.14	-0.11	-0.27	-0.29	-0.19
Abut 2 (Avg)	0.01	0.03	-0.01	-0.03	0.03	0.047	-0.00	-0.06	-0.01	-0.00	-0.05	-0.07	-0.01	0.001	-0.07	-0.10	-0.02
Abut 2 (Max)	0.04	0.07	0.03	0.02	0.07	0.085	0.036	0.090	0.065	0.161	0.126	0.080	0.164	0.160	-0.00	0.190	0.144

Report b-6 Flange Stresses vs. Time

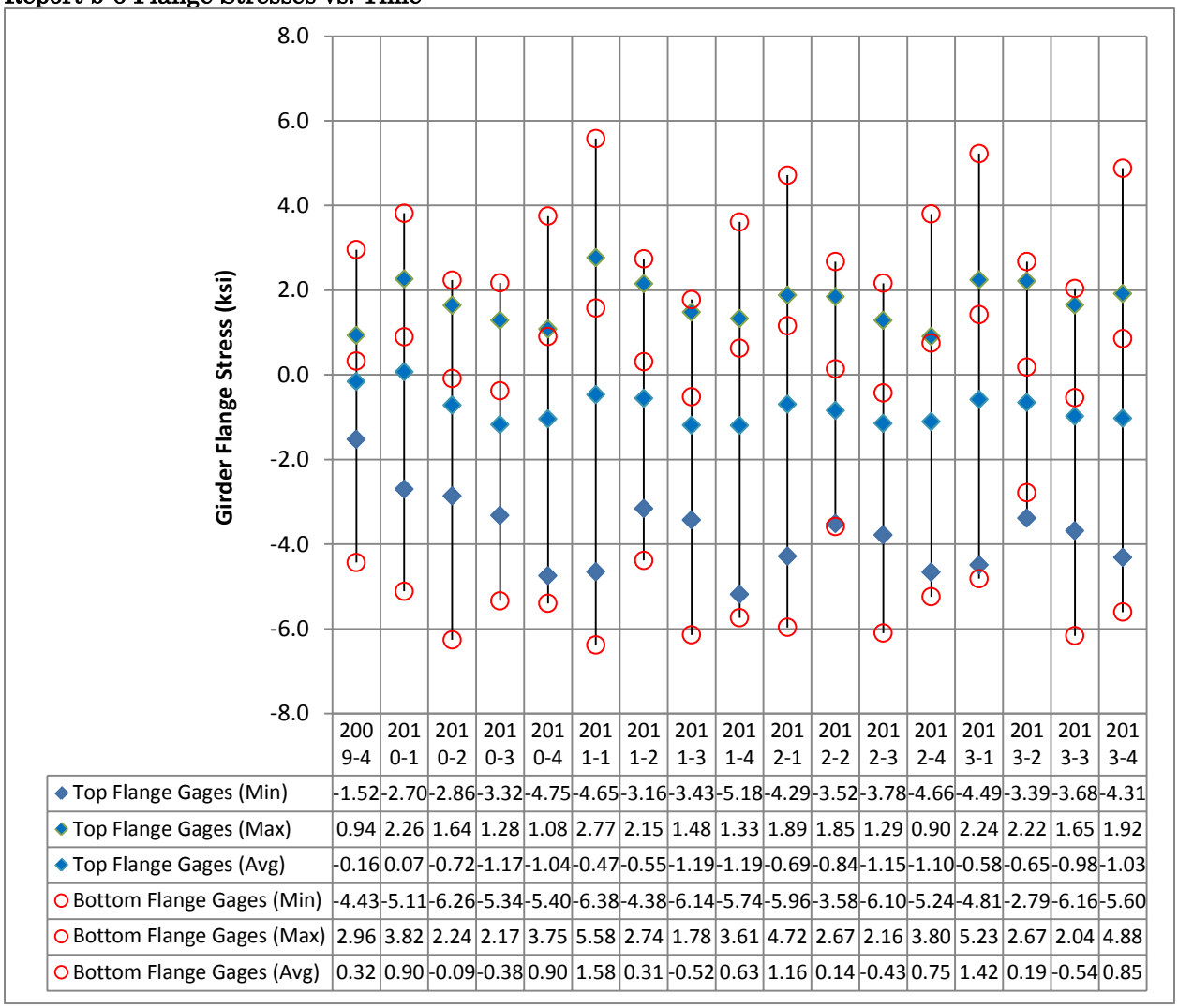

	2009-4	2010-1	2010-2	2010-3	2010-4	2011-1	2011-2	2011-3	2011-4	2012-1	2012-2	2012-3	2012-4	2013-1	2013-2	2013-3	2013-4
Top Flange Gages (Min)	-1.52	-2.70	-2.86	-3.32	-4.75	-4.65	-3.16	-3.43	-5.18	-4.29	-3.52	-3.78	-4.66	-4.49	-3.39	-3.68	-4.31
Top Flange Gages (Max)	0.94	2.26	1.64	1.28	1.08	2.77	2.15	1.48	1.33	1.89	1.85	1.29	0.90	2.24	2.22	1.65	1.92
Top Flange Gages (Avg)	-0.16	0.07	-0.72	-1.17	-1.04	-0.47	-0.55	-1.19	-1.19	-0.69	-0.84	-1.15	-1.10	-0.58	-0.65	-0.98	-1.03
Bottom Flange Gages (Min)	-4.43	-5.11	-6.26	-5.34	-5.40	-6.38	-4.38	-6.14	-5.74	-5.96	-3.58	-6.10	-5.24	-4.81	-2.79	-6.16	-5.60
Bottom Flange Gages (Max)	2.96	3.82	2.24	2.17	3.75	5.58	2.74	1.78	3.61	4.72	2.67	2.16	3.80	5.23	2.67	2.04	4.88
Bottom Flange Gages (Avg)	0.32	0.90	-0.09	-0.38	0.90	1.58	0.31	-0.52	0.63	1.16	0.14	-0.43	0.75	1.42	0.19	-0.54	0.85

Report b-7 Abutment Displacement (Bottom) vs. Abutment Displacement (Top) (2009-2013)

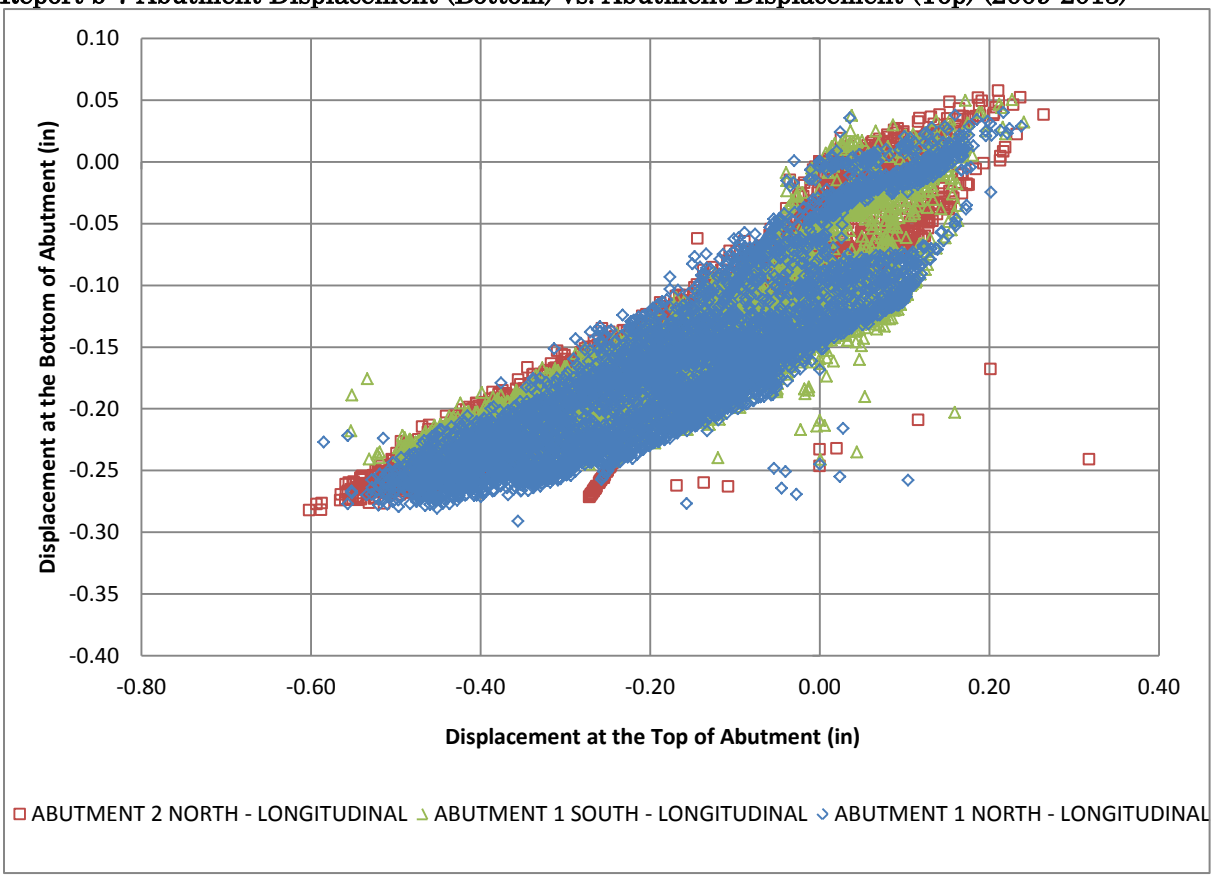

Report b-8 Max Pile Stress at Different Layers vs. Displacement at the Top of Abutment (2009-2013)

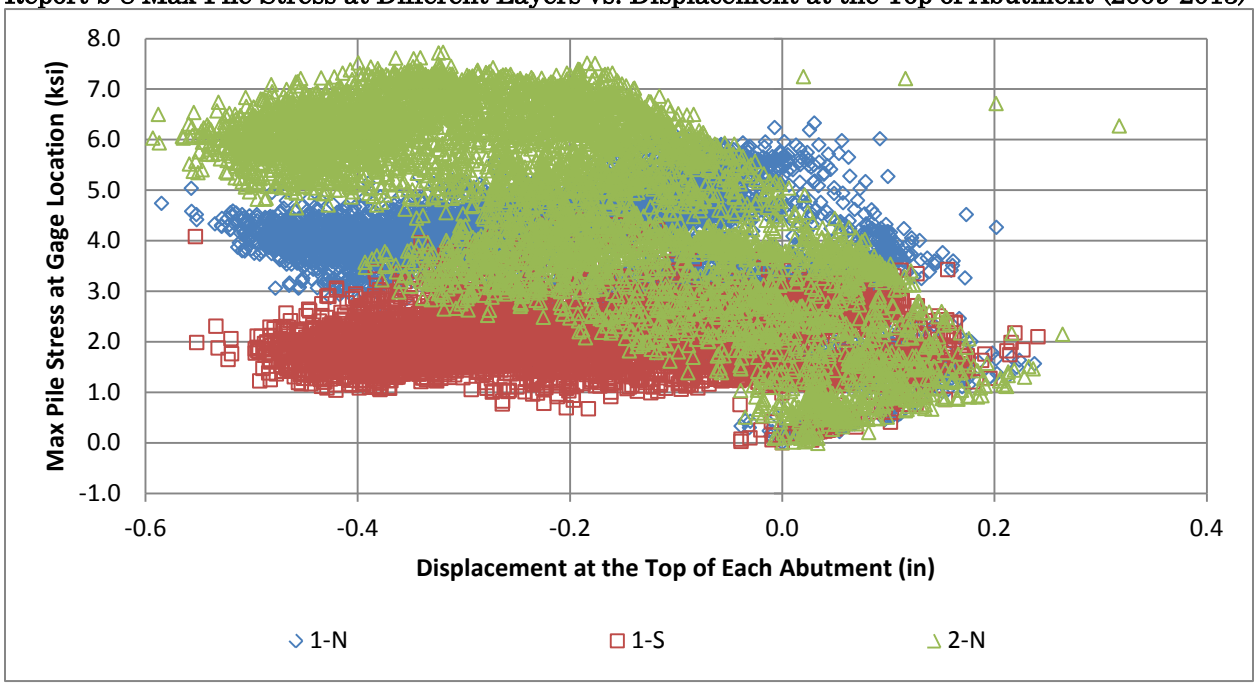

Report b-9 Pile Stress at Gage Location vs. Time

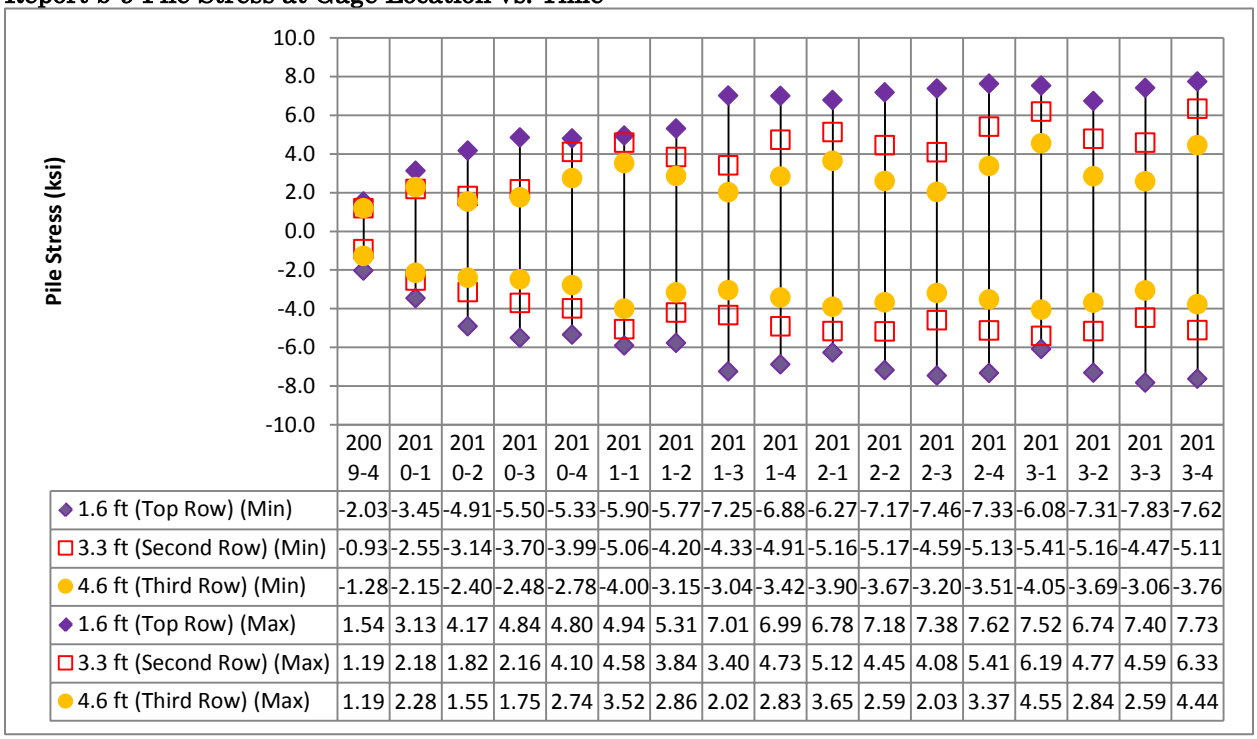

	2009-4	2010-1	2010-2	2010-3	2010-4	2011-1	2011-2	2011-3	2011-4	2012-1	2012-2	2012-3	2012-4	2013-1	2013-2	2013-3	2013-4
1.6 ft (Top Row) (Min)	-2.03	-3.45	-4.91	-5.50	-5.33	-5.90	-5.77	-7.25	-6.88	-6.27	-7.17	-7.46	-7.33	-6.08	-7.31	-7.83	-7.62
3.3 ft (Second Row) (Min)	-0.93	-2.55	-3.14	-3.70	-3.99	-5.06	-4.20	-4.33	-4.91	-5.16	-5.17	-4.59	-5.13	-5.41	-5.16	-4.47	-5.11
4.6 ft (Third Row) (Min)	-1.28	-2.15	-2.40	-2.48	-2.78	-4.00	-3.15	-3.04	-3.42	-3.90	-3.67	-3.20	-3.51	-4.05	-3.69	-3.06	-3.76
1.6 ft (Top Row) (Max)	1.54	3.13	4.17	4.84	4.80	4.94	5.31	7.01	6.99	6.78	7.18	7.38	7.62	7.52	6.74	7.40	7.73
3.3 ft (Second Row) (Max)	1.19	2.18	1.82	2.16	4.10	4.58	3.84	3.40	4.73	5.12	4.45	4.08	5.41	6.19	4.77	4.59	6.33
4.6 ft (Third Row) (Max)	1.19	2.28	1.55	1.75	2.74	3.52	2.86	2.02	2.83	3.65	2.59	2.03	3.37	4.55	2.84	2.59	4.44

Report b-10 Pile Displacement vs. Depth vs. Cap Displacement (2009-2013)

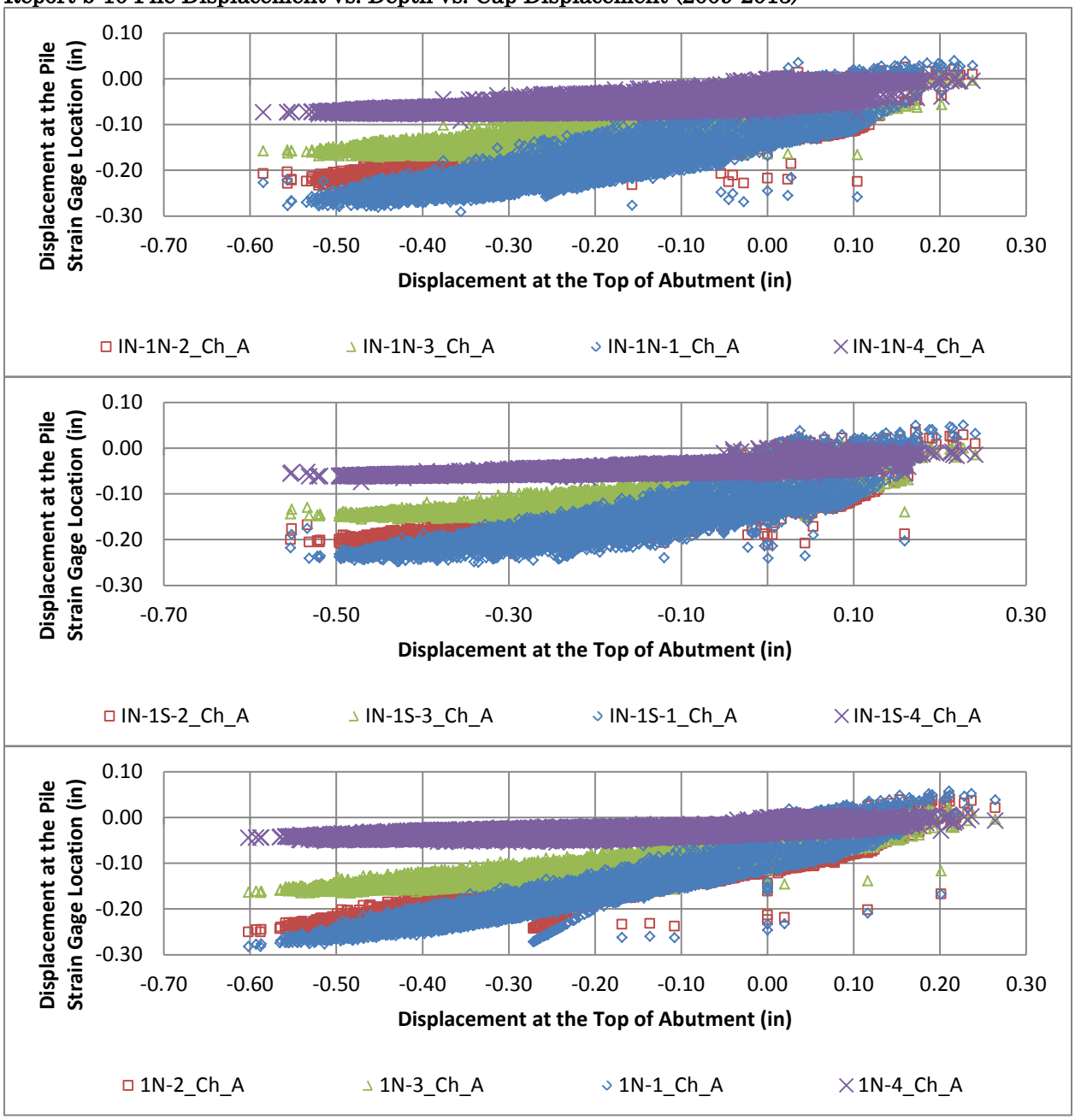

c) Long Term Monitoring of the Stockbridge Bridge

DATES: 11-02-2009/12-31-2013

NOTES:

- All values are relative to the readings from 11-02-2009 at 6.00 pm.
- Temperature on the Bridge Deck during initial reading is 45.4 ^{o}F.
- Highest temperature within the period (on the Bridge Deck): 95.0^{o}F (07/07/2010).
- Lowest temperature within the period (on the Bridge Deck): -16.5^{o}F (01/24/2011).

Report c-1 Max Earth Pressure vs. Time

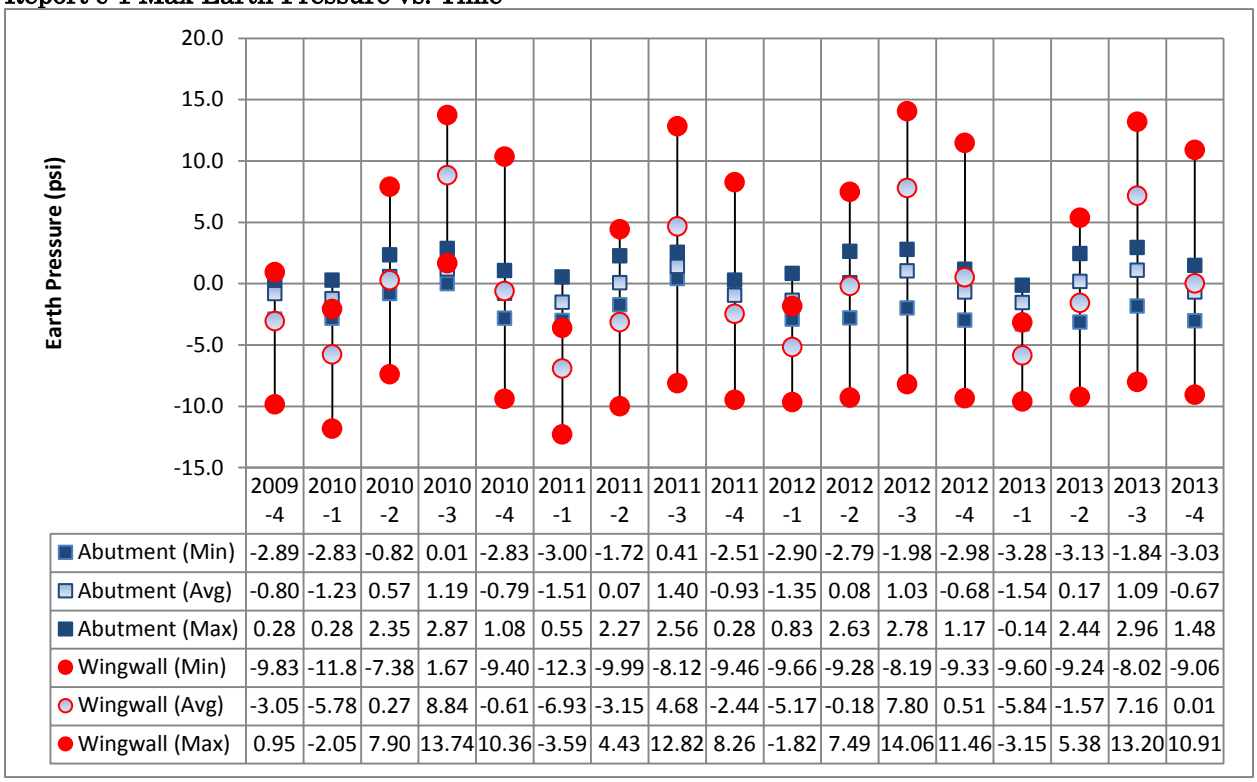

	2009-4	2010-1	2010-2	2010-3	2010-4	2011-1	2011-2	2011-3	2011-4	2012-1	2012-2	2012-3	2012-4	2013-1	2013-2	2013-3	2013-4
Abutment (Min)	-2.89	-2.83	-0.82	0.01	-2.83	-3.00	-1.72	0.41	-2.51	-2.90	-2.79	-1.98	-2.98	-3.28	-3.13	-1.84	-3.03
Abutment (Avg)	-0.80	-1.23	0.57	1.19	-0.79	-1.51	0.07	1.40	-0.93	-1.35	0.08	1.03	-0.68	-1.54	0.17	1.09	-0.67
Abutment (Max)	0.28	0.28	2.35	2.87	1.08	0.55	2.27	2.56	0.28	0.83	2.63	2.78	1.17	-0.14	2.44	2.96	1.48
Wingwall (Min)	-9.83	-11.8	-7.38	1.67	-9.40	-12.3	-9.99	-8.12	-9.46	-9.66	-9.28	-8.19	-9.33	-9.60	-9.24	-8.02	-9.06
Wingwall (Avg)	-3.05	-5.78	0.27	8.84	-0.61	-6.93	-3.15	4.68	-2.44	-5.17	-0.18	7.80	0.51	-5.84	-1.57	7.16	0.01
Wingwall (Max)	0.95	-2.05	7.90	13.74	10.36	-3.59	4.43	12.82	8.26	-1.82	7.49	14.06	11.46	-3.15	5.38	13.20	10.91

Report c-2 Max Earth Pressure vs. Abutment Displacement

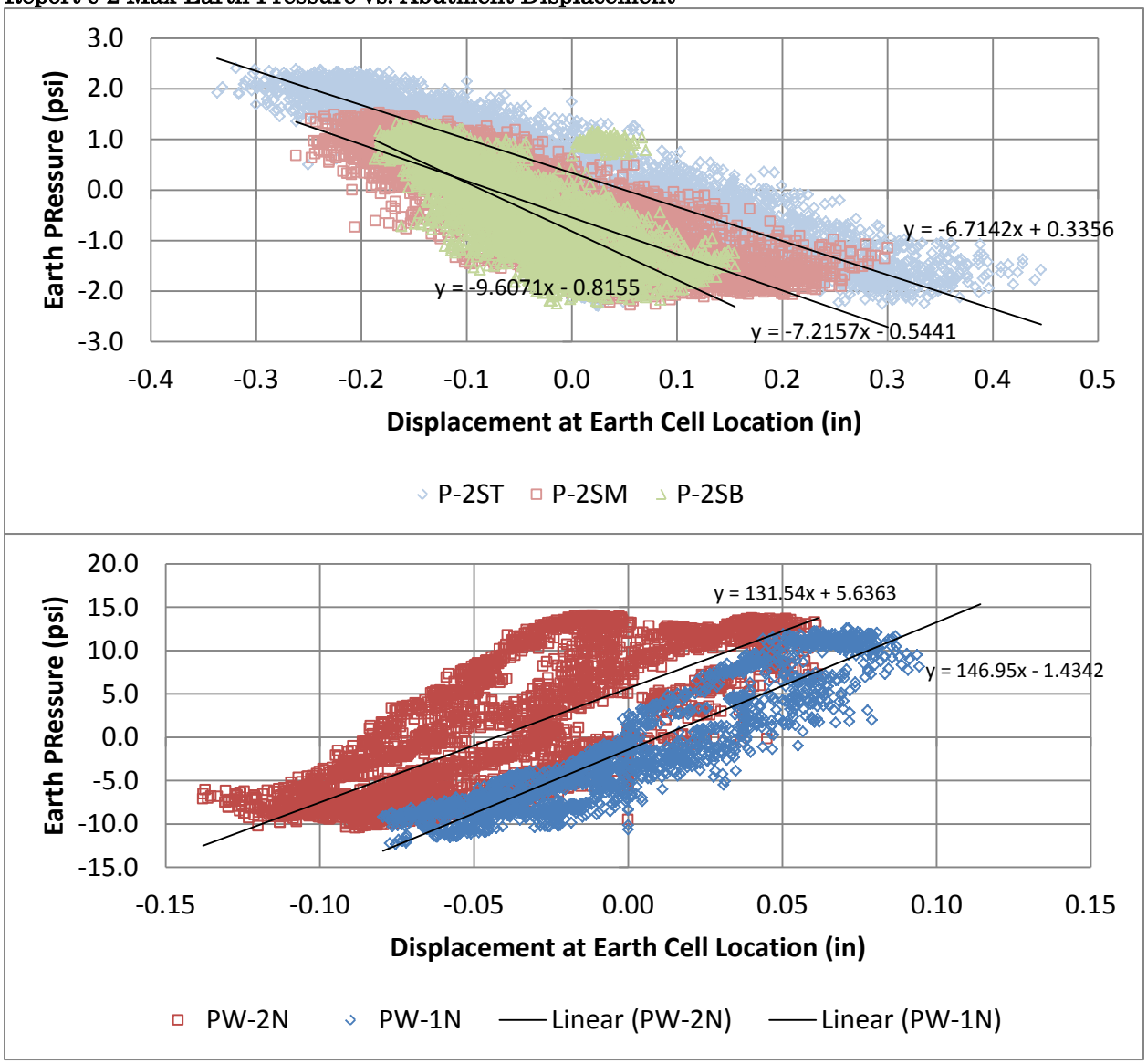

Report c-3 Displacement at the Top of Pile and Abutment vs. Time

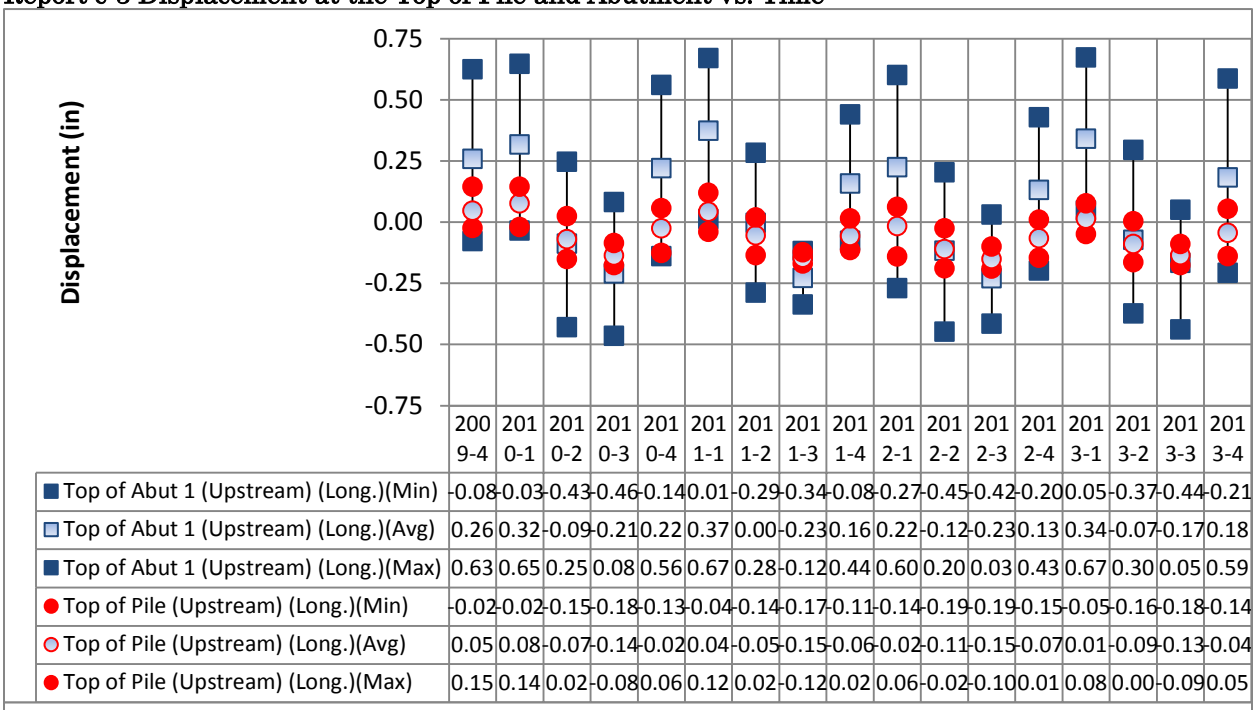

	2009-4	2010-1	2010-2	2010-3	2010-4	2011-1	2011-2	2011-3	2011-4	2012-1	2012-2	2012-3	2012-4	2013-1	2013-2	2013-3	2013-4
Top of Abut 1 (Upstream) (Long.)(Min)	-0.08	-0.03	-0.43	-0.46	-0.14	0.01	-0.29	-0.34	-0.08	-0.27	-0.45	-0.42	-0.20	0.05	-0.37	-0.44	-0.21
Top of Abut 1 (Upstream) (Long.)(Avg)	0.26	0.32	-0.09	-0.21	0.22	0.37	0.00	-0.23	0.16	0.22	-0.12	-0.23	0.13	0.34	-0.07	-0.17	0.18
Top of Abut 1 (Upstream) (Long.)(Max)	0.63	0.65	0.25	0.08	0.56	0.67	0.28	-0.12	0.44	0.60	0.20	0.03	0.43	0.67	0.30	0.05	0.59
Top of Pile (Upstream) (Long.)(Min)	-0.02	-0.02	-0.15	-0.18	-0.13	-0.04	-0.14	-0.17	-0.11	-0.14	-0.19	-0.19	-0.15	-0.05	-0.16	-0.18	-0.14
Top of Pile (Upstream) (Long.)(Avg)	0.05	0.08	-0.07	-0.14	-0.02	0.04	-0.05	-0.15	-0.06	-0.02	-0.11	-0.15	-0.07	0.01	-0.09	-0.13	-0.04
Top of Pile (Upstream) (Long.)(Max)	0.15	0.14	0.02	-0.08	0.06	0.12	0.02	-0.12	0.02	0.06	-0.02	-0.10	0.01	0.08	0.00	-0.09	0.05

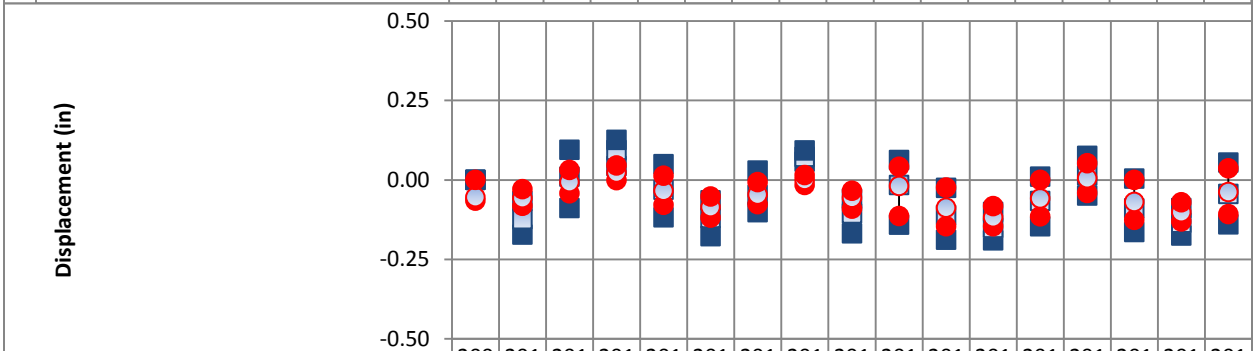

	2009-4	2010-1	2010-2	2010-3	2010-4	2011-1	2011-2	2011-3	2011-4	2012-1	2012-2	2012-3	2012-4	2013-1	2013-2	2013-3	2013-4
Top of Abut 1 (Upstream) (Trans.)(Min)	0.00	-0.17	-0.09	0.04	-0.12	-0.18	-0.10	0.06	-0.17	-0.14	-0.19	-0.19	-0.15	-0.05	-0.16	-0.18	-0.14
Top of Abut 1 (Upstream) (Trans.)(Avg)	0.00	-0.12	0.01	0.09	-0.03	-0.12	-0.05	0.07	-0.11	-0.02	-0.11	-0.15	-0.07	0.01	-0.09	-0.13	-0.04
Top of Abut 1 (Upstream) (Trans.)(Max)	0.00	-0.07	0.09	0.13	0.05	-0.06	0.03	0.09	-0.06	0.06	-0.02	-0.10	0.01	0.08	0.00	-0.09	0.05
Top of Pile (Upstream) (Trans.)(Min)	-0.07	-0.08	-0.04	0.00	-0.08	-0.12	-0.08	-0.02	-0.09	-0.11	-0.15	-0.15	-0.12	-0.04	-0.13	-0.13	-0.11
Top of Pile (Upstream) (Trans.)(Avg)	-0.05	-0.06	-0.01	0.02	-0.03	-0.08	-0.05	0.00	-0.06	-0.02	-0.09	-0.12	-0.06	0.01	-0.07	-0.10	-0.04
Top of Pile (Upstream) (Trans.)(Max)	0.00	-0.03	0.03	0.05	0.01	-0.05	-0.01	0.02	-0.03	0.04	-0.02	-0.08	0.00	0.05	0.00	-0.07	0.04

Report c-4 Displacement at the Top of Pile vs. Temperature (2009-2013)

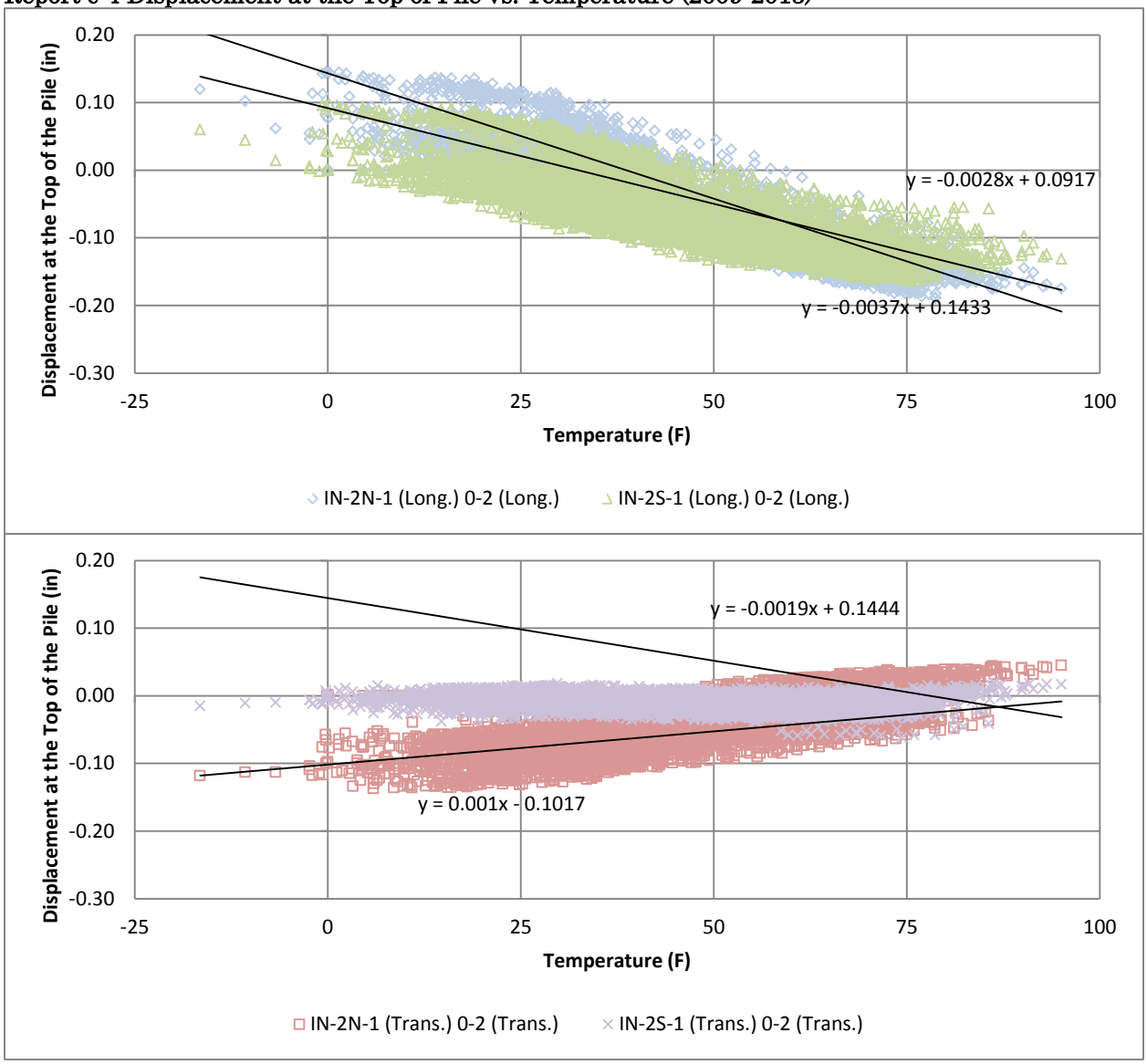

Report c-5Abutment Rotation vs. Time

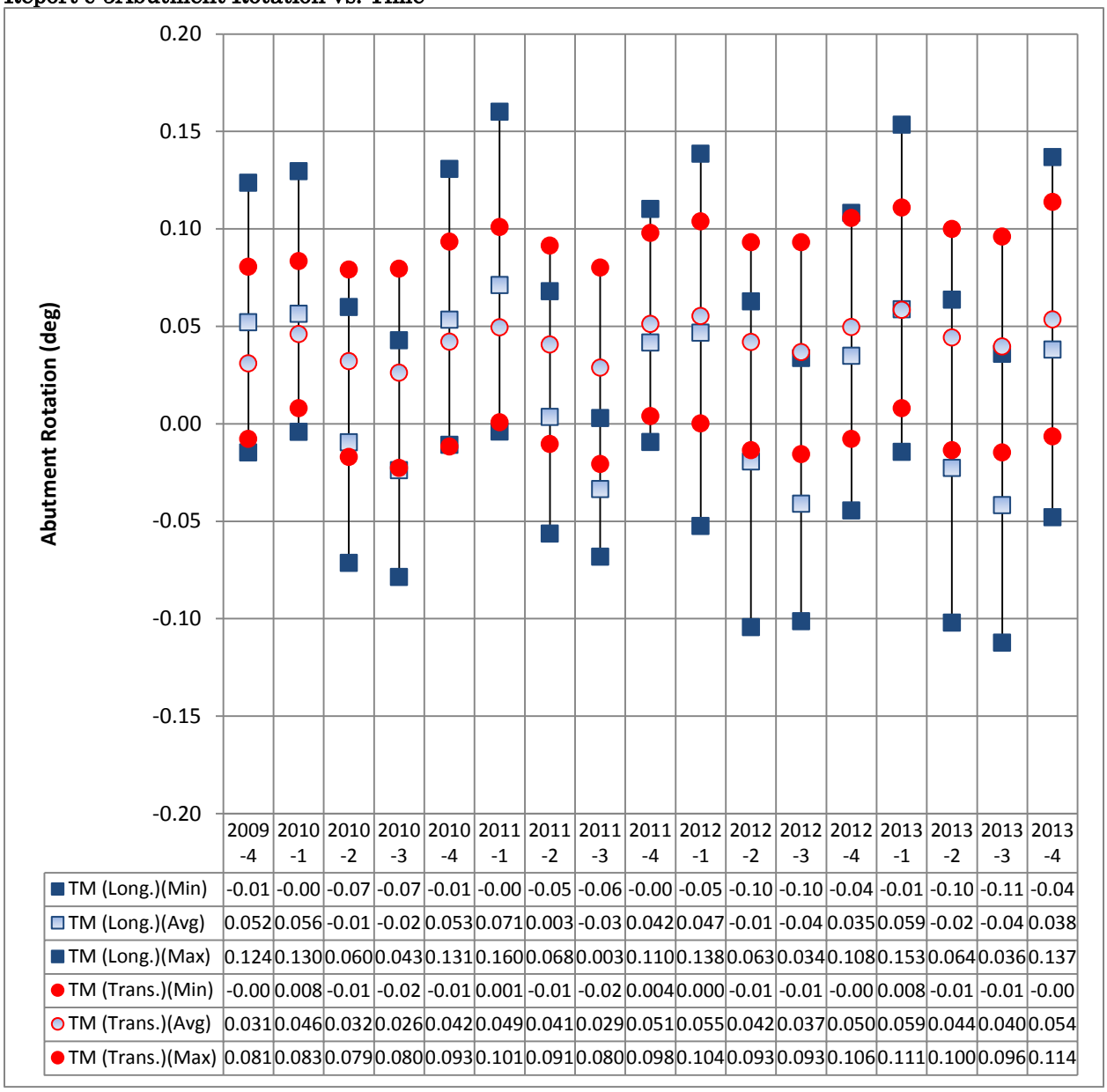

	2009 -4	2010 -1	2010 -2	2010 -3	2010 -4	2011 -1	2011 -2	2011 -3	2011 -4	2012 -1	2012 -2	2012 -3	2012 -4	2013 -1	2013 -2	2013 -3	2013 -4
TM (Long.)(Min)	-0.01	-0.00	-0.07	-0.07	-0.01	-0.00	-0.05	-0.06	-0.00	-0.05	-0.10	-0.10	-0.04	-0.01	-0.10	-0.11	-0.04
TM (Long.)(Avg)	0.052	0.056	-0.01	-0.02	0.053	0.071	0.003	-0.03	0.042	0.047	-0.01	-0.04	0.035	0.059	-0.02	-0.04	0.038
TM (Long.)(Max)	0.124	0.130	0.060	0.043	0.131	0.160	0.068	0.003	0.110	0.138	0.063	0.034	0.108	0.153	0.064	0.036	0.137
TM (Trans.)(Min)	-0.00	0.008	-0.01	-0.02	-0.01	0.001	-0.01	-0.02	0.004	0.000	-0.01	-0.01	-0.00	0.008	-0.01	-0.01	-0.00
TM (Trans.)(Avg)	0.031	0.046	0.032	0.026	0.042	0.049	0.041	0.029	0.051	0.055	0.042	0.037	0.050	0.059	0.044	0.040	0.054
TM (Trans.)(Max)	0.081	0.083	0.079	0.080	0.093	0.101	0.091	0.080	0.098	0.104	0.093	0.093	0.106	0.111	0.100	0.096	0.114

Report c-6 Flange Stresses vs. Time

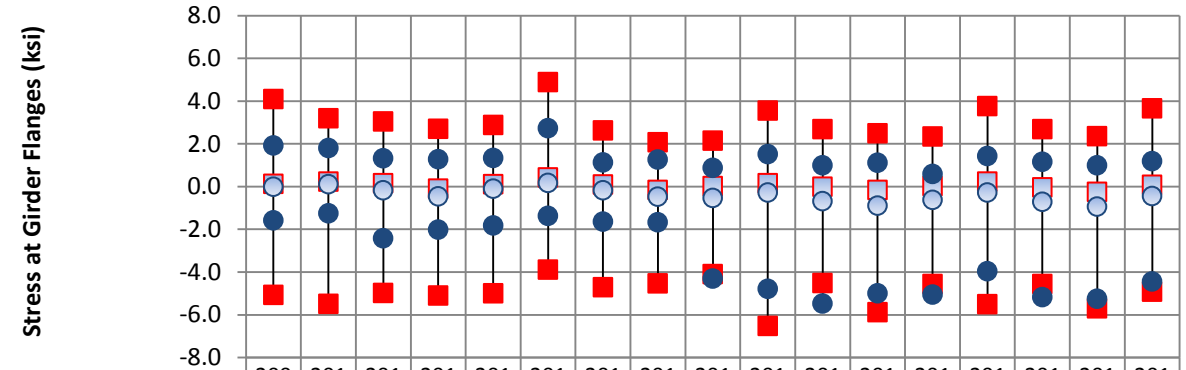

	2009-4	2010-1	2010-2	2010-3	2010-4	2011-1	2011-2	2011-3	2011-4	2012-1	2012-2	2012-3	2012-4	2013-1	2013-2	2013-3	2013-4
Bottom Flange (Min)	-5.1	-5.5	-5.0	-5.1	-5.0	-3.9	-4.7	-4.5	-4.1	-6.5	-4.5	-5.9	-4.6	-5.5	-4.6	-5.7	-4.9
Bottom Flange (Avg)	0.1	0.2	0.2	-0.1	0.1	0.4	0.1	-0.2	0.0	0.2	0.0	-0.2	0.0	0.2	0.0	-0.2	0.1
Bottom Flange (Max)	4.1	3.2	3.0	2.7	2.9	4.9	2.6	2.1	2.1	3.6	2.7	2.5	2.3	3.8	2.7	2.4	3.7
Top Flange (Min)	-1.6	-1.3	-2.4	-2.0	-1.8	-1.4	-1.6	-1.7	-4.3	-4.8	-5.5	-5.0	-5.1	-4.0	-5.2	-5.2	-4.4
Top Flange (Avg)	0.0	0.1	-0.2	-0.5	-0.1	0.2	-0.2	-0.5	-0.5	-0.3	-0.7	-0.9	-0.6	-0.3	-0.7	-0.9	-0.4
Top Flange (Max)	1.9	1.8	1.3	1.3	1.3	2.7	1.1	1.3	0.9	1.5	1.0	1.1	0.6	1.4	1.2	1.0	1.2

Report c-7 Abutment Displacement (Bottom) vs. Abutment Displacement (Top)

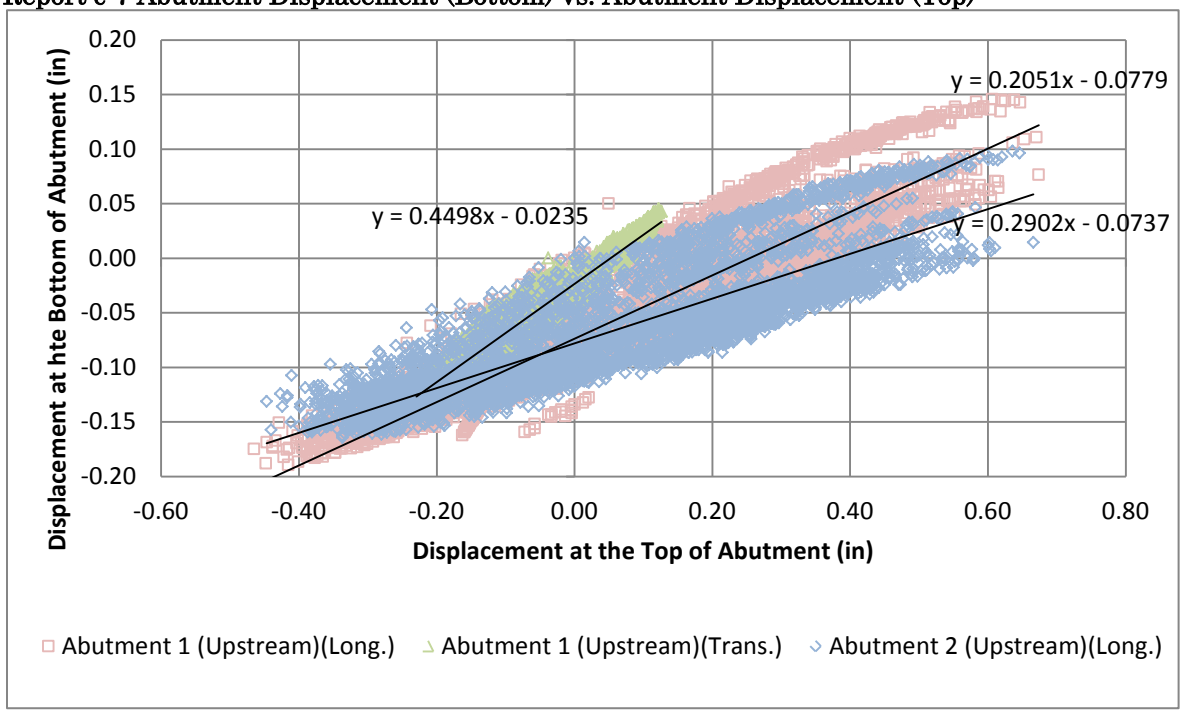

Report c-8 Max Pile Stress at Different Layers vs. Displacement at the Top of Abutment

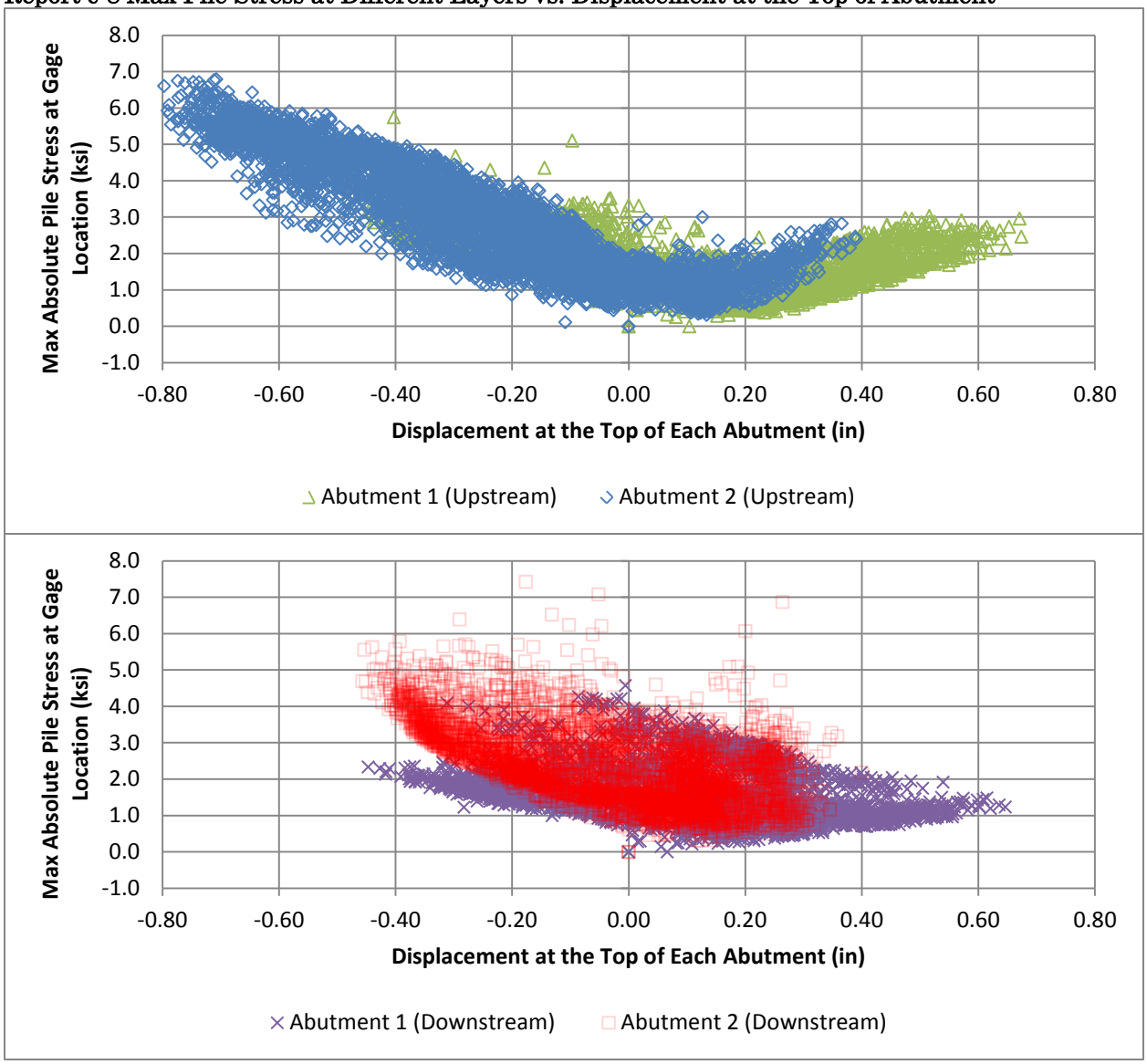

Report c-9 Pile Stress at Gage Location vs. Time

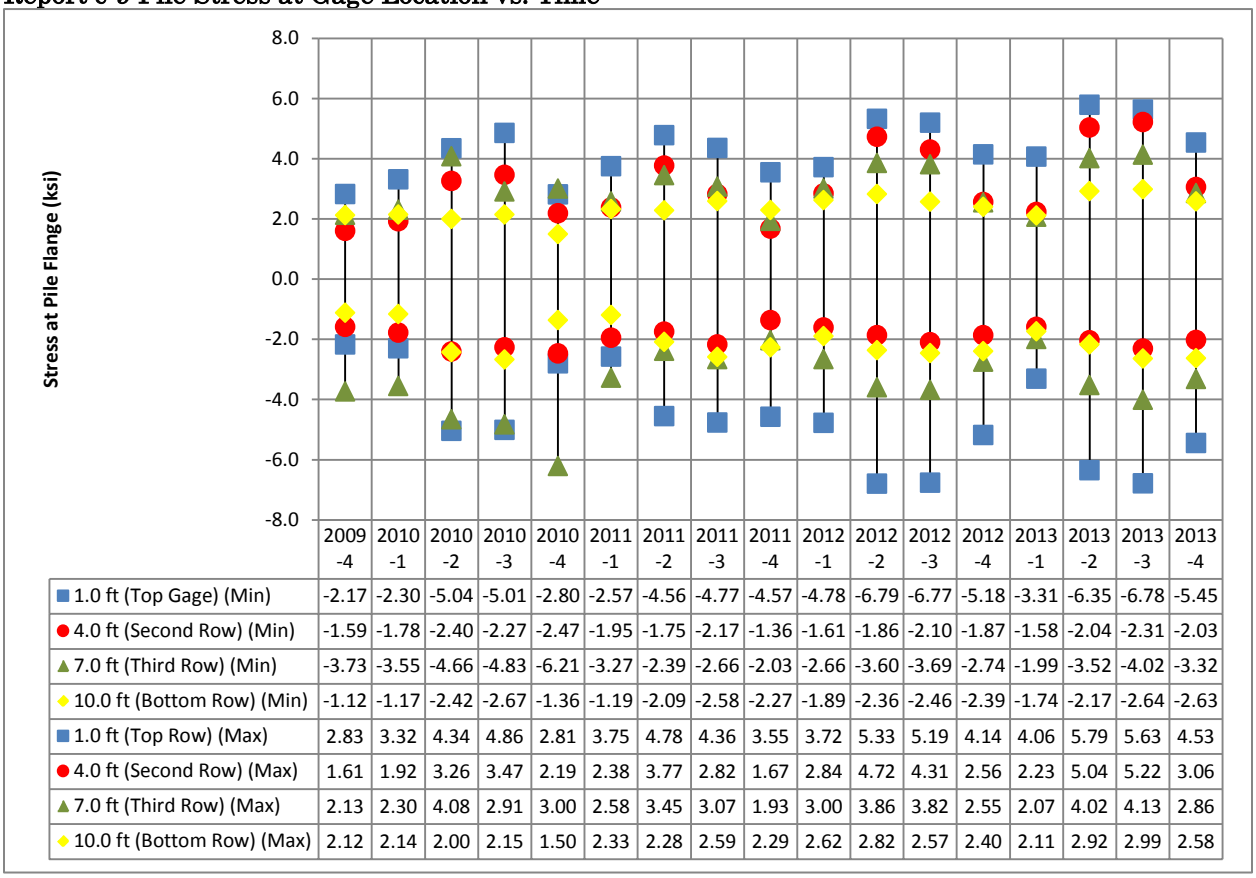

	2009 -4	2010 -1	2010 -2	2010 -3	2010 -4	2011 -1	2011 -2	2011 -3	2011 -4	2012 -1	2012 -2	2012 -3	2012 -4	2013 -1	2013 -2	2013 -3	2013 -4
1.0 ft (Top Gage) (Min)	-2.17	-2.30	-5.04	-5.01	-2.80	-2.57	-4.56	-4.77	-4.57	-4.78	-6.79	-6.77	-5.18	-3.31	-6.35	-6.78	-5.45
4.0 ft (Second Row) (Min)	-1.59	-1.78	-2.40	-2.27	-2.47	-1.95	-1.75	-2.17	-1.36	-1.61	-1.86	-2.10	-1.87	-1.58	-2.04	-2.31	-2.03
7.0 ft (Third Row) (Min)	-3.73	-3.55	-4.66	-4.83	-6.21	-3.27	-2.39	-2.66	-2.03	-2.66	-3.60	-3.69	-2.74	-1.99	-3.52	-4.02	-3.32
10.0 ft (Bottom Row) (Min)	-1.12	-1.17	-2.42	-2.67	-1.36	-1.19	-2.09	-2.58	-2.27	-1.89	-2.36	-2.46	-2.39	-1.74	-2.17	-2.64	-2.63
1.0 ft (Top Row) (Max)	2.83	3.32	4.34	4.86	2.81	3.75	4.78	4.36	3.55	3.72	5.33	5.19	4.14	4.06	5.79	5.63	4.53
4.0 ft (Second Row) (Max)	1.61	1.92	3.26	3.47	2.19	2.38	3.77	2.82	1.67	2.84	4.72	4.31	2.56	2.23	5.04	5.22	3.06
7.0 ft (Third Row) (Max)	2.13	2.30	4.08	2.91	3.00	2.58	3.45	3.07	1.93	3.00	3.86	3.82	2.55	2.07	4.02	4.13	2.86
10.0 ft (Bottom Row) (Max)	2.12	2.14	2.00	2.15	1.50	2.33	2.28	2.59	2.29	2.62	2.82	2.57	2.40	2.11	2.92	2.99	2.58

Report c-10 Pile Displacement vs. Depth vs. Cap Displacement

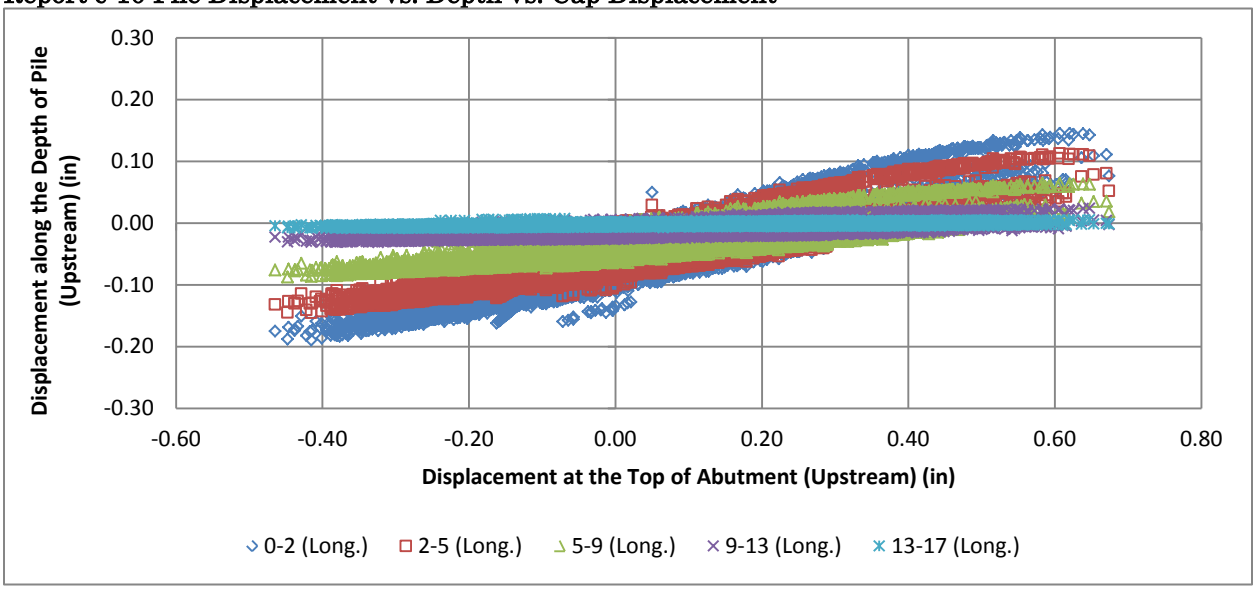

Report c-11 Stress at Gage Location on Pier vs. Time

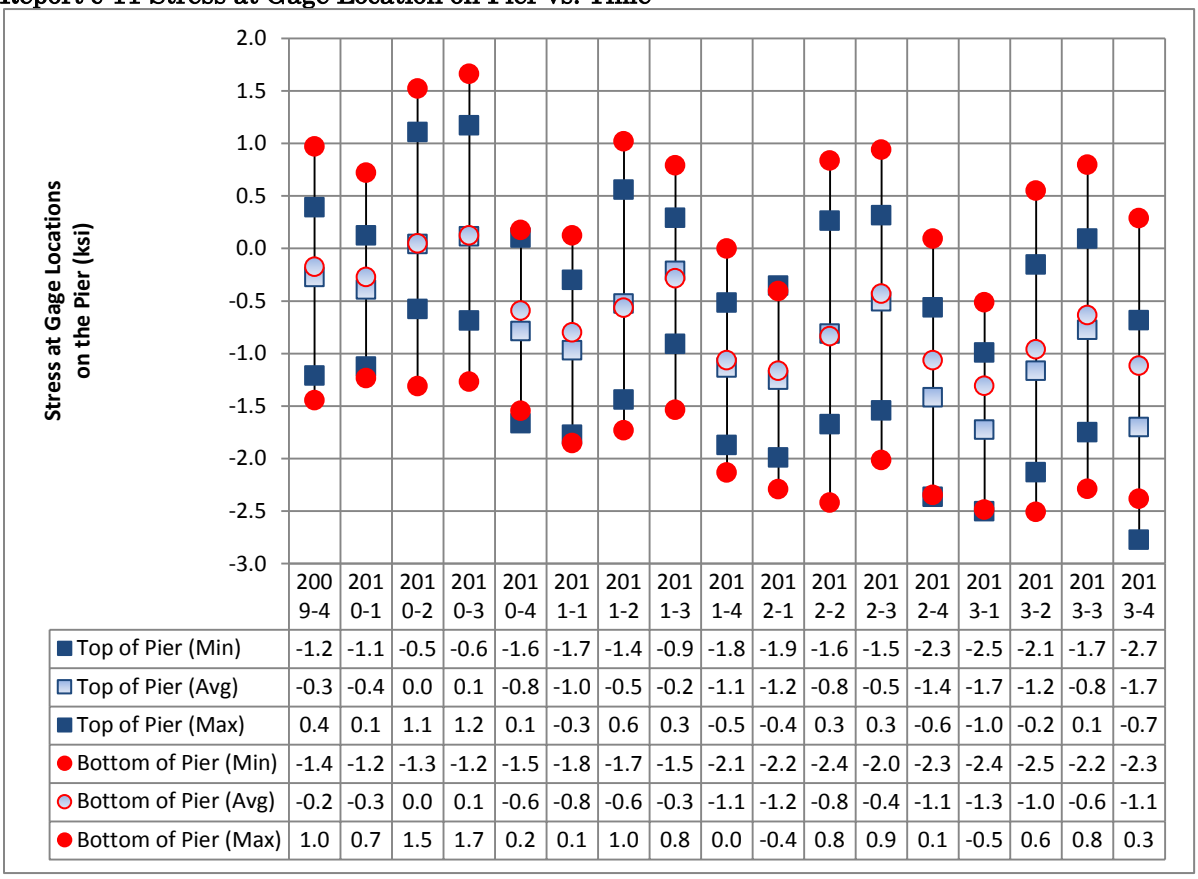

	2009-4	2010-1	2010-2	2010-3	2010-4	2011-1	2011-2	2011-3	2011-4	2012-1	2012-2	2012-3	2012-4	2013-1	2013-2	2013-3	2013-4
Top of Pier (Min)	-1.2	-1.1	-0.5	-0.6	-1.6	-1.7	-1.4	-0.9	-1.8	-1.9	-1.6	-1.5	-2.3	-2.5	-2.1	-1.7	-2.7
Top of Pier (Avg)	-0.3	-0.4	0.0	0.1	-0.8	-1.0	-0.5	-0.2	-1.1	-1.2	-0.8	-0.5	-1.4	-1.7	-1.2	-0.8	-1.7
Top of Pier (Max)	0.4	0.1	1.1	1.2	0.1	-0.3	0.6	0.3	-0.5	-0.4	0.3	0.3	-0.6	-1.0	-0.2	0.1	-0.7
Bottom of Pier (Min)	-1.4	-1.2	-1.3	-1.2	-1.5	-1.8	-1.7	-1.5	-2.1	-2.2	-2.4	-2.0	-2.3	-2.4	-2.5	-2.2	-2.3
Bottom of Pier (Avg)	-0.2	-0.3	0.0	0.1	-0.6	-0.8	-0.6	-0.3	-1.1	-1.2	-0.8	-0.4	-1.1	-1.3	-1.0	-0.6	-1.1
Bottom of Pier (Max)	1.0	0.7	1.5	1.7	0.2	0.1	1.0	0.8	0.0	-0.4	0.8	0.9	0.1	-0.5	0.6	0.8	0.3